Study of conformations in *N*- substituted peptides beyond *N*-methylation
&
Development of bioactive peptide analogs based on Tau derived AcPHF6 and AcPHF6*, and Icosalide A

by

Abha Dangi
10CC17J26034

A thesis submitted to the
Academy of Scientific & Innovative Research
for the award of the degree of
DOCTOR OF PHILOSOPHY
in SCIENCE

Under the supervision of
Dr. Udaya Kiran Marelli

CSIR-National Chemical Laboratory, Pune

Academy of Scientific and Innovative Research
AcSIR Headquarters, CSIR-HRDC campus
Sector 19, Kamla Nehru Nagar
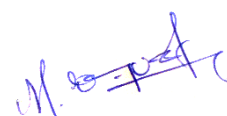Ghaziabad, Uttar Pradesh, 201002 India.

June 2023

Certificate

This is to certify that the work incorporated in this Ph.D. thesis entitled *"Study of conformations in N-substituted peptides beyond N-methylation & Development of bioactive peptide analogs based on Tau derived AcPHF6 and AcPHF6*, and Icosalide A"*, submitted by *Abha Dangi* to the Academy of Scientific and Innovative Research (AcSIR), in fulfillment of the requirements for the award of the Degree of ***Doctor of Philosophy in Science***, embodies original research work carried-out by the student. We, further certify that this work has not been submitted to any other University or Institution in part or full for the award of any degree or diploma. Research materials obtained from other sources and used in this research work has/have been duly acknowledged in the thesis. Images, illustrations, figures, tables, *etc.*, used in the thesis from other sources, have also been duly cited and acknowledged.

Ms. Abha Dangi

Research Student

Date: 26 June 2023

Dr. Udaya Kiran Marelli

Research Supervisor

Date: 26 June 2023

STATEMENT OF ACADEMIC INTEGRITY

I, Abha Dangi, a Ph.D. student of the Academy of Scientific and Innovative Research (AcSIR) with Registration No. 10CC17J26034 hereby undertake that, the thesis entitled "Study of conformations in *N*-substituted peptides beyond *N*-methylation & Development of bioactive peptide analogs based on Tau derived AcPHF6 and AcPHF6*, and Icosalide A" has been prepared by me and that the document reports original work carried out by me and is free of any plagiarism in compliance with the *UGC* Regulations on *"Promotion of Academic Integrity and Prevention of Plagiarism in Higher Educational Institutions (2018)"* and the CSIR Guidelines for "*Ethics in Research and in Governance (2020)"*.
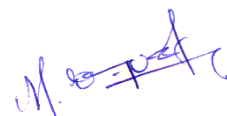
Signature of the Student

Ms. Abha Dangi

Date: 26 June 2023

Place: CSIR-NCL, Pune

It is hereby certified that the work done by the student, under my/our supervision, is plagiarism-free in accordance with the UGC Regulations on *"Promotion of Academic Integrity and Prevention of Plagiarism in Higher Educational Institutions (2018)"* and the CSIR Guidelines for "*Ethics in Research and in Governance (2020)"*.

Signature of the Supervisor

Dr. Udaya Kiran Marelli

Date: 26 June 2023

Place: CSIR-NCL, Pune

DECLARATION

The research work embodied in this thesis has been carried out at CSIR-National Chemical Laboratory, Pune under the supervision of **Dr. Udaya Kiran Marelli**, Central NMR Facility and Organic Chemistry Division, CSIR-National Chemical Laboratory, Pune-411 008. This work is original and has not been submitted in part or full, for any degree or diploma of this or any other university.

Abha Dangi

Central NMR Facility and Organic Chemistry Division

CSIR-National Chemical Laboratory

411008 Pune, India.

My Ph.D. journey has been a very memorable and enjoyable portion of my life, and it would not have been possible without the help and encouragement of some very special people. I'd like to show my gratitude to them for their invaluable help throughout my research journey directly or indirectly.

*First and foremost, I want to express my sincere gratitude to my research supervisor **Dr. Udaya Kiran Marelli**, for giving me the opportunity to work with him and for his unwavering support and encouragement throughout this journey, thank you sir for everything that you have taught me from the day one to completion of my thesis. I sincerely acknowledge your helpful advice and patience during my research work and achieving the endeavour. No words would be suffice to express my gratitude, in my opinion, the utmost way to express my gratefulness to him would be through my future contributions to science and by improving myself through implementing what I have learnt from him.*

*I would like to thank my Doctoral Advisory Committee members, **Dr. Rajesh Gonnade**, **Dr. Moneesha Fernandes**, and **Dr. Pradip Maity** for their continuous support, guidance, and suggestions during the DAC meetings. I am grateful to Prof. A. K. Nangia (former Director), and Dr. Ashish Lele, Director of CSIR-NCL. Dr. Chepuri V. Ramana, (Head, Organic Chemistry Division), Dr. N.P. Argade and Dr. S. P. Chavan (Former Head, Organic Chemistry Division), for giving me this opportunity and providing all necessary infrastructure and facilities to carry out my research work. I thank the Council for Scientific and Industrial Research (CSIR) for providing me with a research scholarship and financial assistance.*

I would especially want to thank central NMR facility team, Dr. P. R. Rajamohanan, T. G. Ajithkumar, Dr. Sapna Ravindranathann, Prashant Mane, and Umesh, as well as Dr. Santhakumari, Ganesh Sevi Nilam from the HRMS division. I would like to express my sincere thanks to the AcSIR coordinators, Dr. B. L. V. Prasad, Dr. Mahesh Kulkarni, Dr. M. Sashidhar, Dr. Santosh Mhaske, and the student academic office staff, P. K. Purushothaman, Poornima Kohle, Vaishali, Komal, Vijaya, and Purnima, for their assistance and cooperation, Glass Blowing section, and DIRC, for their continuous help and support.

I also like to thank the library's personnel, including Mr. Gati Krushna Nayak, Dr. Sunita Barve, and others, for all of their help and for granting access to the collection. I would like to

Chapter 1: Introduction to peptides

Chapter 2: Exploration of N-arylation of backbone amides as a novel tool for conformational modification in peptides

Section A: Design and synthesis of N-aryl cyclic-hexaalanine peptides and their conformational studies by NMR

Section B: Design and synthesis of N-aryl cyclic-hexaalanine peptides and their conformational studies by NMR

Chapter 3: Development of bioactive peptide analogs based on Tau derived AcPHF6 and AcPHF6*

Section A: Residue-based propensity of aggregation in the Tau amyloidogenic hexapeptides AcPHF6* and AcPHF6

Section B: Macrocyclic peptides derived from AcPHF6* and AcPHF6 to selectively modulate the Tau aggregation

Chapter 4: Synthesis, stereochemistry assignment, and NMR structure elucidation of Icosalide A, and its analogues: Evaluation of their antibacterial and antituberculosis activity

NMR	Nuclear magnetic resonance
SPPS	Solid phase peptide synthesis
TEM	Transmission electron microscopy
ACN	Acetonitrile
CD	Circular dichroism
DIPEA	*N*, *N*-Diisopropylethylamine
DMF	*N*, *N*-Dimethylformamide
FMOC	Fluorenylmethyloxycarbonyl
Boc	tert-Butyloxycarbonyl
PyBroP	Bromotripyrrolidinophosphonium
DIC	*N*,*N′*-Diisopropylcarbodiimide
DCC	*N*,*N′*-Dicyclohexylmethanediimine
CDI	N,N'-Carbonyldiimidazole
HCTU	*O*-(1*H*-6-Chlorobenzotriazole-1-yl)-1,1,3,3-tetramethyluronium hexafluorophosphate
HOAt	1-Hydroxy-7-azabenzotriazole
TIPS	Triisopropylsilane
DMAP	4-Dimethylaminopyridine
BTC	Triphosgene (bis(trichloromethyl) carbonate
HPLC	High-performance liquid chromatography
DCHA	Dicyclohexylamine
DPPA	Diphenylphosphoryl azide
THF	Tetrahydrofuran
Rf	Retention factor
ThS	Thioflavin S
ANS	8-anilinonaphthalene-1-sulfonic acid
µM	Micromolar
mL	Millilitre
mg	Milligram

Synopsis Report

	Synopsis of the Thesis to be submitted to the Academy of Scientific and Innovative Research for Award of the Degree of Doctor of Philosophy in Sciences/ Engineering
Name of the Candidate	Abha Dangi
Degree Enrollment No. &Date	Ph. D. in Chemical Sciences (10CC17J26034); January, 2017
Laboratory	CSIR National Chemical Laboratory, Pune
Title of the Thesis	Study of conformations in *N*-substituted peptides beyond *N*-methylation & Development of bioactive peptide analogs based on Tau derived AcPHF6 and AcPHF6*, and Icosalide A
Research Supervisor/ Co-supervisor	Dr. Udaya Kiran Marelli

1. Introduction

Peptides are a unique class of molecules that have filled the therapeutic niche due to their specific biochemical and therapeutic features.[1,2] They are molecularly sandwiched between small molecules and proteins while being biochemically and therapeutically distinct from both. As their molecular weight is between proteins and small molecules, they have advantages and limitations over both. Peptides are attractive as therapeutic agents because of their strong binding affinity towards target receptors, excellent target specificity, low toxicity, and immunogenicity. Peptides do suffer from limitations such as short half-life, low membrane permeability, and poor oral bioavailability. Further, high manufacturing costs have made peptide drugs less affordable. Despite these limitations, in the last couple of decades, there has been an increasing trend in the approval and commercialization of peptide-based drugs.[1] As many as 80 of peptide drugs have been approved by USFDA, 150 of peptides are in the clinical trial phases and, 400–600 peptides undergoing preclinical studies at present.[3,4]

In general, the bioactivity of the peptides is fundamentally determined by their conformations that define the spatial orientation of the side chain functional groups. The last few decades have witnessed

significant advancement in the area of peptides design and research.[4] Numerous peptide modifications were developed to modulate the peptide folding and to alleviate the limitations of the peptides as drugs.[5] These developments include the use of non-proteinogenic amino acids (D-amino acids, beta/gamma/delta, etc. amino acids, modified amino acids, aminoxy acids etc.), cyclization, retro inverso peptides, foldamers, aza peptides, stapled peptides, beta turn mimics, sulphide bridge peptides, click peptides, *N*-methyl peptides to name a few.[6–8] Such synthetic modifications have played a significant role in optimizing the bioactivity of naturally occurring peptides or designing new bioactive peptides.[3]

The journey of peptide-based drug design relies on both the design and employment of methods that modify the conformation and the functional groups. A combination of these two will lead to the structure activity relationship studies of the peptides and, ultimately, the optimization of the activity and the lead development.

Furthermore, low peptide oral bioavailability is another challenge in peptide-based drug design that has garnered special attention in recent times.[9] The above-mentioned synthetic modification strategies were equally employed to either impart or improve the oral bioavailability in peptides. Most importantly, *N*-methylation of backbone amide bonds or using *N*-methyl amino acids was explored to mask the water-exposed non-hydrogen bonded NHs in peptides to improve oral bioavailability.[10–12] Simultaneously, this replacement of amide by its *N*-methyl version also promotes specific conformations or constrains the peptide bond rotation or flipping in the peptides.

2. Statement of the problem: In this work, we aimed to expand the repertoire of methods available for the conformational modification of the peptides. In this direction, we have explored the *N*-arylation of amides as a new method of modification in peptides. We have employed this method on L/D-Ala containing cyclic hexa/penta alanine peptides and characterized their conformations. Further, we aimed to employ the principles of peptide-based drug design to investigate structure activity relationship studies and folding behaviour of biologically significant peptides and peptides of natural origin. For this purpose, we have chosen AcPHF and AcPHF* peptides from Tau protein that is significant for Alzheimer's and Icosalide A, a cyclic depsipeptide of natural origin. Through this study, we were interested in developing rationally designed peptides for modulating the folding behaviour of Tau protein, AcPHF6 and AcPHF6* peptides and optimizing and expanding the biological activity of Icosalide A.

3. Objective

As per the statement of the problem of the thesis, our objectives are

- Introduction of *N*-arylation as a new backbone amide modification tool for conformational fine-tuning of peptides.
- Development of bioactive peptide analogues for tau aggregation inhibition, based on Tau-derived AcPHF6 and AcPHF6*.
- Synthesis and SAR studies of antibacterial peptide Icosalide A and its analogues.

4. Methodology and Results

<div align="center">

Working chapters

</div>

Chapter-1 Design, Synthesis, and NMR-based Conformational Studies of *N*-aryl Peptides.
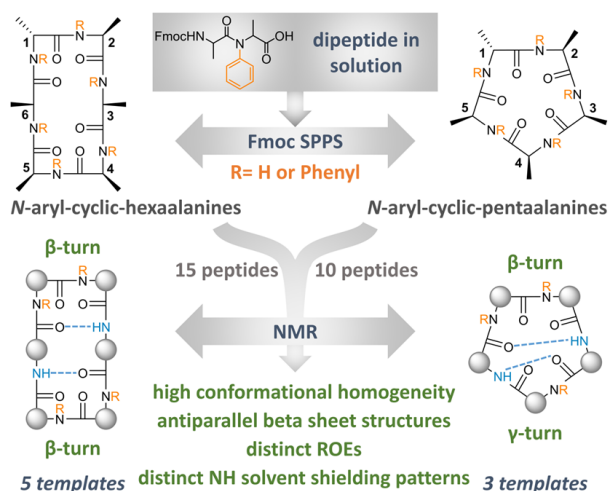
N-aryl-cyclic-hexaalanines   dipeptide in solution   *N*-aryl-cyclic-pentaalanines

Fmoc SPPS
R= H or Phenyl

15 peptides   10 peptides

NMR

high conformational homogeneity
antiparallel beta sheet structures
distinct ROEs
distinct NH solvent shielding patterns

β-turn   γ-turn   5 templates   3 templates

Obtaining a stable, orally available bioactive peptide is a challenging task in the field of peptide therapeutics.[4,5] The biological aspects of peptides are primarily a result of their conformation. Hence, optimizing a peptide's conformation while also bringing in specific functional group changes is a crucial part of the peptide-based drug design. A multitude of peptide design strategies, such as the use of homologous or nonproteinogenic amino acids, cyclization, stereo-inversion, foldamers, stapled peptides, disulphide bridged peptides, and *N*-methylation of backbone amide (extensively studied) are some methods that have been developed and followed to architect peptide folding.[6,7] In the last couple of

decades, *N*-methylation of the backbone amide protons has emerged as one of the multipurpose tools for the chemical modification of cyclic peptides. Kessler's and Lokey's research groups have extensively used *N*-methylation to modify the conformations, bioactivity, lipophilicity or bioavailability in cyclic peptides.[10,13]

As compared to backbone *N*-methylation of amide bonds, other backbone *N*-modifications are underexplored. In this direction, we have hypothesized and explored the backbone amide *N*-arylation as a novel chemical modification in peptides. For our studies, we have considered two model cyclic peptides as parent templates- a cyclic-hexaalanine (CHA) and a cyclic-pentaalanine (CPA)- both containing a D-alanine residue that induces configurational heterogeneity (**Fig 1**). We synthesized a library of 15 *N*-phenyl containing cyclic-hexaalanine (NPCHA; 6 peptides containing one *N*-phenyl-L- or D-alanine and 9 peptides with two *N*-phenyl-L- or D-alanine residues) and 10 *N*-phenyl containing cyclic-pentaalanine (NPCPA; 5 peptides containing one *N*-phenyl-L- or D-alanine and 5 peptides with two *N*-phenyl-L- or D-alanine residues) (**Table 1**) and characterized their conformations by extensive NMR studies.
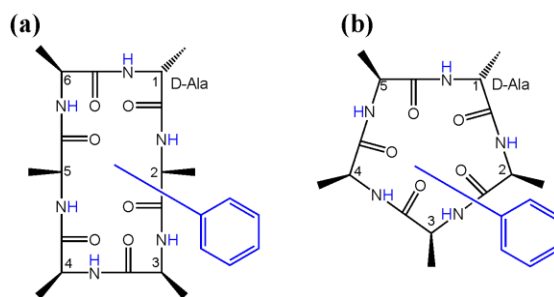
Figure 1. Designed molecules for backbone *N*-aryl modification study.

Section A **Design and synthesis of *N*-aryl cyclic-hexaalanine peptide library and their conformational studies by NMR**

We synthesized a library of 15 *N*-phenyl containing cyclic-hexaalanine (NPCHA; 6 peptides containing one *N*-phenyl-L- or D-alanine and 9 peptides with two *N*-phenyl-L- or D-alanine residues) (**Table 1**). The 15 peptides were synthesized by following a combination of solution and solid phase peptide synthesis chemistry. For the synthesis, *N*-arylation of L- or D-alanine was carried out in solution by following Buchwald-Hartwig method using Iodobenzene to obtain *N*-phenyl-L- or D-alanine.[14] However, due to low nucleophilicity of the arylated amine in *N*-phenyl-L- or D-alanine, the coupling of this monomer turned out to be a very challenging Despite the reaction with various coupling reagents,

the product was either nil or obtained in trace amounts. Finally, the activation of Fmoc-L-Ala-OH to Fmoc-L-Ala-Cl as an acid chloride and coupling to *N*-phenyl-L-ala-OMe in the presence of triethyl amine in dry DCM resulted in reasonable quantities of the dipeptide ester Fmoc-*N*-phenyl-L-Ala-L-Ala-OMe in approximately 55% reaction yield. After having the required dipeptide, we employed solid-phase peptide synthesis to synthesize the library of 15 NPCHA peptides.[15]
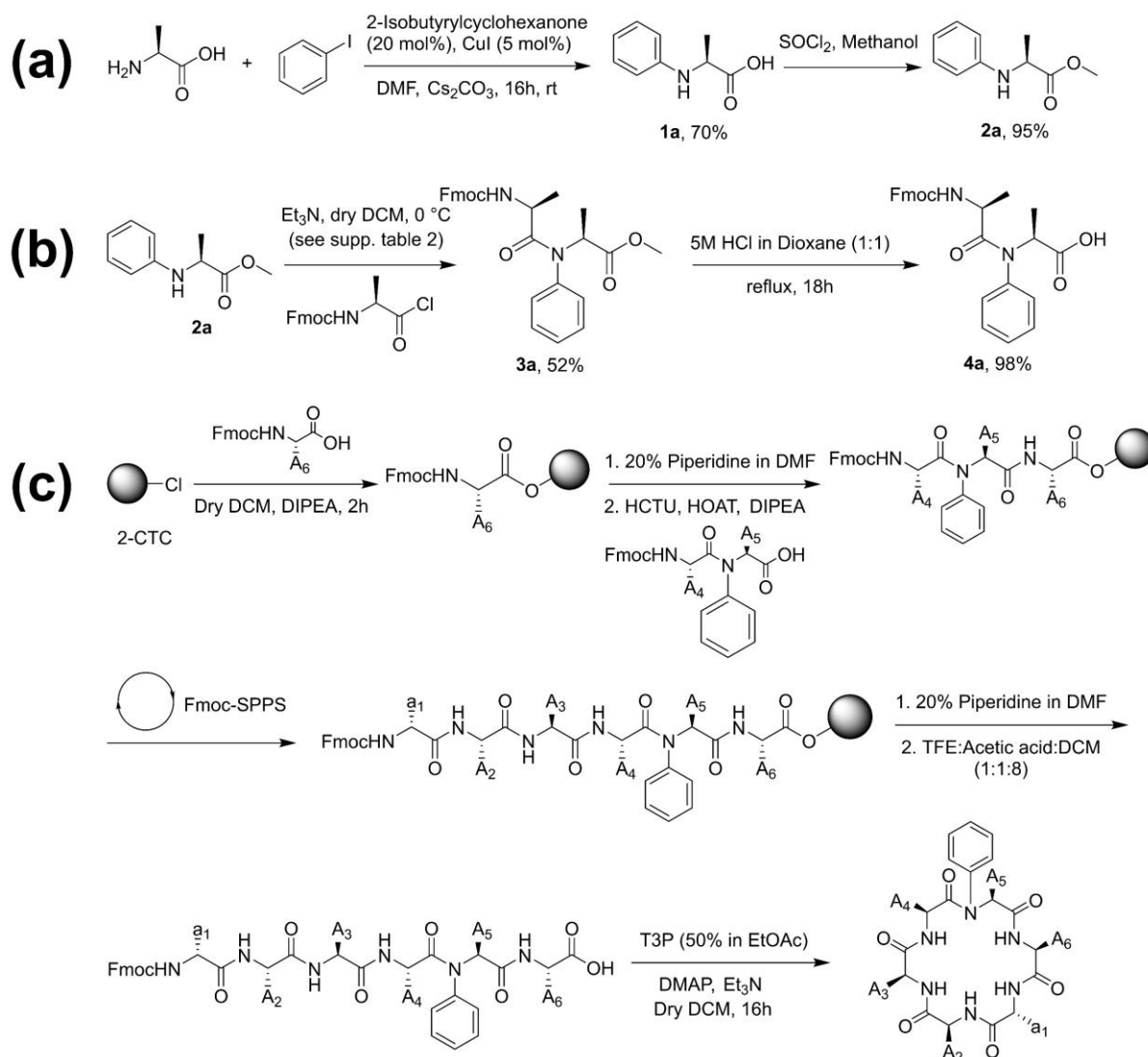
Scheme 1. (a) Synthesis of the *N*-phenyl-L-alanine **(b)** Synthesis of the *N*-aryl dipeptide in solution **(c)** Fmoc-based solid phase peptide synthesis of *N*-aryl peptide on 2-CTC.

Table 1. *N*-aryl cyclic-hexaalanine peptide library synthesized by solid phase peptide synthesis.

S. No.	Name	Sequence					
1	1NPCHA	a	A	A	A	A	A
2	2NPCHA	a	A	A	A	A	A
3	3NPCHA	a	A	A	A	A	A
4	4NPCHA	a	A	A	A	A	A
5	5NPCHA	a	A	A	A	A	A
6	6NPCHA	a	A	A	A	A	A
7	13NPCHA	a	A	A	A	A	A
8	14NPCHA	a	A	A	A	A	A
9	15NPCHA	a	A	A	A	A	A
10	24NPCHA	a	A	A	A	A	A
11	25NPCHA	a	A	A	A	A	A
12	26NPCHA	a	A	A	A	A	A
13	35NPCHA	a	A	A	A	A	A
14	36NPCHA	a	A	A	A	A	A
15	46NPCHA	a	A	A	A	A	A

Note: a = D-Alanine; A= L-Alanine; Shaded cell indicates residue with *N*-phenyl group.
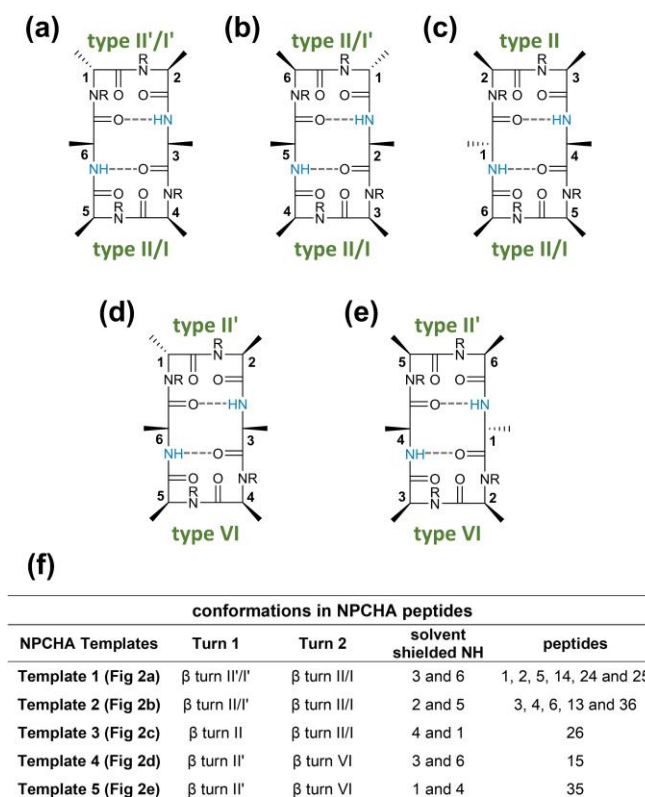
Figure 2. **(a)-(e)** Five different conformational templates observed for NPCHA peptides, **(f)** table showing a summary of the types of conformations observed in NPCHA peptides along with the type of turns in each conformation and the amide NHs that are solvent shielded.

NMR-based Conformational studies of *N*-aryl cyclic-hexaalanine peptides

14 out of 15 NPCHA peptides exhibited an antiparallel beta-sheet structure. The conformational pattern of all the peptides broadly can be divided into five types of template structures based on hydrogen-bonded NHs, structural similarities, and the position of the turn (**Fig. 2a-e**).

First template structure (a): Peptides 1NPCHA, 2NPCHA, 5NPCHA, 14NPCHA, 24NPCHA, and 25NPCHA have type II'/I' β turn around residue 1,2 and type I/II β turn around residue 4,5.

Second template structure (b): Peptides 3NPCHA, 4NPCHA, 6NPCHA, 13NPCHA and 36NPCHA are having type II/I' β turn around residue 6,1 and β-turn II/I around residue 3,4.

Third template structure (c): Peptide 26NPCHA has type II β turn around residue 2,3 and type I/II β turn around residue 5,6.

Fourth template structure (d): 15NPCHA has type II' β turn around residue 1,2 and one signatory type VI β turn around residue 4,5 with a *cis* peptide bond.

Fifth template structure (e): 35NPCHA has type II' β turn around residues 5,6 and one signatory type VI β turn around residues 2,3 with a *cis* peptide bond.

Furthermore, the conformations observed for NPCHA peptides are compared to those in the analogous *N*-Methyl CHA peptides, and we observed distinct differences. To point out some, for 1*N*MeCHA, Beck *et al*. had speculated two fast exchanging conformations with less distinct NMR temperature coefficients for the amide NHs, while the analogous 1NPCHA has a dominant NPCHA Template 1 conformation. For 15NPCHA, the analogous 15*N*MeCHA peptide had the exact same conformation as NPCHA Template 4. On the other hand, the 35NPCHA has starkly differed from its analogous 35*N*MeCHA in populating a single conformation. The four peptides 5NPCHA, 15NPCHA, 25NPCHA and 35NPCHA have revealed conformations that are entirely different from each other, while the analogous 5*N*MeCHA, 15*N*MeCHA, 25*N*MeCHA, and partially the 35*N*MeCHA had identical conformational features.

Section B - Design and synthesis of *N*-aryl cyclic-pentaalanine peptides and their conformational studies by NMR

By following the optimized synthesis conditions described in the above section, we synthesized a library of 10 *N*-phenyl containing cyclic-pentaalanine (NPCPA; 5 peptides containing one *N*-phenyl-L-

or D-alanine and 5 peptides with two *N*-phenyl-L- or D-alanine residues) by a combination of solid and solution phase peptide synthesis (**Scheme 1**) (**Table 2**). Their detailed conformational analysis has been carried out by NMR in which we observed that 9 out of 10 NPCPA peptides showed an antiparallel beta-sheet structure. The conformational pattern in NPCPA peptides is classified into three types of templates based on hydrogen-bonded NHs, structural similarities, and the position of turn (**Fig**. **3a-c**).

Table 2. *N*-aryl cyclic-pentaalanine peptide library synthesized by solid phase peptide synthesis.

S. No.	Name	Sequence					Note:
1	1NPCPA	a	A	A	A	A	
2	2NPCPA	a	A	A	A	A	
3	3NPCPA	a	A	A	A	A	
4	4NPCPA	a	A	A	A	A	
5	5NPCPA	a	A	A	A	A	
6	13NPCPA	a	A	A	A	A	
7	14NPCPA	a	A	A	A	A	
8	15NPCPA	a	A	A	A	A	
9	24NPCPA	a	A	A	A	A	
10	35NPCPA	a	A	A	A	A	

a = D-Alanine; A = L-Alanine; Shaded cell indicates residue with *N*-phenyl group.

(a) type I'/II' — γ-turn
(b) type I/II' — γ-turn
(c) type II — inverse γ-turn

(d)

conformations in NPCPA peptides				
NPCPA Templates	Turn 1	Turn 2	solvent shielded NH	peptides
Template 1 (Fig 3a)	β turn I'/II'	classical γ-turn	3 and 5	2, 4, 5, 14 and 24
Template 2 (Fig 3b)	β turn I/II'	classical γ-turn	5 and 2	1, 3, and 13
Template 3 (Fig 3c)	β turn II	inverse γ-turn	4 and 1	25

Figure 3. **(a)-(c)** Three different conformational templates observed for NPCPA peptides, **(f)** table showing a summary of the types of conformations observed in NPCPA peptides along with the type of turns in each conformation and the amide NHs that are solvent shielded.

First template structure (a): Peptides 2NPCPA, 24NPCPA, 4NPCPA, 5NPCPA, and 24NPCPA have type II/II' beta turn around residue 1,2. One classical gamma turn around residue 4.

Second template structure (b): Peptides 1NPCPA, 3NPCPA, and 13NPCPA have type I/II' beta turn around residue 3,4. The lower classical gamma turn is present around residue 1.

Third template structure (c): 25NPCPA shows beta turn around residue 2,3 and NH of residue 1 and 4 were involved in hydrogen bonding. The lower inverse gamma turn is present around residue 5.

5. Summary- In summary, we have successfully developed a library of 15 cyclohexa and 10 cyclopenta alanine *N*-aryl peptides containing mono and di *N*-aryl motifs, by synthesizing dipeptide in the solution phase. Conformations of all the peptides were established by extensive NMR and MD studies. The data was interpreted and thoroughly compared with the analogous *N*-methyl peptides. We did not observe multiple sets of chemical shifts for any of the peptides, indicating the absence of more than one slow exchanging conformations on the NMR chemical shift time scales. The structural studies on *N*-phenyl series peptides revealed cyclic antiparallel beta sheet conformations with well-defined beta and gamma turns, and hydrogen bonding patterns, which are supported by NMR data. The *N*-phenyl series peptides showcased superior conformational homogeneity compared to their *N*-methyl analogues and exhibited different conformations in the corresponding analogues. We hope that *N*-aryl modification of amide NHs has the potential to be employed as a versatile peptide modification tool in peptide-based drug design approaches.

Chapter 2 Development of bioactive peptide analogues based on Tau-derived AcPHF6 and AcPHF6*

Section A Residue-based propensity of aggregation in the tau amyloidogenic hexapeptides AcPHF6* and AcPHF6

Alanine Mutations on

Ac-VQIINK-NH$_2$ Ac-VQIVYK-NH$_2$

Aggregates

Q → A   A ← Q

✓

V, I, I, N → A   ✗   A ← V, I, V, Y
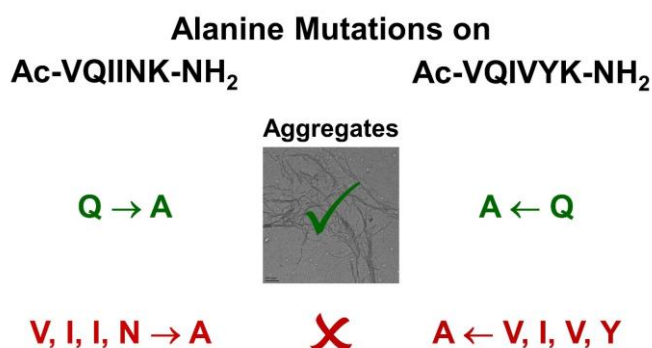
Tau protein is identified to form protein deposits linked with Alzheimer's (AD). The formation of Tau aggregates is prompted by two hexapeptide motifs within Tau; PHF6* and PHF6 NH2 (PHF stands for paired helical filaments). Synthetic analogues of both these hexapeptides, Ac-VQIINK-NH2 (AcPHF6*) and Ac-VQIVYK-NH2 (AcPHF6), which has acetyl protection on the N-terminus and amidation on the C-terminus, are known to form structurally similar fibrils akin to those of Tau. In general, AcPHF6* remains less explored compared to AcPHF6, although recent studies attribute a higher role to ^{275}VQIINK^{280} in Tau aggregation. Despite several studies on these hexapeptides, to our knowledge, the contribution of individual amino acids in AcPHF6 and AcPHF6* towards Tau aggregation has not been examined hitherto, which information is fundamentally important for the design of Tau aggregation inhibitors. Hence, in the present study, the residue-specific propensity of amino acids constituting AcPHF6* and AcPHF6 in their aggregation is investigated.
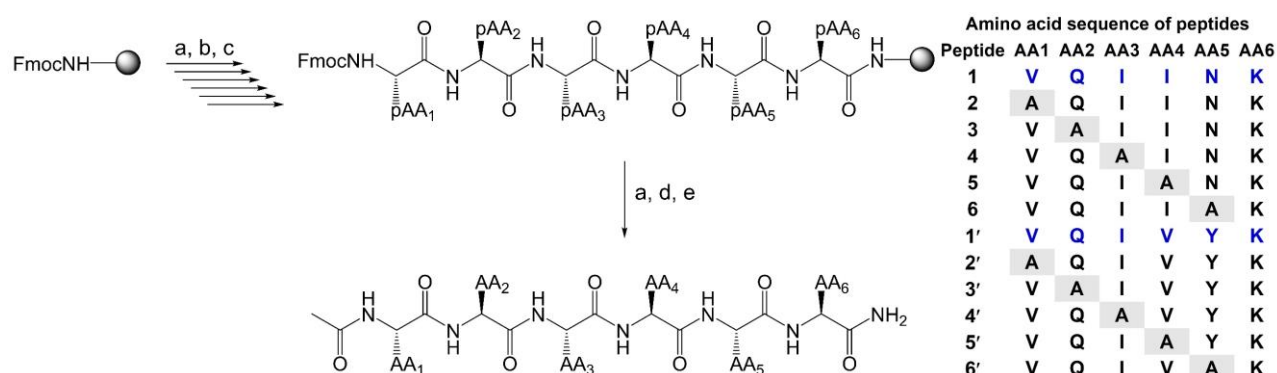
Scheme 2. Scheme showing the synthesis of peptides (**1–6** and **1'–6'**) using Fmoc-based solid phase peptide synthesis on rink amide MBHA resin.

I   **II**
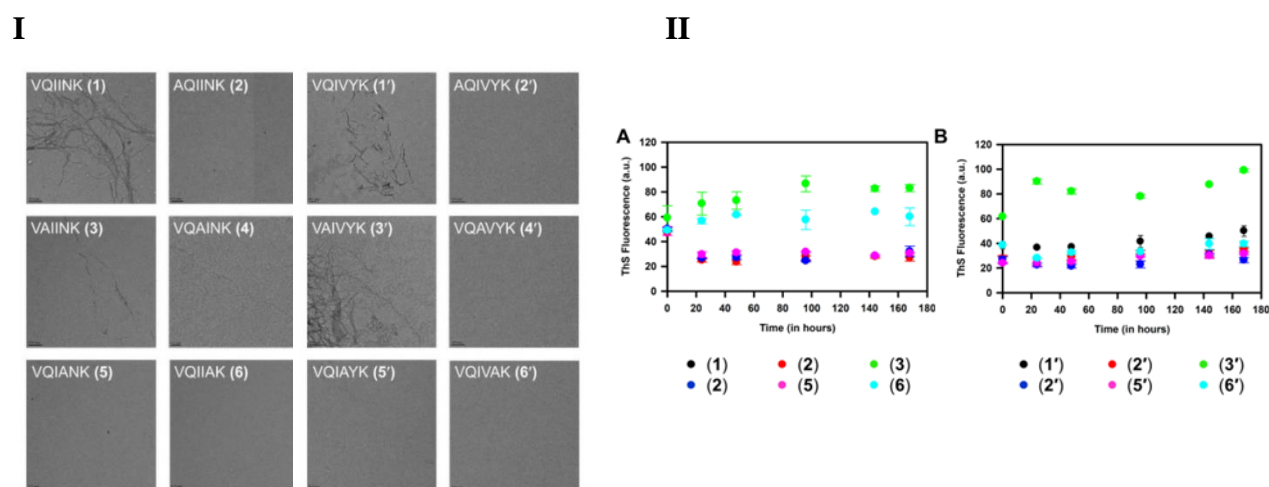
Figure. 4 (I) TEM images for peptides **1–6** and **1'–6'** at the aggregation assay end-point (168 h). **(II)** A) Aggregation of peptides **1-6** monitored by using ThS fluorescence shows the effect of alanine

incorporated at various positions in VQIINK hexapeptide. VQIINK aggregation was found to be affected by substitution of Glu or Asn residues where these substitutions enhanced the aggregation propensity. B) Peptides **1'-6'** showed similar trend in their aggregation propensity as peptide **3'** with glutamine to alanine substitution showed increased aggregation as compared to the other peptides in the group.

For our study, alanine mutation peptides of AcPHF6* and AcPHF6 were synthesized, and their conformational and aggregation properties were characterized using various biophysical and biochemical techniques. A set of twelve peptides consisting of parent peptides AcPHF6* and AcPHF6 and their sequential single-site alanine mutant peptides (**2**–**6** and **2'**–**6'**) were synthesized by employing Fmoc-based solid phase peptide synthesis using rink amide MBHA resin (**Scheme 2**). All of the peptides were subsequently purified by reverse phase semi-preparative HPLC for further studies. Although mutant peptides of **1** and **10** in which lysine is substituted by alanine were synthesized, they could not be purified because of partial solubility in an acetonitrile-water combination and other buffers.

All the peptides were characterized by nuclear magnetic resonance (NMR) spectroscopy, circular dichroism (CD), transmission electron microscopy (TEM) and ThS/ANS fluorescence assay. Our studies show that while the aggregation was suppressed in most of the alanine mutant peptides, while the replacement of glutamine by alanine in both PHF and PHF* enhanced the fibrillization.

Section B AcPHF and AcPHF* based macrocyclic peptides-based inhibitor for tau aggregation

The amyloidogenic hexapeptide sequences VQIVYK and VQIINK from the protein tau not only promote tau aggregation to form neurofibrillary tangles in Alzheimer's disease but also self-aggregate in isolation and act as ideal models to explore the supramolecular chemistry of β-sheet aggregation and amyloid formation related tau protein.[16] Hence, both fragments are interesting targets for the development of Tau aggregation inhibitors (TAI). AcPHF6 and AcPHF6* aggregate in the buffer to form fibrils that resemble those formed by tau. A pair of parallel, in-register, antiparallel-sheets supported by hydrogen bonding, intermolecular zipper locking and Van der Waals interactions make up the fundamental structure of the resultant fibrils in many amyloidogenic proteins and peptides. The atomic structure of AcPHF6 and AcPHF6* fibrils revealed that fibril formation involves hydrogen bond interactions in one direction and non-covalent interactions (hydrophobic) in the opposite direction. Interestingly, the structure of these fibrils contains a 'steric zipper' motif (**Fig. 5**).[17] Hence, we envisaged that breaking any of these interactions by which the hexapeptides packing is propagated, the aggregation

nature of the hexapeptides can be modulated and hence, the aggregation of the Tau protein or its constructs. Therefore, we used the inputs from the residue-based propensity of aggregation that we obtained in the earlier section along with the amide *N*-methylation (to block hydrogen bonds) and the design principles for obtaining macrocyclic peptides with antiparallel beta sheet structure to develop 10 macrocyclic peptides (**Table 3**) based on VQIINK and VQIVYK. All the peptides were characterized for their aggregation behaviour.

MCP1 is derived from the VQIINK sequence and MCP2 is from VQIVYK and MCP3 is the hybrid of both MCP1 and MCP2. In our previous residue-based propensity study it has been revealed that except glutamine, rest of the amino acids in AcPHF peptides show the highest aggregation propensity than alanine.[18] So, in all three macrocyclic peptides (MCP1, MCP2, and MCP3) we have replaced glutamine with alanine in both upper and lower strands and obtained MCP4, MCP5, and MCP6 respectively. Macrocyclic peptides MCP7 and MCP8 obtained by alternate *N*-methylation on the lower strand of MCP1 and MCP2. MCP9 and MCP10 are designed based on our previous study by replacing Val and Ile with alanine (to reduce Van der Waals interaction) along with alternate *N*-methylation on the lower strand to block the further stacking by hydrogen bonding in tau aggregatio

Peptide	Peptide Sequence	Peptide	Peptide Sequence
P1	A V Q I I N a / a V Q I I N A	P6	A V A I V Y a / a V A I I N A
P2	A V Q I V Y a / a V Q I V Y A	P7	A V Q I I N a / a V Q I I N A
P3	A V Q I V Y a / a V Q I I N A	P8	A V Q I V Y a / a V Q I V Y A
P4	A V A I I N a / a V A I I N A	P9	A V Q I I N a / a V Q A A N A
P5	A V A I V Y a / a V A I V Y A	P10	A V Q I V Y a / a V Q A A Y A

🟠 - *N*-Methyl residue, A-alanine mutation

Scheme 3. General scheme for solid phase peptide synthesis of macrocyclic peptides.

Figure 5. **(a)** Tau protein repeat region; **(b)** aggregation model for Tau protein showing hydrogen bonded amides.

All the macrocyclic peptides were synthesized by Fmoc-based solid phase peptide synthesis (**Scheme 3**.) and purified by reverse phase HPLC. All peptides have shown the antiparallel beta-sheet structure as analysed by NMR. The representative conformational model for all the peptides is shown in **Fig. 6** (MCP2). The distant NOEs (**Fig. 6**) NH of Val-1 NH to Val-12 NH, Ile-3 NH to Ile-10 NH, Tyr-5 NH to Tyr-8 NH, Val-1 NH to D-ala-13 Hα and Tyr-8 NH to D-ala-6 Hα and the hydrogen bonded amide NHs (**Table 4**) support the antiparallel beta sheet conformation for MCP2. All the peptides MCP1-MCP10 had similar pattern of temperature coefficients and NOE data.

Figure 6. Scheme showing antiparallel beta-sheet structure of MCP2.

Table 4. Amide NMR chemical shift temperature coefficient for MCP2 showing hydrogen bonded NHs (in blue).

Residue	**V1**	**Q2**	**I3**	**V4**	**Y5**
Temp. Coefficient	0.8	-7	-2.5	-6	-1.6
Residue	**Y8**	**V9**	**I10**	**Q11**	**V12**
Temp. Coefficient	-0.4	-5.5	-2	-4.4	-2.9
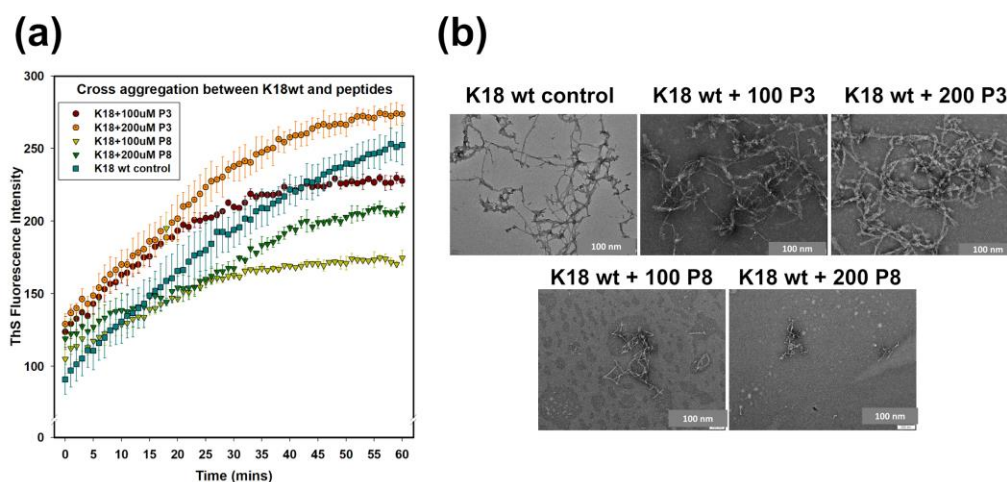
Figure 7. Effect of macrocyclic peptides on Tau aggregation. **(a)** ThS Fluorescence intensities were plotted against time for the cross-aggregation mixtures of K18wt in presence of P3 and P8. 100 µM K18wt with 200 µM P3 showed the highest intensity increase, followed by the 100 µM P3. 100 uM P8 showed higher inhibition, followed by 200 µM P8. **(b)** HR-TEM images for the cross-aggregation mixtures of K18w in presence of P3 and P8. Compared to the K18wt control, K18wt+100 µM P3 shows more mature fibrils and the number increases in K18wt+200P3. K18wt+100 µM P8 shows smaller immature fibers, while K18wt+200µM P8 shows almost complete inhibition of fiber/aggregation formation.

Before going for the tau aggregation inhibition study, first we have done self-aggregation study of MCP1-10. In self-aggregation studies MCP3 is found to exhibit highest aggregation and MCP8 the lowest aggregation. Based on this, we have taken MCP3 and MCP8 peptides for cross aggregation study with AcPHF, AcPHF* and repeat Tau (**Fig. 7**), in which it is observed that MCP3 has promoted the aggregation whereas MCP8 has reduced the aggregation of repeat Tau. Therefore, we could identify two macrocycle peptides that modulated the tau aggregation in pro (MCP3) and contrary (MCP8).

5. Summary- In summary by employing alanine mutation, we explored the residue-based propensity of aggregation in both VQIINK and VQIVYK. Taking inputs from these results and other peptide modification tools, 10 macrocyclic peptides have been designed and synthesized to develop a peptide-based tau-aggregation inhibitor. A conformational study of all macrocyclic peptides was done by NMR, all the peptides exhibited antiparallel beta-sheet structure. From this study, we identified two macrocycle peptides that modulated the tau aggregation in a pro (MCP3) and (MCP8) contrary manner.

Chapter 3 Synthesis, stereochemistry assignment, and NMR structure elucidation of Icosalide A, and its analogues: Evaluation of their antibacterial and antituberculosis activity

Icosalides (**Fig. 8**), new members of the peptolide class of cyclic depsipeptides, were discovered by Boros *et al.* as isolated from a fungal culture. Icosalides are lipodepsipeptidic comprised of six residues, namely, L-Serine, L/D-Leucine alongside beta hydroxy acids having 8 or 10 carbon chains, which form a 20-atom macrocycle core. Unlike most lipopeptides, which contain only one fatty acid chain, the Icosalides are considered unusual for possessing two lipophilic chains as beta-hydroxy acids. Among the three isolated Icosalides, Icosalide **1a** exhibited an antimicrobial activity of MIC 8-16 µg/mL against *Streptococcus pyogenes, S. pneumoniae (Felton),* and *Enterococcus faecalis*. Interestingly, Icosalide **1a** was also found to inhibit the swarming behaviour of the bacteria, a mechanism of antibiotic activity, which is being thoroughly explored.[19,20]

The stereochemistry of the constituent beta hydroxy acids in Icosalides was not identified initially when isolated by Boros *et al.* Dose *et al.* assigned the stereochemistry of beta hydroxy acids as 3-*S*-hydroxy decanoic acid and 3-*R*-hydroxy octanoic acid based on Moscher ester analysis and molecular modeling. In contrary, Jenner *et al.* established the biosynthetic pathway of Icosalides and reported the configurations of both beta hydroxy acids in Icosalide **1a** as *R*. These two studies have left the stereochemistry of the beta hydroxy acids in Icosalides ambiguous.

Structure of Icosalide analogues   **Icosalide 1a**
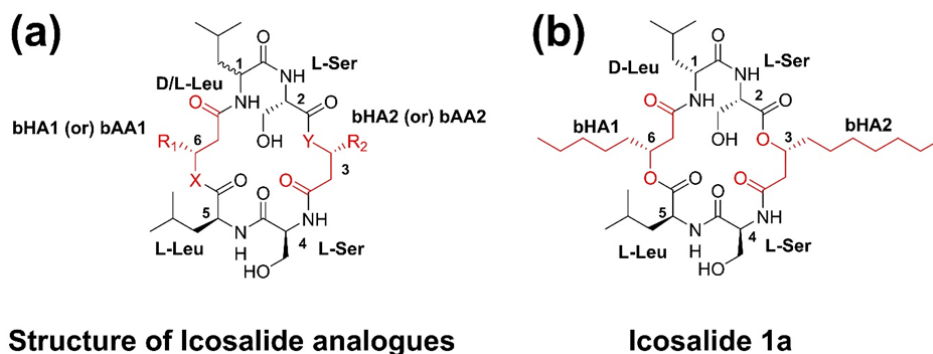
Figure 8. (**a**) General structure representing the Icosalide analogues; and (**b**) the structure of Icosalide **1a**, whose analogues were developed in this study.

Table 5. Sequences of isolated and synthesized Icosalides

Icosalides			Residues			
	1	2	3 (bHA2) $Y=O$, R2=	4	5	6 (bHA1) $X=O$, R1=
1a	I	S	C_7H_{15}	S	L	C_5H_{11}
1a'	I	S	$C_7H_{15}*$	S	L	C_5H_{11}
1a''	I	S	C_7H_{15}	S	L	$C_5H_{11}*$
1a'''	I	S	$C_7H_{15}*$	S	L	$C_5H_{11}*$
1b	L	S	C_7H_{15}	S	L	C_5H_{11}
1c	L	S	C_5H_{11}	S	L	C_5H_{11}
Ester containing Icosalide analogues						
2	I	S	C_3H_7	S	L	CH_3
3	I	S	C_5H_{11}	S	L	C_3H_7
4	I	S	C_9H_{19}	S	L	C_7H_{15}
5	I	S	$C_{11}H_{23}$	S	L	C_9H_{19}
6	I	S	*i*-Pr	S	L	*i*-Pr
7	I	S	Cp	S	L	Cp
Amide containing Icosalide analogues						
	1	2	3 (bHA2) $Y=O$, R2=	4	5	6 (bAA1) $X=NH$, R1=
8	I	S	C_7H_{15}	S	L	H
9	I	S	C_7H_{15}	S	L	C_5H_{11}
	1	2	3 (bAA2) $Y=NH$, R2=	4	5	6 (bHA1) $X=O$, R1=
10	I	S	H	S	L	C_5H_{11}
11	I	S	C_7H_{15}	S	L	C_5H_{11}
	1	2	3 (bAA2) $Y=NH$, R2=	4	5	6 (bAA1) $X=NH$, R1=
12	I	S	H	S	L	H
13	I	S	C_7H_{15}	S	L	C_5H_{11}

L = L-Leucine; I = D-Leucine; S = L-Serine; bHA = beta hydroxy acid; bAA = beta amino acid; *= Chiral centre of this beta hydroxy acid is *S*

The swarming inhibitive nature, unusual lipophilic composition, antibiotic activity of the Icosalide **1a,** and the ambiguity in its structure have attracted us to investigate it. Through this study, we established its precise stereochemical structure via its total synthesis, NMR-based three-dimensional conformation, and further the influence of the lipophilic sidechains and the ester bonds on its activity by synthesizing various analogues (**Table 5**).

Scheme 4. Synthetic schemes, reagents, and conditions (yields). (**A**). stereoselective synthesis of *R*-beta hydroxy acid (a) LAH (1.7 eq.), Dry THF 12 h reflux; (b) CS$_2$ (5 eq.), KOH (5 M); (c) AcCl (1.5 eq.), DMAP (0.1 eq) NEt$_3$ (1.5 eq.), DCM; (d) aldehyde (1 eq.), TiCl$_4$ (1.8 eq.), DIPEA (1.8 eq.), DCM; (e) LiOH (4 eq., 1 M, H$_2$O), THF. (**B**) stereoselective synthesis of *R*-beta amino acid (bAA), (f) EDCI (1.5 eq.), BnONH$_2$ (2.0 eq.), THF-H$_2$O (90%); (g) DEAD (1.0 eq.), PPh$_3$ (1.1 eq.), THF (80%); (h) LiOH, THF MeOH-H$_2$O, 0 °C (95%); (i) Pd/C, H$_2$, MeOH (98%); (j) Fmoc-Cl (1.1 eq.), 10% Na2CO3, dioxane: water. (**C**) Solid phase synthesis of Icosalide A and its analogue - (a) bHA1 or Fmoc-Baa1, DIPEA, DCM (b) 20% piperidine in DMF 20 min (2*10 min) (c) Fmoc-Leu, DIPEA, HCTU, HOAt, NMP (d) Fmoc-Leu, DIC, DMAP DCM (e) Fmoc-Ser(tBu), DIPEA, HCTU, HOAt, NMP (f) bHA2 or Fmoc-bAA2, DIPEA, HCTU, HOAt, NMP 2 h (g) Fmoc-D-Leu, DIPEA, HCTU, HOAt, NMP 2 h (h) Fmoc-D-Leu , DIC DMAP DCM 2 h (i) TFE:AcOH:DCM (1:1:8) (j) HCTU HOAt, DIPEA (k) 50% TFA in DCM.

The Icosalide **1a** and its analogues were synthesized by employing the solid phase peptide synthesis protocol using the Fmoc strategy. The required *R*-beta hydroxy acids (**18a-f**) and *R*- beta-amino acids (**22c-d**) needed for the analogues were synthesized by stereoselective aldol condensation using chiral auxiliary (see Scheme **a, b**). To determine the correct stereochemistry of the constituent beta hydroxy acids in the Icosalide **1a**, we synthesized Icosalide **1a** containing beta hydroxy octanoic acid and beta hydroxy decanoic acid both in *R* configuration as per Jenner *et al*. Further, we have also synthesized the analogue Icosalide **1a'** containing 3-*R*-hydroxy octanoic acid and 3-*S*-hydroxy decanoic acid. Our synthesis studies have shown that Icosalide **1a** with both hydroxy acids in *R* configuration have matched the NMR data reported by Boros *et al.*, Dose *et al.*, and Jenner *et al.*, thus resolving the structural ambiguity associated with Icosalide **1a** while also achieving its total synthesis.

To understand the three-dimensional folding in Icosalide **1a**, NMR-based conformation of **Icosalide 1a** (**Fig. 9**) was determined in DMSO-d_6 at 298 K on Schrodinger Maestro macro model 13.1 using inter-proton distance restraints derived from ROESY experiments. The depsipeptide exhibited a conformation akin to an antiparallel beta-sheet structure in cyclic peptides. A unique feature of the Icosalide **1a** conformation (**Fig. 9**) is the amphiphilic orientation of all the lipophilic chains (from 1-D-Leu, 3-*R*-hydroxy octanoic acid, 3-*R*-hydroxy decanoic acid, and 5-Leu) towards one face of the macrocycle ring and the orientation of the polar sidechains of 2-Ser and 4-Ser towards the opposite face. It is very likely that such orientation promotes Van der Waals interactions and leads to a stable conformation
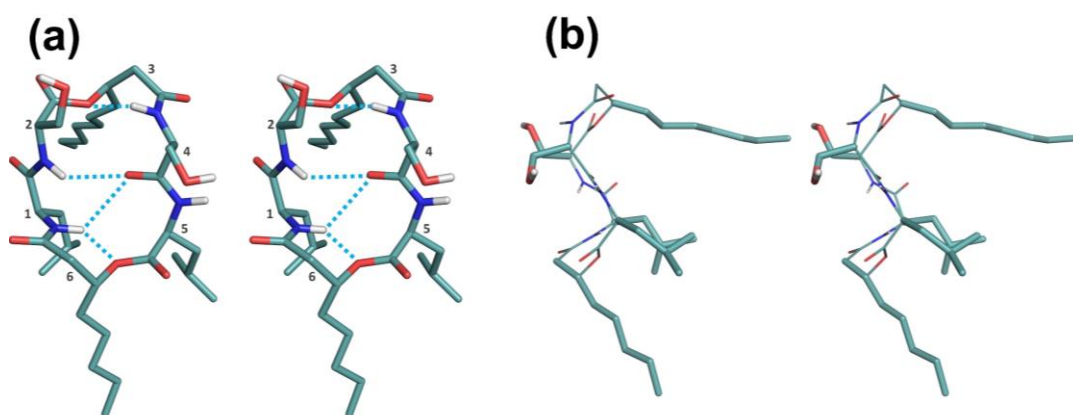
Figure 9. (**a**) Stereoview (top view) of the solution state conformation of Icosalide **1a**. For clarity, all the non-polar hydrogens are omitted. The possible hydrogen bonds are indicated as dashed lines in cyan.

(**b**) Stereoview (side view) of the NMR-derived conformation of Icosalide **1a**. The molecule's backbone is shown as lines to highlight the orientation of the sidechains (shown as sticks).

We have tested all the icosalide analogues for their antibacterial activity (against *B. thuringenesis* and *P. dendritiformis*), swarming inhibiton, anti-mycobacterial (against *M. tuberculosis* H37Ra RFP strain) and anticancer activities (on Hela cervical cancerous cell lines).

5. Summary

The synthesis of Icosalide **1a** antibacterial peptide by solid phase peptide synthesis has been achieved, and 12 analogues were synthesized which varied in the chain length of the lipophilic sidechains and with ester to amide substitution. The absolute stereochemistry of Icosalide A has been unambiguously established via its synthesis and NMR comparison. The conformation of Icosalide A has been determined by NMR spectroscopy and its salient feature is the amphiphilic orientation of sidechains. Peptides with higher lipophilic chain length showed similar antibacterial activity as Icosalide **1a**. Most of the Icosalide analogues have shown AntiTB activity up to 10 μg/mL. Icosalide **1a** is found to be anticancerous against HeLa and ThP1 cell lines.

6. Future direction

Almost all the *N*-aryl peptides exhibited a well-defined conformation and the majority of them present in a single conformation, which implies the potential use of *N*-arylation as a tool for robust conformational control in peptides (**chapter 1**). In addition, the preliminary study of macrocyclic peptide-based inhibitors derived from tau aggregating core sequences shows the potential to inhibit the PHF, PHF*, and R-tau aggregation. As a result, developing more analogues of these macrocyclic peptides through their SAR findings could lead to the discovery of a new peptide Tau inhibitor (**chapter 2**). The work described in **chapter 3** lays the foundation for generating analogues of Icosalide **1a** to develop potential candidates for the treatment of TB and Gram-positive infections.

7. Publication

1. **Dangi, A**.; Bharat Pande, Sonia Agrawal, Dhiman Sarkar, Koteswara Rao Vamkudoth, Kiran Marelli, U. Total synthesis, structure elucidation and expanded bioactivity of Icosalide A: Effect of lipophilicity and ester to amide substitution on its bioactivity. *Org. Biomol. Chem.* **2023 -** OB-COM-05-2023-000809.R1(**Accepted**)

2. **Dangi, A**.; Kiran Marelli, U. Exploration of N-Arylation of Backbone Amides as a Novel Tool for Conformational Modification in Peptides. ***Cover Feature Article*** *Chem. A Eur. J.* 2023.

3. **Dangi, A**.; Balmik, A. A.; Ghorpade, A. K.; Gorantla, N. V.; Sonawane, S. K.; Chinnathambi, S.; Marelli, U. K. Residue-Based Propensity of Aggregation in the Tau Amyloidogenic Hexapeptides AcPHF6∗ and AcPHF6. *RSC Adv.* **2020**, *10* (46), 27331-27335.

4. **Dangi, A**.; Tazeen Qureshi, Subashchandrabose Chinnathambi U. Macrocyclic peptides derived from AcPHF6* and AcPHF6 to selectively modulate the Tau aggregation. *(***Under review***)*

5. Meena, C. L.; Singh, D.; Weinmüller, M.; Reichart, F.; **Dangi, A**.; Marelli, U. K.; Zahler, S.; Sanjayan, G. J. Novel Cilengitide-Based Cyclic RGD Peptides as Avβ3 Integrin Inhibitors. *Bioorganic and Medicinal Chemistry Letters*. **2020** https://doi.org/10.1016/j.bmcl.2020.127039.

6. Sonawane, S. K.; Chidambaram, H.; Boral, D.; Gorantla, N. V.; Balmik, A. A.; **Dangi, A**.; Ramasamy, S.; Marelli, U. K.; Chinnathambi, S. EGCG Impedes Human Tau Aggregation and Interacts with Tau. *Sci. Rep.* **2020**, *10* (1), 1–17.

7. Balmik, A. A.; Chidambaram, H.; **Dangi, A**.; Marelli, U. K.; Chinnathambi, S. HDAC6 ZnF UBP as the Modifier of Tau Structure and Function. *Biochemistry* **2020**, *59* (48), 4546–4562.

8. Balmik, A. A.; Das, R.; **Dangi, A**.; Gorantla, N. V.; Marelli, U. K.; Chinnathambi, S. Melatonin Interacts with Repeat Domain of Tau to Mediate Disaggregation of Paired Helical Filaments. *Biochim. Biophys. Acta - Gen. Subj.* **2020**, *1864* (3), 23–26.

9. Di Leva, F. S.; Tomassi, S.; Di Maro, S.; Reichart, F.; Notni, J.; **Dangi, A**.; Marelli, U. K.; Brancaccio, D.; Merlino, F.; Wester, H. J.; Novellino, E.; Kessler, H.; Marinelli, L. From a Helix to a Small Cycle: Metadynamics-Inspired αvβ6 Integrin Selective Ligands. *Angew. Chemie Int. Ed.* **2018**, *57* (44), 14645–14649.

8. References

1. Muttenthaler, M., King, G. F., Adams, D. J. & Alewood, P. F. Trends in peptide drug discovery. *Nat. Rev. Drug Discov.* **20**, 309–325 (2021).

2. Lau, J. L. & Dunn, M. K. Therapeutic peptides: Historical perspectives, current development trends, and future directions. *Bioorganic Med. Chem.* **26**, 2700–2707 (2018).

3. Lee, A. C. L., Harris, J. L., Khanna, K. K. & Hong, J. H. A comprehensive review on current advances in peptide drug development and design. *Int. J. Mol. Sci.* **20**, 1–21 (2019).

4. Wang, L. *et al.* Therapeutic peptides: current applications and future directions. *Signal Transduct. Target. Ther.* **7**, (2022).

5. Bock, J. E., Gavenonis, J. & Kritzer, J. A. Getting in shape: Controlling peptide bioactivity and bioavailability using conformational constraints. *ACS Chem. Biol.* **8**, 488–499 (2013).

6. Moiola, M., Memeo, M. G. & Quadrelli, P. Stapled peptides-a useful improvement for peptide-based drugs. *Molecules* **24**, (2019).

7. Rinaldi, S. The diverse world of foldamers: Endless possibilities of self-assembly. *Molecules* **25**, (2020).

8.   Otvos, L. Peptide-based drug design: Here and now. *Methods Mol. Biol.* **494**, 1–8 (2008).

9.   Lamers, C. Overcoming the shortcomings of peptide-based therapeutics. *Futur. Drug Discov.* **4**, (2022).

10. Beck, J. G. *et al.* Intestinal permeability of cyclic peptides: Common key backbone motifs identified. *J. Am. Chem. Soc.* **134**, 12125–12133 (2012).

11. Räder, A. F. B. *et al.* Orally Active Peptides: Is There a Magic Bullet? *Angew. Chemie - Int. Ed.* **57**, 14414–14438 (2018).

12. Nielsen, D. S. *et al.* Improving on Nature: Making a Cyclic Heptapeptide Orally Bioavailable. *Angew. Chemie - Int. Ed.* **53**, 12059–12063 (2014).

13. White, T. R. *et al.* On-resin N-methylation of cyclic peptides for discovery of orally bioavailable scaffolds. *Nat. Chem. Biol.* **7**, 810–817 (2011).

14. Sharma, K. K., Sharma, S., Kudwal, A. & Jain, R. Room temperature N-arylation of amino acids and peptides using copper(i) and β-diketone. *Org. Biomol. Chem.* **13**, 4637–4641 (2015).

15. Merrifield, R. B. Solid phase peptide synthesis. *Excerpta Med., I.C.S.* **No.374**, 29–39 (1976).

16. Chaudhary, N., Singh, S. & Nagaraj, R. Morphology of self-assembled structures formed by short peptides from the amyloidogenic protein tau depends on the solvent in which the peptides are dissolved. *J. Pept. Sci.* **15**, 675–684 (2009).

17. Sawaya, M. R. *et al.* Atomic structures of amyloid cross-β spines reveal varied steric zippers. *Nature* **447**, 453–457 (2007).

18. Dangi, A. *et al.* Residue-based propensity of aggregation in the Tau amyloidogenic hexapeptides AcPHF6∗ and AcPHF6. *RSC Adv.* **10**, 27331–27335 (2020).

19. Jenner, M. *et al.* An unusual: Burkholderia gladioli double chain-initiating nonribosomal peptide synthetase assembles 'fungal' icosalide antibiotics. *Chem. Sci.* **10**, 5489–5494 (2019).

20. Boros, C. *et al.* Isolation and identification of the icosalides - Cyclic peptolides with selective antibiotic and cytotoxic activities. *J. Antibiot. (Tokyo).* **59**, 486–494 (2006).

CHAPTER-1

Introduction to Peptides

1.1. Peptides and their therapeutic significance

Peptides are a unique class of molecules that have filled the therapeutic niche due to their specific biochemical and therapeutic features.[1–4] They are molecularly sandwiched between small molecules and proteins while being biochemically and therapeutically distinct from both. Their molecular weight is between proteins and small molecules and they exhibit advantages and limitations over both. Peptides are attractive therapeutic agents because of their unique properties like- strong binding affinity towards target receptors, excellent target specificity, low toxicity, and low immunogenicity- that make them potentially valuable drug molecules.[5–7] Due to their high target specificity, peptide-based drugs provide the potential for minimum side effects, which is a severe drawback in the case of small molecule-based drugs. Furthermore, their low systemic toxicity is a significant advantage compared to small molecules because their degradation products are only amino acids and small peptide fragments. Another unique characteristic of peptides is their structural similarity to the biologically active parent molecules from which they are derived, which helps to reduce the possibility of undesired side effects. Interestingly, peptide-based drug candidate also offers various advantages over proteins and antibodies due to their smaller size. As compared to proteins and antibodies, peptides show better penetration into tissue.[8] Also, peptide-based therapies typically have less complex production processes than protein-based biopharmaceuticals, resulting in reduced production costs, sometimes even comparable to those of small molecules,[9,10] which makes them more affordable compared to proteins and antibodies-based therapeutics. Therefore, peptides are distinctively positioned between small molecules and biopharmaceuticals in several ways (**Table 1.1**).

However, peptides suffer from limitations such as short half-life, low membrane permeability, and poor oral bioavailability.[11,12] These limitations are roadblocks to the development of peptide drugs.[13] When exposed to the gastrointestinal tract environment without any protection, the amide bonds rapidly get hydrolyzed by enzymes *in vivo*. Because of this peptide bond hydrolysis by enzymes, peptides are chemically and physically unstable, with a short half-life and rapid elimination *in vivo*. The membrane permeability of peptides is determined by various parameters, including peptide length, type, composition of different amino acids and their conformations.[14] Peptides, in general, are unable to permeate the cell membrane and target intracellular targets, limiting their use in drug development. According to Lau *et al.* (2018), more than 90% of peptides in the clinical development stage currently target extracellular targets such as G-protein coupled receptors (GPCRs), gonadotropin-releasing hormone (GnRH) receptors, and Glucagon-like peptide 1 (GLP-1) receptors.[15] Further, the high

manufacturing costs of peptides compared to the small molecules have made peptide-based drugs less affordable.

Table 1.1. **Advantages and limitations of peptide-based therapeutics**

Advantages		Drawbacks
▪ High potency and selectivity toward a broad range of targets ▪ High chemical and biological diversity ▪ High target specificity ▪ Minimum risk of systemic toxicity (as the degradation products are amino acids and peptide fragments)		▪ Poor metabolic stability ▪ Poor membrane permeability ▪ Poor oral bioavailability ▪ Rapid systemic clearance ▪ High production costs (in comparison to small molecule drugs)
As compared to small molecule drugs: ▪ Fewer side effects (due to their high target specificity) ▪ Lower accumulation in tissues (due to their short half-life) ▪ Discoverable from the encoded nucleic acids	As compared to proteins and antibodies: ▪ Higher efficacy ▪ Better penetration into tissues (owing to their smaller size) ▪ Potential for less immunogenicity ▪ The defined chemical structure that can be synthesized chemically ▪ Lower manufacturing costs (chemical versus recombinant production) ▪ Greater stability (can be stored at room temperature)	

Despite all these limitations, there has been an increasing trend in the approval and commercialization of peptide-based drugs in the last couple of decades.[15–17] Peptides have proven to be a great starting point for the development of novel treatments due to their exceptional target specificity, which translates into remarkable safety, tolerability, and efficacy. Peptide-based drugs have increased significantly since the beginning of the twenty-first century. Structural biology, recombinant biologics, and new synthetic and analytical tools have considerably accelerated the process of peptide drug development.[19–22] A meticulous system of peptide-based drug development has been built, which involves the design, synthesis, structural modification by incorporating various modification tools, and finally, their activity evaluation. As a result of the sophisticated drug development procedure, since 2000, 33 non-insulin peptide medications have been approved globally (**Table 1.2**).[23] The pharmaceutical industry and academia have been paying more attention to the medicinal potential of peptides. As many as 80 peptide drugs have been approved by the FDA, 150 peptides are in the clinical

trial phases, and 400-600 peptides are currently undergoing preclinical studies.[1] This is expected to grow significantly in the coming period.[23]

Table 1.2. **Peptide drugs approved since 2000, with their targets and function**.[2]

Target name	Peptide name	First approval	Function
GLP-1 receptor	Exenatide	2005	Indicated for Type 2 Diabetes Mellitus
	Liraglutide	2009	
	Lixisenatide	2013	
	Albiglutide	2014	
	Dulaglutide	2014	
	Semaglutide	2017	
GLP-2 receptor	Teduglutide	2012	Treatment of short bowel syndrome and malabsorption
GC-C receptor	Linaclotide	2012	Treatment of irritable bowel syndrome (IBS)
Calcitonin receptor	Pramlintide	2005	Treatment of Type 1 and Type 2 Diabetes Mellitus
GnRH receptor	Abarelix	2003	Treatment of advanced prostate cancer
	Degarelix	2008	
Binding to the active site of the 20S proteasome	Carfilzomib	2012	Treatment of multiple myeloma
NOD2 protein	Mifamurtide	2009	Treatment of high-grade, resectable, non-metastatic osteosarcoma
OT receptor	Carbetocin	2001	Used for postpartum haemorrhage
TRH receptor	Taltirelin	2000	Spinocerebellar degeneration
MC receptors	Bremelanotide	2019	Indicated for hypoactive sexual desire disorder
PTH1 receptor	Teriparatide	2002	Treatment of osteoporosis
	Abaloparatide	2017	
Guanylate cyclase C	Plecanatide	2017	Treatment of chronic idiopathic constipation

Target name	Peptide name	First approval	Function
NPR-A	Nesiritide	2001	Treatment of acute decompensated heart failure
AT$_1$ receptor	Angiotensin II	2017	Indicated for sepsis and septic shock
Beta2-receptor	Icatibant	2008	Approved for use in acute attacks of hereditary angioedema
gp41	Enfuvirtide	2003	Used in combination therapy for the treatment of HIV-1
GHRH receptor	Tesamorelin	2010	Reduction of HIV lipodystrophy
N-type calcium channels	Ziconotide	2004	Management of severe chronic pain
Thrombopoietin receptor	Romiplostim	2008	Treatment of chronic immune thrombocytopenic purpura
Human erythropoietin receptor	Peginesatide	2012	Treatment of anemia associated with chronic kidney disease
Pulmonary surfactant	Lucinactant	2012	Prevention of respiratory distress syndrome
CaSR	Etelcalcetide	2016	Indicated for secondary hyperparathyroidism
MC1 receptor	Afamelanotide	2014	Prevention of phototoxicity
Somatostatin receptors	Pasireotide	2012	Treatment of Cushing's disease
	Lutetium Lu 177 dotatate	2018	Treatment of somatostatin receptor-positive gastroenteropancreatic neuroendocrine tumors
	Edotreotide gallium Ga-68	2019	Indicated for diagnosing somatostatin receptor positive neuroendocrine tumors
Melanocortin-4 receptor	Setmelanotide	2020	Indicated for chronic weight management of obesity

Most of the cellular activities involve protein-protein interactions (PPIs), which have an impact on biological processes by causing changes in protein properties like enzymatic activity and binding capabilities. Therefore, the PPIs are viewed as one of the best possible sources for the design of the next-generation peptide therapies.[4] The molecules which can efficiently bind with proteins and interfere with protein-protein interactions are considered novel candidates for drug development. By using such a

structure-based method, PPI inhibitors can be designed by starting with peptide binding region obtained from protein interaction sites. The secondary structure of the polypeptide chain in the binding domain or interaction region in the PPI, which aligns the side chains of amino acids in a specific way, serves as a conceptual starting design. So, obtaining a peptide such that it is constrained and resembles the bioactive conformation in the PPI interaction is one of the main goals in peptide chemistry.[24] For this purpose several methodologies have been developed and are in use for shaping the peptides to match the target bioactive conformations; this branch is referred to as peptidomimetics.[25–27]

These intrinsic advantages and disadvantages provide both difficulties and opportunities in the journey of peptide-based drug development.

1.2. History and the key inventions in peptides and peptide-based therapeutics

The first synthetic glycylglycine dipeptide was developed in 1901 by Emil Fischer and Ernest Fourneau, which is regarded as the beginning of the peptide research field.[28] Later, for the next 50 years, developments in the peptide field were modest. Further, in 1922, the first medicinal use of insulin, derived from the animal pancreas, transformed the treatment of type 1 diabetes. Following world war II, the use of synthetic peptides for medical purposes began. The initial research of peptide-based therapeutics started with fundamental studies of natural human hormones, insulin, oxytocin, vasopressin, and gonadotropin-releasing hormone (GnRH) and their specific physiological activities in the human body.[29,30] Later, it took almost four decades for chemically synthesized peptide hormones, oxytocin and vasopressin to reach the clinic. Oxytocin and vasopressin were first chemically synthesized in 1953 by Vincent du Vigneaud's group[29,30], for which Vigneaud was recognized with the Nobel Prize in Chemistry in 1955. However, the synthesis of peptides via solution-phase chemistry is a very time-consuming procedure, as it required months to years of labor for the synthesis. Later the development of solid-phase peptide synthesis (SPPS) in 1963 by Merrifield transformed the field of peptide synthesis, for which invention, he was awarded the Nobel Prize in chemistry in 1984.[31]

The therapeutic peptides market first emerged in the 1970s, when Novartis developed Lypressin a synthetic version of porcine, and a Vasopressin mimic. Peptides and proteins, excluding vaccines, made up more than 10% of the industry in 2000, when the overall ethical pharmaceutical business was estimated to be worth $265 billion.[32] Between 1970 and 2003, about 30 peptides were available on the market and later on, industrial groups like Ciba's Robert Schwyzer and Sandoz's Charles Huguenin entered the field of peptides and increased the commercial interest in peptides as therapeutics.

Further, as numerous peptide-based drugs were discovered, the finding and approval of cyclosporine A, an immunosuppressant drug that is orally available, surfaced a new way for peptide-based drug development.[33] Cyclosporine was approved as an immunosuppressive drug in 1983, and it remains an inspiring example that peptides and their mimetics can be orally available.[33] It is a cyclic undecapeptide having 7 *N*-methylated amino acids and one D-amino acid with unique structural features. It is a naturally occurring and membrane-permeable peptide with all remarkable drug-like properties and continues to inspire peptide chemists and peptide drug designers.

All the above mentioned inventions and discoveries led to remarkable advancements in this field and resulted in the approval of more than 80 peptide drugs worldwide, and since 2000, 33 non-insulin peptide medications have been approved globally.[34] As a result, the development of peptide drugs has become one of the most important areas in pharmaceutical research.
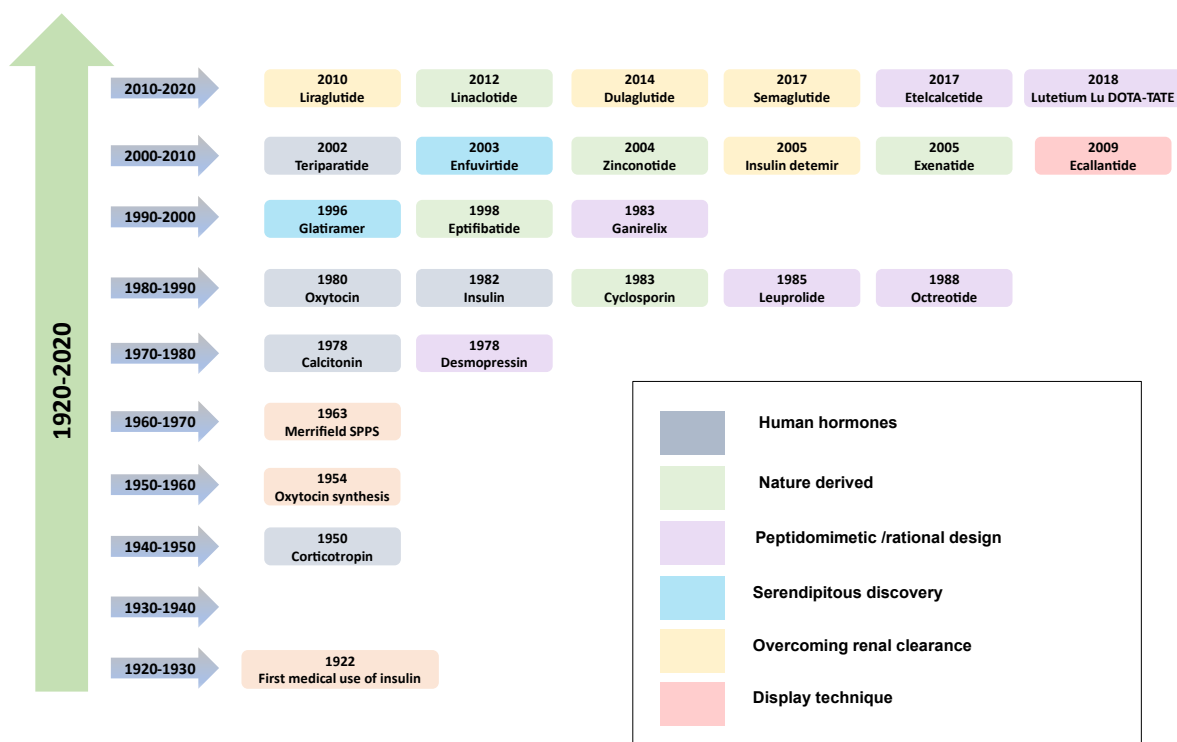
Figure 1.1. Remarkable discoveries (decade-wise) in the field of peptide therapeutics.[35]

Peptides have essential regulatory roles in many physiological processes and they can interact with a variety of biological targets under pathological conditions, which opens up a broad spectrum of possibilities for their biomedical applications. Due to the advancement of synthetic strategies like SPPS and its advanced version- the microwave solid phase peptide synthesis,[36] the synthesis of isolated and modified peptides has become easy and fast. Furthermore, the advancements in synthetic strategies have

expanded the peptidomimetic approaches.[37,38] The effect of these developments can be seen in the trends of peptide-based drug approvals in each decade, which has significantly increased over the years.[35]

1.3. Synthetic strategies for peptides

The chemical synthesis of peptides is well-developed, especially by the invention of solid-phase peptide synthesis. Generally, there are two synthetic strategies available for peptides (1) solution phase synthesis (SPS) and (2) solid phase peptide synthesis (SPPS). Sometimes the combination of both strategies, called hybrid synthesis, is also being used for the development of peptides and their mimetics.

1.3.1. Solution Phase Synthesis (SPS)

Solution phase synthesis is the traditional method for peptide synthesis in which each amino acid is coupled sequentially. Long peptides are synthesized by utilizing the fragment condensation approach. In this synthesis, the target peptide is first broken down into short fragments by retro design approach, and then each required fragment is synthesized separately. Finally, once all the required fragments are obtained, they are joined sequentially to get the desired peptide. The main benefit of solution phase synthesis is that one can deprotect and purify intermediate products at each step to get the required peptide in high quantity and purity (**Figure 1.2**).

Initially, most of the peptides were synthesized by SPS, which include oxytocin (a neuromodulating nonapeptide),[30] porcine gastrin-releasing peptide (a hormone that stimulates the secretion of gastric acid in the stomach), and human insulin (a 51 amino acid peptide hormone that controls carbohydrate metabolism in the body).[39,40].

Synthesis

Separation

Purification
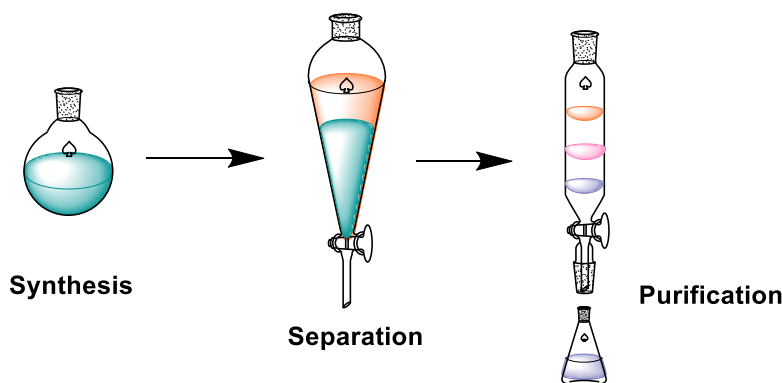
Figure 1.2. Block diagram representation of solution phase peptide synthesis.

Even though SPS is simple and affordable to scale up, the slow reaction time still needs to be improved, which is a major disadvantage of this method.

1.3.2. **Solid Phase Peptide Synthesis (SPPS)**

Solid Phase Peptide Synthesis methodology is well established and has been significantly improved in both methodology as well as synthetic materials, since its discovery, and now it plays an important role in modern peptide synthesis. SPPS, first established by Merrifield in 1963, has quickly emerged as one of the most effective and efficient methodologies for synthesizing peptides. The attachment (loading) of the first amino acid to an insoluble polymeric resin by a covalent bond is the first step of this method. Later, a series of deprotections and amide coupling reactions are carried out to increase the peptide chain length in a sequential manner. The peptide synthesis by using insoluble solid support has several benefits. First, filtration and washing are used to separate resin-bound peptides from soluble reagents and solvents, which takes less time and effort than the workup approach for the separation of compounds used for solution phase synthesis. This automated peptide synthesis made the development of peptides very easy and fast as compared to solution-phase synthesis by removing the purification at each step. The solid phase peptide synthesis consists of three components, resin, amino acid, and coupling reagent. Various resins, such as 4-methyl benzhydryl amine (HMBA) resin, Wang resin, 2-chlorotrityl chloride (CTC) resin, and Merrifield resin, are commonly used resins in SPPS and peptides are linked to them via the C-terminal carboxylic groups.

1.3.2.1. **Types of resins used for solid phase peptide synthesis**

(i) Merrifield resin

Merrifield resin is used to immobilise carboxylic acids and alcohols of the amino acids at the C-terminus for the solid-phase synthesis of peptides. It is also utilised as a starting point to develop a range of modified resins. Merrifield resin can be used to generate single compounds as well as libraries of compounds in either a mixed or parallel method. It uses the Boc/Bzl strategy in solid phase peptide synthesis. Boc group is a temporary amino protecting group and benzyl is used for side chain amine or hydroxyl group protection. While the boc group can be removed by simple acidolysis with TFA, the benzyl-type protecting groups are resistant to repeated exposure to relatively powerful acids, such as 30% TFA in CH_2Cl_2, which is required to remove the boc group. After the peptide has been synthesised, it is separated from the solid support by treating it with strong acids, mostly with anhydrous HF or trifluoromethanesulfonic acid.
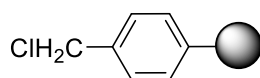
Merrifield resin

(ii) PAM resin

PAM (*p*-Hydoxymethylphenylacetamidomethyl polystyrene) is also used for solid phase peptide synthesis by using the Boc strategy. In the case of Merrifield resin, the frequent Boc deprotection reactions by trifluoroacetic acid (TFA) during synthesis lead to significant losses of peptides. PAM resin provides better stability to TFA, however, this resin has found limited use in solid phase organic chemistry because its peptide cleavage conditions are very harsh such as the use of HF.
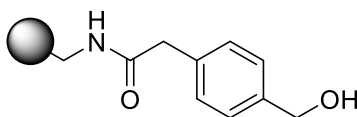
PAM resin

(iii) Wang resin

Wang resin is the most commonly used resin for acid substrates. 4-hydroxybenzyl alcohol linker keeps the polystyrene core together. A phenyl ether bond connects the linker to the resin, while a benzylic ester or ether bond connects the linker to the substrate. Despite its high resistance to a wide range of reaction conditions, this benzylic ester or ether bond is quickly destroyed by moderate treatment with an acid, most commonly with trifluoroacetic acid.
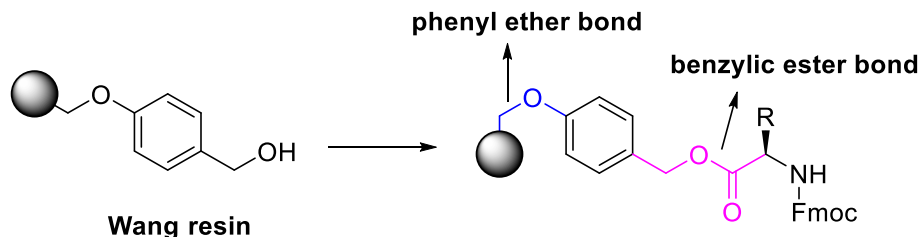
Wang resin

(iv) Amide terminal forming resin

Rinkamide and PAL resins are the two most widely used solid phase supports for the synthesis of amide compounds. All of these resins were initially developed for the Fmoc method of peptide synthesis. Cleavage of the peptides from these resins can occur under mild conditions of using 1% TFA. Each of these resins is supplied with an amine covered by a Fmoc group to ensure stability during

9

storage, therefore piperidine pretreatment is necessary to liberate the free amine. Standard amide-forming conditions, such as DIC/HOBt, HBTU, or BOP, can be used for the coupling of acids.

Rink Amide resin   **PAL resin**   **Sieber Amide resin**
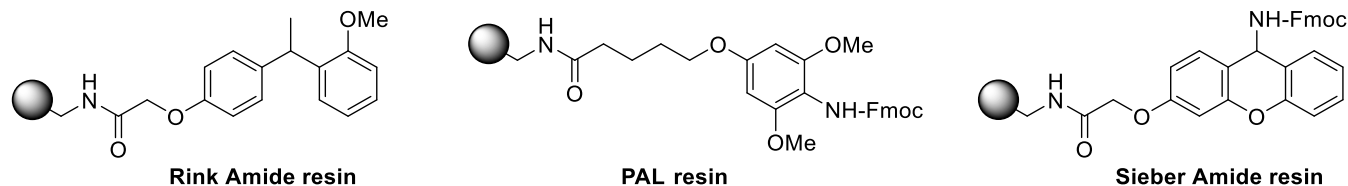
(v) MBHA Resin

MBHA (methylbenzhydryl amine) is an amide-forming resin similar to Rink amide in terms of structure. Although it is not Fmoc protected, diisopropylethylamine or another base must be used to activate it.

MBHA resin
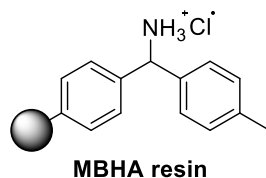
(vi) 2-Chlorotrityl Chloride Resin

2-Chlorotrityl choride resin is a highly acid sensitive resin used in Fmoc-based solid phase peptide synthesis. Peptides from this resin can be cleaved by mild acidic conditions.

2-Chlorotrityl resin
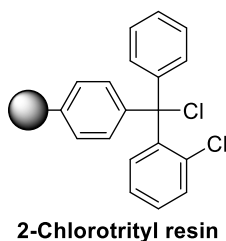
1.3.2.2. Coupling reagents

The chemical synthesis of peptides involves the formation of peptide bonds. This process involves two steps- activation of the carboxyl group to make the carboxyl OH a good leaving group and the amine activation with a base. The acid can be converted to an activated ester by using various coupling reagents containing uronium, phosphonium and triazole groups (**Figure 1.3**).[41]
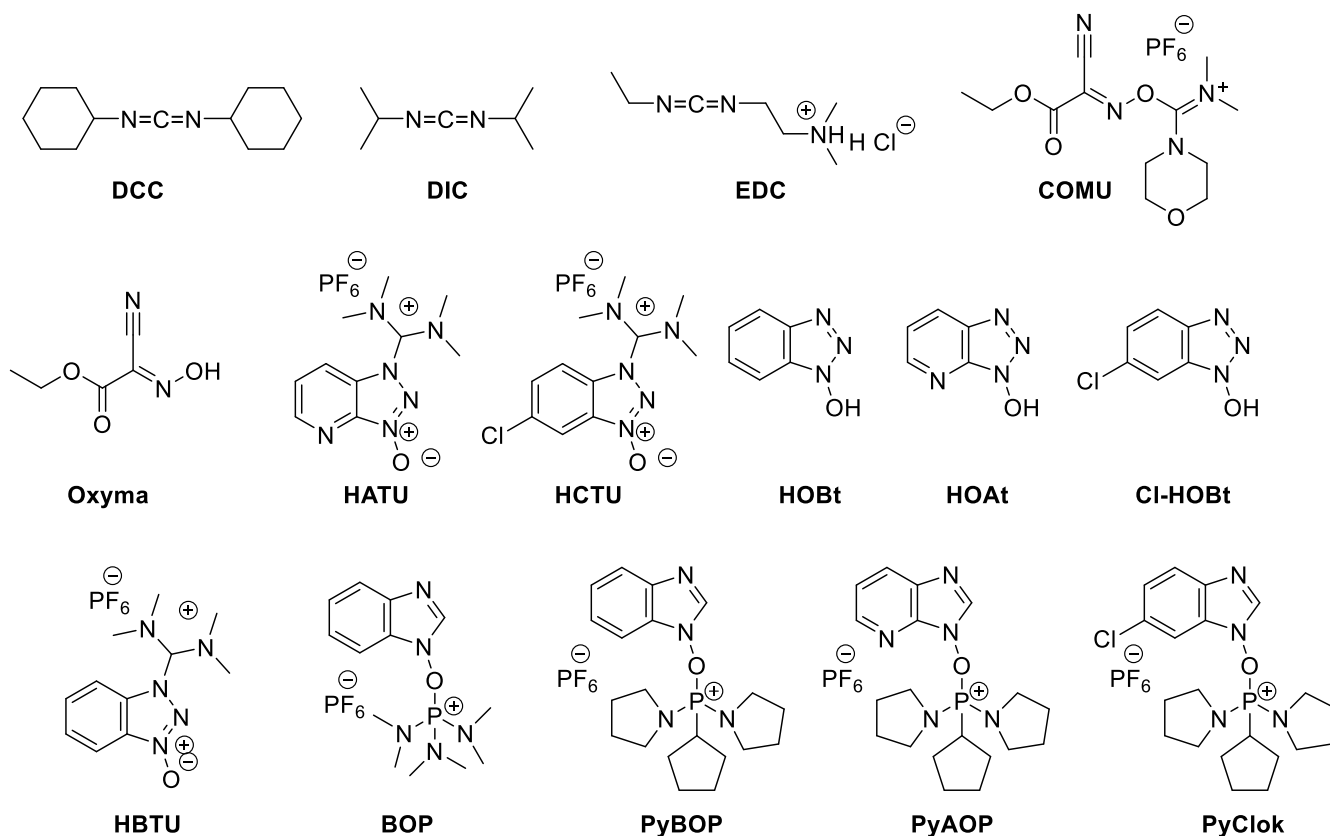
Figure 1.3. Various coupling reagents and additives used in SPPS.

1.3.2.3. The general protocol for SPPS

For solid phase peptide synthesis, the initial step is the attachment of the first amino acid (the C-terminal residue) to the resin (**Figure 1.4**). Then unreacted sites of the resin are capped by suitable reagents. The alpha-amino group and the reactive side chains of amino acids are protected by a transient protective group to stop the self-polymerization of the amino acid. Following this, the *N*-alpha protecting group of the resin-bound amino acid or peptide is removed in a deprotection process and the resin is washed to remove by-products and excess reagents. After that, the next amino acid is coupled to the resin-bound amino acid or peptide. Further, the cycle of coupling and deprotection is repeated until the desired peptide sequence is achieved. Finally, the desired linear peptide is cleaved from the resin. The cleaved linear peptide can further be cyclized in the solution phase if required. Moreover, the impurities in the final SPPS product are primarily produced from incomplete or side reactions during the synthesis procedure, which makes the subsequent purification quite simpler by HPLC. Based on the orthogonal protecting groups, the SPPS has two strategies, namely, Fmoc/tert-butyl and Boc/benzyl based solid phase peptide synthesis. Fmoc solid phase peptide synthesis is more preferable as compared to Boc strategy because the later requires deprotection by harsh TFA at every step.
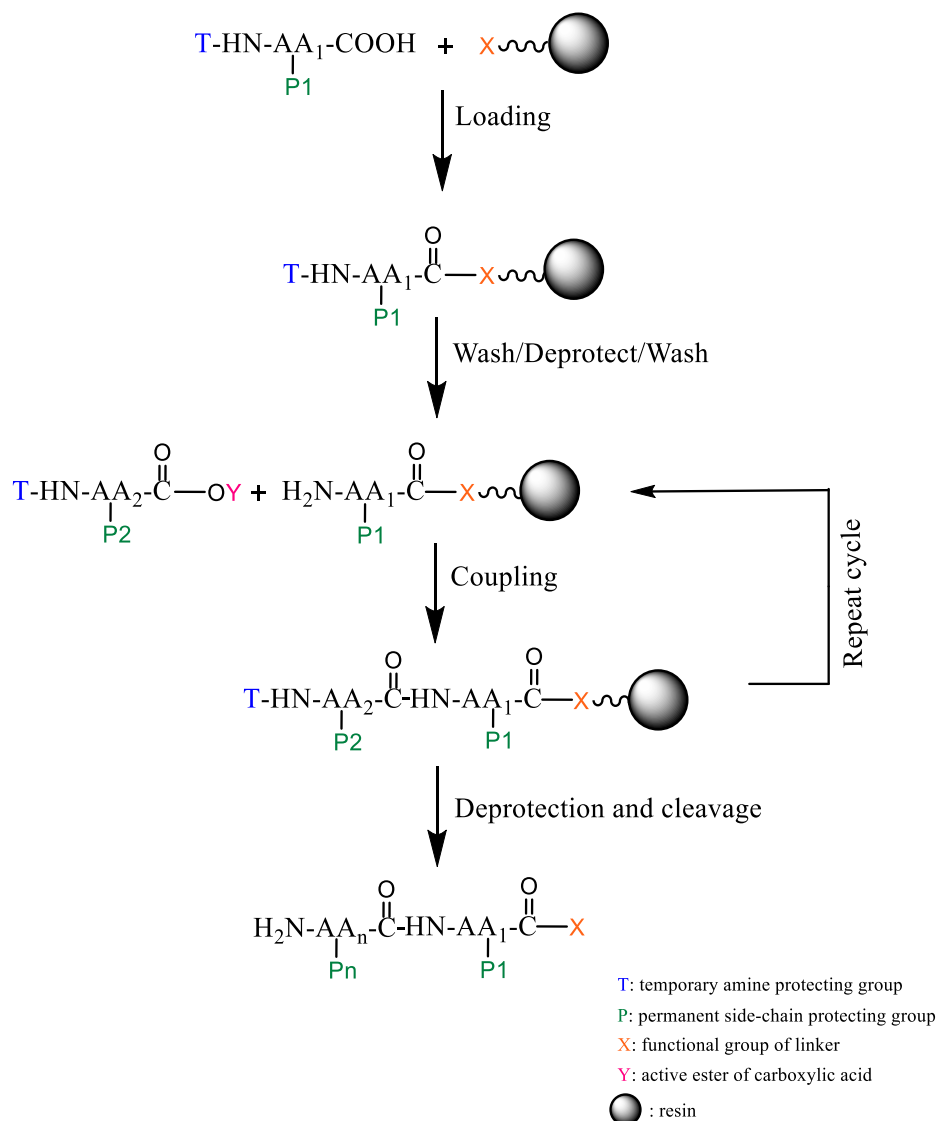
Figure 1.4. Schematic representation of solid phase peptide synthesis protocol.

1.4. Conformations in peptides and their effect on biological activity

Synthetic modifications have played a significant role in optimizing the bioactivity of naturally occurring peptides or designing new bioactive peptides that display organized three-dimensional folding. The alpha-helix, beta-pleated sheet, and random coils are the most common folds in biochemistry that are widely occurring or can be introduced in synthetic peptides by logical modifications like stapling, or by using turn inducers.

(a) Alpha helix

Alpha helix is a commonly occurring secondary structure in proteins in which the main chain's CO and NH groups form a hydrogen bond, to stabilize the helix. The CO group of each $(i)^{th}$ amino acid interacts with the NH group of the $(i+4)^{th}$ amino acid to form a hydrogen bond. Hence, except for the amino acids near the end of the helix, all main-chain CO and NH groups in an alpha helix are hydrogen bonded (**Figure 1.5**). This tight packing of hydrogen bonding offers a very high rigidity, which eventually provides high stability to the molecule.
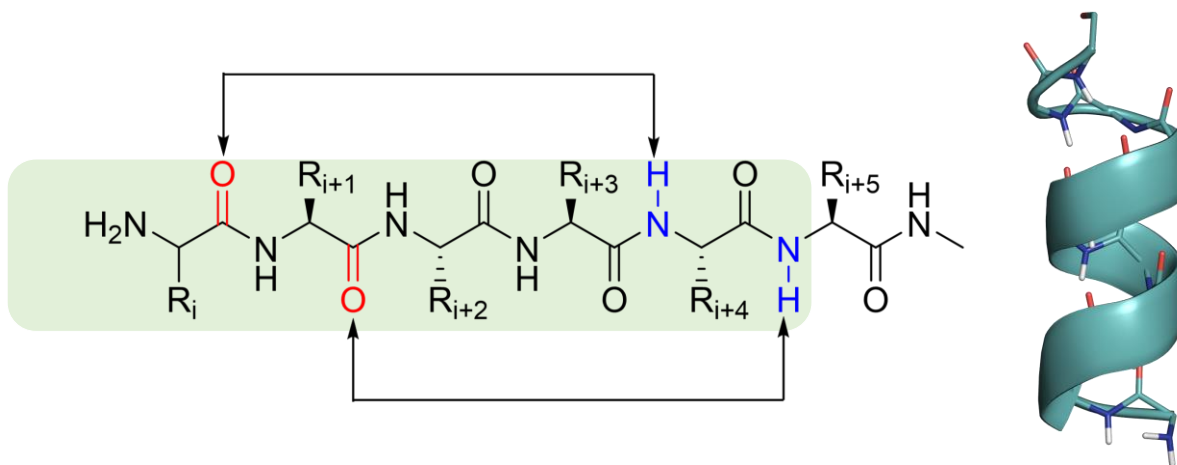
Figure 1.5. Schematic and 3D representation of hydrogen bonding pattern in alpha helix conformation.

(b) Beta-pleated sheet

Beta-pleated sheet is a common secondary structure present in medium sized peptides and proteins.[42] They are made up of beta strands that are joined laterally by backbone hydrogen bonds, resulting in a sheet that is typically twisted and pleated. A beta strand typically has three to ten amino acid residues, and they are organized next to one another to form a dense network of hydrogen bonds. In this instance, the NH groups in one strand's backbone form hydrogen bonds with the CO groups in the backbones of the adjacent strands. To show the orientation, the N- and C- termini are given to both ends of the peptide chain, respectively. N-terminus represents the location at which a free amine group is present. In the beta-sheet structure, two strands run either in the same direction (parallel) or opposite direction (antiparallel) while forming the hydrogen bonds between the residues of both strands.

Based on the N to C terminus direction of running strands, the beta sheet conformations are divided into two types, parallel beta-sheet, and antiparallel beta-sheet (**Figure 1.6**).

(a)

(b)
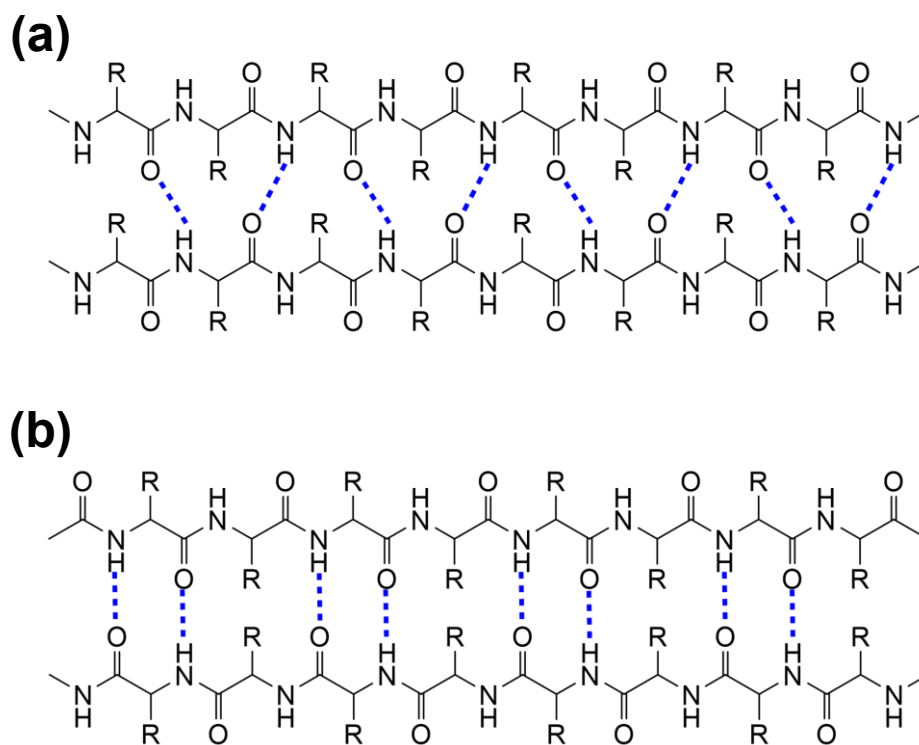
Figure 1.6. Schematic representation of beta-sheet conformations (**a**) parallel beta-sheet, (**b**) antiparallel beta-sheet.

Beta turn

Beta turn is formed when the proteins or peptide chain reverse their direction to join two different secondary structural elements. Beta turn involves a hydrogen bond between the CO of ith residue and the NH of $(i+3)^{th}$ residue (**Figure 1.7**). The "beta hairpin" is a beta turn that connects two antiparallel beta strands. Beta turns are classified into several varieties based on the orientation, shape and dihedral angle (**Figure 1.7**).

Gamma turn

Gamma turns are three-residue turns that commonly have a hydrogen bond interaction between the CO of residue i^{th} and the NH of $(i+2)^{th}$ residue (**Figure 1.7**). Gamma turns are of two types; classical (φ, ψ) (75°, -65°) and inverse (φ, ψ) (-75°, 65°) gamma turns.
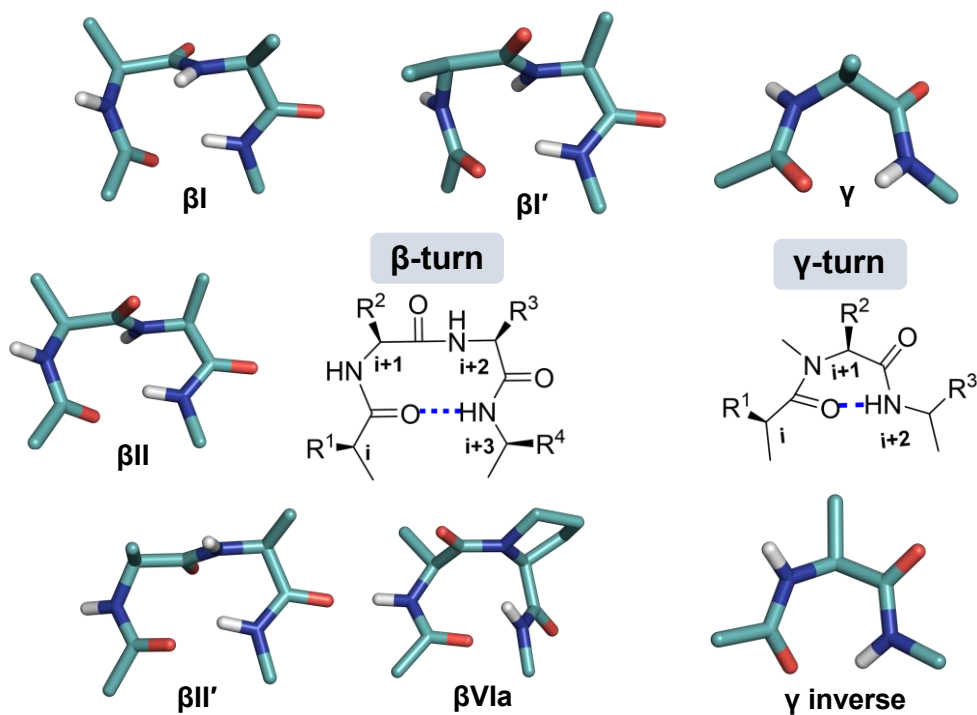
Figure 1.7. Representation of types of beta and gamma turns in peptides.

Dihedral angles

The angle formed by two planes that both pass through the same bond is known as a dihedral angle.[43] Dihedral angles play a significant role in three dimensional structure prediction of proteins and peptides because they define the backbone of proteins and peptides, which, together with side chains, determines the overall protein conformation. The two dihedral angles for an α-amino acid are defined as, phi (φ) = C(i-1), N(i), Cα(i), C(i) and psi (ψ) = N(i), Cα(i), C(i), N(i+1)
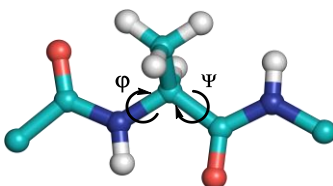
Figure 1.8. Representation of dihedral angles (φ and ψ) in a dipeptide.

Table 1.3. Dihedral angle table for different β and γ-turns.

Type	φ_{i+1}	ψ_{i+1}	φ_{i+2}	ψ_{i+2}
I	−60°	−30°	−90°	0°
II	−60°	120°	80°	0°
VIII	−60°	−30°	−120°	120°
I′	60°	30°	90°	0°
II′	60°	−120°	−80°	0°
VIa1	−60°	120°	−90°	0°*
VIa2	−120°	120°	−60°	0°*
γ-turn	−75°	65°		
Inverse γ-turn	75°	−65°		

* Type VIa1 and VIa2 have *cis* peptide bond at i+2 position.

(c) Random coil

In a protein′s secondary structure certain regions lack the normal secondary structure and the regular hydrogen bonding pattern. These regions are known as random coils, and they can be found in two places in proteins- terminal regions (either N or C terminus) and loop regions where there is no secondary structure. Random coil conformations are always found in proteins and peptides.
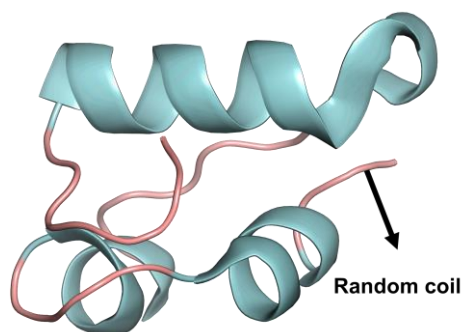
Figure 1.9. Representation of random coil conformations (in a rose colour) in Insulin.

Ramachandran plot

The N-Cα and Cα-C bonds in the main chain of a polypeptide are comparatively free to rotate and hence the torsion angles φ and ψ, respectively, stand in for these rotations. In order to find stable conformations, G. N. Ramachandran used computer models of small polypeptides to repeatedly change φ and ψ. The structure was analysed for atom-atom interactions in each configuration. Atoms were viewed as solid spheres with van der Waals radii-based dimensions. As a result, φ and ψ angles that

cause spheres to collide correspond to conformations of the polypeptide backbone that are sterically forbidden.
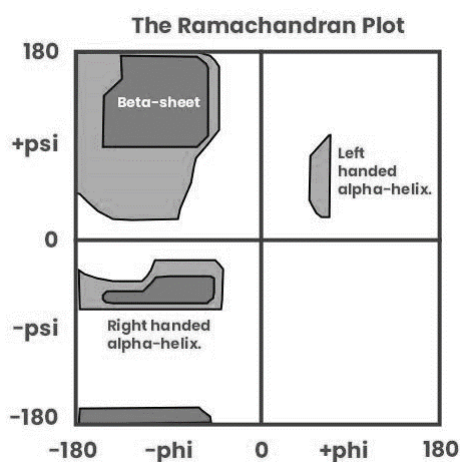
Figure 1.10. Representation of Ramachandran plot showing different regions of secondary structure.

The white regions in the diagram above depict polypeptide atoms that are closer together than the sum of their van der Waals radii (**Figure 1.10**). With the exception of glycine, which is unique in that it lacks a side chain, all amino acids are sterically banned in these positions. The permitted zones are alpha-helical and beta-sheet conformations, while the shaded regions correspond to conformations with no steric collisions. If a shorter van der Waals radius is employed in the computation, or if the atoms are allowed to grow closer together, the dark shaded areas reflect the allowed zones. As a result, the extra region of the left-handed alpha-helix is revealed.

1.5. **Peptide modifications to modulate the peptide folding**

In general, the bioactivity of the peptides is fundamentally determined by their conformations that define the spatial orientation of the side chain functional groups. As mentioned earlier, the last few decades have witnessed significant advancement in the area of peptides design and research.[2,44] Numerous peptide modifications were developed to modulate the peptide folding and to alleviate the limitations of the peptides as drugs.[45,46] These developments include use of non-proteinogenic amino acids (D-amino acids, beta/gamma/delta etc. amino acids, modified amino acids, aminoxy acids etc.), cyclization, retro inverso peptides,[47] foldamers,[48–50] aza peptides,[51,52] stapled peptides,[53–55] beta turn mimics,[56] sulphide bridge peptides,[57,58] click peptides,[59,60] use of *N*-methyl peptides to name a few.[10,49,55] Such synthetic modifications have played a significant role in optimizing the bioactivity of

naturally occurring peptides or designing new bioactive peptides.[61–63] These peptidomimetic modifications strengthen the enzymatic stability of peptides.

The journey of peptide-based drug design relies on both i) the design and ii) the employment of methods that modify the conformation and the functional groups. A combination of these two will lead to the structure activity relationship studies of the peptides and ultimately, the optimization of the activity and the lead development. The basic strategies used for peptide modification are outlined in Figure **1.11**, which are briefly described below.
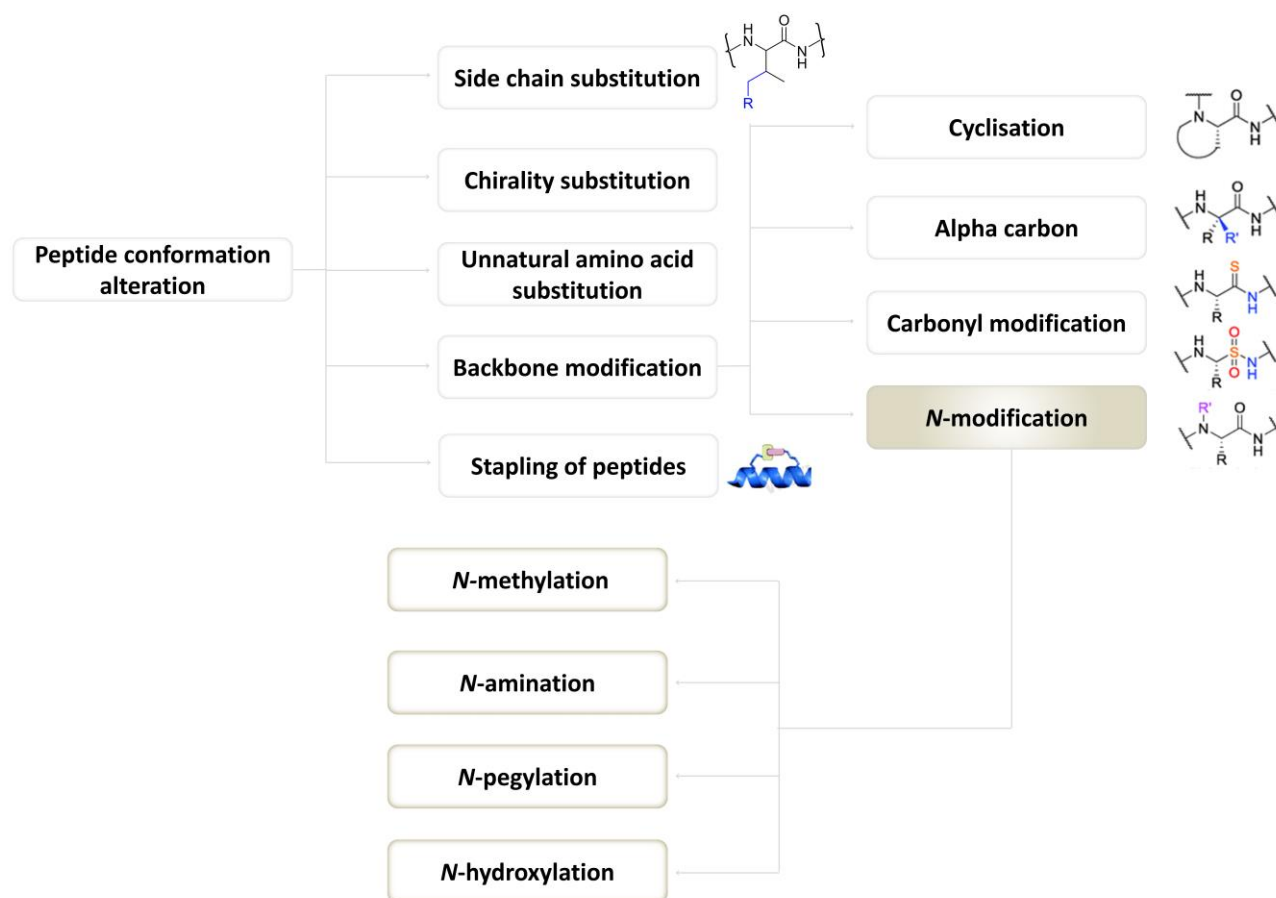
Figure 1.11. A broad classification of the strategies used for the alteration of peptide conformation.

1.5.1. **Cyclization**

Cyclization is a typical modification approach for constraining a peptide into its bioactive target-bound shape and thereby enhancing its pharmacological effects and cell permeability.[64] Biologically active peptides with cyclic ring structures are found in both natural as well as chemically modified peptides.[65–69]

Traditional methods for cyclizing peptide chains include head-tail amidation, disulfide bond formation between cysteines, sidechain amine to C-terminal carboxyl group, and sidechain carboxyl group to *N*-terminal amidation (**Figure 1.12**).[70,71] Among these methods of cyclization, head-to-tail, and side chain-to-side chain cyclizations are the most commonly used. There are lots of biologically active N-to-C cyclic peptides in nature. Some examples include vancomycin, which has antibacterial activity, cyclosporin A, which has the immunosuppressive function, gramicidin, lysobactin[72,73] and tyrocidine,[74] which have bactericidal activity. Cyclization provides conformational rigidity to the peptides as compared to their linear counterparts by restricting the available freedom of rotations. As a result, the cyclization makes peptides enzymatically more stable and permeable due to the lack of the free acid and amine termini, which can be easily recognized and cleaved by enzymes. The cyclization strategy is one of the best methods for increasing membrane permeability in combination with other modifications.[2] Broadly four types of cyclization are in practice (**Figure 1.12**).
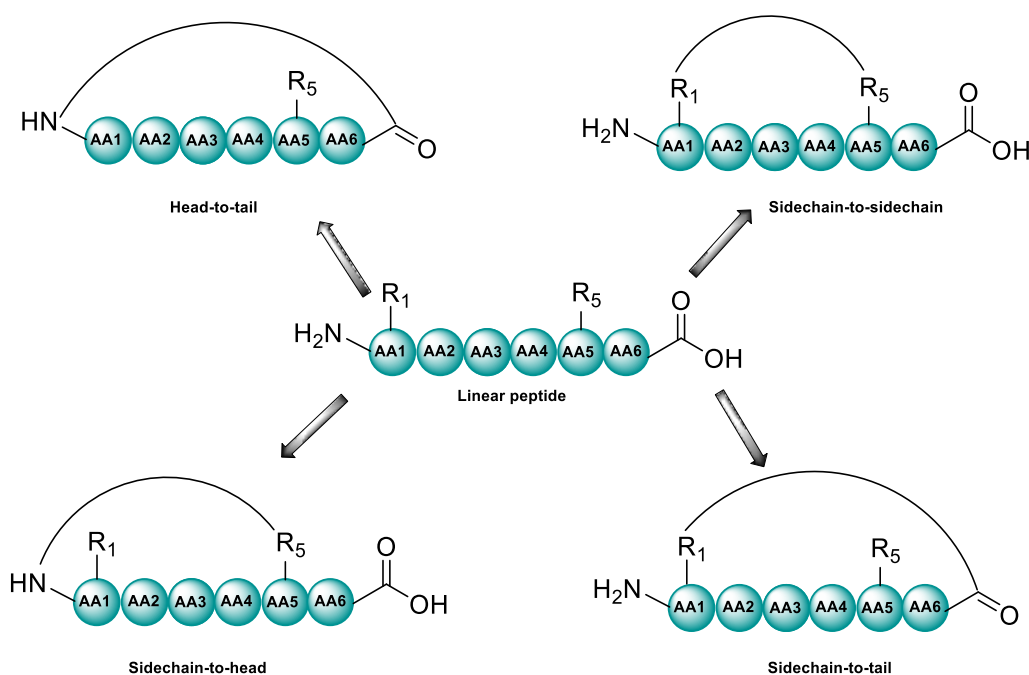
Figure 1.12. Four possible ways to constrain a peptide in a macrocycle. N-terminus is considered the head of peptides, and C-terminus is the tail of peptides.

1.5.2. **Peptide foldamers**

Synthetic oligomers which can fold into a specific 3D shape in solution, in order to mimic the structural behaviour of naturally occurring peptides, proteins, and nucleotides are known as "foldamers".[75,76] Numerous studies have been conducted dealing with the design, synthesis, characterization, and application of foldamers since their first description nearly two decades ago.

Foldamers have the capacity to overcome various drawbacks of peptide and protein based therapeutics, such as protease susceptibility, ultimately resulting in potentially increased half-life and higher oral bioavailability compared to standard peptides.[48,50,77] Foldamers are composed of a mixture of different types of α, β, and γ amino acids, peptoids, oligoureas as well as aza-and aminoxy peptides. By varying the types of amino acids forming the foldamer, its folding nature can be modified, sometimes even with a calculated design.
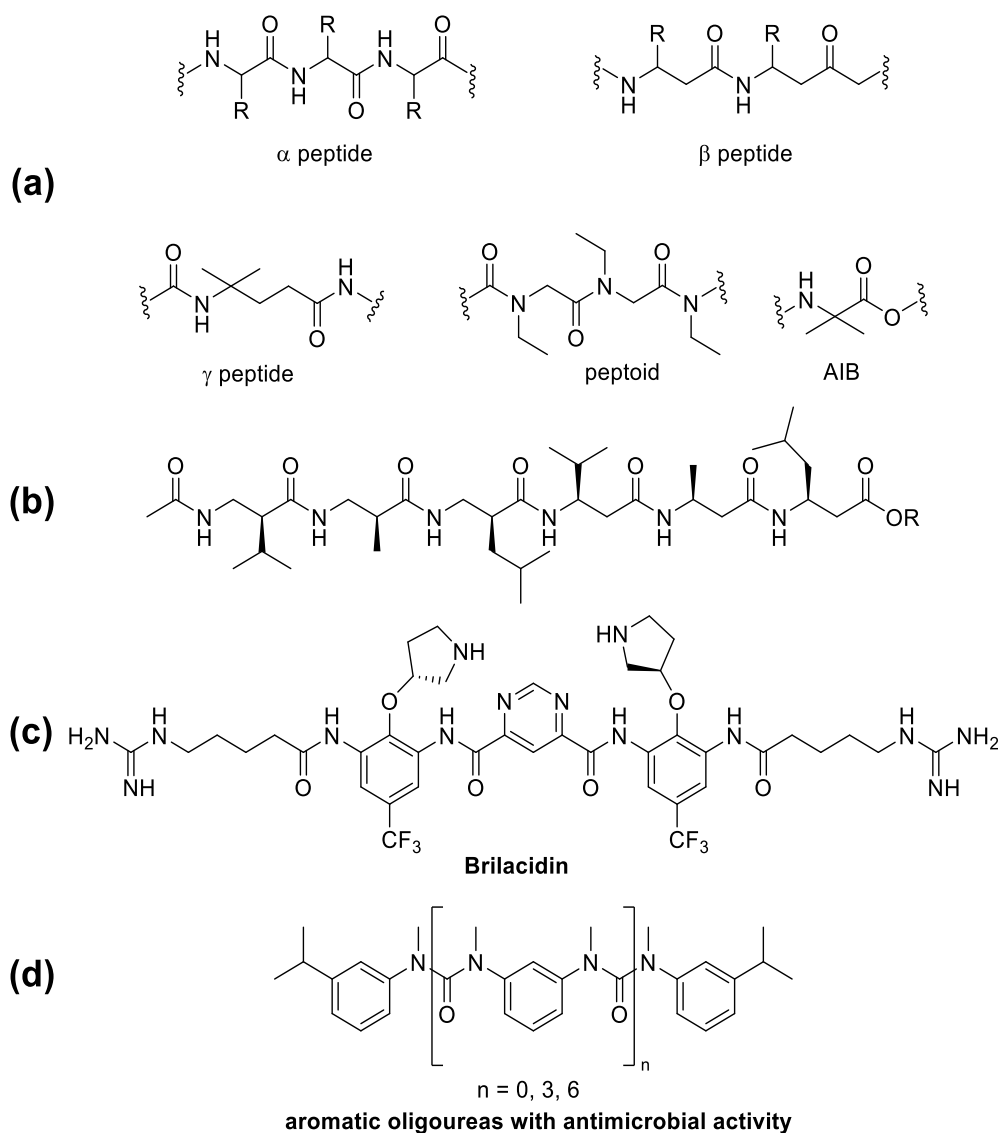
Figure 1.13. (**a**) Different types of peptide backbones in foldamer, (**b**) mixed beta peptide which has shown helical structure in Seebach *et al.* study.[78] (**c**) Brilacidin," a short arylamide foldamer, (**d**) aromatic oligourea based foldamer with antimicrobial activity.

In addition to peptide foldamers fully made of non-natural amino acids, other heterogeneous foldamers having a mixture of natural and non-natural amino acids like αβ, αβα, αβγ etc. amino acid combinations have also been developed. Many of these substances have the potential to be used as antiviral, anticancer, and antibacterial medicines as well as in gene therapy.[79–81] A notable example is the recently concluded phase 2 clinical trials of "Brilacidin," a short arylamide foldamer, for the treatment of bacterial skin infections brought on by *S. aureus (*Figure **1.13c***).*[82]

1.5.3. Peptide stapling

Peptide stapling is a technique for short peptides in which the conformation is enforced to helical form by a synthetic brace (staple).[83] The peptide stapling was first introduced by Helen E. Blackwell and Robert H. Grubbs.[84]

This stapling is done by a covalent bond between two amino acid side chains that are present one above the other in the helical conformation. Peptide stapling is one of the most commonly used strategies that affect the physiological behaviour of peptides.[53,55,85–87] It is done by using different functional groups like alkene, alkyne, azide, triazole etc., leading to stabilized conformations and enhanced biological profiles. In recent years, several research groups have attempted to use various reactions for peptide stapling with varying reagents and linkers.[88–94] Size, chain length and position of the two stapled amino acids are crucial for stapling of peptides such that the conformation is stabilized. Primarily the (i, i+3) or (i, i+4) and (i, i+7) are the most suitable positions for stapling the peptides. One-component stapling forms a bond directly between the sidechains of the two non-native amino acids, whereas two-component stapling uses a second bifunctional linker to connect the two different side chains. (**Figure 1.14**).

1.5.4. Substitution of L-amino acids with D-amino acids (chirality inversion)

The structure and functions of peptides and proteins are also dependent on the chirality of the constituent amino acids and their stereo composition. All natural amino acids, with the exception of glycine, contain two different enantiomers, L- and D. Although the L-form predominates among the enantiomers found in nature, D-amino acid-containing peptides and proteins are also known. Their incorporation into peptides typically modifies the conformation, orientation of the functional groups and can affect the efficacy of peptides.[95] Compounds containing D-residues are significantly more resistant to proteolytic degradation than natural peptides, as they do not match the amino acid stereospecificity

demands of the majority of the exo- or endoproteases. Furthermore, D-residue stabilizes the peptide turns due to the characteristic position in Ramachandran space (**Figure 1.10**).[96]
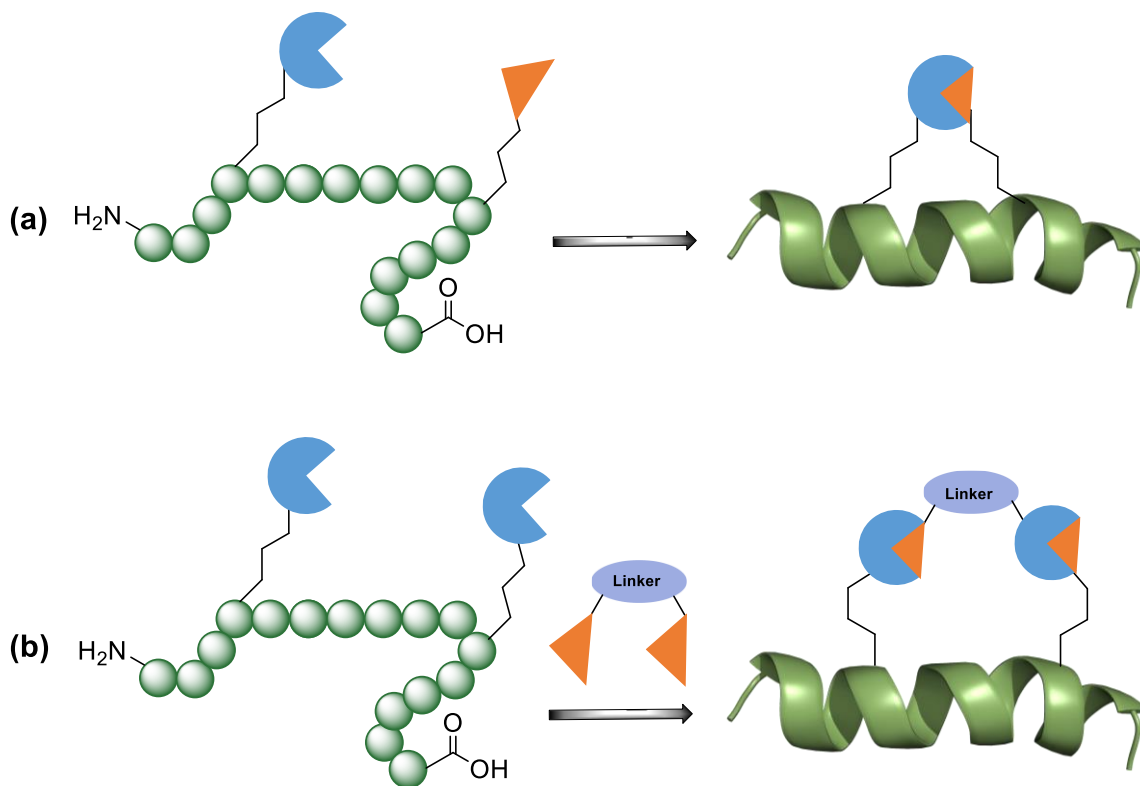
Figure 1.14. Peptide stapling, (**a**) one component stapling, (**b**) two-component stapling.

1.5.5. Backbone modifications

The goal of backbone alteration is to increase proteolytic stability and tune their conformations. The replacement of L-amino acids with D-amino acids, the insertion of *N*-alkyl amino acids, the inclusion of β-amino acids, and the addition of peptoids are some examples of backbone modifications.[97,98] An efficient method for increasing the plasma half-life of peptide drugs is to incorporate these non-natural or modified amino acids into the peptide sequence, particularly at the site of proteolysis. Selepressin, which was developed from vasopressin, has a comparable target selectivity like the parent peptide but with a longer plasma half-life, and is an effective example of backbone modified peptide.[29,99]

1.5.5.1. Backbone *N*-modifications

From numerous aspects, direct alkylation of nitrogen atoms forming the amide bond in a peptide chain is a preferred modification. Most of the naturally occurring peptides, especially *N*-methylated

peptides, mostly show unusual biological activities like Cyclosporin, Omphalotine and Enniatins (**Figure 1.15**.)[100–102]

Removal of the proton-donating NHs by *N*-methyl groups also lowers the potential for inter- and intramolecular hydrogen bonding. Both, by using conformational control or steric hindrance, *N*-methylation of amide bonds can boost metabolic stability, and the absence of hydrogen bonds affects a peptide's secondary structure by modifying the substructures like turns, β-sheets, or helices. Furthermore, *N*-alkylated peptides are less susceptible to enzymatic cleavage.[103] Hence, rationally substituting *N*-alkylated analogues for naturally occurring peptides frequently enhances their pharmacological characteristics, such as bioavailability, metabolic stability, and receptor selectivity.

Cyclosporin A   **Omphalotin**
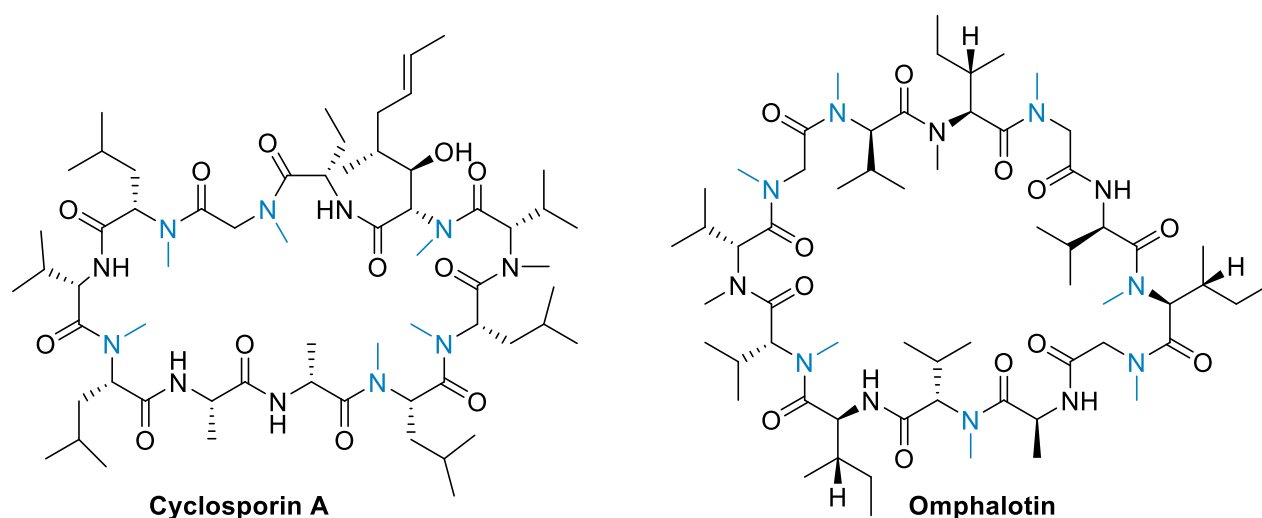
Figure 1.15. Naturally occurring *N*-methylated Cyclosporin A and Omphalotin.

Among various backbone *N*-modification tools, *N*-methylation is the most extensively studied modification. Some of the best peptide *N*-methylation studies and their effects on biological activity and permeability are summarized below.

1.5.5.2. **Backbone *N*-Methylation**: **key roles in improving the permeability of cyclic peptides and their conformational modulation**

The *N*-Methylation of the amide nitrogen has many structural and chemical effects: (1) The hydrogen-bonding property of the peptide bond is altered by the loss of hydrogen on the amide nitrogen. (2). All the peptide bonds are in *trans* form except few exceptions, however, where the nitrogen is methylated, the *cis* isomers are energetically more favorable as compared to non-methylated peptide amide bonds. (3) *N*-Methylation results in steric constraints, thereby decreasing the local flexibility of

the amide bond and restraining the conformation, and it also results in a more hydrophobic peptide bond. These properties make peptide analogues containing *N*-methylated amino acids interesting in biological and structural characterization. The *N*-methyl modifications were pioneered by Kessler′s group.[104] Further, they have developed a strategy for *N*-methylation of amino acids in solution as well as on resin *N*-methylation by modified Mitsonobu method for solid phase peptide synthesis.[105] Further the *N*-methylation modification was extensively studied by Kessler and Lokey′s group and proved it to be an effective modification for the development of various bioactive peptides (**Figure 1.16**).[72,106–110]
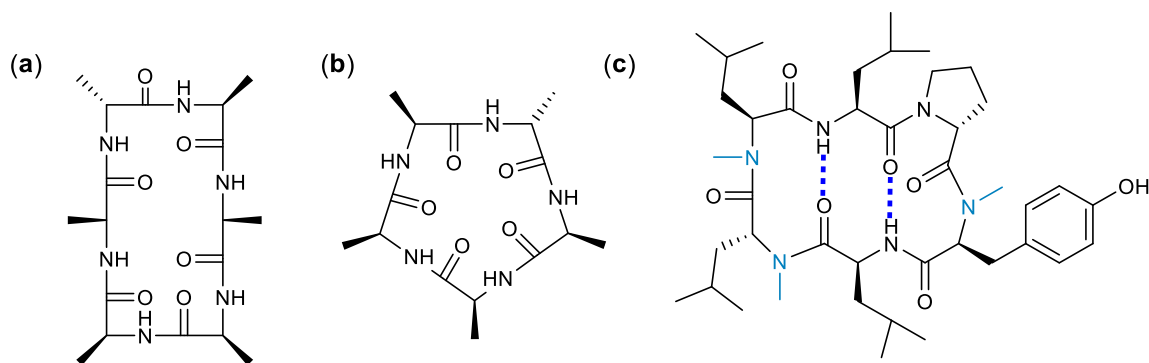
Figure 1.16. (a) cyclic hexaalanine, (b) cyclic pentaalanine templates on which multiple *N*-methylation study was carried out by Kessler *et al.*; (c) rationally designed peptide by Lokey′s group which showed 29% oral bioavailability.

Kessler group has done an extensive study of conformations in backbone *N*-methylated polyalanine cyclic peptides. They have synthesized a library of cyclic pentaalanine peptides containing 30 peptides which vary in number and position *N*-methyl groups and evaluated their conformational preference.[111] Ovadia *et al.* in 2011 have synthesized a library of 54 *N*-methylated cyclohexaalanine peptides and studied the effect of *N*-methylation on permeability.[112] They found that peptides that are mono *N*-methylated have not shown any permeability but 10 out of 54 peptides with 2 or more *N*-methyl groups showed excellent permeability (**Figure 1.16a**). Later, in 2012 G. Beck *et al.* discussed the conformations of these *N*-methyl peptides and identified two highly Caco-2 permeable template structures.[113] The identified template conformations were found to be similar to the conformations in the orally bioavailable somatostatin analogue (Veber-Hirschmann) and cyclosporin A. In another study, the potential role of *cis* peptide bonds[114] and enantiomeric peptides on intestinal permeability of peptides was investigated.[115] Furthermore, sequential *N*-methylation of a cyclic hexapeptide cyclo(GRGDfL) resulted in an *N*-methyl version with increased selectivity towards certain integrin subtypes.[116] These results suggest that the incorporation of bioactive sequences on the highly Caco-2 permeable templates could lead to the potent orally bioavailable peptide.

Lokey's group designed 17 sanguinamide A analogues to test the relative contributions of β-branching, *N*-methylation, and side chain size to passive membrane permeability and aqueous solubility. The results have shown less effect of β-branching on permeability as compared to *N*-methylation of exposed NH groups. From this study, they found one *N*-methylated Sanguinamide A analogue with Leu substitution, that showed higher permeability compared to the parent peptide (**Figure 1.17**).[62]

Sanguinamide A

Sanguinamide A analogue
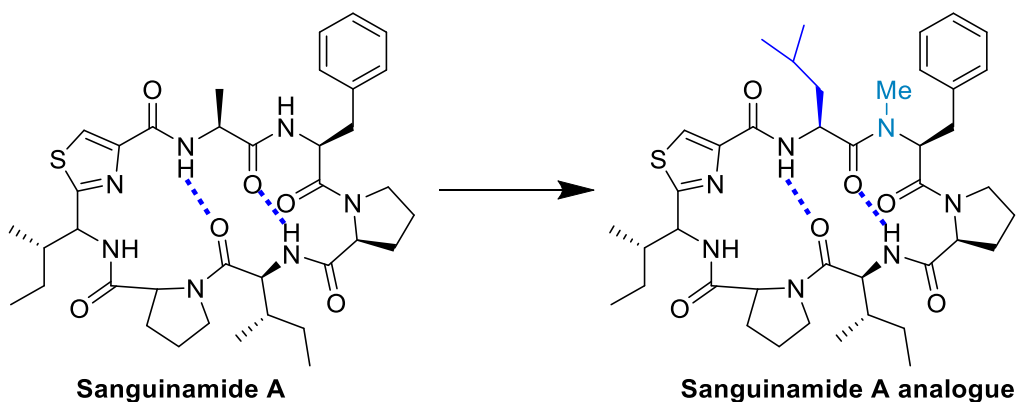
Figure 1.17. Sanguinamide A and it's analogue which has shown higher permeability.

1.5.5.3. Backbone *N*-amination

The concept of *N*-amination was first introduced by Michel Maraud in 1993, where they investigated the conformations in dipeptide (Pro-Gly or Ala-Gly) having *N*-hydroxyl and *N*-aminated amide bonds.[26,117]
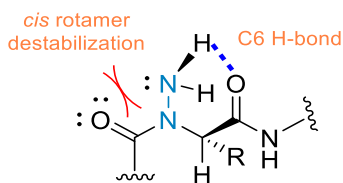
N-amination of peptides, results in unique backbone geometries and maintains H-bond donor capacity.[118] The repulsion of lone pair in *cis* geometry destabilizes the conformation. Pargamicin A is a naturally occurring N-aminated peptide,[119] which is anti methicillin-resistant *Staphylococcus aureus* (MRSA) and anti vancomycin-resistant *Enterococcus faecalis/faecium* (VRE), which are the most intractable pathogens and frequently isolated from patients. L-156, 373 is also a naturally isolated peptide which is Oxytocin antagonist (OT) (**Figure 1.18**).[120]
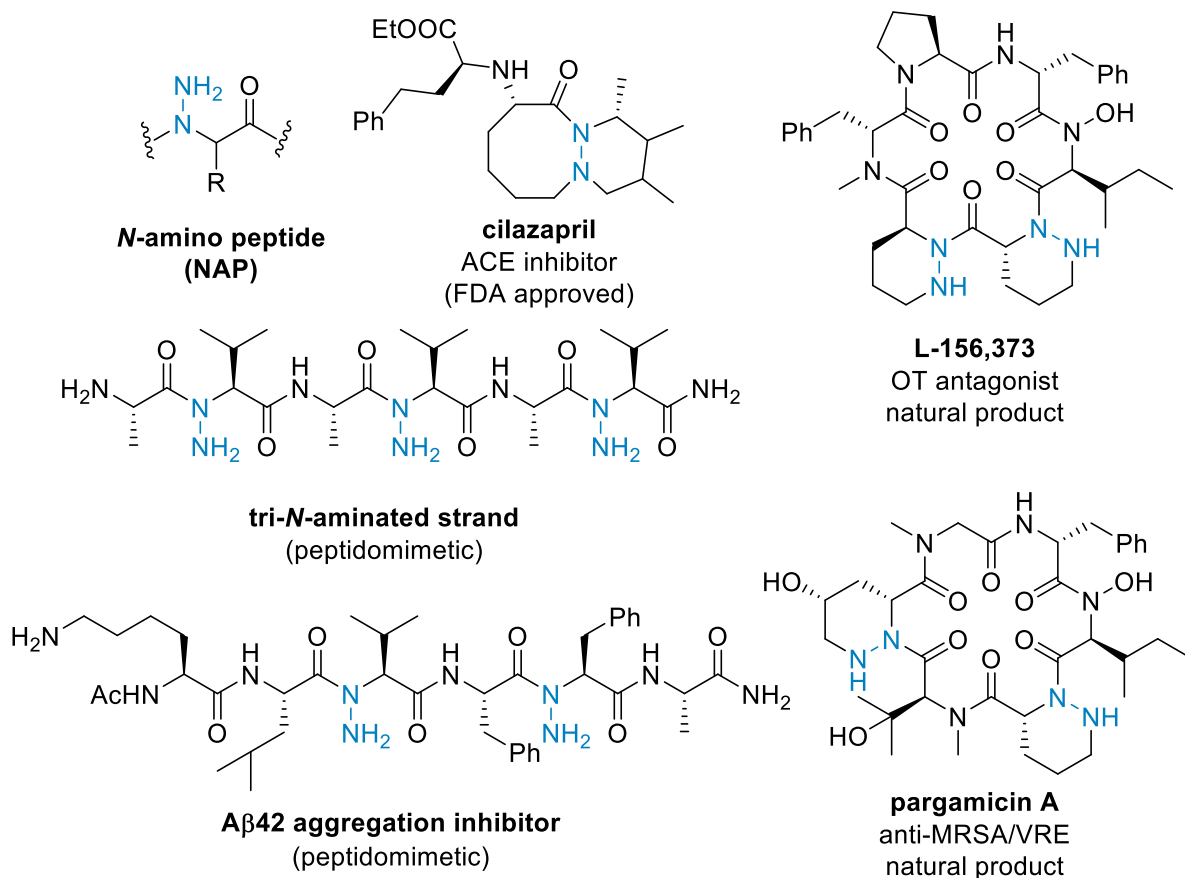
Figure 1.18. Examples of naturally occurring and modified *N*-amino amide peptides.

Recently R. Del Valle′s group developed a class of *N*-amino peptide (NAP) derivatives that are constrained by both covalent and noncovalent interactions.[121,122] In contrast to the *N*-methylated *cis* amide bond NAP has a *trans* amide bond preference. Matthew P. Sarnowski *et.al.* in 2017 described the first solid phase synthesis of diverse *N*-amino peptide (NAP) derivatives and demonstrated their unique ability to adopt β-sheet folds stabilized by non-covalent interactions.[122] Information derived from model *N*-amino peptides suggests that extended conformations are stabilized through cooperative steric, electrostatic, and hydrogen-bonding interactions.[121,123] Benjamin *et al*. did the *N*-amination on Gramicidin S which is a C2-symmetrical cyclic decapeptide and studied the effect on conformation.[61,123] It adopts an antiparallel β-sheet like structure and it shows severe toxicity toward human red blood cells. Further Makwana *et al.* extended the effect of N-amination on beta amyloid protein, by sequential scan on protein segment (peptides), and showed that amide N-amination completely abolishes the tendency of these peptides to self-aggregate.[124]

1.5.5.4. **Backbone amide *N*-PEGylation**

Ana I. Ferna´ndez *et al*. designed and synthesized backbone modified *N*-Triethylene glycol (TEG) analogue of sansalvamide and compared its conformations and lipophilicity with its *N*-methyl versions.[99,125] Also, in another study, they incorporated *N*-Oligoethylene glycol in cilengitide, cyclo[RGDf*N*MeV]. In both cases, there was no effect of the *N*-modification on activity and conformation, but they observed higher lipophilicity as compared to the *N*-methyl analogue in both the studies, as TEG and OEG are lipophilic and larger in size for interaction (**Figure 1.19**).[107]
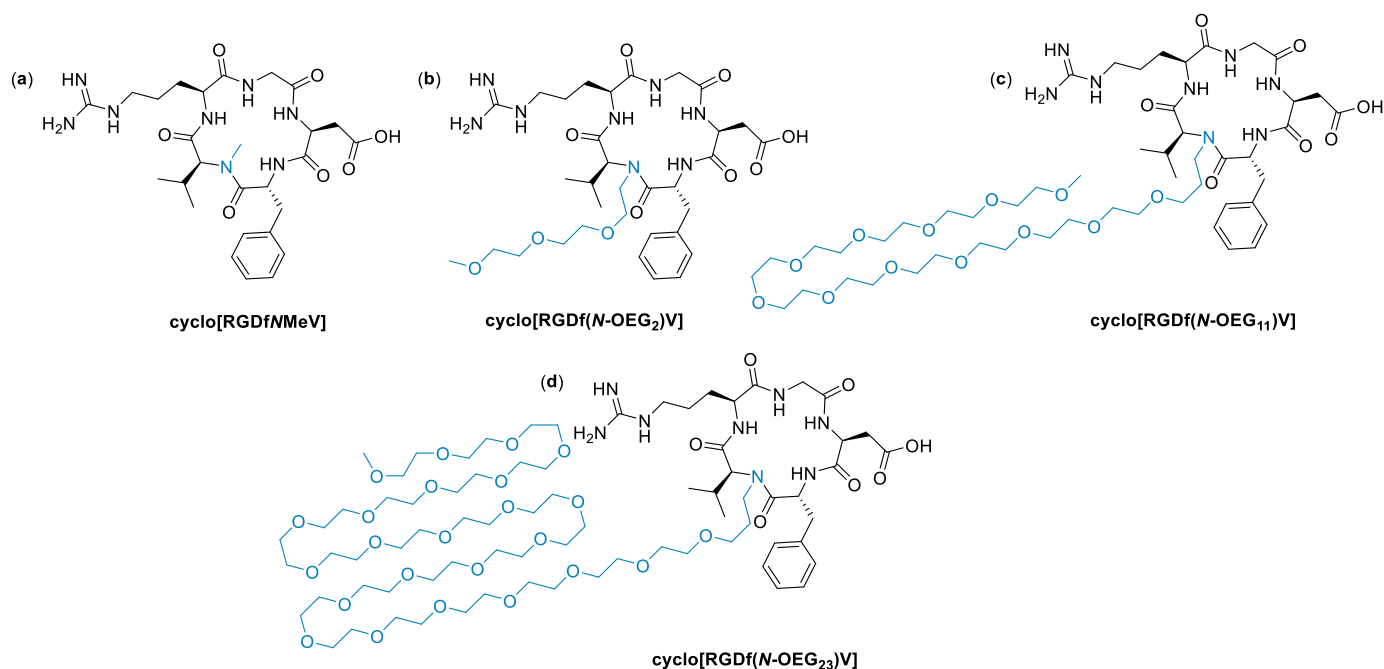
Figure 1.19. (**a**) Structure of cilengitide, cyclo[RGDf*N*MeV] and (**b-d**) the *N*-OEG cyclopeptides synthesized and tested for biological activity and lipophilcity.[107]

1.5.5.5. **Peptide bond isosteres**

Peptide bond isosteres are molecular scaffolds that mimic an amide bond and are used as replacements for amide bonds.[126] Though amide bonds are one of the most important functional groups in medicinal chemistry and are a necessary component of many biologically active molecules, they have a permeability challenge due to hydrolysis and polarity.[127] Furthermore, amides may become inert as a result of resonance stabilisation, which is primarily caused by the differing electronegativities of oxygen and nitrogen. As a result, the carbonyl functional group of amides is less electrophilic than the carbonyl functional group of other carboxylic acid derivatives. In such circumstances, replacing the amide moiety with a surrogate structure may be helpful. Examples of amide isosteres (**Figure 1.20**) are ester,

thioamide,[128,129] triazole,[60] amidine,[130] alkenes, and fluoroalkene,[131,132] etc. The isostere of the amide bond can be used to provide conformational stability to the peptide and increased bioactivity.[60,133,134] There are several reported peptide bond isosteres that mimic the electrostatic characteristics of amides and secondary structures in peptides.[131,135,136] In medicinal chemistry, the isosteres of the carbonyl group containing a heavy atom favourably impact local and overall peptide conformations.[137] Several investigations have indicated that substituting peptide bonds with isosteres influences their bioactivity; for example, sansalvamide ester analogue showed superior activity than amide. (**Figure 1.21**).[138]
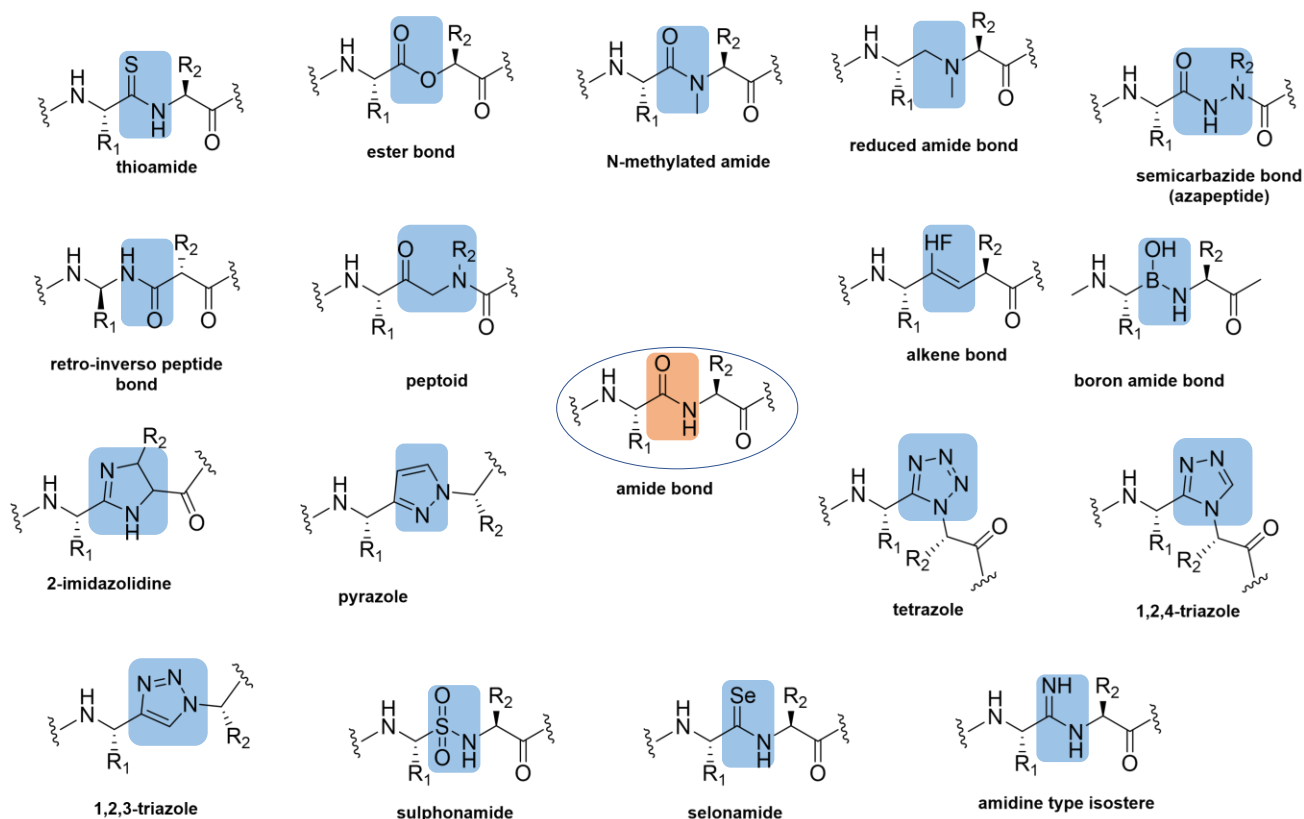
Figure 1.20. Representation of various types of peptide bond isosteres.
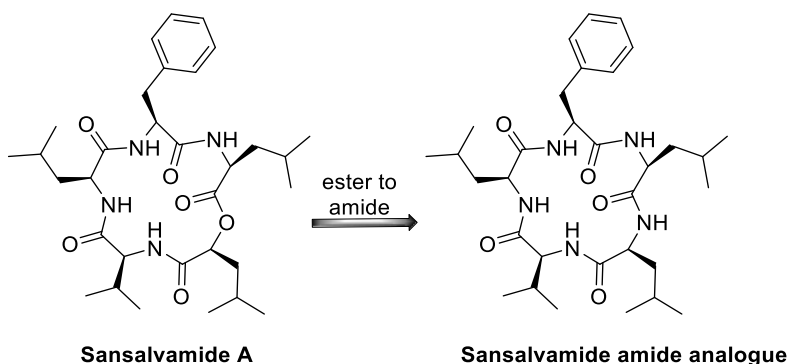
Figure 1.21. Sansalvamide ester amide analogue.

In general, to obtain stable, bioactive as well as orally bioavailable peptide-based drugs, two approaches are in practice.

1. Structural optimization of biological activity in peptides and subsequent conversion of lead peptides to orally bioavailable derivatives while retaining their biological activity. The development of Cilengitide,[108,139–141] (a cyclic pentapeptide discovered by Kessler *et al*. by successfully applying three chemical strategies to RGD sequence, (1) cyclization (2) spatial screening of cyclic peptides[142,143], and (3) *N*-methyl scan) Veber-Hirschmann peptide[110,144,145] and octreotide derived from somatostatin are the best examples of peptide development starting from a bioactive sequence.

Cilengitide   **Veber-Hirschmann peptide**
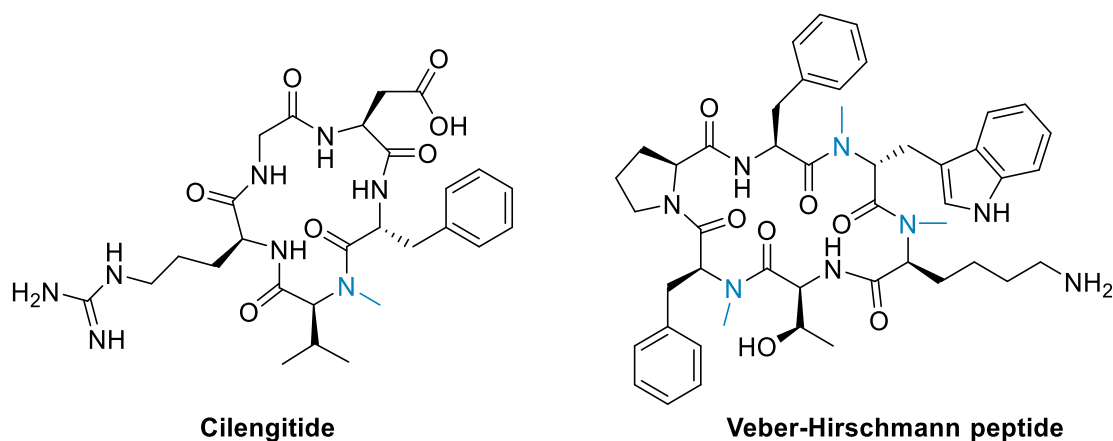
Figure 1.22. Cilengitide and Veber-Hirschmann peptides developed by structural optimization.

2. Development of orally available peptide backbones and utilizing them as scaffolds for the subsequent introduction of functional peptide groups in a stereo-controlled manner to achieve biological activity.[146]
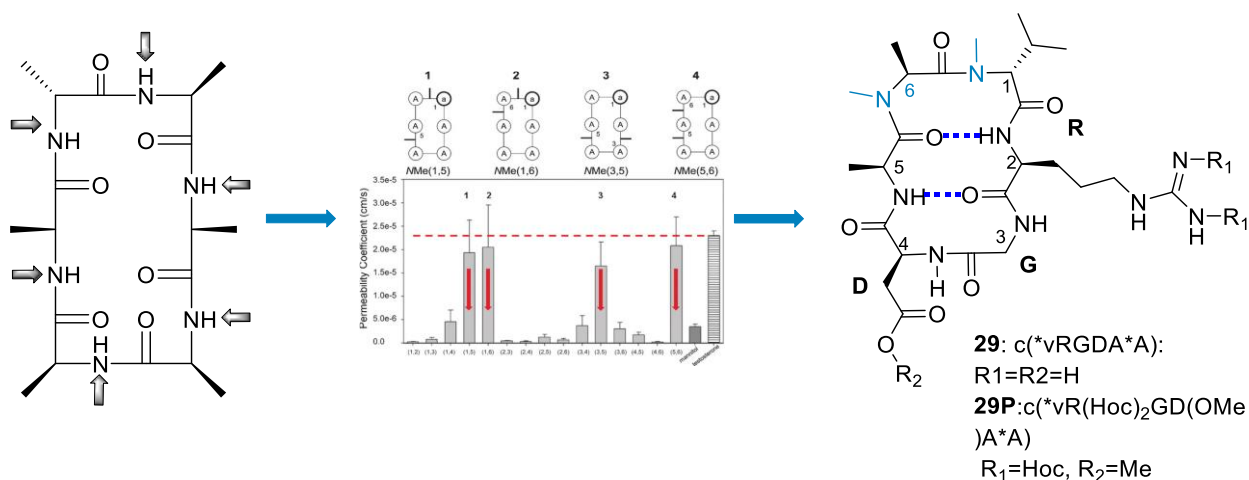
Figure 1.23. Development of a selective and orally available ligand for the integrin αvβ3.[146]

29

1.6. **Conclusions and future perspectives**

Peptides have emerged as a unique class of therapeutic drugs due to their diverse biochemical features and therapeutic potential. Although peptides outperform small molecules and large biologics in several aspects, they usually have poor *in vivo* stability and membrane impermeability due to the amino acid limitations. Extensive research has been conducted on the development, production, and optimization of peptide-based drugs in an attempt to overcome these challenges. The field of peptides started with natural hormones. From the last couple of decades, the trends in peptide discovery and development is shifting from natural hormones or peptides to the development of the rational design of peptides with desirable biochemical and physiological functions. Due to the advancement in the field of molecular biology, peptide synthetic chemistry, and peptide delivery technologies, the approval rate of peptide based drugs improved significantly. Hundreds of peptides are currently undergoing preclinical research and clinical development, and more than 80 therapeutic peptides have already entered the global market.

During the COVID-19 pandemic, the antiviral peptides have gained lots of attention, particularly the development of peptide vaccines against SARS-CoV-2.[147] Locating and designing of potential peptide vaccine candidates has been accelerated by the rapid application of novel technologies such as immunoinformatics characterization, epitope-based design, *in silico* identification, and molecular docking. Despite that, no peptide vaccines have been authorised for the treatment of COVID-19, but sufficient experience has been acquired in the development of peptide vaccines, not only against SARS-CoV-2 but also against potential future viruses.

Peptide therapies are currently providing the pharmaceutical and biotechnology industries with new economic opportunities. By seeing the advantages of this growing field, prominent pharmaceutical and biotech corporations are aggressively investing in the discovery of peptides for various purposes, as well as in newer methods for peptide synthesis and their modification. The role of peptides in the field of protein-protein interaction inhibition is one of the significant areas of peptide drug discovery. Particularly because inhibiting the PPI interactions requires ligands with large surface area, peptide based ligands have an advantage and can interact with the targeted protein effectively as compared to the small molecules.

The peptide-based drugs are one of the leading drug markets, and it is increasing exponentially. The market for peptide therapies has been estimated at USD 42.05 billion in 2022, and from 2023 to 2030, it is estimated to expand at a compound annual growth rate (CAGR) of 6.3%.[148] Because of their immense

medicinal potential, market potential, and economic importance, therapeutic peptides are expected to continue to attract research attention.

1.7. References

(1) Muttenthaler, M.; King, G. F.; Adams, D. J.; Alewood, P. F. Trends in Peptide Drug Discovery. *Nat. Rev. Drug Discov.* **2021**, *20* (4), 309–325.

(2) Wang, L.; Wang, N.; Zhang, W.; Cheng, X.; Yan, Z.; Shao, G.; Wang, X.; Wang, R.; Fu, C. Therapeutic Peptides: Current Applications and Future Directions. *Signal Transduct. Target. Ther.* **2022**, *7* (1).

(3) Goodwin, D.; Simerska, P.; Toth, I. Peptides As Therapeutics with Enhanced Bioactivity. *Curr. Med. Chem.* **2012**, *19* (26), 4451–4461.

(4) Apostolopoulos, V.; Bojarska, J.; Chai, T. T.; Elnagdy, S.; Kaczmarek, K.; Matsoukas, J.; New, R.; Parang, K.; Lopez, O. P.; Parhiz, H.; Perera, C. O.; Pickholz, M.; Remko, M.; Saviano, M.; Skwarczynski, M.; Tang, Y.; Wolf, W. M.; Yoshiya, T.; Zabrocki, J.; Zielenkiewicz, P.; Alkhazindar, M.; Barriga, V.; Kelaidonis, K.; Sarasia, E. M.; Toth, I. A Global Review on Short Peptides: Frontiers and Perspectives. *Molecules* **2021**, *26*.

(5) Greber, K. E.; Dawgul, M. Current Topics in Medicinal Chemistry The International Journal for In-Depth Reviews on Current Topics in Medicinal Chemistry Impact Factor: 2.9. *Curr. Top. Med. Chem.* **2017**, *17*, 620–628.

(6) Hill, T. A.; Shepherd, N. E.; Diness, F.; Fairlie, D. P. Constraining Cyclic Peptides to Mimic Protein Structure Motifs. *Angew. Chemie Int. Ed.* **2014**, *53*, 13020–13041.

(7) Rathman, B. M.; Allen, J. L.; Shaw, L. N.; Del Valle, J. R. Synthesis and Biological Evaluation of Backbone-Aminated Analogues of Gramicidin S. *Bioorganic Med. Chem. Lett.* **2020**, *30* (15), 1–5.

(8) Zorzi, A.; Deyle, K.; Heinis, C. Cyclic Peptide Therapeutics: Past, Present and Future. *Curr. Opin. Chem. Biol.* **2017**, *38*, 24–29.

(9) Henninot, A.; Collins, J. C.; Nuss, J. M. The Current State of Peptide Drug Discovery: Back to the Future? *J. Med. Chem.* **2018**, *61* (4), 1382–1414.

(10) Otvos, L. Peptide-Based Drug Design: Here and Now. *Methods Mol. Biol.* **2008**, *494*, 1–8.

(11) Fosgerau, K.; Hoffmann, T. Peptide Therapeutics: Current Status and Future Directions. *Drug Discov. Today* **2015**, *20* (1), 122–128.

(12) Craik, D. J.; Fairlie, D. P.; Liras, S.; Price, D. The Future of Peptide-Based Drugs. *Chem. Biol. Drug Des.* **2013**, *81* (1), 136–147.

(13) Derakhshankhah, H.; Jafari, S. Cell Penetrating Peptides: A Concise Review with Emphasis on Biomedical Applications. *Biomed. Pharmacother.* **2018**, *108* (September), 1090–1096.

(14) Ahlbach, C. L.; Lexa, K. W.; Bockus, A. T.; Chen, V.; Crews, P.; Jacobson, M. P.; Lokey, R. S. Beyond Cyclosporine A: Conformation-Dependent Passive Membrane Permeabilities of Cyclic Peptide Natural Products. *Future Med. Chem.* **2015**, *7* (16), 2121–2130.

(15) Lau, J. L.; Dunn, M. K. Therapeutic Peptides: Historical Perspectives, Current Development Trends, and Future Directions. *Bioorg. Med. Chem.* **2018**, *26* (10), 2700–2707.

(16) Vlieghe, P.; Lisowski, V.; Martinez, J.; Khrestchatisky, M. Synthetic Therapeutic Peptides: Science and Market. *Drug Discov. Today* **2010**, *15* (1–2), 40–56.

(17) Aminov, R. I. A Brief History of the Antibiotic Era: Lessons Learned and Challenges for the Future. *Front. Microbiol.* **2010**, *1*, 1–7.

(18) Zhang, H.; Chen, S. Cyclic Peptide Drugs Approved in the Last Two Decades (2001-2021). *RSC Chem. Biol.* **2022**, *3* (1), 18–31.

(19) Akram, O. N.; DeGraff, D. J.; Sheehan, J. H.; Tilley, W. D.; Matusik, R. J.; Ahn, J. M.; Raj, G. V. Tailoring Peptidomimetics for Targeting Protein-Protein Interactions. *Mol. Cancer Res.* **2014**, *12* (7), 967–978.

(20) Bhat, A.; Roberts, L. R.; Dwyer, J. J. Lead Discovery and Optimization Strategies for Peptide Macrocycles. *Eur. J. Med. Chem.* **2015**, *94*, 471–479.

(21) Hamley, I. W. Small Bioactive Peptides for Biomaterials Design and Therapeutics. *Chem. Rev.* **2017**, *117* (24), 14015–14041.

(22) Pelay-Gimeno, M.; Glas, A.; Koch, O.; Grossmann, T. N. Structure-Based Design of Inhibitors of Protein-Protein Interactions: Mimicking Peptide Binding Epitopes. *Angew. Chemie Int. Ed.* **2015**, *54* (31), 8896–8927.

(23) Research. *Peptide Therapeutics Market - Global Industry Analysis, Size, Share, Growth, Trends, and Forecast 2016 - 2024*; **2016**.

(24) THAYER, A. M. IMPROVING PEPTIDES. *Chem. Eng. News Arch.* **2011**, *89* (22), 13–20.

(25) Lenci, E.; Trabocchi, A. Peptidomimetic Toolbox for Drug Discovery. *Chem. Soc. Rev.* **2020**, *49* (11), 3262–3277.

(26) Marraud, M.; Dupont, V.; Grand, V.; Zerkout, S.; Lecoq, A.; Boussard, G.; Vidal, J.; Collet, A.; Aubry, A. Modifications of the Amide Bond and Conformational Constraints in Pseudopeptide Analogues. *Biopolymers* **1993**, *33* (7), 1135–1148.

(27) Kordbacheh, S.; Kasko, A. M. Peptide and Protein Engineering by Modification of Backbone and Sidechain Functional Groups. *Polym. Int.* **2021**, *70* (7), 889–896.

(28) Fischer, E.; Fourneau, E. Ueber Einige Derivate Des Glykocolls. *Berichte der Dtsch. Chem. Gesellschaft* **1901**, *34* (2), 2868–2877.

(29) Bryan, W. M.; Hempel, J. C.; Huffman, W. F.; Marshall, G. R.; Moore, M. L.; Silvestri, J.; Stassen, F. L.; Stefankiewicz, J. S.; Sulat, L.; Webb, R. L. Design, Synthesis, and Biological Activity of a Peptide Mimic of Vasopressin. *J. Med. Chem.* **1988**, *31* (4), 742–744.

(30) Vigneaud, V. du; Ressler, C.; Swan, C. J. M.; Roberts, C. W.; Katsoyannis, P. G.; Gordon, S. THE SYNTHESIS OF AN OCTAPEPTIDE AMIDE WITH THE HORMONAL ACTIVITY OF OXYTOCIN. *J. Am. Chem. Soc.* **1953**, *75* (19), 4879–4880.

(31) Merrifield, R. B. Solid Phase Peptide Synthesis. *Excerpta Med., I.C.S.* **1976**, *No.374*, 29–39.

(32) Loffet, A. Peptides as Drugs: Is There a Market? *J. Pept. Sci.* **2002**, *8* (1), 1–7.

(33) Rüegger, A.; Kuhn, M.; Lichti, H.; Loosli, H.-R.; Huguenin, R.; Quiquerez, C.; von Wartburg, A. Cyclosporin A, Ein Immunsuppressiv Wirksamer Peptidmetabolit Aus *Trichoderma Polysporum Rifai*. *Helv. Chim. Acta* **1976**, *59* (4), 1075–1092.

(34) Grand View Research. *Peptide Therapeutics Market Size, Share & Trends Analysis Report By*

Application, By Type, By Type of Manufacturers, By Route of Administration, By Synthesis Technology, By Region, And Segment Forecasts, 2022 - 2030; **2022**.

(35) Muttenthaler, M.; King, G. F.; Adams, D. J.; Alewood, P. F. Trends in Peptide Drug Discovery. *Nat. Rev. Drug Discov.* **2021**, *20* (4), 309–325.

(36) Vanier, G. S. Microwave-Assisted Solid-Phase Peptide Synthesis Based on the Fmoc Protecting Group Strategy (CEM); **2013**; pp 235–249.

(37) Uhlig, T.; Kyprianou, T.; Martinelli, F. G.; Oppici, C. A.; Heiligers, D.; Hills, D.; Calvo, X. R.; Verhaert, P. The Emergence of Peptides in the Pharmaceutical Business: From Exploration to Exploitation. *EuPA Open Proteomics* **2014**, (*4*), 58–69.

(38) Barman, P.; Joshi, S.; Sharma, S.; Preet, S.; Sharma, S.; Saini, A. Strategic Approaches to Improvise Peptide Drugs as Next Generation Therapeutics. *Int. J. Pept. Res. Ther.* **2023**, *29* (4), 61.

(39) Akaji, K.; Fujino, K.; Tatsumi, T.; Kiso, Y. Total Synthesis of Human Insulin by Regioselective Disulfide Formation Using the Silyl Chloride-Sulfoxide Method. *J. Am. Chem. Soc.* **1993**, *115* (24), 11384–11392.

(40) Sieber, P.; Kamber, B.; Hartmann, A.; Jöhl, A.; Riniker, B.; Rittel, W. Totalsynthese von Humaninsulin. IV. Beschreibung Der Endstufen. *Helv. Chim. Acta* **1977**, *60* (1), 27–37.

(41) Valeur, E.; Bradley, M. Amide Bond Formation: Beyond the Myth of Coupling Reagents. *Chem. Soc. Rev.* **2009**, *38* (2), 606–631.

(42) Chung, D. M.; Nowick, J. S. Enantioselective Molecular Recognition between β-Sheets. *J. Am. Chem. Soc.* **2004**, *126* (10), 3062–3063.

(43) Dayalan, S.; Gooneratne, N. D.; Bevinakoppa, S.; Schroder, H. Dihedral Angle and Secondary Structure Database of Short Amino Acid Fragments. *Bioinformation* **2006**, *1* (1), 78–80.

(44) Lubell, W. D. Peptide-Based Drug Development. *Biomedicines* **2022**, *10* (8), 2037.

(45) Bock, J. E.; Gavenonis, J.; Kritzer, J. A. Getting in Shape: Controlling Peptide Bioactivity and Bioavailability Using Conformational Constraints. *ACS Chem. Biol.* **2013**, *8* (3), 488–499.

(46) Hill, T. A.; Shepherd, N. E.; Diness, F.; Fairlie, D. P. Constraining Cyclic Peptides to Mimic Protein Structure Motifs. *Angew. Chemie Int. Ed.* **2014**, *53* (48), 13020–13041.

(47) Kang, C. W.; Sarnowski, M. P.; Elbatrawi, Y. M.; Del Valle, J. R. Access to Enantiopure α-Hydrazino Acids for N-Amino Peptide Synthesis. *J. Org. Chem.* **2017**, *82* (3), 1833–1841.

(48) Girvin, Z. C.; Gellman, S. H. Foldamer Catalysis. *J. Am. Chem. Soc.* **2020**, *142*, 17211–17223.

(49) Rinaldi, S. The Diverse World of Foldamers: Endless Possibilities of Self-Assembly. *Molecules* **2020**, *25*, 49.

(50) Huc, I. Aromatic Oligoamide Foldamers. *European J. Org. Chem.* **2004**, *2004*, 17–29.

(51) Proulx, C.; Sabatino, D.; Hopewell, R.; Spiegel, J.; García Ramos, Y.; Lubell, W. D. Azapeptides and Their Therapeutic Potential. *Future Med. Chem.* **2011**, *3*, 1139–1164.

(52) Altiti, A.; He, M.; VanPatten, S.; Cheng, K. F.; Ahmed, U.; Chiu, P. Y.; Mughrabi, I. T.; Jabari, B. Al; Burch, R. M.; Manogue, K. R.; Tracey, K. J.; Diamond, B.; Metz, C. N.; Yang, H.; Hudson, L. K.; Zanos, S.; Son, M.; Sherry, B.; Coleman, T. R.; Al-Abed, Y. Thiocarbazate Building Blocks Enable the Construction of Azapeptides for Rapid Development of Therapeutic

Candidates. *Nat. Commun.* **2022**, *13*, 7127.

(53)   Li, B.; Wang, L.; Chen, X.; Chu, X.; Tang, H.; Zhang, J.; He, G.; Li, L.; Chen, G. Extendable Stapling of Unprotected Peptides by Crosslinking Two Amines with O-Phthalaldehyde. *Nat. Commun.* **2022**, *13* (1), 1–9.

(54)   Walensky, L. D.; Bird, G. H. Hydrocarbon-Stapled Peptides: Principles, Practice, and Progress. **2014**.

(55)   Moiola, M.; Memeo, M. G.; Quadrelli, P. Stapled Peptides a Useful Improvement for Peptide-Based Drugs. *Molecules* **2019**, *24*.

(56)   Hayward, S. Peptide-Plane Flipping in Proteins. *Protein Sci.* **2008**, *10* (11), 2219–2227.

(57)   Wedemeyer, W. J.; Welker, E.; Narayan, M.; Scheraga, H. A. Disulfide Bonds and Protein Folding. *Biochemistry* **2000**, *39* (15), 4207–4216.

(58)   Góngora-Benítez, M.; Tulla-Puche, J.; Albericio, F. Multifaceted Roles of Disulfide Bonds. Peptides as Therapeutics. *Chem. Rev.* **2014**, *114*, 901–926.

(59)   Testa, C.; D'addona, D.; Scrima, M.; Tedeschi, A. M.; D'ursi, A. M.; Bernhard, C.; Denat, F.; Bello, C.; Rovero, P.; Chorev, M.; Papini, A. M. Design, Synthesis, and Conformational Studies of [DOTA]-Octreotide Analogs Containing [1,2,3]Triazolyl as a Disulfide Mimetic. *Pept. Sci.* **2018**, *110*.

(60)   Rečnik, L.-M.; Kandioller, W.; Mindt, T. L. 1,4-Disubstituted 1,2,3-Triazoles as Amide Bond Surrogates for the Stabilisation of Linear Peptides with Biological Activity. *Molecules* **2020**, *25*, 3576.

(61)   Guan, Q.; Huang, S.; Jin, Y.; Campagne, R.; Alezra, V.; Wan, Y. Recent Advances in the Exploration of Therapeutic Analogues of Gramicidin S, an Old but Still Potent Antimicrobial Peptide. *J. Med. Chem.* **2019**, *62*, 7603–7617.

(62)   Bockus, A. T.; Schwochert, J. A.; Pye, C. R.; Townsend, C. E.; Sok, V.; Bednarek, M. A.; Lokey, R. S. Going Out on a Limb: Delineating the Effects of β-Branching, *N*-Methylation, and Side Chain Size on the Passive Permeability, Solubility, and Flexibility of Sanguinamide A Analogues. *J. Med. Chem.* **2015**, *58* (18), 7409–7418.

(63)   Liu, S.; Gu, W.; Lo, D.; Ding, X. Z.; Ujiki, M.; Adrian, T. E.; Soff, G. A.; Silverman, R. B. N-Methylsansalvamide a Peptide Analogues. Potent New Antitumor Agents. *J. Med. Chem.* **2005**, *48* (10), 3630–3638.

(64)   Perry, S. R.; Hill, T. A.; de Araujo, A. D.; Hoang, H. N.; Fairlie, D. P. Contiguous Hydrophobic and Charged Surface Patches in Short Helix-Constrained Peptides Drive Cell Permeability. *Org. Biomol. Chem.* **2018**, *16* (3), 367–371.

(65)   Zhang, H.; Chen, S. Cyclic Peptide Drugs Approved in the Last Two Decades (2001-2021). *RSC Chem. Biol.* **2022**, *3* (1), 18–31.

(66)   Kitagaki, J.; Shi, G.; Miyauchi, S.; Murakami, S.; Yang, Y. Cyclic Depsipeptides as Potential Cancer Therapeutics. *Anticancer. Drugs* **2015**, *26*, 259–271.

(67)   Gang, D.; Kim, D. W.; Park, H. S. Cyclic Peptides: Promising Scaffolds for Biopharmaceuticals. *Genes (Basel).* **2018**, *9* (11).

(68)   Li, B.; Brown, K. V.; Wenke, J. C.; Guelcher, S. A. Sustained Release of Vancomycin from Polyurethane Scaffolds Inhibits Infection of Bone Wounds in a Rat Femoral Segmental Defect

Model. *J. Control. Release* **2010**, *145* (3), 221–230.

(69)   Vu, Q. N.; Young, R.; Sudhakar, H. K.; Gao, T.; Huang, T.; Tan, Y. S.; Lau, Y. H. Cyclisation Strategies for Stabilising Peptides with Irregular Conformations. *RSC Med. Chem.* **2021**, *12* (6), 887–901.

(70)   Nielsen, D. S.; Shepherd, N. E.; Xu, W.; Lucke, A. J.; Stoermer, M. J.; Fairlie, D. P. Orally Absorbed Cyclic Peptides. *Chem. Rev.* **2017**, *117* (12), 8094–8128.

(71)   White, C. J.; Yudin, A. K. Contemporary Strategies for Peptide Macrocyclization. *Nat. Chem.* **2011**, *3* (7), 509–524.

(72)   Kawai, M.; Ohya, M.; Fukuta, N.; Butsugan, Y.; Saito, K. Preparation, Stereochemistry, and Antibacterial Activity of Gramicidin s Analogs Containing N-Methyl Groups. *Bulletin of the Chemical Society of Japan.* 1991, pp 35–41.

(73)   Guzman-Martinez, A.; Lamer, R.; VanNieuwenhze, M. S. Total Synthesis of Lysobactin. *J. Am. Chem. Soc.* **2007**, *129* (18), 6017–6021.

(74)   Mootz, H. D.; Marahiel, M. A. The Tyrocidine Biosynthesis Operon Of. *Microbiology* **1997**, *179* (21), 6843–6850.

(75)   Gellman, S. H. Foldamers: A Manifesto. *Acc. Chem. Res.* **1998**, *31* (4), 173–180.

(76)   Hill, D. J.; Mio, M. J.; Prince, R. B.; Hughes, T. S.; Moore, J. S. A Field Guide to Foldamers. *Chem. Rev.* **2001**, *101* (12), 3893–4012.

(77)   Horne, W. S. Peptide and Peptoid Foldamers in Medicinal Chemistry. *Expert Opin. Drug Discov.* **2011**, *6* (12), 1247–1262.

(78)   Seebach, D.; Matthews, J. L. β-Peptides: A Surprise at Every Turn. *Chem. Commun.* **1997**, No. 21, 2015–2022.

(79)   Diedrich, D.; Moita, A. J. R.; Rüther, A.; Frieg, B.; Reiss, G. J.; Hoeppner, A.; Kurz, T.; Gohlke, H.; Lüdeke, S.; Kassack, M. U.; Hansen, F. K. α-Aminoxy Oligopeptides: Synthesis, Secondary Structure, and Cytotoxicity of a New Class of Anticancer Foldamers. *Chem. A Eur. J.* **2016**, *22* (49), 17600–17611.

(80)   Raguse, T. L.; Porter, E. A.; Weisblum, B.; Gellman, S. H. Structure−Activity Studies of 14-Helical Antimicrobial β-Peptides: Probing the Relationship between Conformational Stability and Antimicrobial Potency. *J. Am. Chem. Soc.* **2002**, *124* (43), 12774–12785.

(81)   Porter, E. A.; Wang, X.; Lee, H.-S.; Weisblum, B.; Gellman, S. H. Non-Haemolytic β-Amino-Acid Oligomers. *Nature* **2000**, *404* (6778), 565–565.

(82)   Gopalakrishnan, R.; Frolov, A. I.; Knerr, L.; Drury, W. J.; Valeur, E. Therapeutic Potential of Foldamers: From Chemical Biology Tools To Drug Candidates? *J. Med. Chem.* **2016**, *59* (21), 9599–9621.

(83)   Lau, Y. H.; de Andrade, P.; Wu, Y.; Spring, D. R. Peptide Stapling Techniques Based on Different Macrocyclisation Chemistries. *Chem. Soc. Rev.* **2015**, *44* (1), 91–102.

(84)   Blackwell, H. E.; Grubbs, R. H. Highly Efficient Synthesis of Covalently Cross-Linked Peptide Helices by Ring-Closing Metathesis. *Angew. Chemie Int. Ed.* **1998**, *37* (23), 3281–3284.

(85)   Tsomaia, N. Peptide Therapeutics: Targeting the Undruggable Space. *Eur. J. Med. Chem.* **2015**, *94*, 459–470.

(86)   Guarracino, D. A.; Bullock, B. N.; Arora, P. S. Protein-Protein Interactions in Transcription: A Fertile Ground for Helix Mimetics. *Biopolymers* **2011**, *95* (1), 1–7.

(87)   Walensky, L. D.; Bird, G. H. Hydrocarbon-Stapled Peptides: Principles, Practice, and Progress. *J. Med. Chem.* **2014**, *57* (15), 6275–6288.

(88)   Bird, G. H.; Madani, N.; Perry, A. F.; Princiotto, A. M.; Supko, J. G.; He, X.; Gavathiotis, E.; Sodroski, J. G.; Walensky, L. D. Hydrocarbon Double-Stapling Remedies the Proteolytic Instability of a Lengthy Peptide Therapeutic. *Proc. Natl. Acad. Sci.* **2010**, *107* (32), 14093–14098.

(89)   Klein, M. J.; Schmidt, S.; Wadhwani, P.; Bürck, J.; Reichert, J.; Afonin, S.; Berditsch, M.; Schober, T.; Brock, R.; Kansy, M.; Ulrich, A. S. Lactam-Stapled Cell-Penetrating Peptides: Cell Uptake and Membrane Binding Properties. *J. Med. Chem.* **2017**, *60* (19), 8071–8082.

(90)   de Araujo, A. D.; Hoang, H. N.; Kok, W. M.; Diness, F.; Gupta, P.; Hill, T. A.; Driver, R. W.; Price, D. A.; Liras, S.; Fairlie, D. P. Comparative α-Helicity of Cyclic Pentapeptides in Water. *Angew. Chemie Int. Ed.* **2014**, *53* (27), 6965–6969.

(91)   Tian, Y.; Jiang, Y.; Li, J.; Wang, D.; Zhao, H.; Li, Z. Effect of Stapling Architecture on Physiochemical Properties and Cell Permeability of Stapled α-Helical Peptides: A Comparative Study. *ChemBioChem* **2017**, *18* (21), 2087–2093.

(92)   Sakagami, K.; Masuda, T.; Kawano, K.; Futaki, S. Importance of Net Hydrophobicity in the Cellular Uptake of All-Hydrocarbon Stapled Peptides. *Mol. Pharm.* **2018**, *15* (3), 1332–1340.

(93)   Tian, Y.; Li, J.; Zhao, H.; Zeng, X.; Wang, D.; Liu, Q.; Niu, X.; Huang, X.; Xu, N.; Li, Z. Stapling of Unprotected Helical Peptides via Photo-Induced Intramolecular Thiol–Yne Hydrothiolation. *Chem. Sci.* **2016**, *7* (5), 3325–3330.

(94)   Hui, E. Y.-L.; Rout, B.; Tan, Y. S.; Verma, C. S.; Chan, K.-P.; Johannes, C. W. An Intramolecular Tryptophan-Condensation Approach for Peptide Stapling. *Org. Biomol. Chem.* **2018**, *16* (3), 389–392.

(95)   Lu, J.; Xu, H.; Xia, J.; Ma, J.; Xu, J.; Li, Y.; Feng, J. D- and Unnatural Amino Acid Substituted Antimicrobial Peptides With Improved Proteolytic Resistance and Their Proteolytic Degradation Characteristics. *Front. Microbiol.* **2020**, *11*, 1–17.

(96)   Imperiali, B.; Moats, R. A.; Fisher, S. L.; Prins, T. J. A Conformational Study of Peptides with the General Structure Ac-L-Xaa-Pro-D-Xaa-L-Xaa-NH2: Spectroscopic Evidence for a Peptide with Significant .Beta.-Turn Character in Water and in Dimethyl Sulfoxide. *J. Am. Chem. Soc.* **1992**, *114* (9), 3182–3188.

(97)   Fukuda, Y.; Yokomine, M.; Kuroda, D.; Tsumoto, K.; Morimoto, J.; Sando, S. Peptoid-Based Reprogrammable Template for Cell-Permeable Inhibitors of Protein-Protein Interactions. *Chem. Sci.* **2021**, *12* (40), 13292–13300.

(98)   Morimoto, J.; Fukuda, Y.; Kuroda, D.; Watanabe, T.; Yoshida, F.; Asada, M.; Nakamura, T.; Senoo, A.; Nagatoishi, S.; Tsumoto, K.; Sando, S. A Peptoid with Extended Shape in Water. *J. Am. Chem. Soc.* **2019**, *141* (37), 14612–14623.

(99)   Cui, Q.; Xu, Q. jun; Liu, L.; Guan, L. li; Jiang, X. yun; Inam, M.; Kong, L. cong; Ma, H. X. Preparation, Characterization and Pharmacokinetic Study of N-Terminal PEGylated D-Form Antimicrobial Peptide OM19r-8. *J. Pharm. Sci.* **2021**, *110* (3), 1111–1119.

(100)   Wang, C. K.; Swedberg, J. E.; Harvey, P. J.; Kaas, Q.; Craik, D. J. Conformational Flexibility Is

a Determinant of Permeability for Cyclosporin. *J. Phys. Chem. B* **2018**, *122* (8), 2261–2276.

(101) Mayer, A.; Anke, H.; Sterner, O. Omphalotin, A New Cyclic Peptide with Potent Nematicidal Activity from *Omphalotus Olearius* I. Fermentation and Biological Activity. *Nat. Prod. Lett.* **1997**, *10* (1), 25–32.

(102) Cai, M.; Marelli, U. K.; Bao, J.; Beck, J. G.; Opperer, F.; Rechenmacher, F.; McLeod, K. R.; Zingsheim, M. R.; Doedens, L.; Kessler, H.; Hruby, V. J. Systematic Backbone Conformational Constraints on a Cyclic Melanotropin Ligand Leads to Highly Selective Ligands for Multiple Melanocortin Receptors. *J. Med. Chem.* **2015**, *58* (16), 6359–6367.

(103) Kaminker, R.; Anastasaki, A.; Gutekunst, W. R.; Luo, Y.; Lee, S.-H.; Hawker, C. J. Tuning of Protease Resistance in Oligopeptides through *N* -Alkylation. *Chem. Commun.* **2018**, *54* (69), 9631–9634.

(104) Chatterjee, J.; Rechenmacher, F.; Kessler, H. N-Methylation of Peptides and Proteins: An Important Element for Modulating Biological Functions. *Angew. Chemie Int. Ed.* **2013**, *52* (1), 254–269.

(105) Nielsen, D. S.; Hoang, H. N.; Lohman, R. J.; Hill, T. A.; Lucke, A. J.; Craik, D. J.; Edmonds, D. J.; Griffith, D. A.; Rotter, C. J.; Ruggeri, R. B.; Price, D. A.; Liras, S.; Fairlie, D. P. Improving on Nature: Making a Cyclic Heptapeptide Orally Bioavailable. *Angew. Chemie Int. Ed.* **2014**, *53* (45), 12059–12063.

(106) Nguyen, A. M. T.; Brettell, S.; Douanne, N.; Duquette, C.; Corbeil, A.; Fajardo, E. F.; Olivier, M.; Fernandez-Prada, C.; Lubell, W. D. Influence of N-Methylation and Conformation on Almiramide Anti-Leishmanial Activity. *Molecules* **2021**, *26* (12).

(107) Fernández-Llamazares, A. I.; Adan, J.; Mitjans, F.; Spengler, J.; Albericio, F. Tackling Lipophilicity of Peptide Drugs: Replacement of the Backbone n -Methyl Group of Cilengitide by N -Oligoethylene Glycol (N -OEG) Chains. *Bioconjug. Chem.* **2014**, *25* (1), 11–17.

(108) Mas-Moruno, C.; Beck, J. G.; Doedens, L.; Frank, A. O.; Marinelli, L.; Cosconati, S.; Novellino, E.; Kessler, H. Increasing Avβ3 Selectivity of the Anti-Angiogenic Drug Cilengitide by N-Methylation. *Angew. Chemie Int. Ed.* **2011**, *50* (40), 9496–9500.

(109) Chatterjee, J.; Gilon, C.; Hoffman, A.; Kessler, H. N-Methylation of Peptides: A New Perspective in Medicinal Chemistry. *Acc. Chem. Res.* **2008**, *41* (10), 1331–1342.

(110) Biron, E.; Chatterjee, J.; Ovadia, O.; Langenegger, D.; Brueggen, J.; Hoyer, D.; Schmid, H. A.; Jelinek, R.; Gilon, C.; Hoffman, A.; Kessler, H. Improving Oral Bioavailability of Peptides by Multiple N-Methylation: Somatostatin Analogues. *Angew. Chemie Int. Ed.* **2008**, *47* (14), 2595–2599.

(111) Chatterjee, J.; Mierke, D.; Kessler, H. N-Methylated Cyclic Pentaalanine Peptides as Template Structures. *J. Am. Chem. Soc.* **2006**, *128* (47), 15164–15172.

(112) Ovadia, O.; Greenberg, S.; Chatterjee, J.; Laufer, B.; Opperer, F.; Kessler, H.; Gilon, C.; Hoffman, A. The Effect of Multiple N-Methylation on Intestinal Permeability of Cyclic Hexapeptides. *Mol. Pharm.* **2011**, *8* (2), 479–487.

(113) Beck, J. G.; Chatterjee, J.; Laufer, B.; Kiran, M. U.; Frank, A. O.; Neubauer, S.; Ovadia, O.; Greenberg, S.; Gilon, C.; Hoffman, A.; Kessler, H. Intestinal Permeability of Cyclic Peptides: Common Key Backbone Motifs Identified. *J. Am. Chem. Soc.* **2012**, *134* (29), 12125–12133.

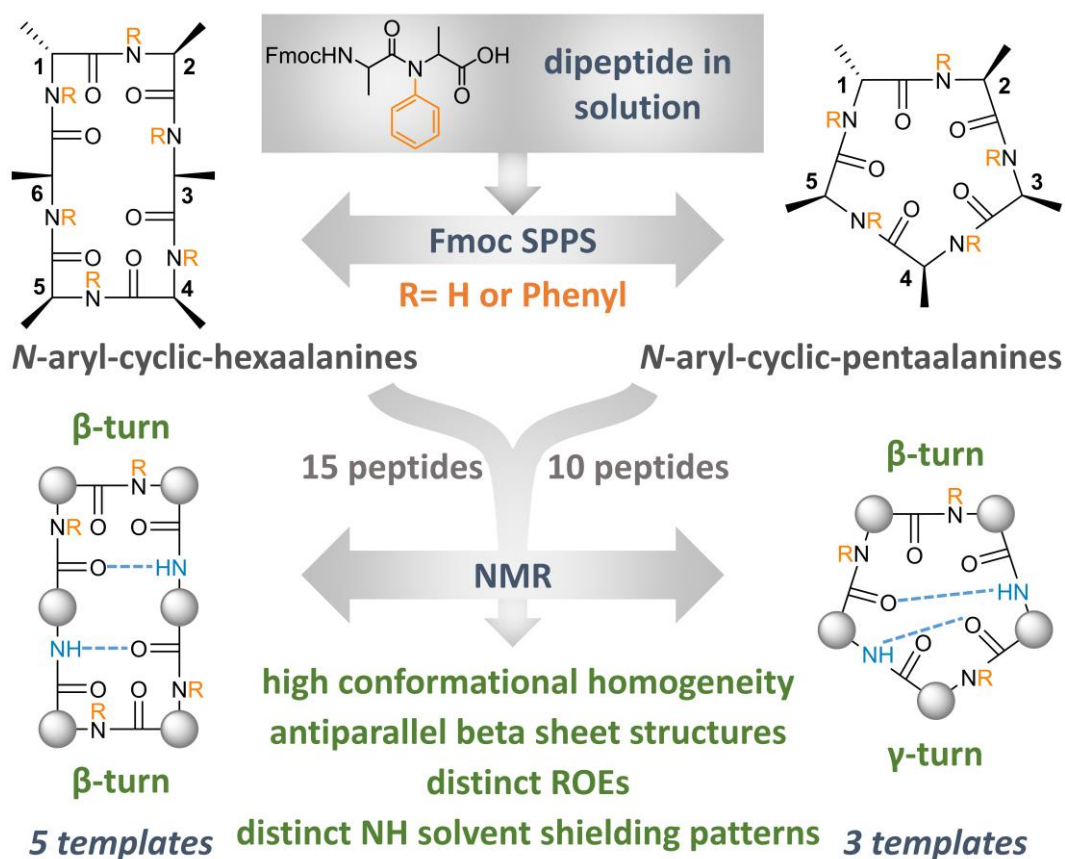(114) Marelli, U. K.; Ovadia, O.; Frank, A. O.; Chatterjee, J.; Gilon, C.; Hoffman, A.; Kessler, H. Cis-

Peptide Bonds: A Key for Intestinal Permeability of Peptides? *Chem. A Eur. J.* **2015**, *21* (43), 15148–15152.

(115) Marelli, U. K.; Bezençon, J.; Puig, E.; Ernst, B.; Kessler, H. Enantiomeric Cyclic Peptides with Different Caco-2 Permeability Suggest Carrier-Mediated Transport. *Chem. A Eur. J.* **2015**, *21* (22), 8023–8027.

(116) Dechantsreiter, M. A.; Planker, E.; Mathä, B.; Lohof, E.; Hölzemann, G.; Jonczyk, A.; Goodman, S. L.; Kessler, H. *N* -Methylated Cyclic RGD Peptides as Highly Active and Selective α $_V$ β $_3$ Integrin Antagonists. *J. Med. Chem.* **1999**, *42* (16), 3033–3040.

(117) Dupont, V.; Lecoq, A.; Boussard, G.; Marraud, M.; Mangeot, J. P.; Aubry, A. Conformational Perturbations Induced by N-Amination and N-Hydroxylation of Peptides. *J. Am. Chem. Soc.* **1993**, *115* (20), 8898–8906.

(118) Rathman, B. M.; Rowe, J. L.; Del Valle, J. R. Synthesis and Conformation of Backbone N-Aminated Peptides. *Methods Enzymol.* **2021**, *656*, 271–294.

(119) Hashizume, H.; Adachi, H.; Igarashi, M.; Nishimura, Y.; Akamatsu, Y. Biological Activities of Pargamicin A, a Novel Cyclic Peptide Antibiotic from Amycolatopsis Sp. *J. Antibiot. (Tokyo).* **2010**, *63* (6), 279–283.

(120) Zhang, H.; Nielsen, A. L.; Boesgaard, M. W.; Harpsøe, K.; Daly, N. L.; Xiong, X. F.; Underwood, C. R.; Haugaard-Kedström, L. M.; Bräuner-Osborne, H.; Gloriam, D. E.; Strømgaard, K. Structure–Activity Relationship and Conformational Studies of the Natural Product Cyclic Depsipeptides YM-254890 and FR900359. *Eur. J. Med. Chem.* **2018**, *156*, 847–860.

(121) Tillett, K. C.; Del Valle, J. R. *N* -Amino Peptide Scanning Reveals Inhibitors of Aβ42 Aggregation. *RSC Adv.* **2020**, *10* (24), 14331–14336.

(122) Sarnowski, M. P.; Kang, C. W.; Elbatrawi, Y. M.; Wojtas, L.; Del Valle, J. R. Peptide N-Amination Supports β-Sheet Conformations. *Angew. Chemie Int. Ed.* **2017**, *56* (8), 2083–2086.

(123) Rathman, B. M.; Allen, J. L.; Shaw, L. N.; Del Valle, J. R. Synthesis and Biological Evaluation of Backbone-Aminated Analogues of Gramicidin S. *Bioorganic Med. Chem. Lett.* **2020**, *30* (15), 127283.

(124) Makwana, K. M.; Sarnowski, M. P.; Miao, J.; Lin, Y. S.; Del Valle, J. R. N-Amination Converts Amyloidogenic Tau Peptides into Soluble Antagonists of Cellular Seeding. *ACS Chem. Neurosci.* **2021**, *12* (20), 3928–3938.

(125) Fernández-Llamazares, A. I.; García, J.; Soto-Cerrato, V.; Pérez-Tomás, R.; Spengler, J.; Albericio, F. N-Triethylene Glycol (*N*-TEG) as a Surrogate for the N-Methyl Group: Application to Sansalvamide A Peptide Analogs. *Chem. Commun.* **2013**, *49* (57), 6430–6432.

(126) Choudhary, A.; Raines, R. T. An Evaluation of Peptide-Bond Isosteres. *ChemBioChem* **2011**, *12* (12), 1801–1807.

(127) Huestis, M. P.; Terrett, J. A. Simple Strategy towards Amide Bioisosteres. *Nat. Chem.* **2022**, *14* (2), 120–121.

(128) Mundlapati, V. R.; Gautam, S.; Sahoo, D. K.; Ghosh, A.; Biswal, H. S. Thioamide, a Hydrogen Bond Acceptor in Proteins and Nucleic Acids. *J. Phys. Chem. Lett.* **2017**, *8* (18), 4573–4579.

(129) Yang, J.; Wang, C.; Yao, C.; Chen, C.; Hu, Y.; He, G.; Zhao, J. Site-Specific Incorporation of

Multiple Thioamide Substitutions into a Peptide Backbone via Solid Phase Peptide Synthesis. *J. Org. Chem.* **2020**, *85* (3), 1484–1494.

(130) Inokuchi, E.; Yamada, A.; Hozumi, K.; Tomita, K.; Oishi, S.; Ohno, H.; Nomizu, M.; Fujii, N. Design and Synthesis of Amidine-Type Peptide Bond Isosteres: Application of Nitrile Oxide Derivatives as Active Ester Equivalents in Peptide and Peptidomimetics Synthesis. *Org. Biomol. Chem.* **2011**, *9* (9), 3421.

(131) Wipf, P.; Henninger, T. C.; Geib, S. J. Methyl- and (Trifluoromethyl)Alkene Peptide Isosteres: Synthesis and Evaluation of Their Potential as β-Turn Promoters and Peptide Mimetics. *J. Org. Chem.* **1998**, *63* (18), 6088–6089.

(132) Oishi, S.; Kamitani, H.; Kodera, Y.; Watanabe, K.; Kobayashi, K.; Narumi, T.; Tomita, K.; Ohno, H.; Naito, T.; Kodama, E.; Matsuoka, M.; Fujii, N. Peptide Bond Mimicry by (E)-Alkene and (Z)-Fluoroalkene Peptide Isosteres: Synthesis and Bioevaluation of α-Helical Anti-HIV Peptide Analogues. *Org. Biomol. Chem.* **2009**, *7* (14), 2872.

(133) Choudhary, A.; Raines, R. T. An Evaluation of Peptide-Bond Isosteres. *ChemBioChem* **2011**, *12* (12), 1801–1807.

(134) Ecker, A. K.; Levorse, D. A.; Victor, D. A.; Mitcheltree, M. J. Bioisostere Effects on the EPSA of Common Permeability-Limiting Groups. *ACS Med. Chem. Lett.* **2022**, *13* (6), 964–971.

(135) Christos, T. E.; Arvanitis, A.; Cain, G. A.; Johnson, A. L.; Pottorf, R. S.; Tam, S. W.; Schmidt, W. K. Stable Isosteres of Neurotensin C-Terminal Pentapeptides Derived by Modification of the Amide Function. *Bioorg. Med. Chem. Lett.* **1993**, *3* (6), 1035–1040.

(136) Lin, J.; Toscano, P. J.; Welch, J. T. Inhibition of Dipeptidyl Peptidase IV by Fluoroolefin-Containing *N*-Peptidyl-*O*-Hydroxylamine Peptidomimetics. *Proc. Natl. Acad. Sci.* **1998**, *95* (24), 14020–14024.

(137) Oishi, S.; Miyamoto, K.; Niida, A.; Yamamoto, M.; Ajito, K.; Tamamura, H.; Otaka, A.; Kuroda, Y.; Asai, A.; Fujii, N. Application of Tri- and Tetrasubstituted Alkene Dipeptide Mimetics to Conformational Studies of Cyclic RGD Peptides. *Tetrahedron* **2006**, *62* (7), 1416–1424.

(138) Otrubova, K.; Lushington, G.; Vander Velde, D.; McGuire, K. L.; McAlpine, S. R. Comprehensive Study of Sansalvamide A Derivatives and Their Structure-Activity Relationships against Drug-Resistant Colon Cancer Cell Lines. *J. Med. Chem.* **2008**, *51* (3), 530–544.

(139) Mas-Moruno, C.; Rechenmacher, F.; Kessler, H. Cilengitide: The First Anti-Angiogenic Small Molecule Drug Candidate. Design, Synthesis and Clinical Evaluation. *Anticancer. Agents Med. Chem.* **2011**, *10* (10), 753–768.

(140) Haubner, R.; Schmitt, W.; Hölzemann, G.; Goodman, S. L.; Jonczk, A.; Kessler, H. Cyclic RGD Peptides Containing β-Turn Mimetics. *J. Am. Chem. Soc.* **1996**, *118* (34), 7881–7891.

(141) Dechantsreiter, M. A.; Planker, E.; Matha, B.; Lohof, E.; Jonczyk, A.; Goodman, S. L.; Kessler, H. Articles. **1999**, 3033–3040.

(142) Kessler, H.; Gratias, R.; Hessler, G.; Gurrath, M.; Müller, G. Conformation of Cyclic Peptides. Principle Concepts and the Design of Selectivity and Superactivity in Bioactive Sequences by "Spatial Screening." *Pure Appl. Chem.* **1996**, *68* (6), 1201–1205.

(143) Haubner, R.; Gratias, R.; Diefenbach, B.; Goodman, S. L.; Jonczyk, A.; Kessler, H. Structural and Functional Aspects of RGD-Containing Cyclic Pentapeptides as Highly Potent and Selective Integrin α(v)B3 Antagonists. *J. Am. Chem. Soc.* **1996**, *118* (32), 7461–7472.

(144) Martín-Gago, P.; Gomez-Caminals, M.; Ramón, R.; Verdaguer, X.; Martin-Malpartida, P.; Aragón, E.; Fernández-Carneado, J.; Ponsati, B.; López-Ruiz, P.; Cortes, M. A.; Colás, B.; Macias, M. J.; Riera, A. Fine-Tuning the π-π Aromatic Interactions in Peptides: Somatostatin Analogues Containing Mesityl Alanine. *Angew. Chemie* **2012**, *124* (8), 1856–1861.

(145) Martín-Gago, P.; Aragón, E.; Gomez-Caminals, M.; Fernández-Carneado, J.; Ramón, R.; Martin-Malpartida, P.; Verdaguer, X.; López-Ruiz, P.; Colás, B.; Cortes, M. A.; Ponsati, B.; Macias, M. J.; Riera, A. Insights into Structure-Activity Relationships of Somatostatin Analogs Containing Mesitylalanine. *Molecules* **2013**, *18* (12), 14564–14584.

(146) Weinmüller, M.; Rechenmacher, F.; Kiran Marelli, U.; Reichart, F.; Kapp, T. G.; Räder, A. F. B.; Di Leva, F. S.; Marinelli, L.; Novellino, E.; Muñoz-Félix, J. M.; Hodivala-Dilke, K.; Schumacher, A.; Fanous, J.; Gilon, C.; Hoffman, A.; Kessler, H. Overcoming the Lack of Oral Availability of Cyclic Hexapeptides: Design of a Selective and Orally Available Ligand for the Integrin Avβ3. *Angew. Chemie Int. Ed.* **2017**, *56* (51), 16405–16409.

(147) Bagwe, P. V.; Bagwe, P. V.; Ponugoti, S. S.; Joshi, S. V. Peptide-Based Vaccines and Therapeutics for COVID-19. *Int. J. Pept. Res. Ther.* **2022**, *28* (3), 94.

(148) Peptide Therapeutics Market Size, Share & Trends Analysis Report By Application, By Type (Generic, Innovative), By Type Of Manufacturer, By Route Of Administration, By Synthesis Technology, By Region, And Segment Forecasts, 2023 - 2030; **2022**.

CHAPTER-2

Exploration of *N*-arylation of backbone amides as a novel tool for conformational modification in peptides

N-aryl-cyclic-hexaalanines

dipeptide in solution

Fmoc SPPS

R= H or Phenyl

N-aryl-cyclic-pentaalanines

β-turn

β-turn

15 peptides   10 peptides

NMR

high conformational homogeneity
antiparallel beta sheet structures
distinct ROEs
distinct NH solvent shielding patterns

β-turn

γ-turn

5 templates   *3 templates*

2.1. Introduction

Obtaining a stable, orally available bioactive peptide is a challenging task in the field of peptide therapeutics.[1–6] The biological aspects of peptides are primarily a result of their conformation.[7–9] Conformations in peptides determine the orientation of the constituent residues and corresponding stereoelectronic and physicochemical features responsible for the biological function of the peptides.[10] Hence, optimizing a peptide's conformation while also bringing in specific functional group changes is a crucial part of the peptide-based drug design.[10] A multitude of peptide design strategies, such as the use of homologous or nonproteinogenic amino acids, cyclization, stereo-inversion, foldamers, stapled peptides, and disulfide bridged peptides are some methods that have been developed and followed to architect peptide folding (Figure **2.1**).[11–19]
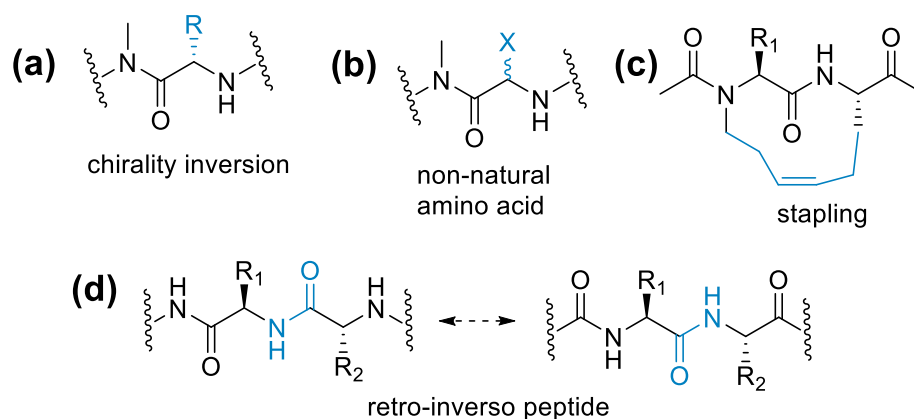
Figure 2.1. Peptide design strategies to constrain peptide folding.

Cyclic peptides are undoubtedly one of the most successful class of peptides that has offered numerous peptide ligands and therapeutics.[20,21] A growing number of peptide drugs that received drug approval in recent times belong to cyclic peptides.[22] The conformational robustness of cyclic peptides enhances their binding affinity and selectivity for specific receptors. Since they lack amino and carboxyl terminals, cyclic peptides are resistant to exopeptidase hydrolysis.[23] Cyclic peptides can show good permeability and are able to pass through cell membranes as compared to linear peptides.[24,25] These characteristics have made cyclic peptides with a stable conformation more drug-like than their linear counterparts. Tailoring the conformations in cyclic peptides is majorly achieved by shaping the turns in the cyclic peptides.[26–28] Because of the cyclic nature, most cyclic peptides display robust structures with well-defined conformational scaffolds such as turns, hairpins, and hydrogen bonding patterns in general. In the last couple of decades, *N*-methylation of the backbone amide protons has emerged as one of the multipurpose tools for the chemical modification of cyclic peptides.[29–34] *N*-methylation has been

demonstrated to modify the conformations, bioactivity, lipophilicity or bioavailability in cyclic peptides.[29,35–37] Cyclosporine, a natural bioavailable peptide and immunosuppressant drug, and Cilengitide, a synthetic peptide from Kessler's research group, are prime examples that portray how a combination of cyclization, stereo inversion, and *N*-methylation can be used to optimize a peptide sequence for a targeted biological activity.[38,39] Kessler's research group has widely employed *N*-methylation as a strategy to develop selective peptide ligands for multiple integrin receptor subtypes, somatostatin and melanocortin receptors, and imaging.[40–42] In parallel, both Kessler and Lokey's group have demonstrated the potential of *N*-methylation in improving the permeability and bioavailability of the peptides.[33,41,43]

Figure 2.2. (a) *N*-methyl containing cyclic hexaalanine template and their permeability study (b) highly membrane permeable orally available (29%) scaffold (cyclo[Leu-*N*Me-D-Leu-*N*Me-Leu-Leu-D-Pro-*N*Me-Tyr]) developed by Lokey's group.

Kessler's group reported extensive conformational studies of *N*-methyl containing oligo-alanine cyclic peptides and used them as templates to investigate the structural requirements for permeability (Figure **2.2a**).[43–48] They developed two highly permeable scaffolds from a library of 54 cyclic-hexaalanine peptides and proved the conformational dependence of permeability, and suggested that the multiple *N*-methylation can dramatically improve the permeability of peptides.[43,45] Biron *et al.* studied the effect of multiple *N*-methylation on the intestinal permeability and enzymatic stability of somatostatin analogue, the Veber-Hirschmann peptide, and had shown that multiple *N*-methylation improved its oral bioavailability without altering its bioactivity.[41] Lokey's group developed a highly membrane permeable orally available (cyclo[Leu-*N*Me-D-Leu-*N*Me-Leu-Leu-D-Pro-*N*Me-Tyr]) (Figure **2.2b**) scaffold.[33] These investigations proved that varying the position and number of *N*-methylations on the backbone amides of a cyclic peptide can significantly impact their permeability and bioactivity.

Other than *N*-methylation, a few individual backbone amide modifications were discussed in the literature recently. Del Valle's group has shown the effect of *N*-amination and *N*-hydroxylation on conformations and activity of peptides.[49–52] Fernando Albericio's group studied the *N*-TEG and *N*-OEG as a surrogate of *N*-Me and found an increase in lipophilicity of the *N*-TEG peptides as compared to the *N*-methylated peptides.[53,54] In an interesting approach, Shinsuke Sando's research group pioneered the synthesis of oligo (*N*-substituted alanine) peptoids via reductive amination of amines in the amino acids with various aldehydes to result in peptoids containing diverse *N*-alkyl groups (Figure **2.3b**). These *N*-alkyl peptoids exhibited extended conformations in water and cell permeability.[55,56] As evident by this discussed literature, the backbone amide modifications are quite versatile in subtle and controlled alteration of the conformations and the resulting stereo-electronic attributes in peptides.[57] As compared to backbone *N*-methylation of amide bonds, other backbone *N*-modifications are underexplored and new modifications are warranted.
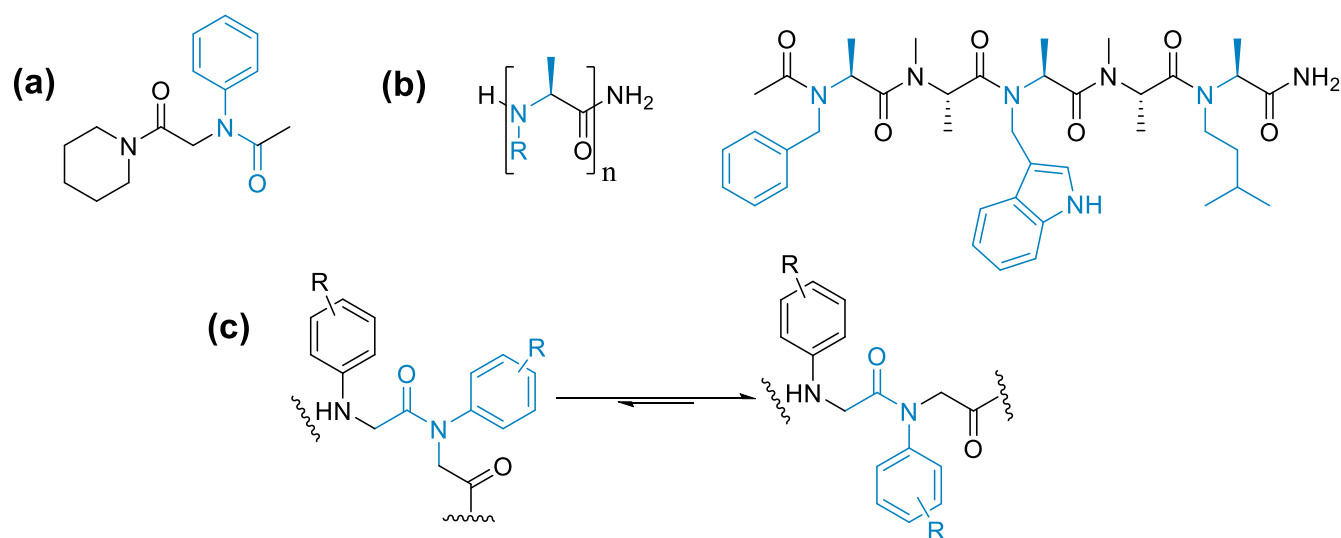
Figure 2.3. (**a**) Representation of *trans* geometry in *N*-aryl amide, (**b**) oligo (*N*-substituted alanine) peptoids by Sando's group, (**c**) study of conformation in oligo (*N*-aryl glycines) and preference for *trans* geometry by Kirshenbaum's group.

In this direction, we have hypothesized and explored the backbone amide *N*-arylation as a novel chemical modification in peptides. We speculate that *N*-arylation would impart the peptides with large steric effects, polarity changes, and pi-pi interaction based conformational changes. For instance, earlier reports on the N-alkylated anilides,[58] oligo (*N*-aryl glycines),[59] and peptoids with *N*-aryl groups[60] have indicated a strong preference of the *N*-aryl amide groups to stay in trans geometry (Figure **2.3c**).[58–61] Further, *N*-arylation would have a much broader substrate scope because of a variety of choices of the aryl groups. In this context, herein we discuss the design, synthesis, NMR based conformational

characterization of 15 cyclic-hexaalanine (section **A**) and 10 cyclic-pentaalanine (section **B**) peptides containing backbone *N*-aryl amide groups.

2.2. **Results and Discussion**

For our studies, we have considered two model cyclic peptides as parent templates- a cyclic-hexaalanine (CHA) and a cyclic-pentaalanine (CPA)- both containing a D-alanine residue that brings in the configurational heterogeneity (Figure **2.4**). We synthesized a library of 15 *N*-phenyl containing cyclic-hexaalanine peptides (NPCHA; 6 peptides containing one *N*-phenyl-L-or D-alanine and 9 peptides with two *N*-phenyl-L-or D-alanine residues) and 10 *N*-phenyl containing cyclic-pentaalanine peptides (NPCPA; 5 peptides containing one *N*-phenyl-L-or D-alanine and 5 peptides with two *N*-phenyl-L-or D-alanine residues). The 25 peptides were synthesized by combining solution and solid phase peptide synthesis chemistry.
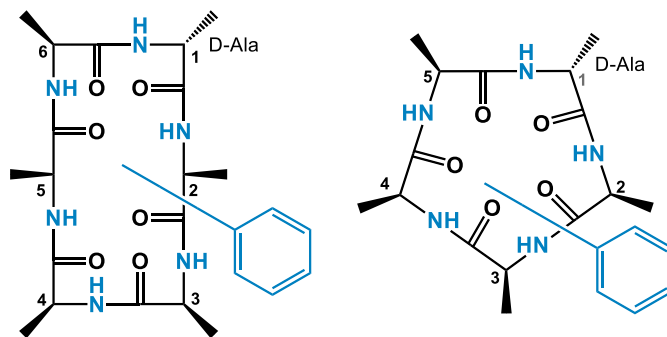
Figure 2.4. Model cyclic peptides as parent templates for *N*-aryl modification study.

For the synthesis of the targeted peptide library (Figure **2.5**), *N*-arylation of L- or D-alanine was carried out in solution by following Buchwald-Hartwig method using Iodobenzene to obtain *N*-phenyl-L- or D-alanine (Scheme **2.1a**).[62] Thus obtained, *N*-phenyl-L- or D-alanine was initially protected with Fmoc to generate Fmoc-*N*-phenyl-L- or D-alanine to use as a building block in Fmoc solid phase peptide synthesis protocol using 2-CTC resin.[63] However, the low nucleophilicity of the arylated amine in *N*-phenyl-L- or D-alanine had posed an insurmountable challenge in its solid phase peptide couplings to Fmoc-L- or D-Ala-OH, despite our trials with various reagent conditions (Table **2.1**) Hence, we attempted to synthesize the dipeptide Fmoc-L-Ala-*N*-phenyl-L-Ala-OH in solution phase under multiple peptide coupling conditions (Table **2.2**). While most coupling conditions have produced nil or trace amounts of the required compound, the activation of Fmoc-L-Ala-OH to Fmoc-L-Ala-Cl as an acid chloride and coupling to *N*-phenyl-L-ala-OMe in the presence of triethyl amine in dry DCM resulted in reasonable quantities of the dipeptide ester Fmoc-L-Ala-*N*-phenyl-L-Ala-OMe in approximately 55 %

reaction yield. This dipeptide ester upon ester hydrolysis with 1:1 aq. 5M HCl and dioxane under reflux yielded the required dipeptide Fmoc-L-Ala-*N*-phenyl-L-Ala-OH in~98 % yield (Scheme **2.1b**).[64]

S.No.	Name	Sequence					
		N-phenyl cyclo-hexaalanine peptides (**NPCHA**)					
1	**1NPCHA**	a	A	A	A	A	A
2	**2NPCHA**	a	A	A	A	A	A
3	**3NPCHA**	a	A	A	A	A	A
4	**4NPCHA**	a	A	A	A	A	A
5	**5NPCHA**	a	A	A	A	A	A
6	**6NPCHA**	a	A	A	A	A	A
7	**13NPCHA**	a	A	A	A	A	A
8	**14NPCHA**	a	A	A	A	A	A
9	**15NPCHA**	a	A	A	A	A	A
10	**24NPCHA**	a	A	A	A	A	A
11	**25NPCHA**	a	A	A	A	A	A
12	**26NPCHA**	a	A	A	A	A	A
13	**35NPCHA**	a	A	A	A	A	A
14	**36NPCHA**	a	A	A	A	A	A
15	**46NPCHA**	a	A	A	A	A	A
		N-phenyl cyclo-pentaalanine peptides (**NPCPA**)					
1	**1NPCPA**	a	A	A	A	A	
2	**2NPCPA**	a	A	A	A	A	
3	**3NPCPA**	a	A	A	A	A	
4	**4NPCPA**	a	A	A	A	A	
5	**5NPCPA**	a	A	A	A	A	
6	**13NPCPA**	a	A	A	A	A	
7	**14NPCPA**	a	A	A	A	A	
8	**15NPCPA**	a	A	A	A	A	
9	**24NPCPA**	a	A	A	A	A	
10	**35NPCPA**	a	A	A	A	A	

Figure 2.5. List of the *N*-phenyl containing peptides designed, synthesized and characterized in this work. 'A′' represents the L-alanine and 'a′' represents D-alanine. The numbers at the start of the peptide name and the amino acid labels highlighted in grey in the sequences indicate the position of the residues with *N*-phenyl amide group.

With the success of dipeptide synthesis in solution phase, we decided to use such suitable Fmoc-*N*-phenyl containing dipeptides as one of the building blocks for solid phase synthesis, instead of Fmoc-*N*-phenyl-L- or D-alanine monomer. Using a dipeptide building block and the lack of N-terminus coupling reactivity of *N*-phenyl-L-or D-alanine on solid phase, therefore, channelled the library to a select 15 NPCHA and 10 NPCPA peptides (Figure **2.5**). As required by the planned sequence of the target peptides, we separately obtained the suitable dipeptides- Fmoc-L-Ala-L-*N*-Ph-Ala-OH (**4a**), Fmoc-D-Ala-L-*N*-Ph-Ala-OH (**4b**) and Fmoc-L-Ala-D-*N*-Ph-Ala-OH (**4c**) by solution phase chemistry (see

experimental section, scheme **2.1b**) to use as coupling units for solid phase peptide synthesis. All the target peptides were synthesized by Fmoc-solid phase peptide synthesis using 2-CTC resin (Scheme **2.1c**) and were purified by reversed phase HPLC.
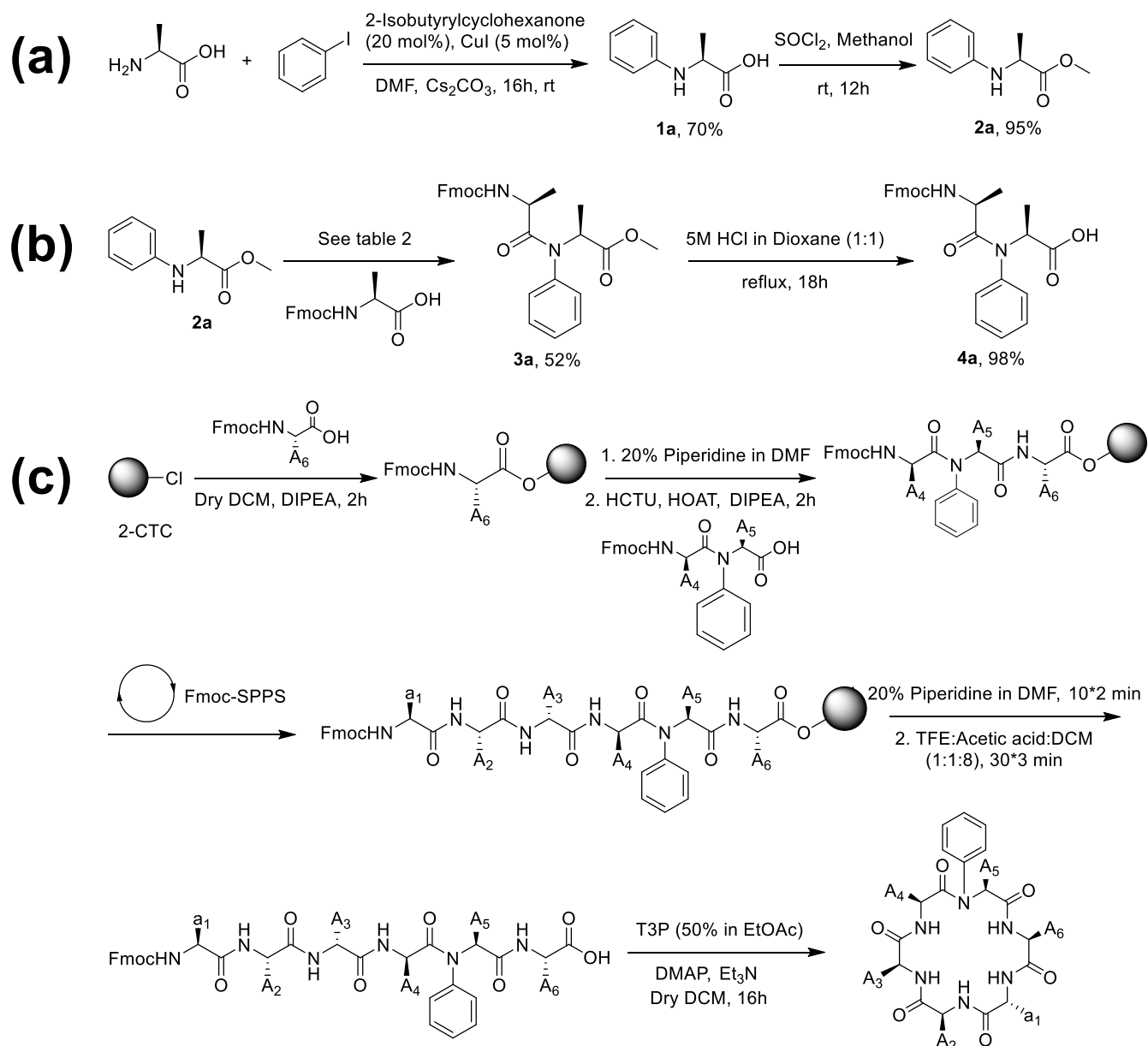
Scheme 2.1. (**a**) Synthesis of *N*-phenyl-L-alanine; (**b**) synthesis of one of the *N*-phenyl containing dipeptides, Fmoc-L-Ala-*N*-phenyl-L-Ala-OH (**4a**), which are used as the building blocks in (**c**) Fmoc based solid phase peptide synthesis of the required peptides on 2-CTC resin, exemplified for 5NPCHA.

Table 2.1. Various conditions under which coupling of resin-bound *N*-phenyl-L-Ala-OH and Fmoc-L-Ala-OH was attempted.

S. No.	Reagents	Conditions	Solvent	Remarks
1	HATU, DIPEA	rt and 45 °C	Dry DCM	No reaction
2	HCTU, DIPEA	60 °C for 16 hrs	Dry DMF	No coupling (Fmoc deprotection of other coupling partners)
3	COMU, DIPEA	rt	DMF	No reaction
5	CDI	rt	DCM	No reaction
6	DCC	rt	DCM	No reaction
7	DIC	rt	DMF	No reaction
8	EDC.HCl	rt	EDC	No reaction
9	HATU, DIPEA	rt	Dry DCM: DMF (6:1)	No reaction
10	HCTU Et$_3$N	rt	DCM	No reaction
11	HATU, DIPEA	Microwave	DMF	No reaction
12	SOCl$_2$ (reflux), Et$_3$N	rt (1.5 hrs)	Dry DCM	product obtained (30%), observed peptide cleavage from resin
13	PyBoP, DIPEA	rt (3 hrs)	NMP	No reaction
14	Oxyma Pure, DIC	rt (3 hrs)	NMP	No reaction
15	DCHA, Pyridine SOCl$_2$, Zn dust	rt (3 hrs)	DCM	No reaction
16	T3P, DMAP, Pyridine	80 ˚C	DMF	No reaction
17	T3P, DMAP, LiHMDS	80 ˚C	DMF	No reaction
18	DCHA, Pyridine, SOCl$_2$, Zn dust	rt (2 hrs)	Dry DCM	No reaction
19	HOAt.DCHA	rt	Dry DCM	No reaction
20	DPPA, Et$_3$N	rt	DMF	No reaction
21	Isobutryl Chloroformate, Et$_3$N	rt (12 hrs)	DCM	No reaction
22	DCHA, Pyridine, SOCl$_2$, Zn dust	50˚C (2 hrs)	Dry DCM	No reaction
23	SOCl$_2$ (reflux), I$_2$	50˚C (2 hrs)	Dry DCM	No reaction
24	PyBroP, Et$_3$N	rt (3 hrs)	NMP	No reaction
25	PyBroP, DIPEA	rt (12 hrs)	NMP	No reaction
27	PyBroP, DIPEA	50˚C (2 hrs)	DMF	No reaction
28	BTC, Collidine, DIPEA	rt (2 hrs)	Dry THF	No reaction
29	BTC, Collidine, DIPEA	50˚C (2 hrs)	Dry THF	product obtained in very trace amounts
30	BTC, Collidine, DIPEA, I$_2$	50˚C (2 hrs)	Dry THF	product obtained in very trace amounts

Table 2.2. Reaction conditions for coupling of *N*-phenyl-L-Ala-OMe to Fmoc-L-ala-OH in solution phase.

S. No.	Reagents	Conditions	Solvent	Remarks
1	HATU, DIPEA	rt and 45 °C	Dry DCM	No reaction
2	HCTU, DIPEA	60 °C for 16 hrs	Dry DMF	No reaction
3	COMU, DIPEA	rt	DMF	No reaction
4	SOCl$_2$, NaH	rt	Dry THF	No reaction
5	HATU, NaH	rt	Dry THF	No reaction
6	CDI	rt	DCM	No reaction
7	DCC	rt	DCM	No reaction
8	DIC	rt	DMF	No reaction
9	EDC.HCl	rt	EDC	No reaction
10	HATU, DIPEA	rt	Dry DCM: DMF (6:1)	No reaction
11	HCTU, Et$_3$N	rt	DCM	No reaction
12	HATU, DIPEA	Microwave	DMF	No reaction
13	SOCl$_2$ (reflux) Pyridine	rt (1.5 hrs)	Dry DCM	product obtained (30%)
14	SOCl$_2$ (reflux) Et$_3$N	rt (1.5 hrs)	Dry DCM	product obtained (50%)
15	SOCl$_2$, Pyridine	0 °C (1.5 hrs)	Dry DCM	product obtained (30%)
16	SOCl$_2$, Et$_3$N	0 °C (1.5 hrs)	Dry DCM	product obtained (50%), no epimerization

2.2.1. HPLC purification of *N*-aryl peptides

All the peptides were purified by reverse phase Semi-prep HPLC on Waters 2545 Quaternary Gradient Module having 2489 UV/Visible Detector. Column specifications- YMC Pack ODS-A-HG C18 column with specifications S-10 µm, 12 nm, 250 mm * 20 mm I.D. Mobile phase ACN and water, and a flow rate of 4 mL/min was used for the purification.

2.2.2. NMR spectroscopic studies of *N*-aryl peptides

For NMR spectroscopic studies, 5 mg of each peptide was dissolved in 0.5 mL of DMSO-d_6. 1D and 2D spectra were recorded at 298 K on Bruker 500 or 700 MHz NMR spectrometer equipped with a BBO or TXI probe respectively. ^{1}H-1D, DQF-COSY, TOCSY, ROESY, ^{1}H-^{13}C HSQC, and ^{1}H-^{13}C HMBC NMR experiments were acquired. A mixing time of 300 ms was used for ROESY. The 2D NMR experiments were acquired with 320 (for DQF-COSY and TOCSY), 512 (for ROESY), 512 (for HSQC and HMBC) data points in the F1 dimension, and 4k (for DQF-COSY, TOCSY, ROESY) and 1k (for HSQC and HMBC) data points in F2 dimension.

2.2.3. Temperature coefficient determination

For the determination of temperature coefficients of amide protons, ^{1}H NMR experiments were recorded at variable temperatures ranging from 300 K to 325 K with 5 K increments. The temperature coefficients were calculated according to $(\Delta\delta*1000)/\Delta T$, wherein $\Delta\delta$ and ΔT are the change in chemical shift of the amide NH and the change in sample temperature, respectively.

Section A

Design and synthesis of *N*-aryl cyclic-hexaalanine peptides and their conformational studies by NMR
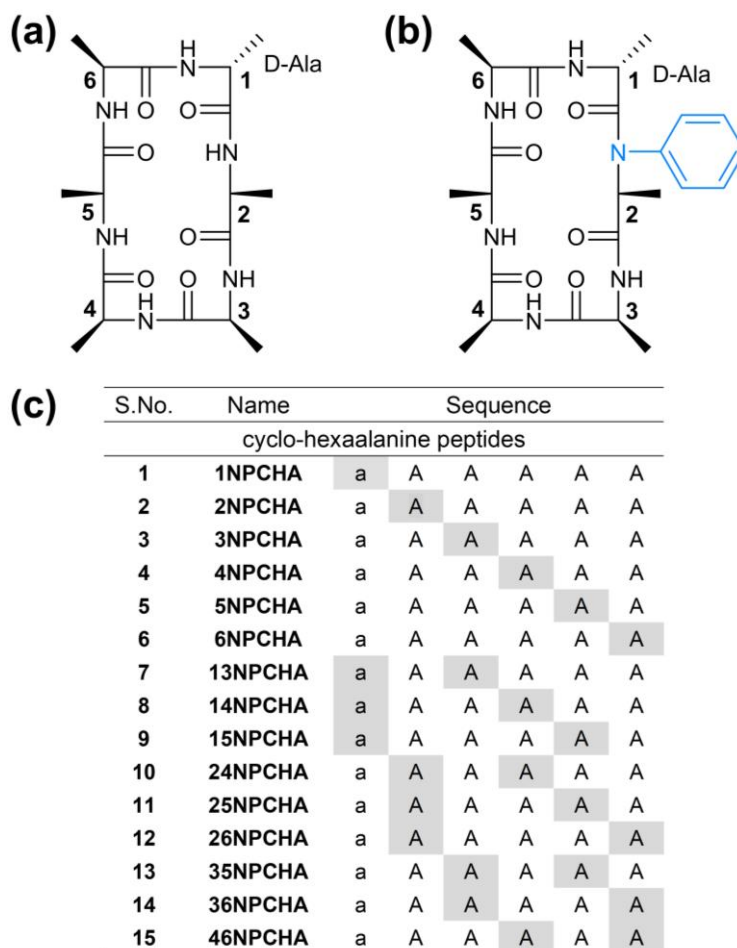
Figure 2A.1. (a) The parent cyclic-hexaalanine peptide template used for *N*-arylation. The residues are numbered starting from D-alanine as position 1; (b) representative example of *N*-phenyl CHA peptide-2NPCHA containing one *N*-phenyl residue; (c) list of the *N*-phenyl containing CHA peptides synthesized and characterized in this work. The numbers at the start of the peptide name and the amino acid labels highlighted in grey in the sequences indicate the position of the residues with *N*-phenyl amide group.
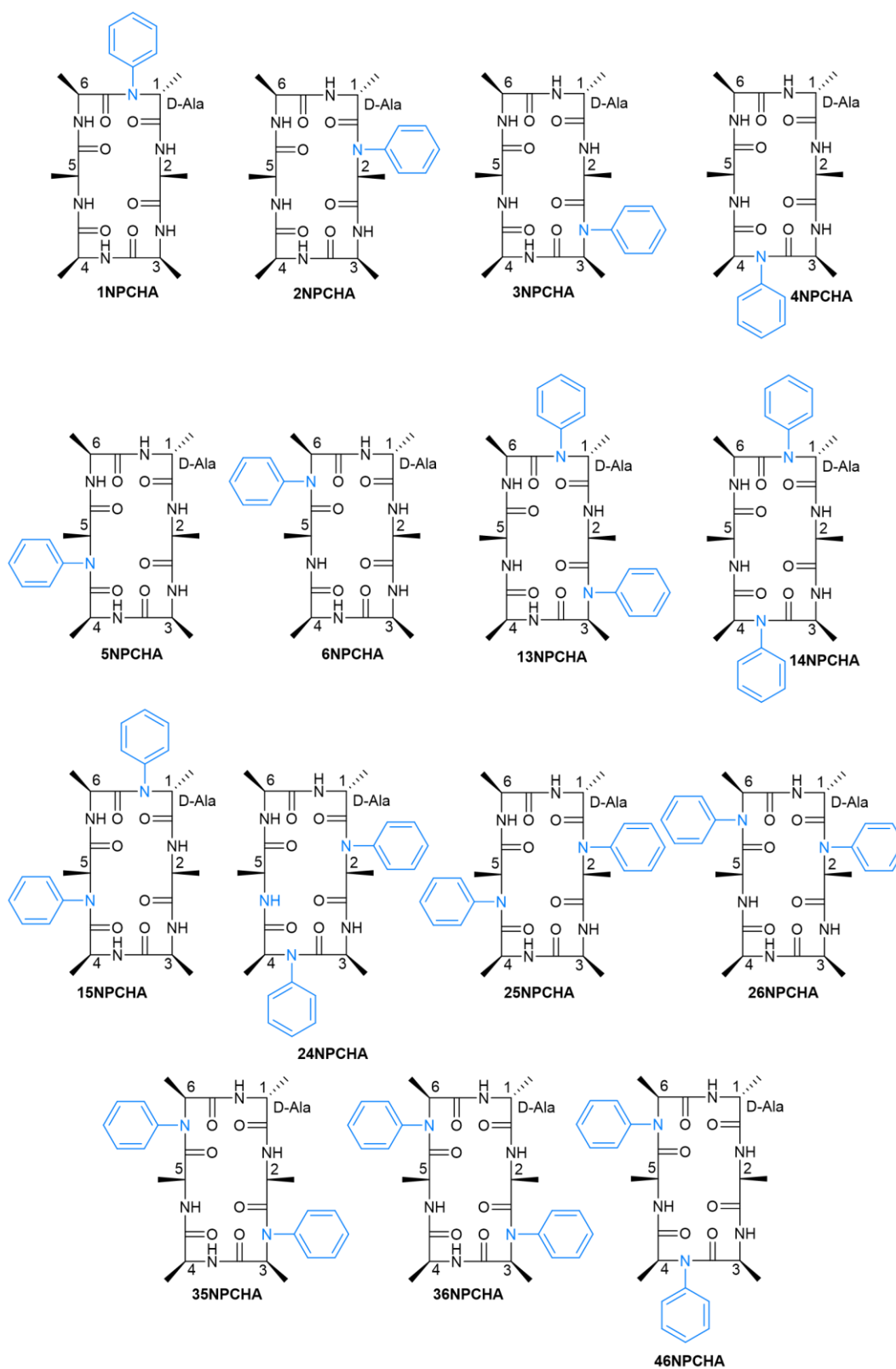
Figure 2A.2. Schematic structures of NPCHA peptides synthesized and studied in this section.

Table 2A.1. HPLC purification methods for **NPCHA** peptides.

S. No.	Peptide	HPLC Method Gradient (ACN : Water)	Retention Time (min)
		Methods used for the HPLC purification of the NPCHA peptides and their corresponding retention times.	
1	1NPCHA	20 % - 50 % ACN in 20 min	14.7
2	2NPCHA	20 % - 50 % ACN in 20 min	17.4
3	3NPCHA	15 % - 50 % ACN in 20 min	14.1
4	4NPCHA	17 % - 50 % ACN in 20 min	14.7
5	5NPCHA	15 % - 50 % ACN in 20 min	15.1
6	6NPCHA	15 % - 50 % ACN in 20 min	12.6
7	13NPCHA	40 % - 50 % ACN in 20 min	13.7
8	14NPCHA	38 % - 48 % ACN in 20 min	12.9
9	15NPCHA	35 % - 45 % ACN in 30 min	14.2
10	24NPCHA	35 % - 60 % ACN in 30 min	18.6
11	25NPCHA	40 % - 70 % ACN in 20 min	11.4
12	26NPCHA	35 % - 45 % ACN in 20 min	17.2
13	35NPCHA	40 % - 70 % ACN in 30 min	13.4
14	36NPCHA	35 % - 55 % ACN in 40 min	16.7
15	46NPCHA	35 % - 60 % ACN in 30 min	12.6

2A.1. **Chemical shift assignments of NPCHA peptides**

The following list of tables **2A.2** – **2A.16** has the chemical shift assignments of the NPCHA peptides. The notations used are ala = L-alanine, ald = D-alanine, lnpa = *N*-phenyl-L-Ala, dnpa = *N*-phenyl-D-Ala.

Table 2A.2. Chemical shift assignments of **1NPCHA**.

Residue	NH	Hα	Hβ	Cα	Cβ	CO	Temp. coeff.
1dnpa	-	4.80	0.90	55.30	16.25	171.7	-
2ala	8.62	4.27	1.30	48.76	18.19	172.23	-4.4
3ala	7.80	4.32	1.40	48.80	18.43	173.10	-2.0
4ala	8.16	3.93	1.23	50.67	16.90	172.29	-4.0
5ala	7.72	3.90	1.19	48.66	16.26	171.89	-3.6
6ala	7.62	3.86	1.10	47.7	17.67	172.58	-1.6

Table 2A.3. Chemical shift assignments of **2NPCHA**.

Residue	NH	Hα	Hβ	Cα	Cβ	CO	Temp. coeff.
1ald	8.43	3.74	1.13	47.78	17.41	173.29	-6.0
2lnpa	-	5.17	0.95	53.77	15.01	170.19	-
3ala	7.98	4.41	1.61	48.14	18.36	172.20	-1.2
4ala	8.09	3.86	1.30	52.05	17.41	173.22	-4.0
6ala	6.87	4.16	1.15	48.64	19.39	173.30	1.2

Table 2A.4. Chemical shift assignments of **3NPCHA**.

Residue	NH	Hα	Hβ	Cα	Cβ	CO	Temp. coeff.
1ald	8.03	4.06	1.12	48.73	18.5	171.89	-4.8
2ala	8.10	3.97	1.04	46.88	17.54	171.49	-4.4
3lnpa	-	3.84	1.47	62.44	14.59	169.70	-
4ala	7.77	4.27	1.29	48.96	17.92	172.32	-1.6
5ala	8.01	4.15	1.29	49.65	18.29	173.01	-2.8
6ala	7.71	4.19	1.16	49.11	17.04	172.09	-4.0

Table 2A.5. Chemical shift assignments of **4NPCHA**.

Residue	NH	Hα	Hβ	Cα	Cβ	CO	Temp. coeff.
1ald	8.44	4.26	1.22	48.25	16.56	172.65	-6.0
2ala	7.52	4.23	1.11	49.01	19.19	171.57	-2.0
3ala	8.31	3.78	1.10	47.35	16.56	173.25	-5.2
4lnpa	-	5.10	0.98	54.15	15.08	169.97	-
5ala	7.88	4.34	1.46	48.10	19.23	172.54	-2.0
6ala	8.23	4.04	1.21	50.22	16.56	172.70	-3.6

Table 2A.6. Chemical shift assignments of **5NPCHA**.

Residue	NH	Hα	Hβ	Cα	Cβ	CO	Temp. coeff.
1ald	8.32	4.16	1.19	49.54	16.9	172.7	-7.2
2ala	8.55	4.07	1.26	49.31	18.05	172.03	-6.4
3ala	7.36	4.28	1.13	48.28	19.79	171.76	-2.4
4ala	8.30	3.82	1.19	47.23	16.77	173.25	-7.2
5lnpa	-	5.07	0.98	54.52	15.94	170.60	-
6ala	7.67	4.35	1.31	48.94	19.27	171.68	-0.8

Table 2A.7. Chemical shift assignments of **6NPCHA**.

Residue	NH	Hα	Hβ	Cα	Cβ	CO	Temp. coeff.
1ald	8.68	4.10	1.3	49.71	17.65	171.68	-6.4
2ala	8.10	4.35	1.27	51.43	16.99	172.44	-2.4
3ala	8.04	4.03	1.286	48.59	19.11	171.42	-4.0
4ala	7.93	4.19	1.175	48.28	17.62	170.96	-3.6
5ala	7.41	4.14	0.856	46.88	17.59	171.79	-0.4
6lnpa	-	4.54	0.925	57.61	15.9	172.71	-

Table 2A.8. Chemical shift assignments of **13NPCHA**.

Residue	NH	Hα	Hβ	Cα	Cβ	CO	Temp. coeff.
1dnpa	-	5.05	0.83	53.78	15.93	170.63	-
2ala	7.97	4.26	1.05	47.05	18.53	171.65	-3.6
3lnpa	-	4.01	1.46	61.94	14.81	170.53	-
4ala	7.94	4.21	1.37	49.30	18.13	171.79	-3.2
5ala	7.86	4.16	1.26	48.32	19.09	172.18	-2.0
6ala	7.93	3.83	1.12	47.35	17.13	173.01	-5.0

Table 2A.9. Chemical shift assignments of **14NPCHA**.

Residue	NH	Hα	Hβ	Cα	Cβ	CO	Temp. coeff.
1dnpa	-	4.73	0.88	54.90	16.15	173.31	-
2ala	8.58	4.10	1.23	48.95	17.64	173.13	-6.8
3ala	7.66	4.24	1.11	46.36	17.97	173.18	-1.6
4lnpa	-	4.06	1.22	60.59	15.16	171.47	-
5ala	8.15	3.82	1.25	49.47	17.38	171.85	-5.2
6ala	7.64	4.15	1.11	47.01	18.04	172.80	0.4

Table 2A.10. Chemical shift assignments of **15NPCHA**.

Residue	NH	Hα	Hβ	Cα	Cβ	CO	Temp. coeff.
1dnpa	-	4.79	0.92	55.75	16.01	172.74	-
2ala	8.79	4.14	1.31	49.81	17.62	172.65	-4.8
3ala	7.50	4.17	1.27	46.95	19.23	172.99	0.8
4ala	8.33	3.70	1.10	48.31	16.06	171.39	-3.6
5lnpa	-	3.25	1.35	63.53	14.35	169.27	-
6ala	7.92	4.33	1.04	47.15	16.78	171.89	-0.4

Table 2A.11. Chemical shift assignments of **24NPCHA**.

Residue	NH	Hα	Hβ	Cα	Cβ	CO	Temp. coeff.
1ald	8.57	3.74	1.16	47.46	16.18	172.05	-8.0
2lnpa	-	5.22	0.87	53.24	15.16	169.84	-
3ala	7.80	4.29	1.27	46.99	18.37	172.35	-2.8
4lnpa	-	4.05	1.25	60.93	15.93	171.55	-
5ala	8.07	4.12	1.37	50.28	17.75	172.31	-4.0
6ala	7.40	4.34	1.16	48.76	19.49	173.46	0.4

Table 2A.12. Chemical shift assignments of **25NPCHA**.

Residue	NH	Hα	Hβ	Cα	Cβ	CO	Temp. coeff.
1ald	8.35	3.90	1.18	47.23	16.91	171.23	-4.4
2lnpa	-	5.20	0.94	53.87	14.96	169.12	-
3ala	7.76	4.08	1.41	48.01	19.03	172.22	-1.6
4ala	8.16	3.87	1.14	47.19	18.26	170.03	-3.5
5lnpa	-	3.77	1.55	45.55	15.74	173.11	-
6ala	7.96	4.32	1.12	49.05	18.25	171.60	0

Table 2A.13. Chemical shift assignments of **26NPCHA**.

Residue	NH	Hα	Hβ	Cα	Cβ	CO	Temp. coeff.
1ald	7.6	4.20	1.09	47.28	16.46	172.50	-1.8
2lnpa	-	4.58	1.11	57.65	15.56	171.04	-
3ala	8.49	4.01	1.35	49.35	16.21	171.14	-6.6
4ala	7.64	4.14	1.25	48.60	18.81	172.31	-1.2
5ala	7.83	3.98	1.08	47.99	16.46	172.50	-6.6
6lnpa	-	3.88	1.46	62.57	14.99	168.40	-

Table 2A.14. Chemical shift assignments of **35NPCHA**.

Residue	NH	Hα	Hβ	Cα	Cβ	CO	Temp. coeff.
1ald	7.58	4.11	1.15	49.22	15.9	171.12	-1.1
2ala	8.10	4.07	1.10	47.57	16.74	170.21	-7.4
3lnpa	-	3.94	1.36	61.50	14.42	172.10	-
4ala	7.48	4.31	1.09	46.29	18.27	171.49	0
5lnpa	-	4.33	1.16	59.21	18.58	169.22	-
6ala	8.35	4.05	1.32	49.67	16.15	172.51	-4.07

Table 2A.15. Chemical shift assignments of **36NPCHA**.

Residue	NH	Hα	Hβ	Cα	Cβ	CO	Temp. coeff.
1ald	8.60	4.01	1.16	49.08	17.4	171.87	-6.0
2ala	7.89	4.11	1.03	47.24	18.01	171.47	-1.6
3lnpa	-	3.91	1.54	62.73	14.57	171.27	-
4ala	8.12	4.15	1.28	49.63	16.90	173.52	-5.2
5ala	7.84	4.29	1.00	46.33	16.97	173.85	-0.8
6lnpa	-	4.56	0.92	57.47	15.79	173.45	-

Table 2A.16. Chemical shift assignments of **46NPCHA**.

Residue	NH	Hα	Hβ	Cα	Cβ	CO	Temp. coeff.
1ald	7.97	4.25	1.22	49.69	18.67	172.89	-5.2
2ala	7.79	4.27	1.22	49.03	18.73	172.73	-3.2
3ala	8.03	4.14	1.02	47.15	17.59	173.32	-6.0
4lnpa	-	4.90	1.05	55.20	15.43	174.43	-
5ala	8.06	4.09	0.94	47.56	17.11	174.22	-6.0
6lnpa	-	4.83	0.97	56.16	15.91	172.36	-

Table 2A.17. NMR chemical shift temperature coefficients (in ppb/K) of amide protons in **NPCHA** peptides (given in the order of peptide names).

cyclic-hexaalanine (CHA) peptides							
S. No.	Peptide	Amides					
		NH1	NH2	NH3	NH4	NH5	NH6
1	**1NPCHA**	-	-4.4	-2	-4	-3.6	-1.6
2	**2NPCHA**	-6	-	-1.2	-4	-4.4	1.2
3	**3NPCHA**	-4.8	-4.4	-	-1.6	-2.8	-4.0
4	**4NPCHA**	-6	-2	-5.2	-	-2	-3.6
5	**5NPCHA**	-7.2	-6.4	-2.4	-7.2	-	-0.8
6	**6NPCHA**	-6.4	-2.4	-4	-3.6	-0.4	-
7	**13NPCHA**	-	-3.6	-	-3.2	-2	-5
8	**14NPCHA**	-	-6.8	-1.6	-	-5.2	0.4
9	**15NPCHA**	-	-4.8	0.8	-3.6	-	-0.4
10	**24NPCHA**	-8	-	-2.8	-	-4	0.4
11	**25NPCHA**	-4.4	-	-1.6	-3.5	-	0
12	**26NPCHA**	-1.8	-	-6.6	-1.2	-6.6	-
13	**35NPCHA**	-1.1	-7.4	-	0	-	-4.07
14	**36NPCHA**	-6	-1.6	-	-5.2	-0.8	-
15	**46NPCHA**	-5.2	-3.2	-6	-	-6	-

2A.2. **NMR based conformational study of NPCHA peptide**

The inter-proton distances required for NMR-based structure calculation were derived from the cross-peak integrals of the ROESY experiment using SPARKY software. These integrated volumes of ROESY cross-peaks were converted to the corresponding inter-proton distances by the linear approximation method. These distances were used for the structural calculation by using Schrodinger Maestro macro model 13.1.[65] For the structure calculation, a minimized starting structure was obtained after a step-wise minimization process of an arbitrary structure by giving the inter-proton distance inputs one by one. The method used for energy minimization was SD (steepest descent) and dielectric constant of DMSO i.e., 47. Thus obtained structure was saved and used as the starting template (beginning structure) for 'Molecular Dynamics Simulations' (MD). MD was run on the structure at 300 K for 10 ns with a simulation time step of 1 fs and by shaking all the bonds of the molecule.

Table 2A.18. List of the number of inter-proton distance restraints that were used for structure calculation of **NPCHA** peptides.

S. No.	Peptide	No. of distance constraints
1	1NPCHA	28
2	2NPCHA	22
3	3NPCHA	21
4	4NPCHA	37
5	5NPCHA	28
6	6NPCHA	31
7	13NPCHA	35
8	14NPCHA	25
9	15NPCHA	26
10	24NPCHA	19
11	25NPCHA	20
12	26NPCHA	36
13	35NPCHA	22
14	36NPCHA	28
15	46NPCHA	17

Figure 2A.3. (a) - (e) Five different conformational templates observed for NPCHA peptides. The first three templates, (a) - (c), are comprised of only beta turns with trans peptide bonds whereas the last two types (d) and (e) consists of one beta VI turn with a *cis* peptide bond. All the residues are numbered starting with D-residue as position 1. Wherever amide group is given as NR, R can be either H or phenyl group depending on the peptide sequence. The possibility of hydrogen bonding for the NHs oriented into the macrocycle are indicated in dashed lines. (f) Table showing a summary of the types of conformations observed in NPCHA peptides along with the type of turns in each conformation and the amide NHs that are solvent shielded as indicated by the NMR chemical shift temperature coefficients. The last column shows the list of peptides (named after the position of *N*-phenyl group) exhibiting the conformations corresponding to each NPCHA template type.

The ^{1}H NMR spectra of all the compounds have shown only one set of chemical shifts implying, in general, either a single predominant conformation or fast exchanging conformations on the NMR chemical shift time scales (see table **2A.2-16**). 13 out of the 15 NPCHA peptides have exhibited distinct antiparallel beta sheet conformations with characteristic beta turns (Figures **2A.3-10**, Table **2A.19-23**). The said conformations are supported by representative NOE correlations and amide chemical shift temperature coefficients that indicated solvent shielding/hydrogen bonding or exposure to the solvent **(**Figure **2A.4**, Table **2A.17**, **19**). Based on the position of the D-alanine in the conformations, the amide NHs that exhibited hydrogen bonding nature and their inward orientation into the macrocycle, and based on the position of beta turn (Table **2A.20**), the conformations observed in NPCHA peptides are broadly classified into five different templates (Figure **2A.3**). In general, NPCHA peptides exhibited the antiparallel beta sheet structures with two beta turns at either end of the 18-atom macrocycle.

.
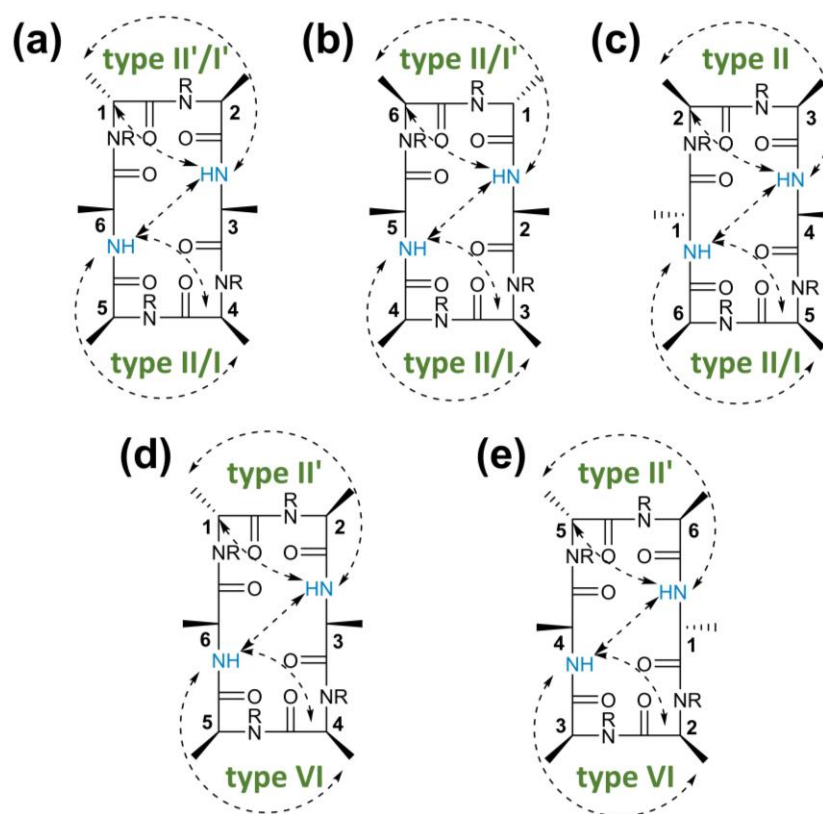
Figure 2A.4. The pattern of characteristic distant ROESY correlations (shown in dashed arrows) observed for each template structure of NPCHA peptides.

Table 2A.19. NMR chemical shift temperature coefficients (in ppb/K) of amide protons in **NPCHA** peptides (given in the order of Template type).

	cyclic-hexaalanine (CHA) peptides							
S. No.	Peptide	Template			Amides			
			NH1	NH2	NH3	NH4	NH5	NH6
1	**1NPCHA**	Template 1	-	-4.4	-2	-4	-3.6	-1.6
2	**2NPCHA**	Template 1	-6	-	-1.2	-4	-4.4	1.2
3	**5NPCHA**	Template 1	-7.2	-6.4	-2.4	-7.2	-	-0.8
4	**14NPCHA**	Template 1	-	-6.8	-1.6	-	-5.2	0.4
5	**24NPCHA**	Template 1	-8	-	-2.8	-	-4	0.4
6	**25NPCHA**	Template 1	-4.4	-	-1.6	-3.5	-	0
7	**3NPCHA**	Template 2	-4.8	-4.4	-	-1.6	-2.8	-4
8	**4NPCHA**	Template 2	-6	-2	-5.2	-	-2	-3.6
9	**6NPCHA**	Template 2	-6.4	-2.4	-4	-3.6	-0.4	-
10	**13NPCHA**	Template 2	-	-3.6	-	-3.2	-2	-5
11	**36NPCHA**	Template 2	-6	-1.6	-	-5.2	-0.8	-
12	**26NPCHA**	Template 3	-1.8	-	-6.6	-1.2	-6.6	-
13	**15NPCHA**	Template 4	-	-4.8	0.8	-3.6	-	-0.4
14	**35NPCHA**	Template 5	-1.1	-7.4	-	0	-	-4.07

Table 2A.20. Template type, turn position, and type of turns observed in NPCHA peptides (given in the order of peptide names).

Peptide Conformation	Template type	Turn position	First turn					Second turn				
			I	I'	II	II'	VI	I	I'	II	II'	VI
1NPCHA	Template 1	1,2 and 4,5				■				■		
2NPCHA-1	Template 1	1,2 and 4,5		■				■				
2NPCHA-2	Template 1	1,2 and 4,5				■		■				
3NPCHA	Template 2	6,1 and 3,4			■			■				
4NPCHA-1	Template 2	6,1 and 3,4			■					■		
4NPCHA-2	Template 2	6,1 and 3,4			■			■				
5NPCHA-1	Template 1	1,2 and 4,5				■				■		
5NPCHA-2	Template 1	1,2 and 4,5				■				■		
6NPCHA	Template 2	6,1 and 3,4			■					■		
13NPCHA	Template 2	6,1 and 3,4			■							
14NPCHA	Template 1	1,2 and 4,5				■						
15NPCHA	Template 4	1,2 and 4,5				■						■
24NPCHA-1	Template 1	1,2 and 4,5		■						■		
24NPCHA-2	Template 1	1,2 and 4,5				■				■		
25NPCHA-1	Template 1	1,2 and 4,5				■				■		
25NPCHA-2	Template 1	1,2 and 4,5				■		■				
26NPCHA-1	Template 3	2,3 and 5,6			■			■				
26NPCHA-2	Template 3	2,3 and 5,6			■			■				
35NPCHA	Template 5	5,6 and 2,3					■					■
36NPCHA	Template 2	6,1 and 3,4		■				■				

Table 2A.21. Template type, turn position, and type of turns observed in NPCHA peptides (given in the order of NPCHA template type).

Peptide Conformation	Template type	Turn position	First turn					Second turn				
			I	I′	II	II′	VI	I	I′	II	II′	VI
1NPCHA	Template 1	1,2 and 4,5				X					X	
2NPCHA-1	Template 1	1,2 and 4,5		X				X				
2NPCHA-2	Template 1	1,2 and 4,5				X		X				
5NPCHA-1	Template 1	1,2 and 4,5				X				X		
5NPCHA-2	Template 1	1,2 and 4,5				X		X				
14NPCHA	Template 1	1,2 and 4,5				X				X		
24NPCHA-1	Template 1	1,2 and 4,5		X						X		
24NPCHA-2	Template 1	1,2 and 4,5				X				X		
25NPCHA-1	Template 1	1,2 and 4,5				X				X		
25NPCHA-2	Template 1	1,2 and 4,5				X		X				
3NPCHA	Template 2	6,1 and 3,4			X			X				
4NPCHA-1	Template 2	6,1 and 3,4			X					X		
4NPCHA-2	Template 2	6,1 and 3,4			X			X				
6NPCHA	Template 2	6,1 and 3,4			X					X		
13NPCHA	Template 2	6,1 and 3,4			X							
36NPCHA	Template 2	6,1 and 3,4		X				X				
26NPCHA-1	Template 3	2,3 and 5,6			X							
26NPCHA-2	Template 3	2,3 and 5,6			X			X				
15NPCHA	Template 4	1,2 and 4,5				X						X
35NPCHA	Template 5	5,6 and 2,3				X						X

Table 2A.22. Beta turn dihedral angles for the conformations observed in NPCHA peptides (given in the order of peptide names).

Peptide Conformation	Template type	Turn 1					Turn 2				
		φi+1	ψi+1	φi+2	ψi+2	Type	φi+1	ψi+1	φi+2	ψi+2	Type
1NPCHA	Template 1	40.5	-98.7	-50.8	-15.8	II'	32.9	93.7	53.9	24.8	II
2NPCHA-1	Template 1	57.7	46.2	62.6	31.7	I'	-56.5	-22.0	-95.1	-26.0	I
2NPCHA-2	Template 1	50.1	-114.5	-99.3	47.2	II'	-60.5	-22.3	-79.7	-26.0	I
3NPCHA	Template 2	-58	81.7	139.3	-25.1	II	-49.5	-21.3	-125.2	66.2	I
4NPCHA-1	Template 2	-44.6	124.1	108.4	-55.2	II	-40.1	148.2	66.8	19.5	II
4NPCHA-2	Template 2	-24.2	129.3	96.6	-59.3	II	-63.4	-46.1	-92.9	25.2	I
5NPCHA-1	Template 1	84.3	-140.4	-97.1	37.0	II'	-23.7	136.7	87.0	-4.4	II
5NPCHA-2	Template 1	84.6	-139.6	-98.1	41.0	II'	-27.2	-56.1	-70.0	19.8	I
6NPCHA	Template 2	-26.5	115.6	67.3	23.8	II	-42.3	123.7	79.3	-24.3	II
13NPCHA	Template 2	-58.6	147	81.8	-31.7	II	-42.8	148.9	54	21.8	II
14NPCHA	Template 1	72.7	-152.2	-87.9	21.8	II'	-44.1	147.2	80.8	-16.1	II
15NPCHA	Template 4	37.2	-111.8	-118.5	15.3	II'	-98	129.5	-107	29.8	VI
24NPCHA-1	Template 1	66.6	40.5	65.3	11.7	I'	-44.4	130.5	73.9	3.5	II
24NPCHA-2	Template 1	47.3	-116.4	-85.7	34.4	II'	-44.5	136.6	44.5	30.6	II
25NPCHA-1	Template 1	70.7	-145	-21.6	-36.9	II'	-66.4	111.1	87.7	-63	II
25NPCHA-2	Template 1	81	-142.9	-18.1	-43.1	II'	-55.6	-45.8	-59.9	-65.6	I
26NPCHA-1	Template 3	19.9	95.9	79.8	-4.4	II	-37.2	153	83.7	-44.2	II
26NPCHA-2	Template 3	18.6	96.3	76.3	-2.6	II	-73.1	-45.4	-62.6	-15.5	I
35NPCHA	Template 5	51.8	-137.3	-85	57.3	II'	-77	125.8	-129	54.8	VI
36NPCHA	Template 2	44.9	73	108.4	-44.3	I'	-39.8	-36.9	-56.1	-70.6	I

Table 2A.23. Beta turn dihedral angles for the conformations observed in NPCHA peptides (given in the order of NPCHA template type).

Peptide	Template type	Turn 1					Turn 2				
		φi+1	ψi+1	φi+2	ψi+2	Type	φi+1	ψi+1	φi+2	ψi+2	Type
1NPCHA	Template 1	40.5	-98.7	-50.8	-15.8	II'	32.9	93.7	53.9	24.8	II
2NPCHA-1	Template 1	57.7	46.2	62.6	31.7	I'	-56.5	-22.0	-95.1	-26.0	I
2NPCHA-2	Template 1	50.1	-114.5	-99.3	47.2	II'	-60.5	-22.3	-79.7	-26.0	I
5NPCHA-1	Template 1	84.3	-140.4	-97.1	37.0	II'	-23.7	136.7	87.0	-4.4	II
5NPCHA-2	Template 1	84.6	-139.6	-98.1	41.0	II'	-27.2	-56.1	-70.0	19.8	I
14NPCHA	Template 1	72.7	-152.2	-87.9	21.8	II'	-44.1	147.2	80.8	-16.1	II
24NPCHA-1	Template 1	66.6	40.5	65.3	11.7	I'	-44.4	130.5	73.9	3.5	II
24NPCHA-2	Template 1	47.3	-116.4	-85.7	34.4	II'	-44.5	136.6	44.5	30.6	II
25NPCHA-1	Template 1	70.7	-145	-21.6	-36.9	II'	-66.4	111.1	87.7	-63	II
25NPCHA-2	Template 1	81	-142.9	-18.1	-43.1	II'	-55.6	-45.8	-59.9	-65.6	I
3NPCHA	Template 2	-58	81.7	139.3	-25.1	II	-49.5	-21.3	-125.2	66.2	I
4NPCHA-1	Template 2	-44.6	124.1	108.4	-55.2	II	-40.1	148.2	66.8	19.5	II
4NPCHA-2	Template 2	-24.2	129.3	96.6	-59.3	II	-63.4	-46.1	-92.9	25.2	I
6NPCHA	Template 2	-26.5	115.6	67.3	23.8	II	-42.3	123.7	79.3	-24.3	II
13NPCHA	Template 2	-58.6	147	81.8	-31.7	II	-42.8	148.9	54	21.8	II
36NPCHA	Template 2	44.9	73	108.4	-44.3	I'	-39.8	-36.9	-56.1	-70.6	I
26NPCHA-1	Template 3	19.9	95.9	79.8	-4.4	II	-37.2	153	83.7	-44.2	II
26NPCHA-2	Template 3	18.6	96.3	76.3	-2.6	II	-73.1	-45.4	-62.6	-15.5	I
15NPCHA	Template 4	37.2	-111.8	-118.5	15.3	II'	-98	129.5	-107	29.8	VI
35NPCHA	Template 5	51.8	-137.3	-85	57.3	II'	-77	125.8	-129	54.8	VI

NPCHA Template 1

The NPCHA Template 1 (Figures **2A.3-2A.5**) conformation is made up of two beta turns- the first beta turn is of type II' or I' positioned between residues 1 and 2 and the second beta turn between residues 4 and 5 is of type II or I (Tables **2A.20-2A.23**). The D-configured residue (D-ala or *N*-Ph-D-ala) is occupying the i+1 position of the first beta turn. The NHs from residues 3 and 6 have internal orientation into the macrocycle with a possibility of hydrogen bonding to the C=O (carbonyl) of 6 and 3 residues, respectively (Table **2A.19**). This is supported by amide NMR chemical shift temperature co-efficients > −2.4 ppb/K for the NHs from residues 3 and 6. Out of the six NPCHA peptides, two peptides, 1NPCHA and 14NPCHA (Figure **2A.5**), have exhibited a single conformation with type II' first turn and type II second turn in the structure calculation. The peptide 2NPCHA, has a conformation in which the second β-turn is of type I and the first β-turn between residues 1 and 2 is either type II' or I', which are a result of 180° peptide bond flip (Figure **2A.5**, **2A.11a**). The distinct observation of type II' or I' turns for the first turn in this peptide could be because of the high energy barrier of rotation for the peptide bond involving the *N*-phenyl amide bond between residues 1 and 2. In support of this peptide bond flip, we have also observed distinct NOEs from the phenyl ring protons to either face of the peptide plane (Figure **2A.11a**). Such peptide bond flip for an unmodified amide bond would be energetically more favorable and thus lead to averaged conformations and NMR data.[44, 45, 66, 67] On similar lines, the conformation for 5NPCHA and 25NPCHA showed a type II' first turn while the second turn between 4 and 5 residues is either type II or I (Figure **2A.5**, **2A.11b**). For 24NPCHA conformation, the first turn being either of the type II' or I' and the second turn is observed to be type II. For the peptides showing the NPCHA Template 1 fold, there are two *N*-methyl CHA peptides whose NMR conformations were discussed by Beck *et al*.[45] 5*N*MeCHA, which is an *N*-methyl analogue of 5NPCHA, had a single conformation with a first beta type II' turn between residues 1 and 2, and a second beta type VI turn between 4 and 5 residues with a *cis* peptide bond (Figure **2A.6** and **2A.12**). In contrast, for 5NPCHA we did not find any signs of *cis* peptide bond and instead observed a population of type II or I turn between 4 and 5 residues. For 1*N*MeCHA, Beck *et al*. had speculated two fast exchanging conformations with less distinct NMR temperature coefficients for the amide NHs, while the analogous 1NPCHA has a dominant NPCHA Template 1 conformation (Figure **2A.7**).
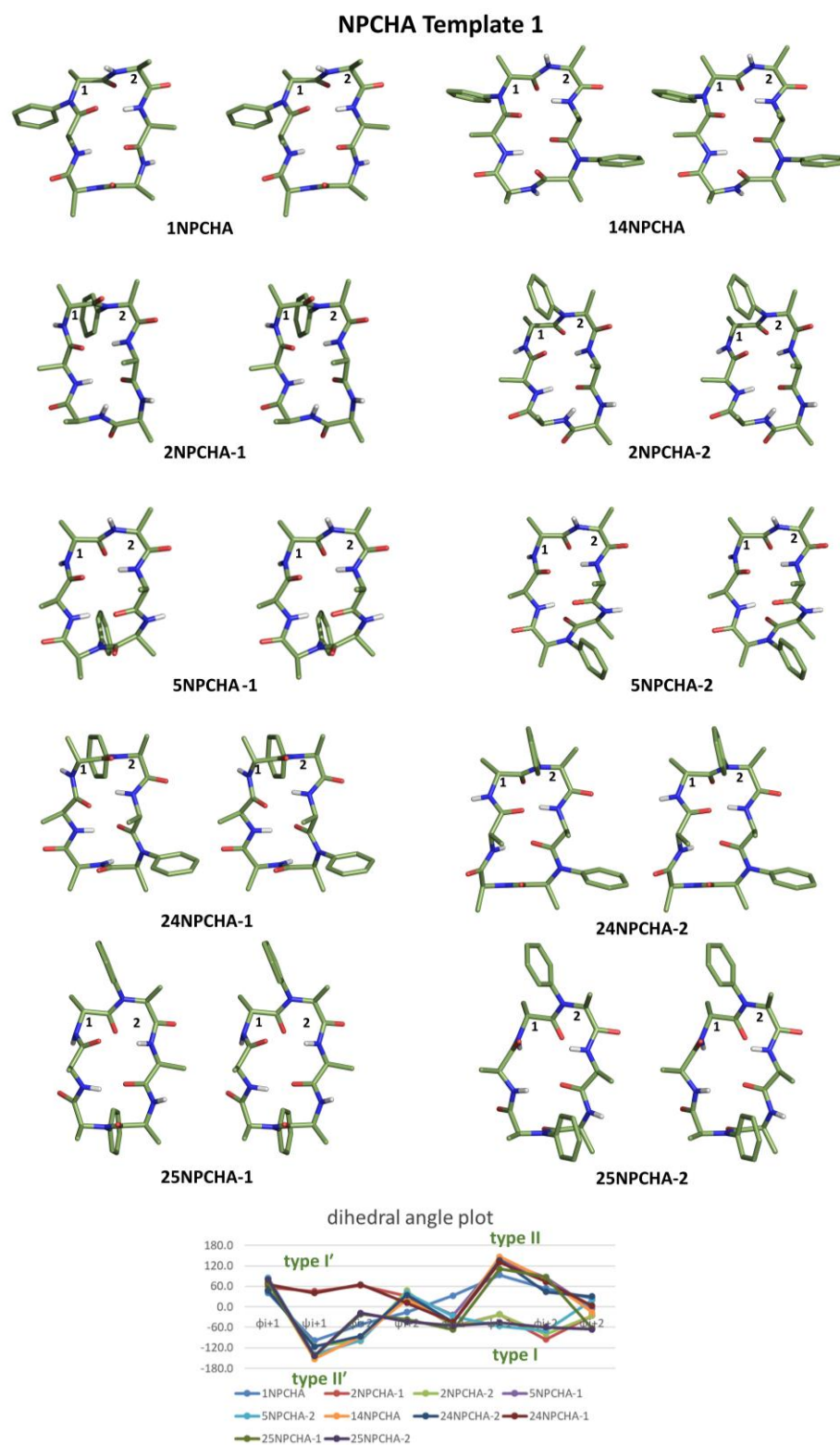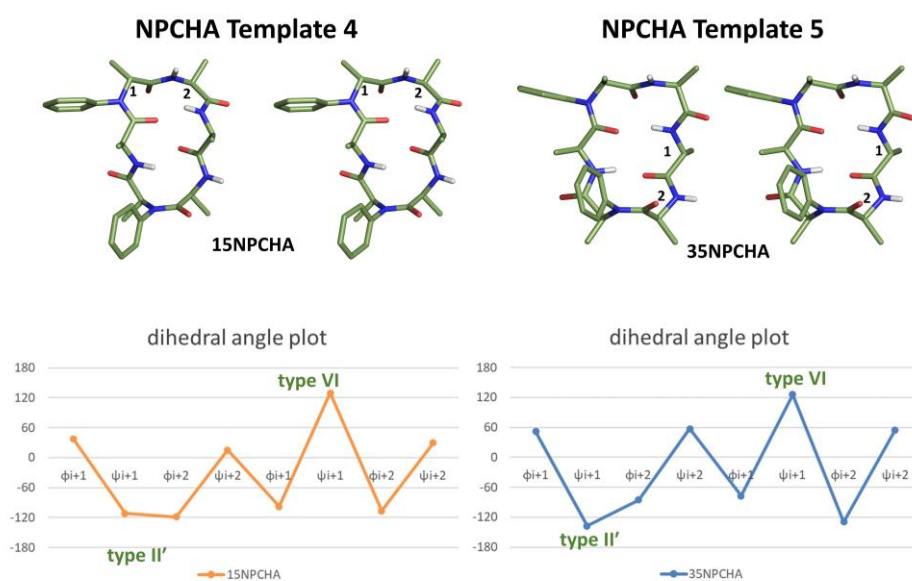
Figure 2A.5. Stereo view (top view) of the NMR-derived conformations and dihedral angle comparison of all peptides from NPCHA template 1.
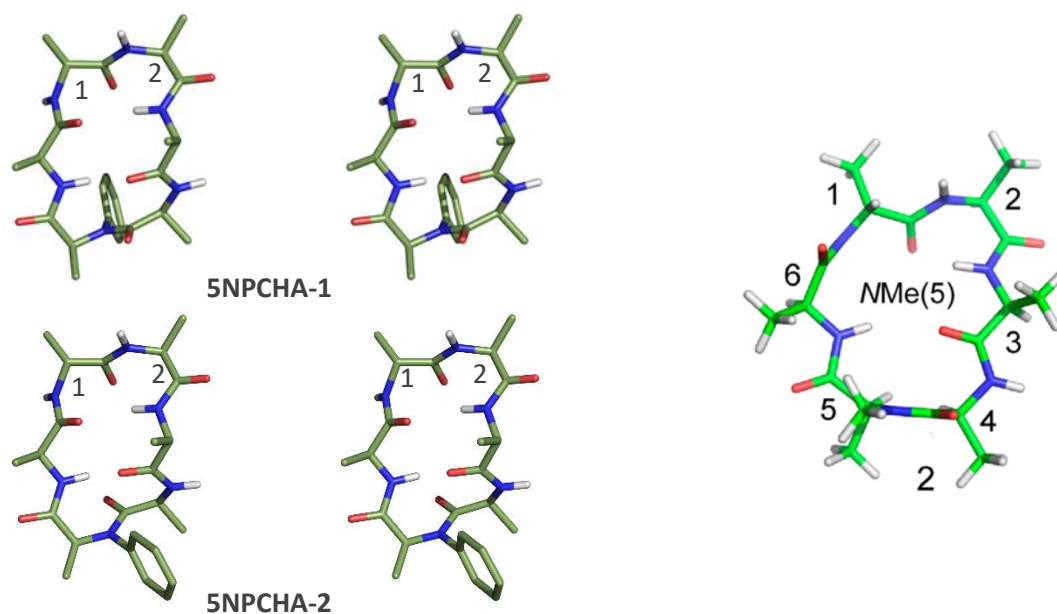
**Figure 2A.6**. Comparison of 5NPCHA and 5*N*MeCHA peptides: For 5NPCHA, two fast exchanging conformations (based on the orientation of 5-Phenyl group) were observed whereas 5*N*Me-CHA has a different conformation with a *cis* peptide bond (beta VI turn) between 4 and 5 residues.
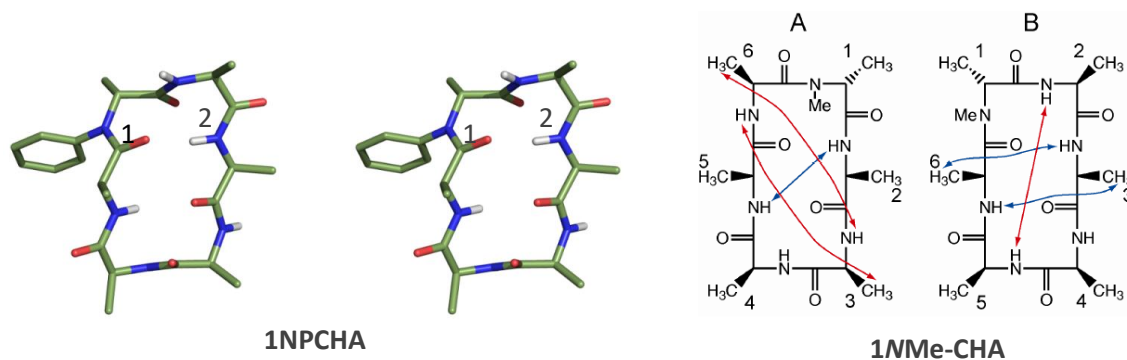
Figure 2A.7. Comparison of 1NPCHA, with 1*N*Me-CHA: For 1NPCHA only single conformation observed while for its *N*-Methylated analogue two fast exchanging conformations were reported.

NPCHA Template 2

The NPCHA Template 2 (Figures **2A.3**, **2A.4**, **2A.8**) structure is comprised of the first beta turn between 6 and 1 residues, which is of type II or I' and the second beta turn of type II/I around 3 and 4 residues, with the D-amino acid occupying the i+2 position of the first turn (Tables **2A.20-2A.23**). The amide NHs of the residues at 2 and 5 positions of the NPCHA Template 2 structure are involved in hydrogen bonding with the C=O of 5 and 2 residues, respectively (Table **2A.19**). Among 3NPCHA, 4NPCHA, 6NPCHA, 13NPCHA and 36NPCHA that have exhibited the NPCHA Template 2

conformation, 6NPCHA and 36NPCHA have predominantly shown one particular beta turn type for each end of the cyclic antiparallel beta sheet conformation (Figure **2A.8a**). 4NPCHA populated peptide bond flip conformations with beta type II first turn and the second turn flipping between type II and type I (Figure **2A.8a**, **2A.11c**). For 3NPCHA and 13NPCHA, the ROE data and temperature coefficients could be more satisfactorily explained when NPCHA Template 2 conformation and NPCHA Template 3 conformation (Figure **2A.8b**) are considered in a fast exchange on the NMR chemical shift time scales.
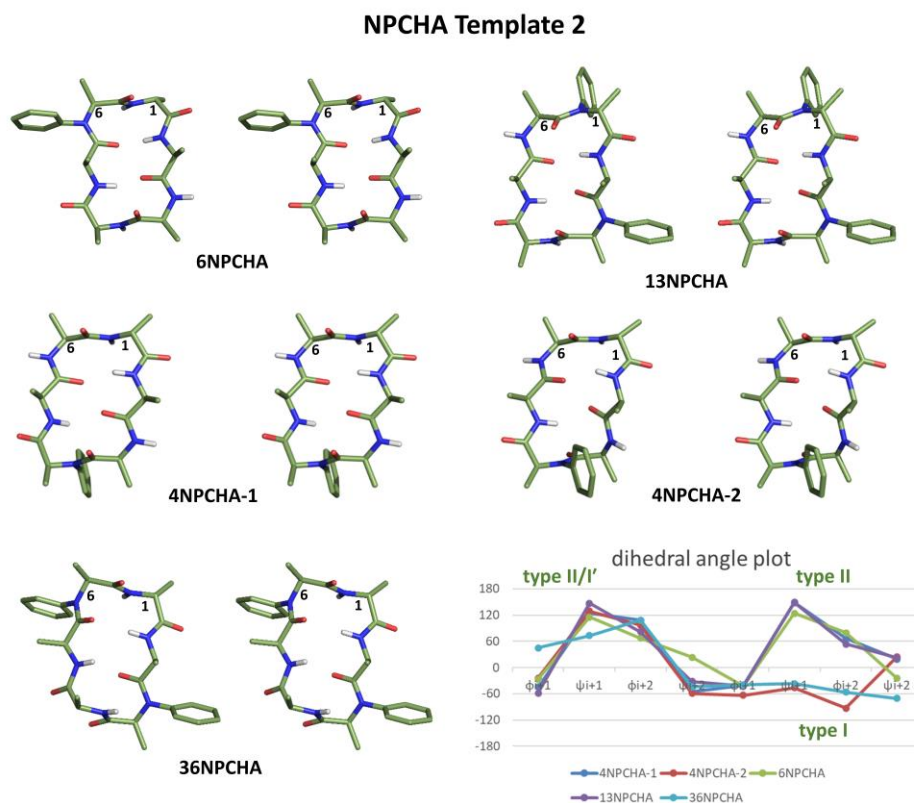
Figure 2A.8a. Stereo view (top view) of the NMR-derived conformations and dihedral angle comparison of all peptides from NPCHA template 2.
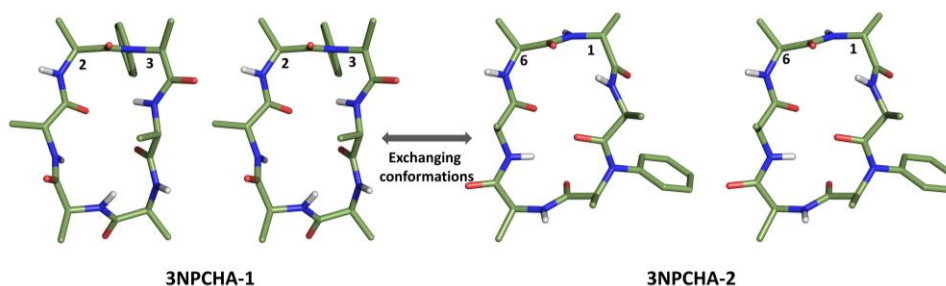
Figure 2A.8b. Stereo view (top view) of the NMR-derived exchanging conformations of 3NPCHA.

NPCHA Template 3

Only one peptide, 26NPCHA has displayed the NPCHA Template 3 (Figures **2A.3**, **2A.4**, **2A.9**) conformation with type II first turn between 2 and 3 amino acids and a type II/I beta turn around 5 and 6 positions with *N*-phenyl amide bond flipping (Figure **2A.11d**) (Tables **2A.20-2A.23**). The D-amino acid in this conformation is simultaneously a part of the first turn as i^{th} residue and as i+3 residue for the second turn. The amide protons of 4 and 1 amino acids are involved in hydrogen bonding with the C=O groups of each other across the macrocycle (Table **2A.19**).
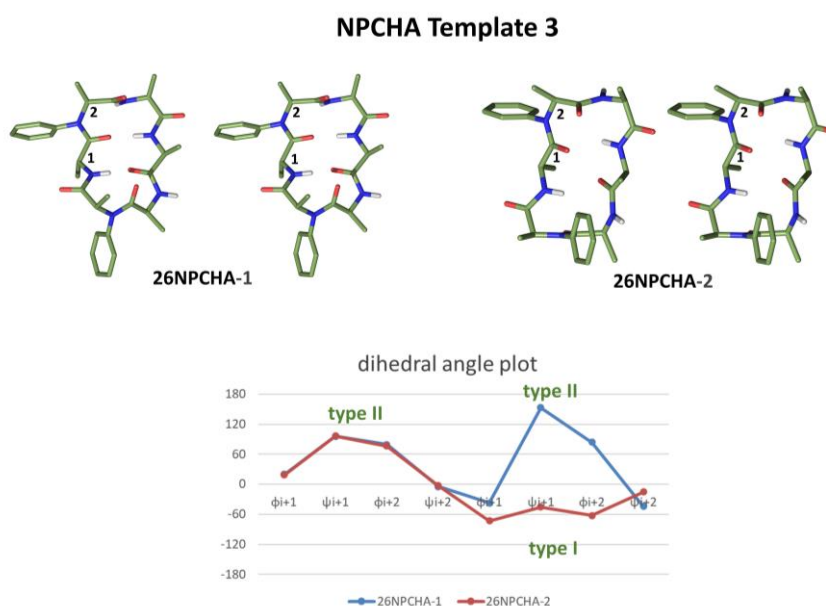
Figure 2A.9. Stereo view (top view) of the NMR-derived conformations and dihedral angle comparison of all peptides from NPCHA template 3.

NPCHA Templates 4 and 5

The last two conformations observed for NPCHA peptides, the NPCHA Template 4 and NPCHA Template 5 (Figures **2A.3**, **2A.4**, **2A.10**), are represented by one peptide each, specifically 15NPCHA and 35NPCHA, respectively. These two templates are distinct from the other NPCHA templates in having a beta VI turn with a *cis* peptide bond as one of the turns. Both the templates have a beta II' and beta VI turn however the position of these turns differ (Tables **2A.20-2A.23**). While the beta II' turn for 15NPCHA is populated around 1 and 2 residues, that for 35NPCHA is between 5 and 6 residues. In accordance, the beta VI turns are centred around 4 and 5 residues for 15NPCHA and 2 and 3 amino acids for 35NPCHA. Similarly, the hydrogen bonding pattern for 15NPCHA is between the amide NHs and C=O groups of the 3 and 6 residues, while it is between those of 1 and 4 amino acids in 35NPCHA

(Table **2A.19**). To draw parallels, for 15NPCHA, the analogous 15*N*MeCHA peptide (Figures **2A.10**, **2A.12**) had the exact same conformation as NPCHA Template 4, which is interesting.[45] On the other hand, the 35NPCHA has starkly differed from its analogous 35*N*MeCHA in populating a single conformation. In contrast, the methyl analogue of 35NPCHA, the 35*N*MeCHA had exhibited two conformations (**2A.12**),[45] one conformation (56 %) with two *cis* peptide bonds between 2 and 3, and 4 and 5 residues, and the other conformation (44 %) with only one *cis* peptide bond between 2 and 3 residues and beta II' turn between 5 and 6 residues. This could be attributed to the role of *N*-aryl group substitution as a bulky restraint on the peptide bond flipping, which leads to distinct conformations.[44,45,66,67]

Figure 2A.10. Stereo view (top view) of the NMR-derived conformations and dihedral angle comparison of all peptides from NPCHA templates 4 and 5.

2A.3. **Key NOE correlations in support of *N*-phenyl amide bond flipping in NPCHA peptides**
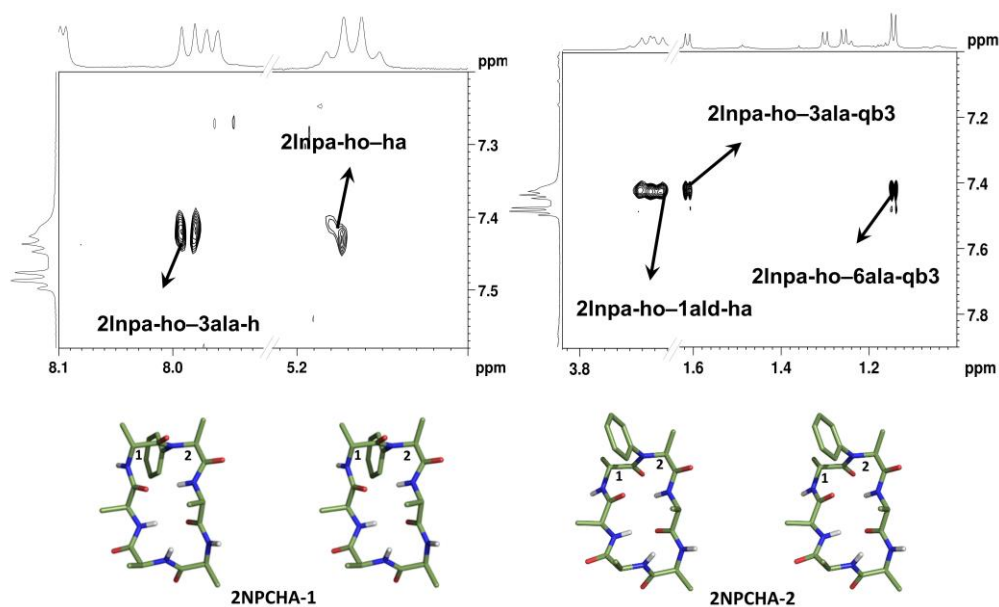
Figure 2A.11a. Key NOE correlations for the orientation of the *N*-phenyl group on either side of the peptide macrocycle face in 2NPCHA. The NOEs 2lnpa-ho to 2lnpa-ha and 2lnpa-ho to 3ala-h support the orientation of the *N*-phenyl group behind the plane of this paper; the NOEs 2lnpa-ho to 3ala-qb3, 2lnpa-ho to 1ald-ha and 2lnpa-ho to 6ala-qb3 support the orientation of the *N*-phenyl group above the plane of the paper. (lnpa=*N*-phenyl-L-ala, ho=ortho protons of the *N*-phenyl ring, ald=D-Alanine, ha=Hα, h=NH, qb3=pseudo position of β protons).
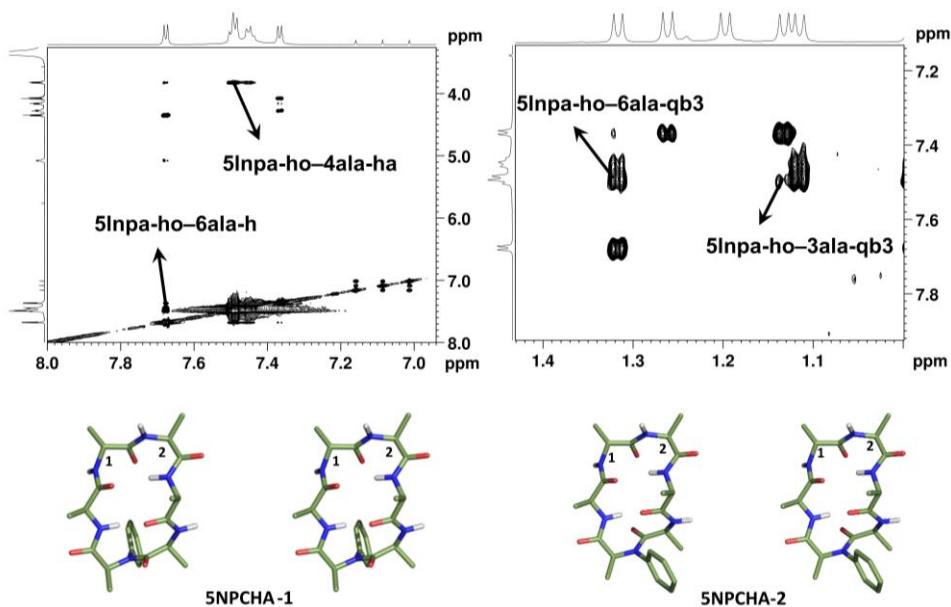
Figure 2A.11b. Key NOE correlations for the orientation of the *N*-phenyl group on either side of the peptide macrocycle face in 5NPCHA. NOE correlation of 5lnpa-ho to 4ala-ha and 5lnpa-ho to 6ala-h support the orientation of the *N*-phenyl group behind the plane of this paper; the NOEs 5lnpa-ho to 6ala-qb3 and 5lnpa-ho to 3ala-qb3 support the orientation of the *N*-phenyl group above the plane of the paper. (lnpa=*N*-phenyl-L-ala, ho=ortho protons of the *N*-phenyl ring, ald=D-Alanine, ha=Hα, h=NH, qb3=pseudo position of β protons).
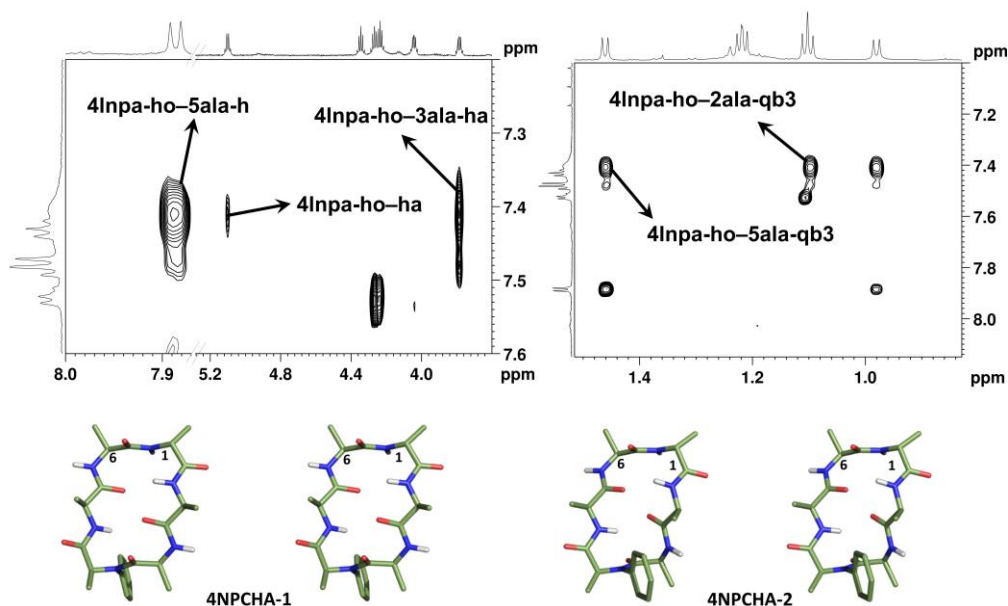
Figure 2A.11c. Key NOE correlations for the orientation of the *N*-phenyl group on either side of the peptide macrocycle face in 4NPCHA. NOE correlation of 4lnpa-ho to 5ala-h, 4lnpa-ho to 3ala-ha and 4lnpa-ho to 4lnpa-ha support the orientation of the *N*-phenyl group behind the plane of this paper; the NOEs 4lnpa-ho to 2ala-qb3, 4lnpa-ho to 5ala-qb3 and 4lnpa-ho to 4lnpa-qb3 support the orientation of the *N*-phenyl group above the plane of the paper. (lnpa=*N*-phenyl-L-ala, ho=ortho protons of the *N*-phenyl ring, ald=D-Alanine, ha=Hα, h=NH, qb3=pseudo position of β protons).
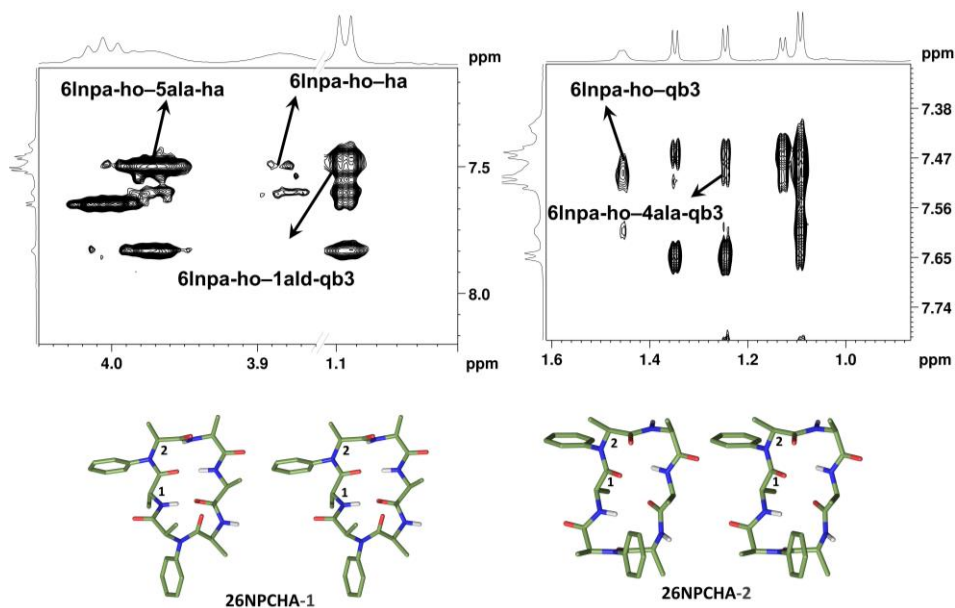
Figure 2A.11d. Key NOE correlations for the orientation of the *N*-phenyl group on either side of the peptide macrocycle face in 26NPCHA. NOE correlation of 6lnpa-ho to 5ala-ha, 6lnpa-ho to 6lnpa-ha and 6lnpa-ho to 1ald-qb3 support the orientation of the *N*-phenyl group of 6lnpa residue behind the plane of this paper; the NOEs 6lnpa-ho to 4ala-qb3 and 6lnpa-ho to 6lnpa-qb3 support the orientation of the *N*-phenyl group 6lnpa residue above the plane of the paper. (lnpa=*N*-phenyl-L-ala, ho=ortho protons of the *N*-phenyl ring, ald=D-Alanine, ha=Hα, h=NH, qb3=pseudo position of β protons).

71
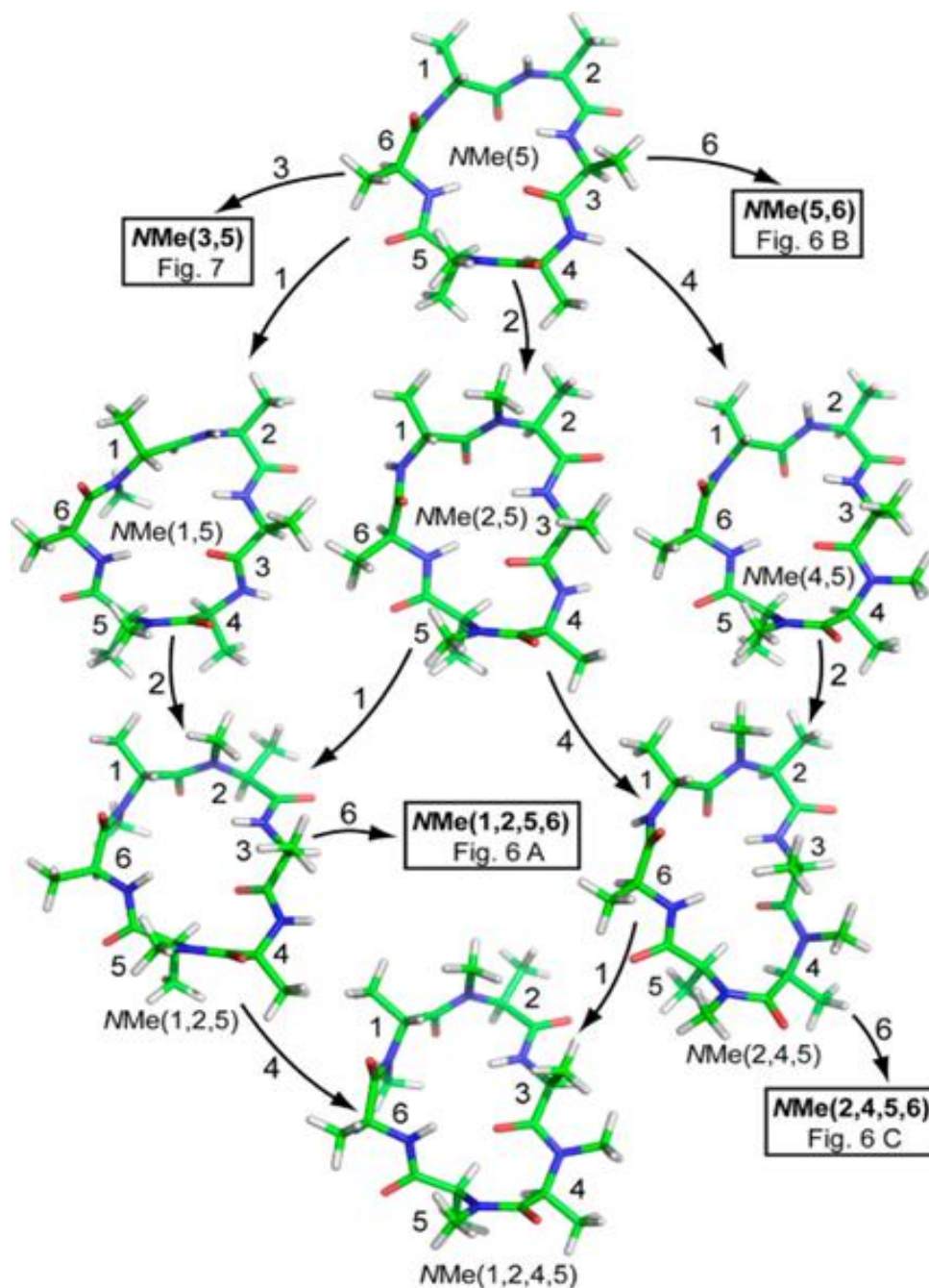
Figure 2A.12. Structures of peptides *N***Me(5)**, *N***Me(1,5)**, *N***Me(2,5)**, *N***Me(4,5)**, *N***Me(1,2,5)**, *N***Me(2,4,5)**, and *N***Me(1,2,4,5)** are very similar. Starting from *N***Me(5)** as the parent peptide that possesses the characteristic *cis* peptide bond between residues Ala4 and Ala5, the other six peptides can be considered as higher *N*-methylated analogues. The numbers given on the arrows indicate the sequence position on which new *N*-methyl groups are attached. Chemical shifts and their temperature dependence further support the high similarity of the structures shown here (reproduced with permission from *J. Am. Chem. Soc.* **2012**, *134*, 12125−12133).

In the *N*-methylation studies of the cyclic-hexaalanine (CHA) scaffold, it was observed that the *N*Me at position 5 was playing a crucial role in conformational control (Figure **2A.12**).[45] When *N*-methylation was present at position 5, the presence or absence of *N*Me at positions 1, 2, 4 and to a certain extent at 3 and 6, had retained the parent conformation observed for 5*N*MeCHA (which is similar to the NPCHA Template 4 conformation). However, in the current studies, although the size of the library is limited, we did not observe any such control over the conformation by the *N*-phenyl group at position 5 or any other position. Especially, the four peptides 5NPCHA, 15NPCHA, 25NPCHA and 35NPCHA have revealed conformations which are entirely different from each other. While the analogous 5*N*MeCHA, 15*N*MeCHA, 25*N*MeCHA and partially the 35*N*MeCHA had identical conformational features (Figure **2A.12**).

Section-B

Design and synthesis of *N*-aryl cyclic-pentaalanine peptides and their conformational studies by NMR
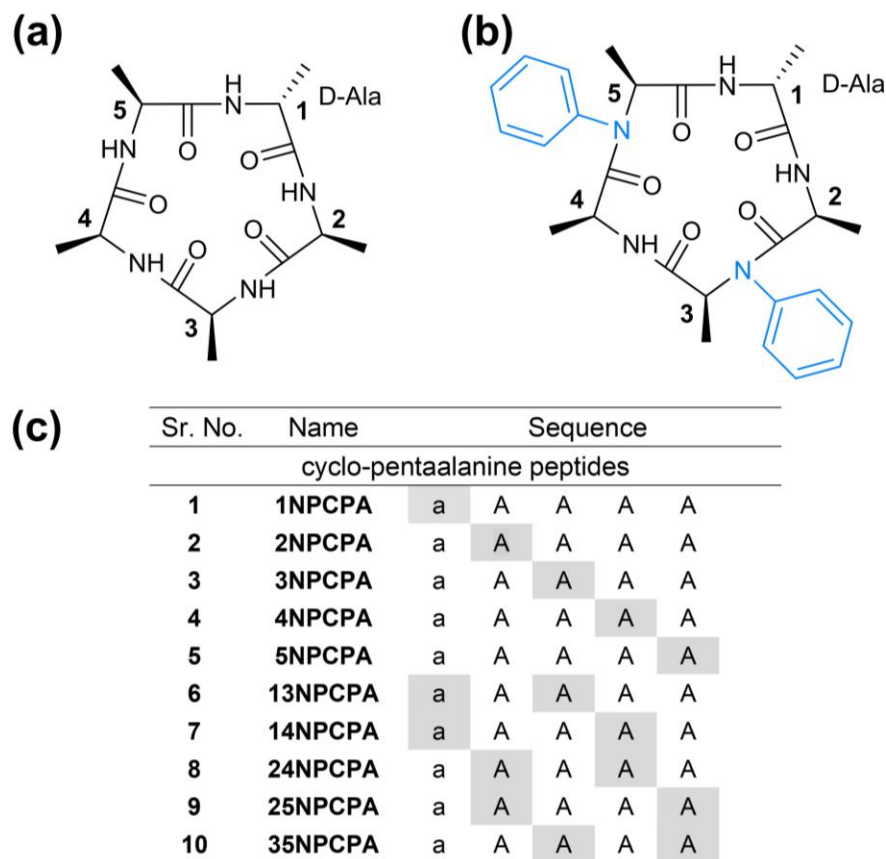
Figure 2B.1. (a) The parent cyclic-pentaalanine peptide template used for *N*-arylation. The residues are numbered starting from D-alanine as position 1; (b) representative example of *N*-phenyl peptide-35NPCPA containing two *N*-phenyl residues; (c) list of the *N*-phenyl containing CPA peptides characterized in this section. The numbers at the start of the peptide name and the amino acid labels highlighted in grey in the sequences indicate the position of the residues with the *N*-phenyl amide group.
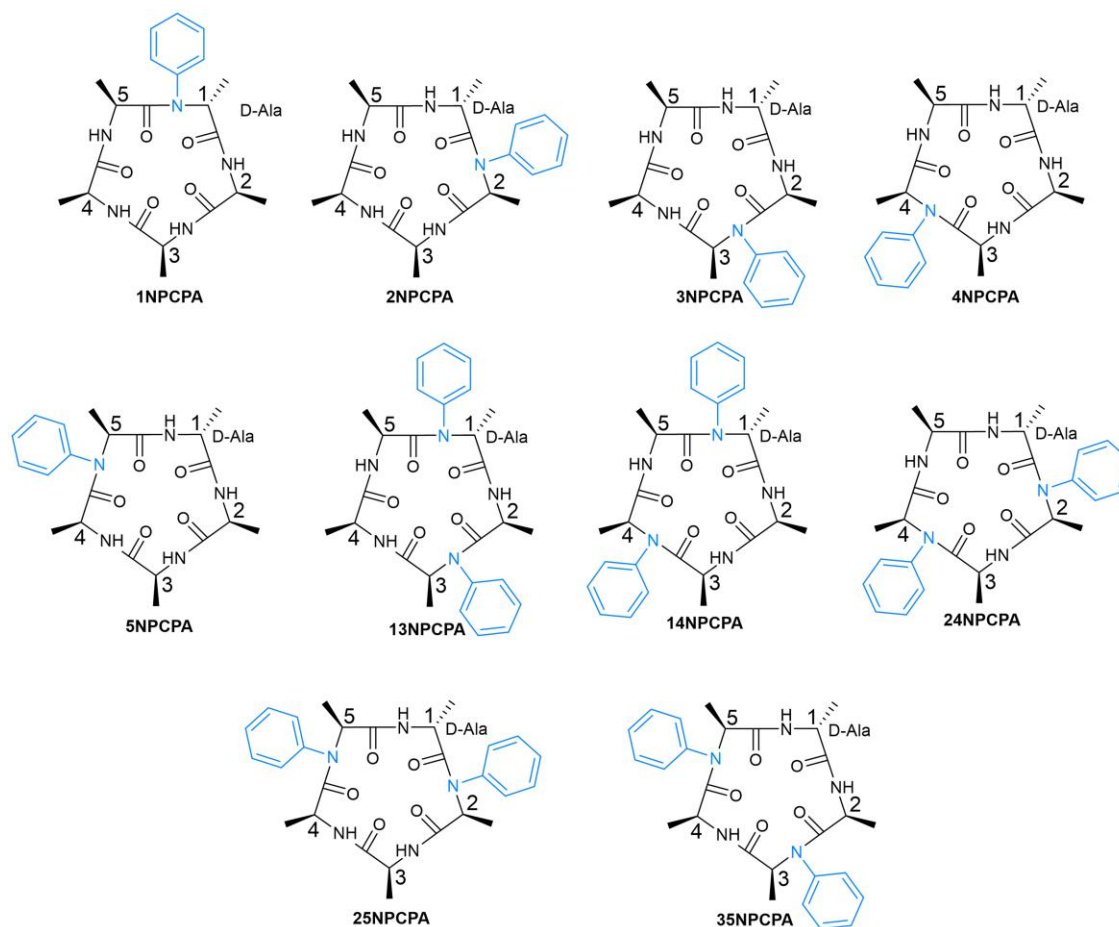
Figure 2B.2. Schematic structures of **NPCPA** peptides synthesized and studied in this section.

Table 2B.1. HPLC purification methods for **NPCPA** peptides

Methods used for the HPLC purification of the NPCPA peptides and their corresponding retention times.			
S. No.	**Peptide**	**HPLC Method Gradient (ACN: Water)**	**Retention Time (min)**
1	1NPCPA	20%-80% ACN in 20 min	9.8
2	2NPCPA	20%-90% ACN in 20 min	10.1
3	3NPCPA	30%-90% ACN in 20 min	9.0
4	4NPCPA	20%-90% ACN in 25 min	9.5
5	5NPCPA	30%-90% ACN in 20 min	9.7
6	13NPCPA	30%-90% ACN in 20 min	12.8
7	14NPCPA	35%-90% ACN in 20 min	11.4
8	24NPCPA	30%-90% ACN in 20 min	13.2
9	25NPCPA	30%-90% ACN in 20 min	11.9
10	35NPCPA	30%-60% ACN in 20 min	12.1

2B.1. Chemical shift assignments of NPCPA peptides

The following list of tables **2B.2 – 2B.11** has the chemical shift assignments of the NPCPA peptides. The notations used are ala = L-alanine, ald = D-alanine, lnpa = *N*-phenyl-L-Ala, dnpa = *N*-phenyl-D-Ala.

Table 2B.2. Chemical shift assignments of **1NPCPA**.

Residue	NH	Hα	Hβ	Cα	Cβ	CO	Temp. coeff.
1dnpa	-	5.07	0.87	53.55	15.01	171.60	-
2ala	8.03	4.34	1.28	49.00	18.31	172.64	-2
3ala	8.28	4.07	1.36	50.31	16.91	171.53	-4.8
4ala	8.10	3.86	1.25	51.05	17.25	171.99	-3.6
5ala	7.71	4.06	1.086	46.44	18.42	172.92	-2

Table 2B.3. Chemical shift assignments of **2NPCPA**.

Residue	NH	Hα	Hβ	Cα	Cβ	CO	Temp. coeff.
1ald	8.73	3.78	1.19	48.01	16.28	174.00	-6.8
2lnpa	-	5.17	0.90	54.09	15.14	170.59	-
3ala	7.71	4.29	1.55	49.68	16.6	172.11	-1.2
4ala	8.16	3.90	1.33	52.81	16.47	173.21	-2.4
5ala	7.29	4.30	1.10	47.23	19.88	173.93	0.8

Table 2B.4. Chemical shift assignments of **3NPCPA**.

Residue	NH	Hα	Hβ	Cα	Cβ	CO	Temp. coeff.
1ald	8.67	4.36	1.09	47.3	14.41	171.54	-8.8
2ala	7.48	4.22	1.08	45.52	13.39	173.02	-3.2
3lnpa	-	3.72	1.63	63.26	14.57	170.94	-
4ala	8.08	4.09	1.35	50.73	17.49	172.31	-4.4
5ala	7.53	4.32	1.18	49.17	17.38	171.45	0.8

Table 2B.5. Chemical shift assignments of **4NPCPA**.

Residue	NH	Hα	Hβ	Cα	Cβ	CO	Temp. coeff.
1ald	8.61	4.2	1.22	49.69	17.66	172.91	-4.2
2ala	8.72	3.89	1.17	50.01	17.62	171.62	-5.2
3aa	7.29	4.0	1.03	46.88	18.3	172.33	-1.2
4lnpa	-	3.7	1.75	66.94	16.19	171.66	-
5ala	8.19	4.54	1.23	48.1	17.82	173.72	-2.8

Table 2B.6. Chemical shift assignments of **5NPCPA**.

Residue	NH	Hα	Hβ	Cα	Cβ	CO	Temp. coeff.
1ald	8.55	4.17	1.24	48.95	17.95	172.6	-5.2
2ala	7.68	4.2	1.26	48.55	18.04	172.5	-5.2
3ala	8.09	4.29	1.16	48.00	17.64	171.59	-2.0
4ala	7.41	4.1	0.94	46.52	17.67	172.5	-3.6
5lnpa	-	4.82	0.91	55.39	16.41	172.48	-

Table 2B.7. Chemical shift assignments of **13NPCPA**.

Residue	NH	Hα	Hβ	Cα	Cβ	CO	Temp. coeff.
1dnpa	-	5.23	0.81	51.57	13.7	170.05	-
2ala	7.44	4.33	1.12	46.24	18.08	171.5	-0.4
3lnpa	-	3.81	1.65	63.99	14.38	169.88	-
4ala	8.07	4.04	1.19	49.40	17.50	171.59	-4.4
5ala	7.73	4.14	1.11	44.08	17.82	173.08	-2.0

Table 2B.8. Chemical shift assignments of **14NPCPA**.

Residue	NH	Hα	Hβ	Cα	Cβ	CO	Temp. coeff.
1dnpa	-	4.71	0.89	55.91	16.04	173.84	-
2ala	8.83	3.98	1.2	49.31	17.6	171.28	-5.2
3ala	7.54	4.05	1.08	47.30	17.76	172.29	-2.0
4lnpa	-	3.61	1.80	68.48	16.62	171.34	-
5ala	8.31	4.2	1.15	46.47	18.54	174.43	0.8

Table 2B.9. Chemical shift assignments of **24NPCPA**.

Residue	NH	Hα	Hβ	Cα	Cβ	CO	Temp. coeff.
1ald	8.84	3.82	1.20	48.1	16.56	173.64	-4.8
2lnpa	-	4.85	0.82	54.91	15.68	169.65	-
3ala	7.76	4.12	1.15	47.61	18.08	172.68	-2.8
4lnpa	-	3.70	1.79	67.47	16.24	172.16	-
5ala	8.19	4.58	1.16	47.8	18.08	173.55	-1.6

Table 2B.10. Chemical shift assignments of **25NPCPA**.

Residue	NH	Hα	Hβ	Cα	Cβ	CO	Temp. coeff.
1ald	6.98	4.13	1.02	46.8	19.78	173.95	0
2lnpa	-	4.59	0.87	56.7	16.38	174.69	-
3ala	8.66	3.71	1.46	54.4	17.07	172.97	-4
4ala	8.35	4.15	1.07	64.3	19.01	171.58	-2.8
5lnpa	-	3.91	1.42	61.6	13.49	169.12	-

Table 2B.11. Chemical shift assignments of **35NPCPA**.

Residue	NH	Hα	Hβ	Cα	Cβ	CO	Temp. coeff.
1ald	8.49	4.19	1.22	49.19	18.01	171.42	-8.8
2ala	7.62	4.01	1.04	46.66	17.2	172.98	-3.2
3lnpa	-	5.31	0.91	53.08	14.9	170.5	-
4ala	7.44	4.24	1.02	46.95	17.5	172.08	-4.4
5lnpa	-	4.74	0.96	56.26	16.3	172.23	0.8

Table 2B.12. NMR chemical shift temperature coefficients (in ppb/K) of amide protons in **NPCPA** peptides (given in the order of peptide names).

cyclic-pentaalanine (CPA) peptides						
S. No.	Peptide	NH1	NH2	NH3	NH4	NH5
1	**1NPCPA**	-	-2	-4.8	-3.6	-2
2	**2NPCPA**	-6.8	-	-1.2	-2.4	0.8
3	**3NPCPA**	-8.8	-2	-	-4.4	0.8
4	**4NPCPA**	-4.2	-5.2	-1.2	-	-2.8
5	**5NPCPA**	-5.2	-5.2	-2	-3.6	-
6	**13NPCPA**	-	-0.4	-	-4.4	-2
7	**14NPCPA**	-	-5.2	-2	-	0.8
8	**24NPCPA**	-4.8	-	-2.8	-	-1.6
9	**25NPCPA**	0	-	-4	-2.8	-
10	**35NPCPA**	-8.8	-3.2	-	-4.4	-

2B.2. NMR-based conformational study of NPCPA peptides

The ^{1}H NMR spectra of all the NPCPA peptides have shown only one set of chemical shifts implying, in general, either a single predominant conformation or fast exchanging conformations on the NMR chemical shift time scales (see table **2B.2-11**). 9 out of the 10 NPCPA peptides have exhibited distinct antiparallel beta sheet conformations with characteristic beta turn and gamma turn (Figures **2B.2-7**). The said conformations are supported by representative NOE correlations and amide chemical shift temperature coefficients that indicated solvent shielding/hydrogen bonding or exposure to the solvent (Figure **2B.3**, Table **2B.12**, **14**). Based on the position of the D-alanine in the conformations, the amide NHs that exhibited hydrogen bonding nature and their inward orientation into the macrocycle, and based on the position of gamma turn (Table **2B.15)**, the conformations observed in NPCPA peptides are broadly classified into three different templates (Figure **2B.2**). The NPCPA compounds displayed three template structures containing one beta-turn and a gamma-turn (Figures **2B.2**) supported by characteristic hydrogen bond and distant NOE pattern (Figures **2B.3**).

Table 2B.13. List of the number of distance restraints that were used for the structure calculation of NPCHA peptides.

S. No.	Name	No. of distance constraints
1	1NPCPA	18
2	2NPCPA	20
3	3NPCPA	19
4	4NPCPA	18
5	5NPCPA	16
6	13NPCPA	19
7	14NPCPA	19
8	24NPCPA	18
9	25NPCPA	14
10	35NPCPA	16

(d)

	conformations in NPCPA peptides			
NPCPA Templates	Turn 1	Turn 2	solvent shielded NH	peptides
Template 1 (Fig 3a)	β turn I'/II'	classical γ-turn	3 and 5	2, 4, 5, 14 and 24
Template 2 (Fig 3b)	β turn I/II'	classical γ-turn	5 and 2	1, 3, and 13
Template 3 (Fig 3c)	β turn II	inverse γ-turn	4 and 1	25

Figure 2B.3. (a)-(c) Three different conformational templates observed for NPCPA peptides. While (a) and (b) have a beta-turn with a *trans* peptide bond in combination with a gamma turn, (c) differs in having an inverse gamma turn along with a beta-turn having a *trans* peptide bond. All the residues are numbered, starting with D-residue as position 1. Wherever the amide group is given as NR, R can be either H or phenyl group depending on the peptide sequence. The possibility of hydrogen bonding for the NHs oriented into the macrocycle is indicated in dashed lines. (d) Table showing a summary of the types of conformations observed in NPCPA peptides along with the type of turns in each conformation and the amide NHs that are solvent shielded as indicated by the NMR chemical shift temperature coefficients. The last column shows the list of peptides (named after the position of the *N*-phenyl group) exhibiting the conformations corresponding to each NPCPA template type.
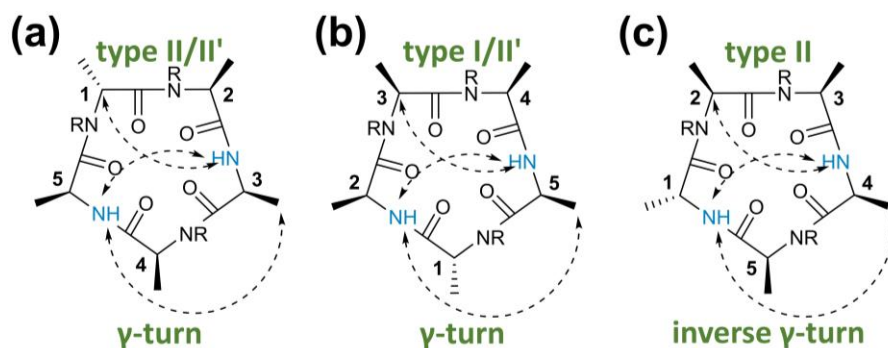
Figure 2B.4. The pattern of characteristic distant ROESY correlations (shown in dashed arrows) was observed for each template structure of NPCPA peptides.

80

Table 2B.14. NMR chemical shift temperature coefficients (in ppb/K) of amide protons in **NPCPA** peptides (given in the order of template type).

			cyclic-pentaalanine (CPA) peptides				
S. No.	**Peptide**	**Template**	**Amides**				
			NH1	NH2	NH3	NH4	NH5
	2NPCPA	Template 1	-6.8	-	-1.2	-2.4	0.8
1	**4NPCPA**	Template 1	-4.2	-5.2	-1.2	-	-2.8
2	**5NPCPA**	Template 1	-5.2	-5.2	-2	-3.6	-
3	**14NPCPA**	Template 1	-	-5.2	-2	-	0.8
4	**24NPCPA**	Template 1	-4.8	-	-2.8	-	-1.6
5	**1NPCPA**	Template 2	-	-2	-4.8	-3.6	-2
6	**3NPCPA**	Template 2	-8.8	-2	-	-4.4	0.8
7	**13NPCPA**	Template 2	-	-0.4	-	-4.4	-2
8	**25NPCPA**	Template 3	0	-	-4	-2.8	-

Table 2B.15. Template type, turn position, and type of turns observed in NPCPA peptides (given in the order of peptide names).

Peptide	Template type	Turn position	Turn 1						Turn 2					
			I	I'	II	II'	γ	γ'	I	I'	II	II'	γ	γ'
1NPCPA	Template 2	3,4 and 1	■										■	
2NPCPA	Template 1	1,2 and 4		■									■	
3NPCPA	Template 2	3,4 and 1				■							■	
4NPCPA	Template 1	1,2 and 4				■							■	
5NPCPA	Template 1	1,2 and 4				■							■	
13NPCPA	Template 2	3,4 and 1				■							■	
14NPCPA	Template 1	1,2 and 4				■							■	
24NPCPA	Template 1	1,2 and 4		■									■	
25NPCPA	Template 3	2,3 and 5			■									■

Table 2B.16. Template type, turn position, and type of turns observed in NPCPA peptides (given in the order of NPCPA template type).

Peptide	Template type	Turn position	Turn 1						Turn 2					
			I	I'	II	II'	γ	γ'	I	I'	II	II'	γ	γ'
2NPCPA	Template 1	1,2 and 4		■									■	
4NPCPA	Template 1	1,2 and 4				■							■	
5NPCPA	Template 1	1,2 and 4				■							■	
14NPCHA	Template 1	1,2 and 4				■							■	
24NPCPA	Template 1	1,2 and 4		■									■	
1NPCPA	Template 2	3,4 and 1	■										■	
3NPCPA	Template 2	3,4 and 1				■							■	
13NPCPA	Template 2	3,4 and 1				■							■	
25NPCPA	Template 3	2,3 and 5			■									■

Table 2B.17. Beta and gamma turn dihedral angles for the conformations observed in NPCPA peptides (given in the order of peptide names).

Peptide	Template type	Turn 1 (beta)					Turn 2 (gamma)		
		φi+1	ψi+1	φi+2	ψi+2	Type	φi+1	ψi+1	Type
1NPCPA	Template 2	-45.5	-34.5	-85.3	-18.1	I	79	-72.3	Classical
2NPCPA	Template 1	61.6	29	79.9	3.3	I'	92.8	-45.2	Classical
3NPCPA	Template 2	61.8	-143.3	-76.1	24.3	II'	88.2	-77.2	Classical
4NPCPA	Template 1	60.7	-125.1	-90	15.8	II'	78.2	-67.5	Classical
5NPCPA	Template 1	76.5	-102.2	-134.8	29.3	II'	106.2	-65.9	Classical
13NPCPA	Template 2	68.7	-102.7	-100.1	1	II'	79	-59.8	Classical
14NPCPA	Template 1	70.9	-132.7	-77.7	-1.6	II'	76	-79.5	Classical
24NPCPA	Template 1	45.8	47	79.4	0.1	I'	72	-67	Classical
25NPCPA	Template 3	-61.9	123.6	67.8	-8	II	-69.8	86.3	Inverse

Table 2B.18. Beta and gamma turn dihedral angles for the conformations observed in NPCPA peptides (given in the order of NPCPA template type).

Peptide	Template type	Turn 1 (beta)					Turn 2 (gamma)		
		φi+1	ψi+1	φi+2	ψi+2	Type	φi+1	ψi+1	Type
2NPCPA	Template 1	61.6	29	79.9	3.3	I'	92.8	-45.2	Classical
4NPCPA	Template 1	60.7	-125.1	-90	15.8	II'	78.2	-67.5	Classical
5NPCPA	Template 1	76.5	-102.2	-134.8	29.3	II'	106.2	-65.9	Classical
14NPCHA	Template 1	70.9	-132.7	-77.7	-1.6	II'	76	-79.5	Classical
24NPCPA	Template 1	45.8	47	79.4	0.1	I'	72	-67	Classical
1NPCPA	Template 2	-45.5	-34.5	-85.3	-18.1	I	79	-72.3	Classical
3NPCPA	Template 2	61.8	-143.3	-76.1	24.3	II'	88.2	-77.2	Classical
13NPCPA	Template 2	68.7	-102.7	-100.1	1	II'	79	-59.8	Classical
25NPCPA	Template 3	-61.9	123.6	67.8	-8	II	-69.8	86.3	Inverse

NPCPA Template 1

The NPCPA Template 1 (Figures **2B.3**-**2B.5**) conformation consists of a beta-turn type I'/II' connecting residues 1 and 2 with the D-residue at the i+1 position, and classical gamma turn centered around residue 4. This arrangement leads to the internal orientation and hydrogen bonding of NH of residue 3 with the C=O of residue 5 in a beta-turn and hydrogen bonding between NH of residue 5 (except for 5NPCPA, where NH at position 5 is modified to *N*-phenyl) with the C=O of residue 3 in the classical gamma turn. While peptides 2NPCPA and 24NPCPA showed a type I' beta-turn, the others, 4NPCPA, 5NPCPA, and 14NPCPA have a type II' turn (Tables **2B.14-2B.18**).
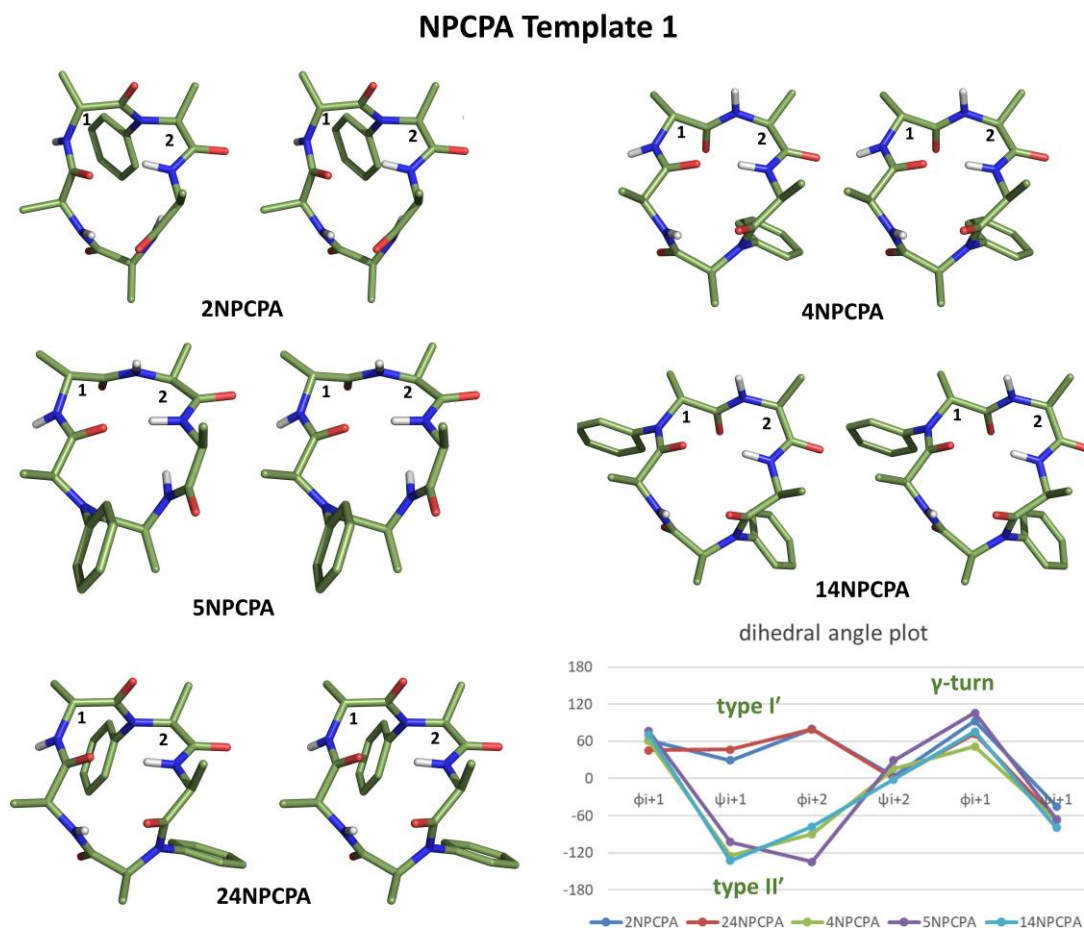
Figure 2B.5. Stereo view (top view) of the NMR-derived conformations and dihedral angle comparison of all peptides from NPCPA template 1.

NPCPA Template 2

1NPCPA, 3NPCPA, and 13NPCPA displayed NPCPA Template 2 conformation (Figures **2B.3**, **2B.4**, **2B.6**) with a type I/II' beta turn around 3 and 4 positions and a classical gamma turn centered at position 1, which is a D-amino acid. The hydrogen bonding pattern involves NH of amino acid 5 with the C=O of residue 2 in the beta-turn and vice versa in the gamma-turn. Among the three peptides of the NPCPA Template 2 structure, the 1NPCPA populated a type I turn, whereas 3NPCPA and 13NPCPA have a type II' beta turn (Tables **2B.14-2B.18**).
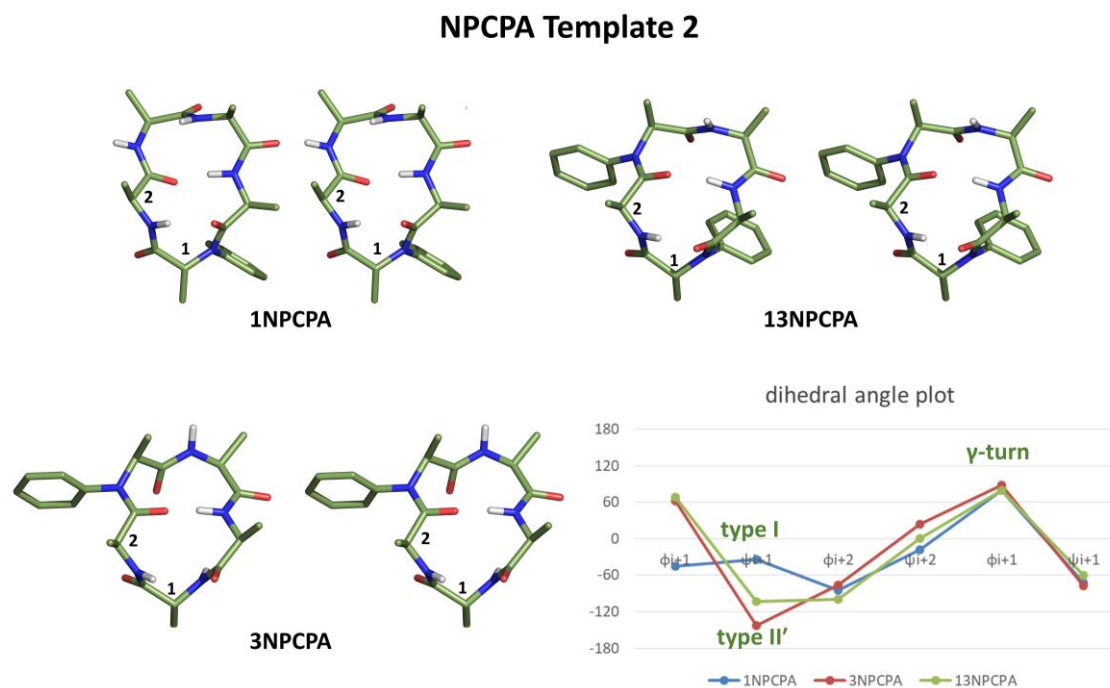
NPCPA Template 2

Figure 2B.6. Stereo view (top view) of the NMR-derived conformations and dihedral angle comparison of all peptides from NPCPA template 2.

NPCPA Template 3

Only one peptide, 25NPCPA, has exhibited NPCPA Template 3 folding (Figures Figures **2B.3**, **2B.4**, **2B.7**) consisting of a type II beta-turn around 2 and 3 residues with D-amino acid occupying the ith position of the turn. In contrast to the NPCPA templates 1 and 2 discussed here, the NPCPA template 3 has an inverse gamma turn centered around amino acid 5. The NPCPA Template 3 has NH of amino acid 4 involved in hydrogen bonding with C=O of residue 1 in the beta II' turn and the NH of amino acid 1hydrogen bonded to C=O of 4 in an inverse gamma turn (Tables **2B.14-2B.18**). We speculate that probably due to the ring constraint in the cyclic-pentaalanine peptides, the peptide bond flipping in the beta turns containing *N*-phenyl groups could be restricted. Therefore, we failed to observe an equilibrium of beta turns with amide bond flipping in the NPCPA peptides, unlike that in the NPCHA series (discussed in the previous section).
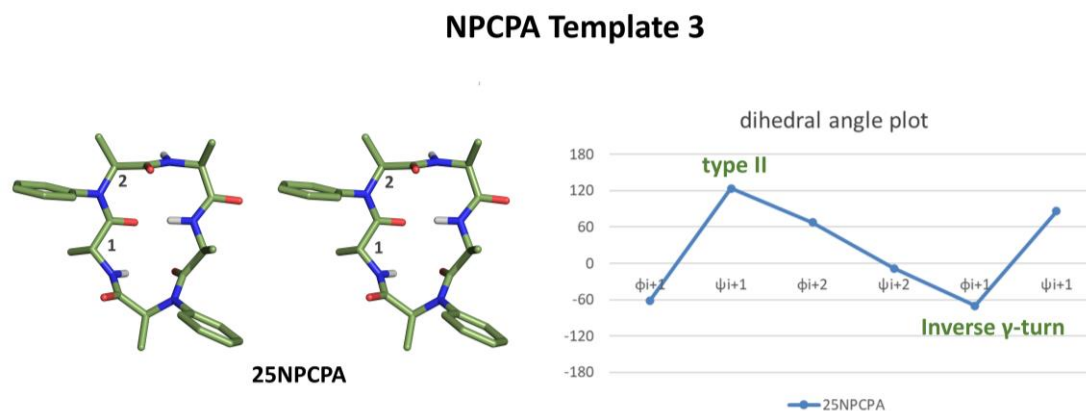
NPCPA Template 3

Figure 2B.7. Stereo view (top view) of the NMR-derived conformations and dihedral angle comparison of all peptides from NPCPA template 2.
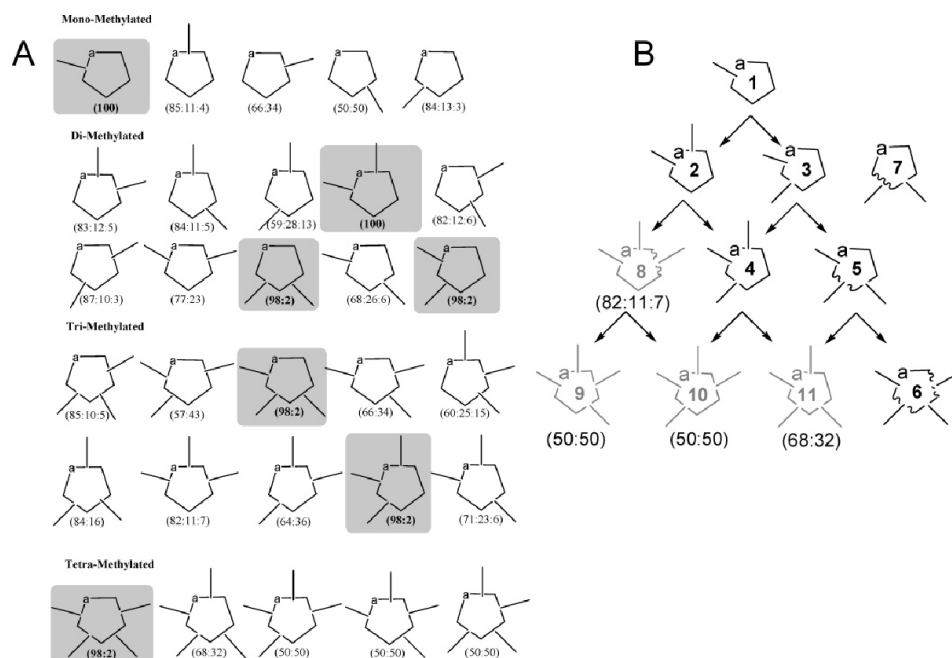
Figure 2B.8. (A) Library of all the synthesized *N*-methylated peptides with their conformational abundance on the NMR time scale of chemical shift separation. The values in parentheses denote the ratio of all the conformers calculated from a ^{1}H spectrum. (B) Schematic diagram illustrating the numbering of the compounds and the correlation between the location and number of *N*-methylated sites and the compounds preferring a single conformation. Conformationally pure peptides are shown in black, and those having multiple conformations on the NMR time scale are shown in gray, with the trans/cis abundance given in the parentheses. The three tetra-*N*-methylated compounds are shown to complete the pattern. The wavy bonds in **5**, **6**, **7**, and **8** denote a cis peptide bond (reproduced with permission from *J. Am. Chem. Soc.* **2006***, 128, 47,* 15164-15172).

It is appealing that in the *N*Me analogues of NPCPA compounds, except for 1*N*MeCPA and 12*N*MeCPA, none others have exhibited a conformational homogeneity (Figure **2B.8**).[44] Furthermore, it is noteworthy that for the NPCPA series, we observed relatively distinct amide NMR chemical shift temperature coefficients (Table **2B.14**) that strongly support a pattern of solvent shielding and involvement in hydrogen bonding. In contrast, the amide NMR chemical shift temperature coefficients for the *N*Me analogues of NPCPAs were ambiguous (Table **2B.19**).[44] We think the large size of the *N*-aryl group, acts as a barrier for the bond rotation and peptide bond flipping, thus restricting the conformational heterogeneity and rotamer populations, in general, for the *N*-aryl peptides.

Table 2B.19. Table depicting the values of temperature gradients of NH Protons ($-\Delta\delta/\Delta T$) in ppb/K; the values shown in parentheses are the respective ^3J (NH−Hα) coupling constants in Hz (reproduced with permission from *J. Am. Chem. Soc.* **2006**, *128, 47,* 15164-15172).

compound	Ala^1	Ala^2	Ala^3	Ala^4	Ala^5
1		2.5 (9.1)	2.7 (8.1)	3.4 (6.9)	2.3 (8.3)
2			3.7 (7.4)	0.6 (7.3)	5.5 (8.2)
3		1.5 (9.4)	2.3 (6.2)	1.1 (7.9)	
4			4.7 (5.7)	−1.3 (7.8)	
5		6.0 (6.9)	0.4 (7.5)		
6		5.1 (9.4)			
7	5.5 (6.2)	5.8 (6.7)	2.3 (7.6)		

2.3. Conclusions

In summary, we have explored the *N*-aryl modification of amide protons in peptides as a novel approach for peptide modifications beyond *N*-methylation. We have designed, synthesized, and carried out the structural characterization of a series of 15 cyclic-hexaalanine peptides and 10 cyclic-pentaalanine peptides containing one or two *N*-phenyl-amino acids. Our studies have shown that the *N*-phenyl peptides are noticeably conformationally homogeneous on the NMR chemical shift time scales. The structural studies on *N*-phenyl series peptides revealed cyclic antiparallel beta sheet conformations with well-defined beta and gamma turns, and hydrogen bonding patterns supported by NMR data. The *N*-phenyl series peptides showcased superior conformational homogeneity compared to their *N*-methyl analogues and exhibited different conformations in the corresponding analogues. We hope that *N*-aryl modification of amide NHs has the potential to be employed as a versatile peptide modification tool in peptide-based drug design approaches.

2.4. Experimental methods

2.4.1. **Synthesis of *N*-phenyl-L/D-Ala-OH (1a/1b):** Into a pre-dried round bottom flask L-alanine (1.2 eq.) Cs_2CO_3 (2.0 eq.) and copper iodide (5 mol %) were weighed in air. After that argon was flushed two to three times, and the flask was sealed under argon. The contents in the flask were dissolved in dry DMF. To this mixture, aryl iodide (2 mmol, 1.0 eq.), and 2-isobutyrylcyclohexanone (20 mol %) were added, and the reaction was stirred at rt for 18h. After the completion of the reaction, the reaction mixture was worked up with cold water and ethyl acetate to remove the DMF. The ethyl acetate layer was washed with 1N NaOH (two times). The aq. phase was acidified with 1N HCl up to 2-3 pH and then extracted with ethyl acetate. The combined organic layer was dried over sodium sulfate and purified by flash column chromatography to obtain the compound in 78 % yield, as a brown oil.

^{1}H NMR (400 MHz, CDCl$_3$): δ 7.23 (t, *J* = 7.6 Hz, 2H), 6.82 (t, *J* = 7.3 Hz, 1H), 6.66 (d, *J* = 7.9 Hz, 2H), 4.16 (q, *J* = 7.1 Hz, 1H), 1.57 (d, *J* = 7.0 Hz, 3H). ^{13}C NMR (125 MHz, CDCl$_3$) δ 178.39, 146.34, 129.61, 119.22, 113.80, 52.58, 19.02. HRMS (ESI-TOF) m/z [M+H+] calculated for $C_9H_{13}NO_2$ 166.0790, found 166.0868.

Following the similar procedure, the arylation of D-alanine was also done.

2.4.2. **Synthesis of *N*-phenyl-L/D-Ala-OMe (2a/2b):** In a round bottom flask *N*-phenyl-L-alanine (1 eq.) was dissolved in MeOH and cooled to 0 °C. To the cooled mixture, $SOCl_2$ (1.5 eq.) was added very slowly, and the reaction was stirred at rt overnight. After the completion of the reaction, thionyl chloride was evaporated to achieve the *N*-phenyl-L-Ala-OMe (**2a**) with 95 % yield as a brown solid.

^{1}H NMR (500 MHz, CDCl$_3$): δ 7.75 – 7.69 (m, 2H), 7.40 (m, 3H), 4.26 (q, *J* = 7.2 Hz, 1H), 3.65 (s, 3H), 1.70 (d, *J* = 7.2 Hz, 3H). ^{13}C NMR (126 MHz, CDCl$_3$) δ 168.79, 134.53, 129.80, 129.23, 124.36, 59.89, 53.07, 15.05. HRMS (ESI-TOF) m/z [M+H+] calculated for $C_{10}H_{14}NO_2$ 180.09460, found 180.1016.

Following a similar procedure, esterification of **1b** was also carried out with 96 % yield to achieve **2b**. ^{1}H NMR (500 MHz, CDCl$_3$) δ 7.25 – 7.17 (m, 2H), 6.81 – 6.74 (m, 1H), 6.67 – 6.61 (m, 2H), 4.19 (q, *J* = 6.9 Hz, 1H), 3.76 (s, 3H), 1.51 (d, *J* = 7.0 Hz, 3H). ^{13}C NMR (126 MHz, CDCl$_3$) δ 175.24, 146.64, 129.45, 118.42, 113.44, 52.34, 52.01, 19.06. HRMS (ESI-TOF) m/z [M+H+] calculated for $C_{10}H_{14}NO_2$ 180.09460, found 180.1016.

2.4.3. **General procedure for the synthesis of dipeptides:** For the synthesis of the dipeptide (**4a-c**), Fmoc-L/D-Ala-OH (1 eq.) was activated by refluxing it with $SOCl_2$ (5 eq.) in dry DCM for 3h. After 3h, the solvent was evaporated on a rotatory evaporator. To remove the excess thionyl chloride, the contents were dissolved in toluene and were evaporated 3-4 times. In an oven-dried round bottom flask *N*-phenyl-L/D-Ala-OMe (1 eq.) was dissolved in dry DCM. Et_3N (1.2 eq.) was added to the solution and stirred for 15 min. Then the Fmoc-L/D-Ala-Cl (2 eq.) dissolved in dry DCM was added slowly at 0 °C to the reaction mixture. The reaction mixture was stirred for 1.5 h. After the completion of the reaction, the contents in the flask were washed with 5 % Na_2CO_3 solution followed by brine. The organic fraction was dried with Na_2SO_4 and concentrated on a rotatory evaporator and purified by column chromatography to get the desired dipeptide as a white solid (51-56 % yield).

2.4.3.1. **Synthesis of Fmoc-L-Ala-*N*-phenyl-L-Ala-OMe (3a):** The synthesis of dipeptide Fmoc-L-Ala-*N*-phenyl-L-Ala-OMe was done by following the general procedure **2.4.3** with a yield of 52 %.

^{1}H NMR (400 MHz, CDCl$_3$): δ 7.75 (d, *J* = 7.5 Hz, 2H), 7.59 (t, *J* = 6.7 Hz, 2H), 7.41 (dt, *J* = 14.8, 6.6 Hz, 7H), 7.34 – 7.26 (m, 2H), 5.55 (d, *J* = 8.4 Hz, 1H), 5.11 (q, *J* = 7.5 Hz, 1H), 4.35 – 4.24 (m, 3H), 4.20 (t, *J* = 7.3 Hz, 1H), 3.78 (s, 3H), 1.23 – 1.15 (m, 6H). ^{13}C NMR (101 MHz, CDCl$_3$) δ 173.50, 172.75, 155.73, 144.13, 144.01, 141.44, 138.31, 129.87, 129.25, 127.84, 127.22, 125.36, 120.12, 67.09, 54.92, 52.55, 48.13, 47.30, 18.78, 15.31.

2.4.3.2. **Synthesis of Fmoc-D-Ala-*N*-phenyl-L-Ala-OMe (3b):** The synthesis of dipeptide Fmoc-D-ala-*N*-phenyl-L-Ala-OMe was done by following the general procedure **2.4.3** with a yield of 55 %.

^{1}H NMR (500 MHz, CDCl$_3$): δ 7.76 (d, *J* = 7.5 Hz, 2H), 7.59 (t, *J* = 6.5 Hz, 2H), 7.49 – 7.38 (m, 6H), 7.38 (s, 1H), 7.36 (s, 1H), 7.31 (t, *J* = 7.4 Hz, 2H), 5.60 (d, *J* = 8.2 Hz, 1H), 4.63 (q, *J* = 7.3 Hz, 1H), 4.34 – 4.24 (m, 3H), 4.20 (t, *J* = 7.3 Hz, 1H), 3.77 (s, 3H), 1.41 (d, *J* = 7.2 Hz, 3H), 1.18 (d, *J* = 6.8 Hz, 3H). ^{13}C NMR (126 MHz, CDCl$_3$) δ 173.05, 171.74, 155.49, 144.11, 143.98, 141.39, 139.62, 130.02, 129.37, 129.18, 127.78, 127.17, 125.32, 120.07, 77.41, 77.16, 76.91, 67.01, 57.81, 52.50, 47.92, 47.24, 18.99, 15.35.

2.4.3.3. **Synthesis of Fmoc-L-Ala-*N*-phenyl-D-Ala-OMe (3c):** The synthesis of dipeptide Fmoc-L-Ala-*N*-phenyl-D-ala-OMe was done by following the general procedure **2.4.3** with a yield of 55 %. ^{1}H NMR (500 MHz, CDCl$_3$) δ 7.76 (d, *J* = 7.6 Hz, 2H), 7.59 (t, *J* = 6.5 Hz, 2H), 7.49 – 7.38 (m, 6H), 7.38 (s, 1H), 7.31 (t, *J* = 7.5 Hz, 2H), 5.59 (d, *J* = 8.4 Hz, 1H), 4.63 (q, *J* = 7.1 Hz, 1H), 4.35 – 4.24 (m, 3H),

4.19 (t, *J* = 7.4 Hz, 1H), 3.77 (s, 3H), 1.40 (d, *J* = 7.4 Hz, 3H), 1.18 (d, *J* = 6.8 Hz, 3H). ^{13}C NMR (126 MHz, CDCl₃) δ 173.08, 171.76, 155.50, 144.13, 143.99, 141.41, 139.62, 130.03, 129.20, 127.80, 127.18, 125.34, 120.08, 67.03, 57.82, 52.52, 47.94, 47.26, 29.84, 19.01, 15.36.

2.4.4. **General procedure for the ester hydrolysis of dipeptides:** For the ester hydrolysis, the dipeptide ester (**3a/3b/3c**) was dissolved in 5M HCl and dioxane (1:1) and the reaction mixture was refluxed for 18 h. After completion of the reaction, the reaction contents were diluted with 5 % Na₂CO₃, and the resulting solution was washed two times with diethyl ether. Further, the aqueous layer was acidified with 3M HCl up to pH 1. The aqueous phase was extracted with DCM 3-4 times, concentrated on rota vapor, and purified by column chromatography to get the desired dipeptide as a white floppy solid (92-95 %).[2]

2.4.4.1. **Fmoc-L-Ala-*N*-phenyl-L-Ala-OH (4a):** By following the general procedure **2.4.4**, the ester hydrolysis of dipeptide **3a** has been carried out with a yield of 90 %.

^{1}H NMR (500 MHz, CDCl₃) δ 7.75 (d, *J* = 7.5 Hz, 2H), 7.60 (t, *J* = 8.0 Hz, 2H), 7.49 – 7.36 (m, 7H), 7.33 – 7.27 (m, 2H), 5.79 (d, *J* = 8.5 Hz, 1H), 5.10 (q, *J* = 7.4 Hz, 1H), 4.37 – 4.27 (m, 3H), 4.21 (t, *J* = 7.3 Hz, 1H), 1.24 (d, *J* = 7.5 Hz, 3H), 1.21 (d, *J* = 7.0 Hz, 3H). ^{13}C NMR (126 MHz, CDCl₃) δ 175.41, 174.43, 155.92, 144.11, 143.99, 141.42, 138.09, 129.97, 129.39, 127.82, 127.20, 125.38, 120.10, 67.14, 55.11, 48.22, 47.25, 18.41, 15.04. HRMS (ESI-TOF) m/z [M+H+] calculated for C₂₇H₂₇N₂O₅ 459.1842, found 459.1914.

2.4.4.2. **Fmoc-D-Ala-*N*-phenyl-L-Ala-OH (4b):** By following the general procedure **2.4.4**, the ester hydrolysis of dipeptide **3b** has been carried out to get the desired dipeptide (91 %). ^{1}H NMR (500 MHz, CDCl₃) δ 7.77 (d, *J* = 7.5 Hz, 2H), 7.63 (t, *J* = 7.2 Hz, 2H), 7.52 – 7.37 (m, 8H), 7.32 (t, *J* = 7.5 Hz, 2H), 5.82 (d, *J* = 8.2 Hz, 1H), 4.64 (q, *J* = 7.2 Hz, 1H), 4.39 – 4.27 (m, 3H), 4.22 (t, *J* = 7.4 Hz, 1H), 1.46 (d, *J* = 7.2 Hz, 3H), 1.24 (d, *J* = 6.8 Hz, 3H).^{13}C NMR (126 MHz, CDCl₃) δ 174.52, 173.77, 155.66, 143.98, 143.84, 141.27, 139.41, 130.01, 129.18, 127.67, 127.06, 125.26, 119.94, 77.28, 77.02, 76.77, 67.00, 58.01, 47.92, 47.09, 18.38, 14.96. HRMS (ESI-TOF) m/z [M+H+] calculated for C₂₇H₂₇N₂O₅ 459.1842, found 459.1814.

2.4.4.3. **Fmoc-L-Ala-*N*-phenyl-D-Ala-OH (4c):** By following the general procedure **2.4.4**, the ester hydrolysis of dipeptide **3c** has been carried out with a yield of 89 %. ^{1}H NMR (500 MHz, CDCl₃) δ 7.77 (d, *J* = 7.5 Hz, 2H), 7.63 (t, *J* = 7.2 Hz, 2H), 7.52 – 7.37 (m, 7H), 7.32 (t, *J* = 7.4 Hz, 2H), 5.85 (d, *J* = 8.4 Hz, 1H), 4.62 (q, *J* = 7.2 Hz, 1H), 4.34 (s, 1H), 4.33 (d, *J* = 2.1 Hz, 1H), 4.30 (d, *J* = 10.7 Hz, 1H),
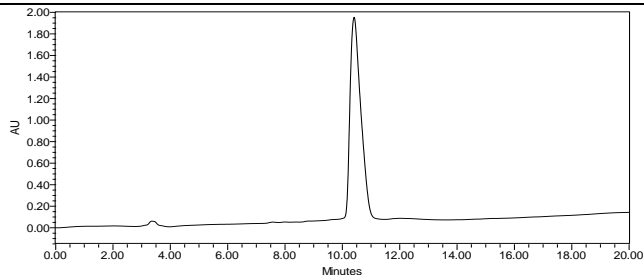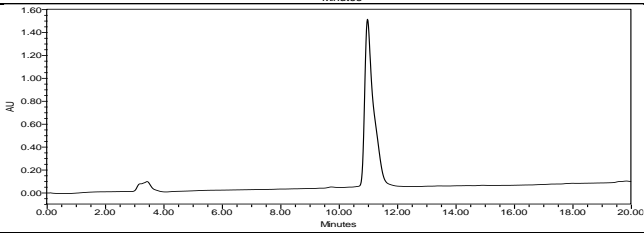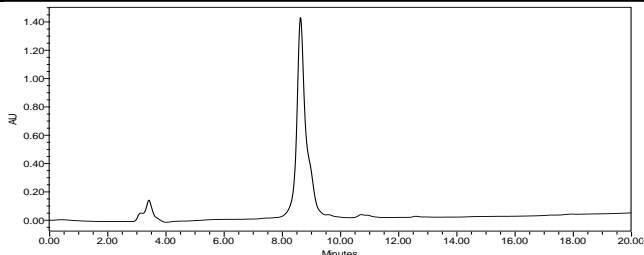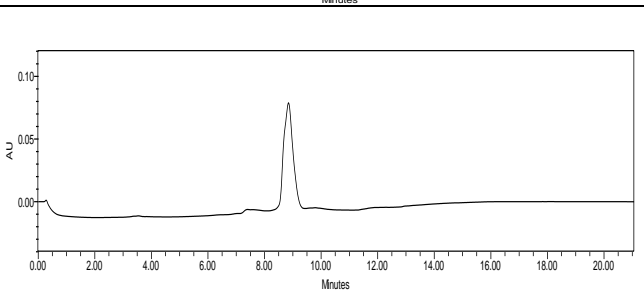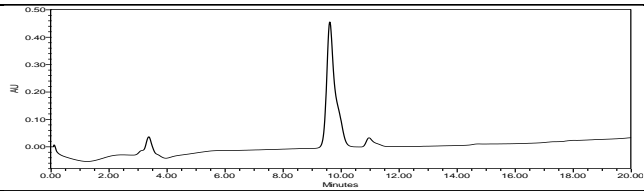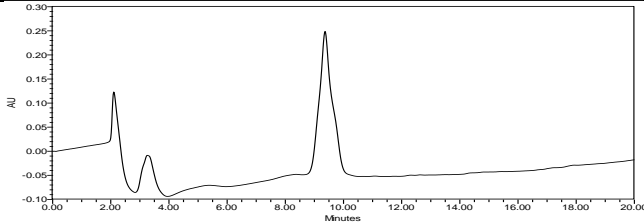
4.22 (t, *J* = 7.3 Hz, 1H), 1.46 (d, *J* = 7.2 Hz, 3H), 1.23 (d, *J* = 6.9 Hz, 3H). ^{13}C NMR (126 MHz, CDCl$_3$) δ 174.80, 173.89, 155.80, 144.11, 143.96, 141.39, 139.57, 130.14, 129.31, 127.80, 127.19, 125.39, 120.07, 67.13, 58.20, 48.04, 47.22, 18.50, 15.09. HRMS (ESI-TOF) m/z [M+H+] calculated for C$_{27}$H$_{27}$N$_2$O$_5$ 459.1842, found 459.1914.

2.4.5. **General protocol for the solid phase peptide synthesis of *N*-aryl peptide library:** Synthesis of **1-25** started with the loading of the required C-terminus Fmoc-protected amino acid or dipeptide building block Fmoc-L/D-Ala-N-phenyl-L/D-Ala-OH (**4a/4b/4c**, 1.2 eq.) as required by their target linear sequences onto the 2-chloro trityl chloride resin (150 mg, 1.6 mmol/g, 0.24 mmol) in dry DCM and DIPEA (3 eq.) for 2 hrs (for example see Scheme 1 for 5NPCHA). After loading of the first building block, capping of the unreacted active sites of the resin was done by MeOH (0.5 ml) and DIPEA (30 μL) for 30 min. After completing the capping, the resin was washed 3 times with DCM, 3 times with NMP, and then the Fmoc deprotection was done with 20 % piperidine in DMF (2*10 min) followed by washing the resin 4 times with NMP. The peptide chain was elongated by coupling of the appropriate Fmoc-protected amino acid or dipeptide building block Fmoc-L/D-Ala-N-phenyl-L/D-Ala-OH (2 eq.), HCTU (2 eq.), HOAt (2 eq.), DIPEA (3 eq.) in NMP for 1.5 hrs following which Fmoc deprotection was done with 20 % piperidine in DMF (2*10 min) and washing of the resin with NMP. The process of coupling of amino acids or dipeptide building blocks and Fmoc deprotection was repeated until the desired length of the peptides was achieved. After obtaining the complete linear peptide sequence, Fmoc deprotection of the terminal residue was carried out with 20 % piperidine in DMF (2*10 min), and then the resin was washed 4 times with NMP, 4 times with DCM. The linear peptide was cleaved from the resin by using TFE: Acetic acid: DCM (1:1:8) for 1.5 hrs (3*30 min). The filtrate was collected and concentrated by removing the excess acetic acid as an azeotrope using chloroform. After the solvent removal, the head-to-tail cyclization of the linear peptide was performed by 50 % 1-propanephosphonic acid cyclic anhydride (T3P) in ethyl acetate. For cyclization, the linear peptide was dissolved in dry DCM (15 mL) and the Et$_3$N (2 eq.) was added at 0 °C. After that DMAP (0.2 eq.) and the T3P (1.5 eq.) reagent was added dropwise. The reaction mixture was brought to room temperature and stirred overnight. After completion of the reaction, the solvent was evaporated on rotavap and the residue was purified by reversed phase HPLC. Following this procedure, all the mono and diarylated cyclic peptides **1**-**25** were synthesized.

2.5. **Analytical HPLC for NPCHA and NPCPA peptides**: The purity of all the peptides was determined by analytical HPLC using YMC Pack ODS-A-HG C18 column with the dimensions S-10
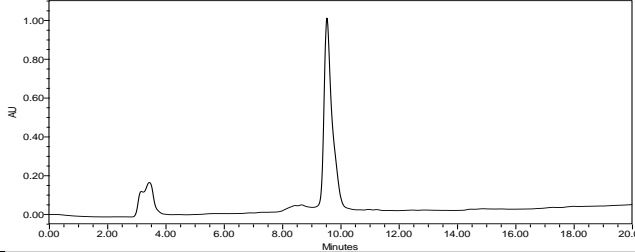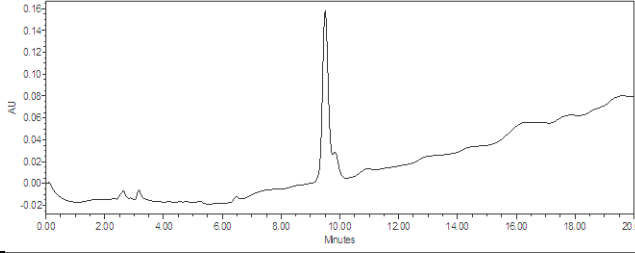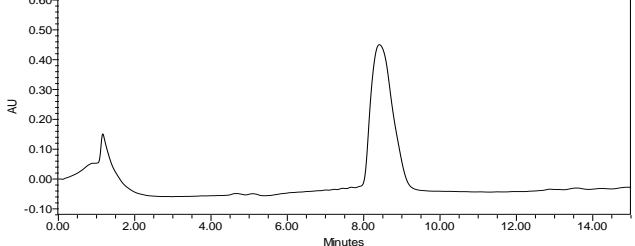
µm, 12 nm, 250 mm * 4.6 mm I.D., on Waters HPLC system 2545 Quaternary Gradient module with 2489 UV/Visible detector. A flow rate of 1 mL/min was used for the analytical run.

Table 2.3. Analytical HPLC of **NPCHA** peptides
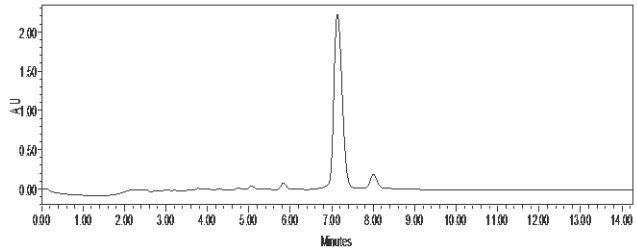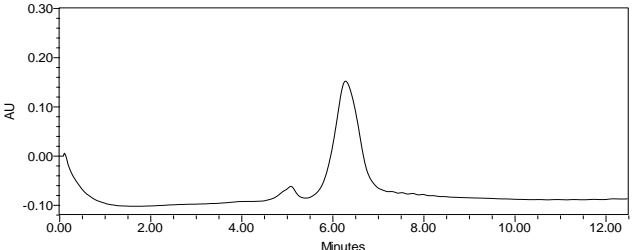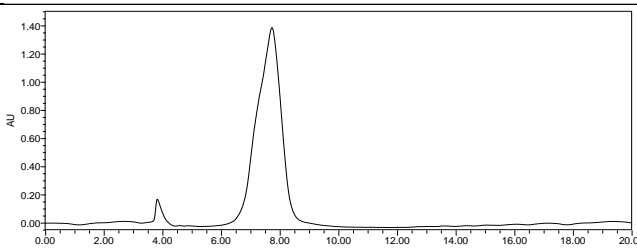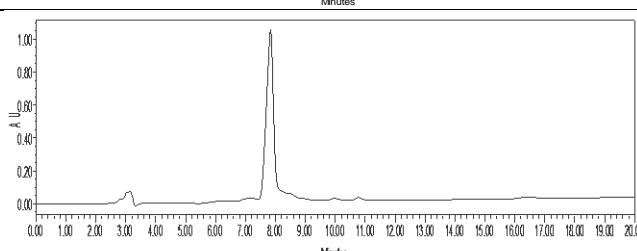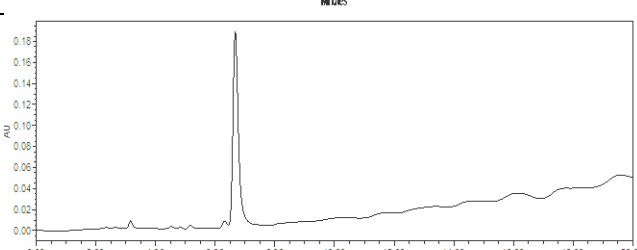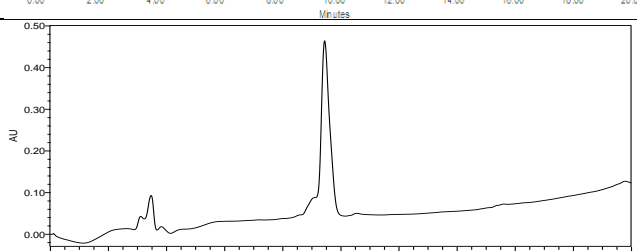
Peptide	HPLC Gradient (ACN: Water)	HPLC Chromatogram
1NPCHA	15 % - 90 % ACN in 20 min	
2NPCHA	15 % - 90 % ACN in 20 min	
3NPCHA	15 % - 90 % ACN in 20 min	
4NPCHA	15 % - 90 % ACN in 20 min	
5NPCHA	15 % - 90 % ACN in 20 min	
6NPCHA	15 % - 90 % ACN in 20 min	

13NPCHA	20 % - 90 % ACN in 20 min	
14NPCHA	20 % - 90 % ACN in 20 min	
15NPCHA	20 % - 90 % ACN in 20 min	
24NPCHA	20 % - 90 % ACN in 20 min	
25NPCHA	20 % - 90 % ACN in 20 min	
26NPCHA	20 % - 90 % ACN in 20 min	

35NPCHA	20 % - 90 % ACN in 20 min	
36NPCHA	20 % - 90 % ACN in 20 min	
46NPCHA	20 % - 90 % ACN in 20 min	

Table 2.4. Analytical HPLC of **NPCPA** peptides

Peptide	HPLC Gradient (ACN : Water)	HPLC Chromatogram
1NPCPA	10% - 90% ACN in 20 min	
2NPCPA	10% - 90% ACN in 20 min	
3NPCPA	10% - 90% ACN in 20 min	
4NPCPA	10% - 90% ACN in 20 min	
5NPCPA	10% - 90% ACN in 20 min	
13NPCPA	10% - 90% ACN in 20 min	

94

14NPCPA	10% - 90% ACN in 20 min	
24NPCPA	60% - 90% ACN in 20 min	
25NPCPA	60% - 90% ACN in 20 min	
35NPCPA	60% - 90% ACN in 20 min	

95
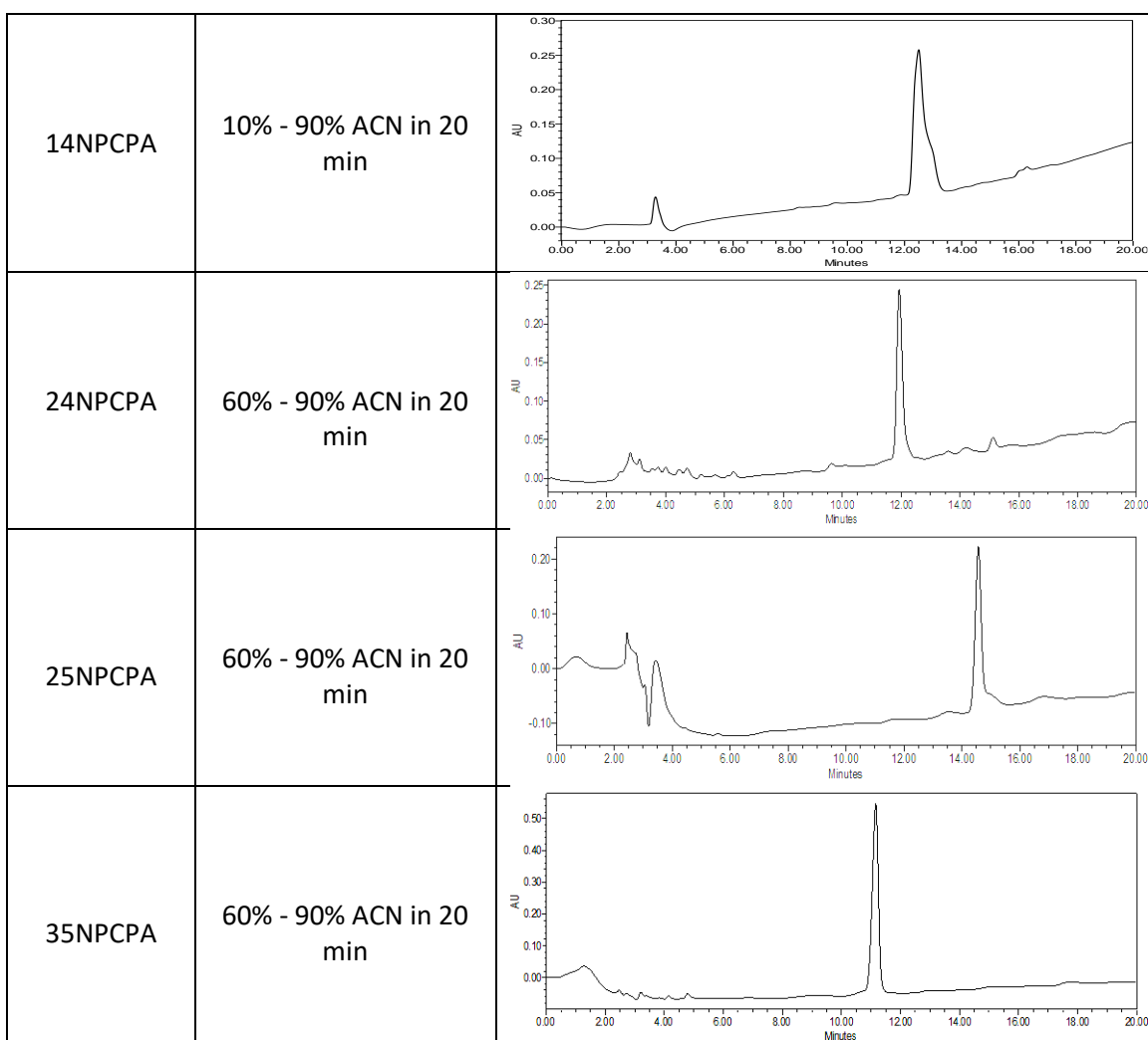
2.6. ¹H and ¹³C NMR spectra of NPCHA and NPCPA peptides

¹H NMR of **1a** on 400 MHz at 298 K in CDCl₃
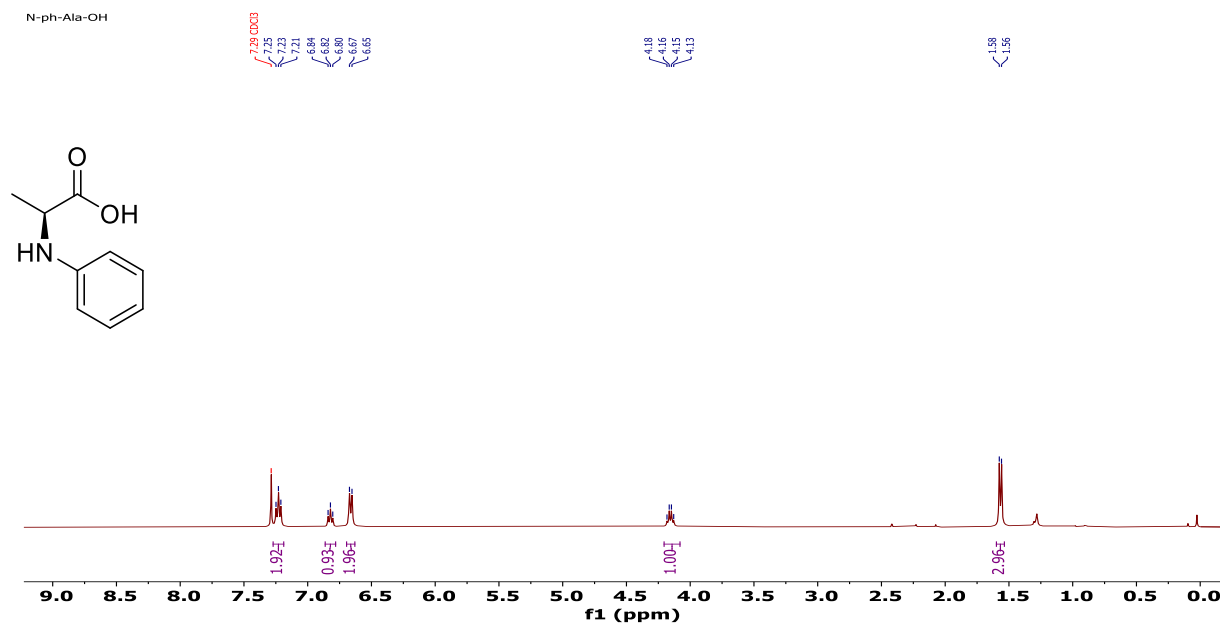
¹³C NMR of **1a** on 500 MHz at 298 K in CDCl₃

96
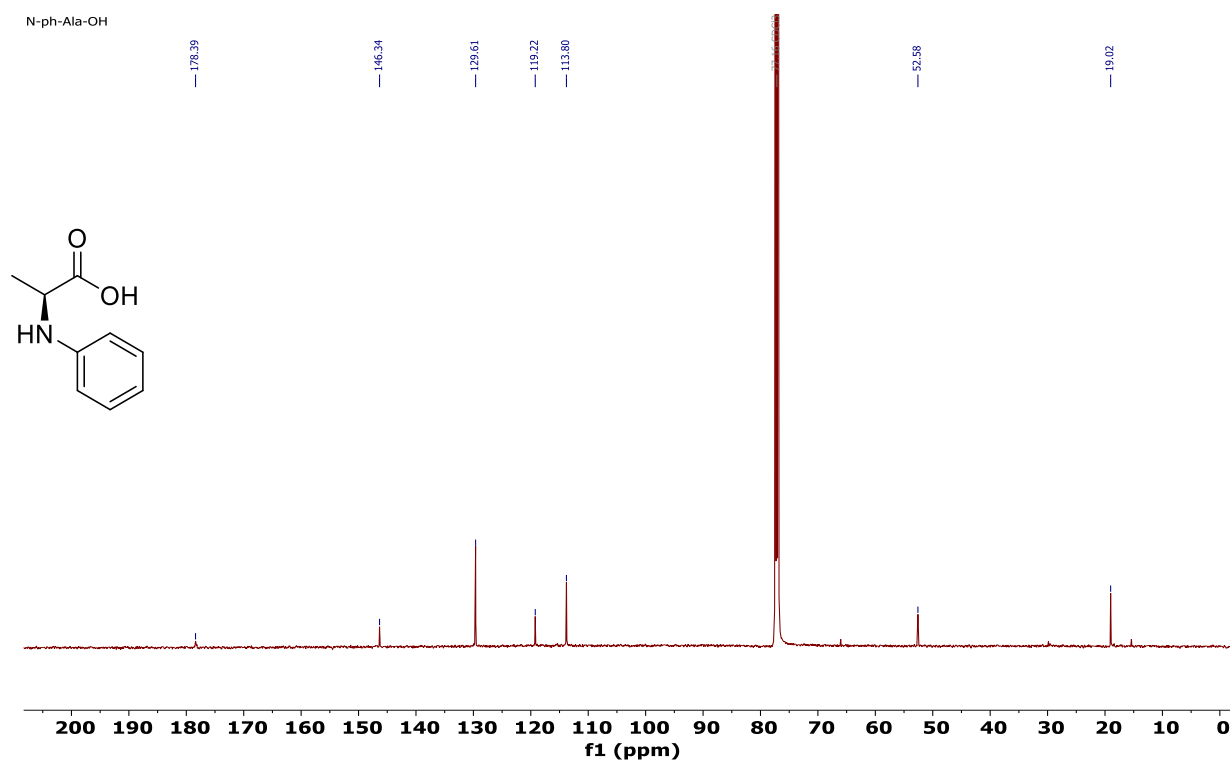
^{1}H NMR of **2a** on 500 MHz at 298 K in CDCl$_3$
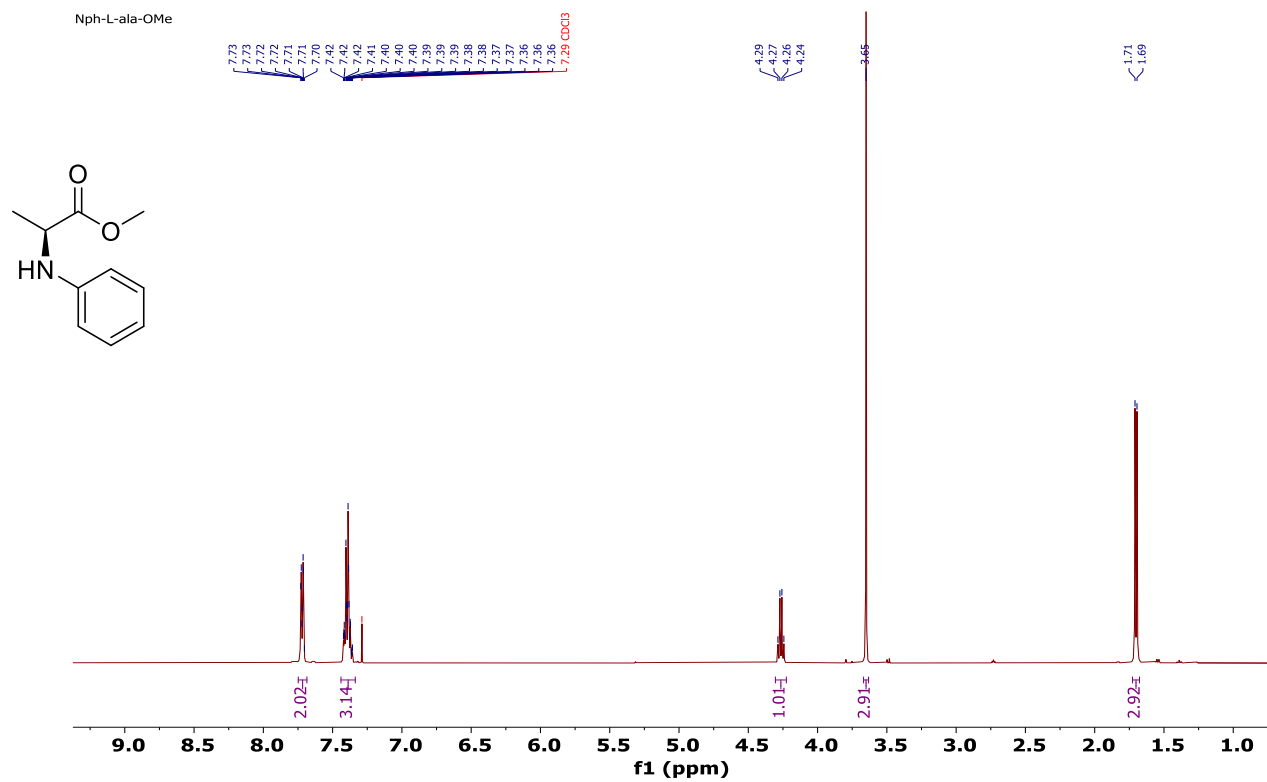
Nph-L-ala-OMe

^{13}C NMR of **2a** on 500 MHz at 298 K in CDCl$_3$
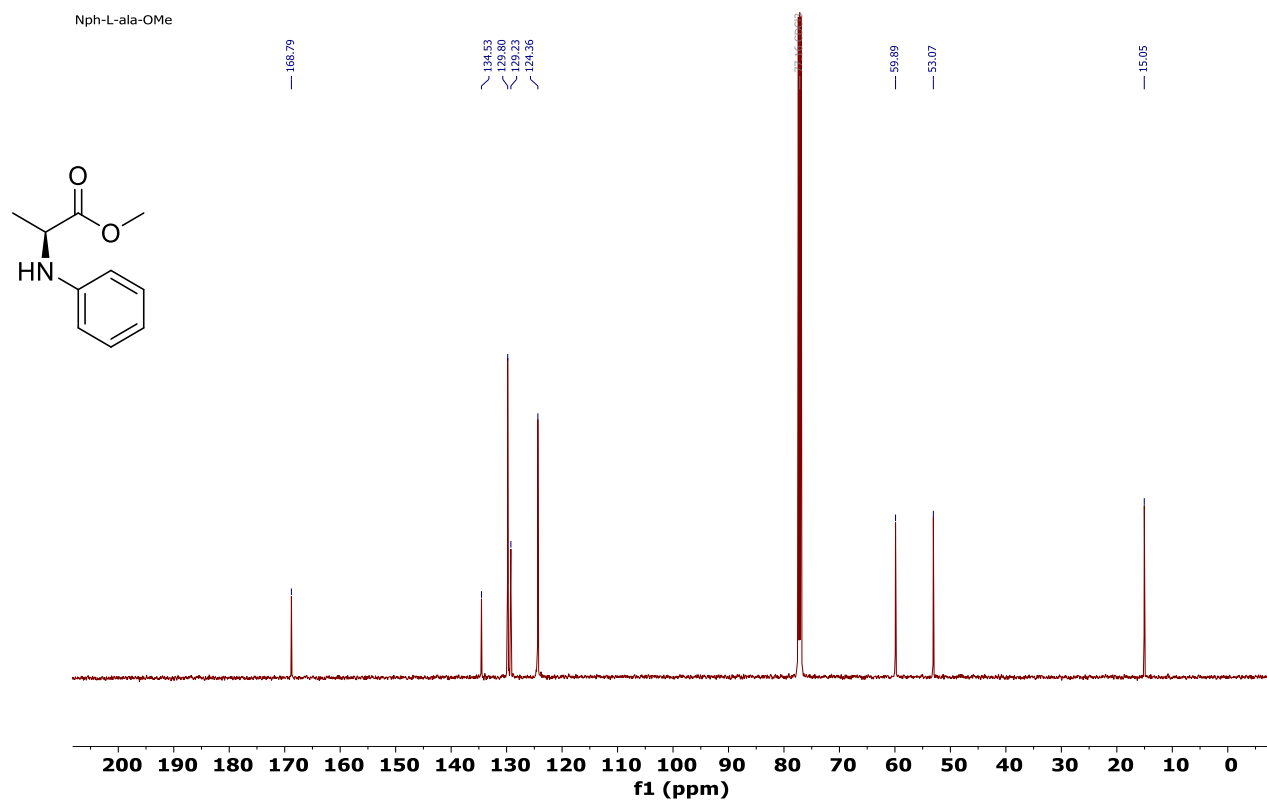
Nph-L-ala-OMe

¹H NMR of **2b** on 500 MHz at 298 K in CDCl₃
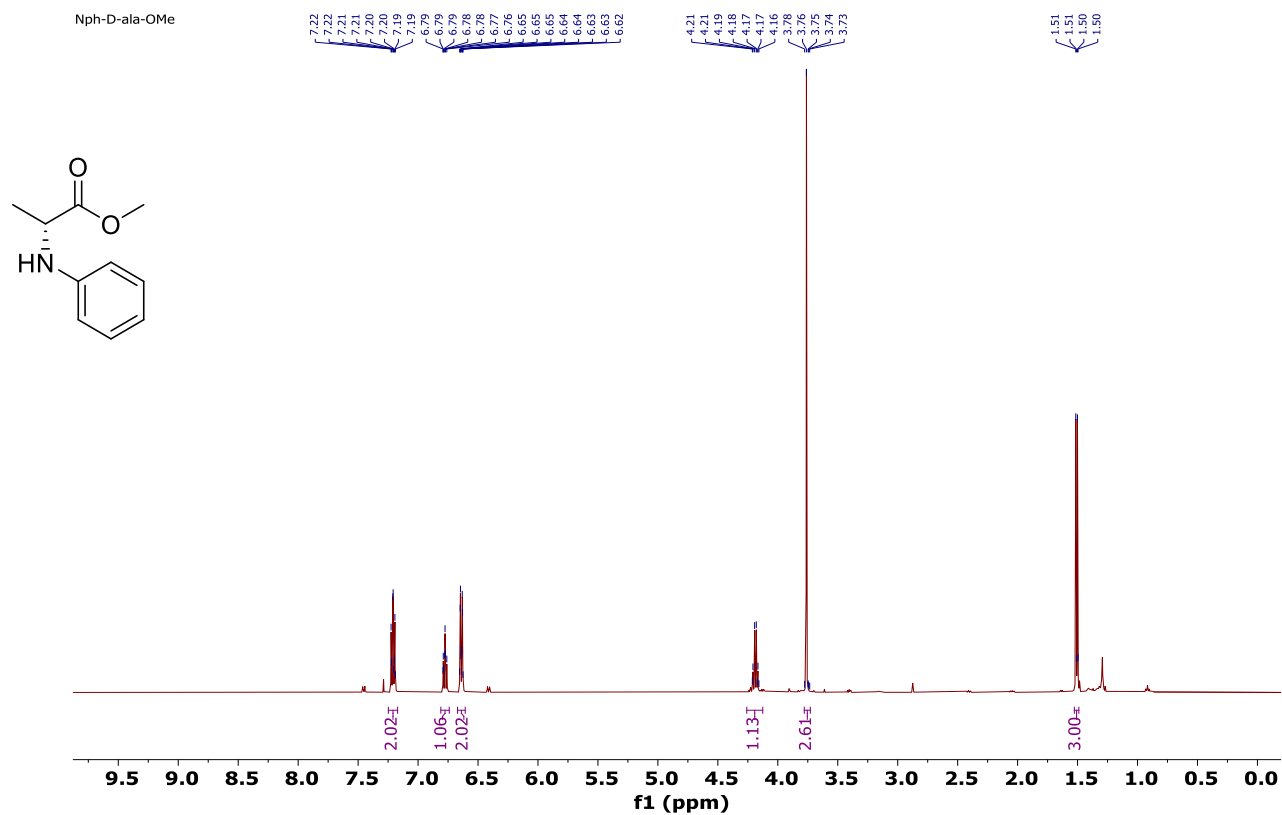
Nph-D-ala-OMe

7.22, 7.22, 7.21, 7.21, 7.20, 7.20, 7.19, 6.79, 6.79, 6.79, 6.78, 6.77, 6.76, 6.65, 6.65, 6.64, 6.64, 6.63, 6.63, 6.62

4.21, 4.21, 4.19, 4.18, 4.17, 4.17, 4.16, 3.78, 3.76, 3.75, 3.74, 3.73

1.51, 1.51, 1.50, 1.50

2.02, 1.06, 2.02, 1.13, 2.61, 3.00

f1 (ppm)

¹³C NMR of **2b** on 500 MHz at 298 K in CDCl₃

Nph-D-ala-OMe

175.24, 146.64, 129.45, 118.42, 113.44, 77.16 CDCl3, 52.34, 52.01, 19.06

f1 (ppm)

^{1}H NMR of **3a** on 500 MHz at 298 K in CDCl$_3$.

Fmoc-A-A-Ph-Ome
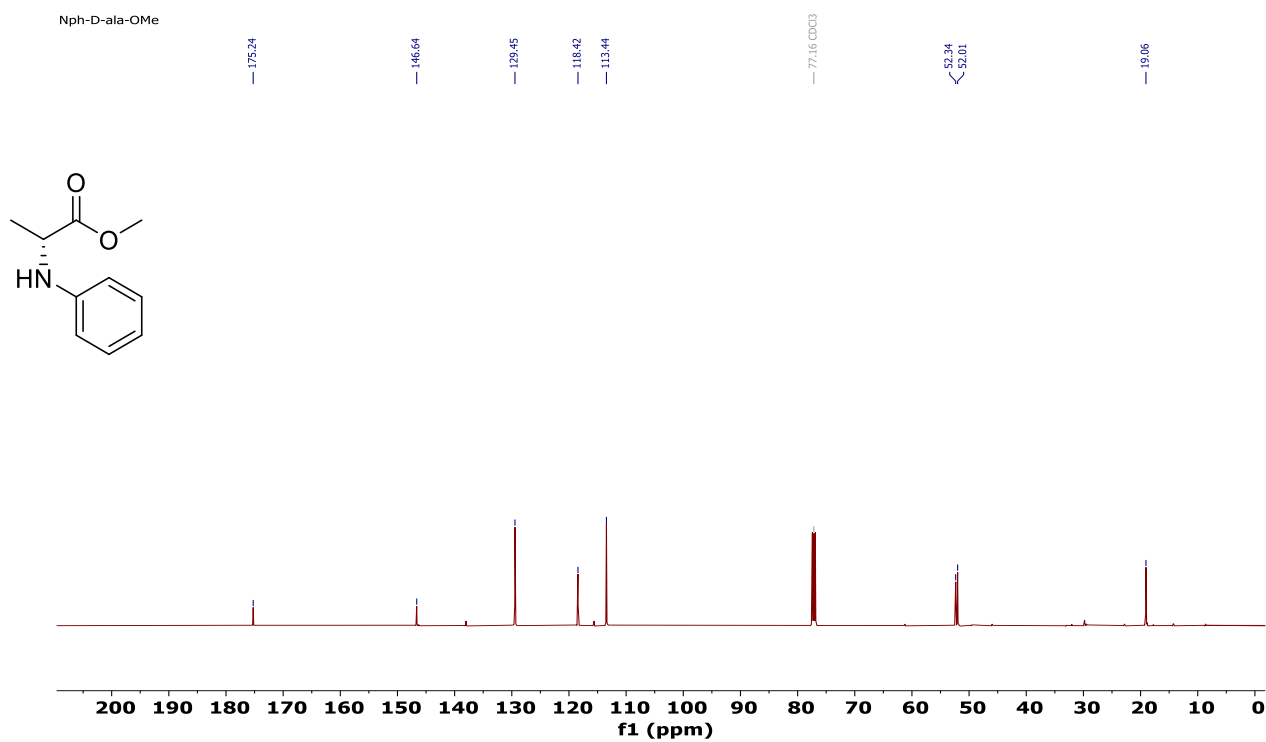
^{13}C NMR of **3a** on 500 MHz at 298 K in CDCl$_3$.

Fmoc-A-A-Ph-Ome
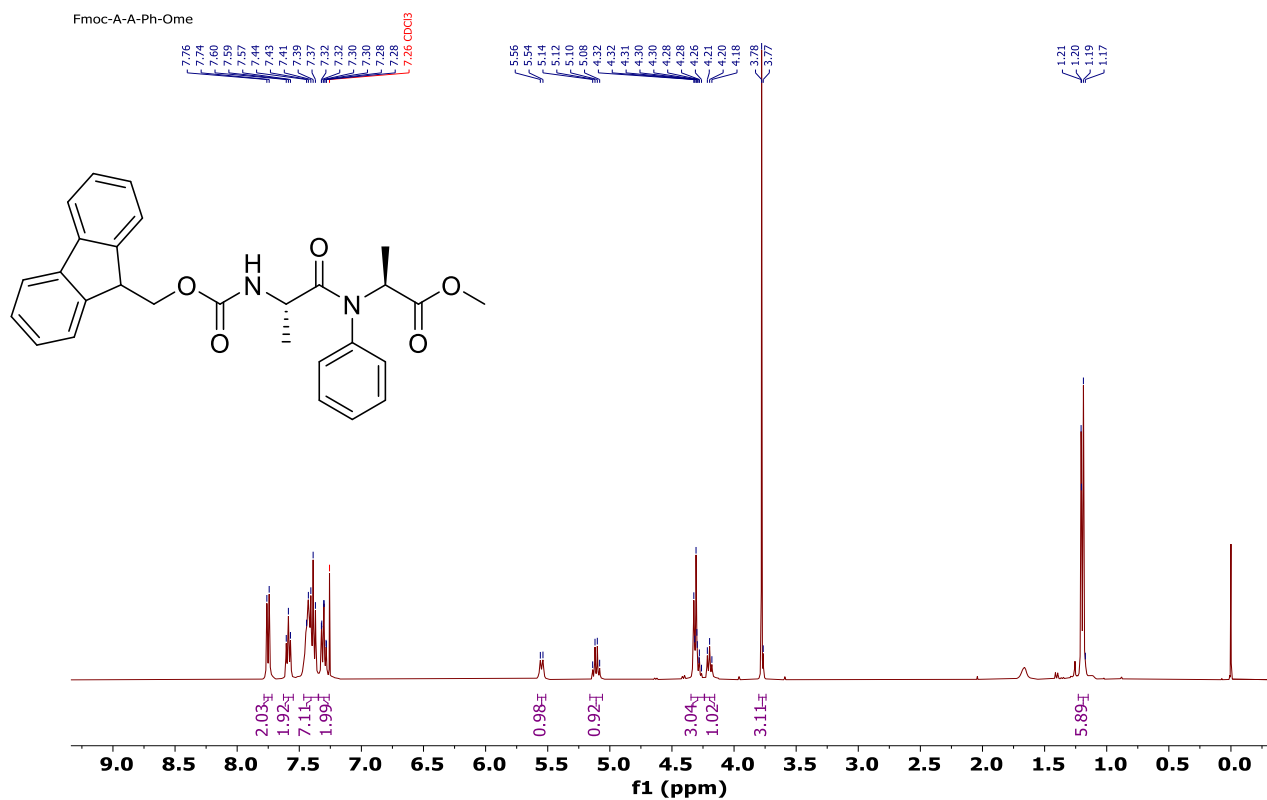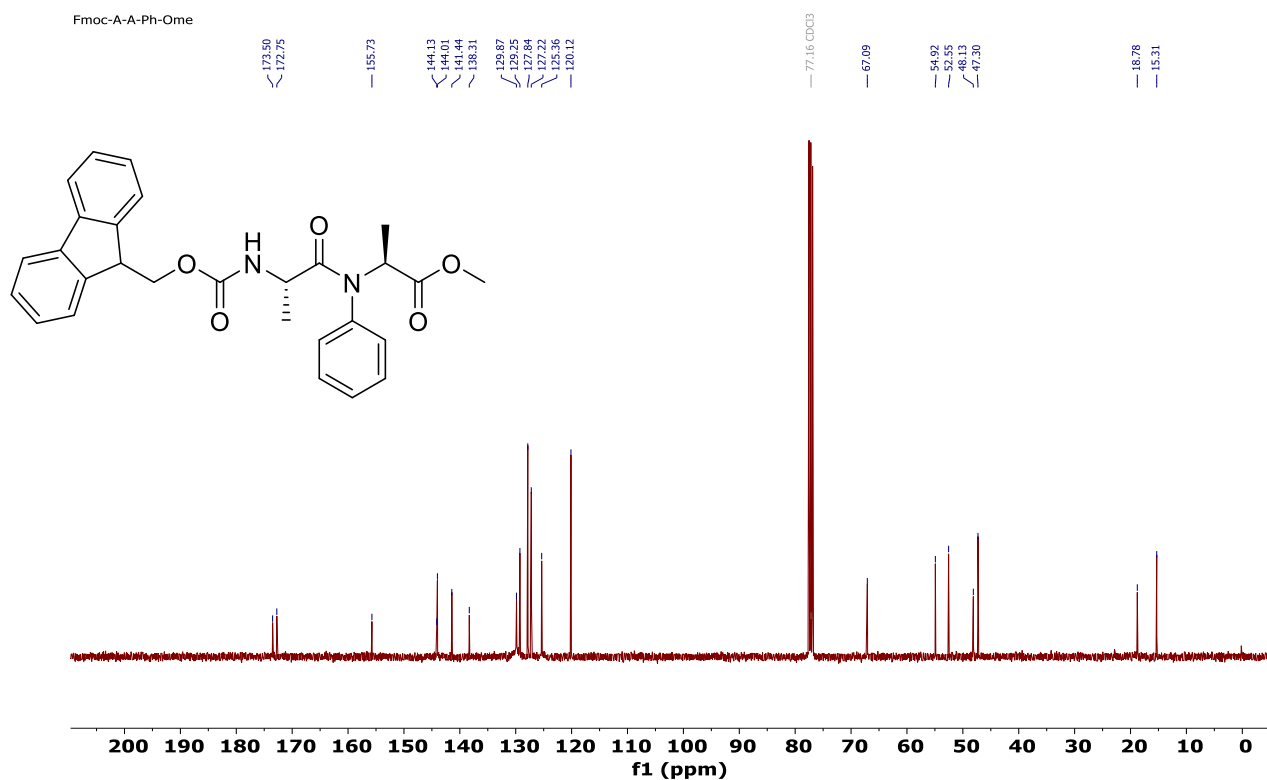
^{1}H NMR of **3b** on 500 MHz at 298 K in CDCl$_3$.

Fmoc-a-A-Ph-OMe
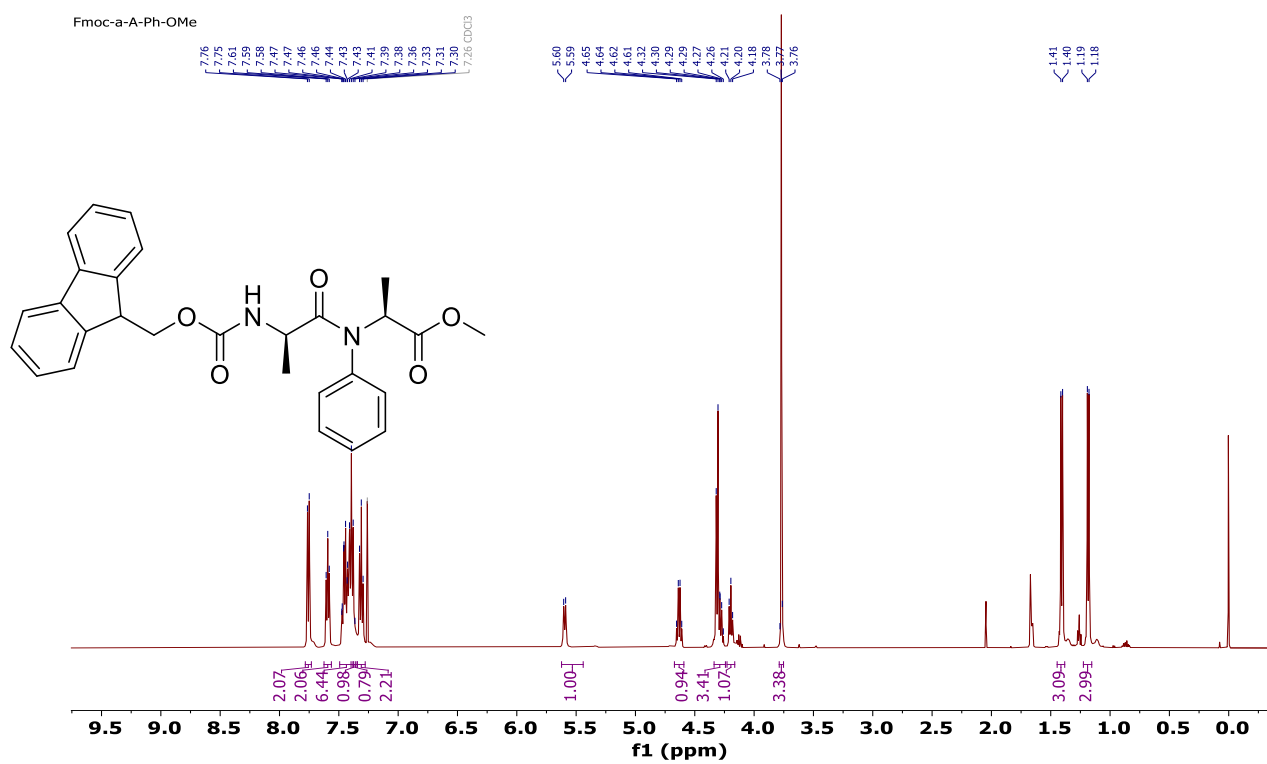
^{13}C NMR of **3b** on 500 MHz at 298 K in CDCl$_3$.

Fmoc-a-A-Ph-OMe
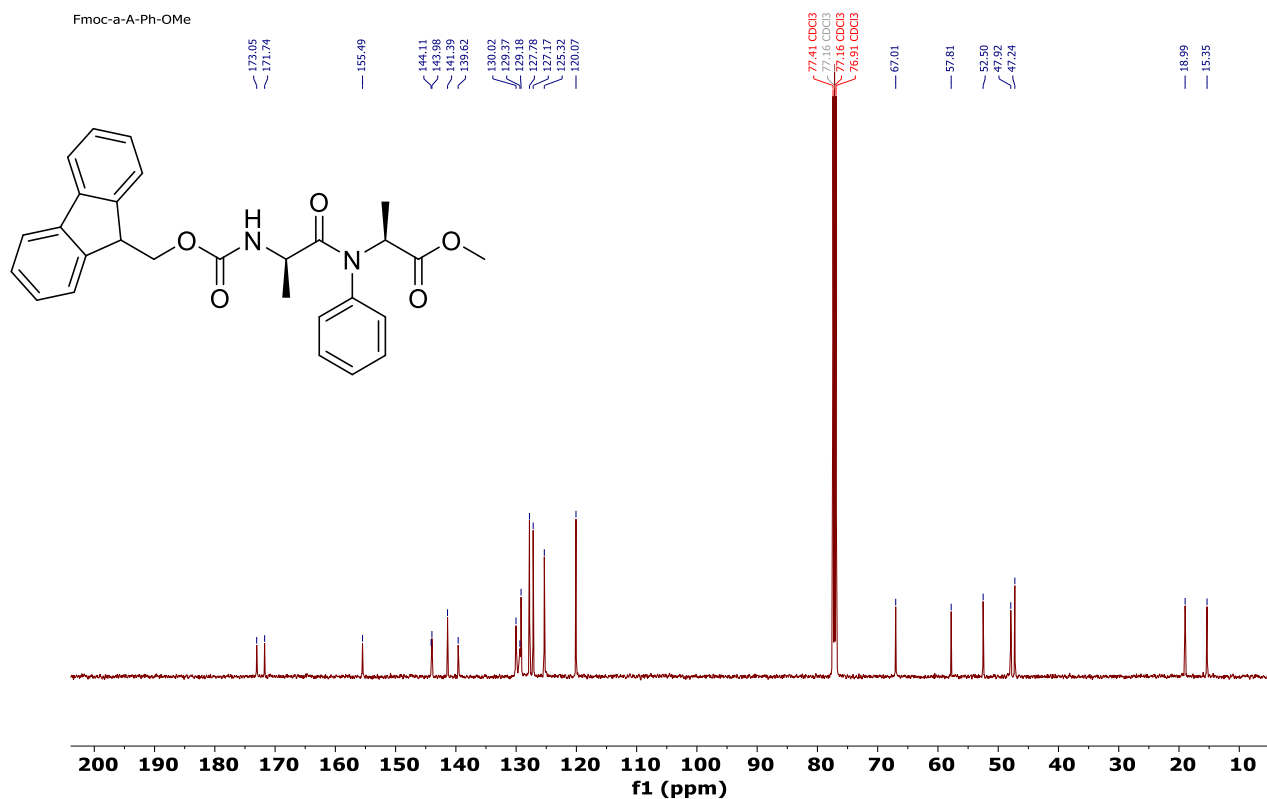
¹H NMR of **3c** on 500 MHz at 298 K in CDCl₃.
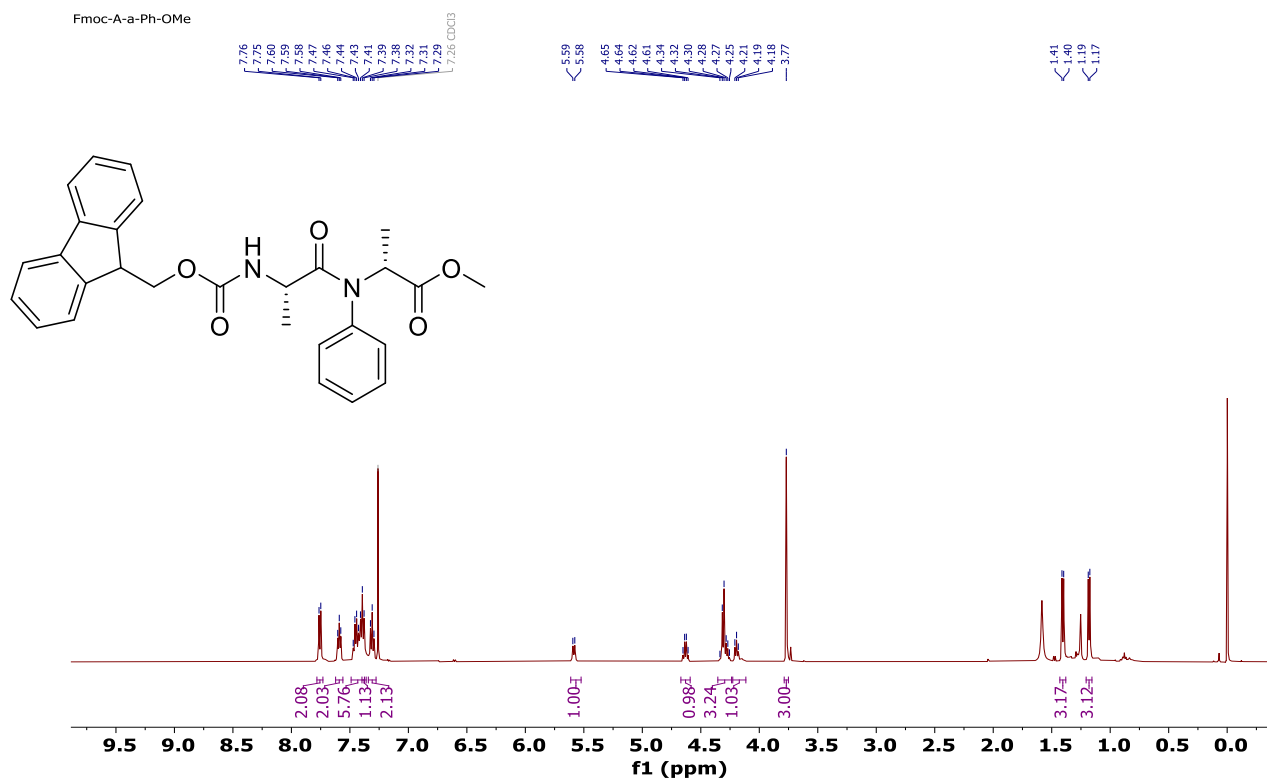
¹³C NMR of **3c** on 500 MHz at 298 K in CDCl₃.
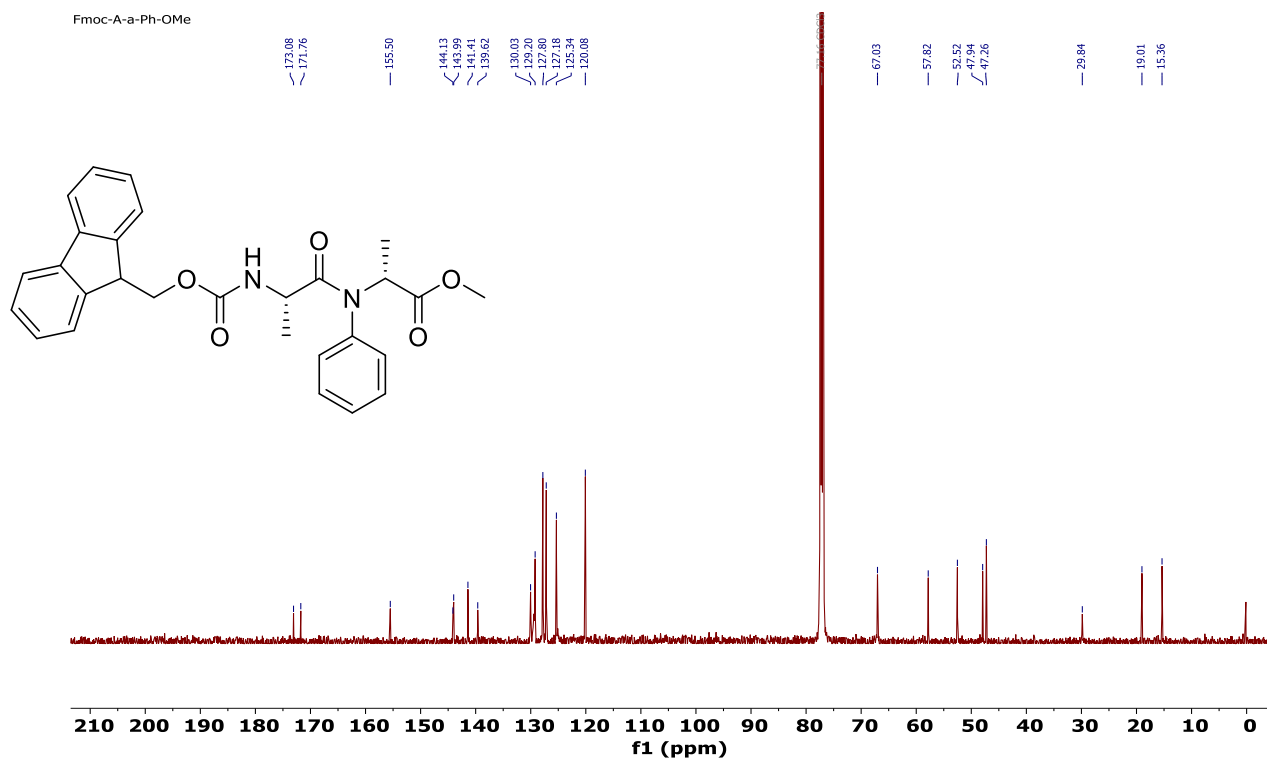
¹H NMR of **4a** on 500 MHz at 298 K in CDCl₃.

Fmoc-A-A-Ph-OH
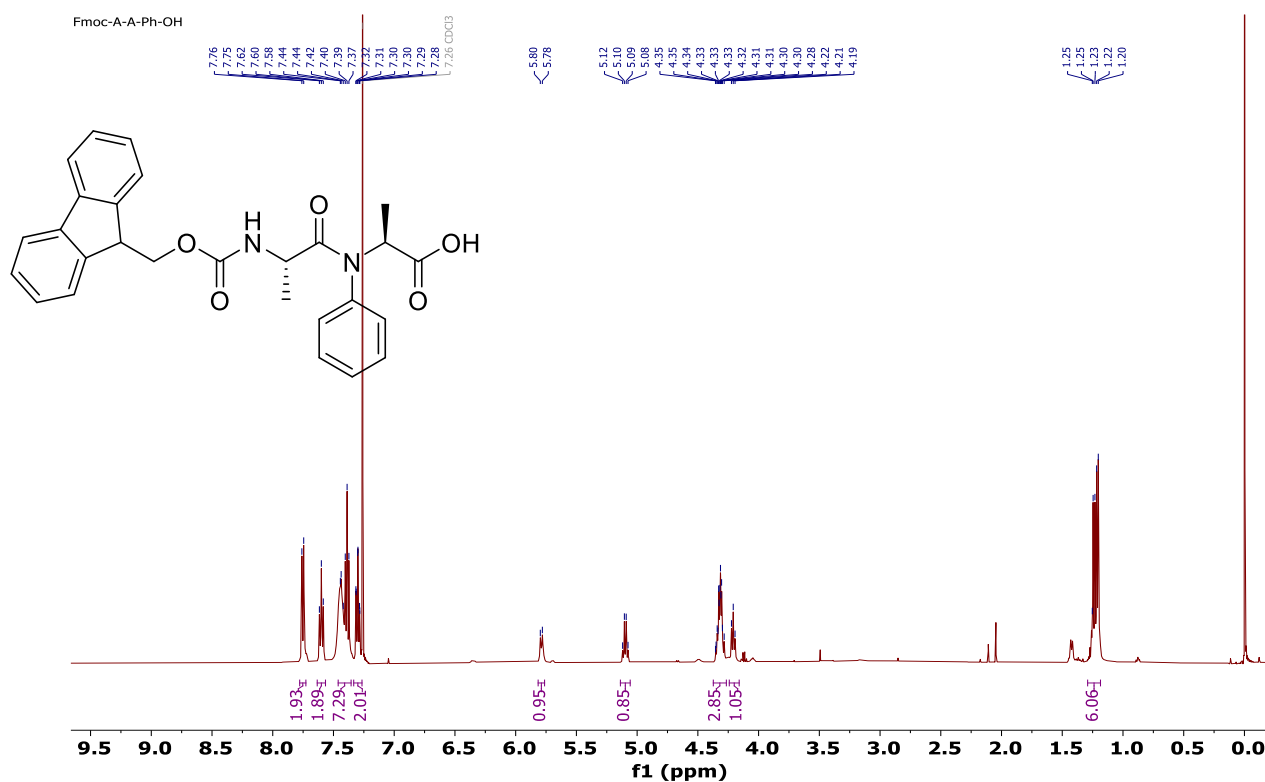
¹³C NMR of **4a** on 500 MHz at 298 K in CDCl₃.

Fmoc-A-A-Ph-OH
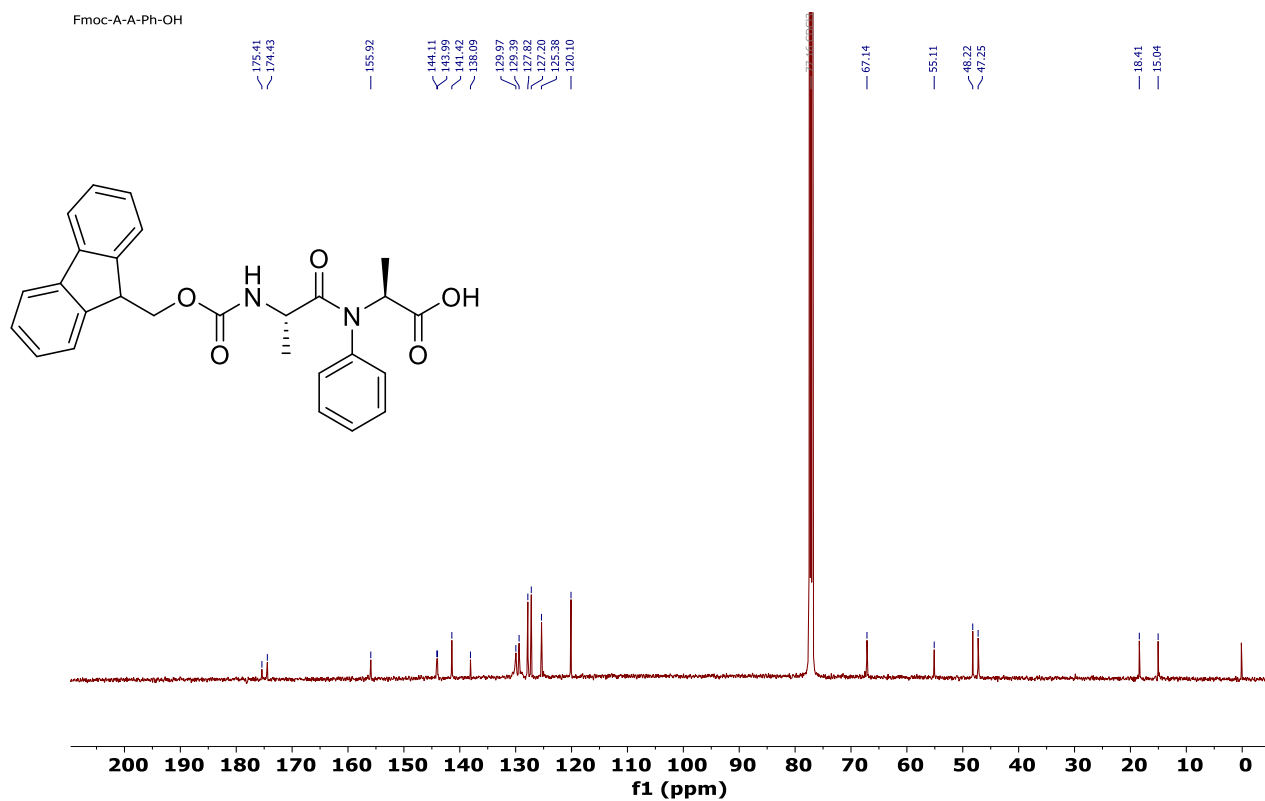
^{1}H NMR of **4b** on 500 MHz at 298 K in CDCl$_3$.
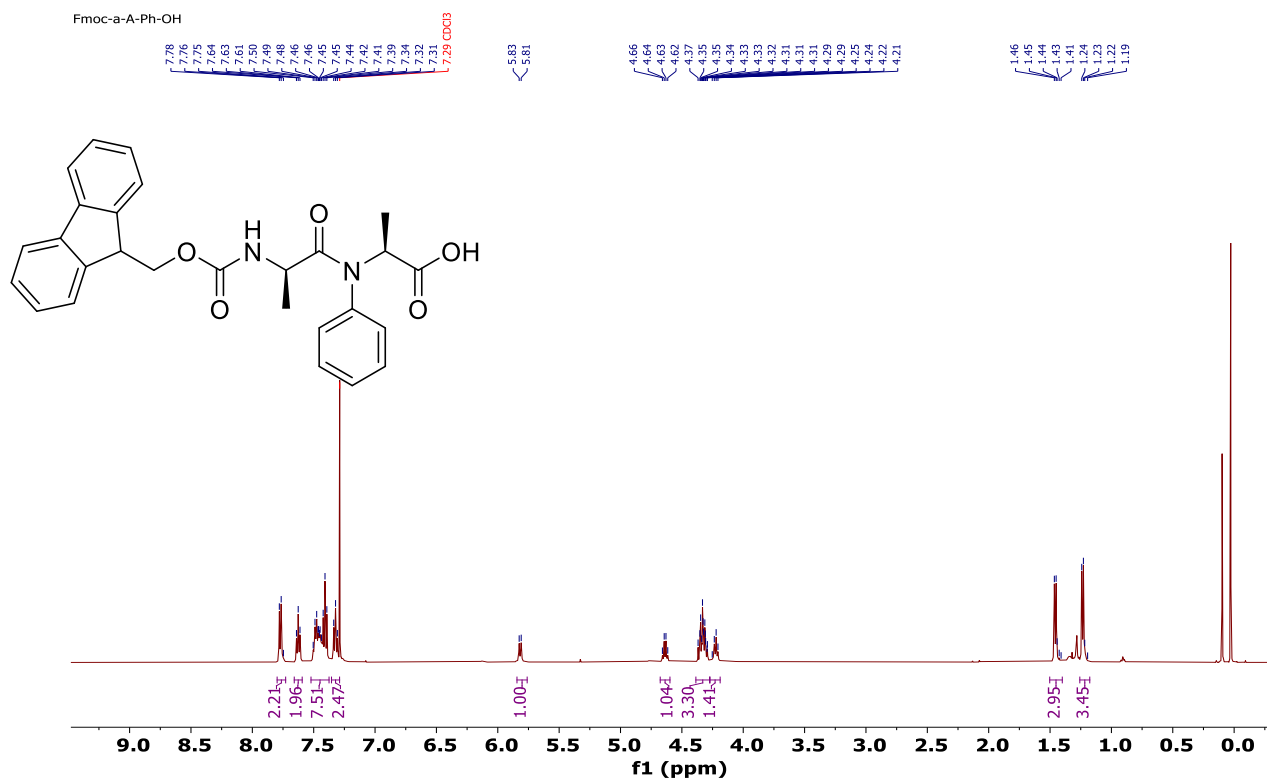
^{13}C NMR of **4b** on 500 MHz at 298 K in CDCl$_3$.
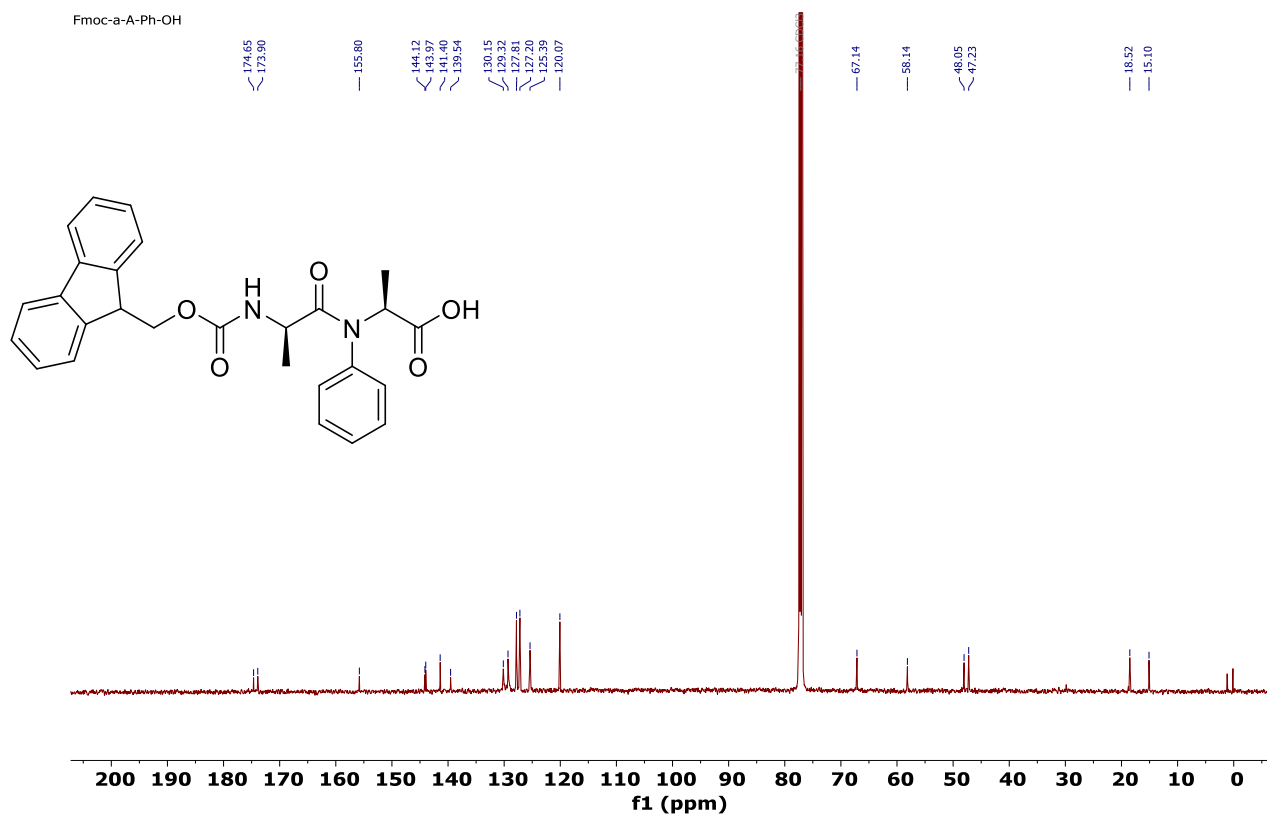
^{1}H NMR of **4c** on 500 MHz at 298 K in CDCl$_3$.

Fmoc-A-a-Ph-OH
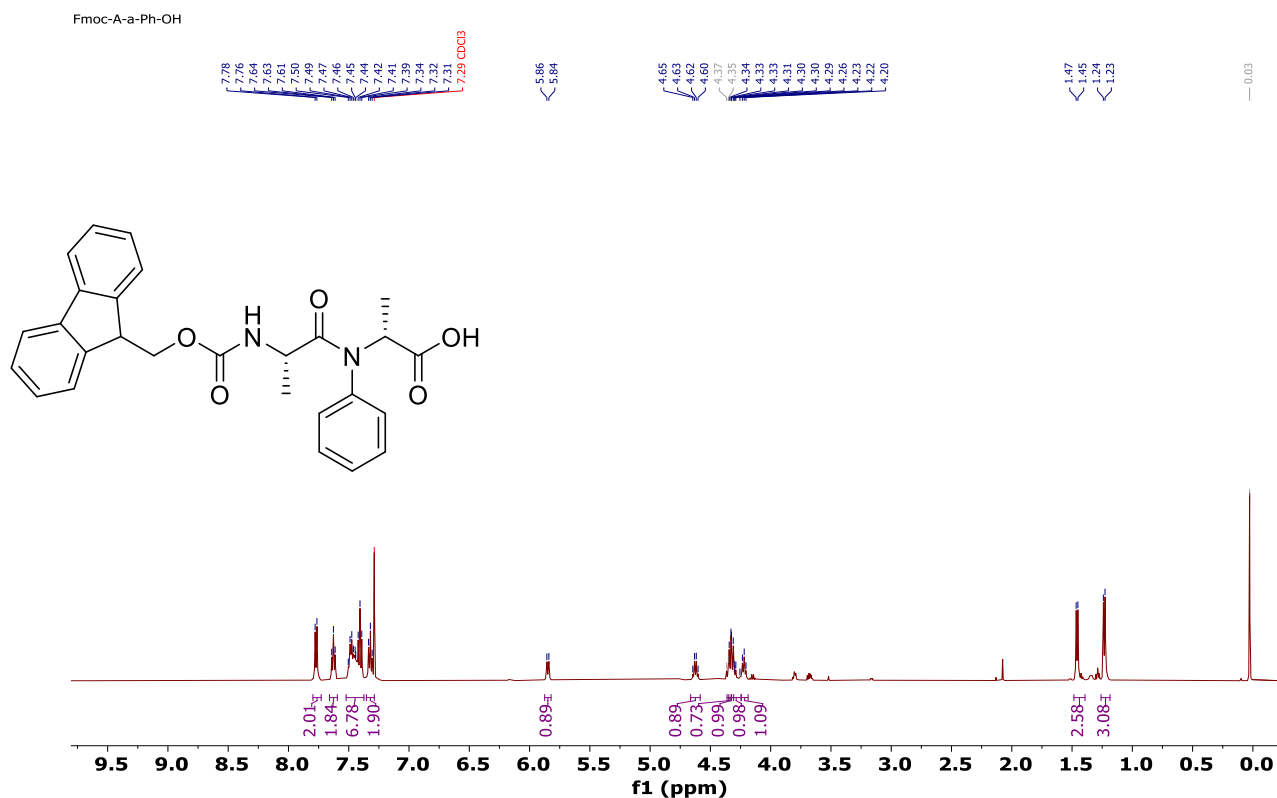
^{13}C NMR of **4c** on 500 MHz at 298 K in CDCl$_3$.

Fmoc-A-a-Ph-OH
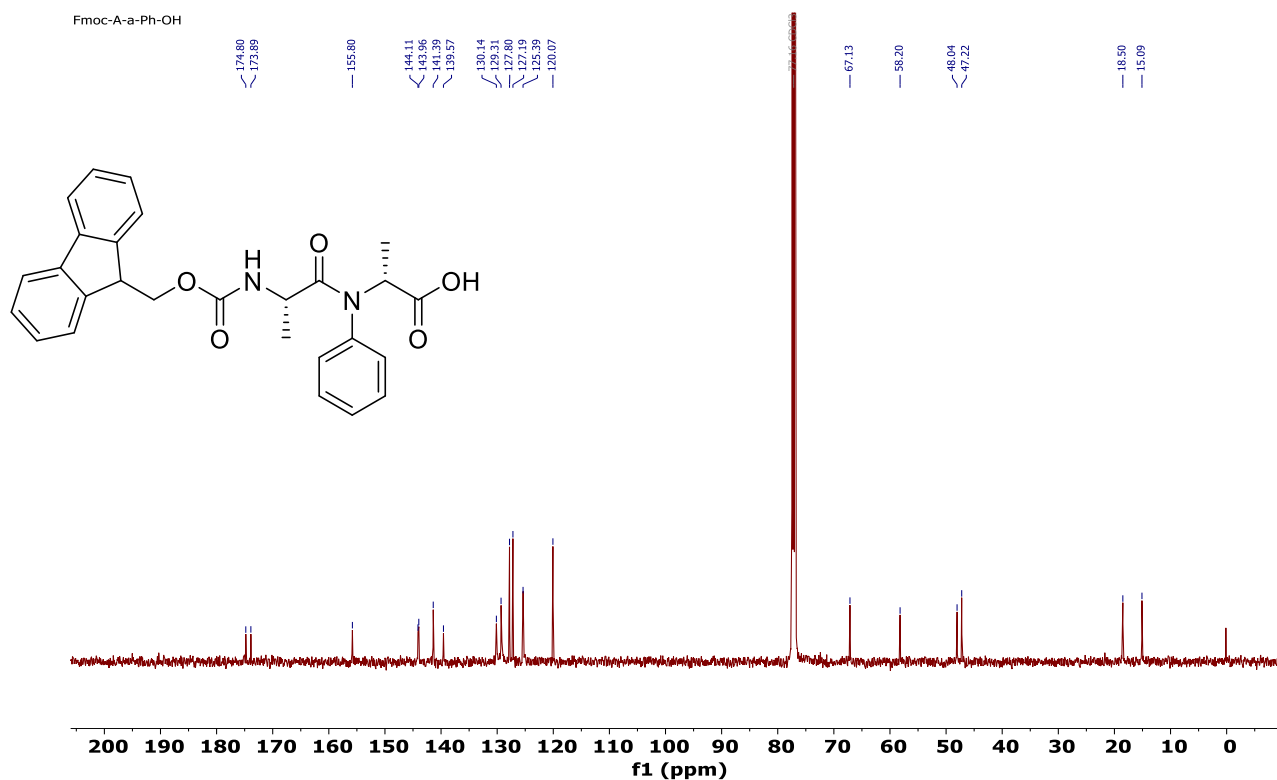
^{1}H NMR of **1NPCHA** on 500 MHz at 298 K in DMSO-d_6.
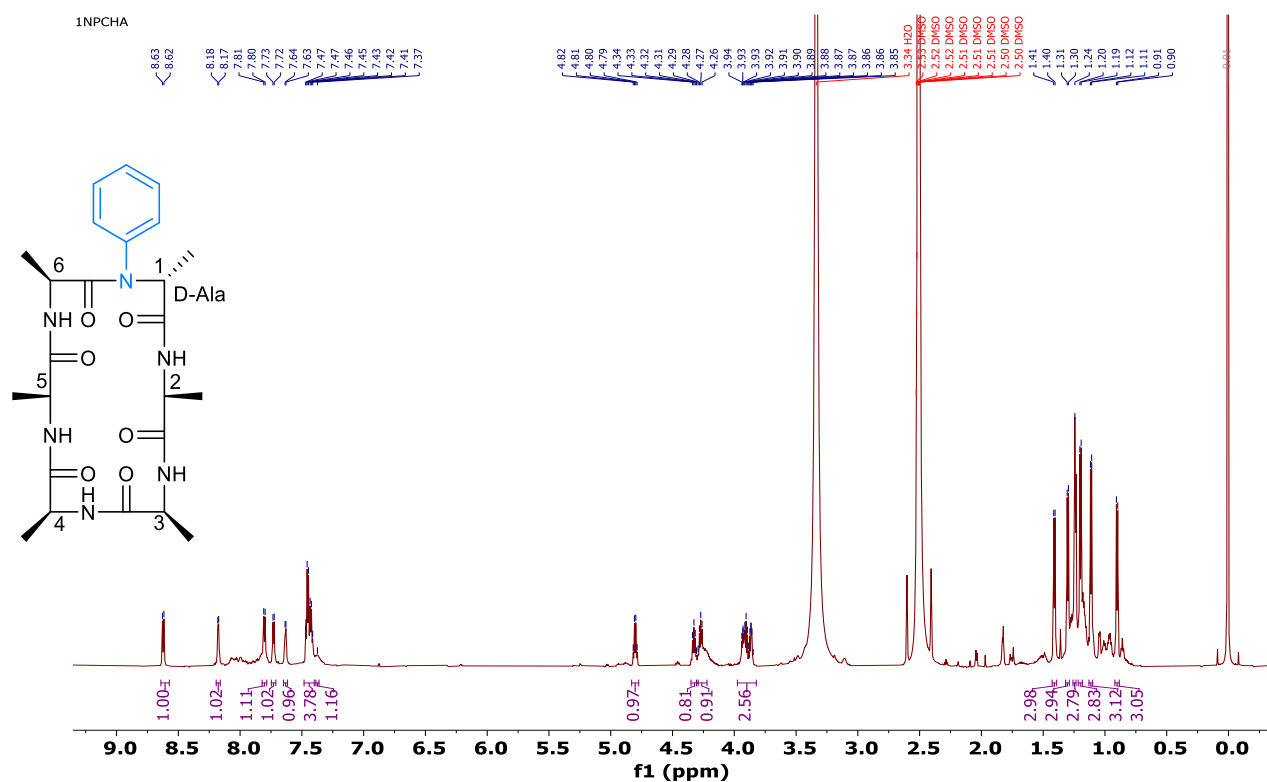
^{1}H NMR of **2NPCHA** on 500 MHz at 298 K in DMSO-d_6.

^{1}H NMR of **3NPCHA** on 500 MHz at 298 K in DMSO-*d*$_6$.

^{1}H NMR of **4NPCHA** on 500 MHz at 298 K in DMSO-*d*$_6$.
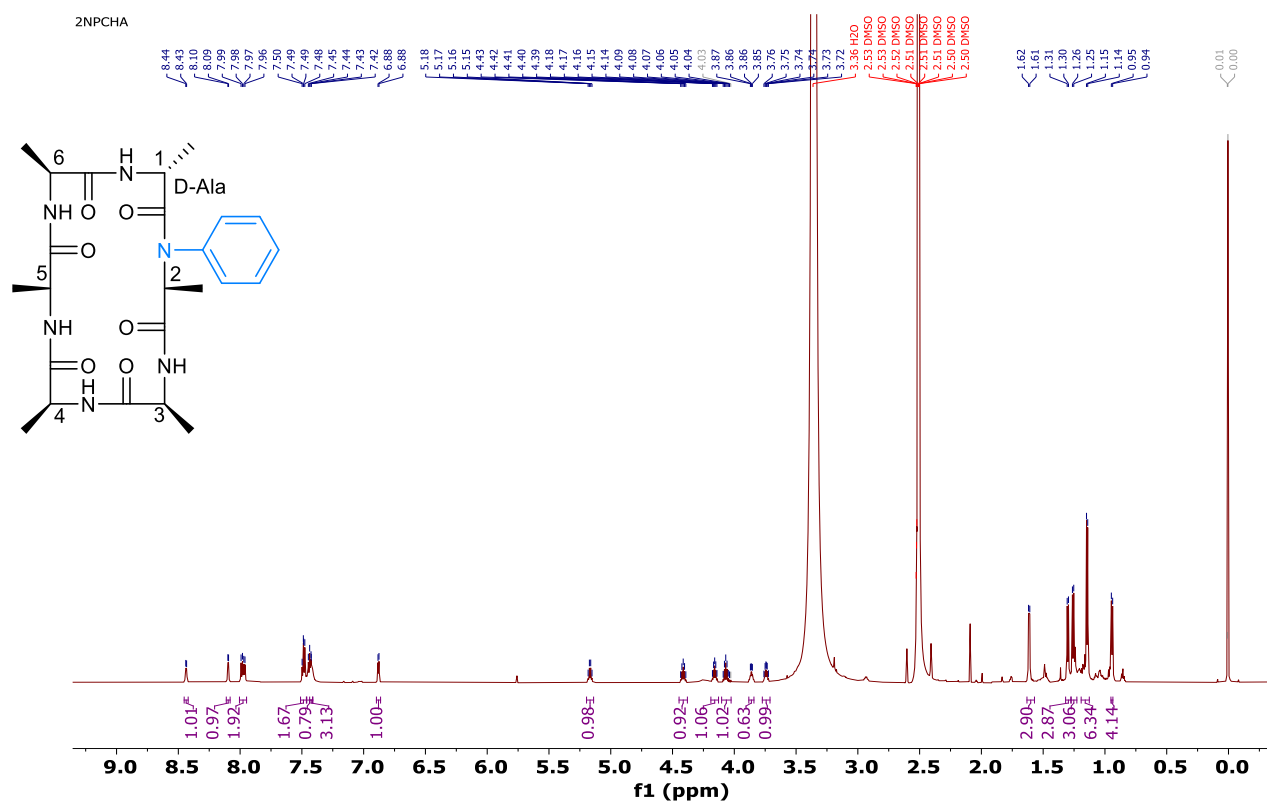
^{1}H NMR of **5NPCHA** on 500 MHz at 298 K in DMSO-d_6.
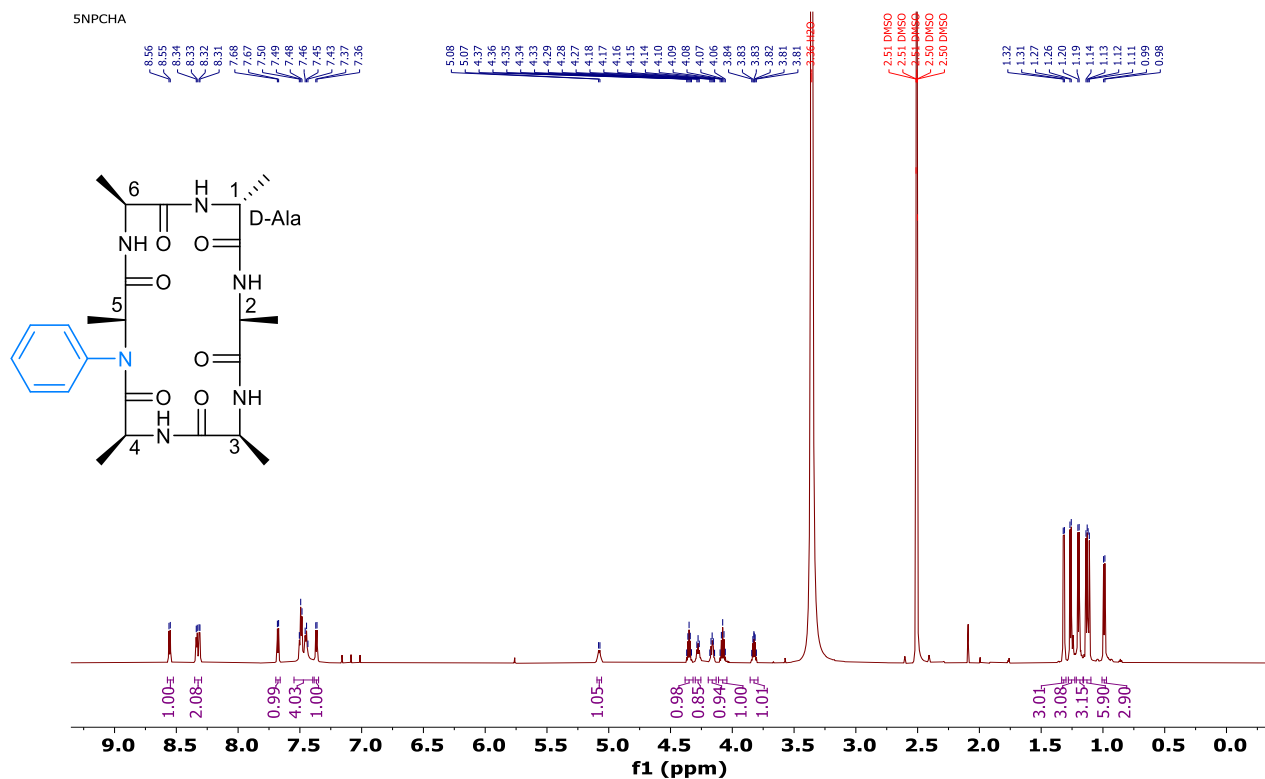
^{1}H NMR of **6NPCHA** on 500 MHz at 298 K in DMSO-d_6.
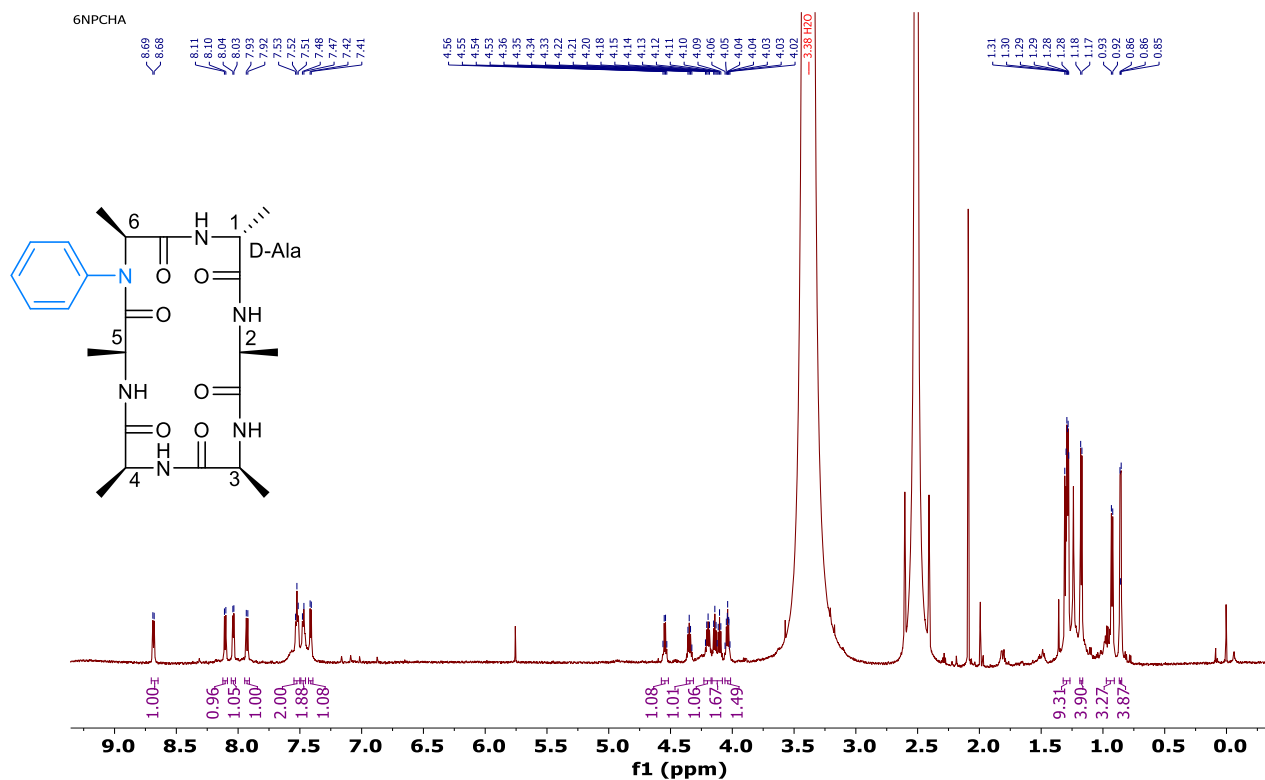
¹H NMR of **13NPCHA** on 500 MHz at 298 K in DMSO-*d*₆.
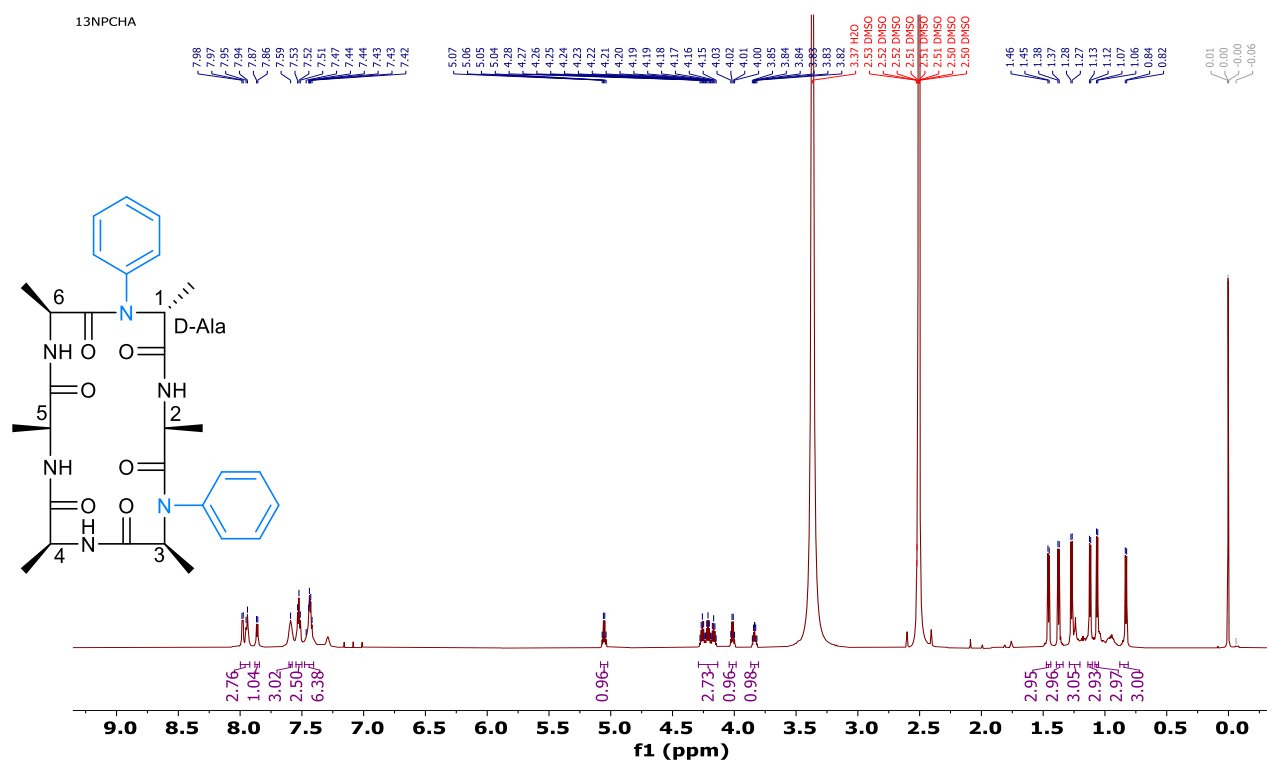
¹H NMR of **14NPCHA** on 500 MHz at 298 K in DMSO-*d*₆.
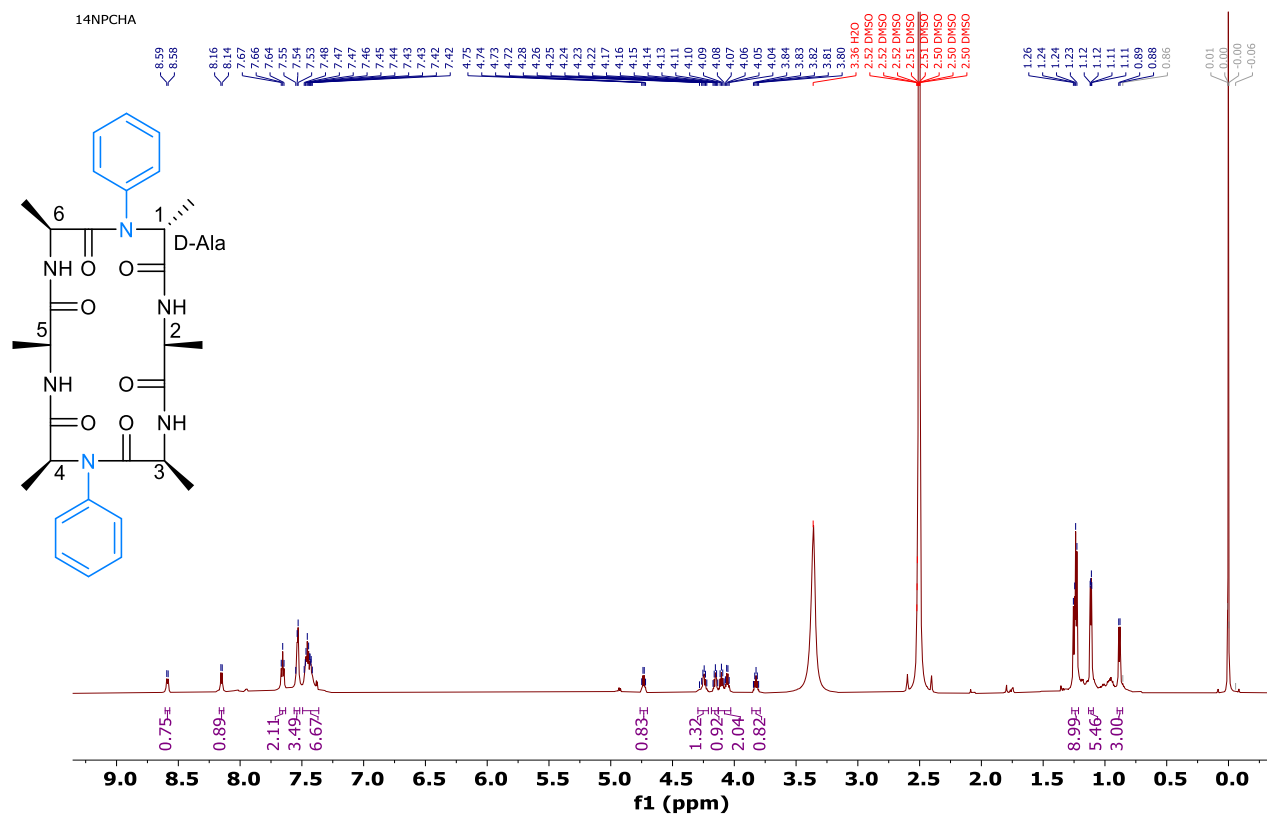
^{1}H NMR of **15NPCHA** on 500 MHz at 298 K in DMSO-d_6.
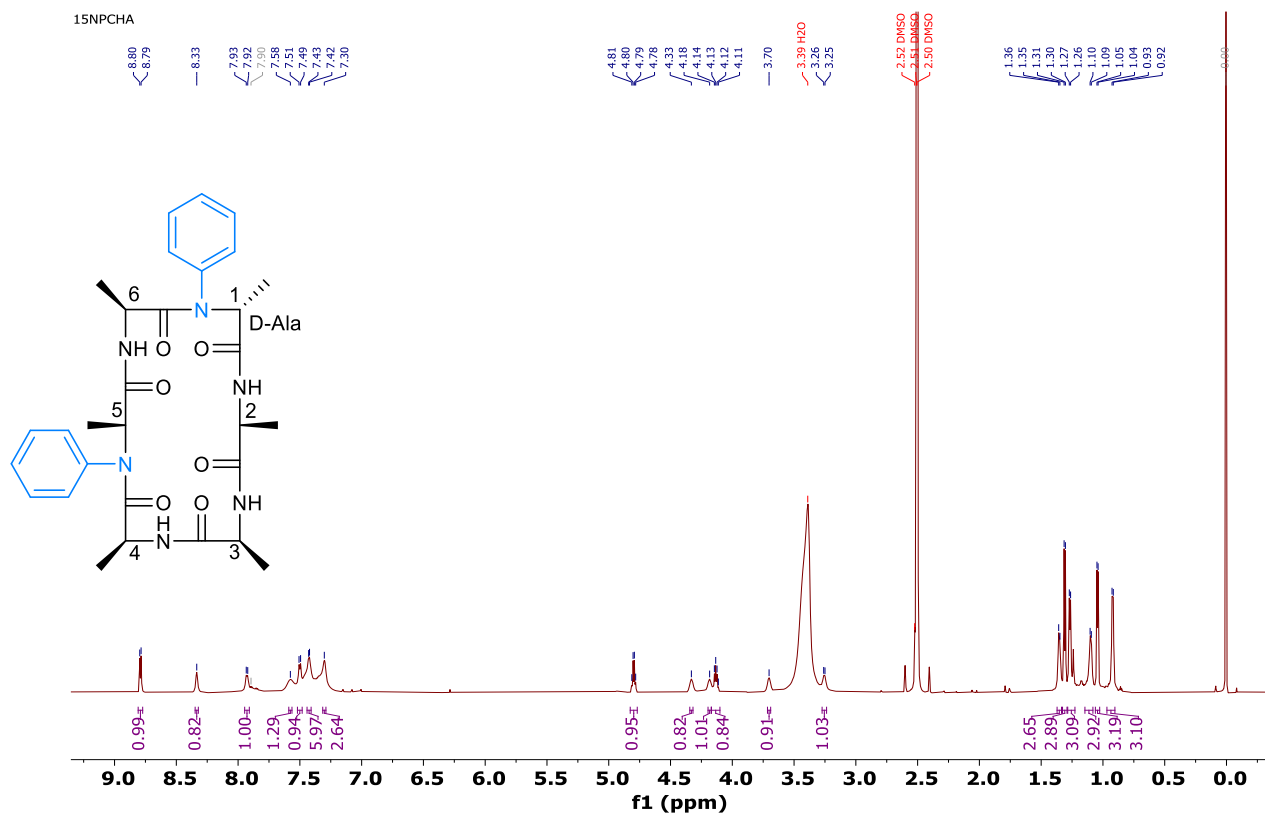
^{1}H NMR of **24NPCHA** on 500 MHz at 298 K in DMSO-d_6.
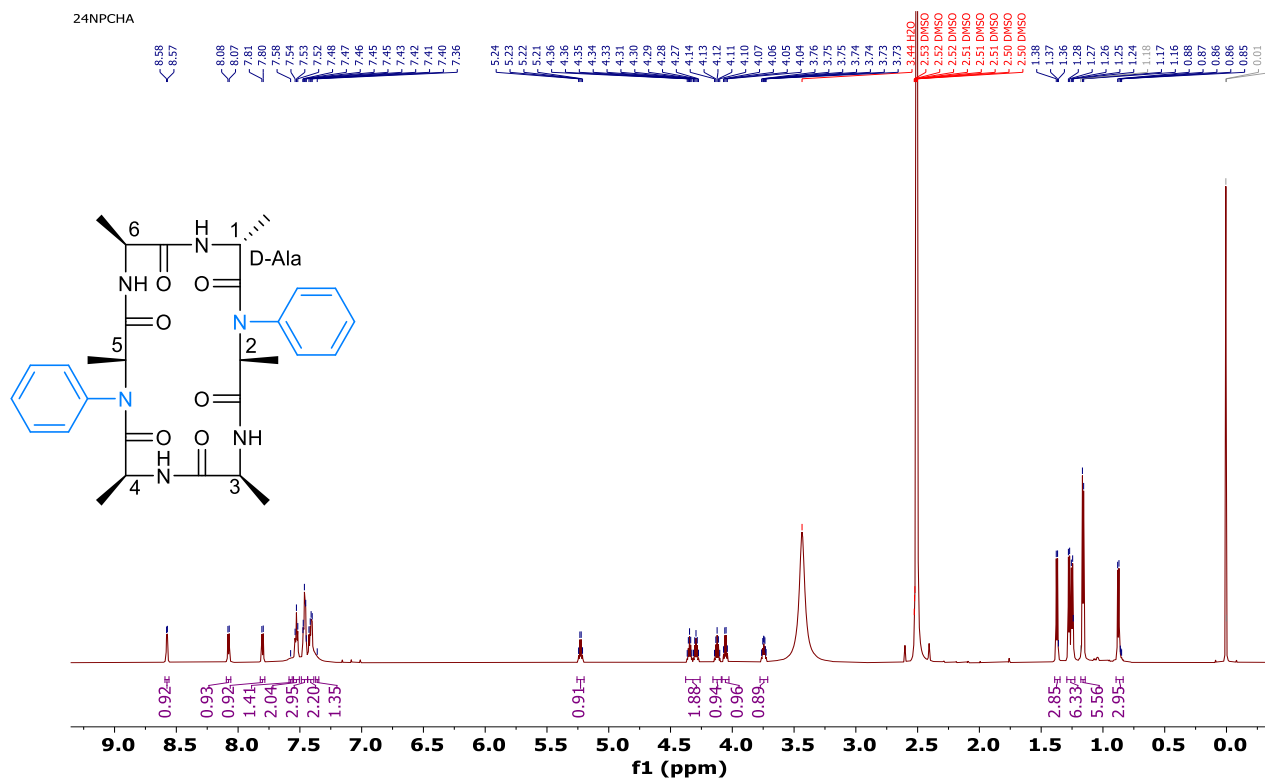
¹H NMR of **25NPCHA** on 500 MHz at 298 K in DMSO-*d₆*.
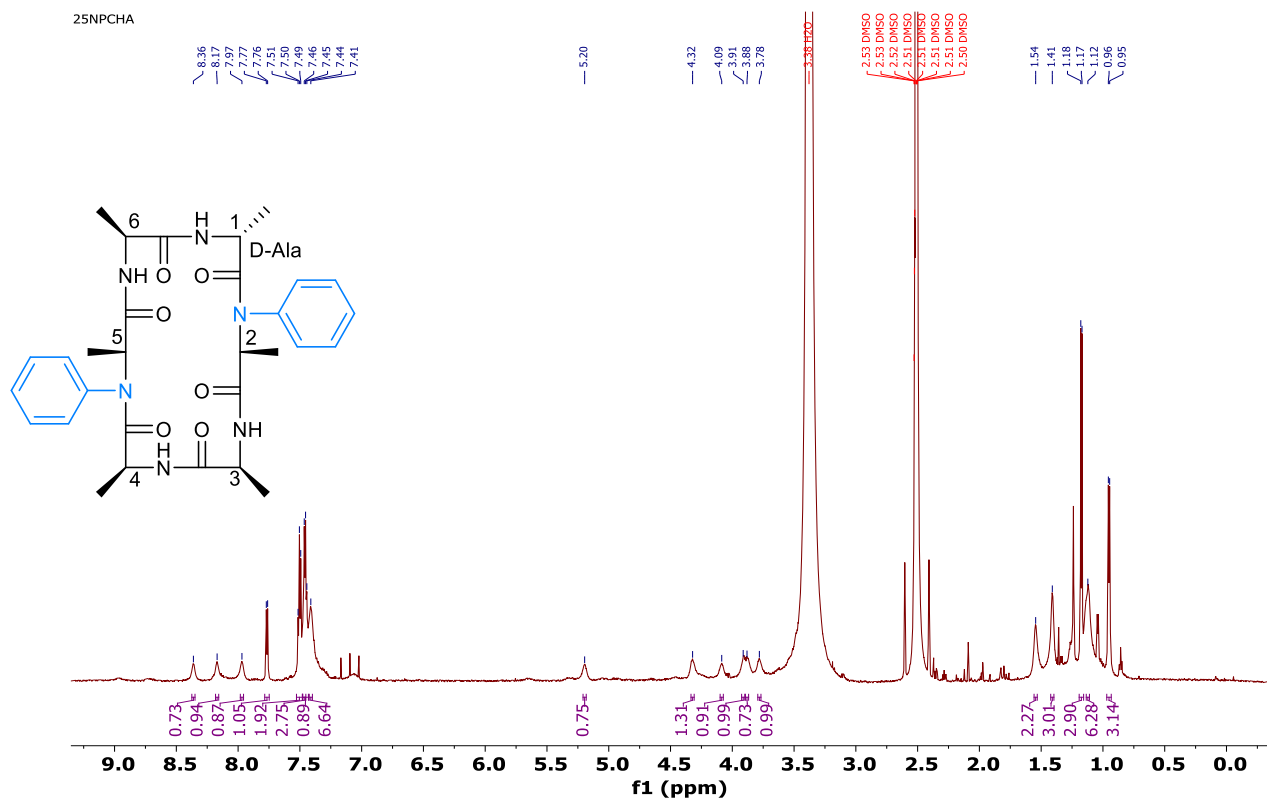
¹H NMR of **26NPCHA** on 500 MHz at 298 K in DMSO-*d₆*.
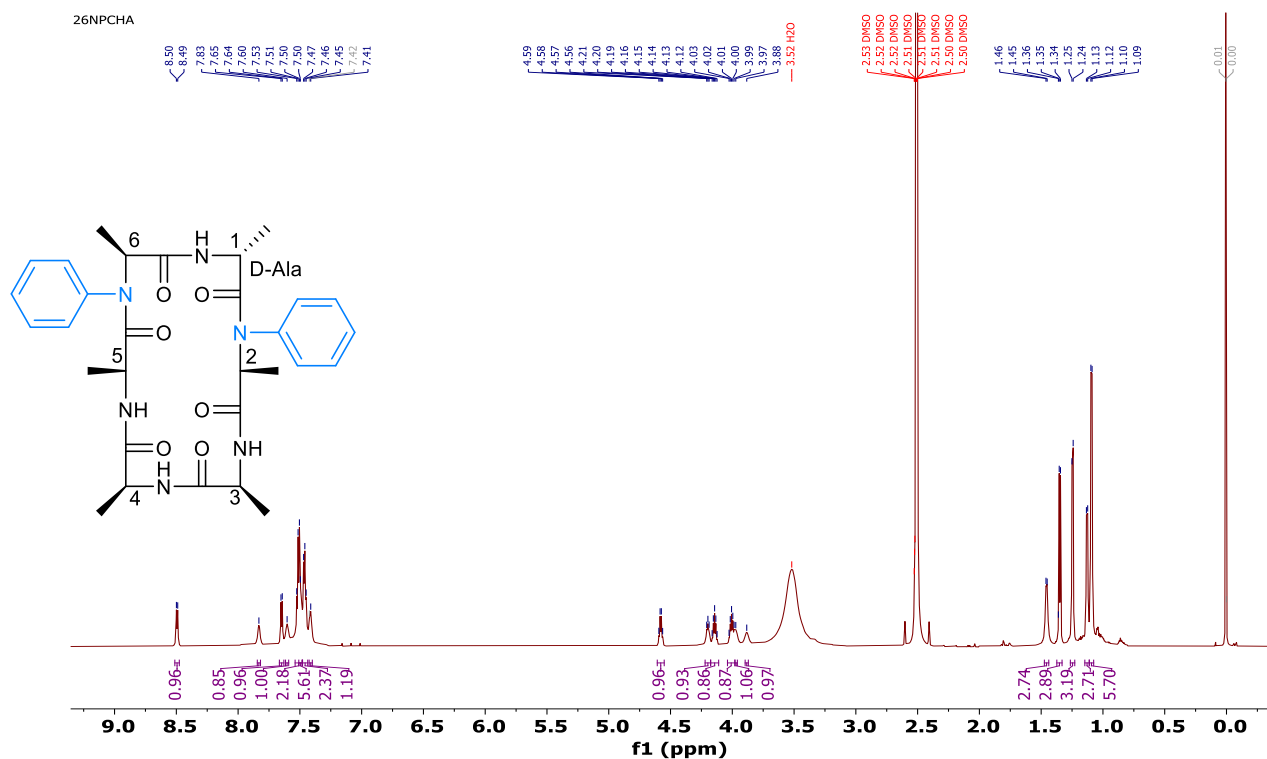
^{1}H NMR of **35NPCHA** on 500 MHz at 298 K in DMSO-d_6.
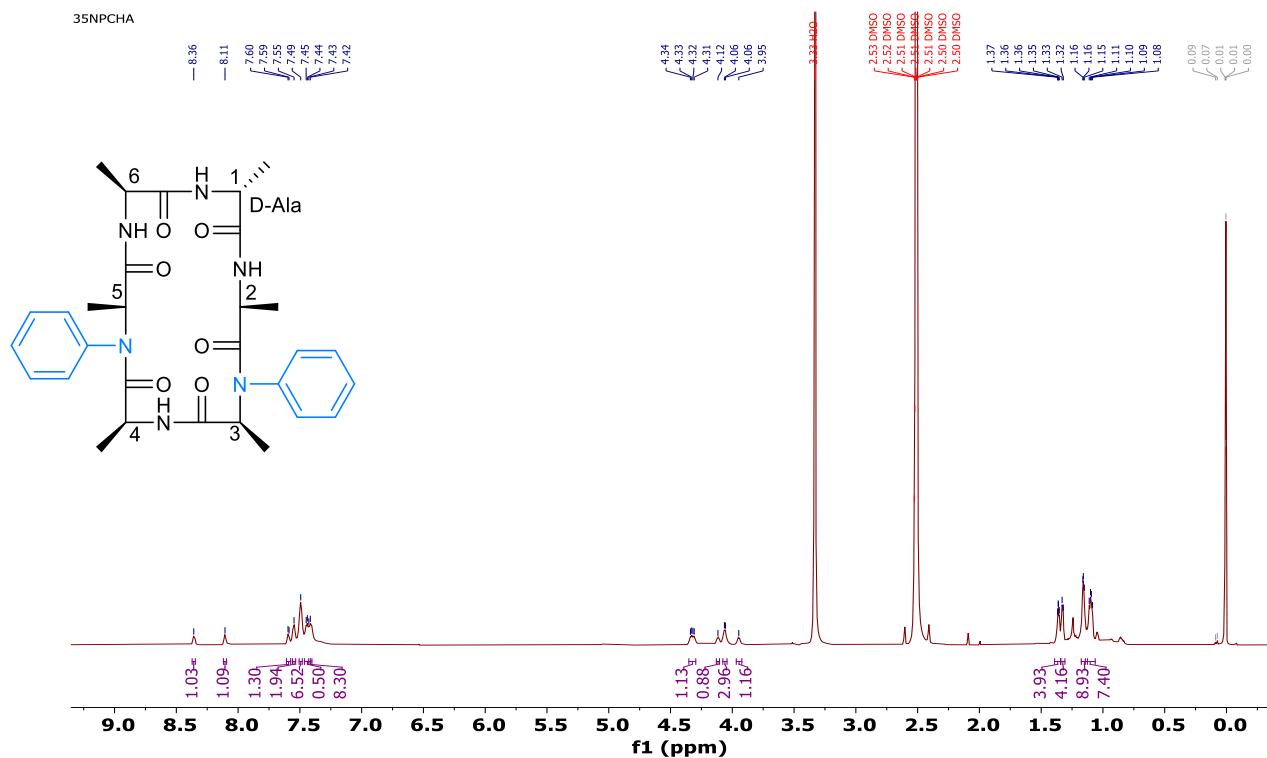
^{1}H NMR of **36NPCHA** on 500 MHz at 298 K in DMSO-d_6.
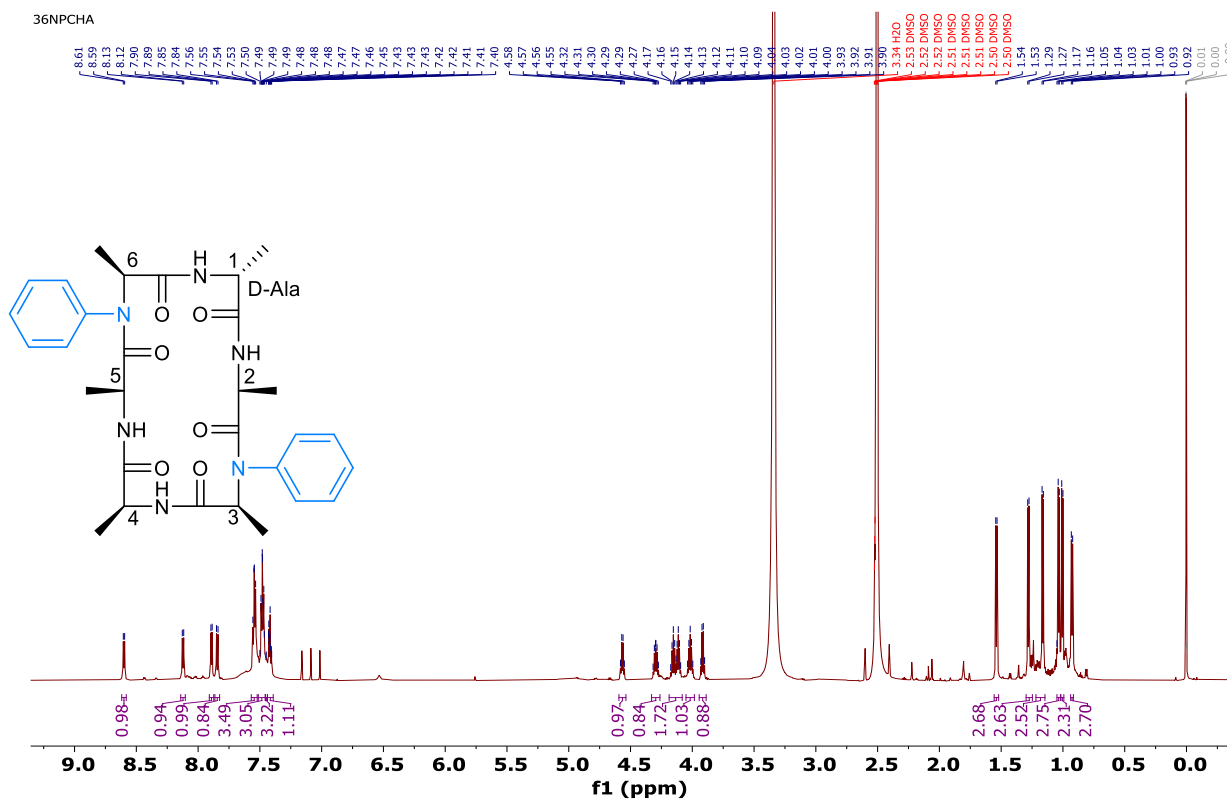
¹H NMR of **46NPCHA** on 500 MHz at 298 K in DMSO-*d₆*.
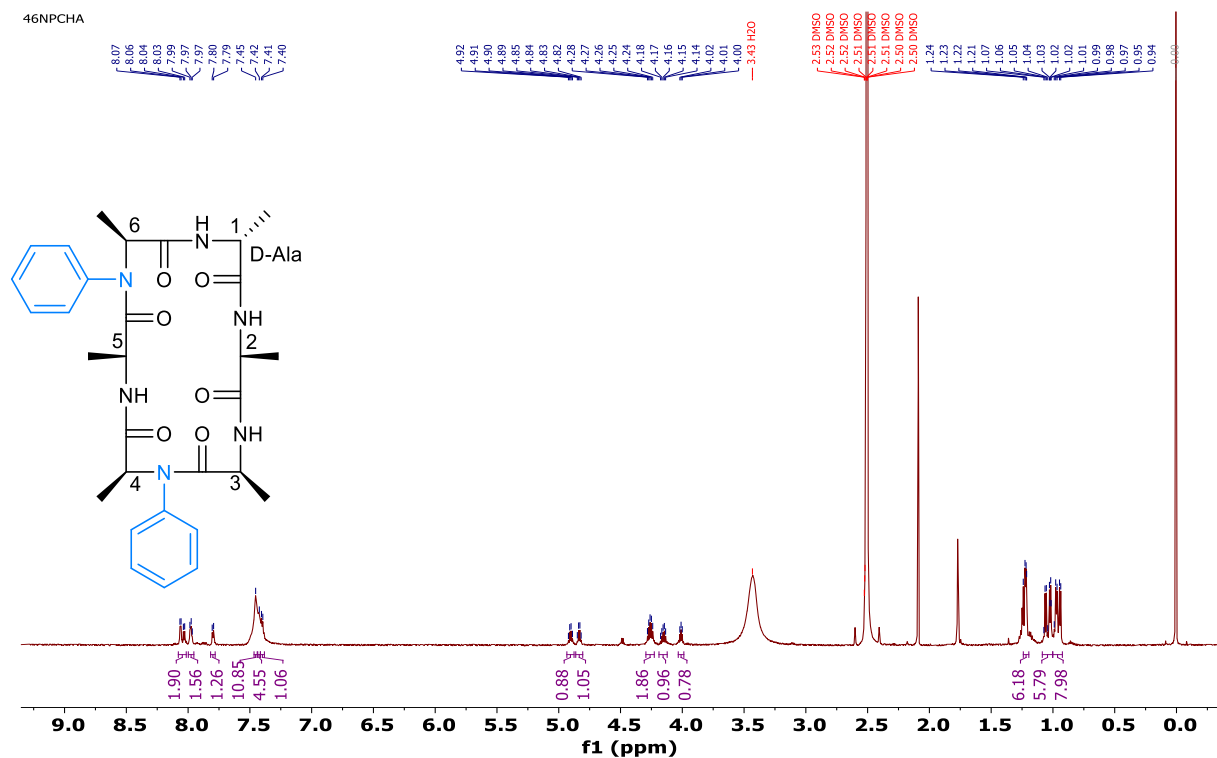
¹H NMR of **1NPCPA** on 500 MHz at 298 K in DMSO-*d₆*.
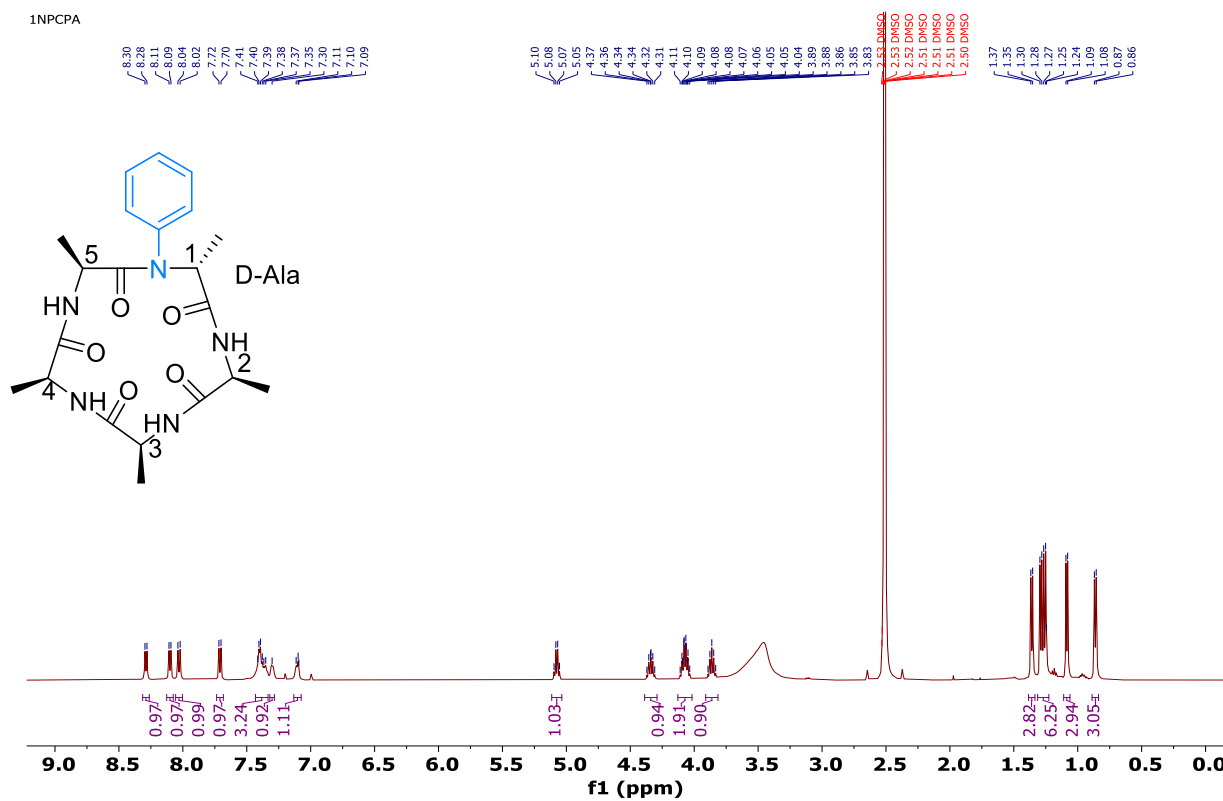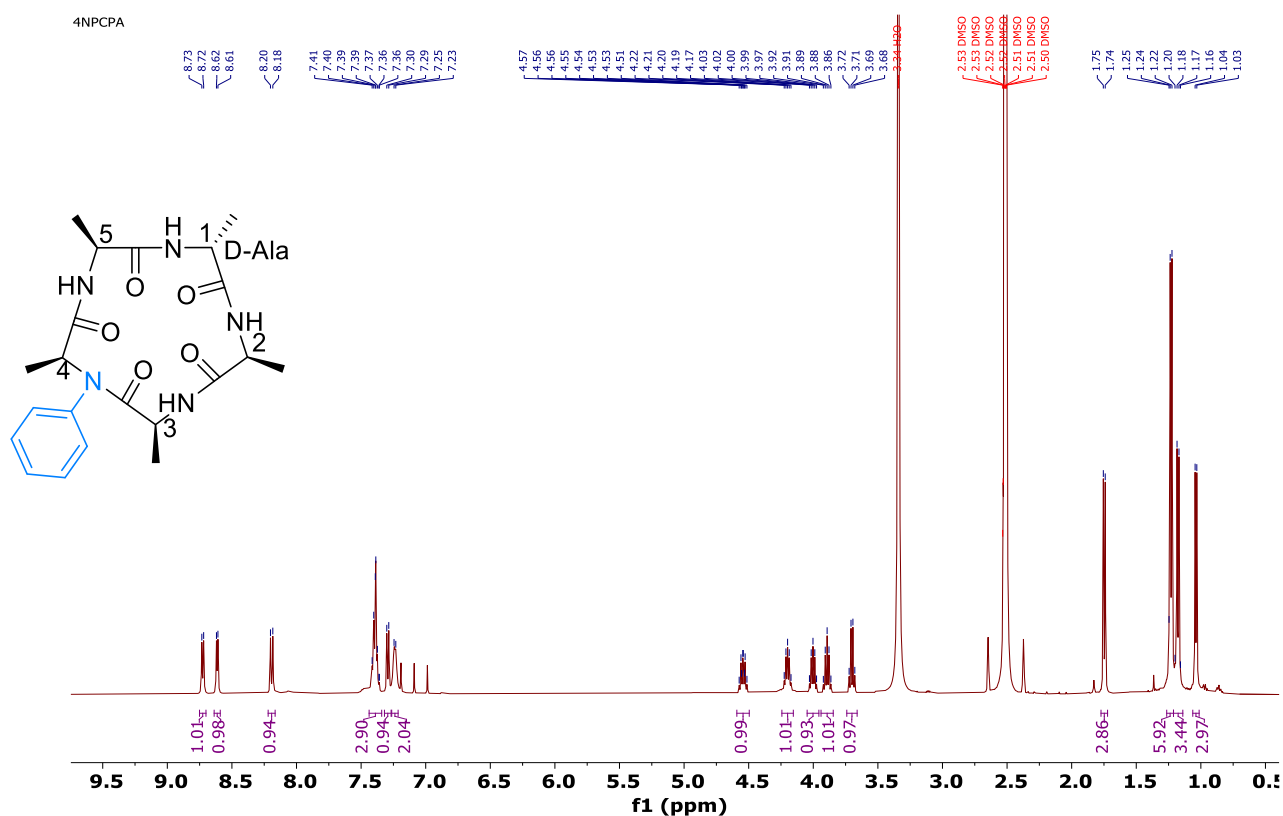
^{1}H NMR of **2NPCPA** on 500 MHz at 298 K in DMSO-d_6.
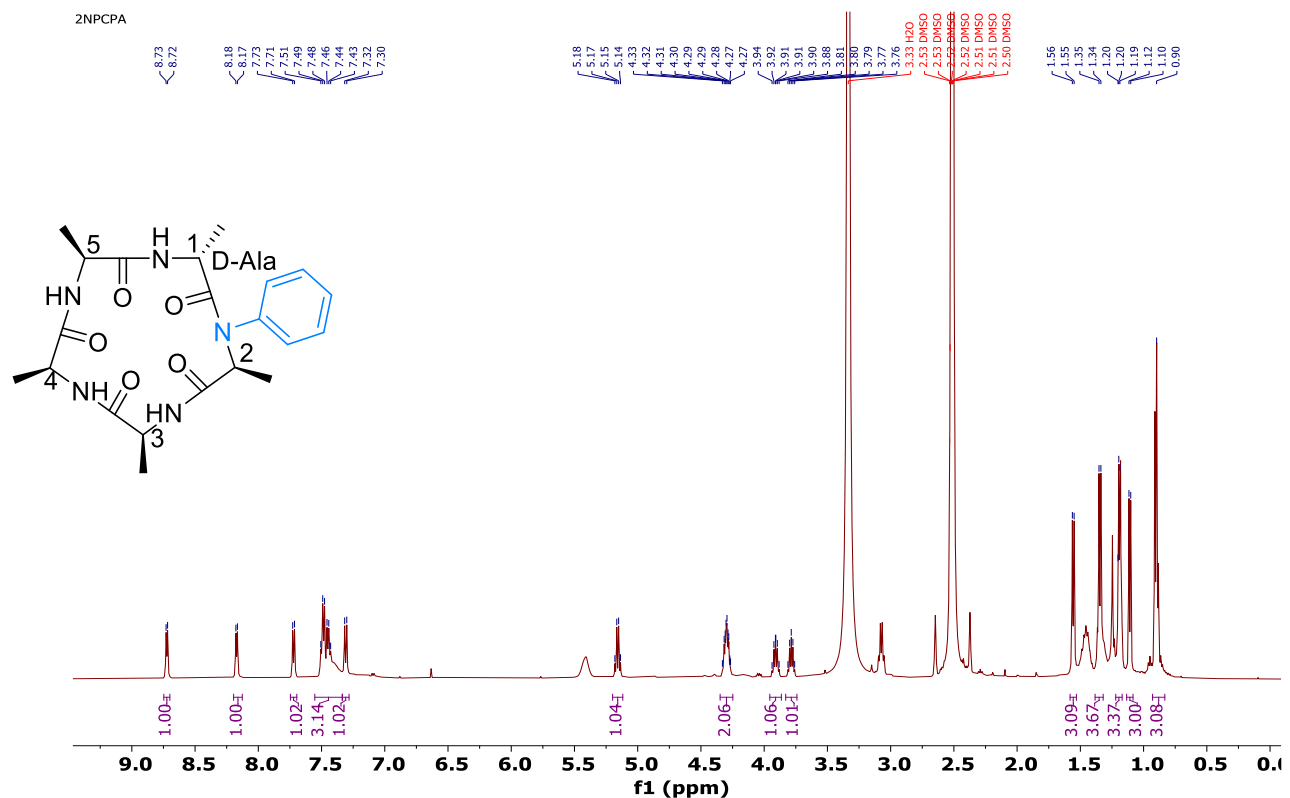
^{1}H NMR of **3NPCPA** on 500 MHz at 298 K in DMSO-d_6.
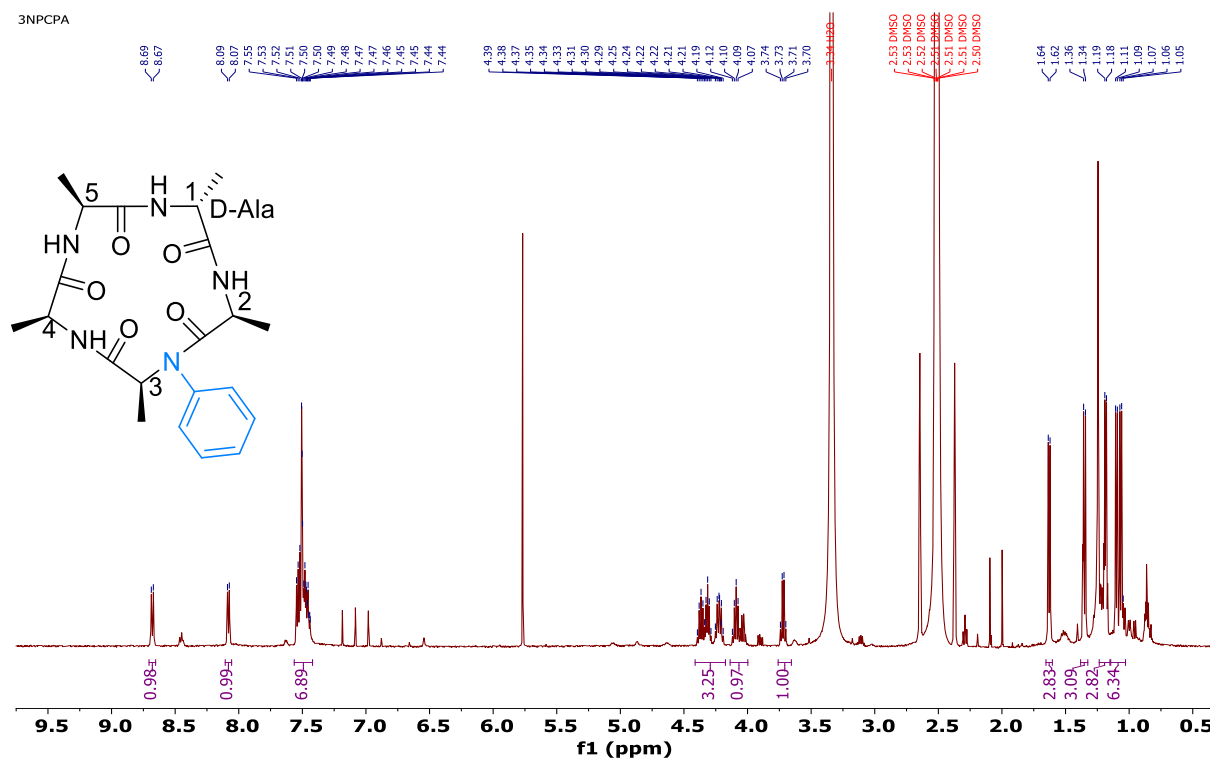
^{1}H NMR of **4NPCPA** on 500 MHz at 298 K in DMSO-*d*$_6$.

^{1}H NMR of **5NPCPA** on 500 MHz at 298 K in DMSO-*d*$_6$.
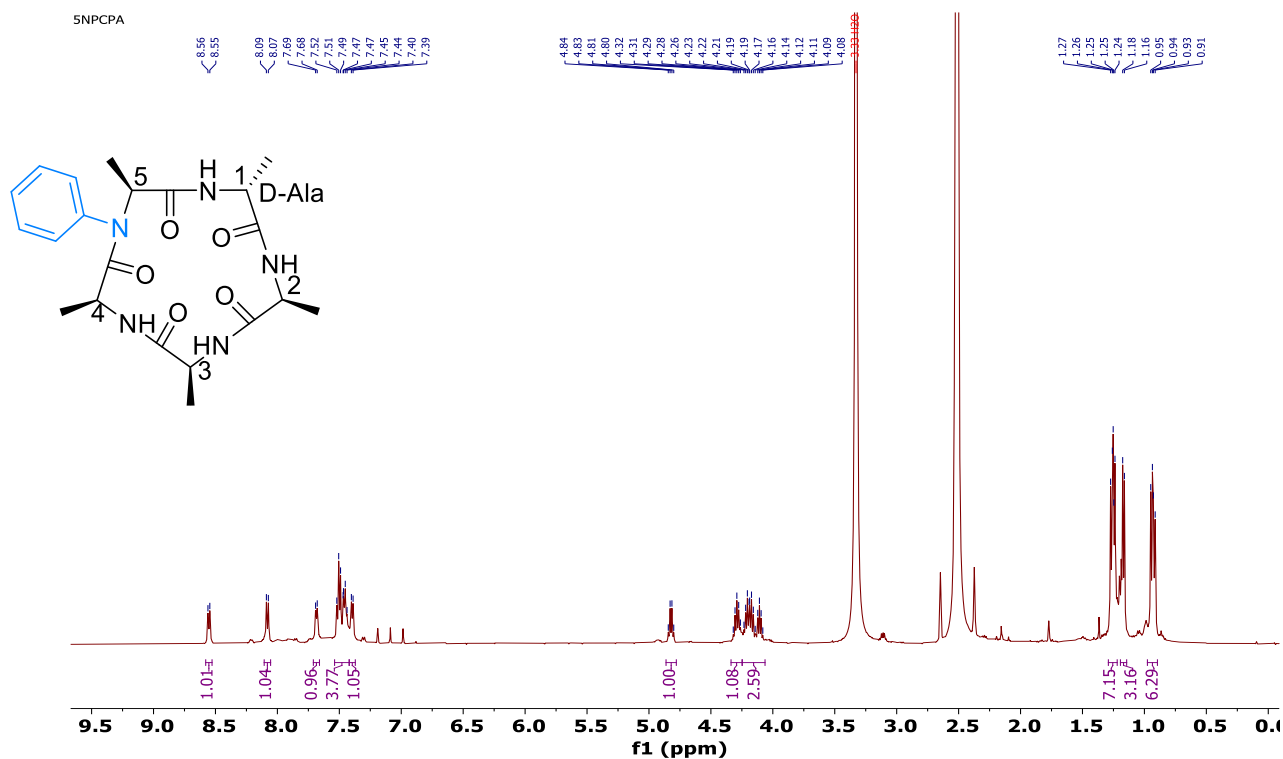
^{1}H NMR of **13NPCPA** on 500 MHz at 298 K in DMSO-d_6.
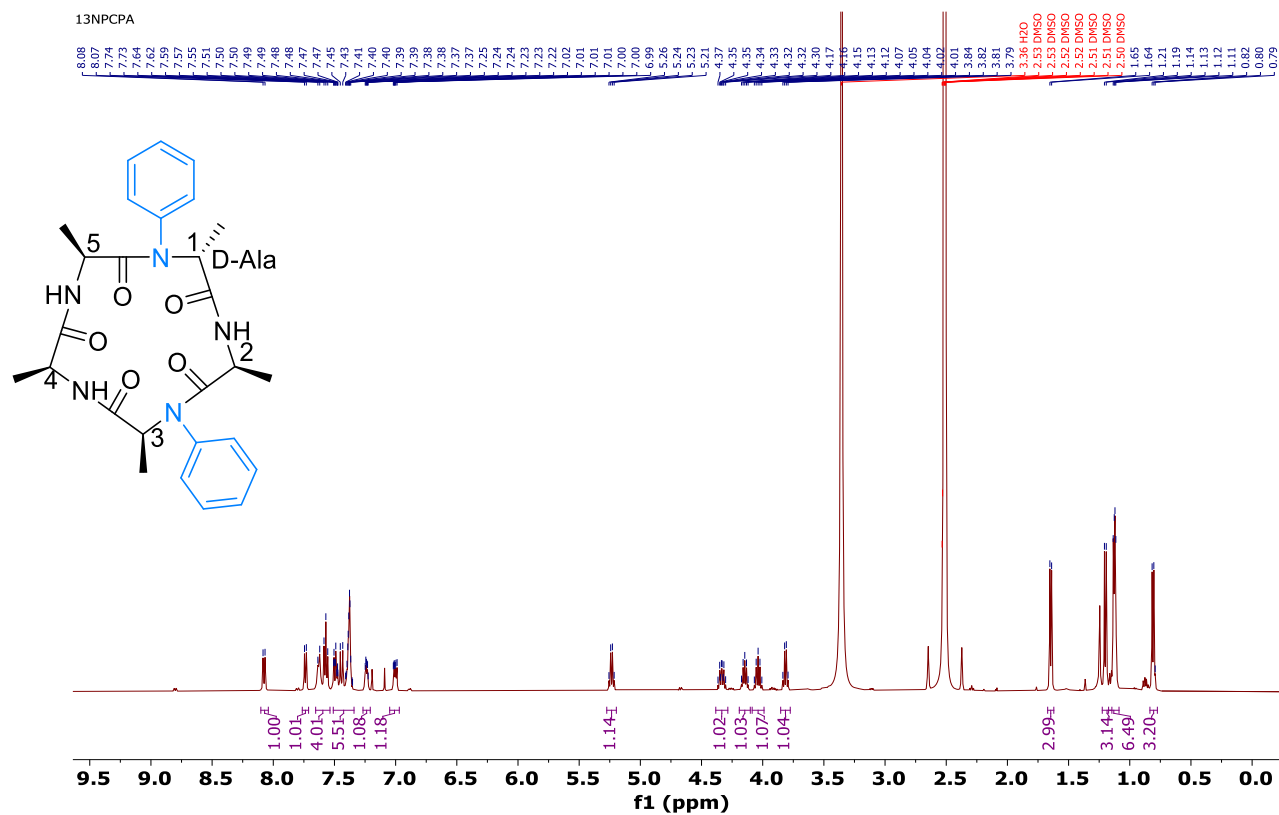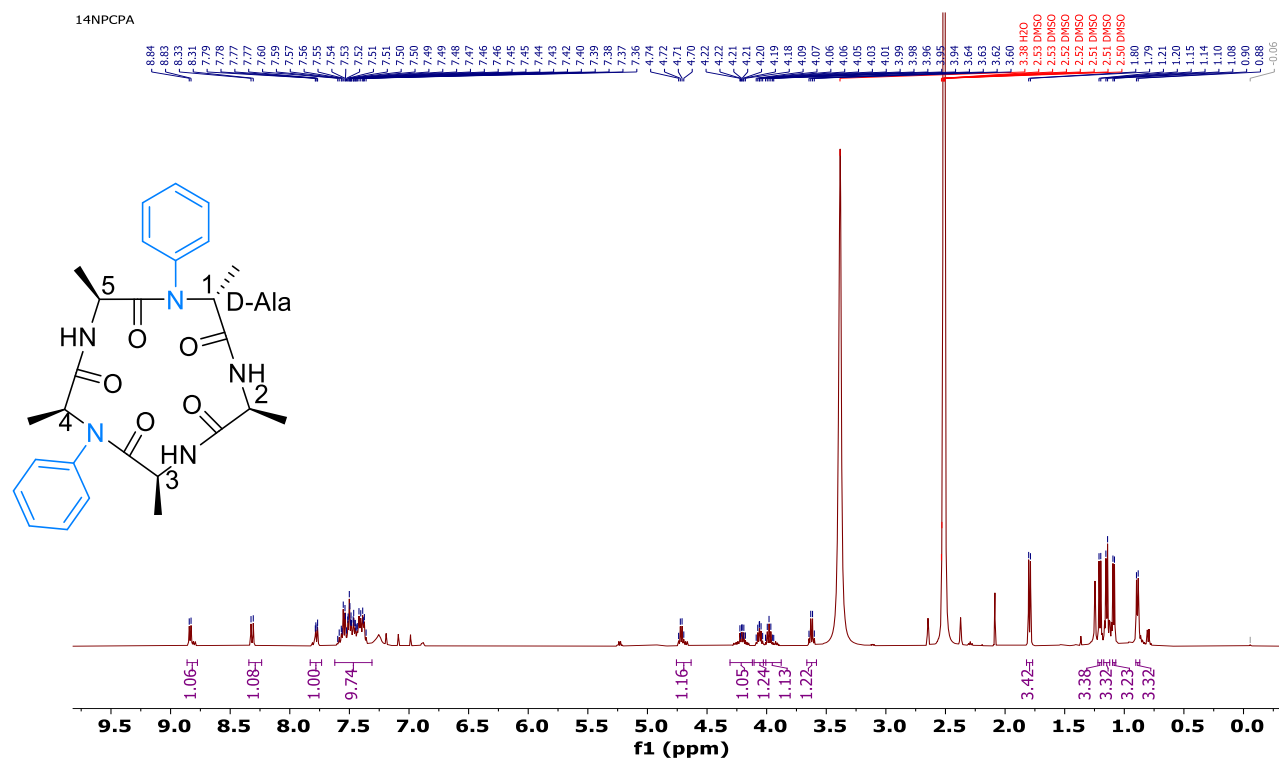

^{1}H NMR of **14NPCPA** on 500 MHz at 298 K in DMSO-d_6.

^{1}H NMR of **24NPCPA** on 500 MHz at 298 K in DMSO-d_6.

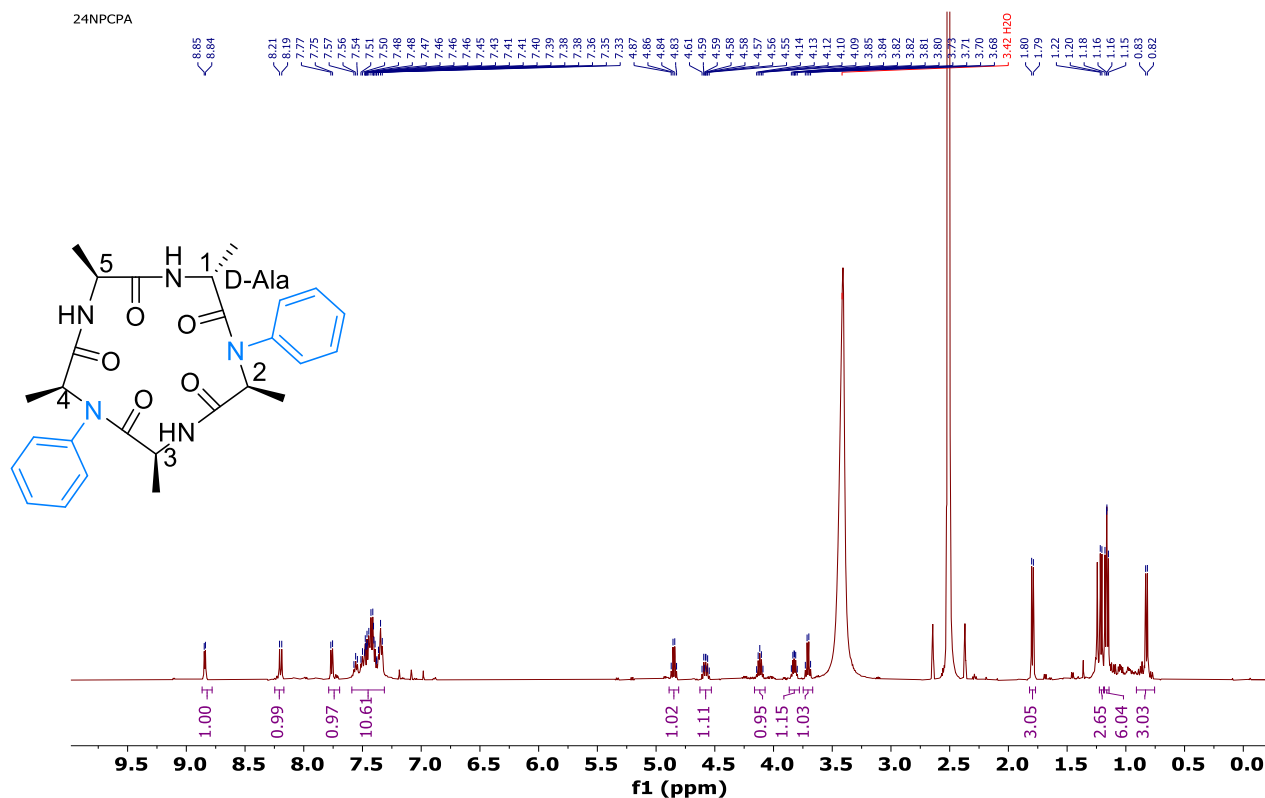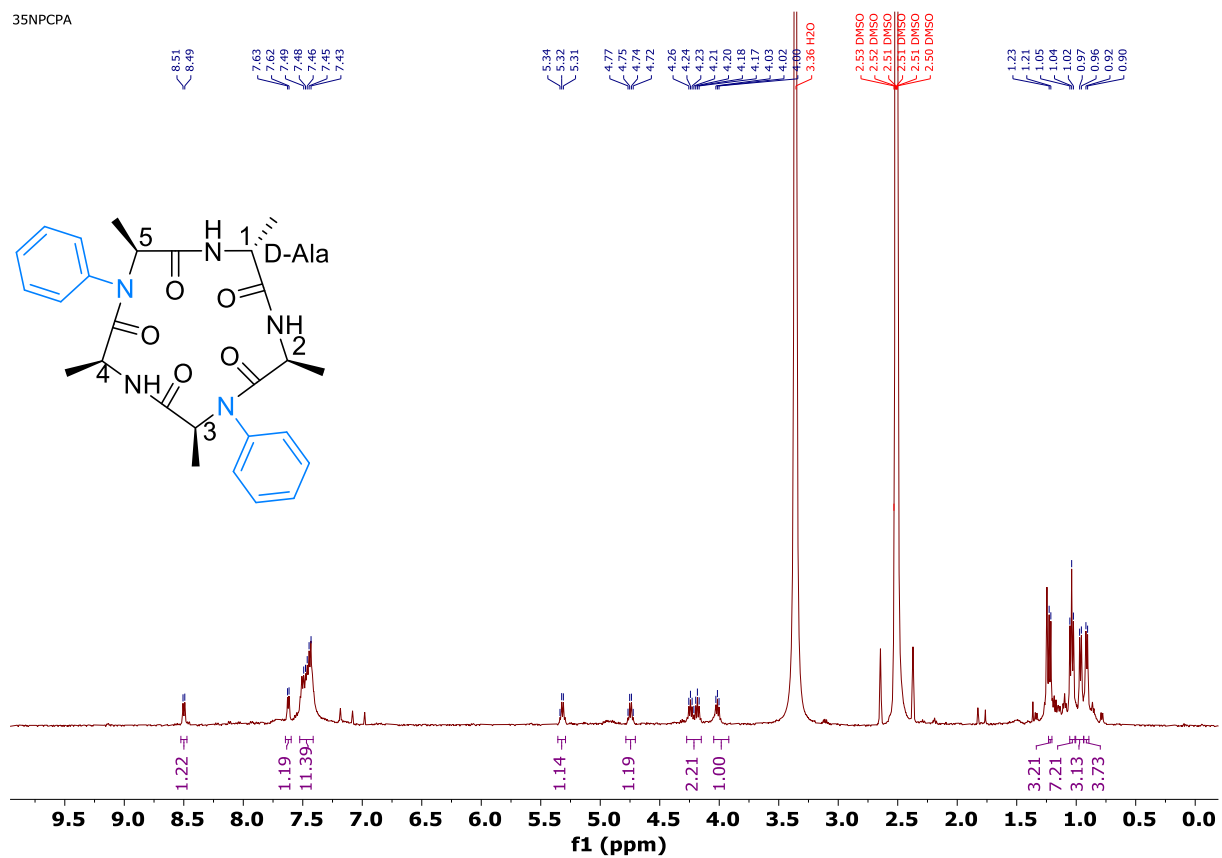^{1}H NMR of **25NPCPA** on 500 MHz at 298 K in DMSO-d_6.
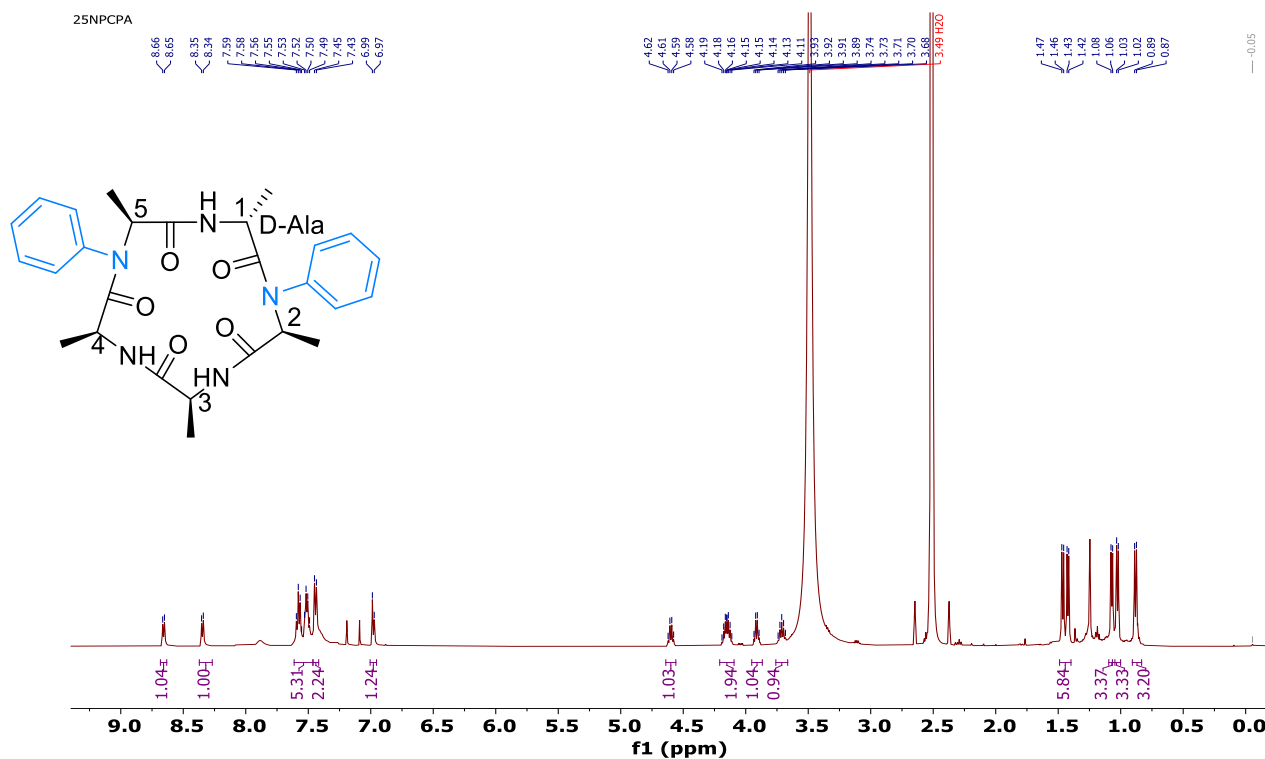
¹H NMR of **35NPCPA** on 500 MHz at 298 K in DMSO-*d*₆.

35NPCPA

2.6. References

(1) Henninot, A.; Collins, J. C.; Nuss, J. M. The Current State of Peptide Drug Discovery: Back to the Future? *J. Med. Chem.* **2018**, *61* (4), 1382–1414.

(2) Fosgerau, K.; Hoffmann, T. Peptide Therapeutics: Current Status and Future Directions. *Drug Discov. Today* **2015**, *20* (1), 122–128.

(3) Lau, J. L.; Dunn, M. K. Therapeutic Peptides: Historical Perspectives, Current Development Trends, and Future Directions. *Bioorg. Med. Chem.* **2018**, *26* (10), 2700–2707.

(4) Wang, L.; Wang, N.; Zhang, W.; Cheng, X.; Yan, Z.; Shao, G.; Wang, X.; Wang, R.; Fu, C. Therapeutic Peptides: Current Applications and Future Directions. *Signal Transduct. Target. Ther.* **2022**, *7* (1).

(5) Vlieghe, P.; Lisowski, V.; Martinez, J.; Khrestchatisky, M. Synthetic Therapeutic Peptides: Science and Market. *Drug Discov. Today* **2010**, *15* (1–2), 40–56.

(6) Lee, A. C. L.; Harris, J. L.; Khanna, K. K.; Hong, J. H. A Comprehensive Review on Current Advances in Peptide Drug Development and Design. *Int. J. Mol. Sci.* **2019**, *20* (10), 1–21.

(7) Lamers, C. Overcoming the Shortcomings of Peptide-Based Therapeutics. *Futur. Drug Discov.* **2022**, *4* (2).

(8) Muttenthaler, M.; King, G. F.; Adams, D. J.; Alewood, P. F. Trends in Peptide Drug Discovery. *Nat. Rev. Drug Discov.* **2021**, *20* (4), 309–325.

(9) Craik, D. J.; Fairlie, D. P.; Liras, S.; Price, D. The Future of Peptide-Based Drugs. *Chem. Biol. Drug Des.* **2013**, *81* (1), 136–147.

(10) Bock, J. E.; Gavenonis, J.; Kritzer, J. A. Getting in Shape: Controlling Peptide Bioactivity and Bioavailability Using Conformational Constraints. *ACS Chem. Biol.* **2013**, *8* (3), 488–499.

(11) Buckton, L. K.; Rahimi, M. N.; McAlpine, S. R. Cyclic Peptides as Drugs for Intracellular Targets: The Next Frontier in Peptide Therapeutic Development. *Chem. - A Eur. J.* **2021**, *27* (5), 1487–1513.

(12) Bhat, A.; Roberts, L. R.; Dwyer, J. J. Lead Discovery and Optimization Strategies for Peptide Macrocycles. *Eur. J. Med. Chem.* **2015**, *94*, 471–479.

(13) Moiola, M.; Memeo, M. G.; Quadrelli, P. Stapled Peptides-a Useful Improvement for Peptide-Based Drugs. *Molecules* **2019**, *24* (20).

(14) Rinaldi, S. The Diverse World of Foldamers: Endless Possibilities of Self-Assembly. *Molecules* **2020**, *25* (14).

(15) Girvin, Z. C.; Gellman, S. H. Foldamer Catalysis. *J. Am. Chem. Soc.* **2020**, *142* (41), 17211–17223.

(16) Roche, S. P.; Richaud, A. D. Structure-Property Relationship Study of n-(Hydroxy)Peptides for the Design of Self-Assembled Parallel β-Sheets. *J. Org. Chem.* **2020**, *85* (19), 12329–12342.

(17) Tsomaia, N. Peptide Therapeutics: Targeting the Undruggable Space. *Eur. J. Med. Chem.* **2015**, *94*, 459–470.

(18) Kimmerlin, T.; Seebach, D. "100 Years of Peptide Synthesis": Ligation Methods for Peptide and Protein Synthesis with Applications to β-Peptide Assemblies. *J. Pept. Res.* **2005**, *65* (2), 229–260.

(19) Räder, A. F. B.; Weinmüller, M.; Reichart, F.; Schumacher-Klinger, A.; Merzbach, S.; Gilon, C.;

Hoffman, A.; Kessler, H. Orally Active Peptides: Is There a Magic Bullet? *Angew. Chemie Int. Ed.* **2018**, *57* (44), 14414–14438.

(20) Zorzi, A.; Deyle, K.; Heinis, C. Cyclic Peptide Therapeutics: Past, Present and Future. *Curr. Opin. Chem. Biol.* **2017**, *38*, 24–29.

(21) Gang, D.; Kim, D. W.; Park, H. S. Cyclic Peptides: Promising Scaffolds for Biopharmaceuticals. *Genes (Basel).* **2018**, *9* (11).

(22) Zhang, H.; Chen, S. Cyclic Peptide Drugs Approved in the Last Two Decades (2001-2021). *RSC Chem. Biol.* **2022**, *3* (1), 18–31.

(23) Nielsen, D. S.; Shepherd, N. E.; Xu, W.; Lucke, A. J.; Stoermer, M. J.; Fairlie, D. P. Orally Absorbed Cyclic Peptides. *Chem. Rev.* **2017**, *117* (12), 8094–8128.

(24) Gudmundsson, O. S.; Jois, S. D. S.; Vander Velde, D. G.; Siahaan, T. J.; Wang, B.; Borchardt, R. T. The Effect of Conformation on the Membrane Permeation of Coumarinic Acid- and Phenylpropionic Acid-Based Cyclic Prodrugs of Opioid Peptides. *J. Pept. Res.* **1999**, *53* (4), 383–392.

(25) Rezai, T.; Yu, B.; Millhauser, G. L.; Jacobson, M. P.; Lokey, R. S. Testing the Conformational Hypothesis of Passive Membrane Permeability Using Synthetic Cyclic Peptide Diastereomers. *J. Am. Chem. Soc.* **2006**, *128* (8), 2510–2511.

(26) Pelay-Gimeno, M.; Glas, A.; Koch, O.; Grossmann, T. N. Structure-Based Design of Inhibitors of Protein-Protein Interactions: Mimicking Peptide Binding Epitopes. *Angew. Chemie Int. Ed.* **2015**, *54* (31), 8896–8927.

(27) Jwad, R.; Weissberger, D.; Hunter, L. Strategies for Fine-Tuning the Conformations of Cyclic Peptides. *Chem. Rev.* **2020**, *120* (17), 9743–9789.

(28) Hill, T. A.; Shepherd, N. E.; Diness, F.; Fairlie, D. P. Constraining Cyclic Peptides to Mimic Protein Structure Motifs. *Angew. Chemie Int. Ed.* **2014**, *53* (48), 13020–13041.

(29) Li, Y.; Li, W.; Xu, Z. Improvement on Permeability of Cyclic Peptide/Peptidomimetic: Backbone n-Methylation as a Useful Tool. *Mar. Drugs* **2021**, *19* (6).

(30) Sharma, A.; Kumar, A.; Abdel Monaim, S. A. H.; Jad, Y. E.; El-Faham, A.; de la Torre, B. G.; Albericio, F. N-Methylation in Amino Acids and Peptides: Scope and Limitations. *Biopolymers* **2018**, *109* (10).

(31) Chatterjee, J.; Gilon, C.; Hoffman, A.; Kessler, H. N-Methylation of Peptides: A New Perspective in Medicinal Chemistry. *Acc. Chem. Res.* **2008**, *41* (10), 1331–1342.

(32) Chatterjee, J.; Rechenmacher, F.; Kessler, H. N-Methylation of Peptides and Proteins: An Important Element for Modulating Biological Functions. *Angew. Chemie Int. Ed.* **2013**, *52* (1), 254–269.

(33) White, T. R.; Renzelman, C. M.; Rand, A. C.; Rezai, T.; McEwen, C. M.; Gelev, V. M.; Turner, R. A.; Linington, R. G.; Leung, S. S. F.; Kalgutkar, A. S.; Bauman, J. N.; Zhang, Y.; Liras, S.; Price, D. A.; Mathiowetz, A. M.; Jacobson, M. P.; Lokey, R. S. On-Resin N-Methylation of Cyclic Peptides for Discovery of Orally Bioavailable Scaffolds. *Nat. Chem. Biol.* **2011**, *7* (11), 810–817.

(34) Turner, R. A.; Hauksson, N. E.; Gipe, J. H.; Lokey, R. S. Selective , On-Resin N - Methylation of Peptide N - Trifluoroacetamides. **2013**, *65* (7), 5981–5984.

(35) Liu, S.; Gu, W.; Lo, D.; Ding, X. Z.; Ujiki, M.; Adrian, T. E.; Soff, G. A.; Silverman, R. B. N-Methylsansalvamide a Peptide Analogues. Potent New Antitumor Agents. *J. Med. Chem.* **2005**, *48* (10), 3630–3638.

(36) Nguyen, A. M. T.; Brettell, S.; Douanne, N.; Duquette, C.; Corbeil, A.; Fajardo, E. F.; Olivier, M.; Fernandez-Prada, C.; Lubell, W. D. Influence of N-Methylation and Conformation on Almiramide Anti-Leishmanial Activity. *Molecules* **2021**, *26* (12).

(37) Sciabola, S.; Goetz, G. H.; Bai, G.; Rogers, B. N.; Gray, D. L.; Duplantier, A.; Fonseca, K. R.; Vanase-Frawley, M. A.; Kablaoui, N. M. Systematic N-Methylation of Oxytocin: Impact on Pharmacology and Intramolecular Hydrogen Bonding Network. *Bioorg. Med. Chem.* **2016**, *24* (16), 3513–3520.

(38) Mas-Moruno, C.; Rechenmacher, F.; Kessler, H. Cilengitide: The First Anti-Angiogenic Small Molecule Drug Candidate. Design, Synthesis and Clinical Evaluation. *Anticancer. Agents Med. Chem.* **2011**, *10* (10), 753–768.

(39) Wang, C. K.; Swedberg, J. E.; Harvey, P. J.; Kaas, Q.; Craik, D. J. Conformational Flexibility Is a Determinant of Permeability for Cyclosporin. *J. Phys. Chem. B* **2018**, *122* (8), 2261–2276.

(40) Weinmüller, M.; Rechenmacher, F.; Kiran Marelli, U.; Reichart, F.; Kapp, T. G.; Räder, A. F. B.; Di Leva, F. S.; Marinelli, L.; Novellino, E.; Muñoz-Félix, J. M.; Hodivala-Dilke, K.; Schumacher, A.; Fanous, J.; Gilon, C.; Hoffman, A.; Kessler, H. Overcoming the Lack of Oral Availability of Cyclic Hexapeptides: Design of a Selective and Orally Available Ligand for the Integrin Avβ3. *Angew. Chemie Int. Ed.* **2017**, *56* (51), 16405–16409.

(41) Biron, E.; Chatterjee, J.; Ovadia, O.; Langenegger, D.; Brueggen, J.; Hoyer, D.; Schmid, H. A.; Jelinek, R.; Gilon, C.; Hoffman, A.; Kessler, H. Improving Oral Bioavailability of Peptides by Multiple N-Methylation: Somatostatin Analogues. *Angew. Chemie Int. Ed.* **2008**, *47* (14), 2595–2599.

(42) Cai, M.; Marelli, U. K.; Bao, J.; Beck, J. G.; Opperer, F.; Rechenmacher, F.; McLeod, K. R.; Zingsheim, M. R.; Doedens, L.; Kessler, H.; Hruby, V. J. Systematic Backbone Conformational Constraints on a Cyclic Melanotropin Ligand Leads to Highly Selective Ligands for Multiple Melanocortin Receptors. *J. Med. Chem.* **2015**, *58* (16), 6359–6367.

(43) Ovadia, O.; Greenberg, S.; Chatterjee, J.; Laufer, B.; Opperer, F.; Kessler, H.; Gilon, C.; Hoffman, A. The Effect of Multiple N-Methylation on Intestinal Permeability of Cyclic Hexapeptides. *Mol. Pharm.* **2011**, *8* (2), 479–487.

(44) Chatterjee, J.; Mierke, D.; Kessler, H. N-Methylated Cyclic Pentaalanine Peptides as Template Structures. *J. Am. Chem. Soc.* **2006**, *128* (47), 15164–15172.

(45) Beck, J. G.; Chatterjee, J.; Laufer, B.; Kiran, M. U.; Frank, A. O.; Neubauer, S.; Ovadia, O.; Greenberg, S.; Gilon, C.; Hoffman, A.; Kessler, H. Intestinal Permeability of Cyclic Peptides: Common Key Backbone Motifs Identified. *J. Am. Chem. Soc.* **2012**, *134* (29), 12125–12133.

(46) Marelli, U. K.; Ovadia, O.; Frank, A. O.; Chatterjee, J.; Gilon, C.; Hoffman, A.; Kessler, H. Cis-Peptide Bonds: A Key for Intestinal Permeability of Peptides? *Chem. - A Eur. J.* **2015**, *21* (43), 15148–15152.

(47) Marelli, U. K.; Bezençon, J.; Puig, E.; Ernst, B.; Kessler, H. Enantiomeric Cyclic Peptides with Different Caco-2 Permeability Suggest Carrier-Mediated Transport. *Chem. - A Eur. J.* **2015**, *21* (22), 8023–8027.

(48) Räder, A. F. B.; Reichart, F.; Weinmüller, M.; Kessler, H. Improving Oral Bioavailability of Cyclic Peptides by N-Methylation. *Bioorg. Med. Chem.* **2018**, *26* (10), 2766–2773.

(49) Tillett, K. C.; Del Valle, J. R *N* -Amino Peptide Scanning Reveals Inhibitors of Aβ42 Aggregation. *RSC Adv.* **2020**, *10* (24), 14331–14336.

(50) Rathman, B. M.; Rowe, J. L.; Del Valle, J. R. Synthesis and Conformation of Backbone N-Aminated Peptides. *Methods Enzymol.* **2021**, *656*, 271–294.

(51) Rathman, B. M.; Allen, J. L.; Shaw, L. N.; Del Valle, J. R. Synthesis and Biological Evaluation of Backbone-Aminated Analogues of Gramicidin S. *Bioorganic Med. Chem. Lett.* **2020**, *30* (15), 1–5.

(52) Sarnowski, M. P.; Kang, C. W.; Elbatrawi, Y. M.; Wojtas, L.; Del Valle, J. R. Peptide N-Amination Supports β-Sheet Conformations. *Angew. Chemie Int. Ed.* **2017**, *56* (8), 2083–2086.

(53) Fernández-Llamazares, A. I.; García, J.; Soto-Cerrato, V.; Pérez-Tomás, R.; Spengler, J.; Albericio, F. N-Triethylene Glycol (N-TEG) as a Surrogate for the N-Methyl Group: Application to Sansalvamide A Peptide Analogs. *Chem. Commun.* **2013**, *49* (57), 6430–6432.

(54) Fernández-Llamazares, A. I.; Adan, J.; Mitjans, F.; Spengler, J.; Albericio, F. Tackling Lipophilicity of Peptide Drugs: Replacement of the Backbone n -Methyl Group of Cilengitide by N -Oligoethylene Glycol (N -OEG) Chains. *Bioconjug. Chem.* **2014**, *25* (1), 11–17.

(55) Morimoto, J.; Fukuda, Y.; Kuroda, D.; Watanabe, T.; Yoshida, F.; Asada, M.; Nakamura, T.; Senoo, A.; Nagatoishi, S.; Tsumoto, K.; Sando, S. A Peptoid with Extended Shape in Water. *J. Am. Chem. Soc.* **2019**, *141* (37), 14612–14623.

(56) Fukuda, Y.; Yokomine, M.; Kuroda, D.; Tsumoto, K.; Morimoto, J.; Sando, S. Peptoid-Based Reprogrammable Template for Cell-Permeable Inhibitors of Protein-Protein Interactions. *Chem. Sci.* **2021**, *12* (40), 13292–13300.

(57) Erak, M.; Bellmann-Sickert, K.; Els-Heindl, S.; Beck-Sickinger, A. G. Peptide Chemistry Toolbox – Transforming Natural Peptides into Peptide Therapeutics. *Bioorg. Med. Chem.* **2018**, *26* (10), 2759–2765.

(58) Stringer, J. R.; Crapster, J. A.; Guzei, I. A.; Blackwell, H. E. Construction of Peptoids with All Trans -Amide Backbones and Peptoid Reverse Turns via the Tactical Incorporation of N -Aryl Side Chains Capable of Hydrogen Bonding. *J. Org. Chem.* **2010**, *75* (18), 6068–6078.

(59) Shah, N. H.; Butterfoss, G. L.; Nguyen, K.; Yoo, B.; Bonneau, R.; Rabenstein, D. L.; Kirshenbaum, K. Oligo(N-Aryl Glycines): A New Twist on Structured Peptoids. *J. Am. Chem. Soc.* **2008**, *130* (49), 16622–16632.

(60) Pros, G. J.; Bloomfield, A. J. Why Do N-Alkylated Anilides Bend Over? The Factors Dictating the Divergent Conformational Preferences of 2° and 3° N-Aryl Amides. *J. Phys. Chem. A* **2019**, *123* (35), 7609–7618.

(61) Itai, A.; Toriumi, Y.; Saito, S.; Kagechika, H.; Shudo, K. Preference for Cis-Amide Structure in N-Acyl-N-Methylanilines. *J. Am. Chem. Soc.* **1992**, *114* (26), 10649–10650.

(62) Sharma, K. K.; Sharma, S.; Kudwal, A.; Jain, R. Room Temperature N-Arylation of Amino Acids and Peptides Using Copper(i) and β-Diketone. *Org. Biomol. Chem.* **2015**, *13* (16), 4637–4641.

(63) Merrifield, R. B. Solid Phase Peptide Synthesis. *Excerpta Med., I.C.S.* **1976**, *No.374*, 29–39.

(64)   Sladojevich, F.; Trabocchi, A.; Guarna, A. Convenient Route to Enantiopure Fmoc-Protected Morpholine-3-Carboxylic Acid. *J. Org. Chem.* **2007**, *72* (11), 4254–4257.

(65)   Schrödinger Release 2022-2: MacroModel, Schrödinger, LLC, New York, NY, 2021.

(66)   Hayward, S. Peptide-Plane Flipping in Proteins. *Protein Sci.* **2008**, *10* (11), 2219–2227.

(67)   Mierke, D. F.; Kurz, M.; Kessler, H. Peptide Flexibility and Calculations of an Ensemble of Molecules. *J. Am. Chem. Soc.* **1994**, *116* (3), 1042–1049.
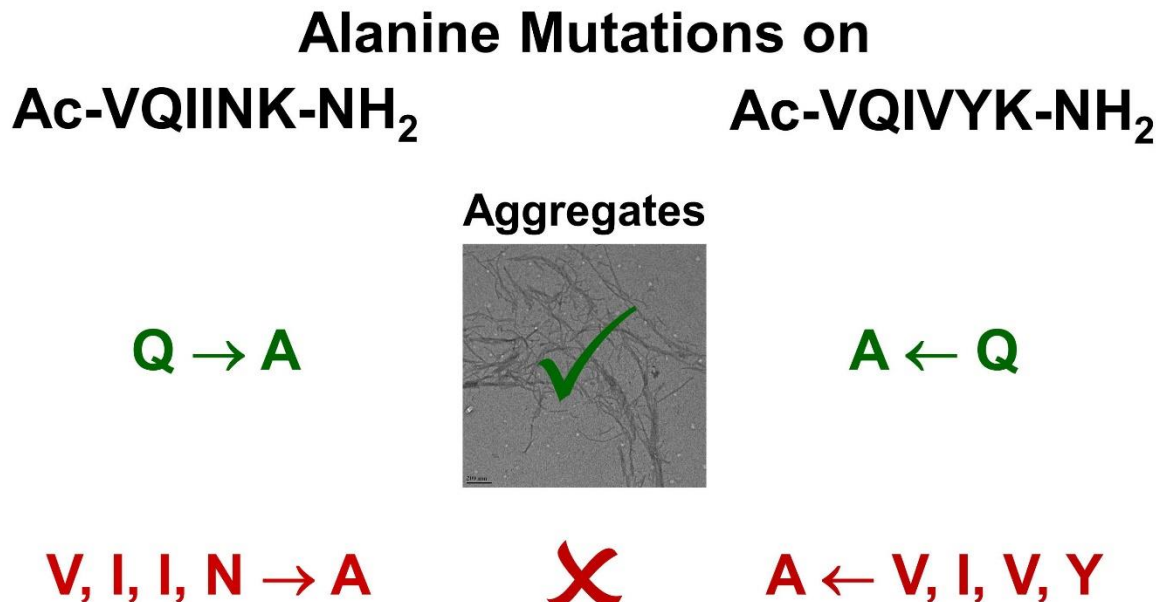
CHAPTER-3

Section-A

Residue-based propensity of aggregation in the Tau amyloidogenic hexapeptides AcPHF6* and AcPHF6

Alanine Mutations on

Ac-VQIINK-NH$_2$ Ac-VQIVYK-NH$_2$

Aggregates

Q $\rightarrow$ A   A $\leftarrow$ Q

V, I, I, N $\rightarrow$ A   ✗   A $\leftarrow$ V, I, V, Y

3A.1. Introduction

Conformational misfolding of proteins leading to protein aggregates, also called as amyloids, is a prime trait of neurodegenerative diseases such as Alzheimer's (AD) and Parkinson's disease (PD).[1,2] Amyloid protein aggregates are also observed in other disease conditions like diabetes and arthritis.[1,3-7] Deposition of amyloids in AD leads to irreversible cell death and chronic dementia resulting in the loss of vital bodily functions, severe behavioural disorders, and ultimately death. As of now, there is no direct cure available for AD. The search for an effective cure for AD is in persistent progress and the majority of the drug discovery research on AD is focused on interfering with the protein deposition mechanisms in neuronal cells and tissues as a rational target.[8-13]

Two proteins, amyloid beta (Aβ) and Tau were identified to form protein deposits linked with AD. Aβ are various small-length protein fragments derived from amyloid precursor protein (APP), among which Aβ-42 has been proven to be toxic and form amyloid plaques.[8,14] However, in recent times, increasing evidence for the pathological role of Tau protein in AD was found.[15-19] Tau, a microtubule-binding protein, forms neurofibrillary tangles (NFTs) in AD *via* soluble oligomers, which are stabilized by beta-sheet interactions. Tau is 441 amino acids long having an N-terminus region, a proline-rich region, followed by the key microtubule-binding domain consisting of 3 or 4 repeat regions depending on the Tau isoform, and a C-terminus domain (Figure **3A.1**).[20]

Figure 3A.1 Schematic diagram of the Full-length tau region.

A high-resolution cryo-EM structure of Tau filaments from the brain of an AD patient was recently established and it highlighted the presence of beta-sheet structures stabilized by hydrogen bonds and hydrophobic interactions.[21] Interestingly, the cryo-EM structure of Tau filaments obtained from the brain of a patient with Pick's disease revealed a different fold for Tau, suggesting disease-specific conformational misfolding of Tau.[22]

Two hexapeptide regions, [275]VQIINK[280] and [306]VQIVYK[311], residing in the second and third repeat units of Tau, respectively, form the core beta-sheet structure in Tau, a structural feature responsible for Tau oligomerization and formation of NFTs.[16,23-26] Synthetic analogues of both these hexapeptides, Ac-VQIINK-NH$_2$ (AcPHF6*, **1**; PHF stands for paired helical filaments) and Ac-VQIVYK-NH$_2$ (AcPHF6, **1'**), having acetyl protection on N-terminus and amidation on C-terminus, are known to form structurally similar fibrils akin to those of Tau and hence AcPHF6 and AcPHF6* stand as model peptides to study the promotion or inhibitory effect of various ligands on Tau aggregation[27-29] and for development of any peptide-based Tau aggregation inhibitors.[30-39] Previous studies showed that even shorter fragments from AcPHF6 are also capable of fibril formation but with a lower rate of polymerization and only upon nucleation with known fibrils.[40] Aggregation properties in lysine mutants of AcPHF6 were explored by the Goux research group and the results showed variable fibril formation tendency for the mutants subject to buffer and salt conditions.[40,41] Recently, Chemerovski-Glikman *et al.* demonstrated that proline mutants of AcPHF6 have inhibited the aggregation of the parent AcPHF6.[42]

In general, AcPHF6* remained less explored compared to AcPHF6 while recent studies attribute a higher role to [275]VQIINK[280] in Tau aggregation.[27] Despite several studies on these hexapeptides, to our knowledge, the contribution of individual amino acids in AcPHF6 and AcPHF6* towards Tau aggregation is not examined hitherto, which information is fundamentally important for the design of Tau aggregation inhibitors. Hence, in the present study, we have investigated the residue specific propensity of amino acids constituting AcPHF6* and AcPHF6 in their aggregation. For the study, a set of alanine mutation peptides of AcPHF6* and AcPHF6 were synthesized, and their conformational and aggregation properties were characterized by various biophysical and biochemical techniques like CD, NMR, TEM, ThS, and ANS assays.

3A.2. Results and Discussion

A set of twelve peptides consisting of parent peptides AcPHF6* (**1**) and AcPHF6 (**1'**) and their sequential single-site alanine mutant peptides (**2-6** and **2'-6'**) were synthesized by employing Fmoc-based solid phase peptide synthesis using rink amide MBHA resin (Figure **3A.2**). All the peptides were subsequently purified by reverse phase semi-preparative HPLC for further studies. Although mutant peptides of **1** and **1'** in which lysine is substituted by alanine were synthesized, they could not be purified because of partial solubility in acetonitrile-water combinations and with other buffers.
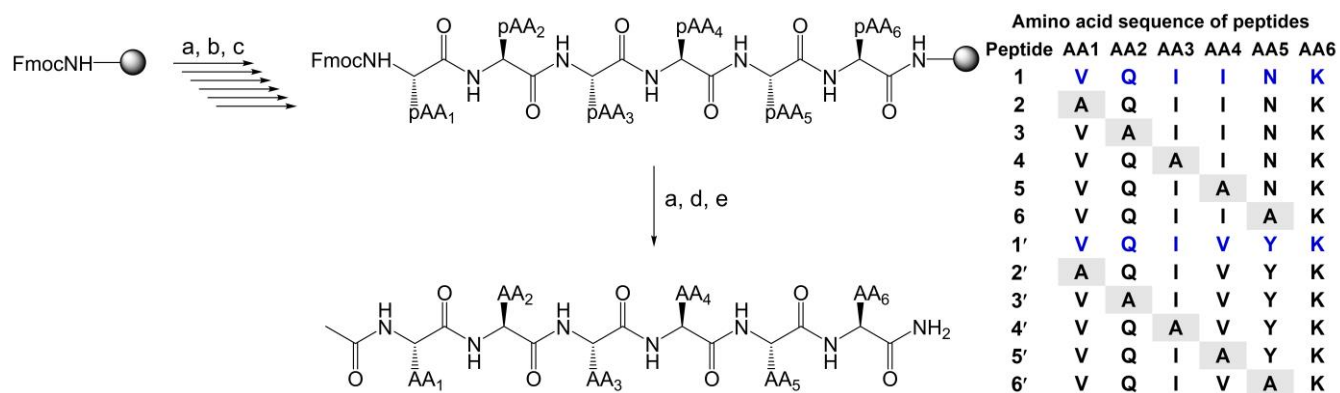
Figure 3A.2. The synthesis of peptides (**1**-**6** and **1'**-**6'**) using Fmoc-based solid phase peptide synthesis on rink amide MBHA resin (150 mg with 0.6 mmol/ gm loading capacity). Reaction conditions: (a) Fmoc deprotection in 20% piperidine in DMF (2*10 min); (b) Fmoc-pAA6-OH (2 eq.), HCTU (2 eq.), HOAt (2 eq.), DIPEA (2 eq.) in NMP, 1.5 hrs.; (c) Capping of free NH groups on resin using acetic anhydride (1.2 mL) and pyridine (0.8 ml), 30 mins. Steps (a) and (b) were repeated for coupling of the rest of the amino acids in sequential order until a linear chain of hexamer is achieved on the resin. (d) acetic anhydride (1 mL), DIPEA (100 µL) in DMF, 1 hr; (e) TFA: H$_2$O: TIPS in 9:0.5:0.5 volume ratio (3 times * 30 mins) for global deprotection of the peptide and cleavage from resin. pAA stands for the side chain protected form of the corresponding amino acid (AA).

### 3A.2.1. HPLC Purification of peptides (1-6, 1′-6′)

All the peptides were purified by reverse phase HPLC on Waters 2545 Quaternary Gradient Module with 2489 UV/Visible Detector using YMC–Pack ODS–A-HG C18 column of pore size S-10 µm, 12 nm, 250 mm * 20 mm I.D. A flow rate of 8 mL/min was used for the purification.

Table 3A.1. **(semi-prep HPLC methods)**

S. No.	Peptide	HPLC Gradient	Retention Time (min)
implied		Methods used for the HPLC purification of the peptides and the corresponding retention times.	
1	VQIINK (**1**)	40 % ACN:60 % water (10 min)	2.7
2	AQIINK (**2**)	40 % ACN:60 % water (15 min)	3.0
3	VAIINK (**3**)	40 % ACN:60 % water (15 min)	3.1
4	VQAINK (**4**)	50 %ACN:50 % water (15 min)	2.5
5	VQIANK (**5**)	50 % ACN:50 % water (12 min)	2.6
6	VQIIAK (**6**)	30 % ACN:70 % water (15 min)	2.3
7	VQIVYK (**1′**)	30 % ACN:70 % water (15 min)	6.4
8	AQIVYK (**2′**)	30 % ACN:70 % water (15 min)	7.6
9	VAIVYK (**3′**)	40 % ACN:60 % water (15 min)	6.3
10	VQAVYK (**4′**)	40 % ACN:60 % water (15 min)	8.3
11	VQIAYK (**5′**)	40 % ACN:60 % water (15 min)	7.2
12	VQIVAK (**6′**)	45 % ACN:55 % water (10 min)	5.3

3A.2.2. NMR spectroscopic study of peptides 1-6 and 1'-6'

For NMR spectroscopic study, ^{1}H NMR spectra for the compounds **1**-**6** and **1'-6'** were recorded in DMSO-*d*6 (Figure **3A.3**) and also in phosphate buffer at 298 K at 5 mM concentration. The chemical shift dispersion of amide and alpha proton regions in NMR reflects about the folded secondary structural nature of the linear peptides. It is evident from the overlay of these regions for peptides **1**-**6** and **1'-6'** (Figure **3A.3**) that none of the peptides have significant chemical shift dispersion either for amide or alpha protons. For all the peptides, amide and alpha region resonances were distributed within
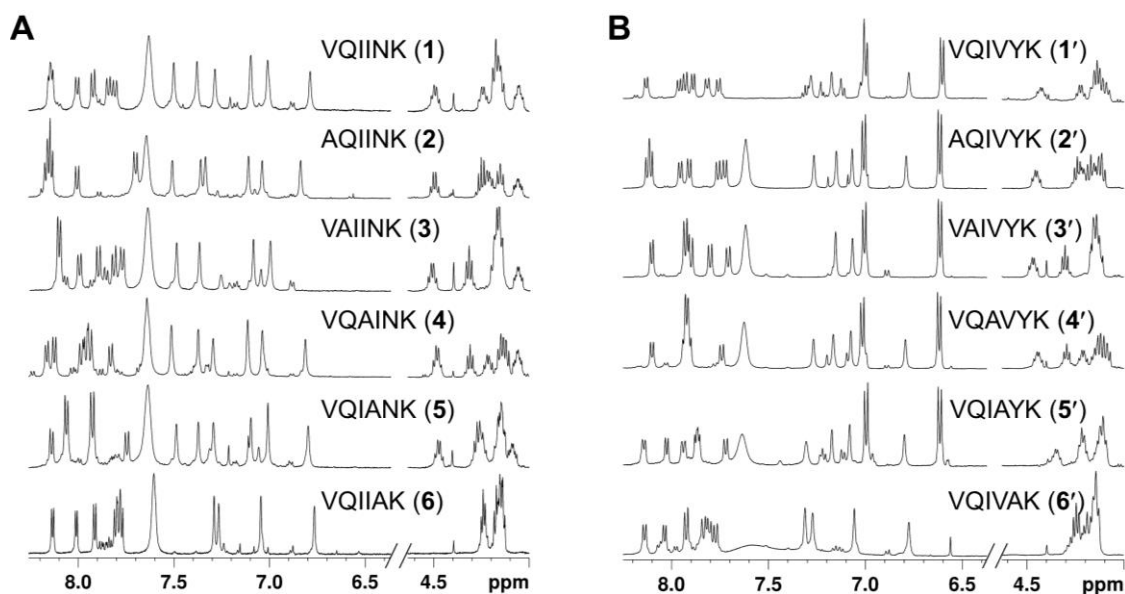
Figure. 3A.3. Overlay of ^{1}H NMR spectra of **1–6** and **1'-6'** recorded in DMSO-d6 at 298 K at 5 mM concentration. For clarity, the amide NH region (6.5–8.25 ppm) and alpha proton region (4–4.6 ppm), which signify the folded nature of the peptides, are shown. An absence of a robust solution-state conformation in these peptides was supported by the lack of resonance dispersion for both the amide and alpha proton regions.

a range of 0.2–0.5 ppm and had severe overlaps, supporting the absence of a well-folded conformation among these peptides. This is in support of the CD spectroscopic studies (Figure **3A.4**) indicating a random coil structure for **1**-**6** and **1'-6'** in monomeric form. ^{1}H NMR-based hydrogen bonding coefficients (calculated based on the change in the chemical shift over a temperature range) for amide NHs convey information about the involvement of NHs in hydrogen bonding or solvent shielding. Constituent backbone amide NH resonances from all the peptides have shown high-temperature coefficients (in the range −3.4 to −7.6 ppb/K; see table **3A.2**), indicating their non-involvement in a strong hydrogen bonding. This complements the lack of chemical shift dispersion for amide and alpha

proton regions, further supporting the absence of a robust conformation for any of the twelve peptides, **1**-**6** and **1'-6'**.

Temperature coefficient determination

The temperature dependence of amide protons resonances was calculated from 1D ^{1}H-NMR spectra by acquiring proton NMR in DMSO-d_6 at 300 K, 305 K, 310 K, 315 K, 320 K, 325 K on 400 MHz.

$$\text{Temperature co-efficient} = (\Delta\delta/\Delta T)\times 1000$$

Table 3A.2. NMR chemical shift temperature coefficients (in ppb/K) of amide protons in peptides **1**-**6** and **1′-6′**.

S. No.	Peptide	Amide NH chemical shifts (downfield to upfield direction) and corresponding temperature coefficients (in parenthesis, ppb/K)					
		NH1	NH2	NH3	NH4	NH5	NH6
1	VQIINK (**1**)	8.105 (-4.0)	8.096 (-5.6)	7.955 (-6.4)	7.883 (-4.8)	7.803 (-4.4)	7.772 (-4.4)
2	AQIINK (**2**)	8.115 (-3.6)	8.105 (-5.2)	8.093 (-4.8)	7.939 (-6.4)	7.666 (-3.2)	7.664 (-3.2)
3	VAIINK (**3**)	8.107 (-0.6)	8.107 (-6.4)	7.989 (-7.6)	7.906 (-6.0)	7.813 (-5.6)	7.770 (-5.2)
4	VQAINK (**4**)	8.116 (-5.2)	8.086 (-4.0)	7.92 (-4.0)	7.913 (-5.2)	7.897 (-5.2)	7.788 (-4.4)
5	VQIANK (**5**)	8.113 (-4.0)	8.033 (-4.8)	8.033 (-5.2)	7.896 (-4.8)	7.896 (-5.6)	7.719 (-4.0)
6	VQIIAK (**6**)	8.135 (-4.0)	8.010 (-6.0)	7.924 (-4.8)	7.790 (-4.8)	7.770 (-4.4)	7.750 (-5.2)
7	VQIVYK (**1′**)	8.109 (-3.6)	7.944 (-5.2)	7.902 (-4.8)	7.891 (-6.0)	7.785 (-4.4)	7.733 (-4.8)
8	AQIVYK (**2′**)	8.105 (-3.2)	8.078 (-4.0)	7.918 (-5.2)	7.865 (-6.0)	7.722 (-4.4)	7.697 (-4.0)
9	VAIVYK (**3′**)	8.068 (-4.8)	7.894 (-4.8)	7.883 (-5.6)	7.865 (-4.8)	7.767 (-4.4)	7.676 (-4.4)
10	VQAVYK (**4′**)	8.074 (-3.6)	7.893 (-3.6)	7.893 (-4.4)	7.880 (-4.4)	7.861 (-5.6)	7.706 (-4.0)
11	VQIAYK (**5′**)	8.121 (-3.6)	7.991 (-4.8)	7.908 (-4.4)	7.830 (-4.8)	7.830 (-5.2)	7.689 (-4.2)
12	VQIVAK (**6′**)	8.112 (-4.0)	8.000 (-4.8)	7.892 (-4.4)	7.799 (-4.4)	7.764 (-5.2)	7.742 (-4.4)

3A.2.3. CD spectroscopic study of peptides 1-6 and 1'-6'

In normal physiological conditions, Tau protein exists in a random coil conformation or natively disordered state.[43,44] CD spectroscopic study of all the twelve peptides was carried out at 1 mg/mL concentration in plain 5 mM MOPS buffer (Figure **3A.4**) in non-aggregating conditions. All the peptides exhibited a similar pattern of CD absorption with only negative mode absorption. Peptides **1** and **4** had similar CD spectra with negative absorption at ~203 nm and a very feeble shoulder around 225 nm. Whereas **2**, **3**, **5,** and **6** exhibited slightly intense CD spectra compared to **1** and **4** with a negative absorption at 205 nm and a weak negative shoulder around 225 nm. This shift for **1** and **4** could be due to the presence of a mixed structure.
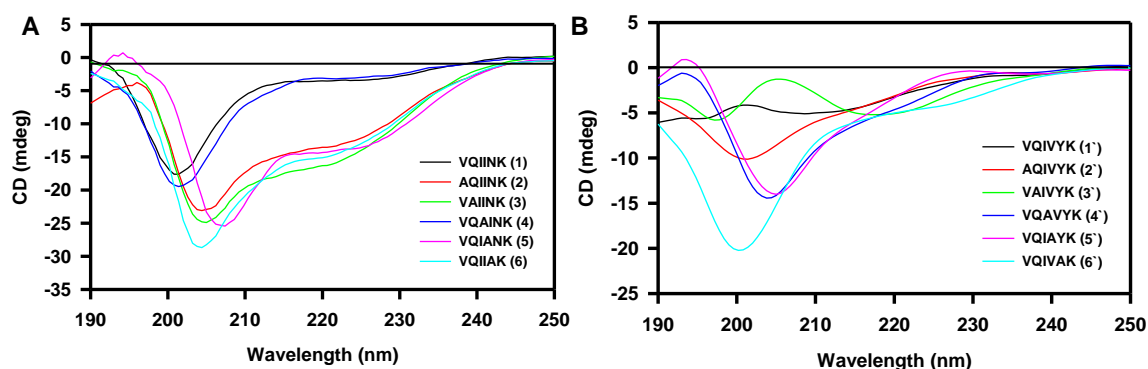

Figure. 3A.4 Circular dichroism (CD) analysis for (A) **1-6** and (B) **1'-6'** recorded at 1 mgmL^{-1} concentration in 5 mM MOPS buffer at 298 K in non-aggregating conditions. None of these peptides showed the CD characteristics of a well-folded alpha helix or a beta-sheet. All of the peptides, in general, showed a random coil conformation with negative absorption at approx. 205 nm, while **1'** and **3'** indicated more inclination towards a β-sheet structure.

Overall, the described CD pattern is primarily indicative of a random coil structure.[40,41] Hence, a possible random coil population may be inferred for all the peptides **1**-**6**. A similar trend was observed for the conformation of peptides in the series **1'-6'** wherein **2'**, **4'**, **5',** and **6'** peptides exhibited negative absorptions around ~203-205 and ~225 nm, with the latter being weak in intensity. A slight rightward shift for **4'** and **5'** compared to **2'** and **6'** could indicate a mixed population of the random coil and beta-sheet. Peptides **1'** and **3'** did not have a characteristic CD pattern corresponding to any of the standard peptide secondary structural scaffolds. The signature obtained for peptides **1'** and **3'** indicates structural orientation towards the β-sheet.

3A.2.4. Self-aggregation study of 1-6 and 1'-6′ peptides

The aggregation of **1-6** peptides was monitored by ThS and ANS fluorescence. It was observed that the substitution of valine or isoleucine in **1** with alanine diminished the aggregation propensity of hexapeptides as compared to the native peptide **1**. However, substituting glutamine by alanine in peptide **3** increased the aggregation propensity (Figure **3A.5**) while a marginally higher aggregation propensity was also observed for **6** in which alanine is substituted for asparagine. On comparing at 168 hours, **3** and **6** gave 83 and 60 a.u. fluorescence, respectively, compared to 30 a.u. for **1**.
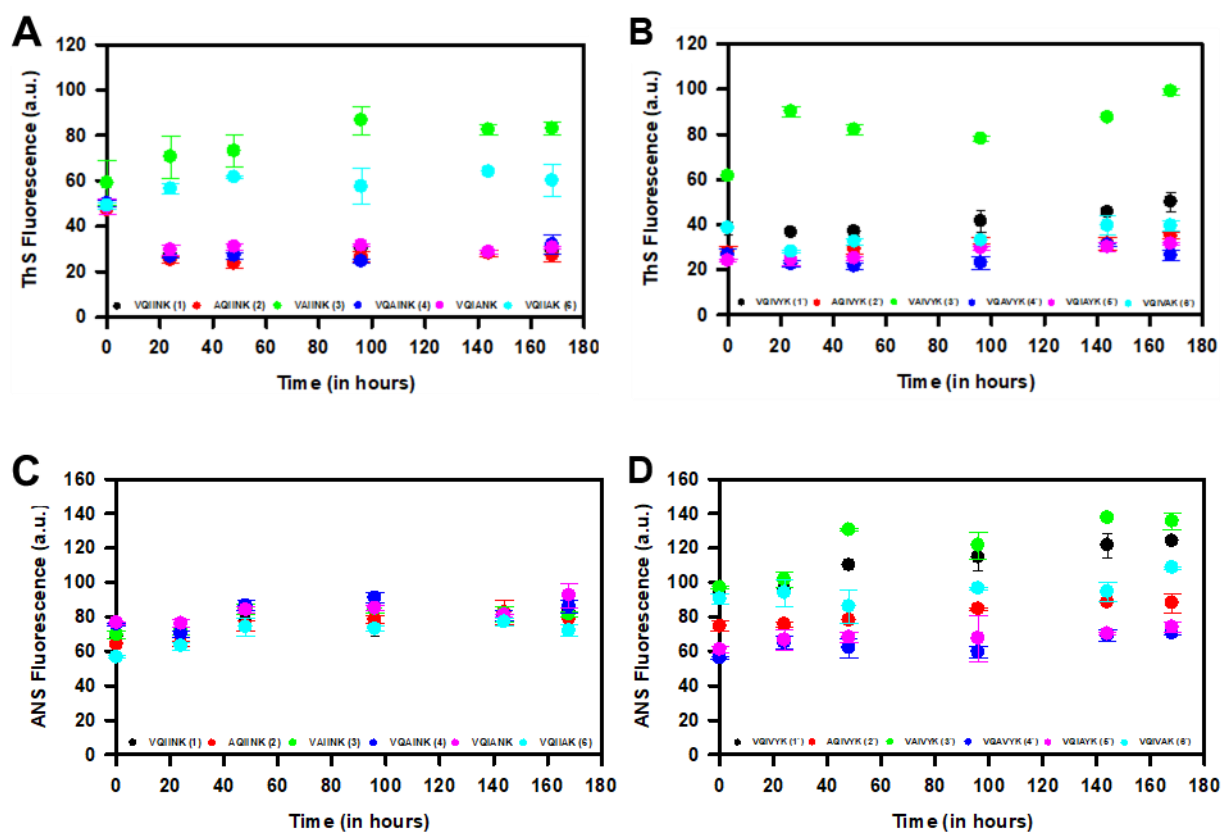
Figure. **3A.5**. (**A**) Aggregation of peptides **1-6** monitored using ThS fluorescence shows the effect of alanine incorporated at various positions in the VQIINK hexapeptide. VQIINK aggregation was found to be affected by the substitution of Glu or Asn residues, where these substitutions enhanced the aggregation propensity. (**B**) Peptides **1′-6′** showed a similar trend in their aggregation propensity, as peptide 30 with Glu to Ala substitution showed increased aggregation compared to the other peptides in the group. (**C**) ANS fluorescence assay was carried out to monitor the change in hydrophobicity of peptides 1-6 and 1'-6'. There was a minimal hydrophobic change in synthetic peptides as compared to peptides 1-6. (**D**) ANS fluorescence assay for peptides 1'-6' showed that hydrophobicity of 1' and 3' increases upon aggregation as compared to other variants.

Similar results were observed for aggregation assay carried out for **1'-6'** peptides and their mono-substituted variants. Aggregation propensity was found to be suppressed for **2'**, **4'**, **5'**, and **6'** when

compared to **1'** and **3'**. The aggregation propensity of **3'** was found to be greatly increased compared to all hexapeptides (Figure **3A.5B**). At 168 hours, **3'** exhibit an absolute fluorescence of 100 a.u., as compared to **1'** where a fluorescence value of 48 a.u. was obtained. Furthermore, peptides **1'** and **3',** which showed high aggregation propensity in ThS fluorescence assay did not present any prominent signature for random coil but showed orientation towards β-sheet structure in their CD spectra (Figure **3A.4**). On the other hand, ANS fluorescence assay for monitoring hydrophobicity change over time did not show a significant difference between **1** and its variants (Figure **3A.5C**). **1'** and its variants in ANS fluorescence assay followed the pattern of the corresponding ThS assay and suggest that glutamine to alanine substitution was associated with increased hydrophobicity (Figure **3A.5D**).

Overall, the current aggregation assay suggests that substitution of glutamine to alanine in **1** and **1'** elevates the aggregation propensity, while alanine replacements for the majority of all other residues suppress the aggregation propensity.
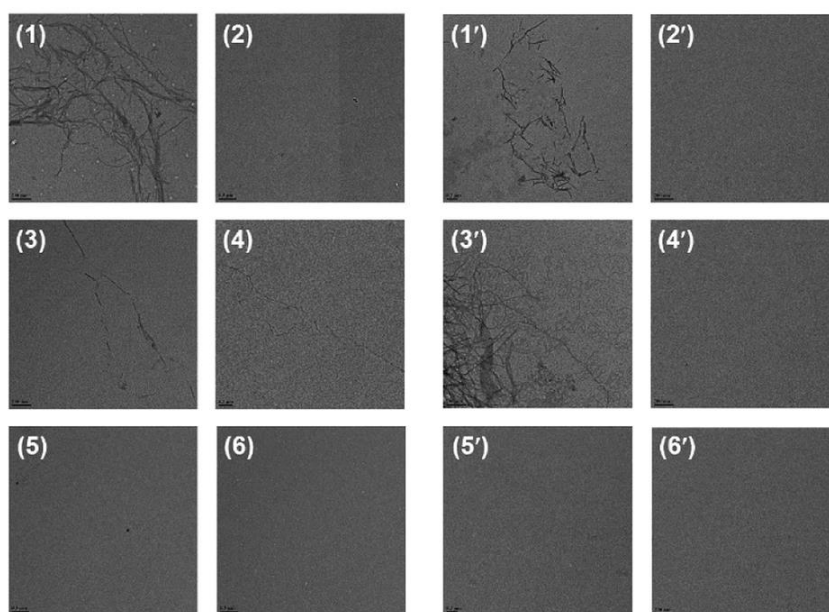

Figure. 3A.6. TEM images for peptides **1–6** and **1′-6′** at the aggregation assay end-point (168 h). The **1** and **1′** hexapeptides can form fibrillar aggregates similar to the full-length Tau protein as they consist of the core upon which aggregates of Tau form. Except for the parent peptides **1** and **1′** and the modified peptides **3** and **3′**, none of the other peptides were observed to form aggregates.

3A.2.4. Self-aggregation study of 1-6 and 1'-6′ peptides by TEM analysis

Further, the self-aggregation properties of peptides **1-6** and **1'-6'** were characterized by TEM analysis (Figure **3A.6**). Aggregation for all the peptides was set up at 100 µM concentrations in 20 mM BES buffer at pH 7.4 with 25 µM heparin as an inducer. After incubation for 168 hours at 37 °C, TEM was

recorded for 2 µM peptides on carbon-coated copper grids. The parent peptides, AcPHF6* (**1**) and AcPHF6 (**1'**), formed aggregates as expected. Out of ten mutant peptides, peptides **3** and **3'**, both having glutamine substituted by alanine, showed filamentous aggregates similar to **1** and **1'**, while no aggregates were observed for the rest of the peptides. Thus, it is interesting to note that out of the first five residues in **1** and **1'** (namely VQIIN in **1** and VQIVY in **1'**), the substitution of any amino acid except glutamine with alanine had nullified their aggregation properties. Conversely, it may be stated that except for glutamine (and asparagine as per fluorescence assay results), the rest of the residues (V and I in **1**, and V, I and Y in **1'**) have higher aggregation propensity than alanine when present in **1** and **1'**. Interestingly, in one of the recent studies where proline, a beta-sheet breaker, is substituted for each amino acid in **1'**, it was reported that the peptide with glutamine to proline substitution had inhibited the aggregation properties of **1'** while the mutant peptide itself being non-aggregating in nature.[42] We speculate that the glutamine in PHF peptides might be in a conformationally favorable position for beta-sheet formation and aggregation, which was disturbed by a cyclically constrained amino acid proline but not by alanine in our case.
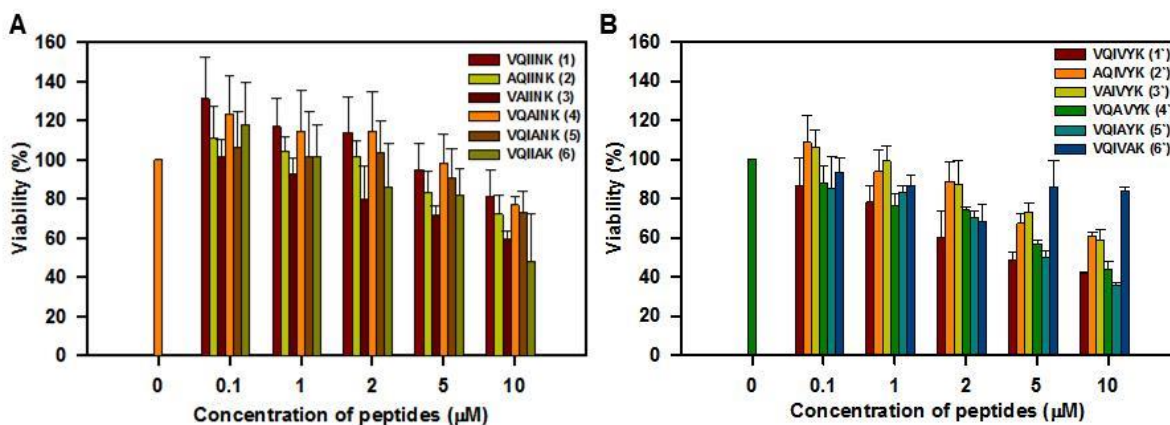
Figure 3A.7: Cell viability assays for aggregated peptides **1**-**6** and **1'**-**6'**. The aggregation assay end-point samples were tested for their effect on the cell viability of neuro2a cells. (**A**) The viability assay for aggregated peptides **1**-**6** does not show toxicity to neuro2a cells. (**B**) The viability assay for aggregated peptides **1'**-**6'** showed a reduction in viability with increasing concentration in comparison to peptides **1**-**6**. Cell viability was found to be sustained for the **6'** peptide.

3A.2.5. Relative toxicity of 1-6 and 1'-6' hexapeptides on neuro2a cells

The formation of Tau aggregates and its deposition in neuronal cells in the form of NFTs is known to be toxic and cause neurodegeneration. Furthermore, aggregated **1**-**6** and **1'**-**6'** peptides at 168 hours were studied for their toxicity in neuro2a cells. The aggregated **1**-**6** peptides did not show toxicity to neuro2a cells up to 5 µM concentration. Thus, we carried out a cell viability assay on neuro2a cells using the end

product of peptide aggregation assay to explore whether alanine substitution imparts toxicity to the peptides. The aggregated **1-6** and **1'-6'** peptides at 168 hours were studied for their toxicity in neuro2a cells (Figure **3A.7**). The cells were treated with 1-10 μM of the aggregated peptides for 24 hours. The aggregated **1-6** peptides did not show toxicity to neuro2a cells up to 5 μM concentration. The highest concentration of 10 μM for all aggregated **1-6** peptides also showed 60% viability as compared to untreated control (Figure **3A.7A**). The cell viability assay suggested that the concentration of 0.1 and 1 μM for all **1'-6'** peptides were not toxic to neuro2a cells. The concentrations of 2-10 μM of peptides **1'-6'** showed reduced viability as compared to untreated control. A relatively better tolerance by cells is observed for **6'** aggregated peptide that resulted in 80% viability at 10 μM concentration whereas the other peptides showed less than 50% viability at the same concentration (Figure **3A.7B**).

3A.3. Conclusions

In conclusion, Alzheimer`s disease is characterized by the deposition of intracellular Tau aggregates and extracellular amyloid-beta plaques. Various treatment strategies have been designed to inhibit or revert this protein aggregation. Especially, PHF6* and PHF6 peptide-based inhibition therapies have gained focus due to their structural mimicry of Tau aggregation. To understand the aggregation nature of these two peptides at individual residue levels, here we have synthesized alanine mutant libraries of AcPHF6* and AcPHF6, and characterized them by various biochemical and biophysical methods. The results showed that all the mutant peptides except for those with glutamine to alanine substitution (**3** and **3'**) had not aggregated as per the general conditions used for the parent peptides **1** and **1'**. While asparagine to alanine mutation (**6**) showed aggregation propensity in fluorescence assays, no aggregates were observed in TEM. Therefore, it was inferred that except glutamine, the residues V and I in AcPHF6* **1**, and V, I, and Y in AcPHF6 **1'** imparts higher aggregation propensity than alanine in the parent peptides. These results are also in alignment with the higher beta sheet propensity of alanine compared to Q but lower than that of V, I and Y.[45,46] Mutational studies using other amino acids that have higher beta sheet/alpha-helical propensities may provide more details on the conformational and aggregation properties of PHF peptides. Overall, alanine substitution in PHF peptides reduces their aggregation propensity without any major change in their conformation. Studying the aggregation properties of these alanine based PHF peptide derivatives provides important and site-specific insight into the aggregation behavior of PHFs, *i.e.,* PHF6 and PHF6*. Hence, this strategy can be potentially employed to selectively control the aggregation in PHFs *via* the rational choice of alanine mutations.

While further expansion studies are in progress in our research group, the current results can form the basis for designing PHF-based Tau aggregation inhibitors by suitable mutations.

3A.4. Experimental procedures and analytical data

3A.4.1. General Procedure for solid phase peptide synthesis

All the peptides were synthesized by Fmoc-based solid phase peptide synthesis using rink amide resin. For the synthesis of each peptide, 150 mg resin was swollen in 5 mL of dry DCM for 1 hr followed by the Fmoc deprotection of the resin using 20% piperidine in DMF. After Fmoc deprotection, the first amino acid was loaded onto the resin using 2 eq. of HCTU, and 4 eq. of DIPEA in 5 mL of NMP for 2 hrs. The fully loaded resin was then subjected to capping using acetic anhydride and pyridine in a 3:2 ratio. From this stage, elongation of the peptide chain was carried out by repeated Fmoc deprotection (using 20 % piperidine in DMF) and coupling of the amino acids (using 2 eq. of Fmoc protected amino acid, 2 eq. of HCTU, 4 eq. of DIPEA in 5 ml of NMP for 2 hrs) up to the desired length of the peptide. After the coupling of the final amino acid and deprotection of its Fmoc group, acetylation of the terminal free amine was carried out using acetic anhydride and DIPEA in DMF. Final linear peptide was cleaved from the resin in three cycles using 5 mL of cleaving cocktail TFA: TIPS: H_2O (9 mL: 0.5 mL: 0.5 mL) each time for 1 hr. The cleaved contents were solvent dried by solvent evaporation on a rotary evaporator and crude peptides were precipitated in ice cold diethyl ether, which was taken forward for reverse phase HPLC purification.

3A.4.2. CD Spectroscopy

CD spectra were acquired for all peptides in a cuvette with a path length of 1 mm under nitrogen atmosphere at 25° Con Jasco J-815 CD spectrometer. For CD, peptides were dissolved in 50 mM MOPS buffer (0.5 mg/mL). The scans were carried out at a scan speed of 100 nm/min and bandwidth of 1 nm with a scan range of 190 nm to 250 nm. The final spectra were taken as an average of 5 acquisitions. The buffer baseline was set with 50 mM MOPS buffer at pH 7.2 and subtracted from the measured spectra for each sample. The final subtracted values were plotted using the origin software.

3A.4.3. NMR Spectroscopy

For NMR experiments, 2 mg of each compound dissolved in 0.5 mL of DMSO-d_6. ^{1}H NMR experiments for all the compounds were recorded at 298 K on Bruker Avance 500 MHz NMR spectrometer equipped with a BBO probe. Variable temperature (VT) experiments for calculating the amide NH temperature coefficients were carried out on Bruker Avance II 400 MHz NMR spectrometer

equipped with BBFO probe. A temperature range of 295 K to 325 K with 5 K increments was used for VT experiments.

3A.4.4. ThS fluorescence assay

100 μM peptides were resuspended in the assembly buffer composed of 20 mM BES at pH 7.4, 25 μM heparin, 25 Mm NaCl, 0.01% NaN$_3$ and 20 μL PIC for aggregation (stock solution). This preparation was incubated at 37 °C and the fluorescence was measured every 24 hours. The peptides were diluted to 5 μM with 20 μM of ThS and incubated in dark for 10 minutes. ThS fluorescence of 20 mM BES was taken as blank. The ThS fluorescence was measured in duplicate for all samples and blank at 521 nm by exciting the fluorophore at 440 nm in Tecan Infinite Series Pro200 spectrofluorimeter.

3A.4.5. TEM Analysis

Transmission electron microscopy was carried out to determine the formation of peptide filaments. After seven days ageing of 100 μM peptide stock solutions that were set up for aggregation, 2 μM of peptides were applied to 400 carbon-coated copper grids for 30 seconds followed by 2 washes with filtered MilliQ water for 30 seconds each. The samples were negatively stained for 1 minute using 2% uranyl acetate. The Grids were dried overnight and the morphology of peptides was mapped using Tecnai G2 20 S – Twin transmission electron microscope.

3A.4.6. ANS fluorescence assay

5 μM of peptides set up for aggregation were incubated with 100 μM of ANS in dark for 10 minutes. The ANS fluorescence was measured with excitation and emission wavelength of 390 and 475 nm respectively in Tecan Infinite Series Pro200 spectrofluorometer. All readings were taken in duplicate and the fluorescence of 20 mM BES buffer was subtracted from each sample.

3A.4.7. Transmission electron microscopy

2 μM of peptides were spotted on carbon-coated copper grids. The peptides were stained by 2% uranyl acetate and dried. The morphology of peptides was mapped using Tecnai G2 20 S – Twin transmission electron microscope.
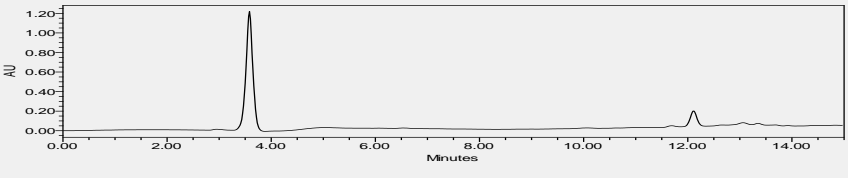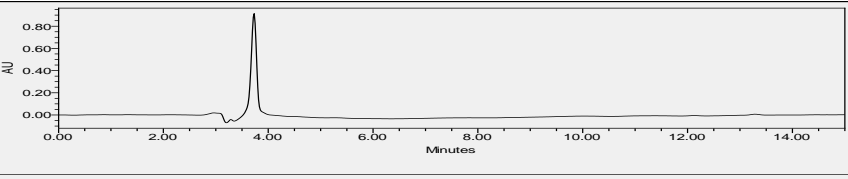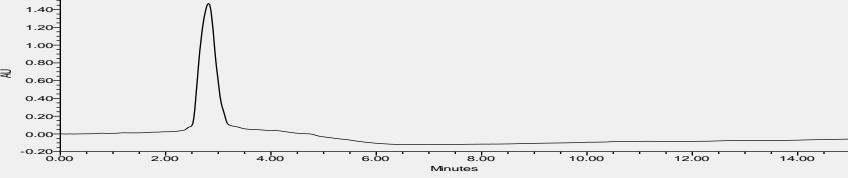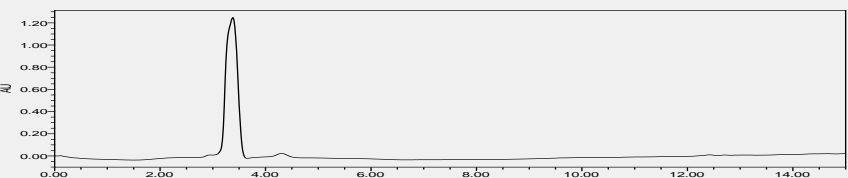
3A.4.8. Cell viability assay

The cell viability assay was performed by MTT (3-(4, 5-dimethylthiazol-2-yl)-2, 5-diphenyltetrazolium bromide) assay. Neuro2a cells were seeded in 96 well plate at the density of $1*10^4$
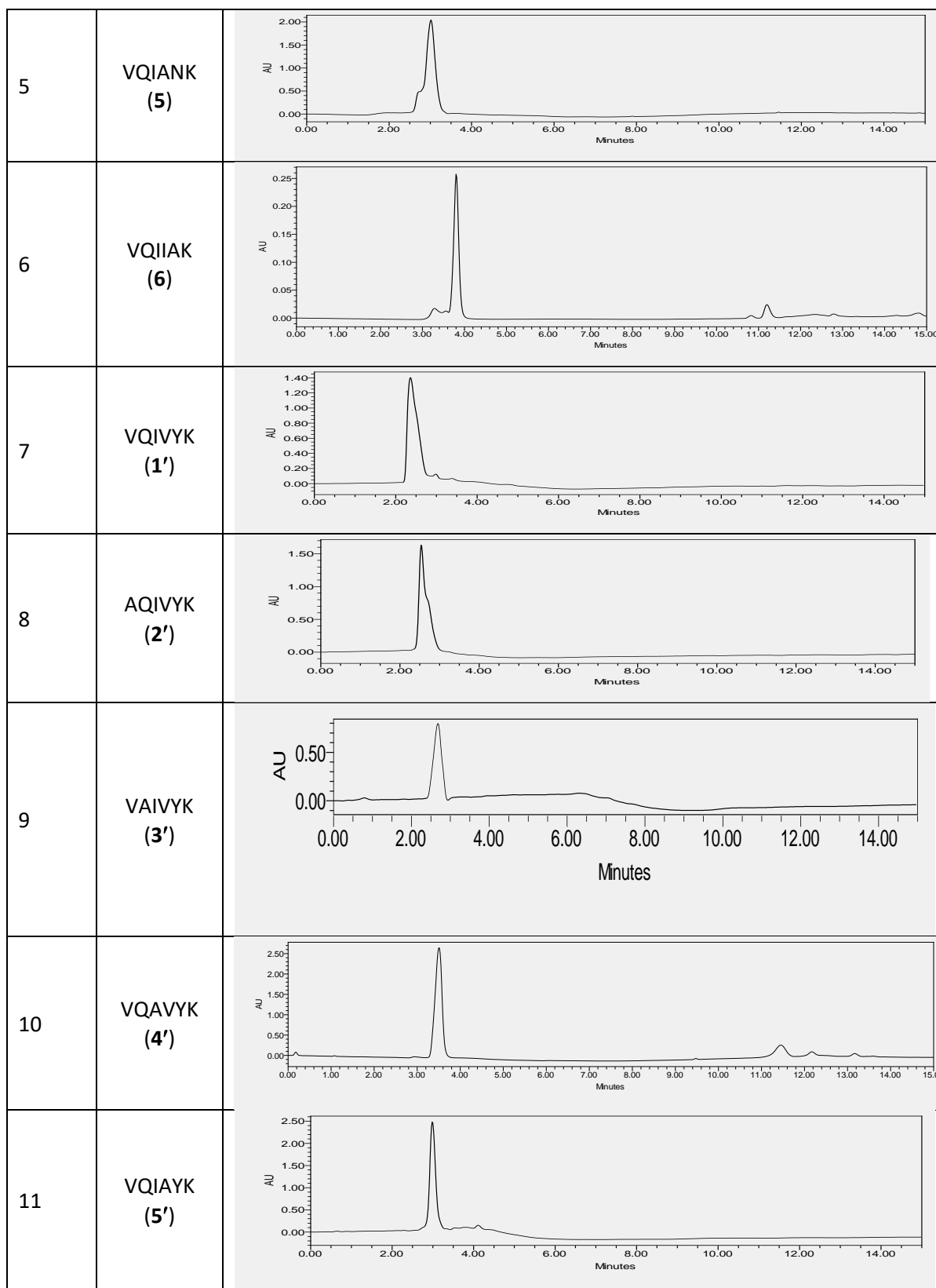
cells/well and incubated for 24 hours. The aggregated peptides from the 168 hours incubated reaction mixture were added to the seeded cells in the serum-starved media for 24 hours. Further, the cells were incubated with 0.5 mg/mL MTT reagent for 4 hours. The formazan crystals formed with dissolved in DMSO, which gave a purple colour to the solution. This absorbance was read in Tecan Infinite Series Pro200 spectrofluorimeter at 570 nm in triplicates and the blank subtraction was made from absorbance by media incubated with MTT reagent in a similar way. The background subtraction was made with the readings at 660 nm.

3A.4.9. Analytical HPLC of peptides (1-6 and 1′-6′)

The purity of all the peptides was determined by analytical HPLC using YMC Pack ODS-A-HG C18 column of pore size S-10 µm, 12 nm, 250 mm * 4.6 mm I.D. on Waters 2545 Quaternary Gradient Module with 2489 UV/Visible detector. ACN and water mobile phase was used for analytical HPLC run, a gradient run of 20 % ACN to 90% in 20 min with a flow rate of 1 mL/min for all the peptides.

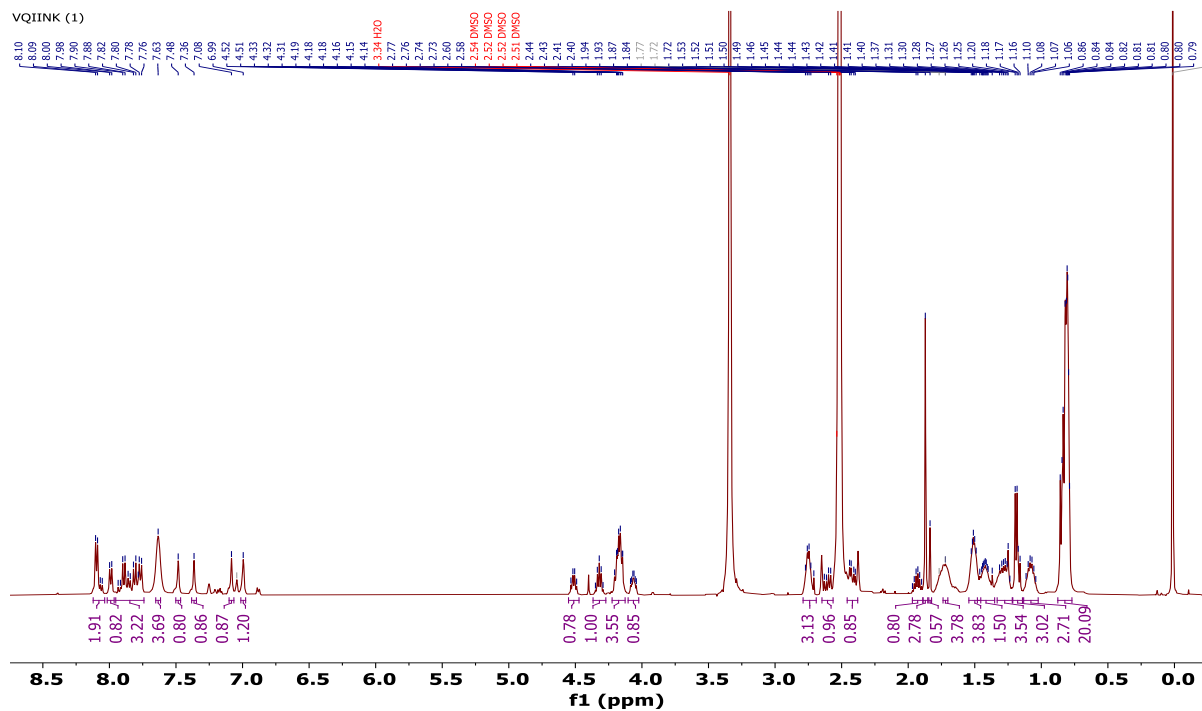**Table 3A.3**. Analytical HPLC chromatograms of the peptides (**1**-**6** and **1′**-**6′**)

S. No.	Peptide	HPLC Chromatogram
1	VQIINK (**1**)	
2	AQIINK (**2**)	
3	VAIINK (**3**)	
4	VQAINK (**4**)	

5	VQIANK (**5**)	
6	VQIIAK (**6**)	
7	VQIVYK (**1′**)	
8	AQIVYK (**2′**)	
9	VAIVYK (**3′**)	
10	VQAVYK (**4′**)	
11	VQIAYK (**5′**)	

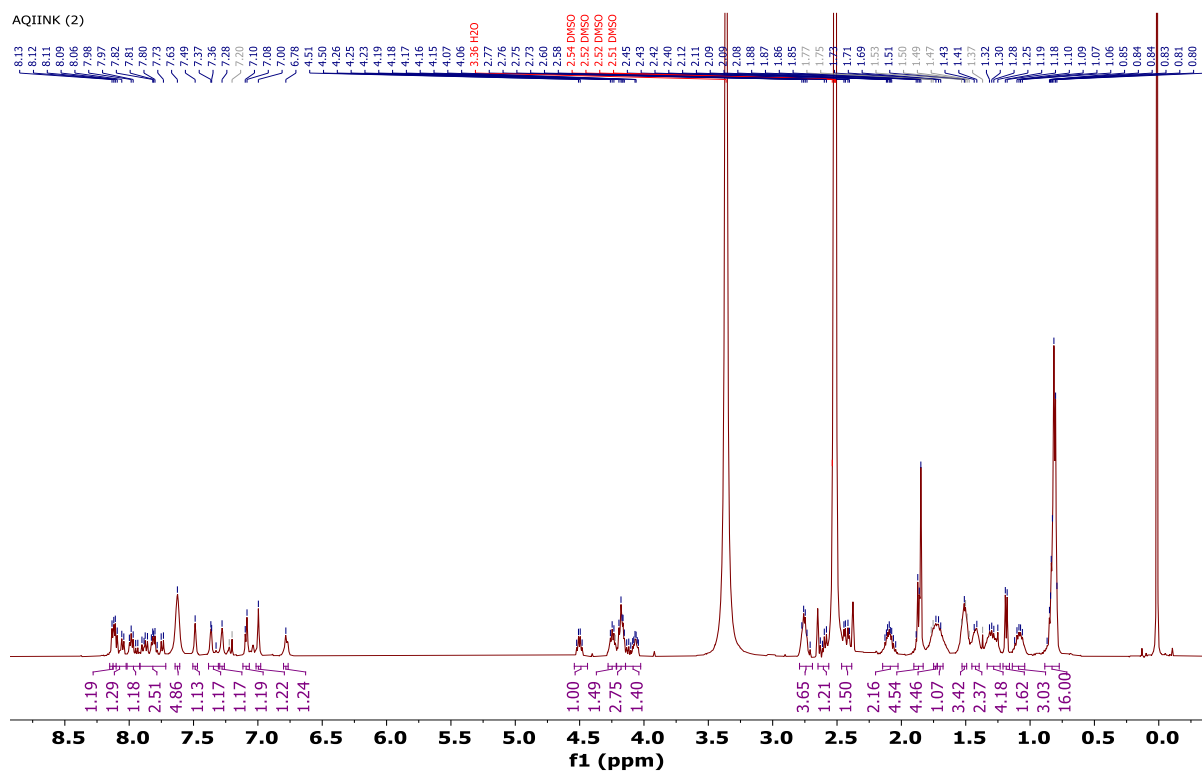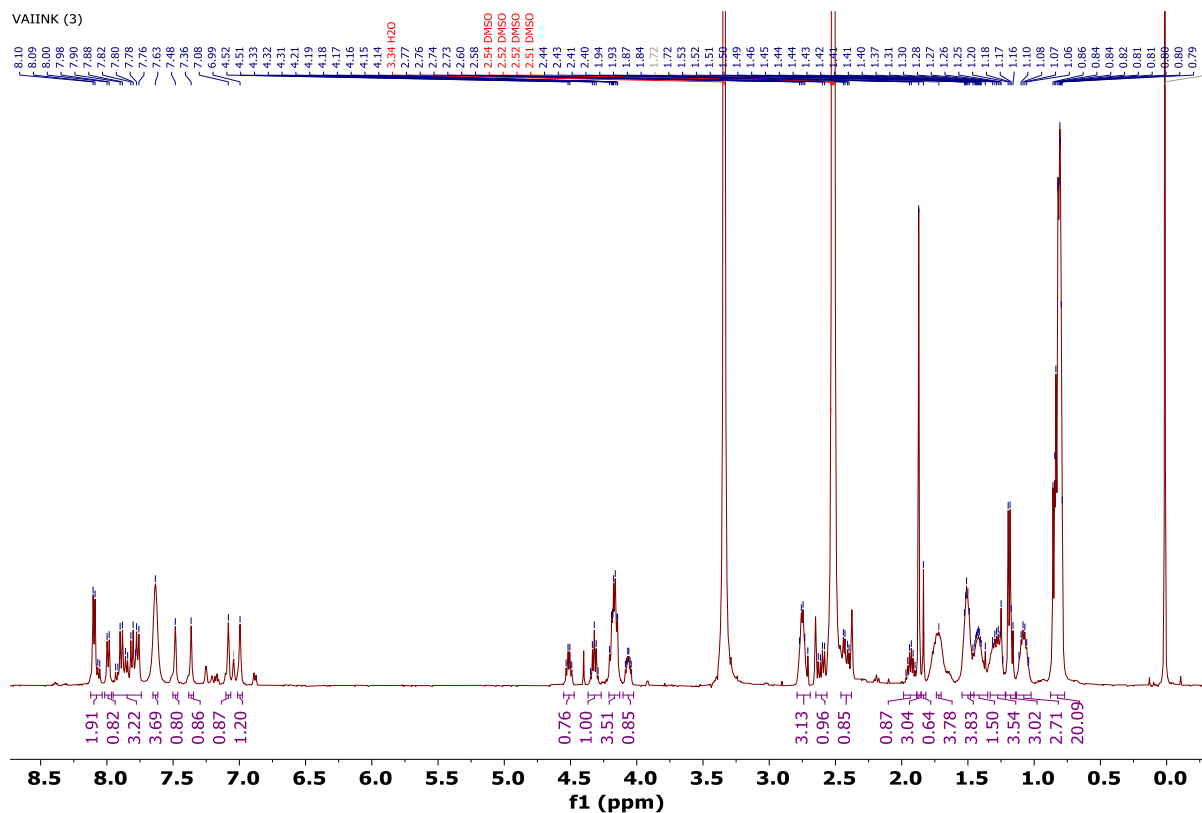| 12	VQIVAK (**6′**)	
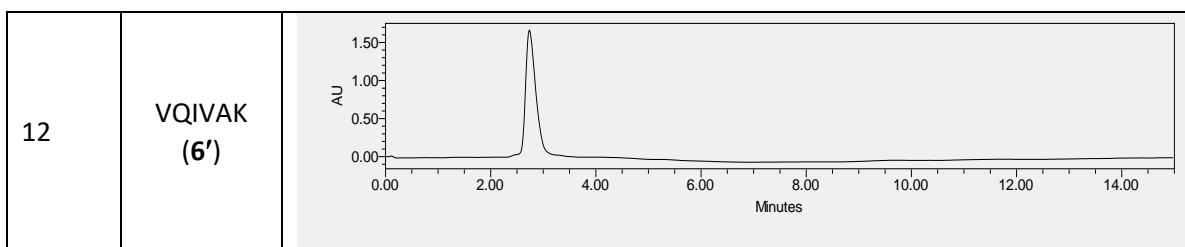
3A.4.10. ¹H NMR spectra of peptides (1-6 and 1′-6′)

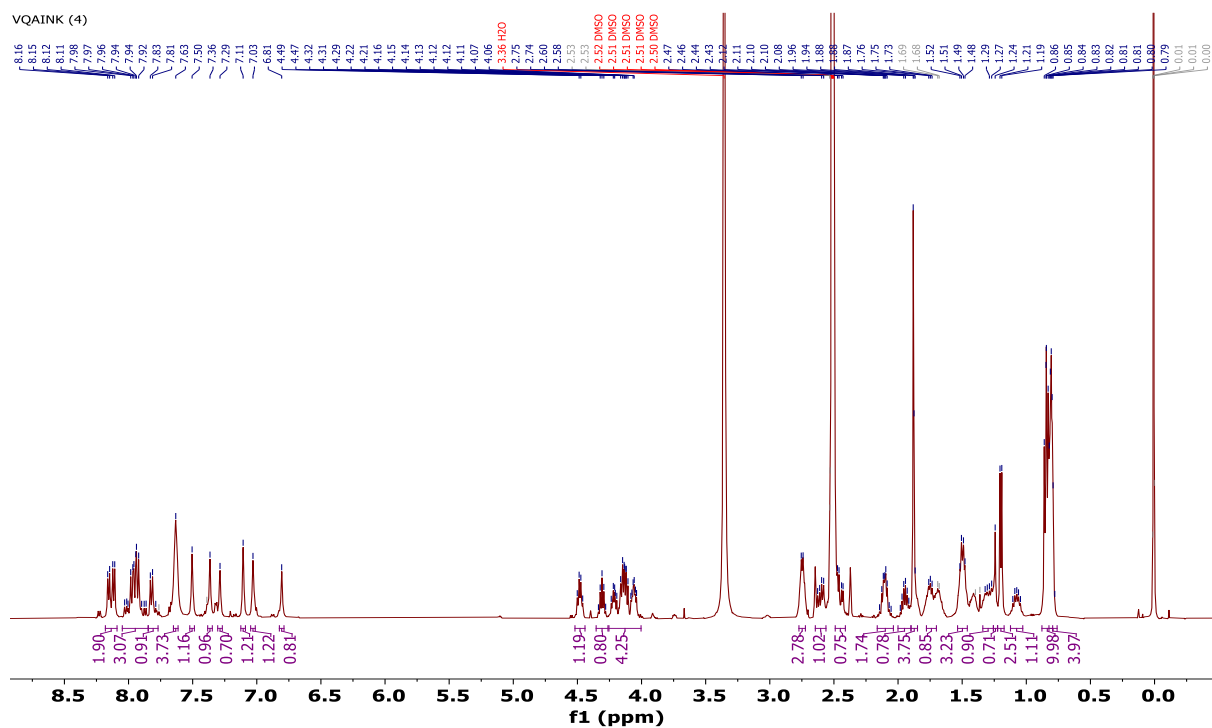¹H NMR of **1** (Ac-VQIINK-NH₂) on 500 MHz at 298 K in DMSO-*d₆*.

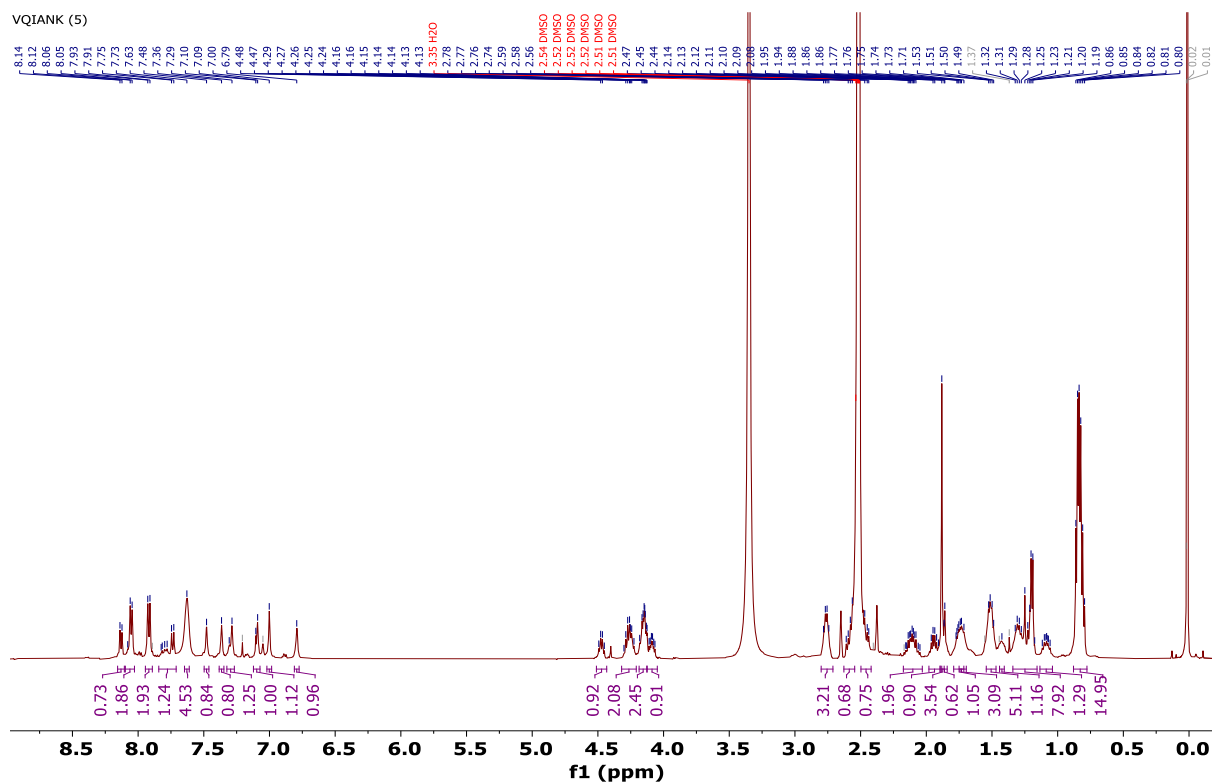^{1}H NMR of **2** (Ac-AQIINK-NH$_2$) on 500 MHz at 298 K in DMSO-*d*$_6$.

^{1}H NMR of **3** (Ac-VAIINK-NH$_2$) on 500 MHz at 298 K in DMSO-*d*$_6$.

^{1}H NMR of **4** (Ac-VQAINK-NH$_2$) on 500 MHz at 298 K in DMSO-d_6.

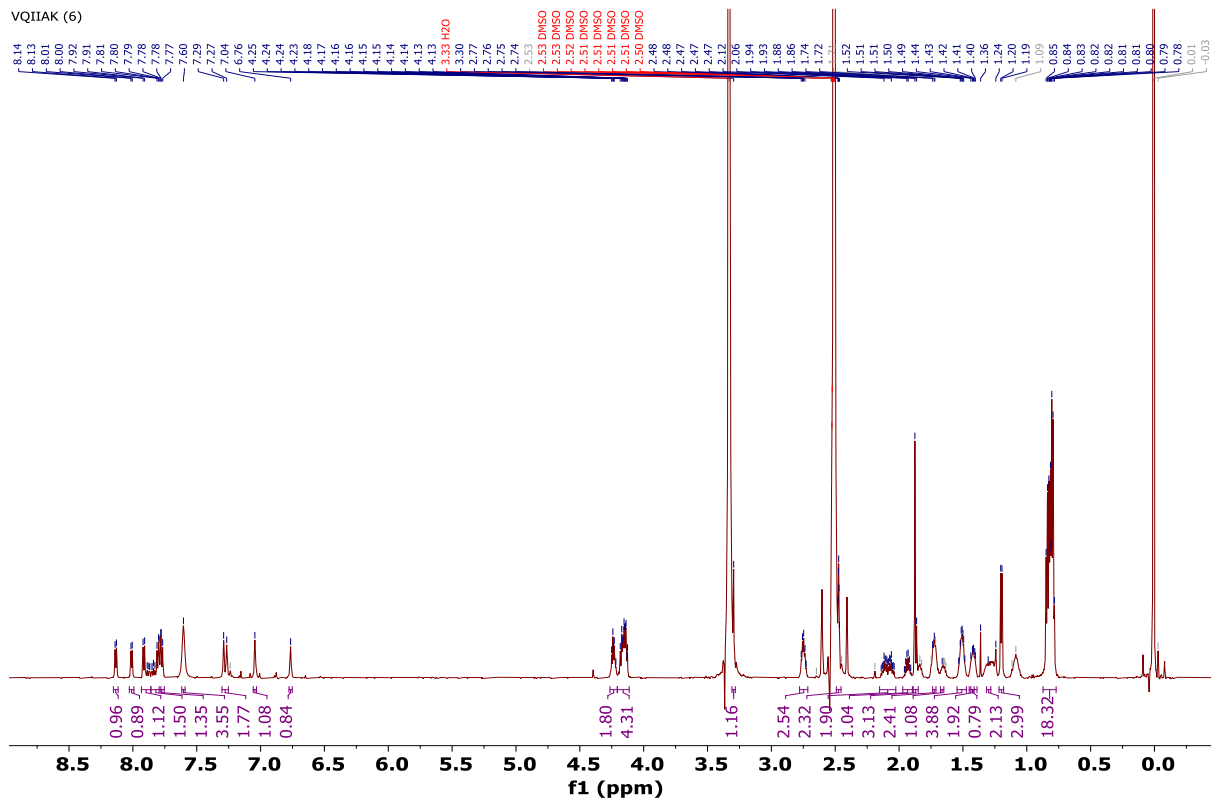^{1}H NMR of **5** (Ac-VQIANK-NH$_2$) on 500 MHz at 298 K in DMSO-d_6.

^{1}H NMR of **6** (Ac-VQIIAK-NH$_2$) on 500 MHz at 298 K in DMSO-*d$_6$*.

^{1}H NMR of **1'** (Ac-VQIVYK-NH$_2$) on 500 MHz at 298 K in DMSO-*d$_6$*.

^{1}H NMR of **2′** (Ac-AQIVYK-NH$_2$) on 500 MHz at 298 K in DMSO-d_6.

^{1}H NMR of **3′** (Ac-VAIVYK-NH$_2$) on 500 MHz at 298 K in DMSO-d_6.

^{1}H NMR of **4′** (Ac-VQAVYK-NH2) on 500 MHz at 298 K in DMSO-*d*6.

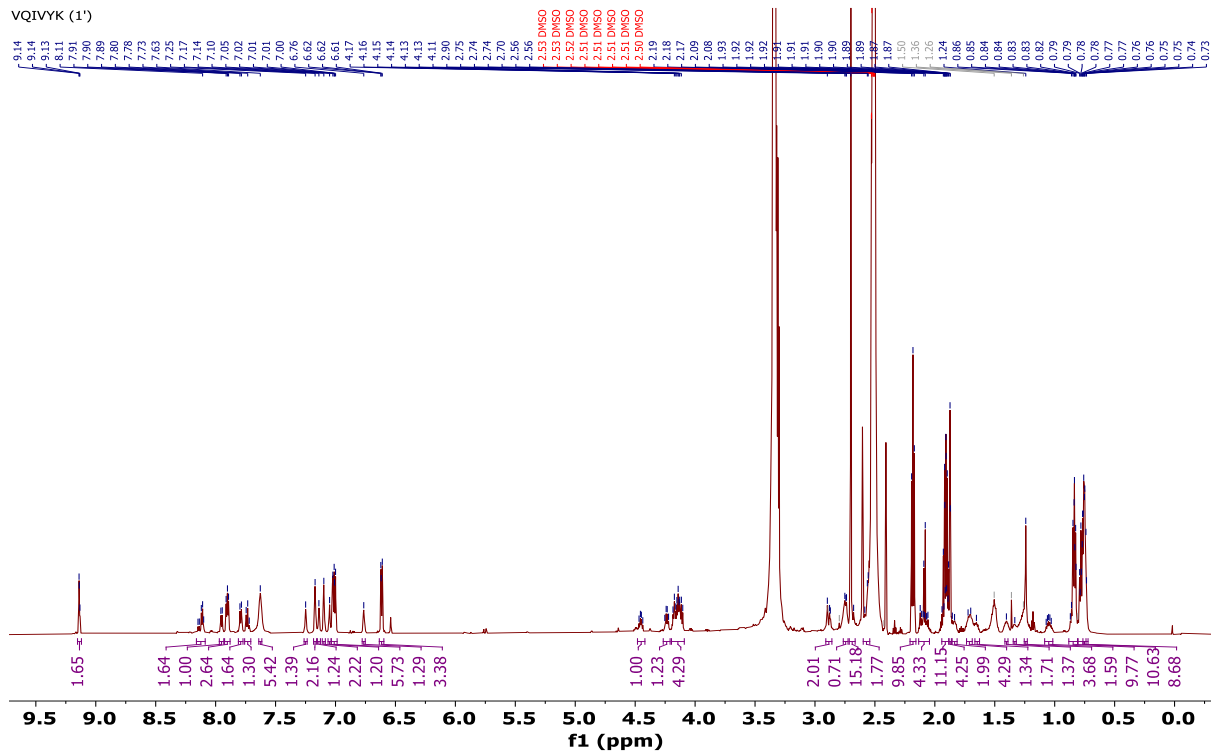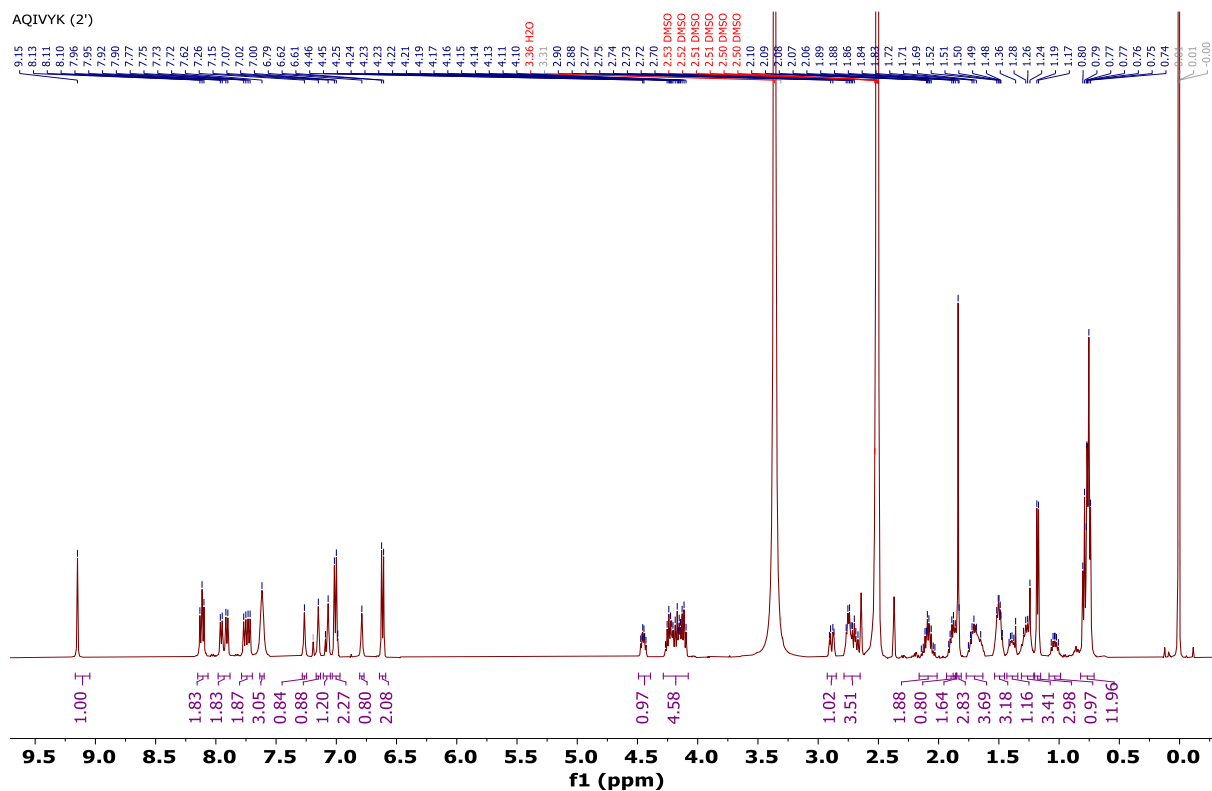^{1}H NMR of **5′** (Ac-VQIAYK-NH2) on 500 MHz at 298 K in DMSO-*d*6.

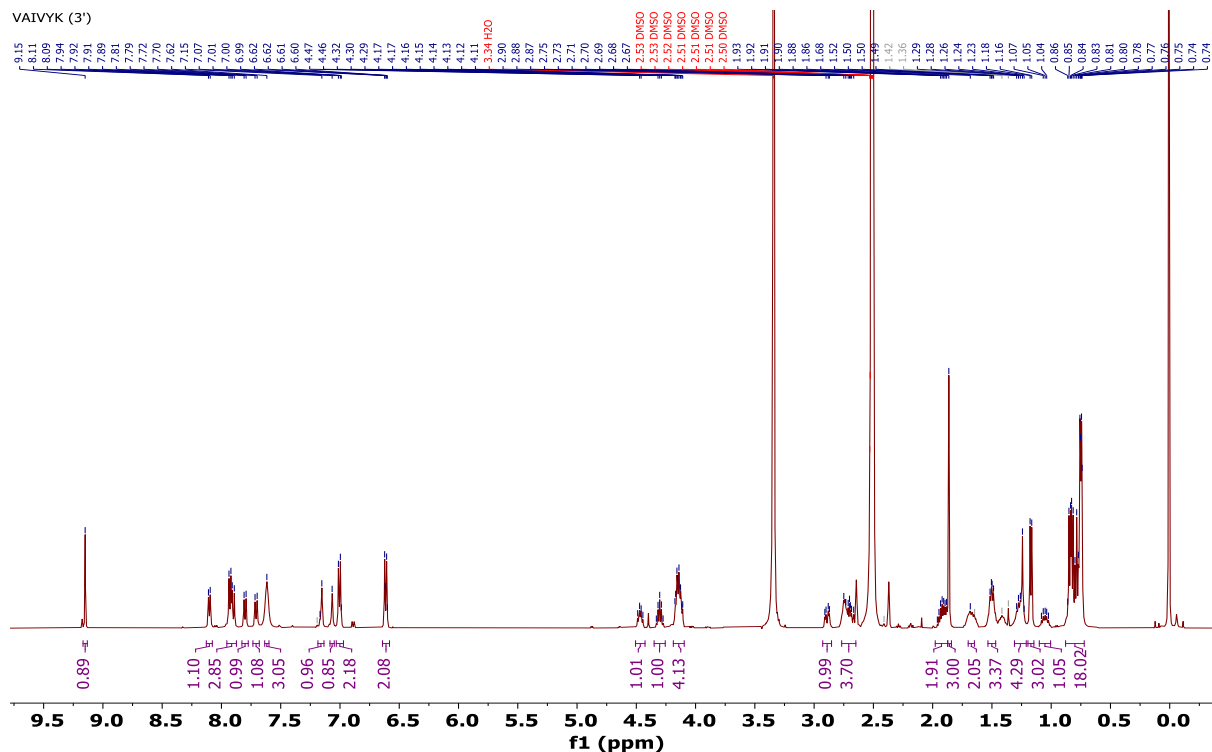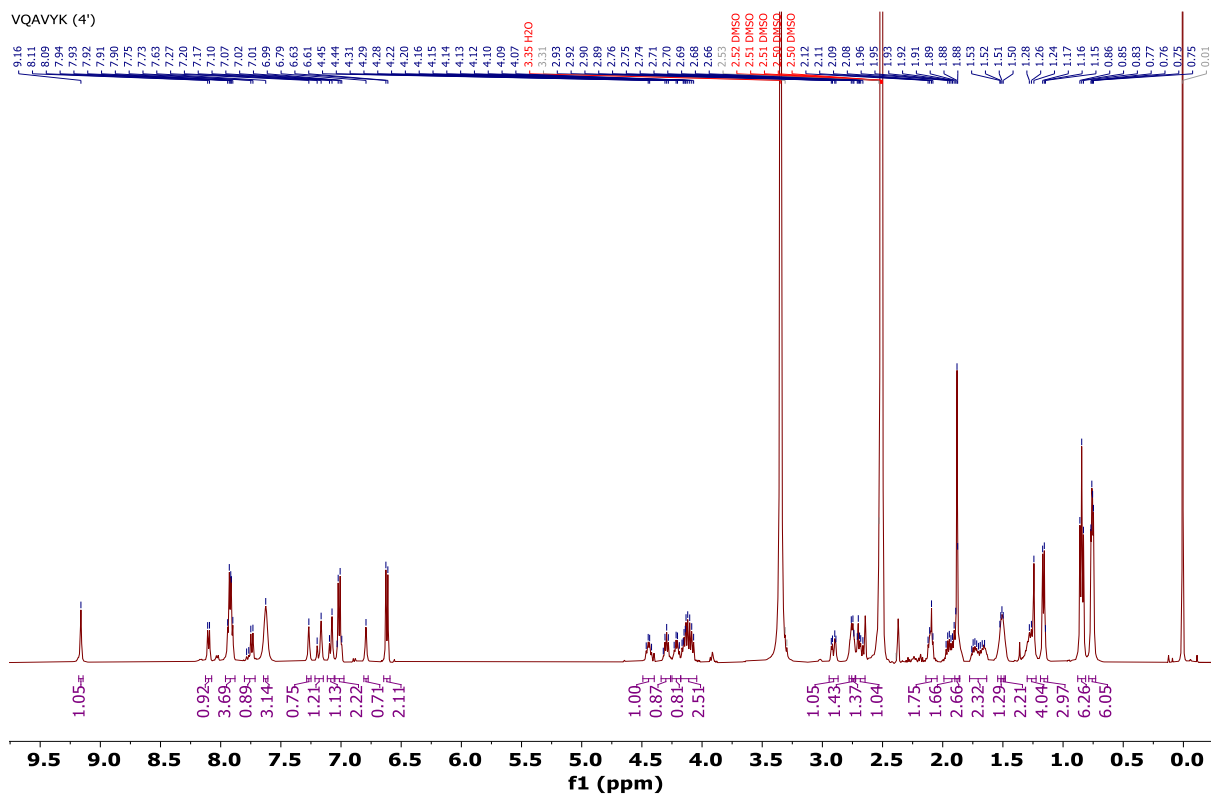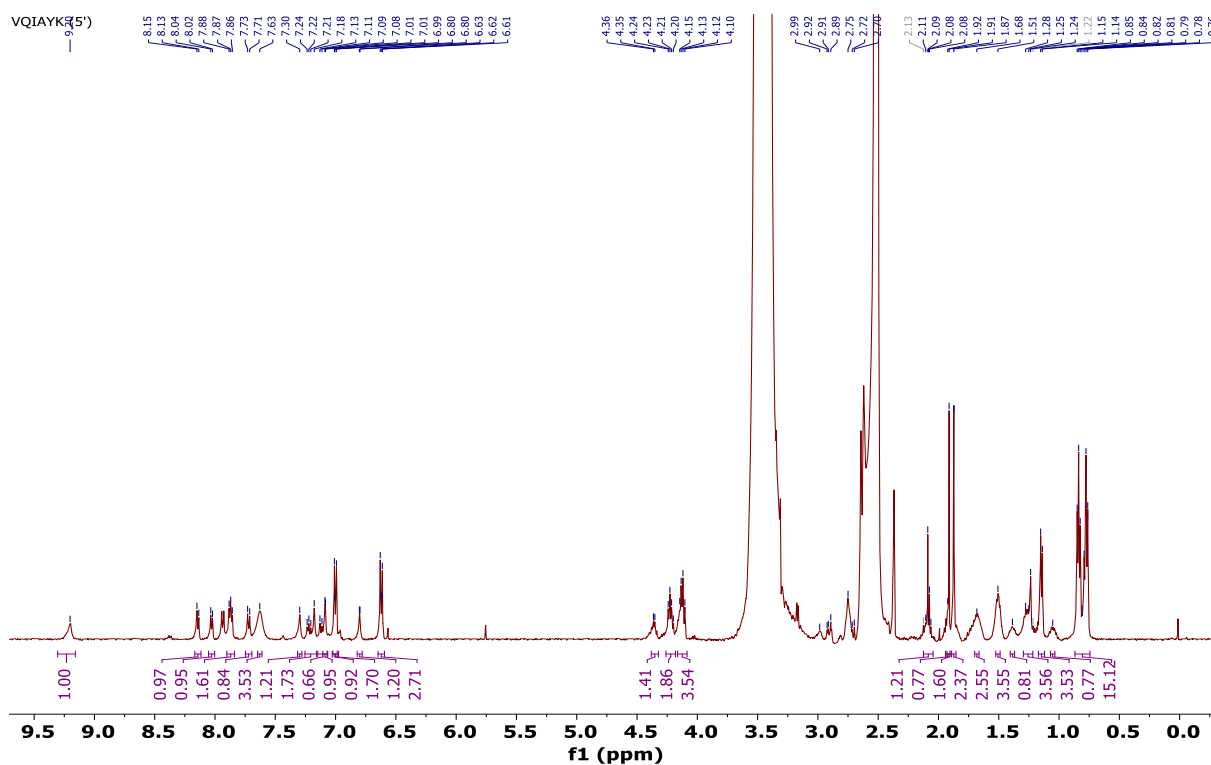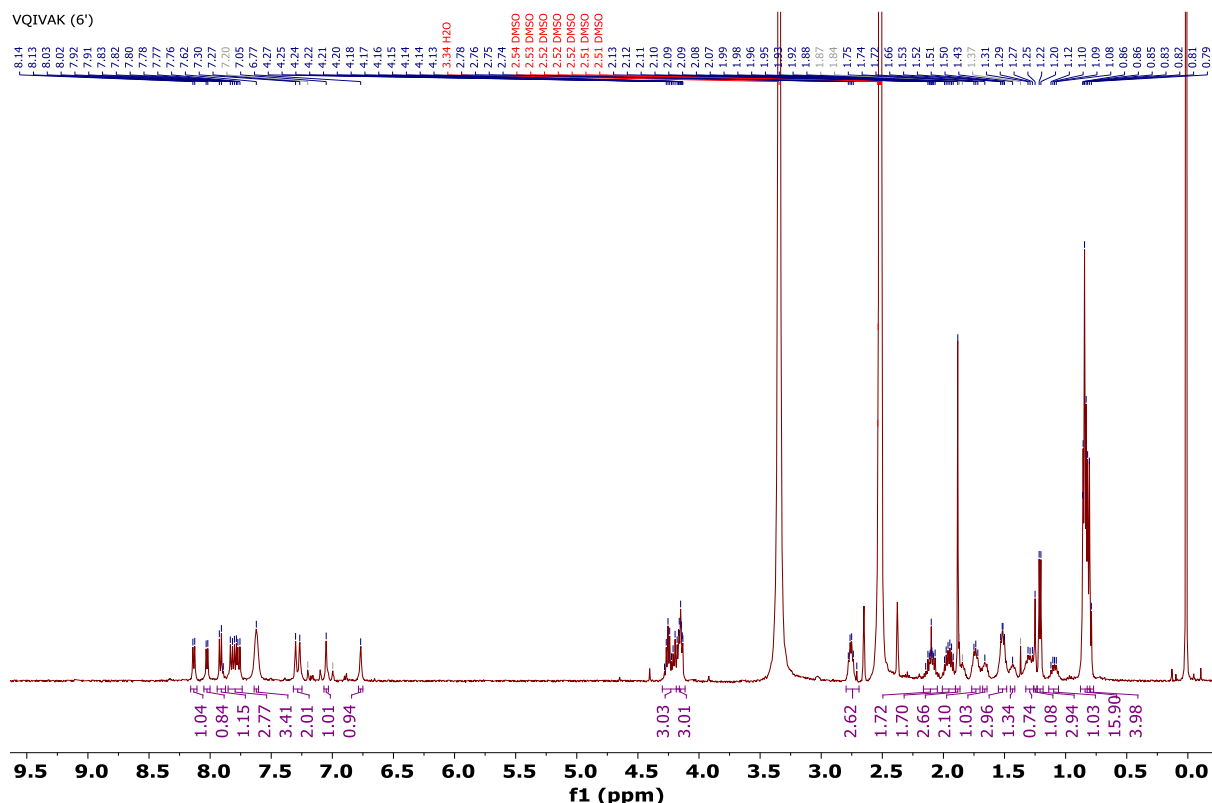^{1}H NMR of **6′** (Ac-VQIVAK-NH$_2$) on 500 MHz at 298 K in DMSO-d_6.

3A.5. References

(1)   Soto, C.; Pritzkow, S. Protein Misfolding, Aggregation, and Conformational Strains in Neurodegenerative Diseases. *Nat. Neurosci.* **2018**, *21* (10), 1332–1340.

(2)   Ross, C. A.; Poirier, M. A. Protein Aggregation and Neurodegenerative Disease. *Nat. Med.* **2004**, *10* (S7), S10–S17.

(3)   Eisenberg, D.; Jucker, M. The Amyloid State of Proteins in Human Diseases. *Cell* **2012**, *148* (6), 1188–1203.

(4)   Eisele, Y. S.; Monteiro, C.; Fearns, C.; Encalada, S. E.; Wiseman, R. L.; Powers, E. T.; Kelly, J. W. Targeting Protein Aggregation for the Treatment of Degenerative Diseases. *Nat. Publ. Gr.* **2015**, *14*.

(5)   Glenner, G. G.; Wong, C. W. Alzheimer's Disease and Down's Syndrome: Sharing of a Unique Cerebrovascular Amyloid Fibril Protein. *Biochem. Biophys. Res. Commun.* **1984**, *122* (3), 1131–1135.

(6)   Masters, C. L.; Simms, G.; Weinman, N. A.; Multhaup, G.; McDonald, B. L.; Beyreuther, K. Amyloid Plaque Core Protein in Alzheimer Disease and Down Syndrome. *Proc. Natl. Acad. Sci.* **1985**, *82* (12), 4245–4249.

(7)   Goedert, M. Alzheimer's and Parkinson's Diseases: The Prion Concept in Relation to Assembled Aβ, Tau, and α-Synuclein. *Science* **2015**, *349* (6248).

(8)   Hardy, J.; Selkoe, D. J. The Amyloid Hypothesis of Alzheimer's Disease: Progress and Problems

on the Road to Therapeutics. *Science* **2002**, *297* (5580), 353–356.

(9) Holtzman, D. M.; Morris, J. C.; Goate, A. M. Alzheimer's Disease: The Challenge of the Second Century. *Sci. Transl. Med.* **2011**, *3* (77).

(10) Li, C.; Götz, J. Tau-Based Therapies in Neurodegeneration: Opportunities and Challenges. *Nat. Rev. Drug Discov.* **2017**, *16* (12), 863–883.

(11) Necula, M.; Kayed, R.; Milton, S.; Glabe, C. G. Small Molecule Inhibitors of Aggregation Indicate That Amyloid β Oligomerization and Fibrillization Pathways Are Independent and Distinct. *J. Biol. Chem.* **2007**, *282* (14), 10311–10324.

(12) Pickhardt, M.; Bergen, M.; Gazova, Z.; Hascher, A.; Biernat, J.; Mandelkow, E.-M.; Mandelkow, E. Screening for Inhibitors of Tau Polymerization. *Curr. Alzheimer Res.* **2005**, *2* (2), 219–226.

(13) Sciarretta, K. L.; Gordon, D. J.; Meredith, S. C. Peptide-Based Inhibitors of Amyloid Assembly; **2006**; 273–312.

(14) Murphy, M. P.; LeVine, H. Alzheimer's Disease and the Amyloid-β Peptide. *J. Alzheimer's Dis.* **2010**, *19* (1), 311–323.

(15) Kosik, K. S.; Joachim, C. L.; Selkoe, D. J. Microtubule-Associated Protein Tau (Tau) Is a Major Antigenic Component of Paired Helical Filaments in Alzheimer Disease. *Proc. Natl. Acad. Sci.* **1986**, *83* (11), 4044–4048.

(16) Von Bergen, M.; Friedhoff, P.; Biernat, J.; Heberle, J.; Mandelkow, E. M.; Mandelkow, E. Assembly of τ Protein into Alzheimer Paired Helical Filaments Depends on a Local Sequence Motif (306VQIVYK311) Forming β Structure. *Proc. Natl. Acad. Sci. U. S. A.* **2000**, *97* (10), 5129–5134.

(17) Goedert, M.; Clavaguera, F.; Tolnay, M. The Propagation of Prion-like Protein Inclusions in Neurodegenerative Diseases. *Trends Neurosci.* **2010**, *33* (7), 317–325.

(18) Jackson, S. J.; Kerridge, C.; Cooper, J.; Cavallini, A.; Falcon, B.; Cella, C. V.; Landi, A.; Szekeres, P. G.; Murray, T. K.; Ahmed, Z.; Goedert, M.; Hutton, M.; O'Neill, M. J.; Bose, S. Short Fibrils Constitute the Major Species of Seed-Competent Tau in the Brains of Mice Transgenic for Human P301S Tau. *J. Neurosci.* **2016**, *36* (3), 762–772.

(19) Friedhoff, P.; von Bergen, M.; Mandelkow, E.-M.; Mandelkow, E. Structure of Tau Protein and Assembly into Paired Helical Filaments. *Biochim. Biophys. Acta Mol. Basis Dis.* **2000**, *1502* (1), 122–132.

(20) Mandelkow, E.-M.; Mandelkow, E. Biochemistry and Cell Biology of Tau Protein in Neurofibrillary Degeneration. *Cold Spring Harb. Perspect. Med.* **2012**, *2* (7), a006247.

(21) Fitzpatrick, A. W. P.; Falcon, B.; He, S.; Murzin, A. G.; Murshudov, G.; Garringer, H. J.; Crowther, R. A.; Ghetti, B.; Goedert, M.; Scheres, S. H. W. Cryo-EM Structures of Tau Filaments from Alzheimer's Disease. *Nature* **2017**, *547* (7662), 185–190.

(22) Falcon, B.; Zhang, W.; Murzin, A. G.; Murshudov, G.; Garringer, H. J.; Vidal, R.; Crowther, R. A.; Ghetti, B.; Scheres, S. H. W.; Goedert, M. Structures of Filaments from Pick's Disease Reveal a Novel Tau Protein Fold. *Nature* **2018**, *561* (7721), 137–140.

(23) Von Bergen, M.; Barghorn, S.; Li, L.; Marx, A.; Biernat, J.; Mandelkow, E. M.; Mandelkow, E. Mutations of Tau Protein in Frontotemporal Dementia Promote Aggregation of Paired Helical Filaments by Enhancing Local β-Structure. *J. Biol. Chem.* **2001**, *276* (51), 48165–48174.

(24)   Inouye, H.; Sharma, D.; Goux, W. J.; Kirschner, D. A. Structure of Core Domain of Fibril-Forming PHF/Tau Fragments. *Biophys. J.* **2006**, *90* (5), 1774–1789.

(25)   von Bergen, M.; Barghorn, S.; Biernat, J.; Mandelkow, E.-M.; Mandelkow, E. Tau Aggregation Is Driven by a Transition from Random Coil to Beta Sheet Structure. *Biochim. Biophys. Acta - Mol. Basis Dis.* **2005**, *1739* (2–3), 158–166.

(26)   Cummings, J.; Lee, G.; Ritter, A.; Sabbagh, M.; Zhong, K. Alzheimer's Disease Drug Development Pipeline: 2019. *Alzheimer's Dement. Transl. Res. Clin. Interv.* **2019**, *5*, 272–293.

(27)   Seidler, P. M.; Boyer, D. R.; Rodriguez, J. A.; Sawaya, M. R.; Cascio, D.; Murray, K.; Gonen, T.; Eisenberg, D. S. Structure-Based Inhibitors of Tau Aggregation. *Nat. Chem.* **2018**, *10* (2), 170–176.

(28)   Perez, M.; Santa-María, I.; Tortosa, E.; Cuadros, R.; Valle, M. del; Hernández, F.; Moreno, F. J.; Avila, J. The Role of the VQIVYK Peptide in Tau Protein Phosphorylation. *J. Neurochem.* **2007**, *103* (4), 1447–1460.

(29)   Mohamed, T.; Hoang, T.; Jelokhani-Niaraki, M.; Rao, P. P. N. Tau-Derived-Hexapeptide [306] VQIVYK [311] Aggregation Inhibitors: Nitrocatechol Moiety as A Pharmacophore In Drug Design. *ACS Chem. Neurosci.* **2013**, *4* (12), 1559–1570.

(30)   Zheng, J.; Baghkhanian, A. M.; Nowick, J. S. A Hydrophobic Surface Is Essential to Inhibit the Aggregation of a Tau-Protein-Derived Hexapeptide. *J. Am. Chem. Soc.* **2013**, *135* (18), 6846–6852.

(31)   Belostozky, A.; Richman, M.; Lisniansky, E.; Tovchygrechko, A.; Chill, J. H.; Rahimipour, S. Inhibition of Tau-Derived Hexapeptide Aggregation and Toxicity by a Self-Assembled Cyclic -α-Peptide Conformational Inhibitor. *Chem. Commun.* **2018**, *54* (47), 5980–5983.

(32)   Frenkel-Pinter, M.; Richman, M.; Belostozky, A.; Abu-Mokh, A.; Gazit, E.; Rahimipour, S.; Segal, D. Selective Inhibition of Aggregation and Toxicity of a Tau-Derived Peptide Using Its Glycosylated Analogues. *Chem. A Eur. J.* **2016**, *22* (17), 5945–5952.

(33)   Wang, C. K.; Northfield, S. E.; Huang, Y.-H.; Ramos, M. C.; Craik, D. J. Inhibition of Tau Aggregation Using a Naturally-Occurring Cyclic Peptide Scaffold. *Eur. J. Med. Chem.* **2016**, *109*, 342–349.

(34)   Dammers, C.; Yolcu, D.; Kukuk, L.; Willbold, D.; Pickhardt, M.; Mandelkow, E.; Horn, A. H. C.; Sticht, H.; Malhis, M. N.; Will, N.; Schuster, J.; Funke, S. A. Selection and Characterization of Tau Binding ᴅ-Enantiomeric Peptides with Potential for Therapy of Alzheimer Disease. *PLoS One* **2016**, *11* (12), e0167432.

(35)   Sievers, S. A.; Karanicolas, J.; Chang, H. W.; Zhao, A.; Jiang, L.; Zirafi, O.; Stevens, J. T.; Münch, J.; Baker, D.; Eisenberg, D. Structure-Based Design of Non-Natural Amino-Acid Inhibitors of Amyloid Fibril Formation. *Nature* **2011**, *475* (7354), 96–103.

(36)   Zheng, J.; Liu, C.; Sawaya, M. R.; Vadla, B.; Khan, S.; Woods, R. J.; Eisenberg, D.; Goux, W. J.; Nowick, J. S. Macrocyclic β-Sheet Peptides That Inhibit the Aggregation of a Tau-Protein-Derived Hexapeptide. *J. Am. Chem. Soc.* **2011**, *133* (9), 3144–3157.

(37)   KrishnaKumar, V. G.; Paul, A.; Gazit, E.; Segal, D. Mechanistic Insights into Remodeled Tau-Derived PHF6 Peptide Fibrils by Naphthoquinone-Tryptophan Hybrids. *Sci. Rep.* **2018**, *8* (1), 71.

(38)   Paul, A.; Kalita, S.; Kalita, S.; Sukumar, P.; Mandal, B. Disaggregation of Amylin Aggregate by Novel Conformationally Restricted Aminobenzoic Acid Containing α/β and α/γ Hybrid

Peptidomimetics. *Sci. Rep.* **2017**, *7* (1), 40095.

(39)   Vaden, T. D.; Gowers, S. A. N.; de Boer, T. S. J. A.; Steill, J. D.; Oomens, J.; Snoek, L. C. Conformational Preferences of an Amyloidogenic Peptide: IR Spectroscopy of Ac-VQIVYK-NHMe. *J. Am. Chem. Soc.* **2008**, *130* (44), 14640–14650.

(40)   Goux, W. J.; Kopplin, L.; Nguyen, A. D.; Leak, K.; Rutkofsky, M.; Shanmuganandam, V. D.; Sharma, D.; Inouye, H.; Kirschner, D. A. The Formation of Straight and Twisted Filaments from Short Tau Peptides. *J. Biol. Chem.* **2004**, *279* (26), 26868–26875.

(41)   Rojas Quijano, F. A.; Morrow, D.; Wise, B. M.; Brancia, F. L.; Goux, W. J. Prediction of Nucleating Sequences from Amyloidogenic Propensities of Tau-Related Peptides. *Biochemistry* **2006**, *45* (14), 4638–4652.

(42)   Chemerovski-Glikman, M.; Frenkel-Pinter, M.; Mdah, R.; Abu-Mokh, A.; Gazit, E.; Segal, D. Inhibition of the Aggregation and Toxicity of the Minimal Amyloidogenic Fragment of Tau by Its Pro-Substituted Analogues. *Chem. A Eur. J.* **2017**, *23* (40), 9618–9624.

(43)   Fink, A. L. Natively Unfolded Proteins. *Curr. Opin. Struct. Biol.* **2005**, *15* (1), 35–41.

(44)   Jeganathan, S.; von Bergen, M.; Mandelkow, E.-M.; Mandelkow, E. The Natively Unfolded Character of Tau and Its Aggregation to Alzheimer-like Paired Helical Filaments. *Biochemistry* **2008**, *47* (40), 10526–10539.

(45)   Minor, D. L.; Kim, P. S. Measurement of the β-Sheet-Forming Propensities of Amino Acids. *Nature* **1994**, *367* (6464), 660–663.

(46)   Fujiwara, K.; Toda, H.; Ikeguchi, M. Dependence of Alpha-Helical and Beta-Sheet Amino Acid Propensities on the Overall Protein Fold Type. *BMC Struct. Biol.* **2012**, *12* (1), 18.

CHAPTER-3

Section-B

Macrocyclic peptides derived from AcPHF6* and AcPHF6 to selectively modulate the Tau aggregation
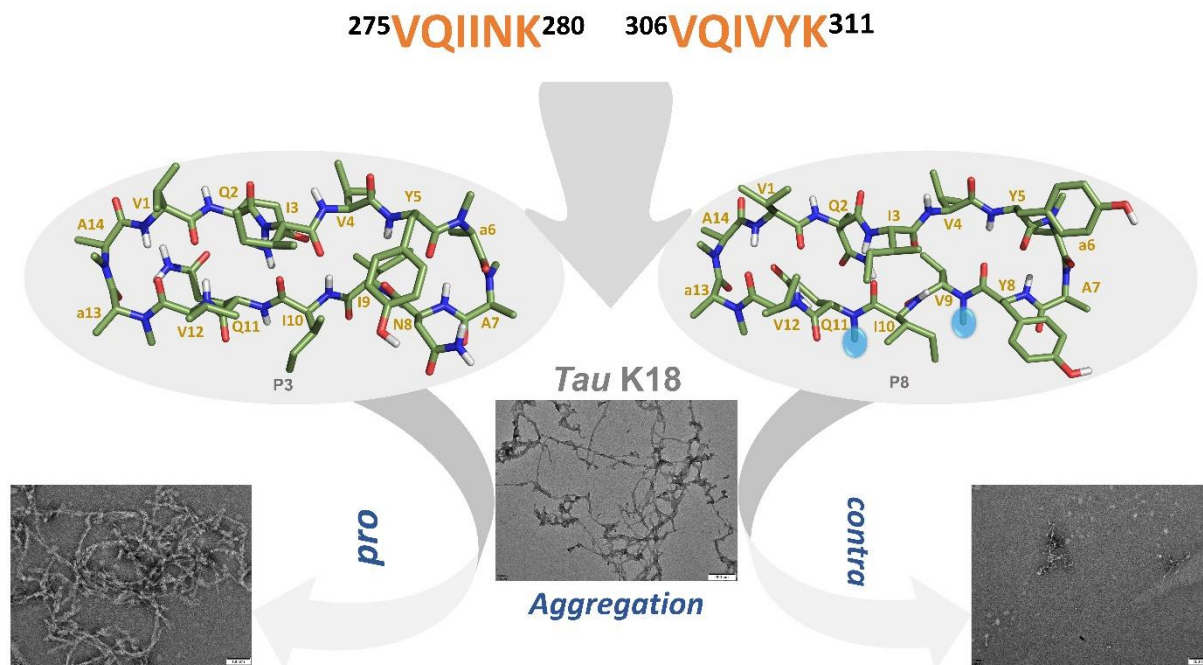
3B.1. Introduction

Alzheimer's disease (AD) is the most common neurodegenerative disease affecting more than 35 million people worldwide.[1,2] The abnormal accumulation of the microtubule-associated protein Tau is one of the prime causes of Alzheimer's disease. Tau protein is mostly unfolded in solution and forms amyloid fibrils in many neuropathologies known as Tauopathies that are toxic to the neural cells.[3,4] Search for potential molecules that can target and inhibit the tauopathies or their underlying cause is a key approach for developing therapeutics for AD.[5–8]

Studies that illustrated the molecular basis of Tau aggregation have established that two specific oligopeptides in Tau, [306]VQIVYK[311] (PHF6) in the third repeat domain and the homologous sequence [275]VQIINK[280] (PHF6*) in the second repeat domain of Tau, are critical in nucleating the β-sheet aggregation of the entire protein.[9–14] The derivatives of these two peptides, Ac-VQIVYK-NH2 (AcPHF6) and Ac-VQIINK-NH2 (AcPHF6*) are proven to form fibrils with biophysical properties similar to full-length Tau fibrils.[15,16] Hence, these two hexapeptides are the standing experimental model systems for investigating the molecular forces that drive Tau aggregation.[12,17–20] The atomic scale structure of AcPHF6 and AcPHF6* fibrils revealed that fibril formation involves hydrogen bond interactions in one direction and non-covalent interactions (hydrophobic) in the opposite direction resulting in a 'steric zipper' structure overall (Figure **3B.1**).[10,21]
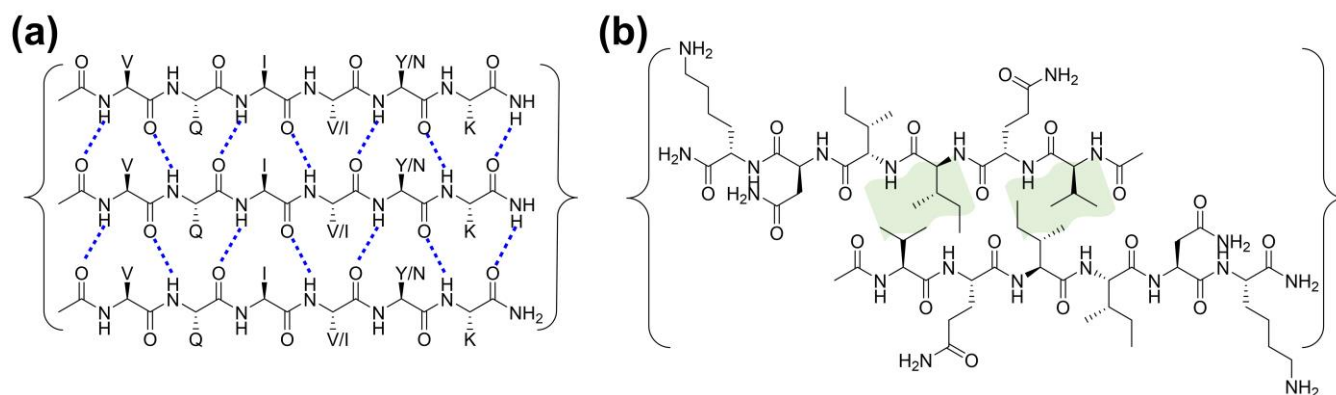
Figure 3B.1. Interactions on the aggregation model of PHF peptides. (**a**) characteristic hydrogen bonding interactions formed between parallelly oriented chains of PHF peptides (**b**) noncovalent steric zipper interactions involving valine and isoleucine sidechains of the antiparallelly oriented chains of PHF peptides.

The concrete aggregation structures of the PHF peptides serve as an excellent starting point to investigate the development of Tau aggregation inhibitors, particularly those based on peptides.[22–24] Nowick's research group has conducted studies on Tau aggregation inhibitors based on a macrocyclic β-

sheet model peptide containing a synthetic amino acid Hao. The designed peptides were shown to be effective in inhibiting the fibril growth of Tau segments and other amyloid-forming proteins.[25–28] Additionally, Funke's research group has identified MMD3 and ISAD1 peptides containing all D-amino acids and their retroinverso peptides that exhibit an inhibitory effect on Tau aggregation.[29] In another study, Craik's group screened naturally occurring disulfide bridge peptides for their potential to inhibit Tau aggregation and identified SFTI-1 peptide as a promising scaffold.[30] They further explored its structure-activity relationships to determine its effect on Tau aggregation.

In general, a well-organized Tau packing model mediated by PHF peptide regions (Figure **3B.1**) offers several rational options for designing peptide-based inhibitors of Tau aggregation.[31] These options include blocking hydrogen bonding propagation, disrupting van der Waals interactions, and blocking aggregation chain propagation through the use of end caps or molecular plugs.[27] By incorporating these rationales, we hypothesized and investigated the use of macrocyclic peptides to modulate Tau aggregation. In this study, we present the design, synthesis, NMR structural studies, and biophysical investigation of 10 macrocyclic peptides (**P1**-**P10**) (Figure **3B.2**) based on PHF and PHF* peptides. Each of these peptides contains 14 amino acids. Aggregation studies of these peptides led to the identification of two peptides with anti-parallel beta-sheet structures that showed a selective pro or contra effect on the aggregation of PHF, PHF*, and the K18wt.

3B.2. Results and Discussion

The design of the current macrocyclic peptides originated from the aggregation model of the PHF peptides (Figure **3B.1**) and our recent study, discussed in the previous section (Chapter 3, Section A), which characterized the residue-based propensity of aggregation in PHF6 and PHF6* peptide by single-point alanine mutations.[32] Our studies established that aggregation was suppressed in most alanine mutant PHF peptides, except for the two peptides with glutamine (Q) to alanine mutation, which enhanced the fibrillization. In the Tau aggregation model (Figure **3B.1**), the VQIINK and VQIVYK peptides are arranged in an array where the amide NH of every amino acid in one chain is hydrogen bonded with the carbonyl groups from the next chain. NHs from alternate residues are oriented in opposite directions from the plane of the hexapeptide leading to a propagation of the hydrogen bonding along the aggregation array. In a second dimension, the hexapeptide arrays are also involved in anti-parallel steric zipper formation, in which the adjacent hexapeptide chains in anti-parallel orientation interlock with each other via van der Waals interactions involving valine and isoleucine residues (**3B.1b**).

Our parent macrocyclic peptides **P1**-**P3** (Figure **3B.2**) consisted of a pair of VQIIN and VQIVY chains from PHFs and are linked to each other at either end via a dipeptide motif *N*HMe-D-ala-*N*Me-L-ala-COOH. These *N*-methylated heterochiral dipeptide amino acids are known to nucleate robust beta turns in peptides and aid the propagation of a beta-sheet having interstrand hydrogen bonds.[33] While peptide **P1** and peptide **P2** are based on VQIVY and VQIIN, respectively, peptide **P3** is a hybrid consisting of a strand each of VQIVY and VQIIN. The peptides **P4**-**P6** are obtained by replacing Q in **P1**-**P3** with Ala as per the results from our earlier studies. Peptides **P7** and **P8** are obtained from the parent macrocycles **P1** and **P2**, respectively, in which the backbone amide NHs on residues Q and I/V that are present at alternate positions on one of the strands are *N*-methylated to block them from participating in hydrogen bonding (Figure **3B.3**). Peptides **P9** and **P10** are derived from peptides **P7** and **P8**, by substituting I and V with Ala to suppress non-covalent interaction which will lead to suppress aggregation and steric zipper interactions. These macrocyclic peptides are hypothesized to act by interacting with themselves and the parent PHF sequences in a manner similar to that depicted for the PHF peptides (Figure **3B.1**). The peptides **P1**-**P6** are expected to propagate the aggregation by supporting elongation of the aggregates via external hydrogen bonding (Figure **3B.3a**). The peptides **P7**-**P10** are expected to lessen the aggregation by inhibiting the external hydrogen bonded propagation and further reduce the steric zipper interactions due to alanine substitutions (Figure **3B.3b**).
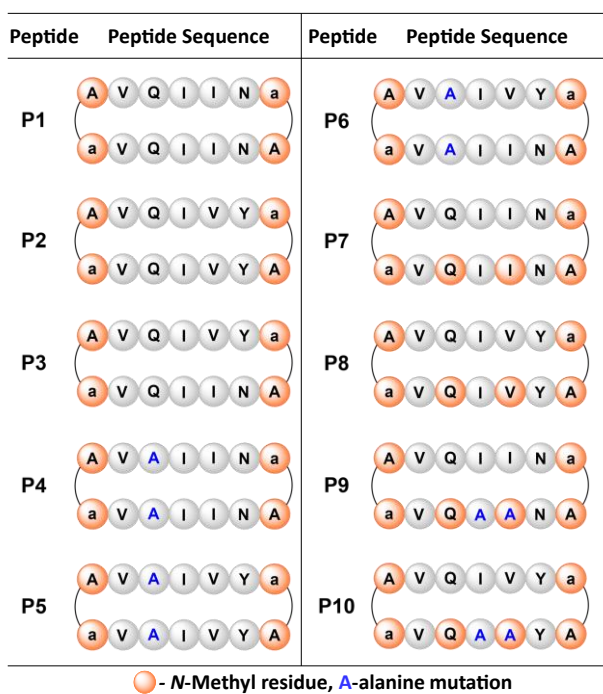
Figure 3B.2. List of macrocyclic peptides **P1**-**P10** synthesized and studied.
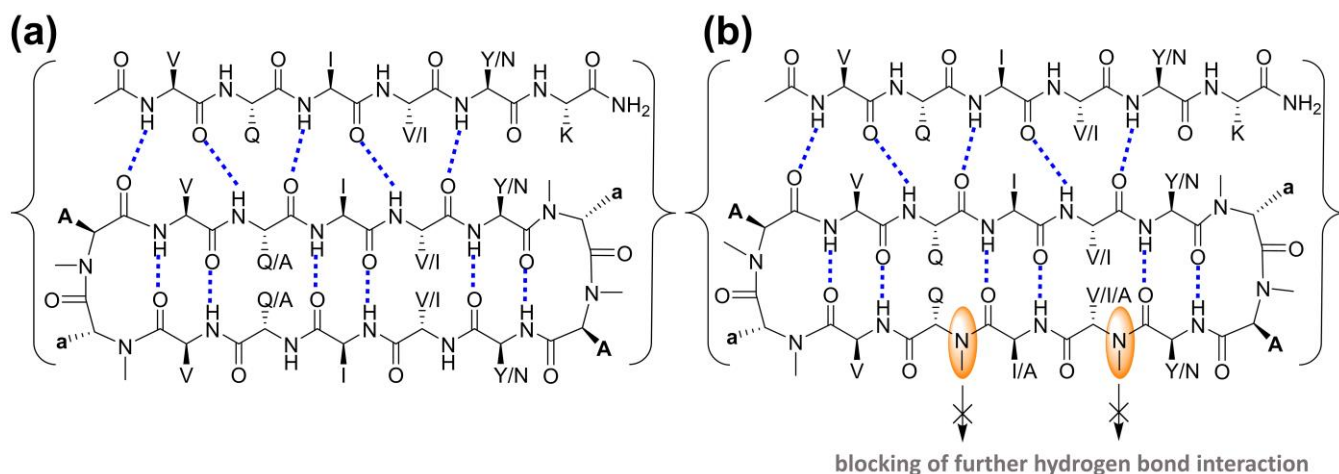
Figure 3B.3. Proposed hydrogen bonding interactions of the designed macrocyclic peptides (**a**) **P1-P6** and (**b**) **P7-P10** with PHF sequences.
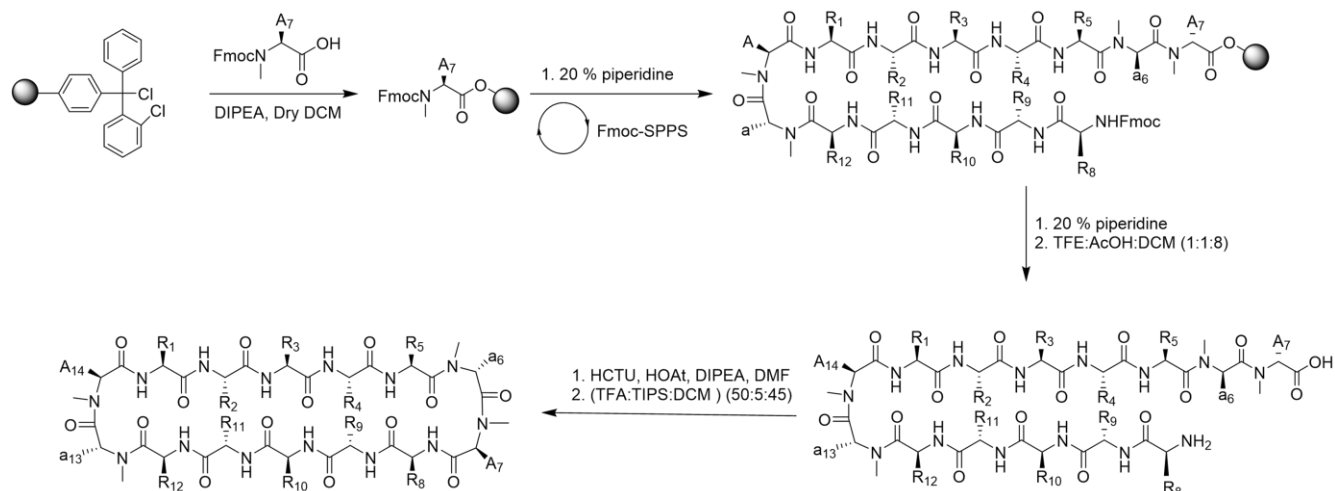
Scheme 3B.1. General solid phase peptide synthesis protocol for the synthesis of all macrocyclic peptides, started with the loading of first amino acid, and further Fmoc-SPPS cycle up to tetradecamer linear peptide, then cleavage from resin followed by cyclisation and global deprotection.

All the peptides were synthesized by following Fmoc solid phase synthesis protocol using 2-CTC resin and solution phase cyclization protocols (Scheme **3B.1** and experimental section **3B.4.1**).[35] All the peptides were purified by reversed-phase HPLC and characterized by HRMS, and NMR spectroscopy further their purity was confirmed by analytical HPLC (Table **3B.15**).

**3B.2.1 NMR spectroscopic studies of macrocyclic peptides (P1-P10)**

For NMR spectroscopic studies, 7 mg of each peptide was dissolved in 0.5 mL of DMSO-d_6. 1D and 2D spectra were recorded at 298 K on Bruker 500 or 700 MHz NMR spectrometer equipped with a BBO probe. ^{1}H-1D, DQF-COSY, TOCSY, ROESY, ^{1}H-^{13}C HSQC, and ^{1}H-^{13}C HMBC NMR experiments were acquired. A mixing time of 300 ms was used for ROESY. The 2D NMR experiments were acquired with 320 (for DQF-COSY and TOCSY), 512 (for ROESY), 512 (for HSQC and HMBC) data points in the F1 dimension, and 4k (for DQF-COSY, TOCSY, ROESY) and 1k (for HSQC and HMBC) data points in F2 dimension.

**3B.2.1.1**. **NMR based conformational study of macrocyclic peptides**

A detailed NMR spectroscopic characterization of all the peptides was done by using 2D NMR experiments (Tables **3B.5-14**) and variable temperature NMR experiments to ascertain the anti-parallel beta-sheet structure in the designed peptides as per our hypothesis (Table **3B.1**). The conformation portrays internal orientation of the amide NHs of residues at positions 1, 3, 5, 8, 10 and 12 into the macrocycle and their hydrogen bonding with the carbonyl groups from the opposite strand. The hydrogen bonding or solvent shielding nature of the mentioned amide NHs is supported by their NMR chemical shift temperature coefficients which are > -3.2 (Table **3B.1**).[37] These characteristic cross-strand NOE patterns and the amide temperature coefficients were observed for all the 10 macrocyclic peptides implying a similar anti-parallel beta sheet conformation (Figure **3B.4-6**).
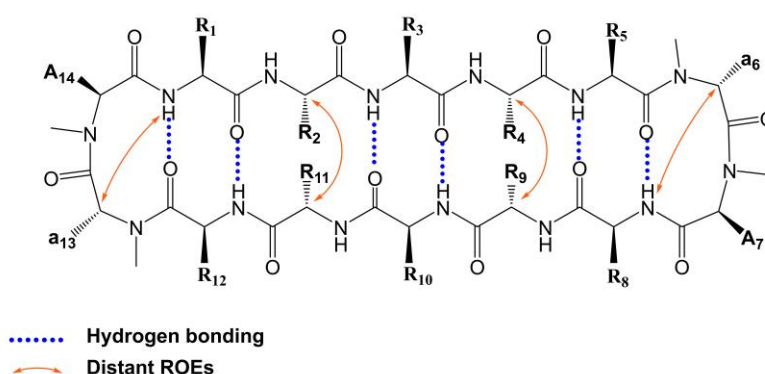
Figure 3B.4. Schematic representation of the characteristic NOEs (orange colour arrows) and hydrogen bonding pattern (dashed blue lines) observed for all the macrocyclic peptides **P1-P10**.
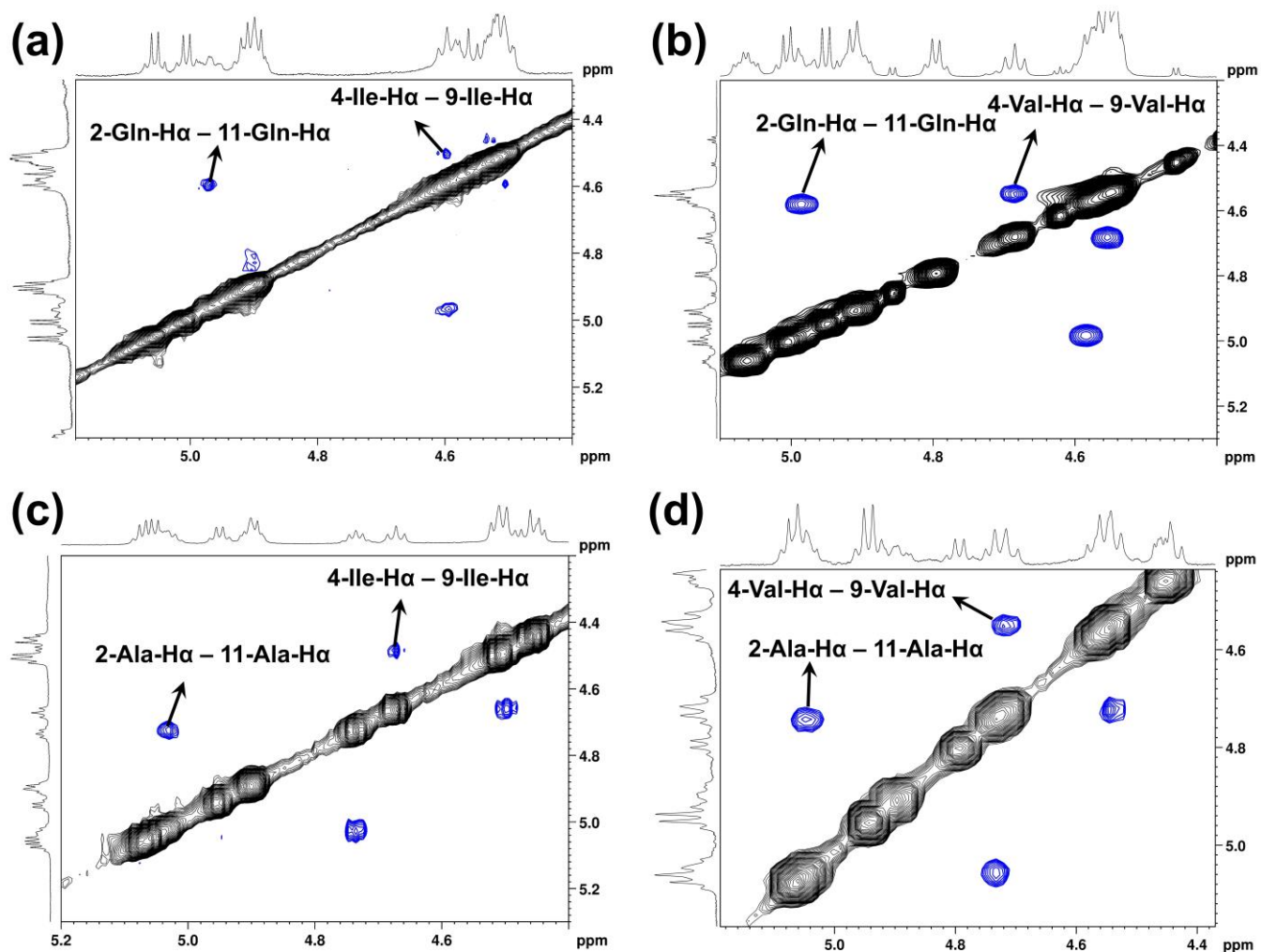
Figure 3B.5. Expansions from the ROESY spectra showing the characteristic cross strands ROESY correlations (**a**) 2-Gln-Hα–11-Gln-Hα and 4-Ile-Hα-9–Ile-Hα for **P1**, (**b**) 2-Gln-Hα–11-Gln-Hα and 4-Val-Hα–9-Val-Hα of **P2**, **(c)** 2-Ala-Hα–11-Ala-Hα and 4-Ile-Hα–9-Ile-Hα for **P4**, (**d**) 2-Ala-Hα–11-Ala-Hα and 4-Val-Hα–9-Val-Hα of **P5** in support of their macrocyclic antiparallel beta-sheet structure.
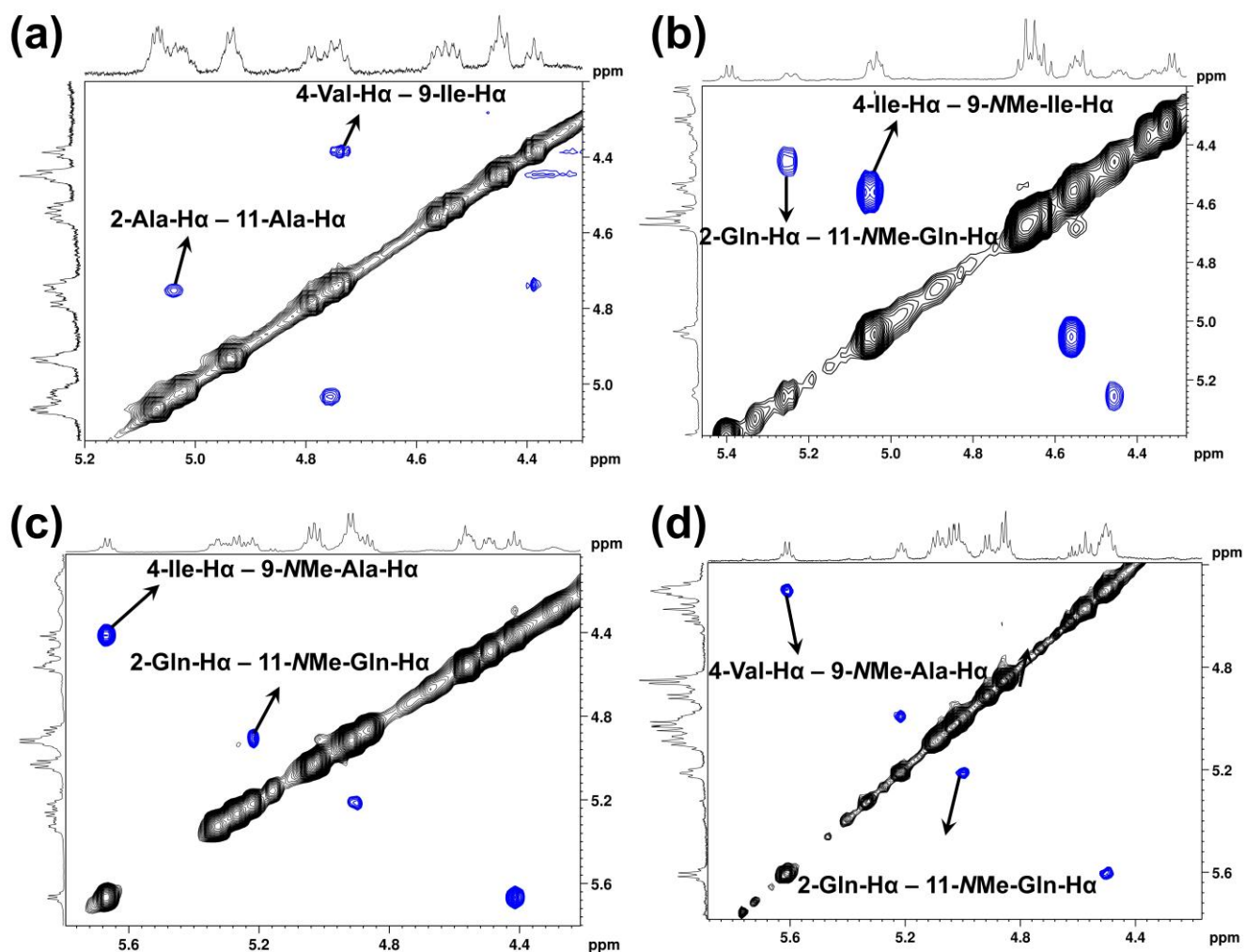
Figure 3B.6. Expansions from the ROESY spectra showing the characteristic cross strands ROESY correlations (**a**) 2-Ala-Hα–11-Ala-Hα and 4-Val-Hα–9Ile-Hα for **P6**, (**b**) 2-Gln-Hα–11-*N*Me-Gln-Hα and 4-Ile-Hα–9-*N*Me-Ile-Hα of **P7**, (**c**) 2-Gln-Hα–11-*N*Me-Gln-Hα and 4-Ile-Hα–9-*N*Me-Ala-Hα for **P9**, (**d**) 2-Gln-Hα–11-*N*Me-Gln-Hα and 4-Val-Hα–9-*N*Me-Ala-Hα of **P10** in support of their macrocyclic antiparallel beta-sheet structure.

3B.2.1.2. Temperature coefficient determination

For the determination of temperature coefficients of amide protons, ^{1}H NMR experiments were recorded at variable temperatures ranging from 300 K to 325 K with 5 K increments. The temperature coefficients were calculated according to (Δδ*1000)/ΔT, wherein Δδ and ΔT is the change in chemical shift of the amide NH and the change in sample temperature, respectively.

153

Table 3B.1. NMR chemical shift temperature coefficients (in ppb/K) of amide protons in peptides **P1-P10**.

| S. No.	Peptide	NMR chemical shift temperature coefficients of amide NHs for P1-P10									
		Upper strand					Lower strand				
		NH1	NH2	NH3	NH4	NH5	NH8	NH9	NH10	NH11	NH12
1.	**P1**	0.8	-4.2	-2.8	-5.2	-2.8	0	-4.8	-3.2	-5.6	-2.8
2.	**P2**	0.8	-7	-2.5	-6	-1.6	-0.4	-5.5	-2	-4.4	-2.9
3.	**P3**	0.4	-5.2	-2.5	-6	-2	0	-3.6	-2	-4.4	-2
4.	**P4**	0.8	-5.6	-2.8	-6.2	-3.2	1.2	-5.2	-2.8	-5.2	-3.2
5.	**P5**	0.8	-5.6	-2.4	-5.8	-2.4	0	-6.4	0.8	-5.6	-3.2
6.	**P6**	0.8	-4.8	-2.8	-5.2	-2	0	-5.6	-3.2	-4.8	-3.2
7.	**P7**	-1.2	-5.6	-2.4	-8.4	-2.4	0	-	-2.4	-	-2.8
8.	**P8**	-0.4	-6	-2.4	-5.6	-2.8	-1.2	-	-2.8	-	-2.8
9.	**P9**	-0.4	-4	-1.2	-4	-2	-1.2	-	-1.6	-	-2.4
10.	**P10**	0	-4.8	-1.6	-5.6	-3.2	0.8	-	-2.8	-	-2.8

After the structural studies by NMR, the aggregation studies of **P1**-**P10** were carried out and analyzed by Thioflavin S (ThS) and Transmission Electron Microscopy (TEM).

3B.2.2. Self-aggregation study of macrocyclic peptides P1-P10

Macrocyclic peptides **P1**-**P10** were allowed to aggregate at 100 µM concentration in 20 mM BES buffer and were monitored by ThS fluorescence every 24 hours for 9 days. It was observed that for all peptides, the aggregate formation increased with time and reached the maximum at ~96 hours (4 days), after which there was a decline in the ThS intensity before reaching a stability (Figure **3B.7**). In general, on comparing the aggregation trend between starting (0 hr) and endpoints (216 hrs), it was noted that **P1**, **P3**, **P4**, **P5**, and **P6** showed increased aggregation compared to **P2**, **P7**, **P8**, **P9**, and **P10** that showed significantly less aggregation (Figure **3B.7b**) suggesting the pro-aggregating nature of the former peptides and the contra-aggregation nature of the latter. The start and endpoint data also show an elevated aggregation for **P1**, **P3**-**P8**, and a stagnated aggregation for **P7**-**P8** and **P2**.

Among all, the hybrid peptide **P3** has shown a strong tendency to aggregate. On the other hand, the peptides **P7**-**P10** have shown a very low aggregation tendency throughout, among which **P8** has the least variation between the start and endpoints compared to the others. Except for **P2**, the aggregation trend displayed by **P1**-**P10** aligns with our hypothesis that the Q to A mutations may work pro-aggregation while the I/V to A mutations and *N*-methylations may have a contra-aggregation effect.
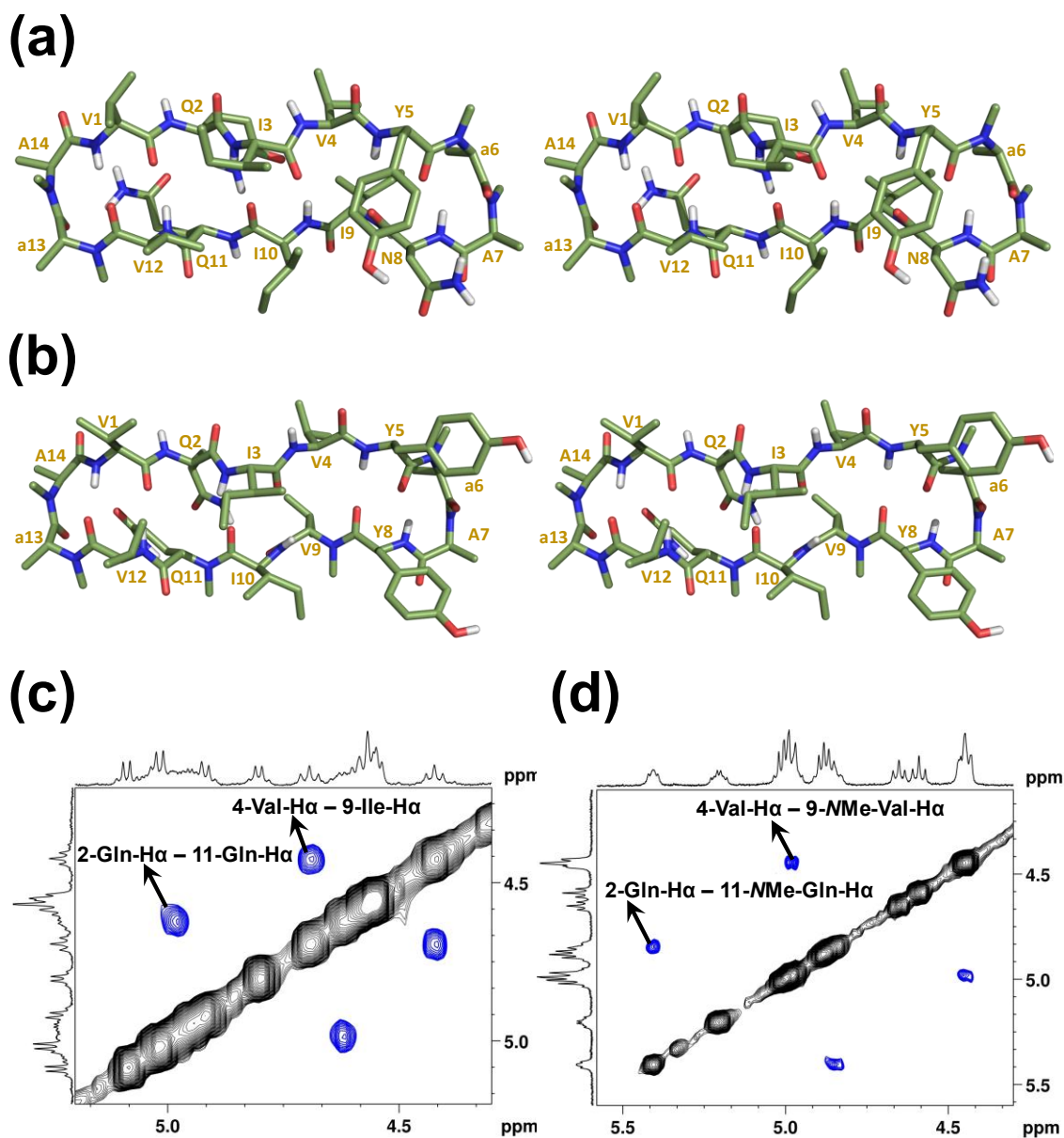
(a)

(b)
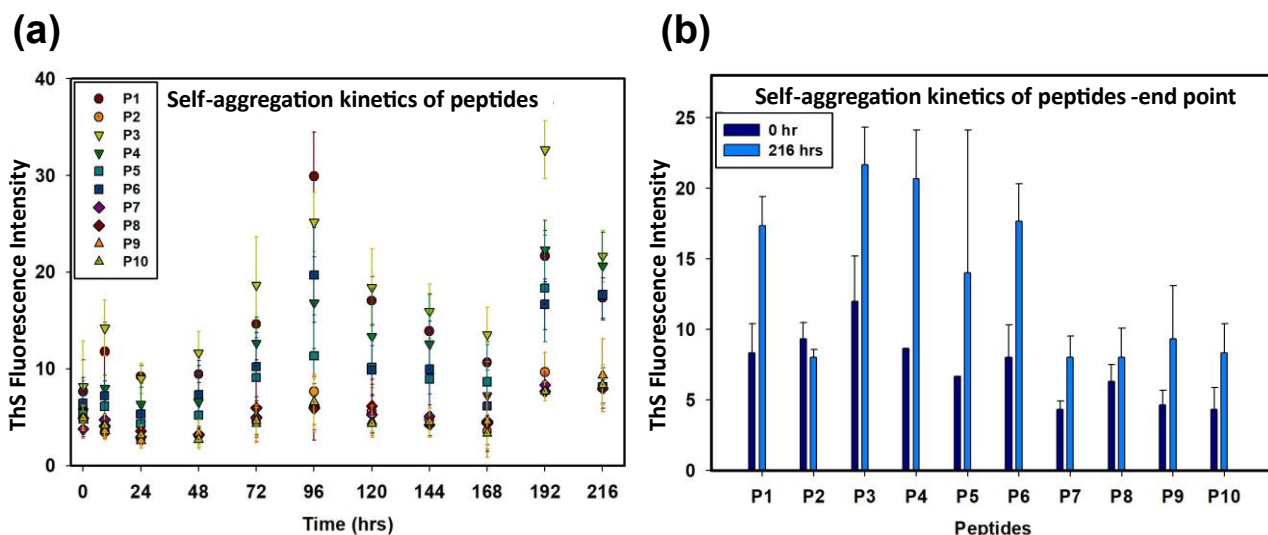
Figure 3B.7. Self-aggregation behaviour of the macrocyclic peptides and determination of aggregation promotor and inhibitor peptides. (**a**) ThS fluorescence assay for monitoring aggregation characteristics of the macrocyclic peptides **P1**-**P10** (100 µM) over a period of 216 hours. Maximum aggregation was observed at 96 hrs. (**b**) The start and end point ThS intensities were plotted for all peptides. **P1**, **P3**-**P6** showed higher aggregation while **P2**, **P7**-**P10** did not show much aggregation.

Based on the self-aggregation result, we have chosen the highest aggregating peptide **P3**, and the lowest aggregating peptide **P8** for a cross-aggregation study.

3B.2.3. Three-dimensional structure elucidation of P3 and P8 peptides

In particular, the three-dimensional conformations for peptides **P3** and **P8** were established by Schrodinger Maestro using NMR-derived internuclear distances as inputs.[36] Both peptides have a robust anti-parallel beta sheet fold, supported by distinct NOEs, Hα of residue 2 from upper strand to Hα of residue 11 from lower strand (Figure **3B.8**) and Hα of residue 4 from upper strand to Hα of residue 9 from lower strand. The inter-proton distances required for NMR-based structure calculation for macrocyclic peptides **P3** and **P8** were derived from the cross-peak integrals of the ROESY experiment using SPARKY software. These integrated volumes of ROESY cross-peaks were converted to the corresponding inter-proton distances by the linear approximation method. These distances were used for the structural calculation by using Schrodinger Maestro macro model 13.1. For the structure calculation, a minimized starting structure was obtained after a step-wise minimization process of an arbitrary structure by giving the inter-proton distance inputs one by one. The method used for energy minimization was SD (steepest descent) and dielectric constant of DMSO i.e., 47.

Thus, obtained structure was saved and used as the starting template (beginning structure) for 'Molecular Dynamics Simulations' (MD). MD was run on the structure at 300 K for 10 ns with simulation time step of 1 fs and by shaking all the bonds of the molecule.

Figure 3B.8. Stereo view (top view) of the solution state conformation of macrocyclic peptides (**a**) **P3**, and (**b**) **P8**. All the non-polar hydrogens are excluded for clarity. Expansions from the ROESY spectra showing the characteristic cross strands ROESY correlations (**c**) 2-Gln-Hα–11-Gln-Hα and 4-Val-Hα-9–Ile-Hα for **P3** and (**d**) 2-Gln-Hα–11-*N*Me-Gln-Hα and 4-Val-Hα-9-*N*Me-Val-Hα of **P8** in support of their macrocyclic antiparallel beta-sheet structure.

Table 3B.2. List of distance restraints that were used for structure calculation of **P3**.

Residue	Atom	Residue	Atom	Distance	Upper	Lower
1val	h	1val	ha	2.75	2.47	3.02
2gln	h	1val	ha	2.10	1.89	2.31
3ile	h	2gln	ha	2.05	1.85	2.26
11gln	ha	2gln	ha	2.18	1.96	2.40
4val	h	3ile	ha	1.85	1.67	2.04
4val	h	4val	ha	3.07	2.76	3.38
5tyr	h	4val	ha	2.09	1.88	2.30
9ile	ha	4val	ha	2.22	1.99	2.44
5tyr	h	5tyr	ha	3.27	2.94	3.60
6dnma	qn3	6dnma	qb3	3.16	2.85	3.48
5tyr	ha	6dnma	qn3	2.32	2.09	2.56
8asn	h	7lnma	ha	2.63	2.37	2.90
6dnma	ha	7lnma	qn3	2.27	2.04	2.49
8asn	h	7lnma	qn3	3.05	2.75	3.36
9ile	h	8asn	ha	2.13	1.92	2.34
10ile	h	9ile	ha	2.07	1.86	2.28
12val	h	11gln	ha	2.12	1.91	2.33
12val	h	12val	ha	2.77	2.49	3.04
12val	ha	13dnma	qn3	2.29	2.06	2.52
1val	h	14lnma	ha	2.55	2.29	2.80
1val	h	14lnma	qn3	3.02	2.72	3.32
13dnma	ha	14lnma	qn3	2.25	2.02	2.47

Note: h=NH, ha=Hα, qb3=pseudo position of β protons, qn3=pseudo position of *N*-methyl proton, lnma=*N*-methyl-L-ala, dnma=*N*-methyl-D-ala.

Table 3B.3. List of distance restraints that were used for structure calculation of **P8**.

| Residue	Atom	Residue	Atom	Distance	Upper	Lower
3ile	h	2gln	ha	2.44	2.20	2.69
11gln	ha	2gln	ha	2.46	2.22	2.71
2gln	h	1val	ha	2.27	2.04	2.49
3ile	h	3ile	ha	3.76	3.38	4.13
4val	h	3ile	ha	2.84	2.55	3.12
5tyr	h	4val	ha	2.27	2.04	2.49
9val	ha	4val	ha	2.59	2.33	2.85
5tyr	ho	5tyr	ha	2.62	2.36	2.89
6dnma	ha	8tyr	h	3.47	3.13	3.82
5tyr	ha	6dnma	qn3	2.51	2.26	2.76
5tyr	ho	6dnma	qn3	3.38	3.04	3.72
8tyr	h	7lnma	ha	2.73	2.46	3.00
6dnma	ha	7lnma	qn3	2.49	2.24	2.74
8tyr	h	7lnma	qn3	3.50	3.15	3.85
8tyr	ho	8tyr	ha	2.62	2.36	2.88
8tyr	ha	9nmval	qn3	2.46	2.22	2.71
12val	h	11nmgln	ha	2.47	2.22	2.72
11nmgln	qn3	11nmgln	hb1	3.16	2.85	3.48
10ile	ha	11nmgln	qn3	2.60	2.34	2.86
13dnma	qn3	13dnma	qb3	3.48	3.13	3.83
12val	ha	13dnma	qn3	2.44	2.20	2.69
1val	h	14lnma	ha	2.83	2.54	3.11
14lnma	qn3	14lnma	qb3	3.28	2.95	3.61
1val	h	14lnma	qn3	3.41	3.07	3.76
13dnma	ha	14lnma	qn3	2.42	2.18	2.66
10ile	h	9nmval	ha	2.42	2.17	2.66

Note: lnma=*N*-methyl-L-ala, dnma=*N*-methyl-D-ala, nmgln=*N*-methyl-L-gln, h=NH, ha=Hα, qb3=pseudo position of β protons, qn3=pseudo position *N*-methyl protons.

3B.2.4. Effect of macrocyclic peptides on the aggregation of Ac-PHFs model peptides

Based on the ThS assay, we have chosen the highest aggregating peptide **P3**, and the lowest aggregating peptide **P8** for a cross-aggregation study with AcPHF and AcPHF* to understand their effect on the aggregation of the latter. The AcPHF and AcPHF* peptides were allowed to aggregate for 60 mins in the presence of 0, 100, and 200 µM of **P3** and **P8**.[12] The ThS data point was acquired at every minute during the aggregation study. It was observed, although there was no significant change in the fluorescence intensities for each individual mixture along this time period, there was a clear distinction of the effect of **P3** and **P8** (Figure **3B.9**) on the aggregation propensity of AcPHF and AcPHF*. In the assay, the fluorescence intensities of AcPHF6 and AcPHF6* controls remained around 40-50 a.u whereas their mixtures with **P3** at 100 and 200 µM displayed higher intensity around 65-75 a.u. and 100-110 a.u., respectively. On the other hand, the mixtures of AcPHF6 and AcPHF6* with **P8** have all showed lower fluorescence intensities of 25-35 a.u., which is less than the controls. These observations suggest that the macrocyclic peptides **P3** and **P8** have the ability to regulate aggregation in the AcPHFs and AcPHF* peptides.

Table 3B.4. Materials and their concentrations that were used for the cross-aggregation assay of **P3** and **P8**.

Sample	Tau	Macrocyclic Peptide	Heparin	Buffer mixture (BES, NaCl, DTT, NaN3, PIC)
PHF6 control	PHF6 (100 µM)	-	Yes	Yes
PHF6* control	PHF6* (100 µM)	-	Yes	Yes
PHF6+100 P3	PHF6 (100 µM)	P3 (100 µM)	Yes	Yes
PHF6*+100 P3	PHF6* (100 µM)	P3 (100 µM)	Yes	Yes
PHF6+200 P3	PHF6 (100 µM)	P3 (200 µM)	Yes	Yes
PHF6*+200 P3	PHF6* (100 µM)	P3 (200 µM)	Yes	Yes
PHF6+100 P8	PHF6 (100 µM)	P8 (100 µM)	Yes	Yes
PHF6*+100 P8	PHF6* (100 µM)	P8 (100 µM)	Yes	Yes
PHF6+200 P8	PHF6 (100 µM)	P8 (200 µM)	Yes	Yes
PHF6*+200 P8	PHF6* (100 µM)	P8 (200 µM)	Yes	Yes
K18wt control	K18wt (100 µM)	-	Yes	Yes
K18+100 P3	K18wt (100 µM)	P3 (100 µM)	Yes	Yes
K18+200 P3	K18wt (100 µM)	P3 (200 µM)	Yes	Yes
K18+100 P8	K18wt (100 µM)	P8 (100 µM)	Yes	Yes
K18+200 P8	K18wt (100 µM)	P8 (200 µM)	Yes	Yes
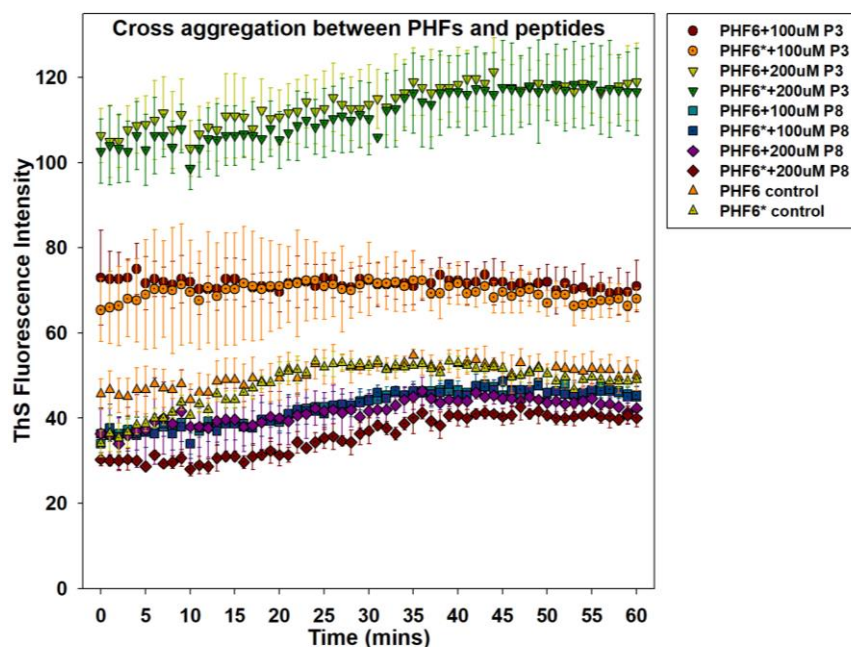
Figure 3B.9 Cross-aggregation assay to study the effect of macrocyclic peptides **P3** and **P8** on the aggregation of AcPHF and AcPHF*. ThS Fluorescence intensities were plotted against time for the cross-aggregation mixtures of AcPHF and AcPHF* with 0, 100 and 200 µM of **P3** and **P8**. We observed an increasing pro-aggregation effect on the aggregation of AcPHF and AcPHF* with increasing concentration of **P3**, whereas the presence of **P8** has led to the diminished aggregation of AcPHF6 and AcPHF6* compared to the controls.

3B.2.5. Tau aggregation is modulated in the presence of macrocyclic peptides

Next, we were keen on understanding whether the effects of **P3** and **P8** on individual PHF hexapeptides could be reproduced in biologically significant Tau species. To understand this, K18wt was allowed to aggregate for 60 mins in the presence of 0, 100 and 200 µM of the macrocyclic peptides **P3** and **P8**. It was found that although there were a couple of overlaps in the aggregation kinetics with the control K18wt, the mixtures of K18wt with **P3** showed higher fluorescence intensities and those with **P8** recorded lower fluorescence intensities than the control K18wt (Figure **3B.10a**). It was noted that 200 µM **P3** showed a better ability to increase K18wt aggregation compared to 100 µM **P3**. Meanwhile, 100 µM **P8** showed a slightly better inhibition compared to 200 µM **P8**. These aggregates of K18wt samples at different concentrations of **P3** and **P8** were loaded on TEM grids for visualization of the aggregate morphology (Figure **3B.10b**). To our delight, the HR-TEM images showed matured and more complex Tau fibrils in the presence of **P3**, whereas fibrils could hardly be formed with **P8**. Hence, it can be inferred that the macrocyclic peptides **P3** and **P8** have the potential to modulate the aggregation of Tau in pro and contra manner, respectively.
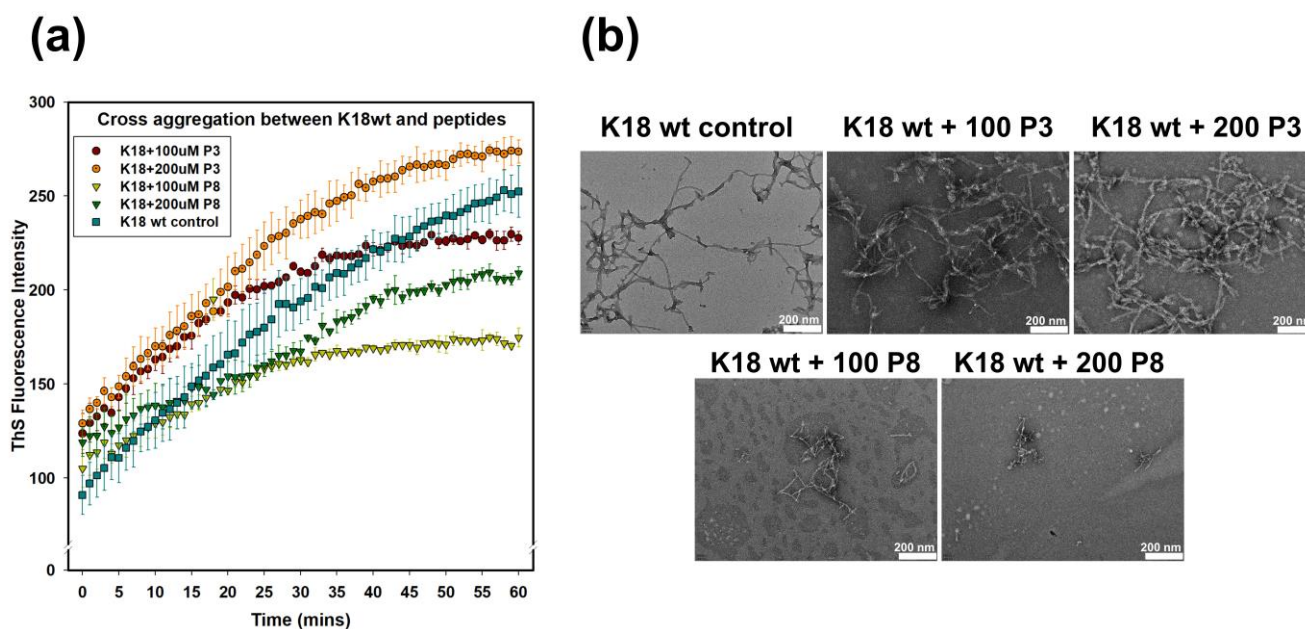
Figure 3B.10 Studies to understand the effect of peptides **P3** and **P8** on Tau aggregation. **(a)** ThS fluorescence intensities were plotted against time for the cross-aggregation mixtures of K18wt with 0, 100, and 200 µM **P3** and **P8**. Aggregation of 100 µM K18wt has increased with the concentration of the **P3** peptide, whereas the aggregation decreased in the presence of **P8**. **(b)** The HR-TEM images for the cross-aggregation mixtures of K18wt with 0, 100, and 200 µM of **P3** and **P8**. Compared to the K18wt control, K18wt+100 µM **P3** shows more mature fibrils and the number of fibrils increased in K18wt+200 µM **P3**. K18wt+100 µM **P8** shows smaller immature fibres, while K18wt+200 µM **P8** shows almost complete inhibition of fibres/aggregation formation.

3B.3. Conclusions

In summary, we have designed 10 macrocyclic peptides based on PHF and PHF* hexapeptides. The peptides were designed in a systematic manner, by taking into account our earlier results on the residue-based propensity of aggregation in AcPHF and AcPHF* peptides and employed peptide structure design principles and *N*-methylation of the backbone amides. The hypothesis was to ultimately obtain peptides that can modulate the aggregation of PHFs and Tau as desired. As expected from the design principles, NMR structural studies have established an anti-parallel beta-sheet fold for all the peptides. The aggregation studies have shown a set of peptides (**P1**, **P3**-**P6**) that have self-aggregated well and another set (**P7**-**P10**) that have diminished aggregation tendency. Through these studies we have identified macrocyclic peptides **P3** and **P8**, that aggregated the most and the least, which behavior also aligned with our hypothetical aggregation model. The presence of peptide **P3** exhibited a pro-aggregation and that of **P8** a contra-aggregation effect on the aggregation of the parent AcPHF6 and AcPHF* peptides. Furthermore, **P3** and **P8** had their natural pro- and contra-aggregation influence also on the Tau protein aggregation, which is evidenced by the corresponding ThS and HR-TEM analysis. This shows the

ability of **P3** and **P8** to act even at the macromolecule level. We hope these results are of potential application for the selective modulation of Tau and PHF aggregation and the design of Tau aggregation inhibitors.

3B.4. Materials and methods

3B.4.1. **Solid phase peptide synthesis protocol**:[35] Synthesis of linear peptides started with the loading of the Fmoc-L-*N*Me-Ala-OH (at position 7 in the peptide sequences,1.2 eq.) to the 2-CTC (150 mg, 1.6mmol/g, 0.24mmol) in dry DCM and DIPEA (3 eq.) for 2 hrs. After loading of the first amino acid, capping of the resin was done by MeOH (0.5 mL) and DIPEA (30 µL) for 30 min. Then Fmoc deprotection was carried out in 20% piperidine in DMF (2*10 min) and resin was washed 4 times with NMP. Coupling of next residue, Fmoc-D-*N*Me-Ala-OH (at position 6, 2 eq.) was done using HCTU (2 eq.), HOAt (2 eq.), DIPEA (5 eq.) in NMP (3 mL) for 1.5 hrs. After which the peptide chains were elongated as per the amino acid sequences by repetitive Fmoc deprotection and coupling of the required amino acids in order. When peptide chains reached the desired tetradecapeptide length, the final Fmoc deprotection was done using 20 % piperidine in DMF. The linear tetra decapeptides with side chain protection groups were cleaved from resin using TFE: AcOH: DCM (1:1:8) for 1.5 hrs. (30 min*3). This filtrate was collected, concentrated and the excess acetic acid was removed as azeotrope with chloroform.

3B.4.2. **General procedure for on resin *N*-methylation**:[38] For the peptides, **P7**-**P10**, *N*-methylation of the externally oriented NHs was performed by modified Fukuyama-Mitsunobu *N*-methylation procedure, which is divided into three steps. The first step is Nosyl protection of the free amine obtained after the Fmoc deprotection. Nosyl protection was performed in presence of Nosyl chloride (3 eq.) and collidine (3 eq.) in NMP for 40 min. The Nosyl protected resin was washed 3 times with NMP and then 3 times with dry THF. Then *N*-methylation was done by using PPh3 (5 eq.), DIAD (5 eq.) and dry methanol (10 eq.) in dry THF for 15 min. After this Mitsonobu alkylation, the Nosyl group was deprotected using DBU (2 eq.) and 2-mercaptoethanol (2 eq.) in 3 mL of NMP for 40 min. This step was performed two times and after completion of the reaction, resin was washed 3 times with NMP.

3B.4.3. **General procedure for cyclization of linear peptides**: The head to tail cyclization of these linear peptides was done using HCTU (2 eq.), HOAt (2 eq.), and DIPEA (5 eq.) in DMF. After overnight stirring, the reaction mixture was concentrated and dissolved in saturated sodium bicarbonate.

The side chain protected cyclic peptides of **P1**-**P10** were extracted from this solution with ethyl acetate and purified by column chromatography.

3B.4.4 Global deprotection of cyclic peptides: Global deprotection of all the side chain protecting groups in cyclic peptides was accomplished with a cocktail of trifluoroacetic acid (TFA) and the carbocation scavenger triisopropylsilane (TIPS) in DCM. (TFA: TIPS: DCM) (50:5:45). After complete deprotection of the sidechain protecting groups, the reaction mixture was concentrated and purified by reversed phase HPLC to obtain peptides **P1**-**P10**.

3B.4.5 HPLC Purification of macrocyclic peptides

Semi-prep HPLC method: All the peptides were purified by reversed phase HPLC on Waters 2545 Quaternary Gradient Module with 2489 UV/Visible Detector using YMC Pack ODS-A-HG C18 column of pore size S-10 μm, 12 nm, 250 mm * 20 mm I.D. A flow rate of 4 mL/min was used for the purification.

3B.4.6. Preparation of repeat Tau

The repeat domain of Tau K18wt (wild type) was cloned in pT7C plasmid and transformed in *BL21** bacterial cells. Bacterial expression was carried out in the stages of primary and secondary inoculation, followed by IPTG induction (0.5 mM) at 37°C, at O.D. at 600 nm. The bacterial cells were harvested after 4 hours and subjected to lysis through homogenization at 15 kPSI (Homogenizer: Constant Cell Disruption). Since Tau is natively unfolded, the lysate is subjected to 90°C treatment for 20 mins in the presence of 0.5 M NaCl and 5 mM DTT. The lysate is then centrifugation at 40,000 rpm, 45 minutes to eliminate all unwanted molecules. The supernatant contains the desired protein and allowed to undergo dialysis overnight for removal of high NaCl concentration. Protein purification is performed in 2 steps – cation exchange chromatography, followed by size-exclusion chromatography. For cation exchange, the dialysate is centrifuged at 40,000 rpm, 45 minutes to remove any precipitate or aggregate formed during the process. This supernatant is loaded onto a super loop for sample application to the cation exchange column (SPFF GE17-0729-01, Sepharose Fast Flow). Column equilibration was done in Buffer A - MES 20 mM (pH 6.8, 50 mM NaCl) while the protein was eluted *via* gradient elution using Buffer B - MES 20 mM (pH 6.8, 1 M NaCl). Absorbance at 214 nm was monitored and the corresponding fractions were collected (~30% Buffer B). The fractions were pooled and concentrated to load for size-exclusion chromatography. The size exclusion column (Superdex 75 Hi-load 16/600 column GE28-9893-33) was equilibrated in PBS 1X, 2 mM DTT. The size exclusion fractions corresponding to the

UV214 peak were collected, pooled and concentrated. Protein concentration was estimated using the Bicinchoninic acid (BCA) assay.

3B.4.7. Preparation of aggregates

Before setting up the aggregates, K18wt, Ac-PHFs and macrocyclic peptides were centrifuged at 60000 rpm for 60 minutes, to get rid of any aggregates already present. All aggregates were prepared in BES 20 mM (pH 7.4), in the presence of ions provided by NaCl (25 mM), DTT (1 mM) for preventing disulphide linkages and sodium azide (0.01%) for protection against microbial contamination. Heparin (17500 Da) was used, in 1:4 proportion (Heparin:Tau), as the inducer for aggregation.

(a) Self-aggregation: Macrocyclic peptides (**P1**-**P10**) were set up for aggregation at 100 µM each by following the above procedure.

(b) Cross-aggregation: The control peptides - PHF6, PHF6* and the K18 repeat region - were subjected to Heparin-based aggregation, in the presence of macrocyclic peptides. The two macrocyclic peptides chosen were **P3** which was pro-aggregation and **P8**, which effectively inhibited aggregation, as seen in the self-aggregation studies. PHFs/K18 and macrocyclic peptides were taken in 1:1 (100 µM PHFs/K18 and 100 µM **P3**/**P8**) and 1:2 (100 µM PHFs/K18 and 200 µM **P3**/**P8**) ratios. The controls for the experiment consisted of systems where the control peptides were allowed to aggregate (Heparin-based) in the absence of the macrocyclic peptides.

3B.4.8. ThS fluorescence assay (Continuous vs. fixed time point)

Thioflavin S emits fluorescence on binding to hydrophobic compounds. It is used here to monitor aggregation of Tau, since aggregates are hydrophobic in nature. Samples were mixed with ThS in 1:4 ratio (Tau:ThS) and fluorescence intensities were taken at excitation 440 nm and emission 521 nm in Tecan microplate reader (Infinite 200 Pro multimode). For determination of aggregation promotors/inhibitors among macrocyclic peptides (self-aggregation), the classical assay was followed where the ThS fluorescence was monitored every 24 hours over a period of 216 hours (9 days). For the cross-aggregation assays, continuous measurement assay was carried out every minute for 60 minutes. Blank reading was taken with BES and ThS and subtracted from all sample intensities.

(a) Classical assay: Aggregates are set at 37º C and at every 24-hour time point, sample was taken out to prepare 2 µM in ThS (8 µM) to make a total of 50 µL volume, which was then added to a 384 well black plate for the measurement.

164

(b) Continuous measurement: All reagents were added for the setting up of aggregates and immediately mixed with ThS (8 µM sample in 32 µM ThS) in the 384 well plate to capture the aggregation kinetics every minute from 0 to 60 minutes. The plate reader is set at 37ºC for the aggregation to take place in the plate over the course of the continuous measurement.

3B.4.9. Electron microscopy or HR-TEM

High Resolution – Transmission electron microscopy (FEI HR-TEM, 300 keV) was performed to understand the aggregate structures in different conditions. 400 mesh carbon coated copper grids were used for the imaging. The grids were incubated with 5 µM sample for 2 minutes, followed by 2 washes with water (filtered Milli Q) for 30 seconds each and negative staining with 2% uranyl acetate for 5 minutes.

3B.4.10. NMR chemical shift assignments of P1-P10.

Table 3B.5. NMR chemical shift assignment of **P1**.

Residue	NH/*N*Me	Hα	Hβ	Hγ	Hδ	Temperature coefficients
Val1	6.98	4.52	2.04	0.87		0.8
Gln2	8.51	4.51	1.63	1.95		-4.2
Ile3	8.50	4.95	1.66	1.24	0.78	-2.8
Ile4	8.45	4.50	1.70	1.19	0.79	-5.2
Asn5	8.25	5.34	2.60/1.92			-2.8
*N*Me-D-ala6	3.12	4.89	1.31			-
*N*Me-L-ala7	2.93	5.05	2.93			-
Asn8	7.09	4.89	2.59			0
Ile9	8.55	4.59	1.47	1.25	0.72	-4.8
Ile10	8.49	4.50	1.61	1.39	0.76	-3.2
Gln11	8.83	4.58	1.79/2.03			-5.6
Val12	8.58	4.56	1.95	0.70		-2.8
*N*Me-D-ala13	3.13	4.91	1.35			-
*N*Me-L-ala14	3.06	5.01	1.26			-

Table 3B.6. NMR chemical shift assignment of **P2**.

Residue	NH/*N*Me	Hα	Hβ	Hγ	Hδ	Temperature coefficients
Val1	6.99	4.54	2.01	0.85		0.8
Gln2	8.50	4.99	1.66	1.96		-7
Ile3	8.46	4.57	1.74	1.34	0.72	-2.5
Val4	8.53	4.55	1.86	0.74		-6
Tyr5	8.60	5.66	2.41/2.98	-		-1.6
*N*Me-D-ala6	3.01	4.79	1.21	-		-
*N*Me-L-ala7	2.89	4.95	1.05	-		-
Tyr8	7.14	4.91	2.95/2.97	-		-0.4
Val9	8.72	4.68	1.74	0.72		-5.5
Ile10	8.56	4.54	1.62	1.29,1.01	0.71	-2
Gln11	8.83	4.58	2.05/1.83	-		-4.4
Val12	8.51	4.51	1.85	0.83		-2.9
*N*Me-D-ala13	3.10	4.90	1.34	-		-
*N*Me-L-ala14	3.05	5.01	1.25	-		-

Table 3B.7. NMR chemical shift assignment of **P3**.

Residue	NH/*N*Me	Hα	Hβ	Hγ	Hδ	Temperature coefficients
Val1	7.01	4.55	2.03	0.86		0.4
Gln2	8.82	4.61	1.78	2.01		-5.2
Ile3	8.49	4.56	2.04	1.60	0.51	-2.5
Val4	8.52	4.43	1.88	0.88		-6
Tyr5	8.38	5.02	2.89/2.35			-2
*N*Me-D-ala6	2.96	4.80	1.24			-
*N*Me-L-ala7	2.94	5.09	1.19			-
Asn8	7.25	4.96	2.62/2.43			0
Ile9	8.55	4.69	1.54	1.40	0.65	-3.6
Ile10	8.52	4.55	1.96	1.86	0.72	-2
Gln11	8.51	4.98	1.65	1.97		-4.4
Val12	8.43	4.56	1.72	0.76		-2
*N*Me-D-ala13	3.13	4.92	1.35	-		-
*N*Me-L-ala14	3.06	5.01	1.25	-		-

Table 3B.8. NMR chemical shift assignment of **P4**.

Residue	NH/*N*Me	Hα	Hβ	Hγ	Hδ	Temperature coefficients
Val1	6.91	4.46	2.05	0.85		0.8
Ala2	8.57	5.03	1.03			-5.6
Ile3	8.45	4.51	1.70	1.28	0.76	-2.8
Ile4	8.48	4.50	1.64	1.38	0.74	-6.2
Asn5	8.23	5.34	2.62			-3.2
*N*Me-D-ala6	3.12	4.89	1.32			-
*N*Me-L-ala7	5.05	2.93	1.20			-
Asn8	7.10	4.89	2.59/2.36			1.2
Ile9	8.56	4.66	1.50	1.45	0.71	-5.2
Ile10	8.46	4.51	1.71	1.29	0.76	-2.8
Ala11	8.73	4.73	1.20			-5.2
Val12	8.33	4.45	1.94	0.75		-3.2
*N*Me-D-ala13	3.04	4.94	1.31			-
*N*Me-L-ala14	3.02	5.07	1.24			-

Table 3B.9. NMR chemical shift assignment of **P5**.

Residue	NH/*N*Me	Hα	Hβ	Hγ	Hδ	Temperature coefficients
Val1	6.88	4.47	2.04	0.84		0.8
Ala2	8.56	5.04	1.02			-5.6
Ile3	8.47	4.57	1.75	0.85	0.74	-2.4
Val4	8.49	4.55	1.64	0.86		-5.8
Tyr5	8.61	5.07	3.01/2.96			-2.4
*N*Me-D-ala6	2.99	4.79	1.22			-
*N*Me-L-ala7	2.58	4.81	1.02			-
Tyr8	7.14	4.91	2.96/2.91			0
Val9	8.74	4.72	1.77	0.74		-6.4
Ile10	8.55	4.55	1.75	0.89	0.71	0.8
Ala11	8.72	4.75	1.20			-5.6
Val12	8.35	4.45	1.91	0.76		-3.2
*N*Me-D-ala13	3.03	4.95	1.23			-
*N*Me-L-ala14	3.01	5.07	1.24			-

Table 3B.10. NMR chemical shift assignment of **P6**.

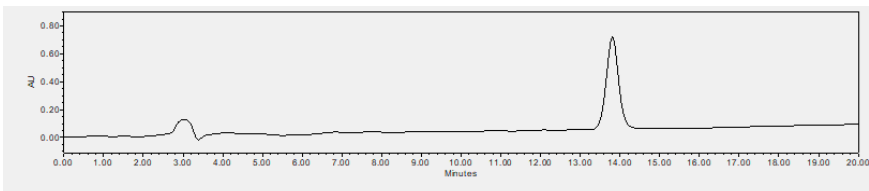| Residue	NH/*N*Me	Hα	Hβ	Hγ	Hδ	Temperature coefficients
Val1	6.91	4.45	2.04	0.84		0.8
Ala2	8.58	5.04	1.04			-4.8
Ile3	8.46	4.57	1.73	1.53		-2.8
Val4	8.51	4.40	1.87	0.86		-5.2
Tyr5	8.38	5.01	2.90/2.37			-2
*N*Me-D-ala6	2.96	4.94	1.32			-
*N*Me-L-ala7	3.02	5.05	1.03			-
Asn8	7.26	4.95	2.46/2.61			0
Ile9	8.55	4.75	1.06	1.54	0.68	-5.6
Ile10	8.59	4.54	1.94	1.46	0.75	-3.2
Ala11	8.71	4.76	1.18			-4.8
Val12	8.34	4.46	2.02			-3.2
*N*Me-D-ala13	3.03	4.79	1.30			-
*N*Me-L-ala14	2.93	5.06	1.18			-

Table 3B.11. NMR chemical shift assignment of **P7**.

Residue	NH/*N*Me	Hα	Hβ	Hγ	Hδ	Temperature coefficients
Val1	8.22	3.84	1.99	0.84		-1.2
Gln2	8.73	4.55	1.10	1.69		-5.6
Ile3	8.62	4.54	1.89	1.46	0.74	-2.4
Ile4	8.81	4.67	1.91	1.26	0.81	-8.4
Asn5	8.64	4.25	2.01/1.80			-2.4
*N*Me-D-ala6	2.90	5.40	1.12			-
*N*Me-L-ala7	2.82	5.04	1.34			-
Asn8	7.52	4.32	1.98			0
*N*Me-Ile9	2.90	5.25	2.21			-
Ile10	8.79	4.45	1.98	1.31	0.76	-2.4
*N*Me-Gln11	2.82	5.03	1.97/2.15			-
Val12	9.06	4.63	2.04	0.89		-2.8
*N*Me-D-ala13	2.89	5.80	1.18			-
*N*Me-L-ala14	2.63	4.22	0.95			-

Table 3B.12. NMR chemical shift assignment of **P8**.

Residue	NH/*N*Me	Hα	Hβ	Hγ	Hδ	Temperature coefficients
Val1	7.12	4.45	2.04	0.86		-0.4
Gln2	8.60	4.85	1.69	1.90		-6
Ile3	8.40	4.46	1.91	1.69	0.76	-2.4
Val4	8.77	4.45	1.89	1.89		-5.6
Tyr5	8.52	5.20	2.52/3.08	-		-2.8
*N*Me-D-ala6	3.07	4.87	1.25	-		-
*N*Me-L-ala7	2.72	5.01	1.10	-		-
Tyr8	7.56	4.97	2.83/3.10	-		-1.2
*N*Me-Val9	3.12	4.98	2.05	2.05		-
Ile10	8.94	4.65	1.91	1.16/1.51	0.74	-2.8
*N*Me-Gln11	3.32	5.40	1.89	2.03		-
Val12	8.43	4.59	1.92	0.84		-2.8
*N*Me-D-ala13	3.16	4.88	1.36	-		-
*N*Me-L-ala14	3.06	5.02	1.27	-		-

Table 3B.13. NMR chemical shift assignment of **P9**.
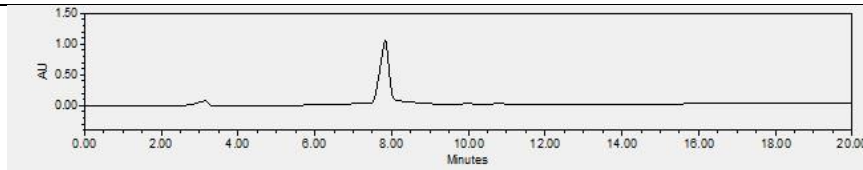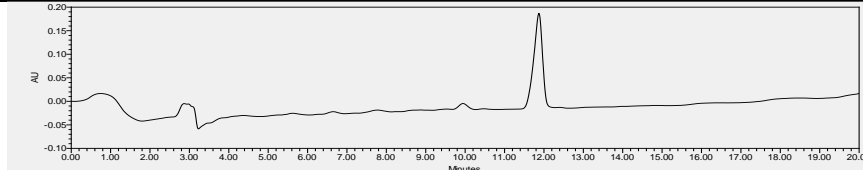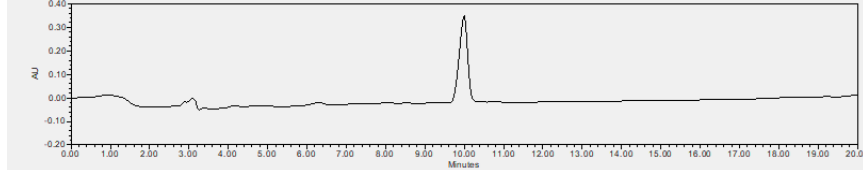
Residue	NH/*N*Me	Hα	Hβ	Hγ	Hδ	Temperature coefficients
Val1	7.07	4.50	2.03	0.84		-0.4
Gln2	8.61	4.91	1.65	1.82/1.94		-4
Ile3	8.22	4.56	1.66	1.29	0.76	-1.2
Ile4	8.60	4.41	1.82	1.13	0.74	-4
Asn5	8.21	5.32	2.86/2.11			-2
*N*Me-D-ala6	3.15	4.91	1.31			-
*N*Me-L-ala7	2.95	5.01	1.21			-
Asn8	7.24	5.27	2.60			-1.2
*N*Me-Ala9	3.22	5.66	1.13			-
Ala10	8.44	4.87	1.18			-1.6
*N*Me-Gln11	3.19	5.22	1.88/2.01			-
Val12	8.37	4.56	1.93	0.76		-2.4
*N*Me-D-ala13	3.14	4.92	1.25			-
*N*Me-L-ala14	3.04	5.07	1.24			-

Table 3B.14. NMR chemical shift assignment of **P10**.
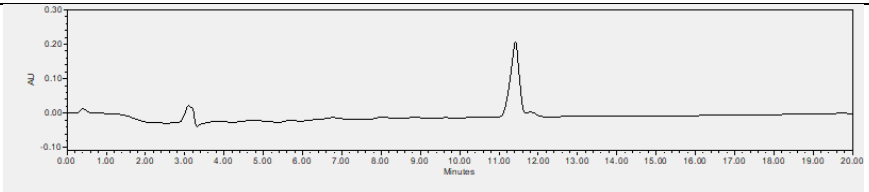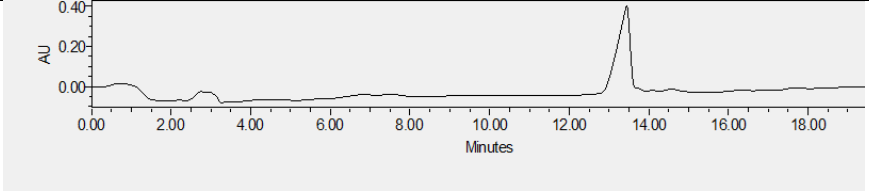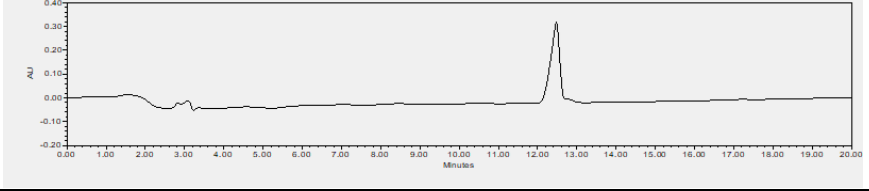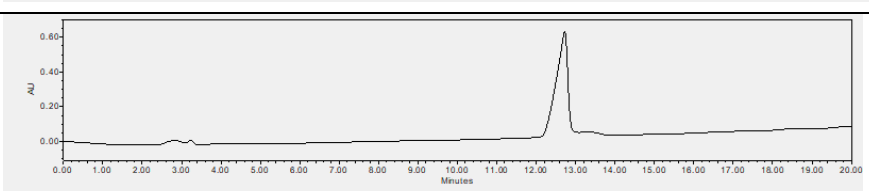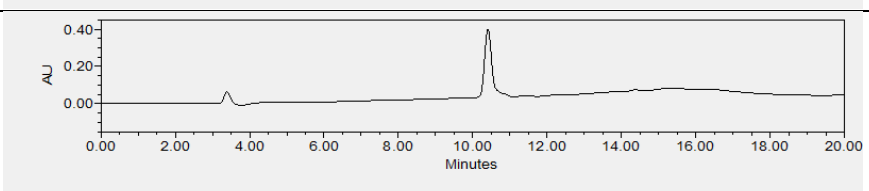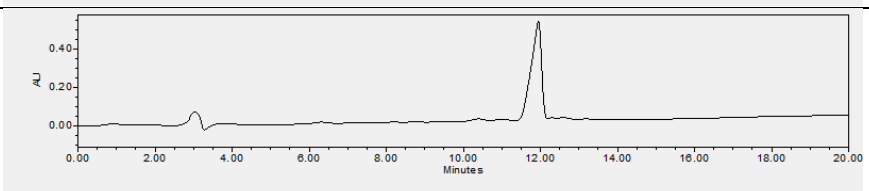
Residue	NH/*N*Me	Hα	Hβ	Hγ	Hδ	Temperature coefficients
Val1	7.06	4.51	2.04	0.87		0
Gln2	8.57	4.94	1.81	1.95		-4.8
Ile3	8.28	4.49	1.68	1.21	0.70	-1.6
Val4	8.60	4.51	1.64	0.73		-5.6
Tyr5	8.54	5.08	2.94/2.67			-3.2
*N*Me-D-ala6	3.06	4.85	1.27			-
*N*Me-L-ala7	2.75	5.02	1.12			-
Tyr8	7.45	5.10	3.08/2.94			0.8
*N*Me-Ala9	3.0	5.61	1.07			-
Ala10	8.65	4.85	1.26			-2.8
*N*Me-Gln11	5.21	1.91	2.02			-
Val12	8.37	4.59	1.94	0.79		-2.8
*N*Me-D-ala13	3.15	4.92	1.35			-
*N*Me-L-ala14	3.05	5.35	1.24			-

3B.4.10. **Analytical HPLC of macrocyclic peptides**: Purity of all the peptides was determined by analytical HPLC using YMC Pack ODS-A-HG C18 column with the dimensions S-10 µm, 12 nm, 250 mm * 4.6 mm I.D., on Waters HPLC 2545 Quaternary Gradient module with 2489 UV/Visible detector. The gradient used for analytical run was 40 to 90% ACN in 20 min with a flow rate of 1 mL/min.

Table 3B.15: Analytical HPLC methods and retention times for the purified peptides.

Peptide	HPLC Gradient	HPLC Chromatogram
P1	70%-90% ACN in 20 min	
P2	60%-90% ACN in 20 min	
P3	60%-90% ACN in 20 min	

P4	60%-90% ACN in 20 min	
P5	50%-90% ACN in 20 min	
P6	40%-90% ACN in 20 min	
P7	60%-90% ACN in 18 min	
P8	40%-90% ACN in 20 min	
P9	60%-90% ACN in 20 min	
P10	20%-90% ACN in 20 min	

3B.4.11. ¹H NMR spectra of P1-P10 peptides.

¹H NMR of **P1** on 500 MHz at 298 K in DMSO-*d*₆.
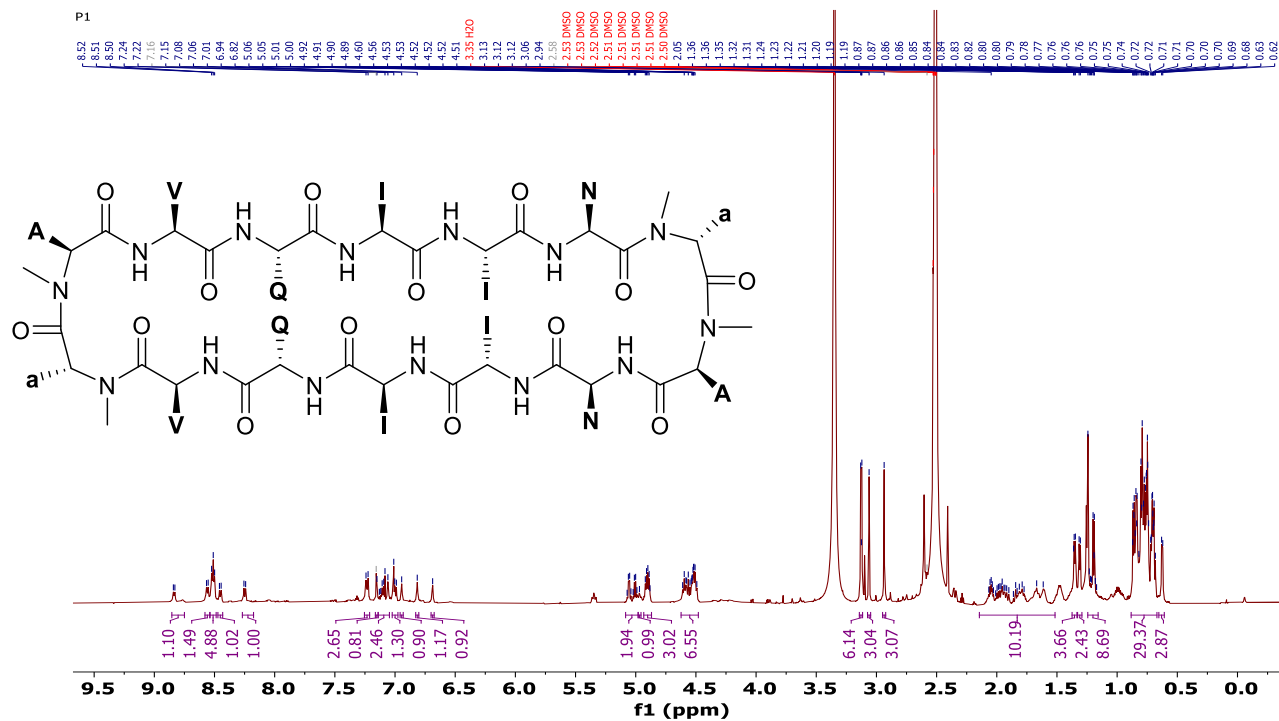
¹H NMR of **P2** on 500 MHz at 298 K in DMSO-*d*₆.
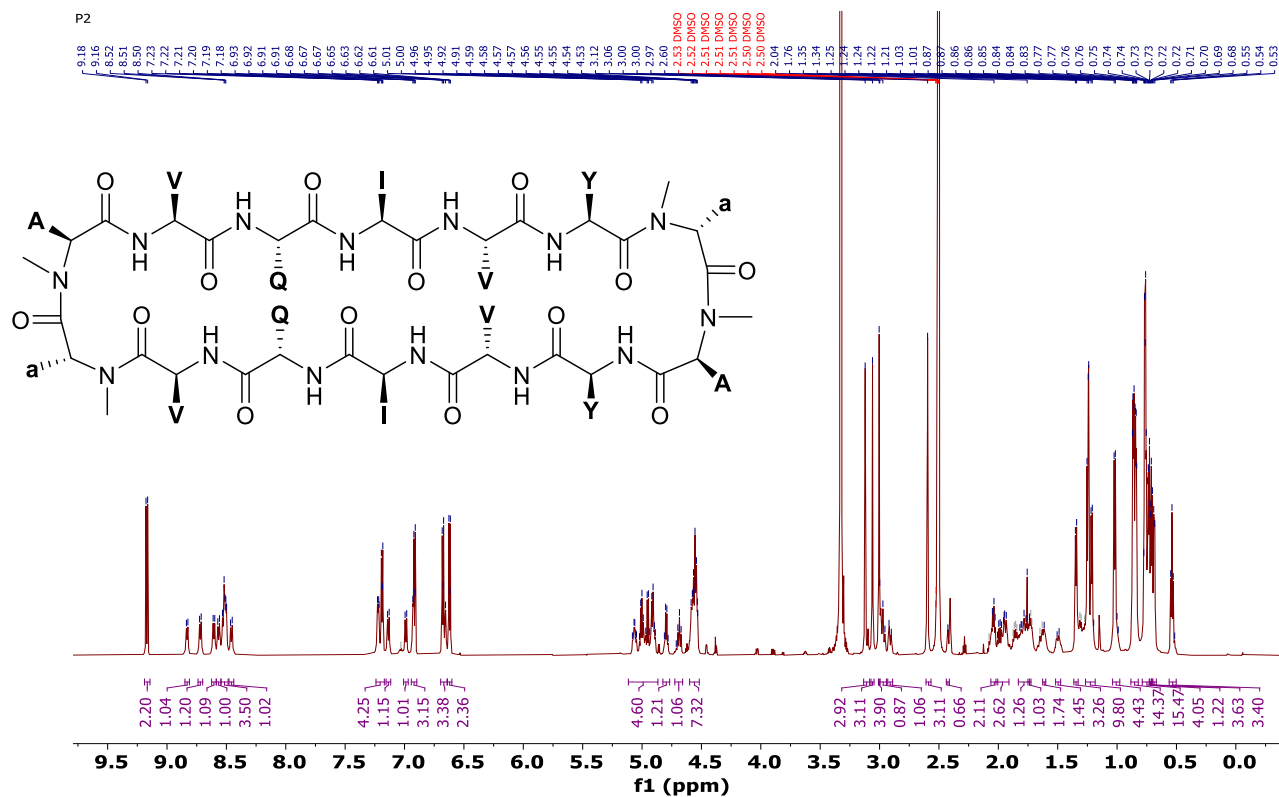
^{1}H NMR of **P3** on 500 MHz at 298 K in DMSO-d_6.
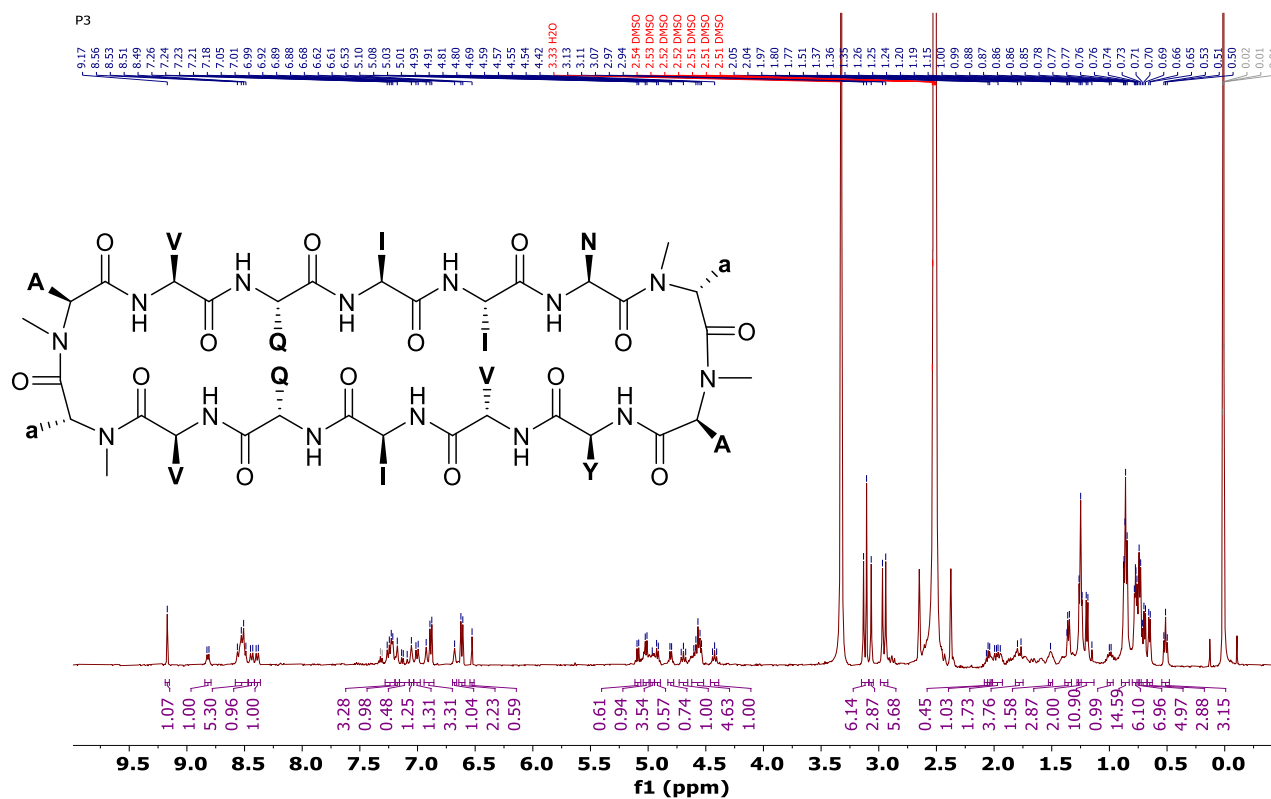
^{1}H NMR of **P4** on 500 MHz at 298 K in DMSO-d_6.
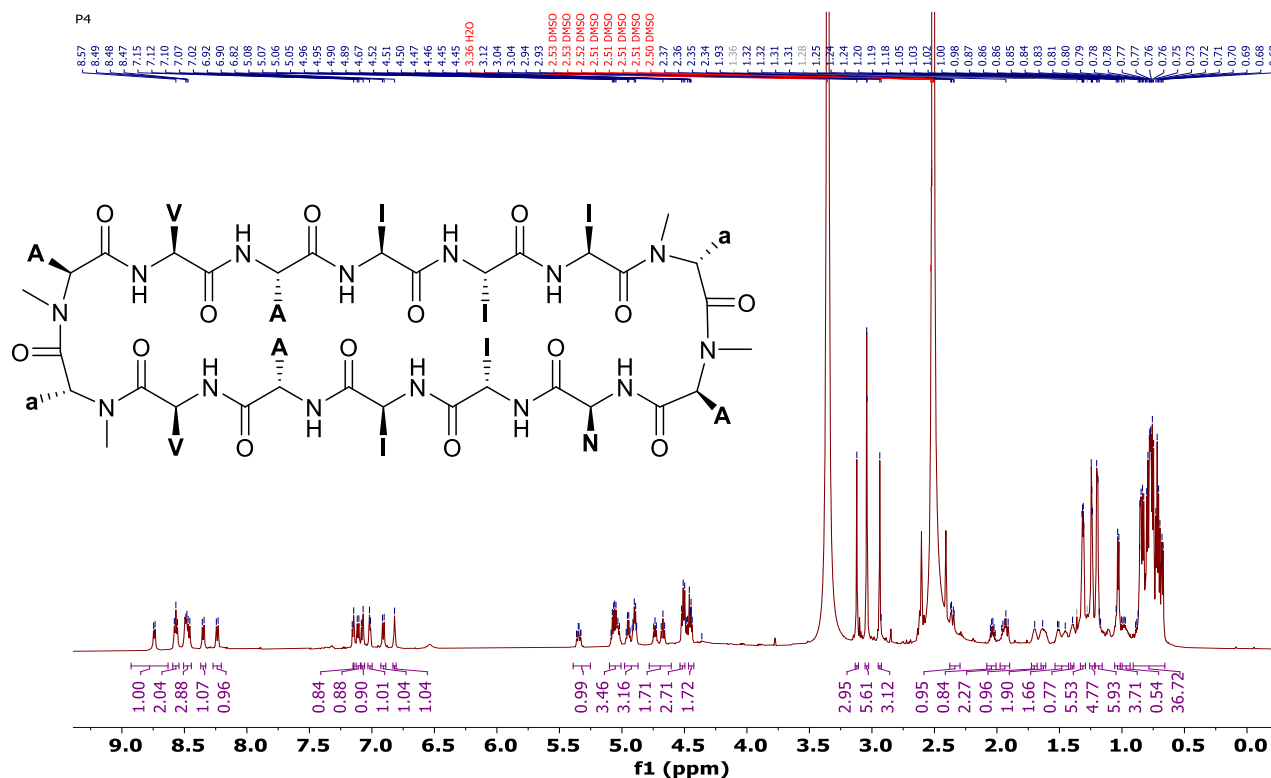
¹H NMR of **P5** on 500 MHz at 298 K in DMSO-*d*₆.
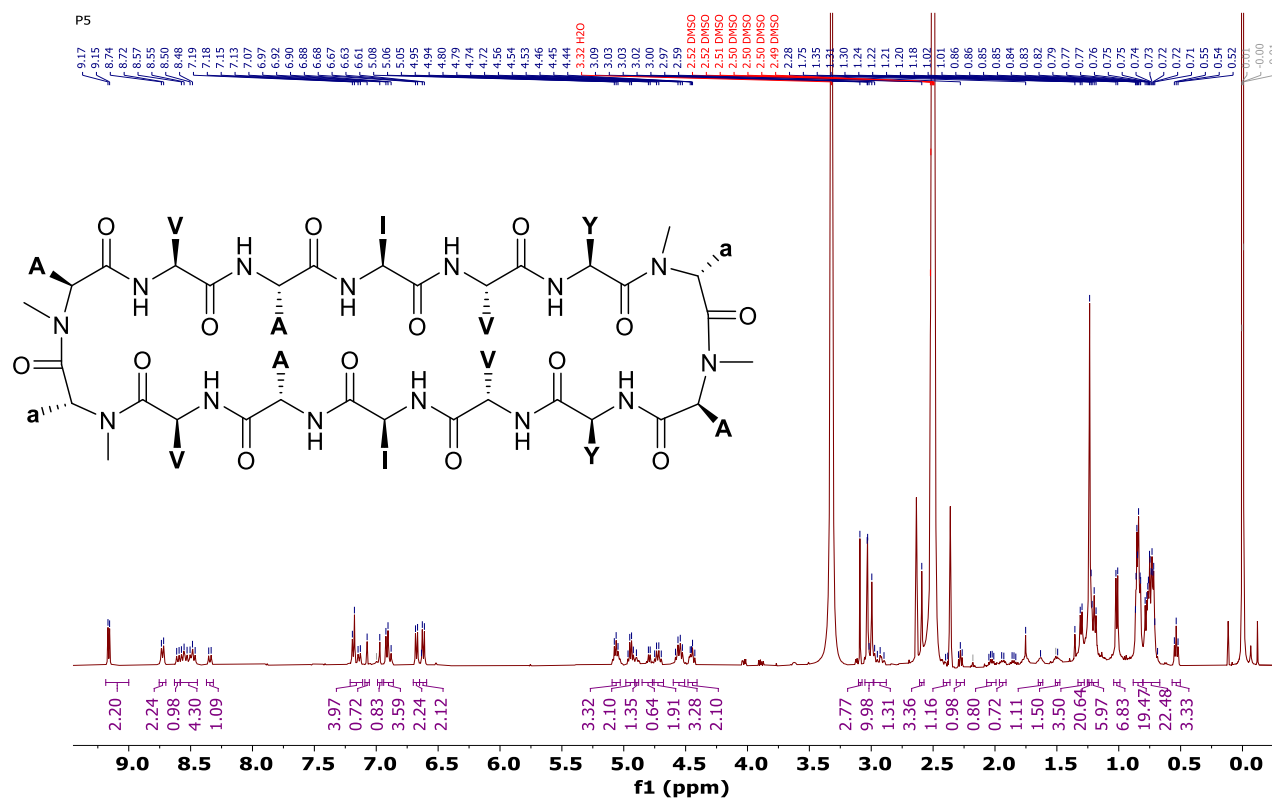
¹H NMR of **P6** on 500 MHz at 298 K in DMSO-*d*₆.
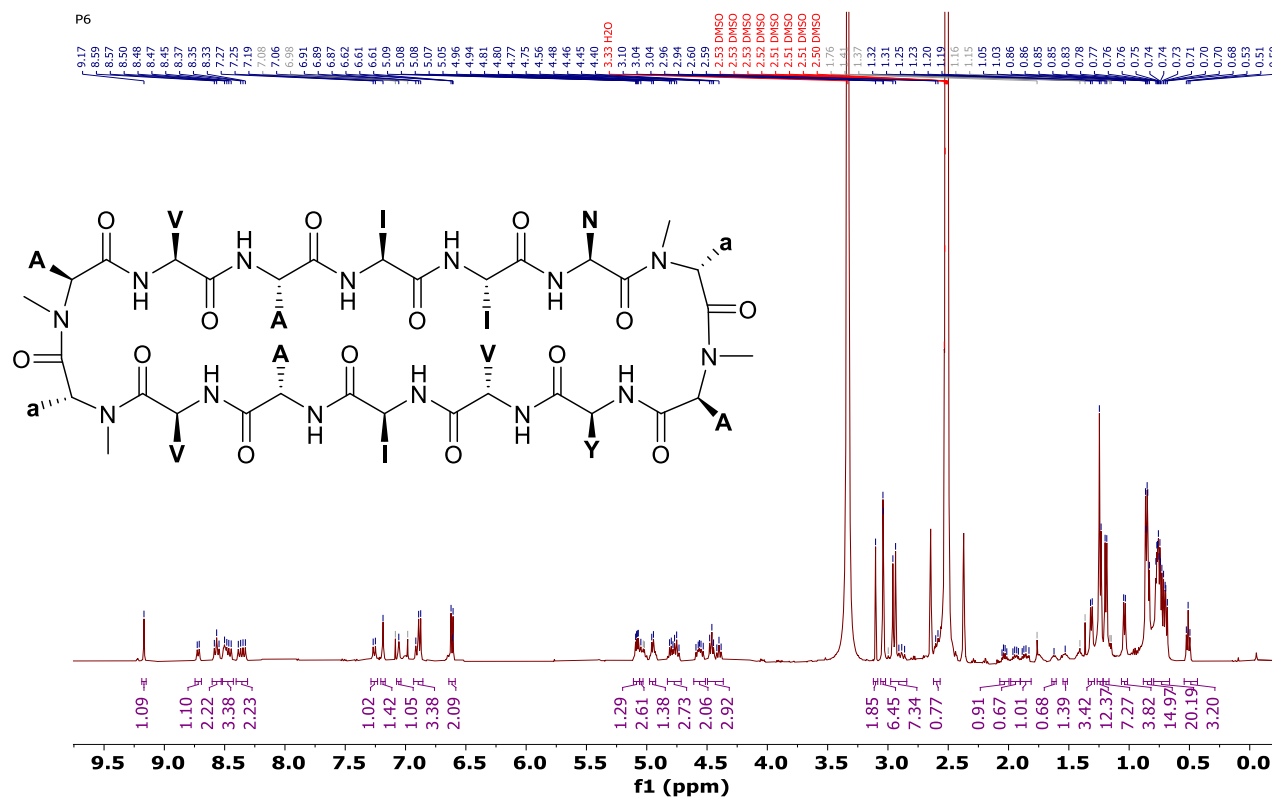
^{1}H NMR of **P7** on 500 MHz at 298 K in DMSO-d_6.
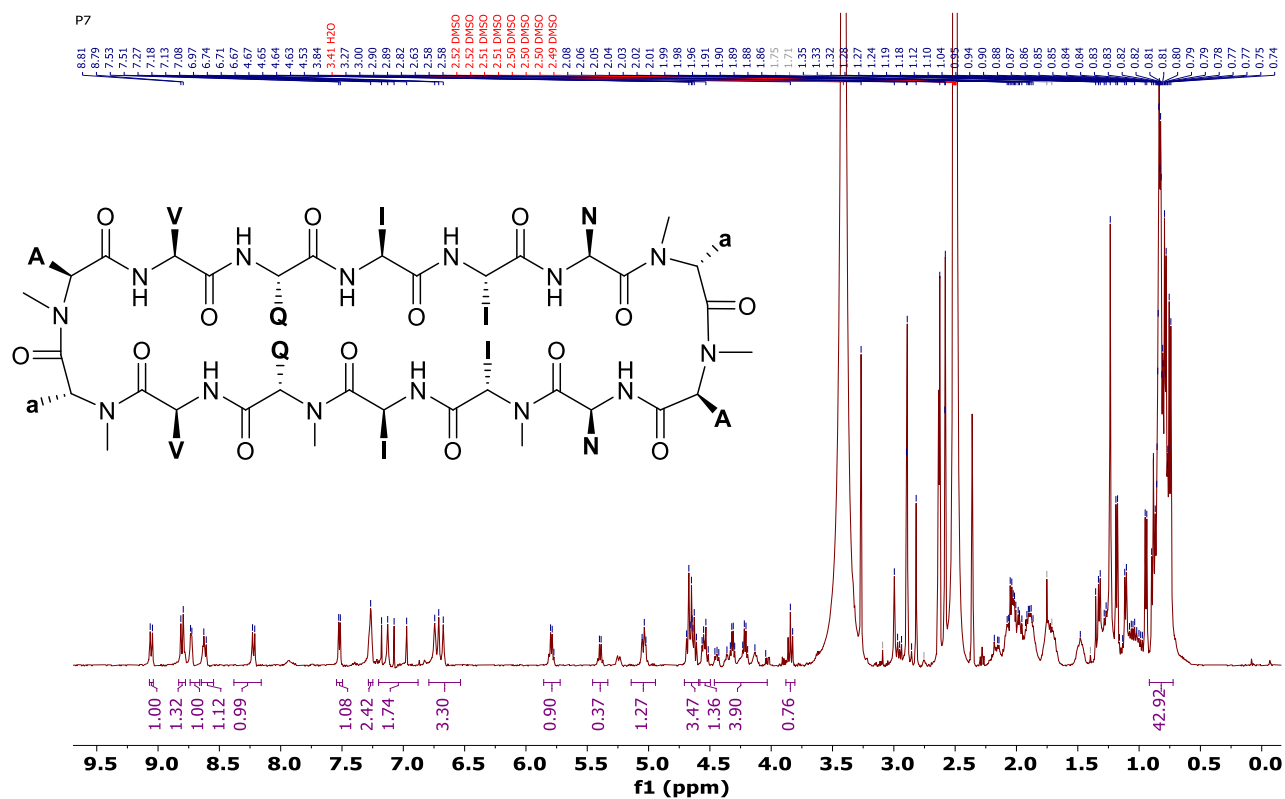
^{1}H NMR of **P8** on 500 MHz at 298 K in DMSO-d_6.
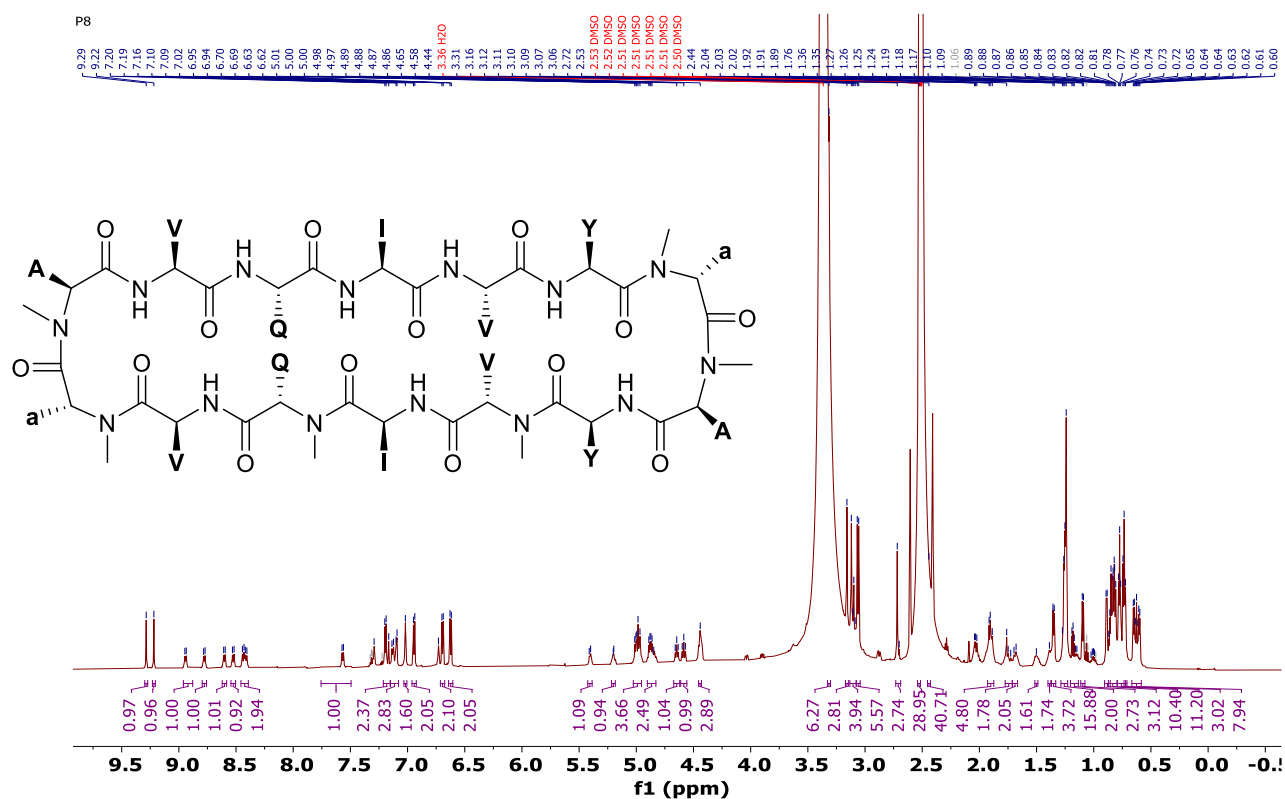
¹H NMR of **P9** on 500 MHz at 298 K in DMSO-*d*₆.
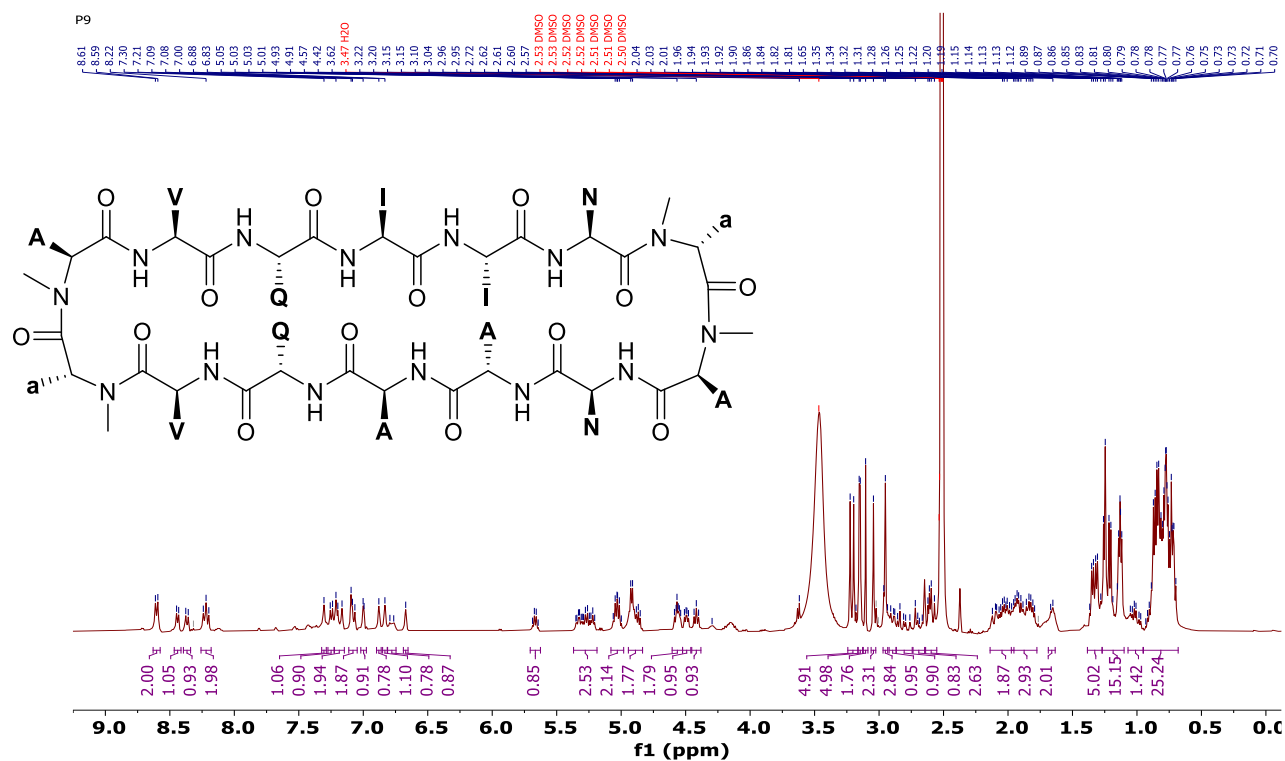
¹H NMR of **P10** on 500 MHz at 298 K in DMSO-*d*₆.
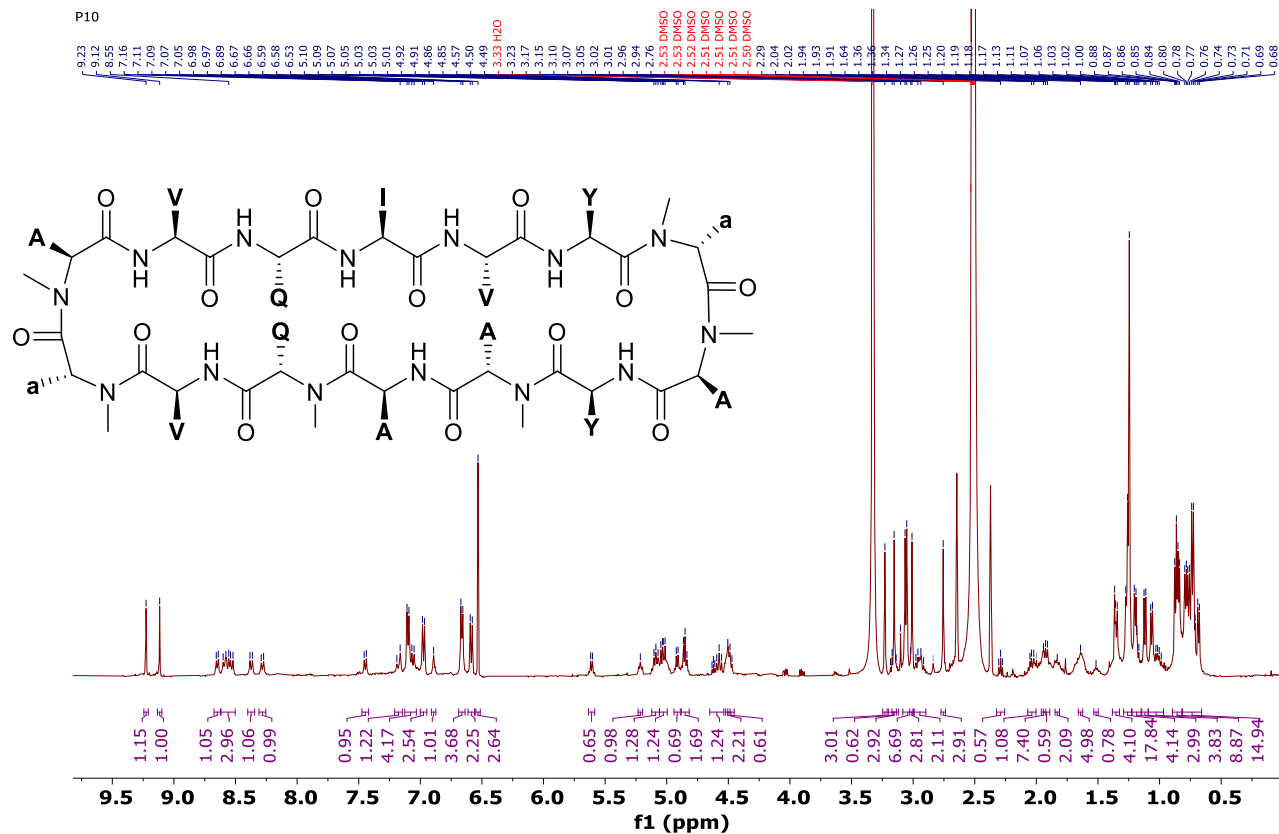
3.5. **Reference**

(1)   Chiti, F.; Dobson, C. M. Protein Misfolding, Amyloid Formation, and Human Disease: A Summary of Progress over the Last Decade. *Annu. Rev. Biochem.* **2017**, *86*, 27–68.

(2)   Cummings, J.; Lee, G.; Ritter, A.; Sabbagh, M.; Zhong, K. Alzheimer's Disease Drug Development Pipeline: 2019. *Alzheimer's Dement. Transl. Res. Clin. Interv.* **2019**, *5*, 272–293.

(3)   Fontaine, S. N.; Sabbagh, J. J.; Baker, J.; Martinez-Licha, C. R.; Darling, A.; Dickey, C. A. Cellular Factors Modulating the Mechanism of Tau Protein Aggregation. *Cell. Mol. Life Sci.* **2015**, *72* (10), 1863–1879.

(4)   Kaufman, S. K.; Sanders, D. W.; Thomas, T. L.; Sharma, A. M.; Miller, T. M.; Diamond, M. I.; Kaufman, S. K.; Sanders, D. W.; Thomas, T. L.; Ruchinskas, A. J.; Vaquer-alicea, J. Tau Prion Strains Dictate Patterns of Cell Pathology , Progression Rate , and Regional Vulnerability In Vivo Article Tau Prion Strains Dictate Patterns of Cell Pathology , Progression Rate , and Regional Vulnerability In Vivo. *Neuron* **2016**, *92* (4), 796–812.

(5)   Soto, C.; Sigurdsson, E. M.; Morelli, L.; Asok Kumar, R.; Castaño, E. M.; Frangione, B. β-Sheet Breaker Peptides Inhibit Fibrillogenesis in a Rat Brain Model of Amyloidosis: Implications for Alzheimer's Therapy. *Nat. Med.* **1998**, *4* (7), 822–826.

(6)   Congdon, E. E.; Sigurdsson, E. M. Tau-Targeting Therapies for Alzheimer Disease. *Nat. Rev. Neurol.* **2018**, *14* (7), 399–415.

(7)   Armiento, V.; Spanopoulou, A.; Kapurniotu, A. Peptide-Based Molecular Strategies To Interfere with Protein Misfolding, Aggregation, and Cell Degeneration. *Angew. Chemie Int. Ed.* **2020**, *59* (9), 3372–3384.

(8)   Iqbal, K.; Grundke-Iqbal, I. Inhibition of Neurofibrillary Degeneration: A Promising Approach to Alzheimers Disease and Other Tauopathies. *Curr. Drug Targets* **2004**, *5* (6), 495–502.

(9)   Von Bergen, M.; Friedhoff, P.; Biernat, J.; Heberle, J.; Mandelkow, E. M.; Mandelkow, E. Assembly of τ Protein into Alzheimer Paired Helical Filaments Depends on a Local Sequence Motif (306VQIVYK311) Forming β Structure. *Proc. Natl. Acad. Sci. U. S. A.* **2000**, *97* (10), 5129–5134.

(10)   Seidler, P. M.; Boyer, D. R.; Rodriguez, J. A.; Sawaya, M. R.; Cascio, D.; Murray, K.; Gonen, T.; Eisenberg, D. S. Structure-Based Inhibitors of Tau Aggregation. *Nat. Chem.* **2018**, *10* (2), 170–176.

(11)   Inouye, H.; Sharma, D.; Goux, W. J.; Kirschner, D. A. Structure of Core Domain of Fibril-Forming PHF / Tau Fragments. *Biophys. J.* **2006**, *90* (5), 1774–1789.

(12)   Rojas Quijano, F. A.; Morrow, D.; Wise, B. M.; Brancia, F. L.; Goux, W. J. Prediction of Nucleating Sequences from Amyloidogenic Propensities of Tau-Related Peptides. *Biochemistry* **2006**, *45* (14), 4638–4652.

(13)   Fitzpatrick, A. W. P.; Falcon, B.; He, S.; Murzin, A. G.; Murshudov, G.; Garringer, H. J.; Crowther, R. A.; Ghetti, B.; Goedert, M.; Scheres, S. H. W. Cryo-EM Structures of Tau Filaments from Alzheimer's Disease. *Nature* **2017**, *547* (7662), 185–190.

(14) Ganguly, P.; Do, T. D.; Larini, L.; LaPointe, N. E.; Sercel, A. J.; Shade, M. F.; Feinstein, S. C.; Bowers, M. T.; Shea, J.-E. Tau Assembly: The Dominant Role of PHF6 (VQIVYK) in Microtubule Binding Region Repeat R3. *J. Phys. Chem. B* **2015**, *119* (13), 4582–4593.

(15) Zhao, J. H.; Liu, H. L.; Chuang, C. K.; Liu, K. T.; Tsai, W. B.; Ho, Y. Molecular Dynamics Simulations to Investigate the Stability and Aggregation Behaviour of the Amyloid-Forming Peptide VQIVYK from Tau Protein. *Mol. Simul.* **2010**, *36* (13), 1013–1024.

(16) Von Bergen, M.; Barghorn, S.; Li, L.; Marx, A.; Biernat, J.; Mandelkow, E. M.; Mandelkow, E. Mutations of Tau Protein in Frontotemporal Dementia Promote Aggregation of Paired Helical Filaments by Enhancing Local β-Structure. *J. Biol. Chem.* **2001**, *276* (51), 48165–48174.

(17) Goux, W. J.; Kopplin, L.; Nguyen, A. D.; Leak, K.; Rutkofsky, M.; Shanmuganandam, V. D.; Sharma, D.; Inouye, H.; Kirschner, D. A. The Formation of Straight and Twisted Filaments from Short Tau Peptides. *J. Biol. Chem.* **2004**, *279* (26), 26868–26875.

(18) Mohamed, T.; Gujral, S. S.; Rao, P. P. N. Tau Derived Hexapeptide AcPHF6 Promotes Beta-Amyloid (Aβ) Fibrillogenesis. *ACS Chem. Neurosci.* **2018**, *9* (4), 773–782.

(19) Mandelkow, E.; Von Bergen, M.; Biernat, J.; Mandelkow, E. M. Structural Principles of Tau and the Paired Helical Filaments of Alzheimer's Disease. *Brain Pathol.* **2007**, *17* (1), 83–90.

(20) Mohamed, T.; Hoang, T.; Jelokhani-Niaraki, M.; Rao, P. P. N. Tau-Derived-Hexapeptide [306]VQIVYK[311] Aggregation Inhibitors: Nitrocatechol Moiety as A Pharmacophore In Drug Design. *ACS Chem. Neurosci.* **2013**, *4* (12), 1559–1570.

(21) Sawaya, M. R.; Sambashivan, S.; Nelson, R.; Ivanova, M. I.; Sievers, S. A.; Apostol, M. I.; Thompson, M. J.; Balbirnie, M.; Wiltzius, J. J. W.; McFarlane, H. T.; Madsen, A.; Riekel, C.; Eisenberg, D. Atomic Structures of Amyloid Cross-β Spines Reveal Varied Steric Zippers. *Nature* **2007**, *447* (7143), 453–457.

(22) Aillaud, I.; Funke, S. A. Tau Aggregation Inhibiting Peptides as Potential Therapeutics for Alzheimer Disease. *Cell. Mol. Neurobiol.* **2022**, No. 0123456789.

(23) Sievers, S. A.; Karanicolas, J.; Chang, H. W.; Zhao, A.; Jiang, L.; Zirafi, O.; Stevens, J. T.; Münch, J.; Baker, D.; Eisenberg, D. Structure-Based Design of Non-Natural Amino-Acid Inhibitors of Amyloid Fibril Formation. *Nature* **2011**, *475* (7354), 96–103.

(24) Press, P.; Ra, D. O. I.; Seidler, X. P. M.; Boyer, D. R.; Murray, K. A.; Yang, T. P.; Bentzel, M.; Sawaya, X. M. R.; Rosenberg, G.; Cascio, D.; Williams, C. K.; Newell, K. L.; Ghetti, B.; Deture, M. A.; Dickson, D. W.; Vinters, H. V; Eisenberg, X. D. S. Cro Structure-Based Inhibitors Halt Prion-like Seeding by Alzheimer 's Disease – and Tauopathy – Derived Brain Tissue Samples. *J. Biol. Chem.* **2019**, *294* (44), 16451–16464.

(25) Zheng, J.; Liu, C.; Sawaya, M. R.; Vadla, B.; Khan, S.; Woods, R. J.; Eisenberg, D.; Goux, W. J.; Nowick, J. S. Macrocyclic β-Sheet Peptides That Inhibit the Aggregation of a Tau-Protein-Derived Hexapeptide. *J. Am. Chem. Soc.* **2011**, *133* (9), 3144–3157.

(26) Cheng, P. N.; Liu, C.; Zhao, M.; Eisenberg, D.; Nowick, J. S. Amyloid β-Sheet Mimics That Antagonize Protein Aggregation and Reduce Amyloid Toxicity. *Nat. Chem.* **2012**, *4* (11), 927–933.

(27) Zheng, J.; Baghkhanian, A. M.; Nowick, J. S. A Hydrophobic Surface Is Essential to Inhibit the Aggregation of a Tau-Protein-Derived Hexapeptide. *J. Am. Chem. Soc.* **2013**, *135* (18), 6846–6852.

(28) Cheng, P.-N.; Spencer, R.; Woods, R. J.; Glabe, C. G.; Nowick, J. S. Heterodivalent Linked Macrocyclic β-Sheets with Enhanced Activity against Aβ Aggregation: Two Sites Are Better Than One. *J. Am. Chem. Soc.* **2012**, *134* (34), 14179–14184.

(29) Malhis, M.; Kaniyappan, S.; Aillaud, I.; Chandupatla, R. R.; Ramirez, L. M.; Zweckstetter, M.; Horn, A. H. C.; Mandelkow, E.; Sticht, H.; Funke, S. A. Potent Tau Aggregation Inhibitor D-Peptides Selected against Tau-Repeat 2 Using Mirror Image Phage Display. *ChemBioChem* **2021**, *22* (21), 3049–3059.

(30) Wang, C. K.; Northfield, S. E.; Huang, Y. H.; Ramos, M. C.; Craik, D. J. Inhibition of Tau Aggregation Using a Naturally-Occurring Cyclic Peptide Scaffold. *Eur. J. Med. Chem.* **2016**, *109*, 342–349.

(31) Wischik, C. M.; Novak, M.; Thogersen, H. C.; Edwards, P. C.; Runswick, M. J.; Jakes, R.; Walker, J. E.; Milstein, C.; Roth, M.; Klug, A. Isolation of a Fragment of Tau Derived from the Core of the Paired Helical Filament of Alzheimer Disease. *Proc. Natl. Acad. Sci. U. S. A.* **1988**, *85* (12), 4506–4510.

(32) Dangi, A.; Balmik, A. A.; Ghorpade, A. K.; Gorantla, N. V.; Sonawane, S. K.; Chinnathambi, S.; Marelli, U. K. Residue-Based Propensity of Aggregation in the Tau Amyloidogenic Hexapeptides AcPHF6∗ and AcPHF6. *RSC Adv.* **2020**, *10* (46), 27331–27335.

(33) Haubner, R.; Schmitt, W.; Hölzemann, G.; Goodman, S. L.; Jonczk, A.; Kessler, H. Cyclic RGD Peptides Containing β-Turn Mimetics. *J. Am. Chem. Soc.* **1996**, *118* (34), 7881–7891.

(34) Merrifield, R. B. Solid Phase Peptide Synthesis. *Excerpta Med., I.C.S.* **1976**, *No.374*, 29–39.

(35) Amblard, M.; Fehrentz, J. A.; Martinez, J.; Subra, G. Methods and Protocols of Modern Solid Phase Peptide Synthesis. *Mol. Biotechnol.* **2006**, *33* (3), 239–254.

(36) Schrödinger Release 2022-2: MacroModel, Schrödinger, LLC, New York, NY, 2021.

(37) Cierpicki, T.; Otlewski, J. Amide Proton Temperature Coefficients as Hydrogen Bond Indicators in Proteins. *J. Biomol. NMR* **2001**, *21* (3), 249–261.

(38) Miller, S. C.; Scanlan, T. S.; Francisco, S. Site-Selective N-Methylation of Peptides on Solid Support Department of Pharmaceutical Chemistry Uni V Ersity of California Conformational Restriction of Peptides Can Yield Useful Information about Their Bioactive Conformation . 1 N - Methyl Amino Acid Sub. **1997**, *7863* (16), 2301–2302.

CHAPTER-4

Synthesis, stereochemistry assignment, and NMR structure elucidation of Icosalide A, and its analogues: Evaluation of their antibacterial and antituberculosis activity
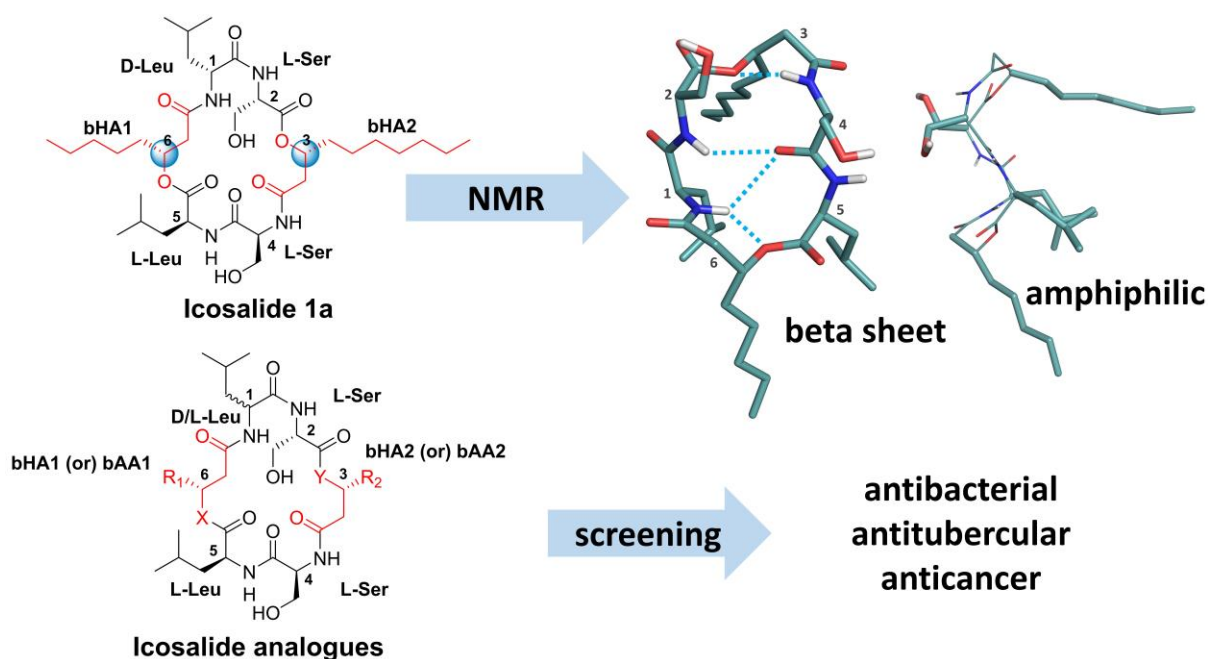
4.1. Introduction

As witnessed by the Covid-19 pandemic, infectious diseases are always a major threat to human health. In addition, antibiotic resistance, an impending reality caused by the inappropriate use of the existing antibiotics and the growing virulence of the microbes, is a challenge to overcome in front of the scientific and medical community.[1,2,3,4] A repertoire of antibiotic molecules that act by distinct mechanisms and which are not extensively used would help tackle infectious diseases more effectively in times of pandemics or widely spreading infections.[5,6,7] Hence, searching for newer antibiotic substances belonging to different structural classes that act efficiently and by novel mechanisms of action is a continuous process.[8,9] Among the various ways of communication among bacterial colonies, swarming behavior in bacteria is a vital phenomenon that has significance in signaling, virulence, pathogenicity, colonization, and antibiotic tolerance.[10] The display of antibiotic activity by inhibiting the swarming behavior of bacteria is a new mechanism of action that has gained significant interest in recent times.[11] Many existing antibiotic drugs and isolated natural products, as reviewed by Rütschlin *et al.*, were tested for their swarming behavior.[11] However, the search for molecules that could inhibit bacterial swarming at less than hundreds of millimolar concentrations is persistently underway.

Nature is a limitless source for discovering several bioactive compounds, including peptides and depsipeptides, for antibiotic activity.[12,13] Many antimicrobial peptides (AMPs) such as defensins, gramicidin S, valinomycin, nisin, phalloidin, amanitins, teixobactin[14,15,16,17] are all isolated from nature and have shown good Gram-positive and Gram-negative bacterial inhibitory action.

Cyclic depsipeptides are a class of cyclic peptides in which one or more amide bonds are replaced with ester bonds.[18,19,20] Numerous cyclic depsipeptides have been discovered that displayed anticancer, antibacterial, antifungal, and anti-inflammatory activities.[21,22,23] Since the discovery of the didemnins, this class of natural compounds has sparked ongoing study in synthetic and medicinal chemistry, clinical oncology, and cell biology.[24,25] Daptomycin 1 and Ramoplanin are excellent antibiotic depsipeptides that act by a different mechanism of action and have proved their clinical potential in drug development.[26,27] While Daptomycin 1 disrupts the cell membrane functions, Ramoplanin interferes with cell wall synthesis. Multiple naturally occurring cyclic depsipeptides exhibiting distinct structural features responsible for antibiotic activity were identified over the years and used as parent scaffolds for structure-activity optimization.[28,29,30]

Icosalides (Figure **4.1**), new members of the peptolide class of cyclic depsipeptides, were discovered by Boros *et al.* as isolated from a fungal culture.[31] Icosalides are lipodepsipeptidic comprised of six

residues, namely, L-Serine, L/D-Leucine alongside beta hydroxy acids having 8 or 10 carbon chains, which form a 20 atom macrocycle core. Unlike most lipopeptides, which contain only one fatty acid chain, the Icosalides are considered unusual for possessing two lipophilic chains as beta-hydroxy acids. Among the three isolated Icosalides (**1a**, **1b** and **1c**), Icosalide **1a** exhibited an antimicrobial activity of MIC 8-16 µg/mL against *Streptococcus pyogenes, S. pneumoniae (Felton),* and *Enterococcus faecalis*. Interestingly, Icosalide **1a** was also found to inhibit the swarming behaviour of the bacteria,[31] a mechanism of antibiotic activity, which is being thoroughly explored.[11,32] The stereochemistry of the constituent beta hydroxy acids in Icosalide was not identified initially when it was isolated by Boros *et al.* However, recently, Dose *et al.*[33] studied the genomic, metabolic profiling of *Burkholderia gladioli* bacteria and attributed the origin of the Icosalides to the bacteria rather than fungi. Further, they assigned the stereochemistry of beta hydroxy acids as 3-*S*-hydroxy decanoic acid and 3-*R*-hydroxy octanoic acid based on Moscher ester analysis and molecular modeling.[33] In contrary, Jenner *et al.*[34] established the biosynthetic pathway of Icosalides and reported the configurations of both beta hydroxy acids in Icosalide **1a** as *R*.[34] These two studies have left the stereochemistry of the beta hydroxy acids in Icosalide **1a** ambiguous.

The swarming inhibitive nature, unusual lipophilic composition, the antibiotic activity of the Icosalide **1a**, and the ambiguity in its structure have attracted us to investigate more about it. Through this study, we established its precise stereochemical structure via its total synthesis, NMR-based three-dimensional conformation, and further the influence of the lipophilic sidechains and the ester bonds on its activity (by switching ester bond to amide).
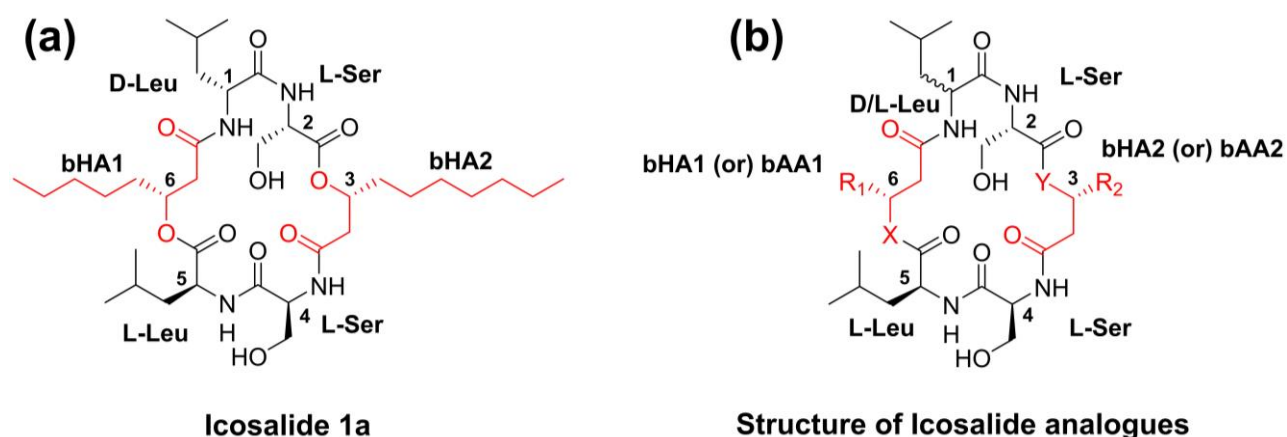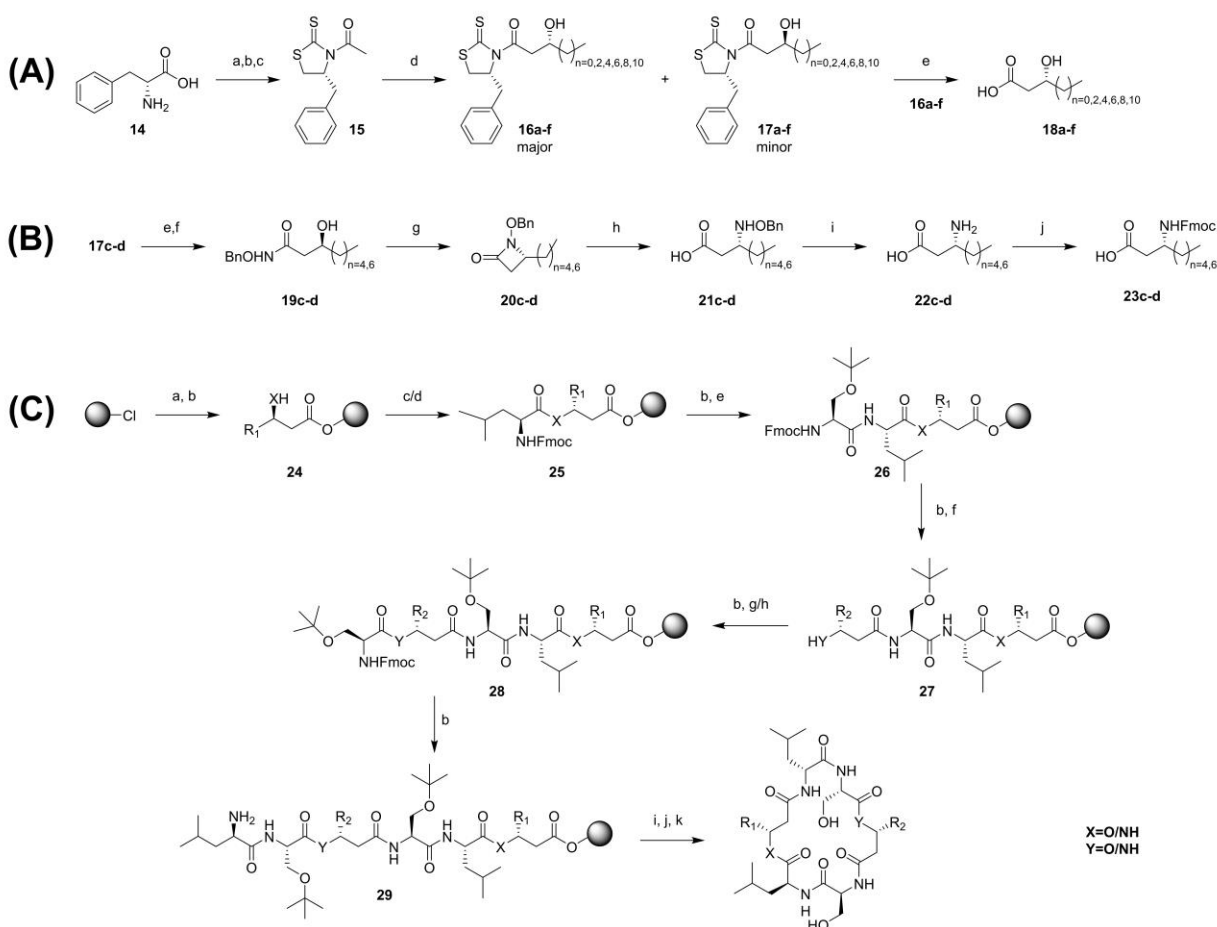

Figure 4.1. (**a**) The structure of Icosalide **1a**, whose analogues were developed in this study; and (**b**) the general structure representing the Icosalide analogues.

Herein, we report the first synthesis of Icosalide **1a** and its analogues, NMR-based structural studies of Icosalide **1a**, and the structure-activity studies of its analogues. The Icosalide **1a** analogues (peptides **1a**, **2**-**13**) planned for this study vary (a) in the length of the beta hydroxy fatty acid chains (peptides **2**-**7**) and (b) substitution of the beta hydroxy acid with beta amino acid (peptides **8**-**13**), which is inspired by the earlier reports on the influence of ester to amide switching on bioactivity (Table **4.1**).[26,35]

Table 4.1. Residue sequences of isolated and synthesized Icosalides (the residue numbering is as given in Figure **4.1a**).

Icosalides	1	2	3 (bHA2) Y=O, R2=	4	5	6 (bHA1) X=O, R1=
			Residues			
1a	I	S	C_7H_{15}	S	L	C_5H_{11}
1a'	I	S	C_7H_{15}*	S	L	C_5H_{11}
1a''	I	S	C_7H_{15}	S	L	C_5H_{11}*
1a'''	I	S	C_7H_{15}*	S	L	C_5H_{11}*
1b	L	S	C_7H_{15}	S	L	C_5H_{11}
1c	L	S	C_5H_{11}	S	L	C_5H_{11}
Ester containing Icosalide analogues						
2	I	S	C_3H_7	S	L	CH_3
3	I	S	C_5H_{11}	S	L	C_3H_7
4	I	S	C_9H_{19}	S	L	C_7H_{15}
5	I	S	$C_{11}H_{23}$	S	L	C_9H_{19}
6	I	S	*i*-Pr	S	L	*i*-Pr
7	I	S	Cp	S	L	Cp
Amide containing Icosalide analogues						

	1	2	3 (bHA2) Y=O, R2=	4	5	6 (bAA1) X=NH, R1=
8	I	S	C_7H_{15}	S	L	H
9	I	S	C_7H_{15}	S	L	C_5H_{11}

	1	2	3 (bAA2) Y=NH, R2=	4	5	6 (bHA1) X=O, R1=
10	I	S	H	S	L	C_5H_{11}
11	I	S	C_7H_{15}	S	L	C_5H_{11}

	1	2	3 (bAA2) Y=NH, R2=	4	5	6 (bAA1) X=NH, R1=
12	I	S	H	S	L	H
13	I	S	C_7H_{15}	S	L	C_5H_{11}

L = L-Leucine; I = D-Leucine; S = L-Serine; bHA = beta hydroxy acid; bAA = beta amino acid; *= Chiral centre of this beta hydroxy acid is *S*

Scheme 4.1. Synthetic schemes, reagents, and conditions (yields). (**A**) **stereoselective synthesis of *R*-beta hydroxy acid (bHA)**[37]; (a) LAH (1.7 eq.), Dry THF 12 h reflux; (b) CS_2 (5 eq.), KOH (5 M); (c) AcCl (1.5 eq.), DMAP (0.1 eq), NEt_3 (1.5 eq.), Dry DCM; (d) aldehyde (1 eq.), $TiCl_4$ (1.8 eq.), DIPEA (1.8 eq.), Dry DCM; (e) LiOH (4 eq., 1M, H_2O), THF. (**B**) **stereoselective synthesis of R-beta amino acid (bAA)**,[38] (f) EDCI (1.5 eq.), $BnONH_2$ (2.0 eq.), THF-H_2O (90%); (g) DEAD (1.0 eq.), PPh_3 (1.1 eq.), Dry THF (80%); (h) LiOH, THF MeOH-H_2O, 0 °C (95%); (i) Pd/C, H_2, MeOH (98%); (j) Fmoc-Cl (1.1 eq.), 10% Na_2CO_3, dioxane:water (1:1) (95%) (**C**) **solid phase peptide synthesis of Icosalide 1a-1a''' and analogues (2-13)**; (a) bHA1 or Fmoc-bAA1 (1.2 eq.), DIPEA (3 eq.), DCM 1.5 h (b) 20% piperidine in DMF 20 min (2*10 min) (c) Fmoc-Leu (2 eq.), DIPEA (3 eq.), HCTU (2 eq.), HOAt (2 eq.), NMP 2 h (d) Fmoc-Leu (2 eq.), DIC (2 eq.) DMAP (0.2 eq.) DCM (e) Fmoc-Ser(*t*Bu) (2 eq.), DIPEA (3 eq.), HCTU (2 eq.), HOAt (2 eq.), NMP (f) bHA2 or Fmoc-bAA2 (2 eq.), DIPEA (3 eq.), HCTU (2 eq.), HOAt (2 eq.), NMP 2 h (g) Fmoc-D-Leu (2 eq.), DIPEA (3 eq.), HCTU (2 eq.), HOAt (2 eq.), NMP 2 h (h) Fmoc-D-Leu (2 eq.), DIC (2 eq.) DMAP (2 eq.) DCM 2 h (i) TFE: AcOH: DCM (1:1:8) (j) HCTU (1.1 eq.) HOAt (1.1 eq), DIPEA (k) 50% TFA in DCM.

4.2. Results and discussion

The Icosalide **1a** and its analogues were synthesized by employing the solid phase peptide synthesis protocol using Fmoc strategy (see scheme **4.1C** and experimental section).[36] The basic L- and D- amino acid building blocks and reagents were obtained from commercial sources. The required *R*-beta hydroxy

acids (**18a-h**) and *R*- beta amino acids (**22c-d**) needed for the analogues were synthesized by stereoselective aldol condensation using chiral auxiliary (see scheme **4.1A, B** and experimental section).[37] To determine the correct stereochemistry of the constituent beta hydroxy acids in the Icosalide **1a**, we synthesized Icosalide **1a** containing beta hydroxy octanoic acid and beta hydroxy decanoic acid both in *R* configuration (3*R*6*R* isomer) as per Jenner *et al*. and the analogue Icosalide **1a'** (3*S*6*R* isomer) containing 3-*R*-hydroxy octanoic acid and 3-*S*-hydroxy decanoic acid as per Dose *et al*.

Table 4.2. Comparison of the ^{1}H and ^{13}C chemical shift data of the synthesized Icosalide **1a** with that of the isolated peptide.

Position	Icosalide 1a (*Burkholderia gladioli HKI0739*)		Icosalide 1a synthesized	
	[13]C (ppm)	[1]H (ppm)	[13]C (ppm)	[1]H (ppm)
1-D-Leu				
C=O	173.0		173.2	
α	51.4	4.37; 1 H (m)	51.7	4.37; 1 H (td), (9.3)
β	40.6	1.58; 1 H (m) 1.34; 1 H (m)	40.5	1.58; 1 H (m) 1.35; 1 H (m)
γ	24.3	1.57; 1 H (m)	24.3	1.84; 1 H (m)
γ-CH3	21.5	0.92; 3 H (d) (5.8)	21.5	0.92; 3 H (d), (5.8)
γ-CH3	22.4	0.88; 3 H (d) (5.9)	22.4	0.88; 3 H (d), (5.9)
NH		7.99; 1 H (d) (9.3)		7.99; 1 H (d), (9.3)
2-Ser				
C=O	170.4		170.5	
α	54.1	4.33; 1 H (dt), (8.8, 2.6)	54.1	4.33; 1 H (dt), (8.8, 2.6)
β	62.2	3.91; 1 H (dd), (10.4, 2.7)) 3.65; 1 H (dd), (10.9, 3.1)	62.5	3.91; 1 H (dd), (10.6, 2.7)) 3.65; 1 H (dd), (10.6, 2.8)
NH		7.44; 1 H (d), (8.7)		7.44; 1 H (d), (8.7)
3-bHA2				
C=O	168.3		168.3	
2	40.4	2.47; 1 H (dd), (3.6) * 2.17; 1 H (dd), (9.4, 3.7)	40.2	2.47; 1 H (dd), (3.6) 2.17; 1 H (dd), (9.4, 3.7)
3	71.5	4.93; 1 H (m)	71.5	4.93; 1 H (m)
4	31.8	1.34; 2 H (m)	31.8	1.34; 2 H (m)
5	25.3	1.11; 2 H (m)	25.3	1.11; 2 H (m)
6	28.9[c]	1.19; 2 H (m)	28.9[c]	1.19; 2 H (m)
7	28.7[c]	1.19; 2 H (m)	28.7[c]	1.19; 2 H (m)
8	30.7	1.19; 2 H (m)	30.7	1.19; 2 H (m)
9	21.8[a]	1.24; 2 H (m)	21.8[a]	1.24; 2 H (m)
10	13.7[b]	0.83; 3 H (m)	13.7[b]	0.83; 3 H (m)

4-Ser				
C=O	172.1		172.1	
α	54.6	4.48; 1 H (td), (8.5, 4.5)	54.9	4.48; 1 H (td), (8.5, 4.5)
β	61.7	3.56; 1 H (dd), (11.0, 4.6) 3.43; 1 H*	61.9	3.56; 1 H (dd), (11.0, 4.6) 3.43; 1 H (dd), (11.0, 8.6)
NH		7.28; 1 H (d), (8.2)		7.28; 1 H (d) (8.2)
5-Leu				
C=O	172.1		172.1	
α	52.3	3.93; 1 H (m)	52.3	3.93; 1 H (dd)
β	38.7	1.57; 2 H (m)	38.33	1.57; 2 H (m)
γ	23.8	1.84; 2 H (m)	23.7	1.57; 1 H (m)
γ-CH3	23.5	0.84; 3 H (m)	23.5	0.84; 3 H (m)
γ-CH3	20.3	0.83; 3 H (m)	20.3	0.83; 3 H (m)
NH		9.03; 1 H (s)		9.03; 1 H (d) (4.3)
6-bHA1				
C=O	168.1		168.1	
2	40.4	2.59; 1 H (dd), (13.9, 3.7) 2.25; 1 H (dd), (14.0, 4.0)	40.1	2.59; 1 H (dd), (13.9, 3.7) 2.25; 1 H (dd), (14.0, 4.0)
3	71.5	4.87; 1 H (m)	71.5	4.87; 1 H (m)
4	31.1	1.47; 2 H (m)	31.1	1.47; 2 H (m)
5	24.5	1.24; 2 H (m)	24.5	1.24; 2 H (m)
6	31.3	1.47; 2 H (m)	31.3	1.47; 2 H (m)
7	22.1	1.24; 2 H (m)	22.1	1.24; 2 H (m)
8	14.0	0.83; 3 H (m)	14.0	0.83; 3 H (m)

[a], [b], [c] interchangeable signals; * signal overlaid with solvent signal.

Further, we have also synthesized the other two diastereomers of Icosalide **1a** in which the beta hydroxy acid configuration at residue positions 3 and 6 are 3*R*6*S* (**1a''**) and 3*S*6*S* (**1a'''**) (Table **4.1**). Our synthesis studies and the comparison of all the four diastereomers with the isolated Icosalide **1a** have shown that Icosalide **1a** with both hydroxy acids in *R* configuration has matched the NMR data (Figure **4.2**) reported by Boros *et al.*, Dose *et al.*, and Jenner *et al*. Thus, the structural ambiguity associated with Icosalide **1a** has been resolved while also achieving its total synthesis.
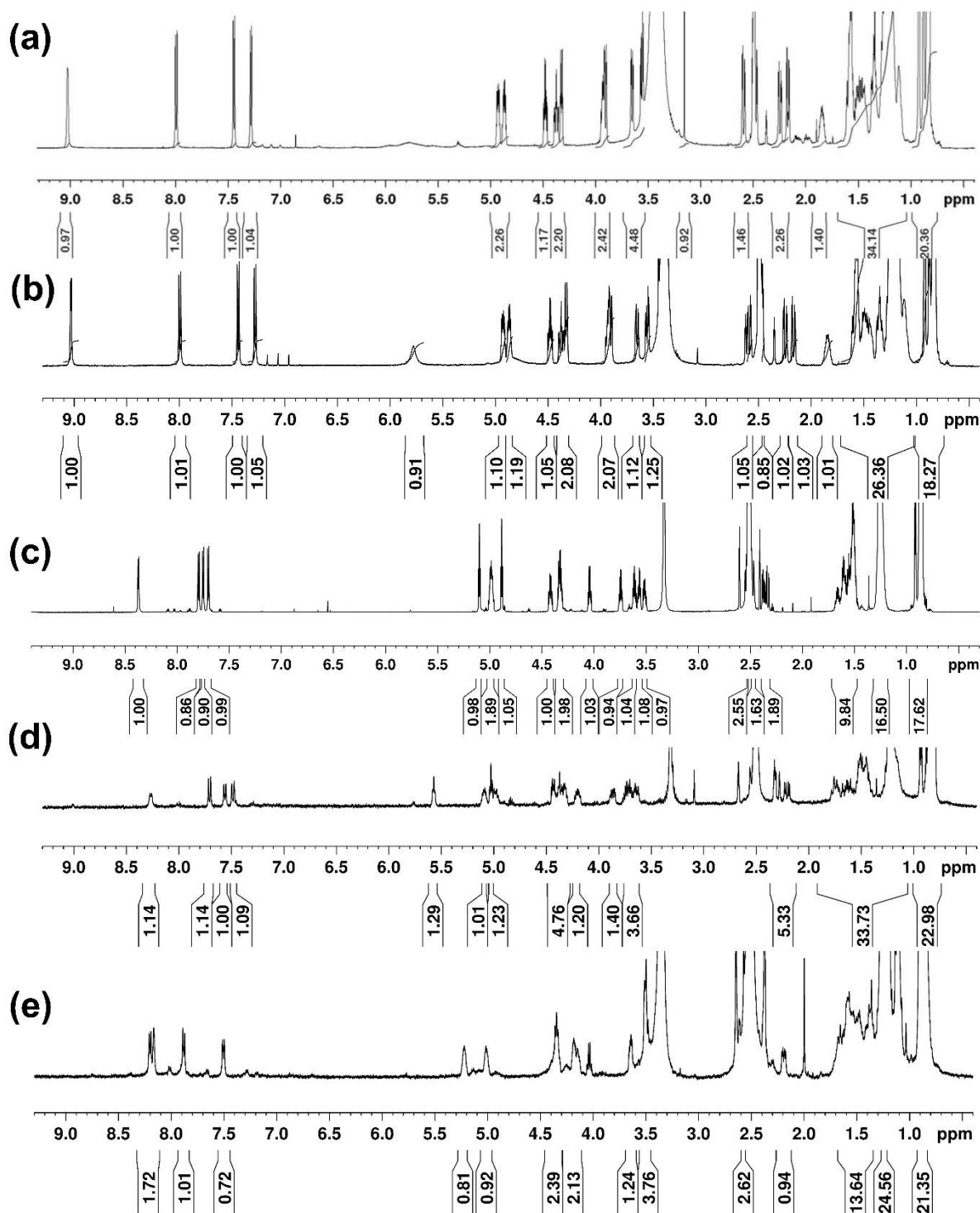
Figure. 4.2. Comparison of the NMR spectra of (**a**) Icosalide **1a** isolated from cell culture,[6] (**b**) the synthesized Icosalide **1a** (3*R*6*R*), (**c**) Icosalide **1a′** (3*S*6*R*), (**d**) Icosalide **1a″** (3*R*6*S*), (**e**) Icosalide **1a‴** (3*S*6*S*). The data shows that the Icosalide **1a** has (3*R*6*R*) configuration.

186

4.2.1. NMR Spectroscopic studies of Icosalide 1a

For NMR spectroscopic studies, 6 mg of Icosalide **1a** was dissolved in 0.5 mL of DMSO-d_6. 1D and 2D spectra were recorded at 298 K on Bruker 500 MHz NMR spectrometer equipped with BBO probe. ^{1}H-1D, DQF-COSY, TOCSY, ROESY, ^{1}H-^{13}C HSQC, and ^{1}H-^{13}C HMBC NMR experiments were acquired. A mixing time of 300 ms was used for ROESY. The 2D NMR experiments were acquired with 320 (for DQF-COSY and TOCSY), 512 (for ROESY), 512 (for HSQC and HMBC) data points in F1 dimension, and 4k (for DQF-COSY, TOCSY, ROESY) and 1k (for HSQC and HMBC) data points in F2 dimension.

4.2.1.1. Temperature coefficients determination

For the determination of temperature coefficients of amide protons, ^{1}H NMR experiments were recorded at variable temperatures ranging from 300 K to 325 K with 5 K increments. The temperature coefficients were calculated according to $(\Delta\delta*1000)/\Delta T$, wherein $\Delta\delta$ and ΔT are the change in chemical shift of the amide NH and the change in sample temperature, respectively. In this study, three of the NHs in Icosalide **1a**, namely, 2-Ser-NH (-0.4), 4-Ser-NH (-1.6 and), and 1-D-Leu-NH (-2.8) exhibited low temperature coefficients, which indicate their involvement in hydrogen bonding and/or shielding from the solvent (Table **4.3**).

Table 4.3. NMR chemical shift temperature coefficients of amide protons in Icosalide **1a**

Name of the NH	Temperature coefficients
1-D-Leu-NH	-2.8
2-Ser-NH	-0.4
4-Ser-NH	-1.6
5-Leu-NH	-6.8

4.2.1.2. Structure calculation of Icosalide 1a

Further, to understand the three-dimensional folding in Icosalide **1a**, NMR-based conformation of Icosalide **1a** was determined by using Schrodinger Maestro macro model 13.1[39] using inter-proton distance restraints derived from ROESY experiments. The inter-proton distances required for NMR-based structure calculation were derived from the cross-peak integrals of the ROESY experiment using SPARKY software. These integrated volumes of ROESY cross-peaks were converted to the corresponding inter-proton distances by the linear approximation method.

These distances were used for the structural calculation by using Schrodinger Maestro macro model 13.1. For the structure calculation, a minimized starting structure was obtained after a step-wise minimization process of an arbitrary structure by giving the inter-proton distance inputs one by one with ±10 relaxation. The method used for energy minimization was SD (steepest descent) and dielectric constant of DMSO i.e., 47. Thus obtained structure was saved and used as the starting template (beginning structure) for 'Molecular Dynamics Simulations' (MD). MD has been run on the structure at 300 K for 10 ns with simulation time step of 1 fs and by shaking all the bonds of the molecule.

Table 4.4. List of distance restraints that were used for structure calculation of Icosalide **1a**.

Residue	Atom	Residue	Atom	d [Å]	d_{Low} [Å]	d_{up} [Å]
1-D-Leu	NH	6-bHA1	Hα1	2.92	2.63	3.22
1-D-Leu	NH	6-bHA1	Hα2	2.92	2.63	3.22
1-D-Leu	NH	5-Leu	Hα	3.21	2.89	3.54
1-D-Leu	NH	1-D-Leu	Hα	3.12	2.81	3.43
6-bHA1	Hβ	5-Leu	Hα	3.99	3.59	4.39
6-bHA1	Hβ	6-bHA1	Hα1	2.42	2.18	2.66
6-bHA1	Hβ	6-bHA1	Hα2	2.51	2.26	2.76
5-Leu	NH	4-Ser	Hα	2.56	2.30	2.82
5-Leu	NH	5-Leu	Hα	3.24	2.92	3.57
4-Ser	NH	3-bHA2	Hα1	2.66	2.39	2.92
4-Ser	NH	3-bHA2	Hα2	2.66	2.39	2.92
4-Ser	NH	3-bHA2	Hβ	3.85	3.46	4.23
4-Ser	Hα	5-Leu	Hα	4.15	3.73	4.56
4-Ser	NH	4-Ser	Hα	3.02	2.72	3.33
3-bHA2	Hβ	2-Ser	Hα	4.18	3.76	4.60
2-Ser	NH	1-D-Leu	NH	3.14	2.82	3.45
2-Ser	NH	1-D-Leu	Hα	3.23	2.91	3.55
2-Ser	NH	4-Ser	NH	4.50	4.05	4.94
2-Ser	NH	2-Ser	Hα	2.89	2.60	3.18

Note: Hα1 and Hα2 of 6-bHA1, Hα1 and Hα2 of 3-bHA2 were considered as pseudo atoms

The depsipeptide exhibited a conformation akin to an anti-parallel beta-sheet structure in cyclic peptides (Figure **4.3**, Table **4.5**). The turn regions are occupied by *R*-3-hydroxy octanoic acid, *R*-3-hydroxy decanoic acid and hence the turns formed here are not the typical beta and gamma turns observed in peptides. The conformation shows the possibility of three amide NHs, namely, 1-D-Leu-NH, 2-Ser-NH, and 4-Ser-NH, internally oriented into the macrocycle and involved in hydrogen bonding with the ester oxygen of *R*-3-hydroxy octanoic acid, 4-Ser-CO, and the ester oxygen of *R*-3-hydroxy decanoic acid, respectively. The ROE between 2-Ser-NH and 4-Ser-NH supports the internal

orientation of the Serine NHs (see Figure **4.4**). The involvement in hydrogen bonding or solvent shielding of these three amide NHs is also supported by the low values (-2.8, -0.4, and -1.6 ppb/K for 1-D-Leu-NH, 2-Ser-NH, and 4-Ser-NH, respectively) of NMR chemical shift temperature coefficients (see table **4.3**) calculated in DMSO-d_6.[40] 3-Leu-NH is externally oriented, and its solvent-accessible nature is supported by a high (-6.8 ppb/K) chemical shift temperature coefficient.
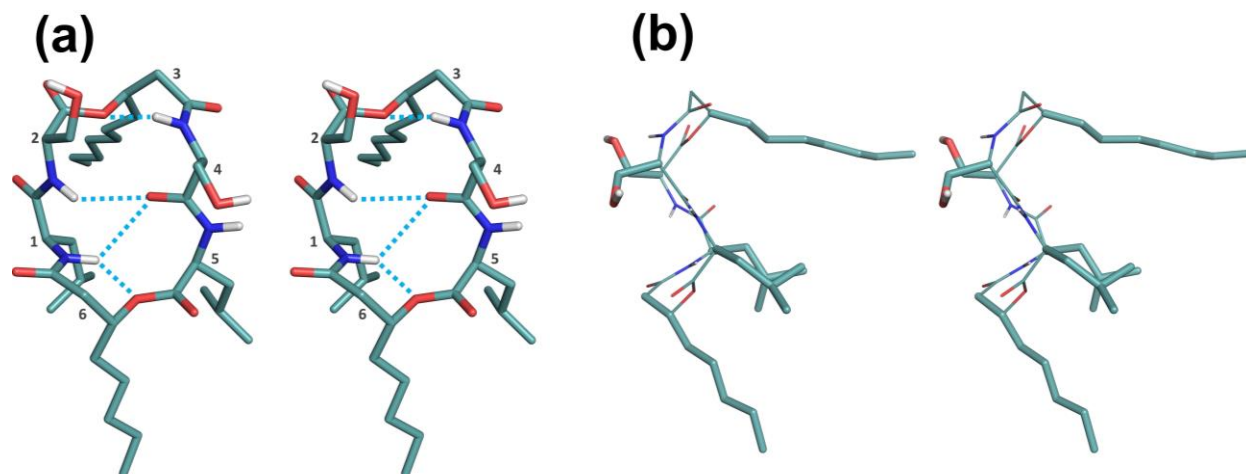
Figure 4.3. (**a**) Stereo view (top view) of the solution state conformation of Icosalide **1a**. For clarity, all the non-polar hydrogens are omitted. The possible hydrogen bonds are indicated as dashed lines in cyan. (**b**) Stereo view (side view) of the NMR-derived conformation of Icosalide **1a**. The molecule's backbone is shown as lines to highlight the orientation of the sidechains (shown as sticks).

A unique feature of the Icosalide **1a** conformation (Figure **4.3b**) is the amphiphilic orientation of all the lipophilic chains (from 1-D-Leu, *R*-3-hydroxy octanoic acid, *R*-3-hydroxy decanoic acid, and 5-Leu) towards one face of the macrocycle ring and the orientation of the polar sidechains of 2-Ser and 4-Ser towards the opposite face. It is very likely that such orientation promotes Van der Waals interactions and led to a stable conformation. Further, the sidechains of 2-Ser and 4-Ser face each other from the opposite sides of the macrocycle ring, which is supported by the ROEs, 4-Ser-NH to 2-Ser-Hβ protons, and 2-Ser-NH to 4-Ser-Hβ protons (Figure **4.4a**). A similar face-to-face position is also observed for the sidechains of 1-D-Leu and 5-Leu and is supported by the ROE between the 5-Leu-Hα proton and 1-D-Leu-Hγ proton (Figure **4.4b**). Further, the inward orientation of 2-Ser-NH, 4-Ser-NH and 1-D-Leu-NH is well supported by their ROESY cross-peaks (Figure **4.4c-d**).
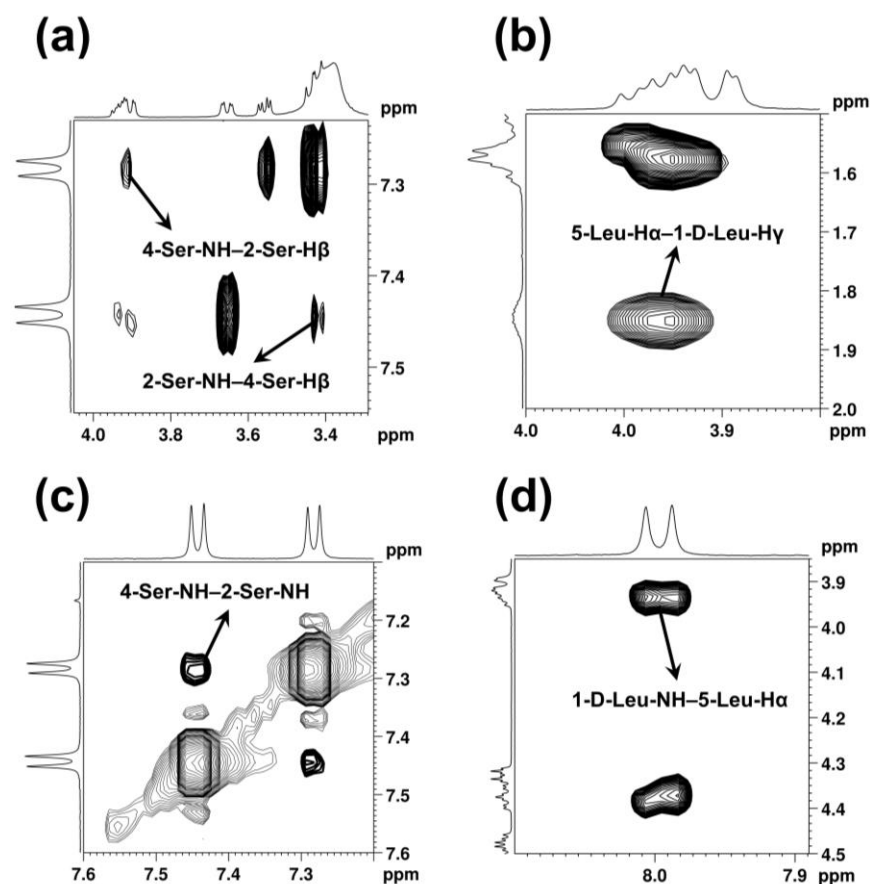
Figure 4.4. Expansions from the ROESY spectrum of Icosalide **1a** showing the cross-peaks between (**a**) 4-Ser-NH to 2-Ser-Hβ protons, and 2-Ser-NH to 4-Ser-Hβ (**b**) 5-Leu-Hα and 1-D-Leu-Hγ, in support of the Serine and Leucine sidechains facing each other (**c**) 2-Ser-NH and 4-Ser-NH, and (**d**) 1-D-Leu-NH and 5-Leu-Hα, in support of the inward orientation of Serine and Leucine NHs in the conformation of Icosalide **1a**.

Table 4.5. The dihedral angles (φ, ψ) measured for all four amino acids from the NMR-derived structure of the Icosalide **1a**.

Amino acid	φ	ψ
1-D-Leu	77.8°	14.0°
2-Ser	-71.0°	-64.8°
4-Ser	-80.0°	145.3°
5-Leu	-77.1°	111.2°

4.2.2. Bioactivity assays

The common appearance of a typical Icosalide complex in different *Burkholderia spp.* indicates that the peptolide has a key role in ecology as evidenced by its lipopeptidic nature that harms the swarming process resulting in its antimicrobial activity.[33] The Icosalide isolated from *Burkholderia* symbionts contains potential therapeutic applications with efficient swarming inhibitory activity and it also showed

antibacterial activity against *Bacillus thuringenesis* and *Paenibacillus larvae* with MIC of 12.5 μg/mL and 3.1 μg/mL respectively. Previous study by Boros *et al.* (2006) reported the activity of Icosalide **1a** against *Streptococcus pneumoniae*, *Enterococcus faecalis* and an MIC of 8-16 μg/mL against *Streptococcus pyogenes*. To understand the effect of the chain length of the lipophilic side chain and the ester to amide modification on the activity of Icosalide **1a**, we have investigated their structure activity relationship studies against *B. thuringenesis* and *P. dendritiformis*.
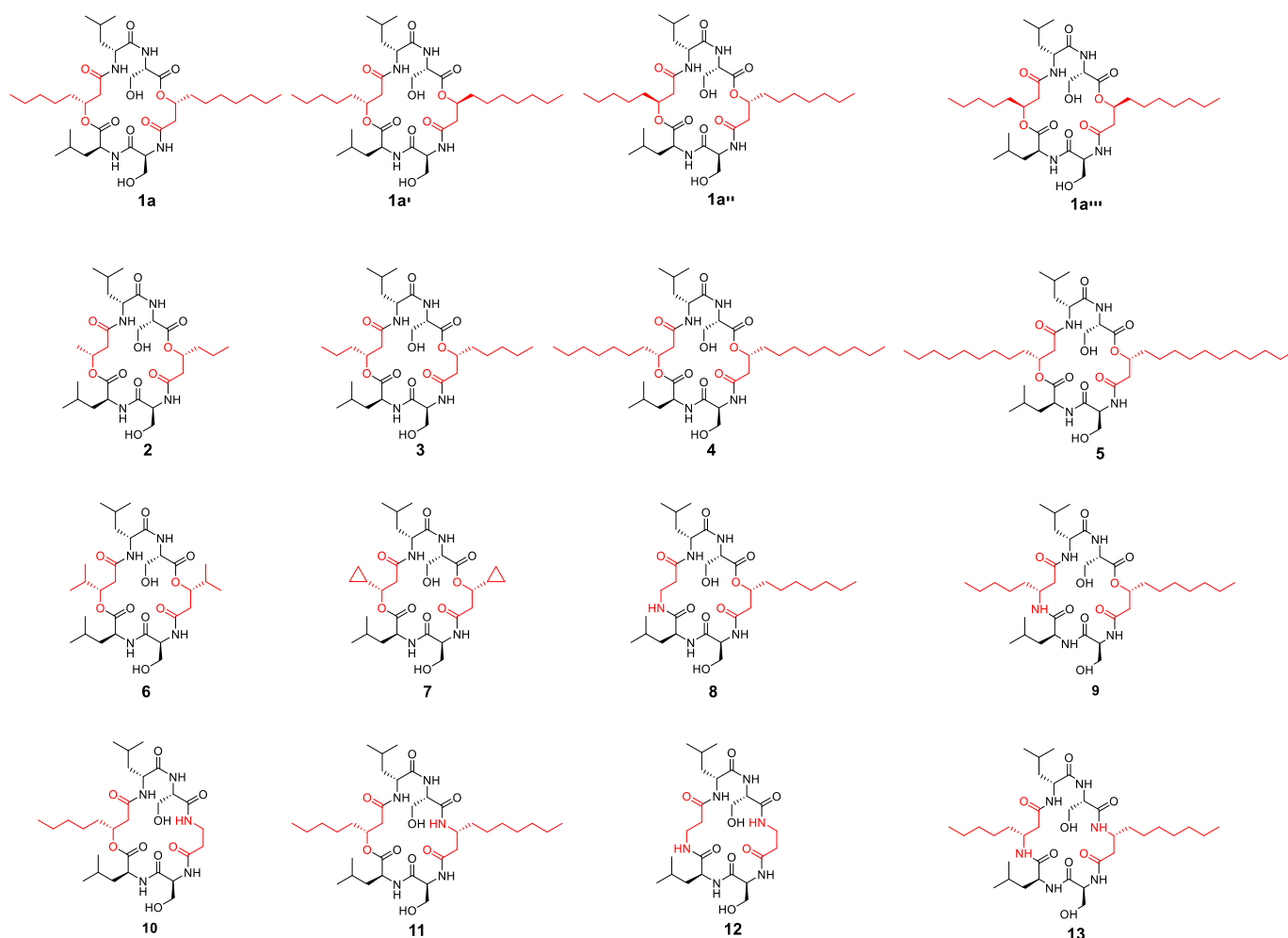
Figure 4.5. Icosalide **1a** and its analogues synthesized in this work.

For the SAR study, 12 analogues (**2-13**) of Icosalide **1a** were designed and synthesized. The analogues **2-7** have the ester linkages but vary in the length of the lipophilic sidechains. Analogues **2** and **3** have shorter lipophilic sidechains than those in Icosalide **1a**, whereas **4** and **5** have longer lipophilic sidechains than those in Icosalide **1a**. Analogue **6** has branched isopropyl sidechains, and **7** has cyclopropyl sidechains. Analogues **8-11** contain one amide bond, and **12-13** have two amide bonds instead of the ester groups. While **8** and **9** have amide linkage between residues 5 and 6, **10** and **11** have amide linkage between residues 2 and 3. Analogues **8** and **10** used β-Alanine for amide bond, **9** and **11**

have 3-*R*-amino octanoic acid and 3-*R*-amino decanoic acid, respectively. **12** has two amide bonds from two β-Alanines and **13** has two amide bonds made from the amide analogues of respective beta hydroxy acids at positions 3 and 6. In principle, **12** is the amide analogue of **1a** without lipophilic chains, and **13** is the amide analogue of **1a** with all the original side chain groups (Figure **4.5**).

4.2.2.1. Time-kill test

In this study, synthesized Icosalide **1a** analogues were primarily evaluated for their antimicrobial activity against *B. thuringenesis* as model strain. All the tested 13 Icosalide analogues showed promising antibacterial activity at 50 µg/mL. The Icosalide **1a** showed the least CFU indicating the highest growth inhibition of the tested bacteria followed by **4** and **5** containing the longest beta hydroxy acid chains, **10** and **12** (Figure **4.6**). Analogues **3**, **8**, **9**, and **13** showed moderate activity. The rest of the analogues showed the least inhibitory activity against *B. thuringenesis*. Further, we evaluated their MIC using dilution and resazurin assay.[41]
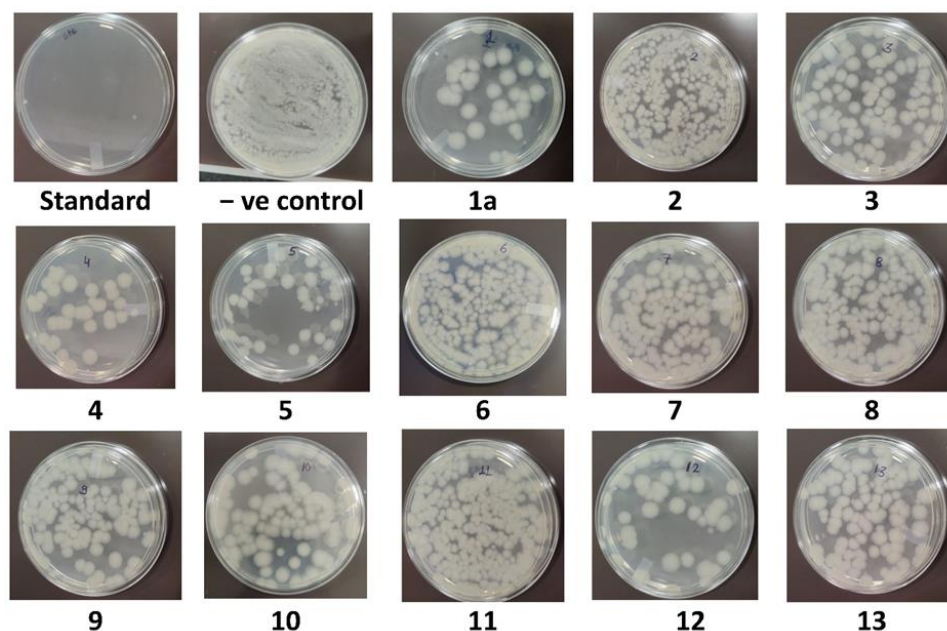
Figure 4.6. Antibacterial activity of Icosalide its analogues against *B. thuringenesis.*

4.2.2.2. Resazurin Assay

To determine the MIC endpoint, the resazurin was used as a growth indicator to differentiate the bacterial growth and inhibition. A 10 µL of resazurin containing 2 mg/mL concentration was added into each well in dark condition and incubated in dark for 2 h results in the color change to violet from pink indicated dead cells (Figure **4.7**).
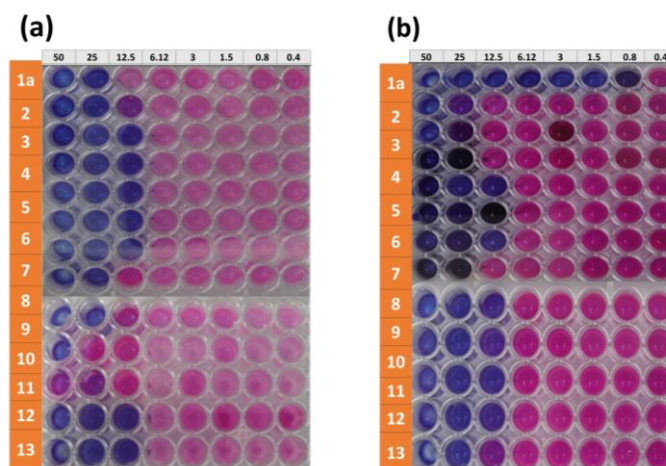
Figure 4.7. (**a**) Antibacterial activity of Icosalides against *B. thuringenesis*; (**b**) antibacterial activity of Icosalides against *P. dendritiformis.*

4.2.2.3. Determination of MIC

MIC assay was carried out for all the Icosalide analogues against *B. thuringenesis* and *P. dendritiformis* (Figure **4.7**, and table **4.6**, **4.7**). Against *B. thuringenesis*, **1a**, **2**, **8** and **9** displayed MIC at 25.0 µg/mL, while **3**, **4**, **5**, **6**, **7**, **12**, and **13** showed MIC at 12.5 µg/mL, which is better than the activity of Icosalide **1a**. The least MIC was noticed for **10** at MIC 50 µg/mL and no or partial activity was observed with **11**. Against *P. dendritiformis,* Icosalide **1a** showed MIC at 0.8 µg/mL, followed by analogues **5, 6, 7, 9, 10, 11**, and **12** that showed MIC at 12.5 µg/mL while the peptides **2, 3, 4, 8** and **13** exhibited the least MIC at 25 µg/mL.

Table 4.6. Effect of icosalides on growth inhibition of *B. thuringiensis*.

Conc. (µg/mL)	Peptide												
	1a	2	3	4	5	6	7	8	9	10	11	12	13
Growth Inhibition (%)													
50	68.31	89.90	84.35	80.71	81.16	84.79	84.65	84.32	87.93	82.92	82.10	79.68	88.71
25	67.04	86.99	83.61	76.03	78.17	84.11	83.97	71.40	85.52	79.73	75.45	78.23	85.27
12.5	39.35	85.35	81.70	64.78	75.14	83.39	77.97	52.31	82.41	78.31	40.34	72.34	83.82
6.25	3.29	3.70	8.21	9.29	2.14	14.58	0	0	0	0	0	15.69	23.99
3.12	0	0	4.73	2.56	0.05	0	0	0	0	0	0	0	18.23
1.5	0	0	0	0	0	0	0	0	0	0	0	0	6.04
0.8	0	0	0	0	0	0	0	0	0	0	0	0	0
0.4	0	0	0	0	0	0	0	0	0	0	0	0	0

Table 4.7. Effect of icosalides on growth inhibition of *P. dendritiformis*.

Conc. (µg/mL)	Peptide												
	1a	2	3	4	5	6	7	8	9	10	11	12	13
	Growth Inhibition (%)												
50	82.72	82.77	79.65	85.76	75.28	81.58	87.53	77.61	84.77	80.64	78.95	79.80	82.26
25	82.70	80.59	76.74	73.63	68.68	81.07	80.19	70.14	82.99	79.69	76.70	76.25	80.65
12.5	82.66	40.41	16.27	46.51	67.77	80.55	73.84	11.91	80.71	77.75	74.26	74.29	71.66
6.25	82.01	0	2.64	0	0	0.515	0	0	0	0	0	0	0
3.12	81.13	0	0	0	0	0	0	0	0	0	0	0	0
1.5	72.27	0	0	0	0	0	0	0	0	0	0	0	0
0.8	70.21	0	0	0	0	0	0	0	0	0	0	0	0
0.4		0	0	0	0	0	0	0	0	0	0	0	0

4.2.2.4. Swarming assay

Swarming inhibition assay was performed to determine the chemotoxicity of the icosalide analogues towards *B. thuringiensis* and *P. dendritiformis* (Figure **4.8**). In this study, Icosalide **1a** has shown complete inhibition against both the bacterial strains at 25 µg/mL. Analogues **2**, **5**, and **8** inhibited about ~8.3% of the swarming activity of *B. thuringiensis* when compared with the icosalide **1a**. On the other hand, for *P. dendritiformis*, analogue **2** demonstrated ~33% of swarming inhibition, followed by **3**, and **4**, which demonstrated ~25% inhibition. The rest of the icosalides displayed about 16–24% inhibition of the swarming area of *P. dendritiformis*.
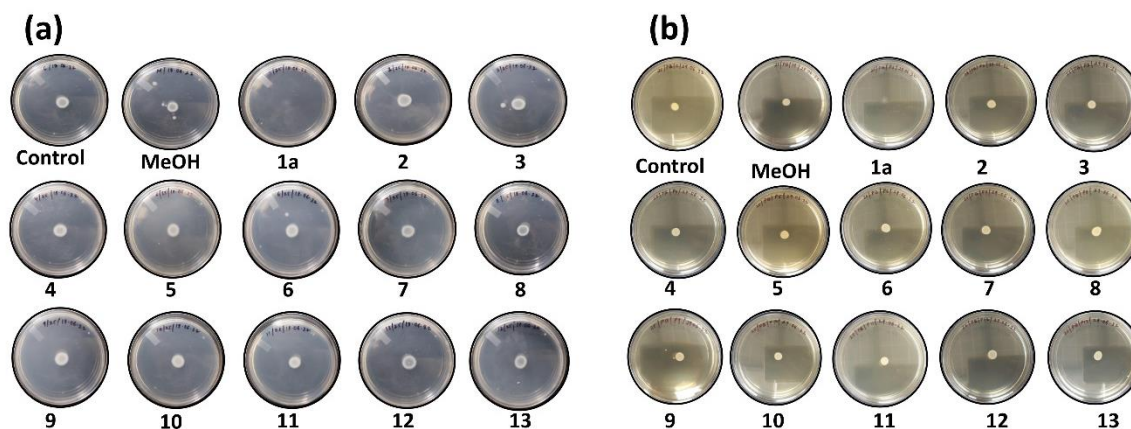
Figure 4.8. **(a)** Swarming inhibitory activities of Icosalides against *B. thuringiensis*, **(b)** swarming inhibitory activities of Icosalides against *P. dendritiformis*.

4.2.2.5. Drop collapse assay

Further, the drop collapse assay was performed to determine the surfactant activity of the various Icosalide analogues on *B. thuringiensis* on parafilm 'M'. The results showed that most of the Icosalide analogues displayed drop collapsing except **2**, **4**, **5**, and **11** (Figure **4.9**).
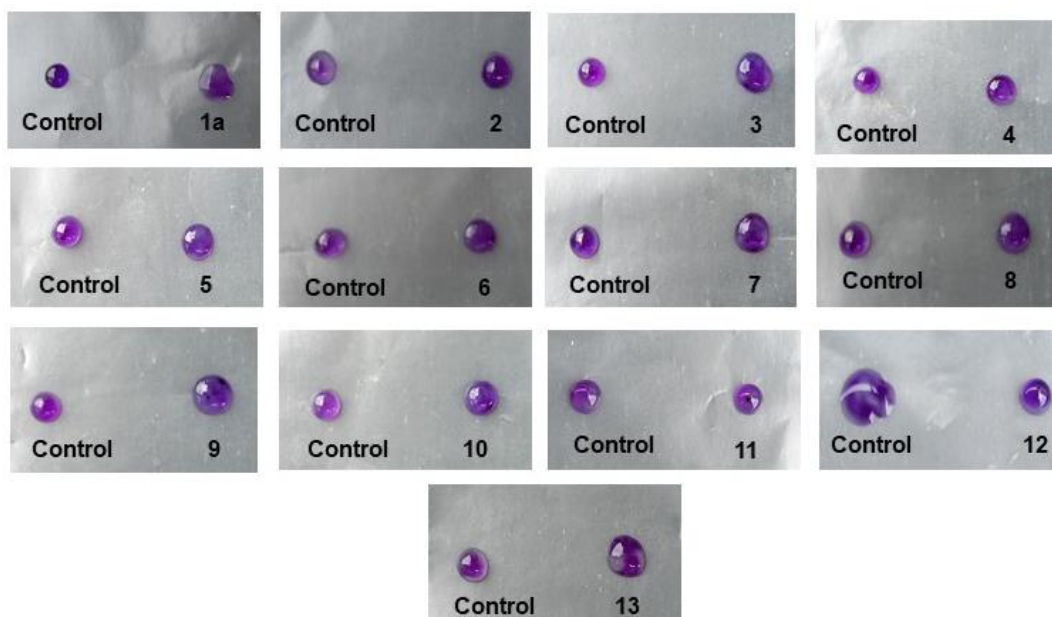
Figure 4.9. Drop-collapsing assay of Icosalides against *Bacillus thuringiensis*.

In further expansion of the biological activity screening of the Icosalides, we have also screened the Icosalides for their anti-mycobacterium and anti-cancer activities.

4.2.2.6. Antitubercular and anticancer activity

The Icosalide **1a** and its analogues were screened for *in vitro* anti-tubercular activity against *M. tuberculosis* H37Ra RFP strain by an established paraffin red fluorescence microplate assay.[42] The MIC of each screened Icosalide (table **4.8**) against *Mycobacterium tuberculosis* is in between 2 to 10 µg/mL except **2** and **9**. Here, Rifampicin and Isoniazid were used as standard molecules for anti-TB studies with MIC 0.005±0.001 & 0.047±0.021 µg/mL. Furthermore, anticancer activity for Icosalides was performed on Hela cervical cancerous cell lines and Thp1 monocytic cell lines by using the anticancer drug Doxorubicin as the standard (table **7**).[43] Among all, Icosalide **1a** has shown IC_{50} of (4.612±0.389 µg/mL) on HeLa and, (4.125±1.271901 µg/mL) against ThP1 cell lines.

Table 4.8. *In vitro* anti-cancer activity of Icosalide **1a** and its analogues against HeLa and ThP1 cell lines and antitubercular activity against *M. tuberculosis* H37RaRFP.

Peptide	Anti-cancer activity		AntiTB activity (Active Stage *M. tb)*
	HeLa IC$_{50}$ (μg/mL)	ThP1 IC50 (μg/mL)	MIC$_{90}$ (μg/mL)
1a	4.612±**0.389**	4.125±1.271901	5.018±**0.254**
2	20.5438±**2.705**	8.816±**4.106**	12.615±**2.149**
3	14.6627±**2.003**	7.068±**2.443**	3.2448±**0.193**
4	8.360±**0.627**	5.9063±**0.414**	2.7422±**0.163**
5	ND	ND	ND
6	14.867±**2.366**	13.31±**3.288**	6.179±**0.277**
7	ND	ND	ND
8	20.093±**6.72**	3.881±**1.856**	8.835±**1.555**
9	23.407±**2.524**	24.028±**3.254**	25.95±**0.256**
10	24.141±**4.916**	34.257±**8.655**	5.1092±**0.538**
11	16.481±**2.592**	6.374±**0.906**	3.2882±**0.043**
12	8.854±**0.507**	13.353±**2.933**	4.7792±**0.0793**
13	21.0015±**7.220**	15.59±**5.435**	5.4082±**0.188**
Standard	Doxorubicin 50 ng/mL	Doxorubicin 50 ng/mL	Rifampicin 0.005±**0.001** Isoniazid 0.047±**0.021**

Through the current SAR study, we could showcase the expanded biological activities of the Icosalide **1a** and its analogues. Amongst all, compound **5** having the longest lipophilic sidechains, had shown positive activity in the majority of the tests (Time-kill test, MIC against *B. thuringenesis* and *P. dendritiformis*, Swarming inhibition assay and antitubercular activity). Analogues of **1a** with beta-branched sidechains, **6** and **7**, also displayed a competitive MIC against both the tested bacterial strains. Compound **12**, the all amide analogue of **1a,** containing two β-Alanines and no lipophilic sidechains showed better Time-kill and MIC activity than compound **13**, which is an all amide compound with lipophilic sidechains as in **1a**. Interestingly, most of the modifications studied here have not affected the newly found antitubercular activity of Icosalide **1a**. However, pronounced trends in the bioactivities to the changes in lipophilic sidechains or amide substitutions in Icosalide **1a** were elusive.

4.3. Conclusions

In summary, we have developed a hybrid synthetic route comprising solid-phase and solution-phase synthesis methods to access Icosalide **1a**, a natural antibacterial product, and its analogues. We have also unequivocally confirmed the stereochemistry of the two hydroxy acids in Icosalide **1a** as *R*-configuration. We have synthesized a set of analogues of Icosalide **1a**, which varied in the length of the constituent lipophilic beta-hydroxy acids and/or have the ester bonds replaced by amide bonds. We found that the ester analogues containing longer beta-hydroxy acid chains (**4** and **5**) have shown antibacterial activity similar to Icosalide **1a**, however, the ones with shorter beta hydroxy acid chain lengths have shown substantially lower activity. On the other hand, Icosalide **1a** and most of its analogues, except for **2** and **9** have exhibited antitubercular activity within 10 μg/mL. Icosalide **1a** is found to be anticancerous against HeLa and ThP1 cell lines. The work described here lays the foundation for generating analogues of Icosalide **1a** with a view to optimize their activity for tuberculosis and Gram-positive infections.

4.4. Experimental procedures and analytical data

4.4.1. **Synthetic procedure for (*R*)-1-(4-benzyl-2-thioxothiazolidin-3-yl) ethan-1-one (15)**: Synthesis of *R*-chiral auxiliary was started by dissolving D-phenyl alanine (3 gm, 18.8 mmol, 1 eq.) in dry THF and thus formed suspension was cooled to 0 °C. To this cooled suspension, LiAlH$_4$ (1 gm, 26.91 mmol, 1.48 eq.) was added in portions over a duration of 10 minutes, and the reaction contents were heated to reflux overnight. Then the reaction mixture was cooled to 0 °C and quenched with slow addition of water for 10 minutes, followed by slow addition of 15% (aq) KOH for 30 min. The quenched mixture was diluted and extracted with ethyl acetate. The ethyl acetate extract was concentrated over rotavapor to afford D-phenylalaninol (2.7 gm, 99%) as a white viscous oil, which was further used without purification.

D-Phenylalaninol (2.7 gm, 19.2 mmol, 1 eq.) was dissolved in aqueous KOH (3 M, 100 mL). CS$_2$, (5.8 mL, 96 mmol, 5 eq.) was added, and the solution was heated to reflux overnight. The solution was extracted with CH$_2$Cl$_2$ (3*200 mL), dried over Na$_2$SO$_4$, filtered, concentrated, and purified by column chromatography to afford (*R*)-4-benzylthiazolidine-2-thione (3.19 gm, 86%) ^{1}H NMR (500 MHz, CDCl$_3$) δ 7.72 (1H, s), 7.38 (2H, t, *J* =7.4 Hz), 7.32 (1H, t, *J* =7.4 Hz), 7.26 – 7.20 (2H, m), 4.49 (1H, p, *J* =7.2 Hz), 3.61 (1H, dd, *J* =11.3, 7.6 Hz), 3.35 (1H, dd, *J* =11.1, 6.8 Hz), 3.03 (2H, qd, *J* =13.6, 7.2 Hz); ^{13}C NMR (126 MHz, CDCl$_3$) δ 201.11, 135.98, 129.29, 129.16, 127.62, 65.20, 40.20, 38.35. HRMS (ESI-TOF) m/z [M+H]$^+$ calculated for C$_{10}$H$_{11}$NS$_2$ 210.0336, found 210.0366.

The above compound (2.3 g, 11 mmol, 1 eq.), DMAP (134 mg, 1.1 mmol, 0.1 eq.), and NEt$_3$ (2.3 mL, 16.5 mmol, 1.5 eq.) were dissolved in dry CH$_2$Cl$_2$ (100 mL) and cooled to 0 °C. To this reaction contents, AcCl (1.2 mL, 16.5 mmol, 1.5 eq.) was added dropwise, and the reaction was allowed to reach room temperature and stirred overnight. Then, the reaction was quenched with saturated NH$_4$Cl (100 mL), and the organic contents were extracted with Et$_2$O (1*50 mL) and EtOAc (2*50 mL). The combined organic phase was washed with water (50 mL) and brine (50 mL), dried over (Na$_2$SO$_4$), filtered, and concentrated to give the crude compound as a yellow solid. Recrystallization of this yellow solid from EtOH afforded the acetylated chiral auxiliary **15** bright yellow crystals (2.8 gm, 80%); $[\alpha]_D^{26}$ = -142.5 (c 0.5, CH$_2$Cl$_2$) ^{1}H NMR (500 MHz, CDCl$_3$) δ 7.41 – 7.34 (2H, m), 7.34 – 7.27 (3H, m), 5.40 (1H, ddd, J = 10.8, 7.2, 3.8 Hz), 3.41 (1H, dd, J = 11.5, 7.2 Hz), 3.25 (1H, dd, J = 13.2, 3.8 Hz), 3.07 (1H, dd, J = 13.2, 10.5 Hz), 2.91 (1H, d, J = 11.4 Hz), 2.82 (3H, s); ^{13}C NMR (126 MHz, CDCl$_3$) δ 201.69, 170.84, 136.63, 129.57, 129.02, 127.34, 68.33, 36.80, 31.94, 27.18. HRMS (ESI-TOF) m/z [M+H]$^+$ calculated for C$_{12}$H$_{13}$NOS$_2$ 252.0439, found 252.0472.

The characterization data was in accordance with the previous report.[1]

4.4.2. **General procedure for aldol reaction**: 0.2 M solution of acetylated auxiliary 15 (1.7 eq.) in DCM was prepared. To this solution, TiCl$_4$ (1.8 eq.) and *i*-Pr$_2$NEt (1.8 eq.) were added dropwise, and the resulting suspension was cooled to -78 °C and stirred for 2 h. To this solution, a solution of the appropriate aldehyde (according to Scheme **1a**, 0.2 M in CH$_2$Cl$_2$, 1 eq.) was added dropwise. The mixture was stirred at -78 °C for 4 to 24 h depending on the reaction. After completion of the reaction, the reaction was quenched with saturated NH$_4$Cl (50 mL) and water (50 mL). The organic phase in CH$_2$Cl$_2$ was separated and washed with water (100 mL) and brine (100 mL), dried over Na$_2$SO$_4$, filtered, and concentrated to give a yellow crude material, which was further purified by column chromatography to obtain the compounds **16a-h** and **17a-h**.

(*R*)-1-((*R*)-4-benzyl-2-thioxothiazolidin-3-yl)-3-hydroxybutan-1-one **(16a)**: Compound **15** was reacted with acetaldehyde according to general procedure **4.6.2** and subsequent flash chromatography furnished title compound **16a** (1.2 g, 53%) as a yellow oil (major diastereomer); Rf 0.16 (pet ether : EtOAc, 4:1) 1H NMR (500 MHz, CDCl$_3$) δ 7.41 – 7.33 (2H, m), 7.36 – 7.28 (3H, m), 5.43 (1H, ddd, J = 10.8, 7.2, 4.1 Hz), 4.36 (1H, ddt, J = 10.2, 6.6, 3.2 Hz), 3.69 (1H, dd, J = 17.7, 2.5 Hz), 3.44 (1H, dd, J = 11.5, 7.2 Hz), 3.25 (1H, dd, J = 13.2, 4.0 Hz), 3.22 – 2.99 (2H, m), 2.93 (1H, d, J = 11.5 Hz), 1.31 (3H, d, J = 6.2 Hz); ^{13}C NMR (126 MHz, CDCl$_3$) δ 201.56, 173.29, 136.53, 129.59, 129.10, 127.46,

68.42, 64.25, 47.44, 37.01, 32.20, 22.45. HRMS (ESI-TOF) m/z [M+H]$^+$ calculated for $C_{14}H_{17}NO_2S_2$ 296.0701, found 296.0703.

(*R*)-1-((*R*)-4-benzyl-2-thioxothiazolidin-3-yl)-3-hydroxyhexan-1-one (16b): Compound **15** was reacted with butanal according to general procedure **4.6.2** and subsequent flash chromatography furnished title compound **16b** (1.1 g, 55%) as a yellow oil (major diastereomer); Rf 0.16 (Pet ether : EtOAc, 4:1) ^{1}H NMR (500 MHz, CDCl$_3$) δ 7.50 – 7.20 (5H, m), 5.44 (1H, ddd, *J* = 10.7, 7.1, 4.0 Hz), 4.10 (1H, tdt, *J* = 7.4, 4.0, 2.4 Hz), 3.59 – 2.89 (7H, m), 1.66 – 1.36 (4H, m), 0.97 (3H, t, *J* = 6.9 Hz); ^{13}C NMR (126 MHz, CDCl$_3$) δ 201.62, 174.03, 136.50, 129.58, 129.09, 127.43, 68.37, 68.33, 45.63, 38.88, 36.93, 32.16, 18.81, 14.14. HRMS (ESI-TOF) m/z [M+H]$^+$ calculated for $C_{16}H_{21}NO_2S_2$ 324.1014, found 324.1104.

(*R*)-1-((*R*)-4-benzyl-2-thioxothiazolidin-3-yl)-3-hydroxyoctan-1-one (16c): Compound **15** was reacted with hexanal according to general procedure **4.6.2** and subsequent flash chromatography furnished title compound **16c** (2 g, 45%) as a yellow oil (major diastereomer). ^{1}H NMR (400 MHz, CDCl$_3$) δ 7.56 – 7.05 (5H, m), 5.41 (1H, ddd, *J* = 10.9, 7.2, 4.0 Hz), 4.05 (1H, tt, *J* = 6.9, 3.4 Hz), 3.57 – 2.70 (6H, m), 1.65 – 1.16 (9H, m), 0.89 (3H, t, *J* = 6.7 Hz); ^{13}C NMR (101 MHz, CDCl$_3$) δ 201.62, 174.03, 136.52, 129.58, 129.09, 127.43, 68.63, 68.38, 45.64, 36.95, 36.76, 32.18, 31.89, 25.30, 22.74, 14.18. HRMS (ESI-TOF) m/z [M+H]$^+$ calculated for $C_{18}H_{25}NO_2S_2$ 352.1327, found 352.1360.

(*R*)-1-((*R*)-4-benzyl-2-thioxothiazolidin-3-yl)-3-hydroxydecan-1-one (16d): Compound **15** was reacted with octanal according to general procedure **4.6.2** and subsequent flash chromatography furnished title compound **16d** (2.2 g, 51%) as a yellow oil (major diastereomer). ^{1}H NMR (700 MHz, CDCl$_3$) δ 7.40 – 7.29 (5H, m), 5.44 (1H, ddd, *J* = 10.8, 7.2, 4.1 Hz), 4.10 – 4.04 (1H, m), 3.48 (1H, dd, *J* = 17.5, 9.4 Hz), 3.43 (1H, ddd, *J* = 11.5, 7.3, 1.0 Hz), 3.36 (1H, dd, *J* = 17.5, 2.5 Hz), 3.25 (1H, dd, *J* = 13.3, 4.0 Hz), 3.12 (1H, d, *J* = 4.1 Hz), 3.07 (1H, dd, *J* = 13.3, 10.4 Hz), 2.93 (1H, d, *J* = 11.5 Hz), 1.55 – 1.43 (1H, m), 1.41 – 1.26 (11H, m), 0.90 (3H, t, *J* = 7.0 Hz). HRMS (ESI-TOF) m/z [M+H]$^+$ calculated for $C_{20}H_{29}NO_2S_2$ 380.1640, found 380.1673.

(*R*)-1-((*R*)-4-benzyl-2-thioxothiazolidin-3-yl)-3-hydroxydodecan-1-one (16e): Compound **15** was reacted with decanal according to general procedure **4.6.2** and subsequent flash chromatography furnished title compound **16e** (1g, 51%) as a yellow oil (major diastereomer). ^{1}H NMR (400 MHz, CDCl$_3$) δ 7.41 – 7.33 (2H, m), 7.33 – 7.25 (3H, m), 5.41 (1H, ddd, *J* = 10.8, 7.1, 4.0 Hz), 4.14 (1H, ddd, *J* = 14.3, 9.2, 5.9 Hz), 3.66 (1H, dd, *J* = 17.9, 2.4 Hz), 3.42 (1H, ddd, *J* = 11.5, 7.2, 1.0 Hz), 3.24 (1H, dd, *J* = 13.2, 4.0 Hz), 3.19 – 3.00 (2H, m), 2.91 (1H, d, *J* = 11.6 Hz), 2.72 (1H, d, *J* = 3.8 Hz), 1.66 –

1.47 (1H, m), 1.50 – 1.41 (1H, m), 1.29 (13H, q, *J* = 4.9 Hz), 0.88 (3H, t); ^{13}C NMR (126 MHz, CDCl$_3$) δ 201.55, 173.51, 136.55, 129.58, 129.09, 127.44, 68.47, 68.00, 46.06, 36.97, 36.51, 32.18, 32.03, 29.70, 29.46, 25.69, 22.82, 14.26. HRMS (ESI-TOF) m/z [M+H]$^+$ calculated for C$_{22}$H$_{33}$NO$_2$S$_2$ 408.1953, found 408.1951.

(*R*)-1-((*R*)-4-benzyl-2-thioxothiazolidin-3-yl)-3-hydroxytetradecan-1-one (16f): Compound **15** was reacted with dodecanal according to general procedure **4.6.2** and subsequent flash chromatography furnished title compound **16f** (0.5 g, 51%) as a yellow oil (major diastereomer); ^{1}H NMR (500 MHz, CDCl$_3$) δ 7.41 – 7.34 (2H, m), 7.34 – 7.28 (3H, m), 5.43 (1H, ddd, *J* = 10.7, 7.0, 3.9 Hz), 4.17 (1H, dddd, *J* = 9.9, 7.5, 4.7, 2.4 Hz), 3.68 (1H, dd, *J* = 17.9, 2.4 Hz), 3.44 (1H, dd, *J* = 11.6, 7.2 Hz), 3.26 (1H, dd, *J* = 13.2, 4.0 Hz), 3.15 (1H, dd, *J* = 17.7, 9.5 Hz), 3.08 (1H, dd, *J* = 13.2, 10.5 Hz), 2.93 (1H, d, *J* = 11.6 Hz), 2.37 (1H, t, *J* = 7.5 Hz), 1.74 – 1.19 (27H, m), 0.91 (4H, t, *J* = 6.8 Hz); ^{13}C NMR (126 MHz, CDCl$_3$) δ 201.57, 173.53, 136.56, 129.59, 129.10, 127.45, 68.49, 68.05, 46.05, 36.99, 36.51, 34.05, 32.20, 32.06, 29.74, 29.58, 29.49, 29.39, 29.21, 25.70, 24.85, 22.83, 14.26. HRMS (ESI-TOF) m/z [M+H]$^+$ calculated for C$_{24}$H$_{37}$NO$_2$S$_2$ 436.2266, found 436.2291.

(*R*)-1-((*R*)-4-benzyl-2-thioxothiazolidin-3-yl)-3-hydroxy-4-methylpentan-1-one (16g): Compound **15** was reacted with isobutyraldehyde according to general procedure **4.6.2** and subsequent flash chromatography furnished title compound **16g** (1 g, 51%) as a yellow oil; ^{1}H NMR (700 MHz, CDCl$_3$) δ 7.41 – 7.35 (2H, m), 7.32 (3H, d, *J* = 7.4 Hz), 5.43 (1H, ddd, *J* = 10.8, 7.2, 4.0 Hz), 3.97 (1H, ddd, *J* = 10.2, 5.6, 2.0 Hz), 3.68 – 3.62 (1H, m), 3.43 (1H, dd, *J* = 11.5, 7.2 Hz), 3.26 (1H, dd, *J* = 13.2, 3.9 Hz), 3.19 (1H, dd, *J* = 17.6, 10.2 Hz), 3.08 (1H, dd, *J* = 13.2, 10.4 Hz), 2.93 (1H, d, *J* = 11.5 Hz), 1.85 – 1.76 (1H, m, *J* = 6.7 Hz), 1.00 (6H, dd, *J* = 15.0, 6.8 Hz); ^{13}C NMR (176 MHz, CDCl$_3$) δ 201.62, 173.88, 136.57, 129.59, 129.09, 127.43, 72.60, 68.54, 43.33, 36.97, 33.30, 32.20, 18.64, 18.06. HRMS (ESI-TOF) m/z [M+H]$^+$ calculated for C$_{16}$H$_{21}$NO$_2$S$_2$ 324.1014, found 324.1047.

(*R*)-1-((*R*)-4-benzyl-2-thioxothiazolidin-3-yl)-3-cyclopropyl-3-hydroxypropan-1-one (16h): Compound **15** was reacted with cyclopropane aldehyde according to general procedure **4.6.2** and subsequent flash chromatography furnished title compound **16h** (0.5 g, 53%) as pale yellow liquid; ^{1}H NMR (700 MHz, CDCl$_3$) δ 7.34 (2H, t, *J* = 7.6 Hz), 7.29 (3H, d, *J* = 7.4 Hz), 5.39 (1H, ddd, *J* = 10.9, 7.1, 3.9 Hz), 3.71 (1H, dd, *J* = 17.4, 2.1 Hz), 3.47 (1H, td, *J* = 9.0, 2.3 Hz), 3.44 – 3.39 (1H, m), 3.41 – 3.35 (1H, m), 3.23 (1H, dd, *J* = 13.3, 4.0 Hz), 3.05 (1H, dd, *J* = 13.3, 10.4 Hz), 2.90 (1H, d, *J* = 11.5 Hz), 1.02 (1H, ddt, *J* = 13.1, 8.2, 4.2 Hz), 0.57 (2H, dqd, *J* = 27.0, 8.8, 4.5 Hz), 0.42 (1H, dq, *J* = 9.7, 5.0 Hz), 0.27 (1H, dq, *J* = 10.0, 5.0 Hz); ^{13}C NMR (500 MHz, CDCl$_3$): 3.35 (1H, td, *J* = 8.6, 3.5 Hz),

2.70 (2H, qd, J = 16.3, 6.3 Hz), 1.07 – 0.87 (2H, m), 0.58 (3H, dtt, J = 17.7, 9.0, 4.2 Hz), 0.42 (1H, dq, J = 8.7, 4.6 Hz), 0.27 (1H, dq, J = 10.0, 4.7 Hz); ^{13}C NMR (176 MHz, CDCl$_3$) δ 201.50, 173.07, 136.56, 129.57, 129.07, 127.41, 72.71, 68.56, 45.88, 45.58, 36.92, 32.22, 16.93. HRMS (ESI-TOF) m/z [M+H]$^+$ calculated for C$_{16}$H$_{19}$NO$_2$S$_2$ 322.0857, found 322.0891.

(*S*)-1-((*R*)-4-benzyl-2-thioxothiazolidin-3-yl)-3-hydroxybutan-1-one (**17a**): Compound **15** was reacted with acetaldehyde according to general procedure **4.6.2** and subsequent flash chromatography furnished title compound **17a** as a yellow oil (minor diastereomer); ^{1}H NMR (500 MHz, CDCl$_3$) δ 7.41 – 7.18 (m, 5H), 5.43 (ddd, J = 10.8, 7.2, 4.1 Hz, 1H), 4.36 (dtt, J = 8.9, 6.3, 3.2 Hz, 1H), 3.69 (dd, J = 17.8, 2.5 Hz, 1H), 3.44 (dd, J = 11.5, 7.2 Hz, 1H), 3.34 – 3.03 (m, 3H), 2.93 (d, J = 11.9 Hz, 1H), 1.31 (d, J = 6.4 Hz, 3H). ^{13}C NMR (126 MHz, CDCl$_3$) δ 201.43, 173.15, 136.40, 129.46, 129.22, 128.97, 128.53, 128.48, 127.32, 126.82, 68.29, 64.10, 47.32, 36.87, 32.06, 22.32., 14.2. HRMS (ESI-TOF) m/z [M+H]$^+$ calculated for C$_{14}$H$_{17}$NO$_2$S$_2$ 296.0701, found 296.0703.

(*S*)-1-((*R*)-4-benzyl-2-thioxothiazolidin-3-yl)-3-hydroxyhexan-1-one (**17b**): Compound **15** was reacted with butanal according to the general procedure **4.6.2** and subsequent flash chromatography furnished title compound **17b** as a yellow oil (minor diastereomer); ^{1}H NMR (500 MHz, CDCl$_3$) δ 7.40 – 7.35 (m, 2H), 7.31 (dd, J = 7.7, 5.6 Hz, 4H), 5.44 (ddd, J = 10.8, 7.1, 4.1 Hz, 1H), 4.08 (s, 1H), 3.48 (dd, J = 17.5, 9.4 Hz, 1H), 3.45 – 3.40 (m, 1H), 3.36 (dd, J = 17.5, 2.5 Hz, 1H), 3.25 (dd, J = 13.3, 4.1 Hz, 1H), 3.12 (s, 1H), 3.10 – 3.00 (m, 1H), 2.93 (d, J = 11.7 Hz, 1H), 1.55 – 1.47 (m, 1H), 1.49 (s, 1H), 1.33 (s, 9H), 1.38 – 1.26 (m, 3H), 0.94 – 0.86 (m, 5H). ^{13}C NMR (126 MHz, CDCl$_3$) δ 201.50, 173.91, 136.39, 129.46, 128.97, 127.31, 68.25, 68.21, 45.51, 38.76, 36.82, 32.05, 18.70, 14.03. HRMS (ESI-TOF) m/z [M+H]$^+$ calculated for C$_{16}$H$_{21}$NO$_2$S$_2$ 324.1014, found 324.1104.

(*S*)-1-((*R*)-4-benzyl-2-thioxothiazolidin-3-yl)-3-hydroxyoctan-1-one (**17c**): Compound **15** was reacted with hexanal according to the general procedure **4.6.2** and subsequent flash chromatography furnished title compound **17c** as a yellow oil (minor diastereomer) ^{1}H NMR (400 MHz, CDCl$_3$) δ 7.44 – 7.26 (m, 6H), 5.43 (ddd, J = 10.6, 7.0, 3.8 Hz, 1H), 4.17 (t, J = 10.4 Hz, 1H), 3.72 – 3.60 (m, 1H), 3.40 (ddd, J = 27.2, 11.3, 6.9 Hz, 1H), 3.29 – 3.17 (m, 1H), 3.17 – 3.00 (m, 2H), 2.92 (d, J = 11.4 Hz, 1H), 1.61 (dt, J = 18.1, 6.6 Hz, 1H), 1.53 (dd, J = 11.2, 6.3 Hz, 1H), 1.52 – 1.37 (m, 1H), 1.41 – 1.30 (m, 5H), 0.92 (t, J = 6.6 Hz, 3H). ^{13}C NMR (101 MHz, CDCl$_3$) δ 201.44, 173.37, 136.42, 129.45, 129.25, 128.99, 128.95, 127.57, 127.30, 68.34, 67.89, 64.97, 45.92, 40.25, 38.42, 36.85, 36.36, 32.07, 31.74, 25.24, 22.61, 14.05. HRMS (ESI-TOF) m/z [M+H]$^+$ calculated for C$_{18}$H$_{25}$NO$_2$S$_2$ 352.1327, found 352.1360.

(*S*)-1-((*R*)-4-benzyl-2-thioxothiazolidin-3-yl)-3-hydroxydecan-1-one (**17d**): Compound **15** was reacted with octanal according to the general procedure **4.6.2** and subsequent flash chromatography furnished title compound **17d** as a pale-yellow oil (minor diastereomer); ^{1}H NMR (700 MHz, CDCl$_3$) δ 7.43 – 7.32 (m, 3H), 7.34 – 7.28 (m, 3H), 5.43 (ddd, *J* = 10.8, 7.1, 4.0 Hz, 1H), 4.20 – 4.14 (m, 1H), 3.67 (dd, *J* = 17.8, 2.4 Hz, 1H), 3.43 (ddd, *J* = 11.5, 7.2, 1.1 Hz, 1H), 3.25 (dd, *J* = 13.3, 4.0 Hz, 1H), 3.15 (dd, *J* = 17.7, 9.5 Hz, 1H), 3.07 (dd, *J* = 13.3, 10.5 Hz, 1H), 2.92 (d, *J* = 11.5 Hz, 1H), 2.73 (d, *J* = 3.9 Hz, 1H), 1.64 – 1.56 (m, 1H), 1.55 – 1.44 (m, 2H), 1.49 (s, 1H), 1.36 – 1.25 (m, 7H), 0.91 (t, *J* = 7.0 Hz, 3H). HRMS (ESI-TOF) m/z [M+H]$^+$ calculated for C$_{20}$H$_{29}$NO$_2$S$_2$ 380.1640, found 380.1673.

(*S*)-1-((*R*)-4-benzyl-2-thioxothiazolidin-3-yl)-3-hydroxydodecan-1-one (**17e**): Compound **15** was reacted with decanal according to general procedure **4.6.2** and subsequent flash chromatography furnished title compound **17e** as a yellow oil (minor diastereomer); ^{1}H NMR (700 MHz, CDCl$_3$) δ 7.40 – 7.35 (m, 2H), 7.33 – 7.28 (m, 3H), 5.44 (ddd, *J* = 10.8, 7.2, 4.1 Hz, 1H), 4.10 – 4.04 (m, 1H), 3.48 (dd, *J* = 17.5, 9.4 Hz, 1H), 3.43 (ddd, *J* = 11.5, 7.3, 1.0 Hz, 1H), 3.36 (dd, *J* = 17.5, 2.5 Hz, 1H), 3.25 (dd, *J* = 13.3, 4.0 Hz, 1H), 3.12 (d, *J* = 4.1 Hz, 1H), 3.07 (dd, *J* = 13.3, 10.4 Hz, 1H), 2.93 (d, *J* = 11.5 Hz, 1H), 1.65 – 1.57 (m, 6H), 1.55 – 1.46 (m, 1H), 1.32 (s, 6H), 1.31 (ddt, *J* = 17.1, 11.9, 8.2 Hz, 6H), 0.90 (t, *J* = 7.0 Hz, 3H). HRMS (ESI-TOF) m/z [M+H]$^+$ calculated for C$_{22}$H$_{33}$NO$_2$S$_2$ 408.1953, found 408.1951.

(*S*)-1-((*R*)-4-benzyl-2-thioxothiazolidin-3-yl)-3-hydroxytetradecan-1-one (**17f**): Compound **15** was reacted with dodecanal according to general procedure **4.6.2** and subsequent flash chromatography furnished title compound **17f** as a yellow oil (minor diastereomer); ^{1}H NMR (500 MHz, CDCl$_3$) δ 7.39 (d, *J* = 7.4 Hz, 2H), 7.32 (s, 1H), 7.23 (d, *J* = 7.3 Hz, 3H), 4.49 (p, *J* = 7.2 Hz, 2H), 3.63 (dd, *J* = 11.1, 7.6 Hz, 2H), 3.39 – 3.22 (m, 2H), 3.12 – 2.97 (m, 4H), 2.36 (t, *J* = 7.5 Hz, 2H), 1.65 (p, *J* = 7.5 Hz, 2H), 1.34 (dd, *J* = 27.0, 11.6 Hz, 5H), 1.31 (s, 5H), 1.28 (s, 10H), 0.91 (d, *J* = 6.6 Hz, 3H). ^{13}C NMR (126 MHz, CDCl$_3$) δ 201.43, 179.08, 173.39, 136.42, 129.45, 128.96, 127.31, 68.35, 67.91, 60.43, 45.91, 36.85, 36.37, 33.91, 32.06, 31.92, 29.67, 29.60, 29.44, 29.35, 29.25, 29.07, 25.56, 24.71, 22.70, 14.13. HRMS (ESI-TOF) m/z [M+H]$^+$ calculated for C$_{24}$H$_{37}$NO$_2$S$_2$ 436.2266, found 436.2291.

Table 4.9. Stereoselectivities observed in the above aldol reactions.

Aldehyde	Compound	*syn:anti*
Acetaldehyde	**16a:17a**	90:10
Butanal	**16b:17b**	88:12
Hexanal	**16c:17c**	95:5
Octanal	**16d:17d**	89:11
Decanal	**16e:17e**	93:7
Dodecanal	**16f:17f**	96:4
Isobutaraldehyde	**16g:17g**	98:2
Cyclopropanecarbaldehyde	**16h:17h**	97:3

4.4.3. **General procedure for the hydrolysis of aldol adducts**: To a 0.2 M solution of aldol adduct (**16a-h**, 1 eq.) in THF, 1 M aqueous LiOH (4 eq.) was added. The reaction mixture was stirred at room temperature for 3-4 h. After the reaction, THF was removed over rotavapor, and the aqueous phase was washed with EtOAc (2*100 mL), then acidified with 2 M HCl to 2-3 pH. The solution was extracted with EtOAc (3*100 mL), which was dried over Na_2SO_4, filtered, and concentrated to afford the corresponding beta hydroxy acid (**18a-h**).

(***R***)-3-hydroxyhexanoic acid (18b): Following the general procedure **4.6.3** hydrolysis of **16b** afforded the desired product **18b** with 95% yield as colourless oil; $[\alpha]_D^{25}$ = -12.2 (c 0.5, CH_2Cl_2); ^{1}H NMR (500 MHz, $CDCl_3$) δ 4.07 – 3.88 (1H, m), 2.57 – 2.22 (2H, m), 1.63 – 1.20 (4H, m), 0.85 (3H, t, *J* = 6.9 Hz); ^{13}C NMR (126 MHz, $CDCl_3$) δ 177.34, 68.02, 42.10, 38.68, 18.55, 13.90. HRMS (ESI-TOF) m/z [M+H]$^+$ calculated for $C_6H_{12}O_3$ 133.0786, found 133.0826; in agreement with previously reported data.[1]

(***R***)-3-hydroxyoctanoic acid (18c): Following the general procedure **4.6.3** hydrolysis of **16c** afforded the desired product **18c** with 96% yield as colourless oil; $[\alpha]_D^{25}$ = -4.45 (c 0.5, CH_2Cl_2) ^{1}H NMR (500 MHz, $CDCl_3$) δ 4.03 (1H, tt, *J* = 8.0, 3.7 Hz), 2.64 – 2.38 (2H, m), 1.62 – 1.21 (8H, m), 0.89 (3H, t, *J* = 6.6 Hz); ^{13}C NMR (126 MHz, $CDCl_3$) δ 177.11, 68.35, 41.48, 36.65, 31.77, 25.24, 22.66, 14.09. HRMS (ESI-TOF) m/z [M+H]$^+$ calculated for $C_8H_{16}O_3$ 161.1099, found 161.1069; data in agreement with previously reported data.[1]

(***R***)-3-hydroxydecanoic acid (18d): Following the general procedure **4.6.3** hydrolysis of **16d** afforded the desired product **18d** with 91% yield as white sticky solid; $[\alpha]_D^{25}$ = -8.68 (c 0.5, CH_2Cl_2) ^{1}H NMR (700 MHz, $CDCl_3$) δ 4.03 (1H, tdd, *J* = 8.1, 4.6, 3.0 Hz), 2.57 (1H, dd, *J* = 16.5, 3.0 Hz), 2.47 (1H, dd, *J* = 16.6, 9.1 Hz), 1.61 – 1.20 (13H, m), 0.88 (3H, t, *J* = 7.0 Hz); ^{13}C NMR (126 MHz, CDCl3) δ

177.74, 68.28, 41.27, 36.61, 31.92, 29.57, 29.35, 25.59, 22.78, 14.22. HRMS (ESI-TOF) m/z [M+H]$^+$ calculated for $C_{10}H_{20}O_3$ 189.1412, found 189.1446

(R)-3-hydroxydodecanoic acid (18e): Following the general procedure **4.6.3** hydrolysis of **16e** afforded the desired product **18e** with 93% yield as white solid; $[\alpha]_D^{25}$ = -16.6 (c 0.5, CH_2Cl_2) ^{1}H NMR (500 MHz, CDCl$_3$) δ 4.06 (1H, tt, *J* = 8.3, 3.9 Hz), 2.60 (1H, dd, *J* = 16.6, 3.0 Hz), 2.50 (1H, dd, *J* = 16.6, 9.0 Hz), 1.63 – 1.42 (2H, m), 1.39 – 1.27 (13H, m), 0.90 (3H, t, *J* = 6.9 Hz); ^{13}C NMR (126 MHz, CDCl3) δ 177.91, 68.20, 41.21, 36.63, 32.03, 29.69, 29.67, 29.62, 29.44, 25.59, 22.82, 14.25; in agreement with previously reported data.[3] HRMS (ESI-TOF) m/z [M+H]$^+$ calculated for $C_{12}H_{24}O_3$ 216.1725, found 216.1759.

(R)-3-hydroxy-4-methylpentanoic acid (18g): Following the general procedure **4.6.3** hydrolysis of **16g** afforded the desired product **18g** with 95% yield as colourless oil; ^{1}H NMR (700 MHz, CDCl3) δ 3.82 (1H, ddd, *J* = 9.8, 5.7, 2.6 Hz), 2.56 (1H, dd, *J* = 16.3, 2.6 Hz), 2.48 (1H, dd, *J* = 16.3, 9.8 Hz), 1.79 – 1.70 (1H, m), 0.96 (3H, d, *J* = 6.8 Hz), 0.94 (3H, d, *J* = 6.8 Hz) ^{13}C NMR (176 MHz, CDCl3) δ 178.33, 72.94, 38.46, 33.31, 18.46, 17.83; in agreement with previously reported data.[4] HRMS (ESI-TOF) m/z [M+H]$^+$ calculated for $C_6H_{12}O_3$ 133.0786, found 133.0756.

(R)-3-cyclopropyl-3-hydroxypropanoic acid (18h): Following the general procedure **4.6.3** hydrolysis of **16h** afforded the desired product **18h** with 88% yield as colourless oil; ^{1}H NMR (500 MHz, CDCl3) δ 3.35 (1H, td, *J* = 8.6, 3.5 Hz), 2.70 (2H, qd, *J* = 16.3, 6.3 Hz), 1.07 – 0.87 (2H, m), 0.58 (3H, dtt, *J* = 17.7, 9.0, 4.2 Hz), 0.42 (1H, dq, *J* = 8.7, 4.6 Hz), 0.27 (1H, dq, *J* = 10.0, 4.7 Hz); ^{13}C NMR (126 MHz, CDCl3) δ 176.92, 72.99, 41.27, 29.83, 17.00. HRMS (ESI-TOF) m/z [M+H]$^+$ calculated for $C_6H_{10}O_3$ 131.0630, found 131.0631.

4.4.4. **General procedure for the synthesis of β-amino acids (22c and 22d)**: Following the literature procedure required β-amino acids (**22c** and **22d**) were synthesized in four steps with an overall yield of 85%.[2]

4.4.4.1. **(S)-N-(benzyloxy)-3-hydroxydecanamide (19d)**: To a stirring mixture of β-hydroxy acid **17d** (1.1 gm, 5.8 mmol, 1 eq.) in THF-H$_2$O (4:1, 50 mL), BnONH$_2$×HCl (1.86 gm, 11.7 mmol, 2eq.) was added. The pH of the solution was adjusted to 4.5 with 1N NaOH, and then EDCI (1.3 gm, 8.7, 1.5 eq.) was added in one portion. The resulting solution was stirred at rt for 2 h while maintaining the pH at 4.5 with 1 M HCl by using a pH meter. After the completion of the reaction, THF was removed, and the residue was extracted with ethyl acetate (3*25 mL). The whole EtOAc organic layer was washed with

10% citric acid, 10 % NaHCO₃, dried over Na₂SO₄, and concentrated to afford **19d** (1.65 gm, 95%) as a white solid which was used further without purification.

The analogous compound **19c** was synthesized by following the same procedure.

4.4.4.2. (*R*)-1-(benzyloxy)-4-heptylazetidin-2-one (20d): To a stirring cooled (0 °C) solution of *o*-benzylhydroxamate **19d** (1.65 gm g, 5.6 mmol) and PPh₃ (1.61 gm, 6.2 mmol) in dry THF (50 mL), DEAD (1.27 mL, 5.6 mmol) was added dropwise. The resulting solution was stirred for 4 h at room temperature. After evaporation of THF, the residue was purified by column chromatography (hexane/EtOAc, 5:1) to give the product **20d** as a colorless oil (1.2 g, 80%) ¹H NMR (500 MHz, CDCl₃) δ 7.42 (5H, ddt, *J* = 15.8, 7.2, 2.9 Hz), 5.03 – 4.93 (2H, m), 3.53 (1H, dtd, *J* = 7.6, 5.0, 2.4 Hz), 2.73 (1H, dd, *J* = 13.5, 5.1 Hz), 2.30 (1H, dd, *J* = 13.6, 2.4 Hz), 1.73 – 1.63 (1H, m), 1.43 – 1.24 (12H, m), 0.91 (3H, t, *J* = 7.0 Hz). HRMS (ESI-TOF) m/z [M+H]⁺ calculated for C₁₇H₂₅NO₂ 276.1877, found 276.1891.

The analogous compound **20c** was synthesized by following the same procedure. ¹H NMR (700 MHz, CDCl₃) δ 7.45 – 7.35 (5H, m), 4.99 (1H, d, *J* = 11.1 Hz), 4.95 (1H, d, *J* = 11.2 Hz), 3.52 (1H, dtd, *J* = 7.5, 5.0, 2.4 Hz), 2.72 (1H, dd, *J* = 13.4, 5.1 Hz), 2.30 (1H, dd, *J* = 13.5, 2.5 Hz), 1.68 (1H, ddt, *J* = 14.2, 10.1, 5.2 Hz), 1.41 – 1.34 (1H, m), 1.34 – 1.20 (6H, m), 0.90 (3H, t, *J* = 7.2 Hz) ¹³C NMR (176 MHz, CDCl₃) δ 135.53, 129.38, 129.02, 128.70, 78.30, 77.34, 77.16, 76.98, 58.23, 37.93, 32.50, 31.66, 25.27, 22.56, 14.05. HRMS (ESI-TOF) m/z [M+H]⁺ calculated for C₁₉H₂₉NO₂ 304.2189, found 304.2168.

4.4.4.3. (*R*)-3-((benzyloxy)amino) decanoic acid (21d): To a cooled (0 °C) solution of β-lactam **20d** (960 mg, 3.88 mmol, 1 eq.) in THF:MeOH (3:1, 8 mL), LiOH (149 mg, 4.6 mmol, 1.2 eq.) in water (2 mL) was added under stirring. The resulting solution was stirred at 0 °C until complete consumption of the starting material. Then the reaction solution was acidified to pH 2 with 4N HCl, and the organic solvents were evaporated. The residue was extracted with ethyl acetate (3*30 mL), and the combined organic layer was washed with brine (2*10 mL), dried over Na₂SO₄, and evaporated to give **21d** (1.02 gm, 98%).

The analogous compound **21c** was synthesized by following the same procedure.

4.4.4.4. (*R*)-3-aminodecanoic acid (22d): A solution of **21d** (1.02 gm, 3.44 mmol) in MeOH (30 mL) was hydrogenated in the presence of 10% Pd/ C (100 mg) at atmospheric pressure. The reaction was

monitored using TLC. After completion of the reaction, Pd/C was filtered off, and the solvent was evaporated to give **22d** as a white solid (650 mg, 99%).

The analogous compound **22c** was synthesized by following the same procedure.

4.4.5. **General procedure for the Fmoc protection of β-amino acids**: To a solution of (*R*)-3-β-amino acid (**22c** or **22d**) (540 mg, 2.88 mmol) in dioxane was added 10% (aq.) Na_2CO_3 (5 mL) and stirred at 0 °C for 10 min. Then the Fmoc-Cl (1.1 gm, 4.33 mmol) in dioxane (5 mL) was added to the stirring solution and further stirred for 2-3 hr at room temperature. After completion of the reaction, dioxane was evaporated on rotavapor and the aqueous layer was washed with diethyl ether. The pH of aq. layer brought up to 2-3 by 2 M HCl, and then the residue was extracted with ethyl acetate (2*50), dried over Na_2SO_4, and evaporated to give corresponding Fmoc-protected (*R*)-3-β-amino acid.

(*R*)-3-((((9H-fluoren-9-yl)methoxy)carbonyl)amino) octanoic acid (23c): Following the general procedure **1.41** to **1.45,** five step afforded the desired product **23c** as white solid with overall yield of 85% ^{1}H NMR (700 MHz, CDCl3) δ 7.78 (2H, d, *J* = 7.6 Hz), 7.61 (2H, d, *J* = 7.5 Hz), 7.41 (2H, t, *J* = 7.5 Hz), 7.33 (2H, t, *J* = 7.4 Hz), 5.19 (1H, d, *J* = 9.2 Hz), 4.52 (1H, s), 4.42 (2H, d, *J* = 7.2 Hz), 4.24 (1H, t, *J* = 7.0 Hz), 4.00 (1H, q, *J* = 7.7 Hz), 2.61 (2H, qd, *J* = 16.0, 5.4 Hz), 1.38 (1H, s), 1.38 – 1.25 (6H, m), 1.22 (1H, s), 0.90 (3H, t, *J* = 6.6 Hz); ^{13}C NMR (176 MHz, CDCl3) 177.03, 156.11, 144.10, 144.02, 141.46, 127.81, 127.18, 125.23, 125.19, 120.11, 66.79, 48.18, 47.42, 39.06, 34.42, 31.59, 25.95, 22.65, 14.15. HRMS (ESI-TOF) m/z [M+H]$^+$ calculated for $C_{23}H_{27}NO_4$ 382.1940, found 382.1914.

(R)-3-((((9H-fluoren-9-yl)methoxy)carbonyl)amino)decanoic acid (23d): Following the general procedure **1.41** to **1.45,** five steps afforded the desired product **23d** with overall yield of 82% ^{1}H NMR (700 MHz, CDCl3) δ 7.78 (2H, d, *J* = 7.6 Hz), 7.61 (2H, d, *J* = 7.4 Hz), 7.41 (2H, t, *J* = 7.5 Hz), 7.33 (2H, t, *J* = 7.4 Hz), 5.16 (1H, d, *J* = 9.1 Hz), 4.42 (2H, dt, *J* = 14.2, 7.3 Hz), 4.24 (1H, t, *J* = 7.0 Hz), 3.99 (1H, q, *J* = 7.7 Hz), 2.62 (2H, qd, *J* = 16.3, 5.3 Hz), 1.57 (2H, h, *J* = 7.4 Hz), 1.40 – 1.18 (13H, m), 0.90 (3H, t, *J* = 7.1 Hz); ^{13}C NMR (176 MHz, CDCl3) δ 176.69, 156.09, 144.10, 144.03, 141.47, 127.82, 127.19, 125.24, 125.19, 120.12, 66.79, 48.19, 47.43, 39.00, 34.48, 31.91, 29.40, 29.32, 26.30, 22.78, 14.23. HRMS (ESI-TOF) m/z [M+H]$^+$ calculated for $C_{25}H_{31}NO_4$ 410.2253, found 410.2245.

4.4.6. **Solid phase peptide synthesis of Icosalide 1a and its analogues**: Synthesis of **1a-1a'''**, and **2-7** started with the loading of *R*-3-hydroxy acid or *S*-3-hydroxy acid (1.2 eq.) at residue position 6 (depending on the peptides sequence) (see Figure **1**) onto the 2-chloro trityl chloride resin (150 mg, 1.6 mmol/g, 0.24 mmol) in dry DCM and DIPEA (3 eq.) for 2 hrs. After loading the first hydroxy acid, capping of the resin's unreacted active sites was done by MeOH (0.5 mL) and DIPEA (30 µL) for 30

min. Then, on resin esterification of hydroxy acid to Fmoc-Leu was performed in the presence of DIC (2 eq.) and DMAP (0.2 eq.) in dry DCM for 1.5 hrs.[5] After completing the esterification, the resin was washed 3 times with DCM, 3 times with NMP, and then the Fmoc deprotection was done with 20% piperidine in DMF (2*10 min) followed by washing the resin 4 times with NMP. The peptide chain was elongated by coupling Fmoc-Ser(tBu)-OH, HCTU (2 eq.), HOAt (2 eq.), DIPEA (3 eq.) in NMP for 1.5 hrs following which Fmoc deprotection was done with 20% piperidine in DMF (2*10 min) and washing the resin with NMP. Coupling of *R*-3-hydroxy acid or *S*-3-hydroxy acid (2 eq.) at residue position 5 (depending on the peptides sequence) (see Figure **1**) using HCTU (2 eq.), HOAt (2 eq.), DIPEA (3 eq.) in NMP was carried out for 1.5 hrs. Later, the resin was washed 3 times with NMP and 3 times with DCM. On resin esterification with Fmoc-Ser (tBu)-OH was done in the presence of DIC (2 eq.), DMAP (0.2 eq.) in dry DCM for 1.5 hrs. After esterification, Fmoc deprotection was done using 20% piperidine in DMF (2*10 min). Coupling of Fmoc-Leu in the presence of HCTU (2 eq.), HOAt (2 eq.), and DIPEA (2 eq.) in NMP was carried out for 2 hrs. The exact procedure described here was also followed for synthesizing linear peptides of **8**-**13**; however, the amide coupling protocol as mentioned above is employed whenever amide coupling was used instead of esterification because of substituting *R*-3-hydroxy acid with *R*-3-amino acid. After obtaining the complete linear sequence, Fmoc deprotection of the terminal residue was carried out with 20% piperidine in DMF (2*10 min), and then the resin was washed 4 times with NMP, 4 times with DCM. The linear hexapeptide was cleaved from the resin using TFE: Acetic acid: DCM (1:1:8) for 1.5 hrs (3*30 min). The filtrate was collected and concentrated by removing the excess acetic acid as an azeotrope using chloroform. The head to tail cyclization of these linear peptides was done using HCTU (2 eq.), HOAt (2 eq.), and DIPEA (5 eq.) in DMF. After overnight stirring, the reaction mixture was concentrated and dissolved in saturated sodium bicarbonate. The sidechain protected cyclic peptides of **1a-1a′′′**, **2-13** were extracted from this solution with ethyl acetate and purified by column chromatography. Global deprotection of the *tert*-Butyl groups of the cyclic peptide was accomplished with 50% (TFA) in DCM. After complete deprotection of sidechain protecting groups, the reaction mixture was concentrated and purified by column chromatography to obtain peptides **1a**-**1a′′′** and **2-13**.

The synthesis of Icosalide **1a** and its analogues was performed following the general procedure **4.7**.

Icosalide 1a: ^{1}H NMR (500 MHz, DMSO) δ 9.03 (d, *J* = 4.6 Hz, 1H), 8.00 (d, *J* = 9.3 Hz, 1H), 7.44 (d, *J* = 8.7 Hz, 1H), 7.28 (d, *J* = 8.2 Hz, 1H), 5.78 (s, 1H), 4.90 (ddq, *J* = 29.5, 8.8, 4.0 Hz, 2H), 4.48 (td, *J* = 8.4, 4.5 Hz, 1H), 4.42 – 4.32 (m, 2H), 3.92 (ddd, *J* = 17.1, 9.4, 3.7 Hz, 2H), 3.66 (dd, *J* = 10.8, 3.0 Hz,

1H), 3.56 (dd, *J* = 10.9, 4.5 Hz, 1H), 2.59 (dd, *J* = 13.9, 3.8 Hz, 1H), 2.51 (d, *J* = 2.0 Hz, 1H), 2.46 (d, *J* = 3.9 Hz, 1H), 2.25 (dd, *J* = 13.9, 3.6 Hz, 1H), 1.85 (s, 1H), 1.58 (dd, *J* = 13.9, 8.3 Hz, 4H), 1.53 – 1.06 (m, 19H), 0.92 (d, *J* = 5.6 Hz, 3H), 0.88 (d, *J* = 5.7 Hz, 3H), 0.83 (t, *J* = 8.1 Hz, 6H). HRMS (ESI$^+$): calculated for $C_{36}H_{65}N_4O_{10}$ [M+H]$^+$ = 713.4620, found 713.4697.

Icosalide 1a′: ^{1}H NMR (700 MHz, DMSO) δ 8.37 (d, *J* = 6.0 Hz, 1H), 7.79 (d, *J* = 8.7 Hz, 1H), 7.75 (d, *J* = 7.8 Hz, 1H), 7.70 (d, *J* = 8.2 Hz, 1H), 5.10 (t, *J* = 5.6 Hz, 1H), 4.98 (tdd, *J* = 10.9, 5.6, 3.3 Hz, 2H), 4.89 (t, *J* = 5.5 Hz, 1H), 4.42 (td, *J* = 9.1, 5.3 Hz, 1H), 4.36 – 4.29 (m, 2H), 4.04 (td, *J* = 7.7, 6.1 Hz, 1H), 3.75 (dt, *J* = 10.7, 5.3 Hz, 1H), 3.59 (ddt, *J* = 31.0, 10.6, 5.2 Hz, 2H), 3.51 (ddd, *J* = 10.8, 7.1, 5.3 Hz, 1H), 2.50 – 2.45 (m, 2H), 2.40 – 2.31 (m, 2H), 1.67 (tt, *J* = 12.7, 6.5 Hz, 1H), 1.64 – 1.46 (m, 9H), 1.25 (q, *J* = 6.6 Hz, 16H), 0.92 (d, *J* = 6.4 Hz, 3H), 0.90 – 0.80 (m, 15H). HRMS (ESI$^+$): calculated for $C_{36}H_{65}N_4O_{10}$ [M+H]$^+$ = 713.4620, found 713.4697.

Icosalide analogue 2: ^{1}H NMR (500 MHz, Acetone) δ 8.31 (s, 1H), 7.91 (d, *J* = 9.3 Hz, 1H), 7.61 (d, *J* = 8.8 Hz, 1H), 7.37 (s, 1H), 5.17 (tq, *J* = 6.7, 3.3 Hz, 1H), 5.11 (dd, *J* = 8.8, 4.4 Hz, 1H), 4.72 – 4.60 (m, 2H), 4.52 (dt, *J* = 8.8, 2.7 Hz, 1H), 4.27 – 4.14 (m, 2H), 3.86 (dd, *J* = 10.4, 2.8 Hz, 1H), 3.78 – 3.66 (m, 2H), 3.48 (s, 1H), 2.79 (d, *J* = 3.8 Hz, 1H), 2.64 (dd, *J* = 13.9, 3.8 Hz, 1H), 2.26 (ddd, *J* = 13.4, 9.3, 3.6 Hz, 2H), 1.87 – 1.65 (m, 4H), 1.62 – 1.49 (m, 3H), 1.38 – 1.23 (m, 4H), 1.02 (d, *J* = 6.4 Hz, 3H), 1.00 – 0.91 (m, 9H), 0.88 (t, *J* = 7.4 Hz, 3H).). HRMS (ESI$^+$): calculated for $C_{28}H_{49}N_4O_{10}$ [M+H]$^+$ = 601.3370, found 601.3433.

Icosalide analogue 3: ^{1}H NMR (500 MHz, Acetone) δ 8.00 (d, *J* = 7.1 Hz, 1H), 7.77 (d, *J* = 8.5 Hz, 1H), 7.37 (s, 1H), 7.24 (d, *J* = 9.4 Hz, 1H), 5.13 (ddd, *J* = 29.4, 10.3, 5.1 Hz, 2H), 4.65 – 4.54 (m, 2H), 4.49 (tt, *J* = 8.9, 4.5 Hz, 2H), 4.14 (dd, *J* = 10.6, 3.0 Hz, 1H), 4.02 (dd, *J* = 11.3, 3.9 Hz, 1H), 3.89 (dd, *J* = 11.3, 4.0 Hz, 1H), 3.80 (dd, *J* = 10.6, 2.8 Hz, 1H), 2.64 (dd, *J* = 13.9, 3.7 Hz, 1H), 2.33 – 2.23 (m, 2H), 1.98 (t, *J* = 10.3 Hz, 1H), 1.89 – 1.76 (m, 1H), 1.79 – 1.67 (m, 2H), 1.66 – 1.52 (m, 4H), 1.35 (dd, *J* = 14.8, 7.3 Hz, 2H), 1.28 (d, *J* = 14.0 Hz, 12H), 0.97 (d, *J* = 6.5 Hz, 4H), 0.96 – 0.83 (m, 18H). HRMS (ESI$^+$): calculated for $C_{32}H_{57}N_4O_{10}$ [M+H]$^+$ = 657.8180, found 657.4065.

Icosalide analogue 4: ^{1}H NMR (500 MHz, Acetone) δ 8.33 (d, *J* = 4.9 Hz, 1H), 7.94 (d, *J* = 9.3 Hz, 1H), 7.58 (d, *J* = 8.9 Hz, 1H), 7.31 (d, *J* = 8.6 Hz, 1H), 5.06 (dq, *J* = 8.6, 4.1 Hz, 1H), 4.99 (dq, *J* = 11.9, 3.5 Hz, 1H), 4.68 (ddd, *J* = 8.6, 7.0, 5.3 Hz, 1H), 4.60 (ddd, *J* = 12.7, 9.4, 3.5 Hz, 1H), 4.49 (dt, *J* = 9.0, 2.7 Hz, 1H), 4.25 – 4.13 (m, 2H), 3.85 (dd, *J* = 10.4, 2.8 Hz, 1H), 3.73 (dd, *J* = 11.1, 5.3 Hz, 1H), 3.66 (dd, *J* = 11.1, 7.0 Hz, 1H), 2.76 (dd, *J* = 13.9, 3.9 Hz, 1H), 2.62 (dd, *J* = 13.9, 3.9 Hz, 1H), 2.27 (ddd, *J* = 13.8, 7.1, 3.3 Hz, 2H), 1.84 – 1.60 (m, 6H), 1.59 – 1.50 (m, 2H), 1.39 (s, 2H), 1.29 (d, *J* = 9.4 Hz,

23H), 1.02 (d, J = 6.1 Hz, 3H), 1.00 − 0.92 (m, 9H), 0.88 (td, J = 6.8, 4.2 Hz, 6H). HRMS (ESI⁺): calculated for $C_{40}H_{73}N_4O_{10}$ [M+H]⁺ = 769.5248, found 769.5323.

Icosalide analogue 5: ¹H NMR (500 MHz, Acetone) δ 8.34 (d, J = 4.9 Hz, 1H), 7.94 (d, J = 9.3 Hz, 1H), 7.58 (d, J = 8.9 Hz, 1H), 7.33 (d, J = 8.6 Hz, 1H), 5.06 (dd, J = 8.7, 4.7 Hz, 1H), 4.67 (td, J = 7.7, 5.3 Hz, 1H), 4.61 (ddd, J = 12.7, 9.3, 3.5 Hz, 1H), 4.49 (dt, J = 9.0, 2.6 Hz, 1H), 4.19 (ddd, J = 28.0, 9.0, 3.7 Hz, 2H), 3.72 (dd, J = 11.1, 5.2 Hz, 1H), 3.66 (dd, J = 11.1, 7.0 Hz, 1H), 2.28 (dd, J = 9.3, 3.4 Hz, 1H), 2.28 − 2.20 (m, 1H), 1.79 (td, J = 13.1, 3.6 Hz, 1H), 1.77 − 1.62 (m, 4H), 1.54 (tt, J = 11.1, 3.7 Hz, 2H), 1.39 (s, 2H), 1.29 (d, J = 6.5 Hz, 33H), 1.05 − 0.93 (m, 12H), 0.91 − 0.85 (m, 6H). HRMS (ESI⁺): calculated for $C_{44}H_{81}N_4O_{10}$ [M+H]⁺ = 825.5874, found 825.5947.

Icosalide analogue 6: ¹H NMR (500 MHz, Acetone) δ 8.29 (d, J = 5.1 Hz, 1H), 7.95 (d, J = 9.2 Hz, 1H), 7.62 (d, J = 8.8 Hz, 1H), 7.38 (d, J = 8.6 Hz, 1H), 4.76 − 4.49 (m, 5H), 4.24 (td, J = 7.6, 5.1 Hz, 1H), 4.15 (dd, J = 10.4, 2.6 Hz, 1H), 3.84 (dd, J = 10.4, 2.8 Hz, 1H), 3.72 (dd, J = 11.1, 5.3 Hz, 1H), 3.66 (dd, J = 11.1, 6.9 Hz, 1H), 2.65 (dd, J = 14.2, 3.8 Hz, 1H), 2.52 (dd, J = 14.1, 3.9 Hz, 1H), 2.45 (ddd, J = 13.9, 9.6, 3.8 Hz, 2H), 1.96 (ddd, J = 10.2, 6.8, 3.7 Hz, 1H), 1.92 − 1.68 (m, 5H), 1.56 (ddd, J = 14.1, 10.7, 3.8 Hz, 1H), 1.05 − 0.87 (m, 21H), 0.84 (d, J = 6.5 Hz, 3H). HRMS (ESI⁺): calculated for $C_{30}H_{53}N_4O_{10}$ [M+H] ⁺ = 629.3683, found 629.3756.

Icosalide analogue 7: ¹H NMR (500 MHz, Acetone) δ 8.27 (d, J = 5.1 Hz, 1H), 7.89 (d, J = 9.2 Hz, 1H), 7.62 (d, J = 9.0 Hz, 1H), 7.39 (d, J = 8.5 Hz, 1H), 4.67 (s, 1H), 4.67 − 4.58 (m, 1H), 4.53 (dt, J = 9.1, 2.9 Hz, 1H), 4.45 (dt, J = 8.3, 3.9 Hz, 1H), 4.26 (dtd, J = 12.9, 8.3, 4.5 Hz, 2H), 4.12 (dd, J = 10.5, 2.8 Hz, 1H), 3.83 (dd, J = 10.5, 2.9 Hz, 1H), 3.75 − 3.63 (m, 2H), 2.76 (dd, J = 13.9, 4.0 Hz, 1H), 2.66 (dd, J = 13.8, 3.9 Hz, 1H), 2.47 − 2.34 (m, 2H), 1.87 (dd, J = 13.8, 9.7 Hz, 1H), 1.76 (dd, J = 14.2, 6.4 Hz, 1H), 1.70 (dd, J = 8.0, 5.9 Hz, 2H), 1.58 (ddd, J = 14.3, 10.6, 4.0 Hz, 1H), 1.12 (ddt, J = 12.8, 8.5, 4.6 Hz, 2H), 1.01 (d, J = 6.2 Hz, 3H), 0.98 − 0.87 (m, 11H), 0.90 − 0.84 (m, 1H), 0.65 − 0.48 (m, 3H), 0.43 (dq, J = 8.4, 4.1 Hz, 1H), 0.42 − 0.32 (m, 2H), 0.29 (ddt, J = 18.8, 9.3, 5.1 Hz, 2H). HRMS (ESI⁺): calculated for $C_{30}H_{49}N_4O_{10}$ [M+H]⁺ = 625.3370, found 625.3443.

Icosalide analogue 8: ¹H NMR (500 MHz, DMSO) δ 8.14 (t, J = 7.9 Hz, 2H), 8.03 (d, J = 8.7 Hz, 1H), 7.77 (t, J = 6.1 Hz, 1H), 7.46 (d, J = 7.4 Hz, 1H), 5.20 (t, J = 5.2 Hz, 1H), 5.11 (d, J = 7.4 Hz, 1H), 4.90 − 4.82 (m, 1H), 4.49 (ddt, J = 15.1, 10.1, 4.6 Hz, 2H), 4.38 − 4.23 (m, 1H), 4.10 (q, J = 7.3 Hz, 1H), 3.67 (s, 0H), 3.63 − 3.57 (m, 2H), 3.19 (dd, J = 13.1, 6.6 Hz, 1H), 2.46 (dd, J = 13.4, 8.1 Hz, 1H), 2.37 − 2.25 (m, 3H), 1.68 (dt, J = 13.6, 6.7 Hz, 1H), 1.55 − 1.48 (m, 5H), 1.48 − 1.35 (m, 1H), 1.30 − 1.23 (m,

3H), 1.24 (s, 11H), 0.92 − 0.81 (m, 17H). HRMS (ESI$^+$): calculated for C$_{31}$H$_{56}$N$_5$O$_9$ [M+H]$^+$ = 642.4000, found 642.4073.

Icosalide analogue 9: ^{1}H NMR (500 MHz, DMSO) δ 8.06 (d, J = 6.4 Hz, 1H), 7.82 − 7.73 (m, 3H), 7.46 (d, J = 8.1 Hz, 1H), 5.41 (s, 1H), 5.01 (s, 1H), 4.83 (s, 1H), 4.43 − 4.35 (m, 2H), 4.29 (s, 1H), 4.08 (dt, J = 10.4, 5.7 Hz, 1H), 3.79 (s, 2H), 3.63 (d, J = 9.2 Hz, 1H), 3.58 − 3.50 (m, 1H), 2.22 (ddd, J = 29.9, 13.6, 5.8 Hz, 2H), 1.70 (d, J = 6.7 Hz, 1H), 1.50 (s, 4H), 1.47 − 1.37 (m, 3H), 1.31 − 1.25 (m, 2H), 1.23 (s, 2H), 1.22 (s, 16H), 0.86 (ddt, J = 15.6, 13.6, 6.5 Hz, 20H). HRMS (ESI$^+$): calculated for C$_{36}$H$_{66}$N$_5$O$_9$ [M+H]$^+$ = 712.4782, found 712.4855.

Icosalide analogue 10: ^{1}H NMR (500 MHz, DMSO) δ 8.59 (d, J = 6.5 Hz, 1H), 7.69 (dd, J = 13.5, 8.2 Hz, 2H), 7.55 (d, J = 7.8 Hz, 1H), 7.39 (dd, J = 8.4, 4.1 Hz, 1H), 4.99 (s, 1H), 4.37 (dtd, J = 30.9, 8.5, 4.4 Hz, 2H), 4.18 (dt, J = 8.9, 4.6 Hz, 1H), 4.12 (q, J = 7.3 Hz, 1H), 3.70 (dd, J = 10.8, 4.5 Hz, 2H), 3.63 (dd, J = 11.0, 4.3 Hz, 1H), 3.57 − 3.50 (m, 2H), 2.94 (dd, J = 13.1, 9.6 Hz, 1H), 2.36 − 2.25 (m, 1H), 2.13 − 2.06 (m, 1H), 1.71 (s, 1H), 1.65 − 1.48 (m, 4H), 1.53 (s, 4H), 1.28 − 1.19 (m, 9H), 0.94 − 0.80 (m, 16H). HRMS (ESI$^+$): calculated for C$_{29}$H$_{52}$N$_5$O$_9$ [M+H]$^+$ = 614.3687, found 614.3760.

Icosalide analogue 11: ^{1}H NMR (500 MHz, DMSO) δ 8.96 (d, J = 6.7 Hz, 1H), 7.48 (d, J = 9.2 Hz, 1H), 7.39 (dd, J = 12.0, 7.5 Hz, 2H), 7.00 (d, J = 9.6 Hz, 1H), 5.36 (t, J = 5.3 Hz, 1H), 4.96 (s, 1H), 4.85 (t, J = 5.5 Hz, 1H), 4.48 − 4.34 (m, 2H), 4.16 − 4.08 (m, 2H), 4.01 (s, 1H), 3.81 − 3.75 (m, 1H), 3.61 (dd, J = 10.7, 5.4 Hz, 2H), 2.58 (dd, J = 14.3, 3.7 Hz, 1H), 2.32 (s, 0H), 2.05 (dd, J = 12.7, 5.4 Hz, 1H), 1.81 − 1.75 (m, 1H), 1.70 − 1.60 (m, 2H), 1.53 (dt, J = 23.1, 8.3 Hz, 6H), 1.37 (d, J = 11.1 Hz, 1H), 1.24 (d, J = 9.0 Hz, 15H), 1.19 (s, 5H), 1.12 (s, 4H), 0.91 (d, J = 6.0 Hz, 3H), 0.89 − 0.80 (m, 17H). HRMS (ESI$^+$): calculated for C$_{36}$H$_{66}$N$_5$O$_9$ [M+H]$^+$ = 712.4782, found 712.4846.

Icosalide analogue 12: ^{1}H NMR (500 MHz, DMSO) δ 8.12 (d, J = 7.9 Hz, 1H), 7.89 (d, J = 8.3 Hz, 1H), 7.83 − 7.72 (m, 4H), 4.92 (s, 2H), 4.27 (tt, J = 9.7, 5.2 Hz, 2H), 4.18 (td, J = 9.0, 5.1 Hz, 1H), 4.12 (q, J = 6.1 Hz, 1H), 3.57 (ddd, J = 28.5, 10.3, 5.5 Hz, 5H), 3.46 (dd, J = 10.5, 5.8 Hz, 1H), 3.22 − 3.15 (m, 1H), 3.11 − 3.02 (m, 1H), 2.37 − 2.24 (m, 2H), 2.29 (s, 2H), 1.61 − 1.41 (m, 5H), 0.89 − 0.79 (m, 13H). HRMS (ESI$^+$): calculated for C$_{24}$H$_{43}$N$_6$O$_8$ [M+H]$^+$ = 543.3064, found 543.3134.

Icosalide analogue 13: ^{1}H NMR (500 MHz, DMSO) δ 8.13 (dd, J = 19.3, 7.4 Hz, 2H), 7.96 (dd, J = 11.0, 8.1 Hz, 2H), 7.64 (d, J = 8.6 Hz, 1H), 7.43 (d, J = 8.8 Hz, 1H), 5.12 (t, J = 5.2 Hz, 1H), 4.80 (t, J = 5.5 Hz, 1H), 4.41 − 4.29 (m, 2H), 4.22 (dq, J = 14.3, 7.4 Hz, 2H), 4.13 (q, J = 5.9 Hz, 1H), 4.06 − 3.98 (m, 2H), 3.61 (dt, J = 10.9, 5.7 Hz, 1H), 3.56 (q, J = 5.3 Hz, 2H), 3.49 (d, J = 5.6 Hz, 1H), 3.27 (dd, J = 10.8, 5.5 Hz, 1H), 2.31 (dd, J = 15.3, 6.2 Hz, 1H), 2.27 (dd, J = 7.3, 3.9 Hz, 3H), 1.84 (s, 3H), 1.59 (d, J

= 8.4 Hz, 3H), 1.45 (dq, *J* = 20.7, 7.7 Hz, 4H), 1.23 (s, 2H), 1.19 (s, 18H), 0.91 − 0.81 (m, 16H), 0.82 (d, *J* = 6.3 Hz, 4H). HRMS (ESI$^+$): calculated for $C_{36}H_{67}N_6O_8$ [M+H]$^+$ = 711.4942, found 711.4993.

4.4.7. Chemicals and media

Nutrient broth, nutrient agar (NA), dimethyl sulfoxide (DMSO), streptomycin sulphate (Hi Media, Mumbai, India), Resazurin (Sigma Aldrich, India). All Icosalide compounds were dissolved in dimethyl sulfoxide (DMSO) and two-fold dilutions (50.0, 12.0, 6.0, 3.0, 1.6, 0.8, 0.4, 0.2, 0.1 and 0 µg/mL) were prepared. *Bacillus thuringiensis* NCIM-5467 and *Paenibacillus dendritiformis* used in this study were cultured in MGY+M9 and LB media, respectively.

4.4.7.1. Time-kill test (time-kill curve)

The antibacterial activity of Icosalide and their analogues were determined using time -kill test method described by Clinical and Laboratory Standards Institute (CLSI).[47] A 50 µL *B. thuringenesis* suspension containing 0.1 OD was mixed in a tube with 50 µl of Icosalide compounds containing 50 µg/ml concentration then the mixture was incubated at 37 °C for 1 h. The standard antibiotic streptomycin was used as a positive control and a tube containing no compound was kept as negative control. The growth inhibition of *B. thuringenesis* was calculated relatively to the growth control by using agar plate count method and percentage inhibition was determined by calculating CFU count (CFU/mL).

4.4.7.2. Antibacterial activity of Icosalide analogues by Dilution method[48]

A 96-well microtiter plate was used for the antimicrobial assay against *Bacillus thuringiensis* and *Paenibacillus dendritiformis*.[33] Briefly, 96 well microtiter plate was filled with 100 µL of MGY+M9 and LB medium used for the growth of *B. thuringiensis* and *P. dendritiformis*, respectively. A 100 µL of Icosalide (1 mg/mL) in DMSO was added into the first well containing 100 µL of respective medium. From this mixture, 100 µL was serially diluted to get the minimum concentration (0.4 µg/mL). Then 5 µL of overnight grown bacterial culture (0.1 OD600) was added, and plates were incubated at 90 rpm, 30 °C, for 18 hrs. After incubation period, the optical density (OD) was measured at 600 nm using multimode microplate reader (Bio-Rad, USA). The MIC of the compound was calculated using standard formula (Growth inhibition (%) = 100-At / Ac × 100

4.4.7.3. Resazurin Assay

To determine the MIC endpoint, the resazurin was used as a growth indicator to differentiate the bacterial growth and inhibition. A 10 µL of resazurin containing 2 mg/mL concentration was added into

each well in dark condition and incubated in dark for 2 h results in the color change to violet from pink indicated dead cells.

4.4.7.4. Swarming assay

Novel Icosalide analogues were tested in a swarming assay against *B. thuringiensis* and *P. dendritiformis* (Dose et al., 2018). As previously mentioned, *B. thuringiensis and P. dendritiformis* were grown for 18 hours in a MGY and LB media, and a 0.4 OD600 set. A 0.7% agar plate with 10 µL of culture was pipetted in the centre, and it was incubated at 30 °C for 48 hours. At the end of the incubation, the agar plates were photographed from a fixed height and the swarming area was calculated using zone sale (Hi Media, India).

4.4.7.5. Drop-collapsing assay

The drop-collapsing assay was used to determine whether surfactants may destabilise liquid droplets (Jain et al. 1991). A single colony of *B. thuringiensis* cells was isolated and resuspended in a 10 µL water droplet. A 10 µL Icosalide droplet was placed on a hydrophobic surface with a 10 µL water droplet on top (Parafilm 'M' Laboratory). Crystal violet was added to the droplet (0.0025%) to help visualise the droplet crumbling. It had no effect on the droplet's form. Crystal violet, water, and *B. thuringiensis* were used to maintain the control.

4.4.7.6. Antitubercular activity of Icosalide analogues against active state of Mycobacterium tuberculosis H37Ra

Mycobacterium tuberculosis (ATCC 25177) H37 Ra RFP culture was grown in Dubos medium containing 10% glycerol with antibiotics hygromycin (50 µg/mL). Once OD600 reached 1 then 1% of the culture was inoculated in Dubos medium and aliquot in 96 black well plates as described in the earlier protocol. Novel red fluorescence protein based microplate assay for drug screening against dormant Mycobacterium tuberculosis by using paraffin.[42] The 2 fold serially dilution of Icosalide **1a** and its analogues were added in plate to reach final concentrations of 100, 50, 25, 12.5, 3.125, 1.5625, and 0.781 µg/mL for aerobic condition. 80 µL Paraffin oil was added in each well and incubated for 8 days. After incubation fluorescence was read at 587/610 nm using a multimode plate reader (Model Spectramax M5e, Molecular Devices, USA). Rifampicin and Isoniazid used as standard antitubercular drug. The data shown are representative of three independent experiments.

4.4.7.7. **Anticancer activity of Icosalide and its analogues against HeLa and Thp1 cell lines**

The anticancer activity was determined by MTT cell sensitivity assays.[43] Briefly, HeLa, Thp1 cells were seeded at 1 x 105/mL density in 96-well plate. An untreated group was kept as a positive control. Icosalide and their analogues were added at following concentrations (100, 50, 25, 12.5, and 6.25 µg/mL) in each triplicate well. After 48 h of addition, MTT solution (5 mg/mL) was added to each well, and the cells were kept for another 4 h at 37°C in 5% CO_2 incubator. The formazan crystals formed were dissolved by addition of SDS-DMF. After 15 mins of incubation, the amount of color formazan was determined by measuring optical density (OD) at 570 nm using a multimode plate reader.

The percentage viability was calculated as:

% Viability = (OD of treated Cells-OD of control/ OD of Control-OD of blank) x 100

4.4.8. **Analytical HPLC of peptides**- The purity of all the peptides (except **4** and **5**, which, due to their high lipophilicity, could not be eluted from the column) was determined by analytical HPLC using YMC Pack ODS-A-HG C18 column with the dimensions S-10 µm, 12 nm, 250 mm * 4.6 mm I.D., on Waters HPLC 2545 Quaternary Gradient module with 2489 UV/Visible detector. A flow rate of 1 mL/min was used for the analytical run.

Table 4.10. Analytical HPLC methods and retention times for the purified peptides, (ACN-Acetonitrile).

Peptide	HPLC Gradient	HPLC Chromatogram
Icosalide 1a	70% to 90% ACN in 20 min	
2	60% to 90% ACN in 20 min	
3	60% to 90% ACN in 20 min	
6	60% to 90% ACN in 20 min	
7	50% to 90% ACN in 20 min	

8	40% to 90% ACN in 20 min	
9	60% to 90% ACN in 18 min	
10	40% to 90% ACN in 20 min	
11	60% to 90% ACN in 20 min	
12	20% to 90% ACN in 20 min	
13	60% to 90% ACN in 20 min	
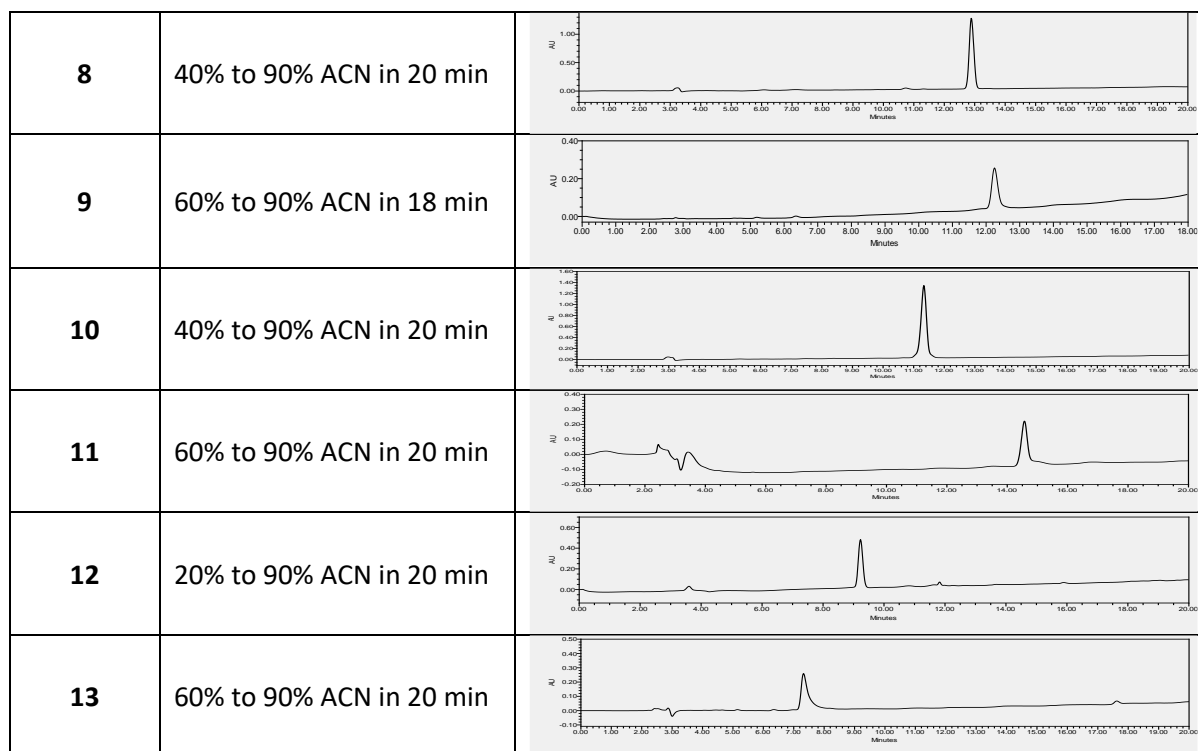
Table 4.11. HRMS Data of peptides **1a** to **13**.
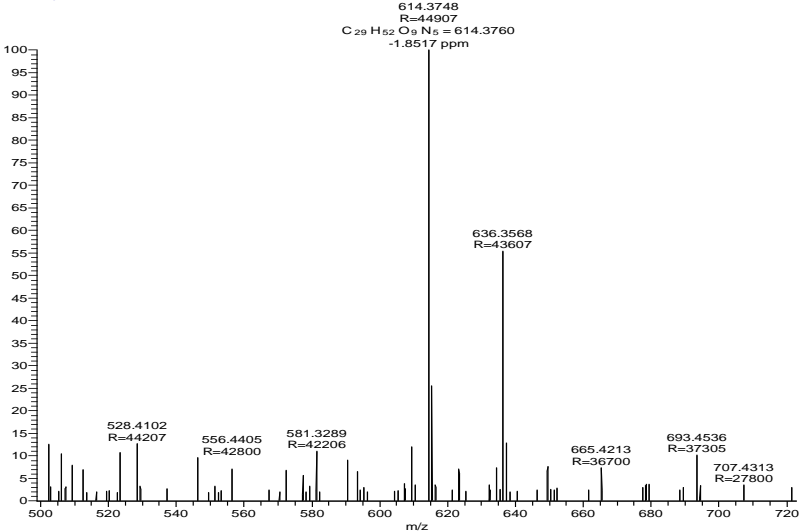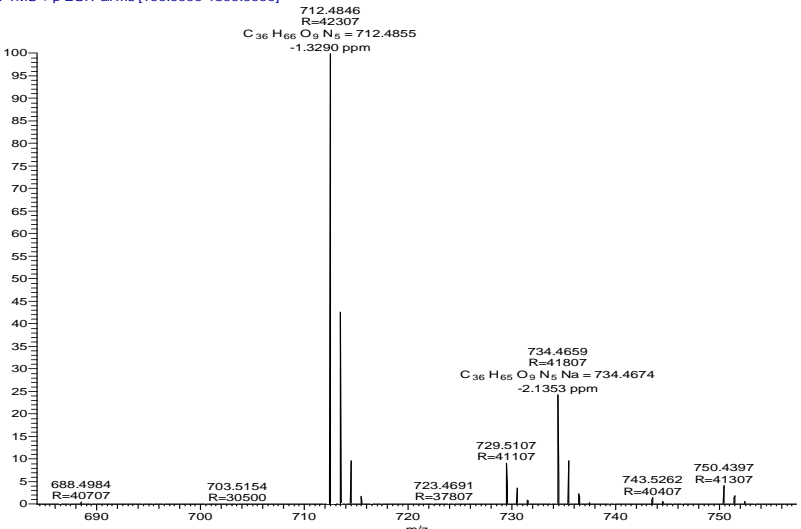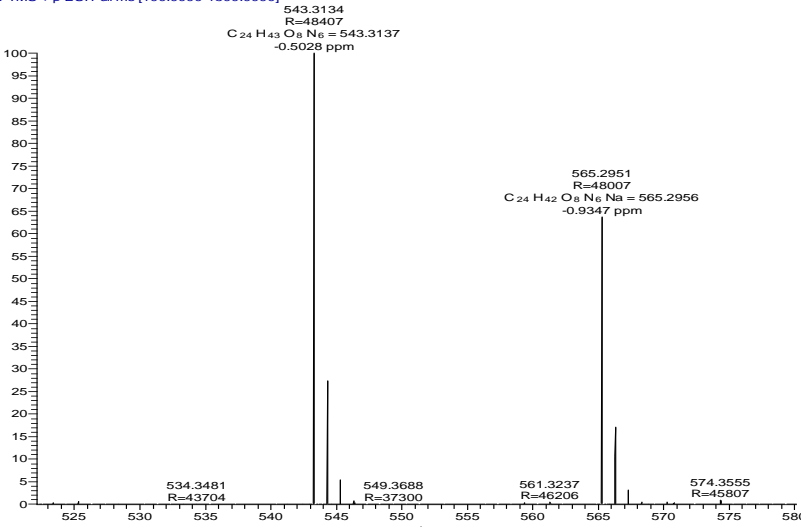
Peptide	Exact Mass	HRMS (M+1)	HRMS Data
Icosalide **1a**	712	713	

Icosalide **1a'**	712	713	
2	600	601	
3	656	657	

4	768	769	
5	824	825	
6	628	629	

ICO-1012 #602 RT: 3.27 AV: 1 NL: 3.13E8
T: FTMS + p ESI Full ms [100.0000-1500.0000]

769.5323
R=40807
$C_{40} H_{73} O_{10} N_4$ = 769.5321
0.2168 ppm

791.5113
R=40407

785.9508
R=47500

717.5359
R=38906
$C_{37} H_{73} O_9 N_4$ = 717.5372
-1.8362 ppm

751.5195
R=39602
$C_{40} H_{71} O_9 N_4$ = 751.5216
-2.7756 ppm

781.0170
R=39306

807.4855
R=39707

800.5718
R=39402

814.5877
R=39607

828.6038
R=38807

842.6191
R=37507

853.4826
R=37907

865.5479
R=28900

876.4910
R=33806

ICO-1214 #846 RT: 4.73 AV: 1 NL: 3.24E7
T: FTMS + p ESI Full ms [100.0000-1500.0000]

847.5760
R=39007
$C_{44} H_{80} O_{10} N_4$ Na = 847.5767
-0.7987 ppm

825.5946
R=39307
$C_{44} H_{81} O_{10} N_4$ = 825.5947
-0.1412 ppm

863.5495
R=38607

791.5137
R=39207
$C_{40} H_{72} O_{10} N_4$ Na = 791.5141
-0.4201 ppm

835.5139
R=32406

857.6381
R=33102

872.7695
R=29400

884.6675
R=28100

898.7854
R=30907

915.5637
R=35907

932.5544
R=35207

948.5269
R=27405

ICO-Isobutryl #266 RT: 1.56 AV: 1 NL: 8.16E8
T: FTMS + p ESI Full ms [100.0000-1500.0000]

629.3739
R=45407
$C_{30} H_{53} O_{10} N_4$ = 629.3756
-2.7310 ppm

646.3997
R=44707

451.2393
R=51006
$C_{18} H_{35} O_9 N_4$ = 451.2399
-1.1207 ppm

558.4196
R=47400

688.4465
R=42707

725.3557
R=38700

761.4653
R=37704

810.4493
R=31800

7	624	625	
8	641	642	
9	711	712	

ICO-Cyclopr_210317125154 #272 RT: 1.55 AV: 1 NL: 2.66E8
T: FTMS + p ESI Full ms [100.0000-1500.0000]
625.3436 R=45507 C₃₀H₄₉O₁₀N₄ = 625.3443 -1.2044 ppm; 647.3242 R=44607 C₃₀H₄₈O₁₀N₄Na = 647.3263 -3.2550 ppm; 642.3697 R=44807; 636.3278 R=44807; 656.3838 R=44007; 663.2975 R=44007; 670.4000 R=43007

ICO-BA1 #203 RT: 1.61 AV: 1 NL: 1.39E7
T: FTMS + p ESI Full ms [100.0000-1500.0000]
642.4059 R=44507 C₃₁H₅₆O₉N₅ = 642.4073 -2.1340 ppm; 624.3967 R=42507 C₃₁H₅₄O₈N₅ = 624.3967 0.0617 ppm; 664.3873 R=44007; 572.4326 R=41807; 590.4271 R=44407; 659.4318 R=43107; 680.3613 R=43807; 701.4805 R=42607; 715.4962 R=31505

ICO-AMD1 #257 RT: 1.73 AV: 1 NL: 3.16E6
T: FTMS + p ESI Full ms [100.0000-1500.0000]
712.4846 R=42307 C₃₆H₆₆O₉N₅ = 712.4855 -1.3290 ppm; 734.4663 R=41907 C₃₆H₆₅O₉N₅Na = 734.4674 -1.5536 ppm; 722.5049 R=31000; 729.5089 R=34404; 739.4449 R=27100; 743.5268 R=39507

217

10	613	614	ICO-BA2 #138 RT: 1.09 AV: 1 NL: 9.93E4 T: FTMS + p ESI Full ms [100.0000-1500.0000] 614.3748 R=44907 $C_{29} H_{52} O_9 N_5 = 614.3760$ -1.8517 ppm 636.3568 R=43607 528.4102 R=44207 556.4405 R=42800 581.3289 R=42206 665.4213 R=36700 693.4536 R=37305 707.4313 R=27800
11	711	712	ICO-AMD2 #308 RT: 2.39 AV: 1 NL: 2.81E6 T: FTMS + p ESI Full ms [100.0000-1500.0000] 712.4846 R=42307 $C_{36} H_{66} O_9 N_5 = 712.4855$ -1.3290 ppm 734.4659 R=41807 $C_{36} H_{65} O_9 N_5 Na = 734.4674$ -2.1353 ppm 688.4984 R=40707 703.5154 R=30500 723.4691 R=37807 729.5107 R=41107 743.5262 R=40407 750.4397 R=41307
12	542	543	ICO-BA3 #223 RT: 1.67 AV: 1 NL: 4.15E6 T: FTMS + p ESI Full ms [100.0000-1500.0000] 543.3134 R=48407 $C_{24} H_{43} O_8 N_6 = 543.3137$ -0.5028 ppm 565.2951 R=48007 $C_{24} H_{42} O_8 N_6 Na = 565.2956$ -0.9347 ppm 534.3481 R=43704 549.3688 R=37300 561.3237 R=46206 574.3555 R=45807

218

13	710	711	
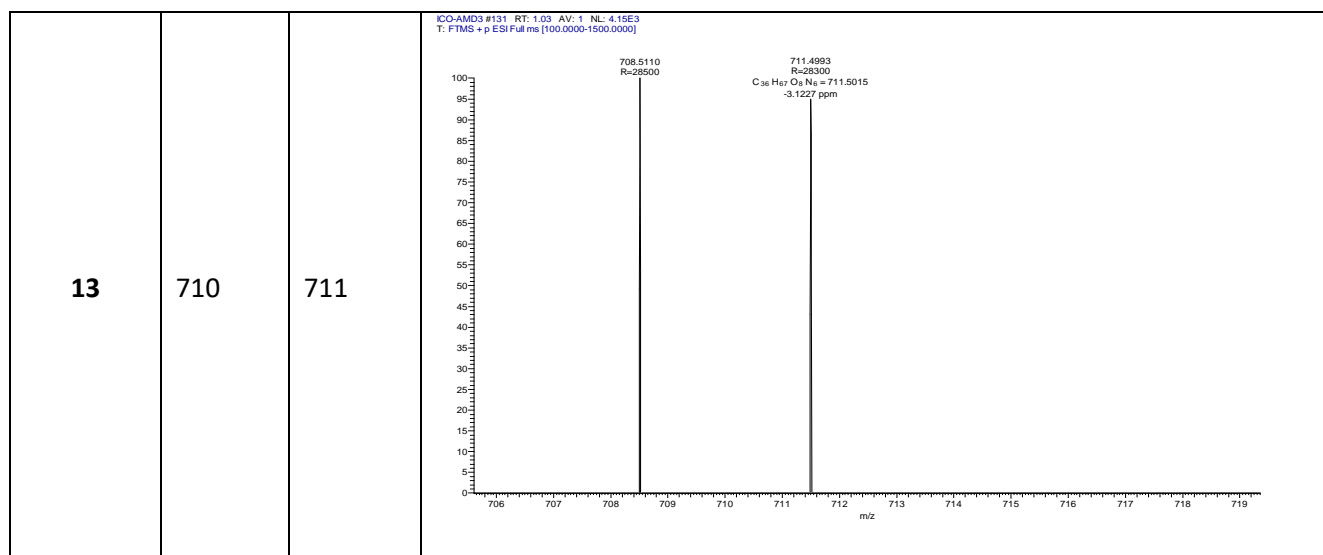
4.4.9. ^{1}H and ^{13}C NMR spectra of Icosalide analogues and building blocks

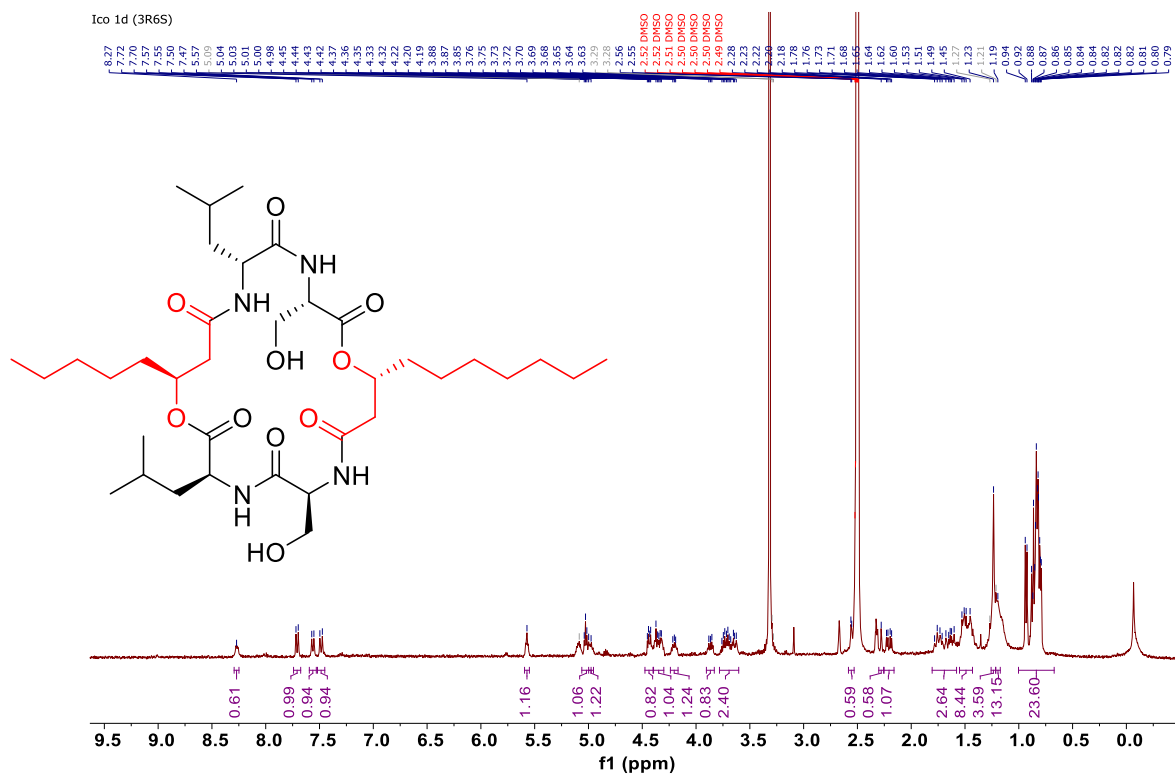^{1}H NMR of Icosalide **1a** on 500 MHz at 298 K in DMSO-d_6.
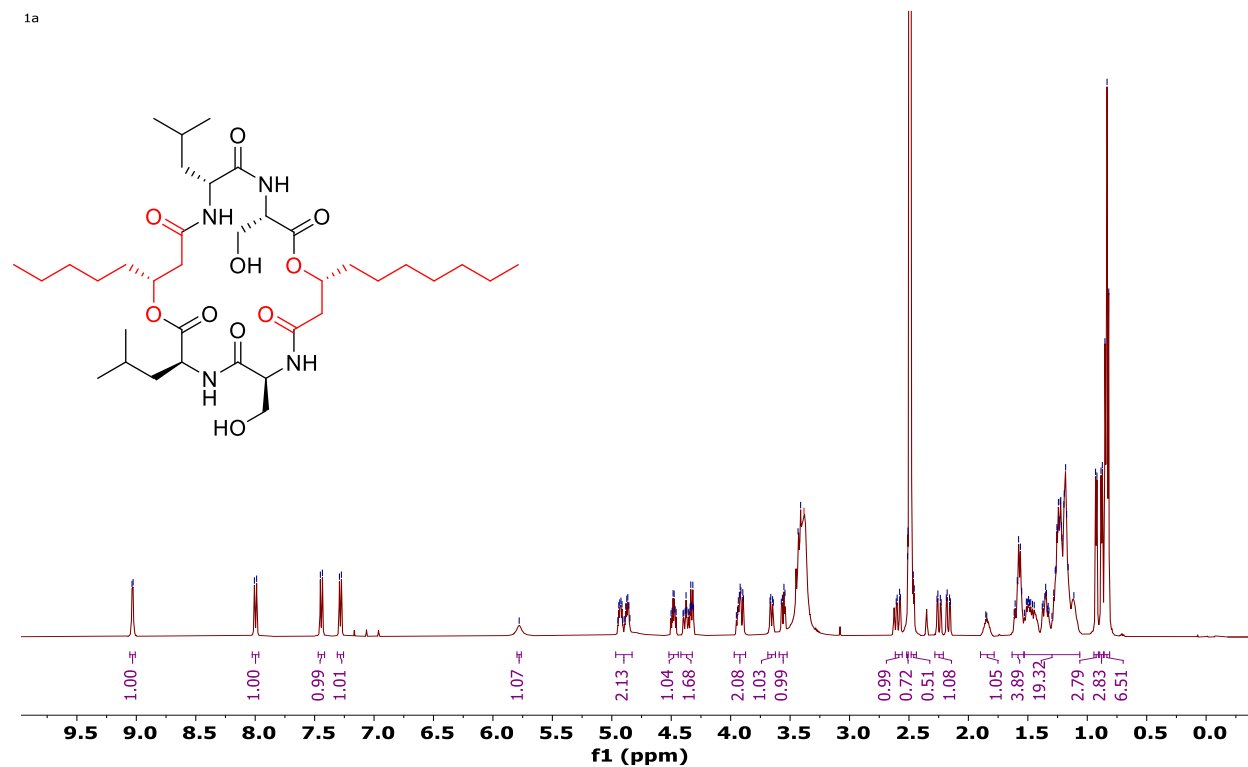
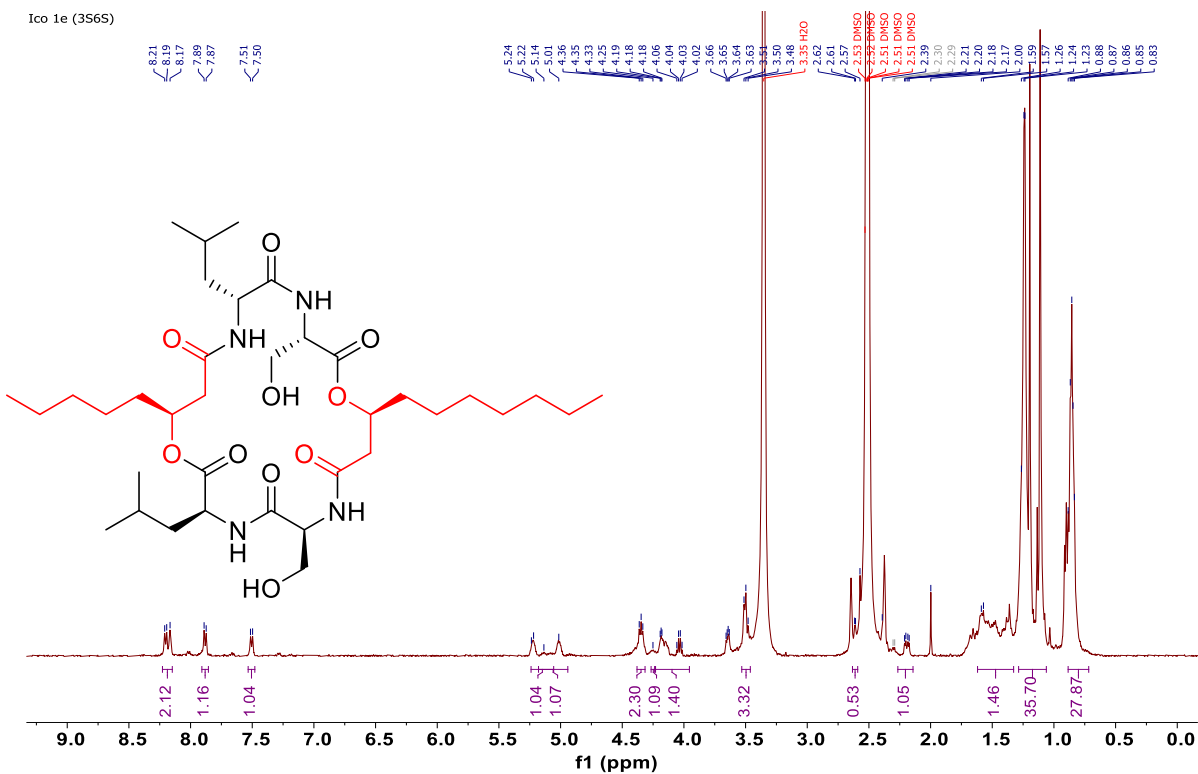^{1}H NMR of Icosalide **1a'** on 700 MHz at 298 K in DMSO-*d*6.
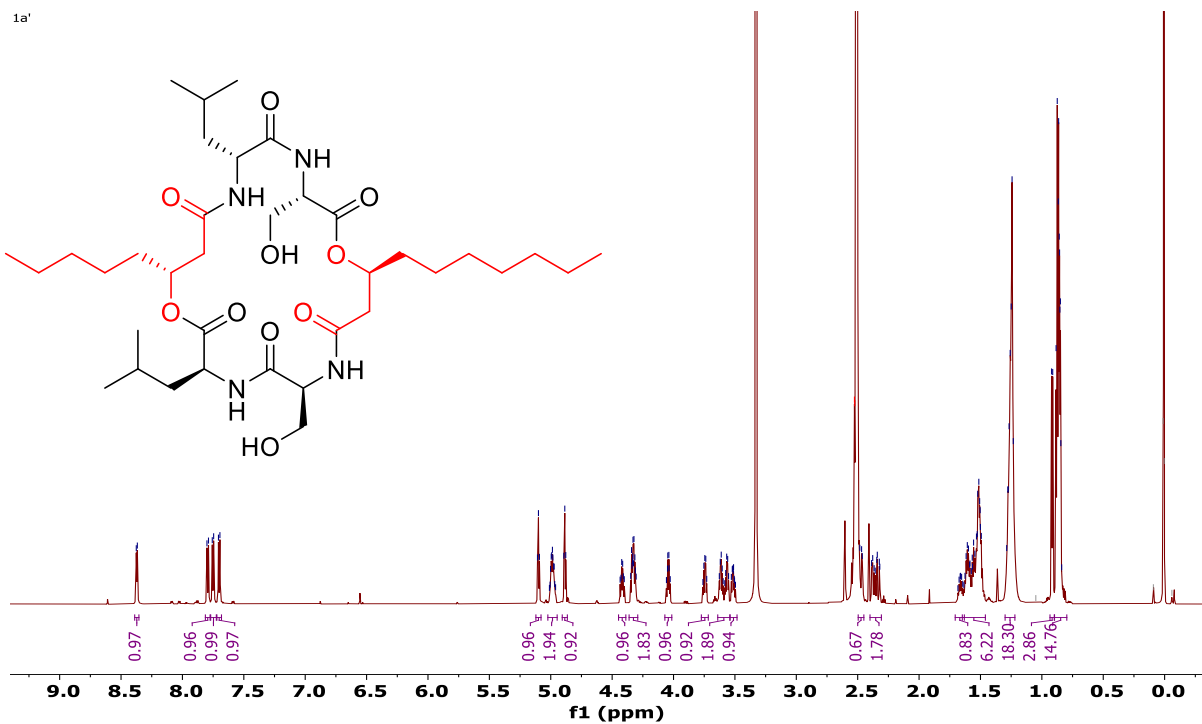
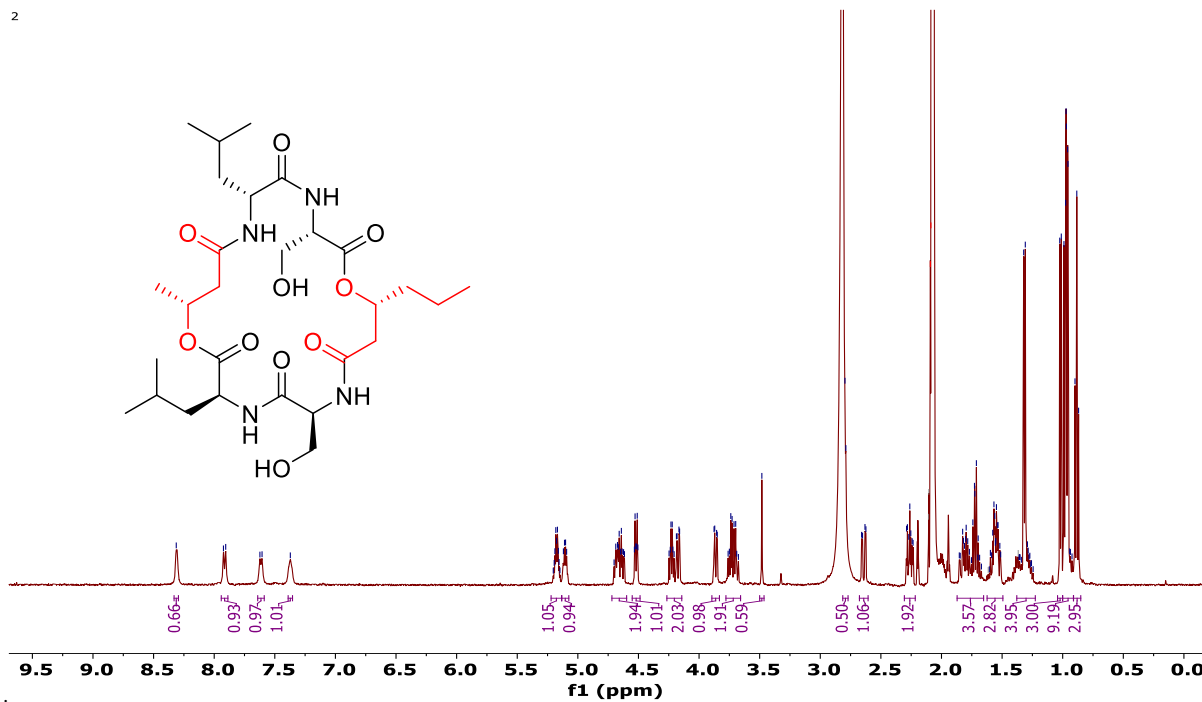^{1}H NMR of Icosalide **1a''** on 500 MHz at 298 K in DMSO-*d*6.

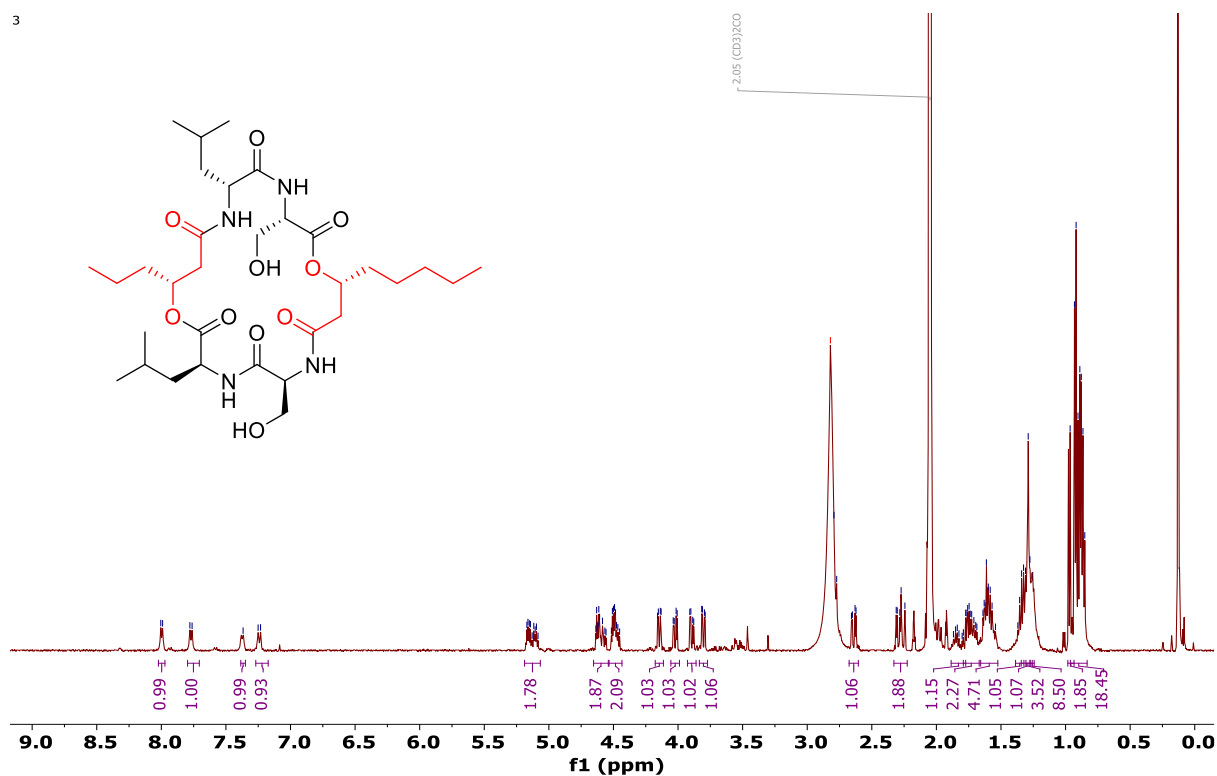¹H NMR of Icosalide **1a'''** on 500 MHz at 298 K in DMSO-*d*₆.

¹H NMR of compound **2** on 500 MHz at 298 K in Acetone-*d*₆

^{1}H NMR of compound **3** on 500 MHz at 298 K in Acetone-*d₆.*
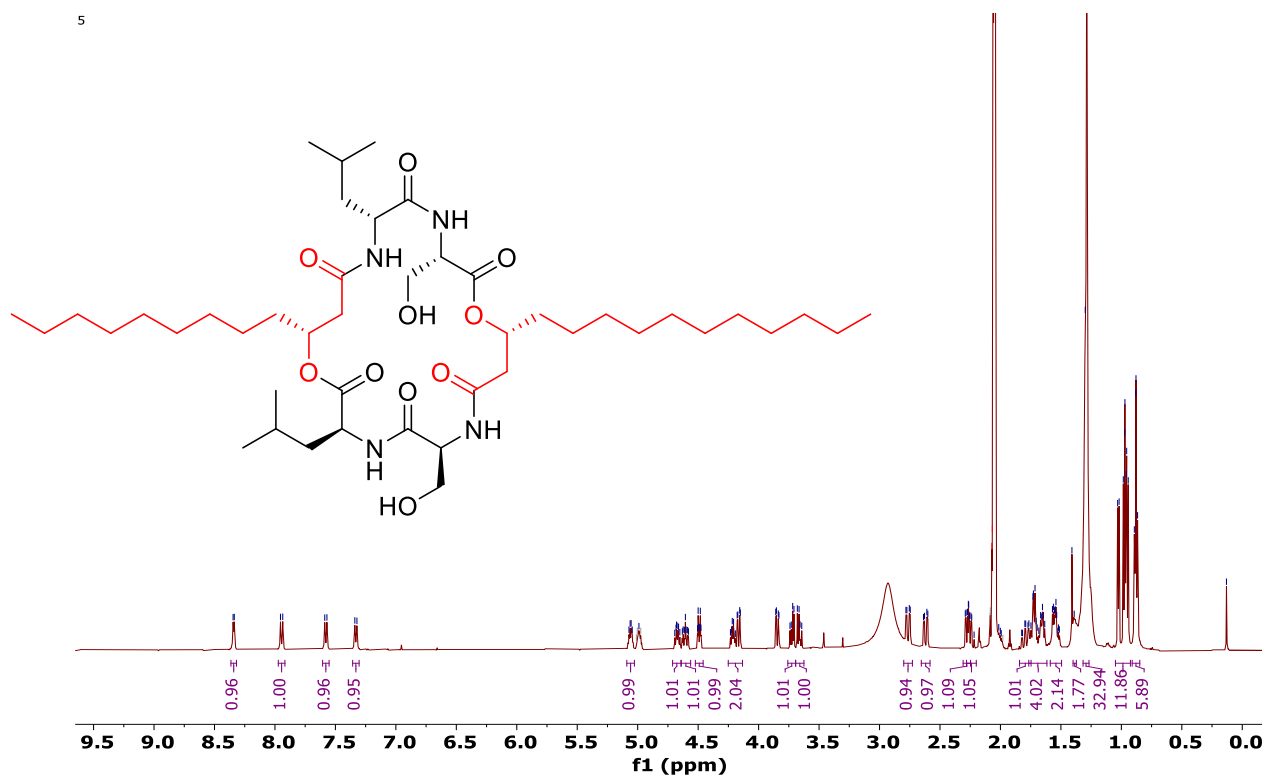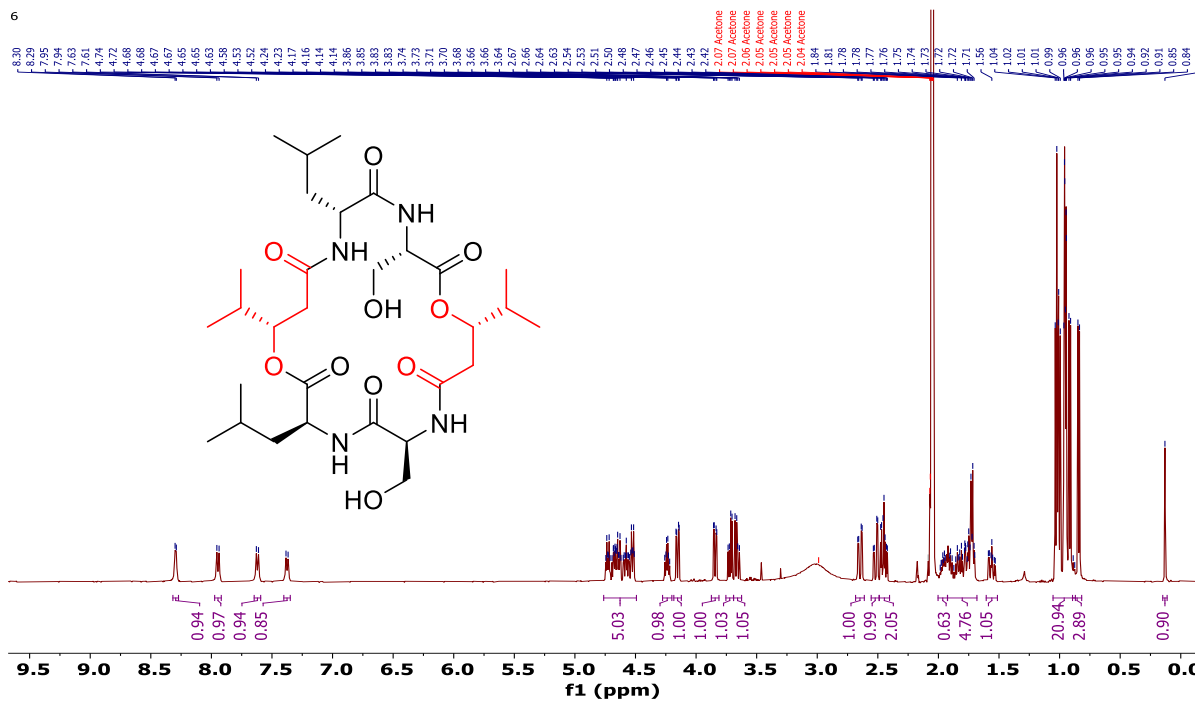

^{1}H NMR of compound **4** on 500 MHz at 298 K in Acetone-*d₆.*
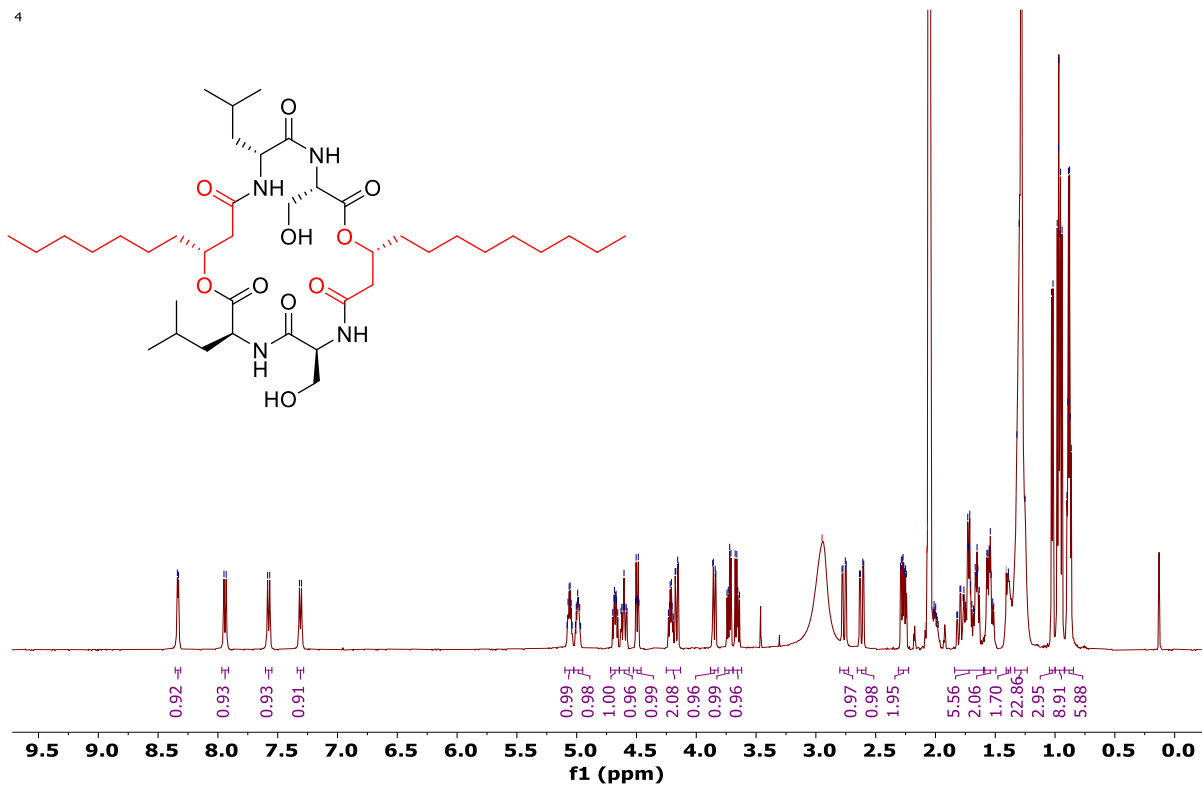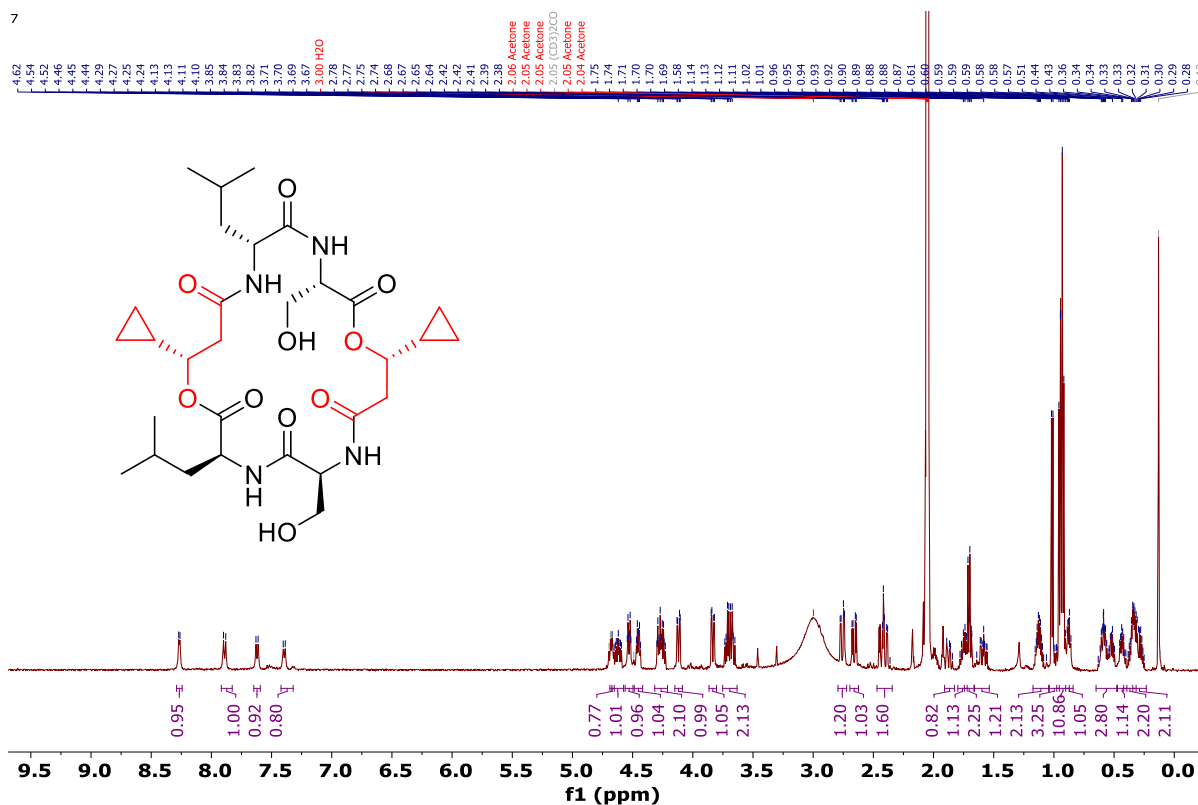
^{1}H NMR of compound **5** on 500 MHz at 298 K in Acetone-d_6.

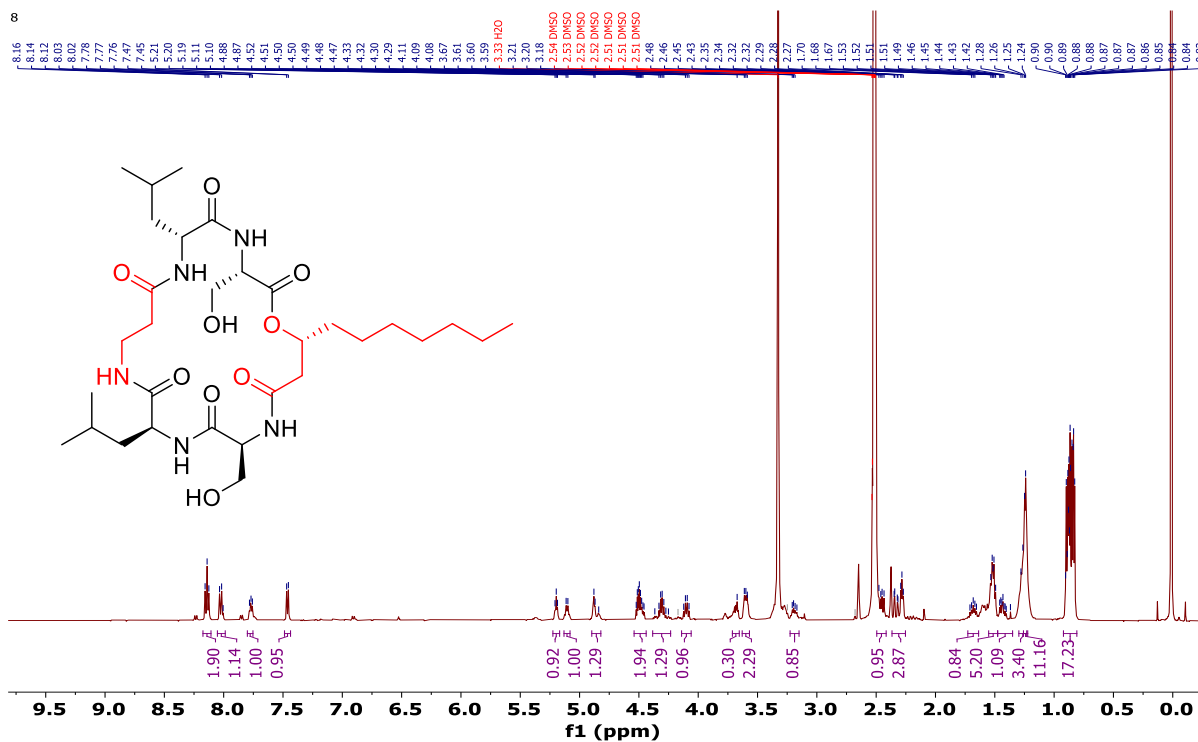^{1}H NMR of compound **6** on 500 MHz at 298 K in Acetone-d_6.

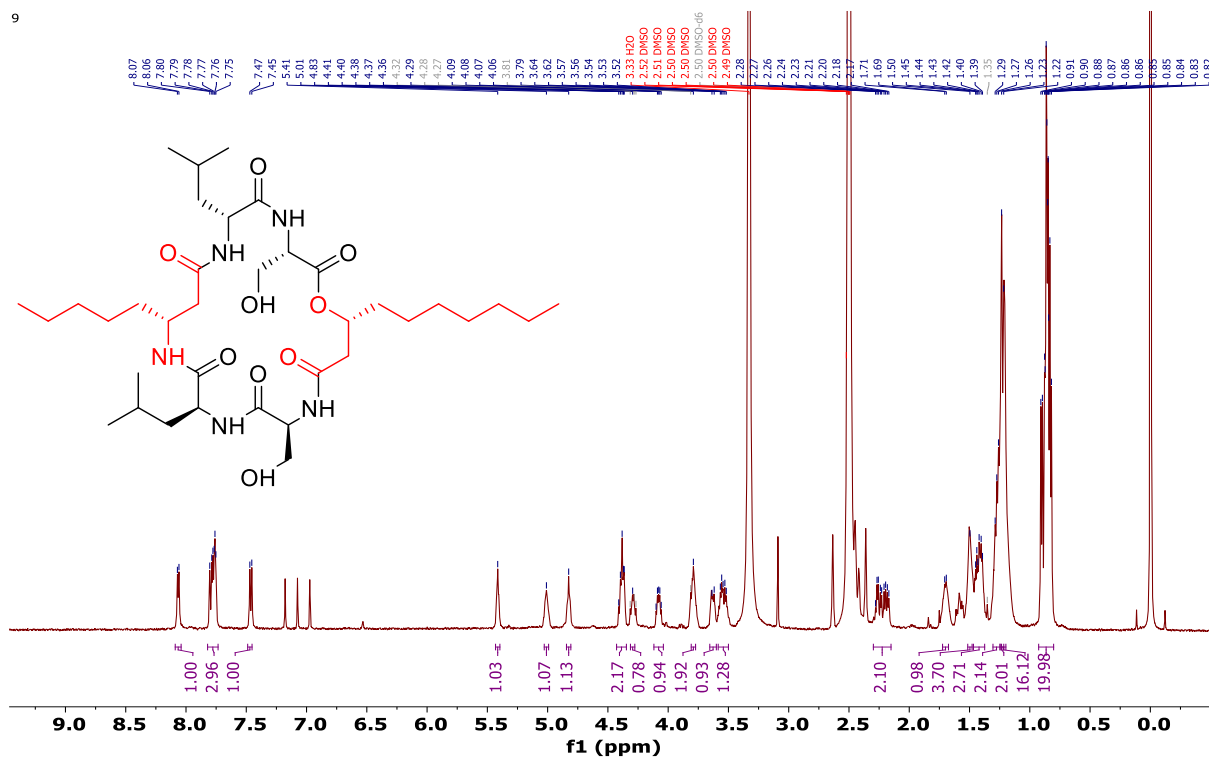^{1}H NMR of compound **7** on 500 MHz at 298 K in Acetone-d_6.

^{1}H NMR of compound **8** on 500 MHz at 298 K in DMSO-d_6.

^{1}H NMR of compound **9** on 500 MHz at 298 K in DMSO-*d*[6].

^{1}H NMR of compound **10** on 500 MHz at 298 K in DMSO-*d*[6].

¹H NMR of compound **11** on 500 MHz at 298 K in DMSO-*d₆*.

¹H NMR of compound **12** on 500 MHz at 298 K in DMSO-*d₆*.
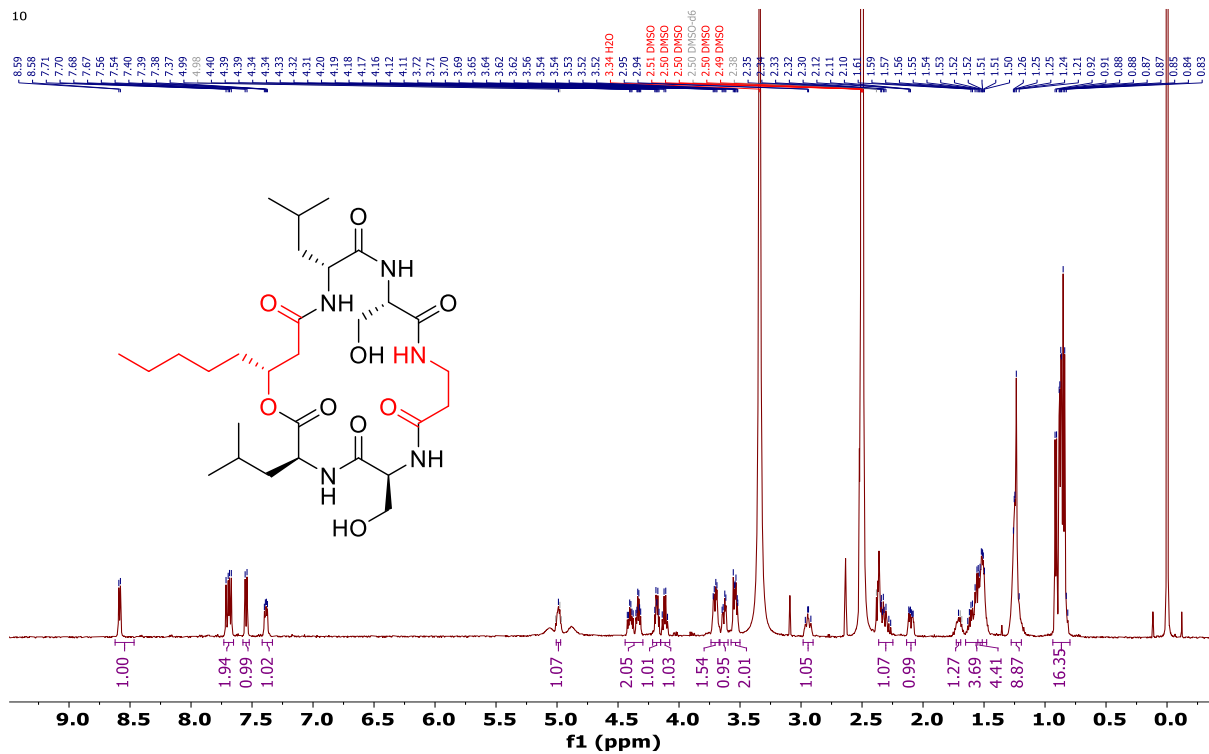
^{1}H NMR of compound **13** on 500 MHz at 298 K in DMSO-d_6.
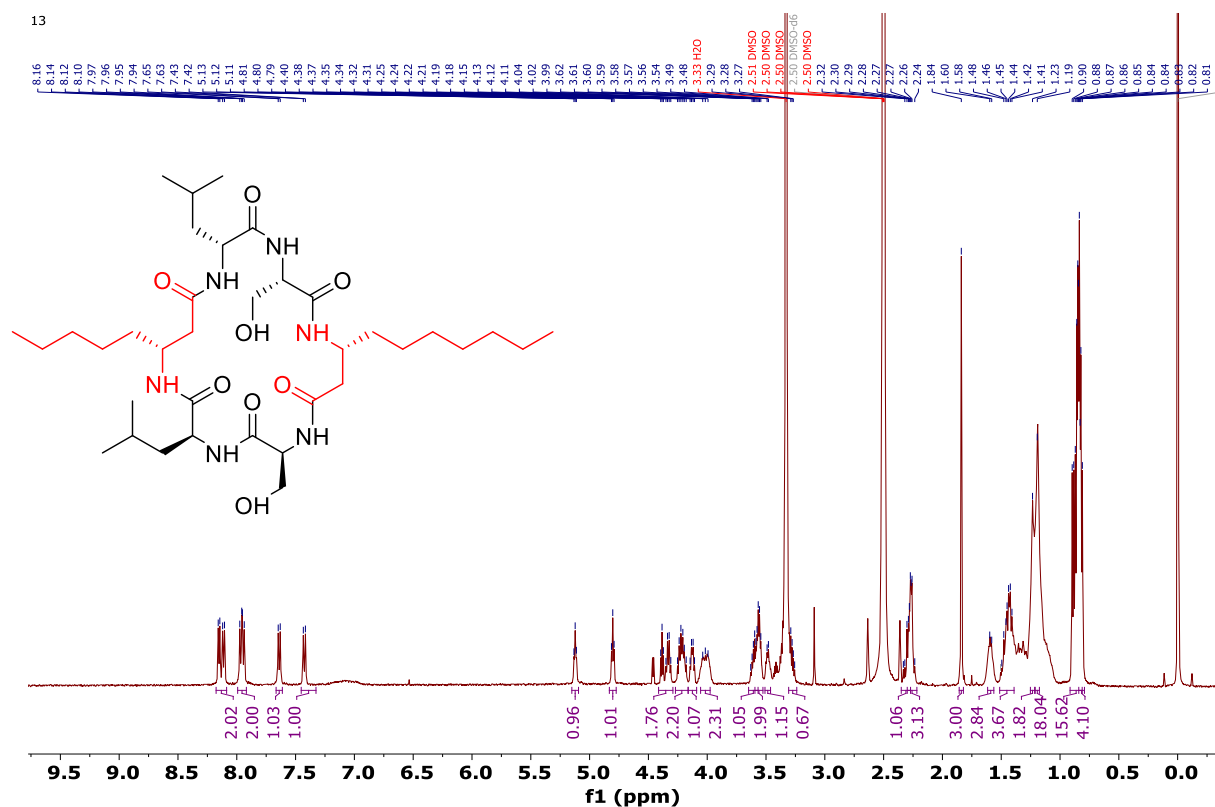
^{1}H NMR of compound ***R*-chiral auxillary (15)** on 500 MHz at 298 K in CDCl$_3$.
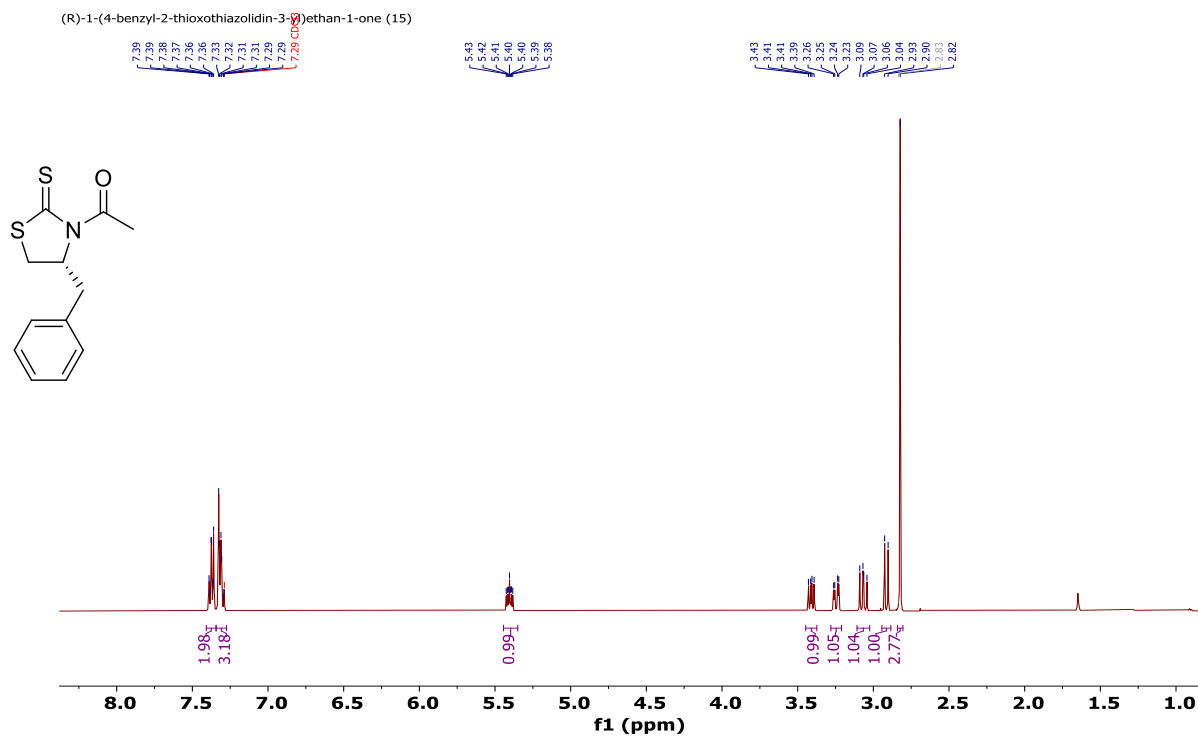
^{13}C NMR of compound ***R*-chiral auxillary (15)** on 125 MHz at 298 K in CDCl$_3$.

(R)-1-(4-benzyl-2-thioxothiazolidin-3-yl)ethan-1-one (15)
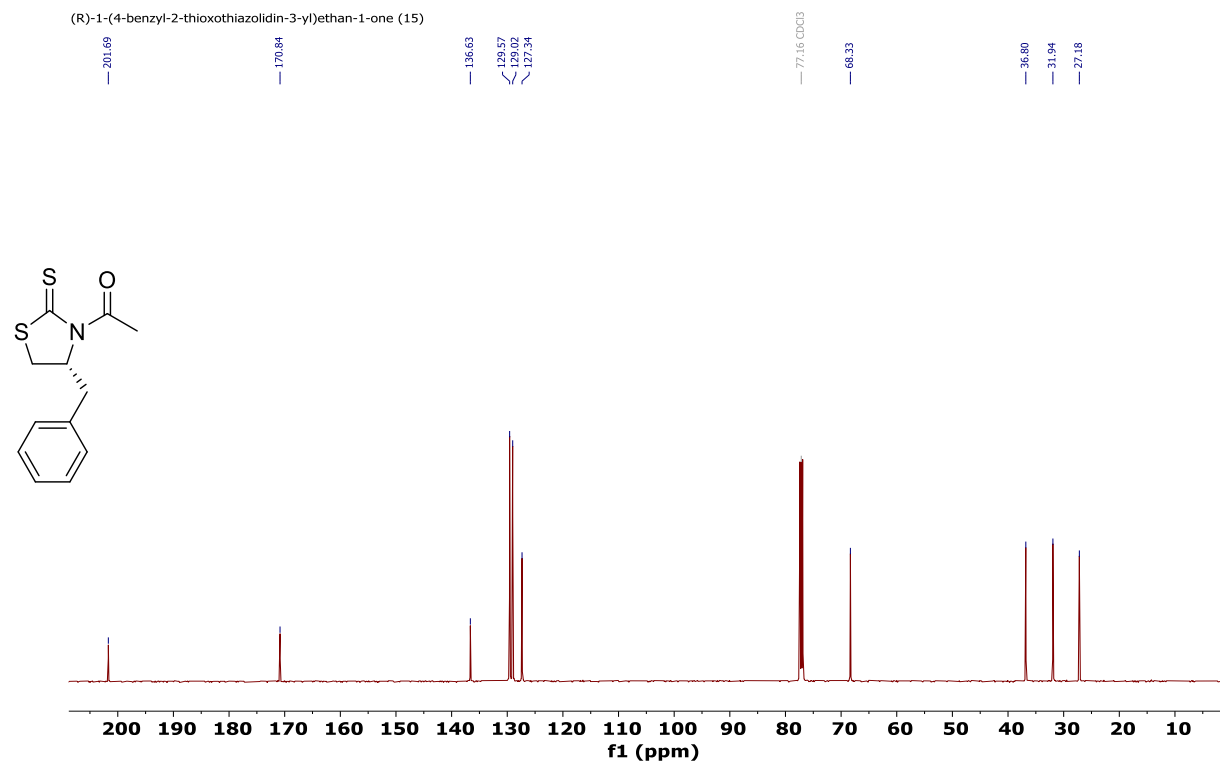
^{1}H NMR of compound **16a** on 500 MHz at 298 K in CDCl$_3$.

(R)-1-((R)-4-benzyl-2-thioxothiazolidin-3-yl)-3-hydroxybutan-1-one (16a)
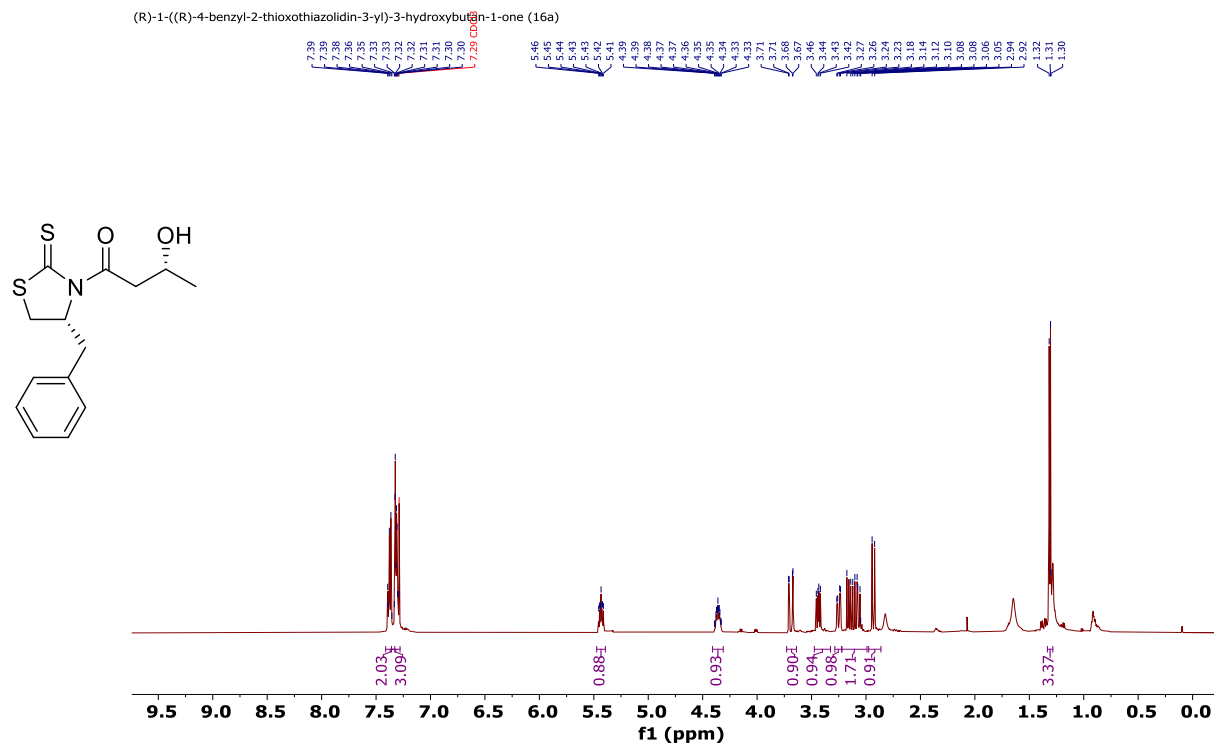
^{13}C NMR of compound **16a** on 125 MHz at 298 K in CDCl$_3$.

(R)-1-((R)-4-benzyl-2-thioxothiazolidin-3-yl)-3-hydroxybutan-1-one (16a)
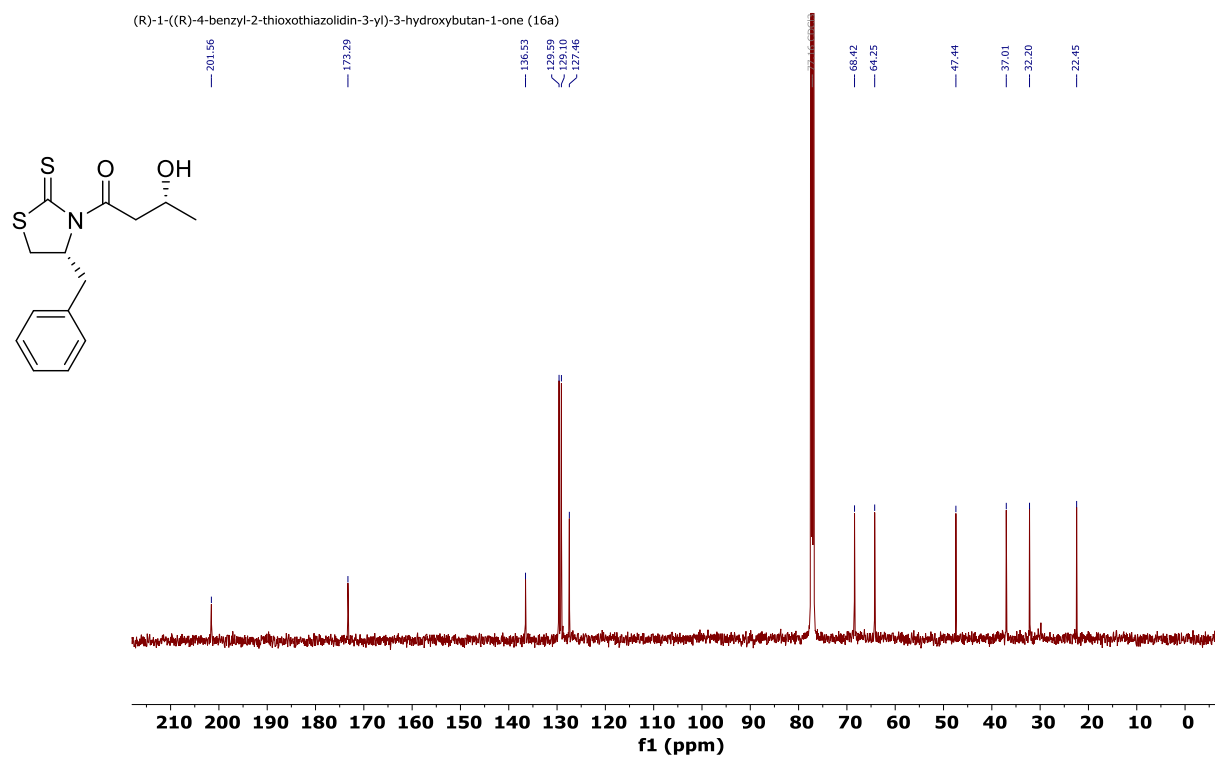
^{1}H NMR of compound **16b** on 500 MHz at 298 K in CDCl$_3$

(R)-1-((R)-4-benzyl-2-thioxothiazolidin-3-yl)-3-hydroxyhexan-1-one (16b)
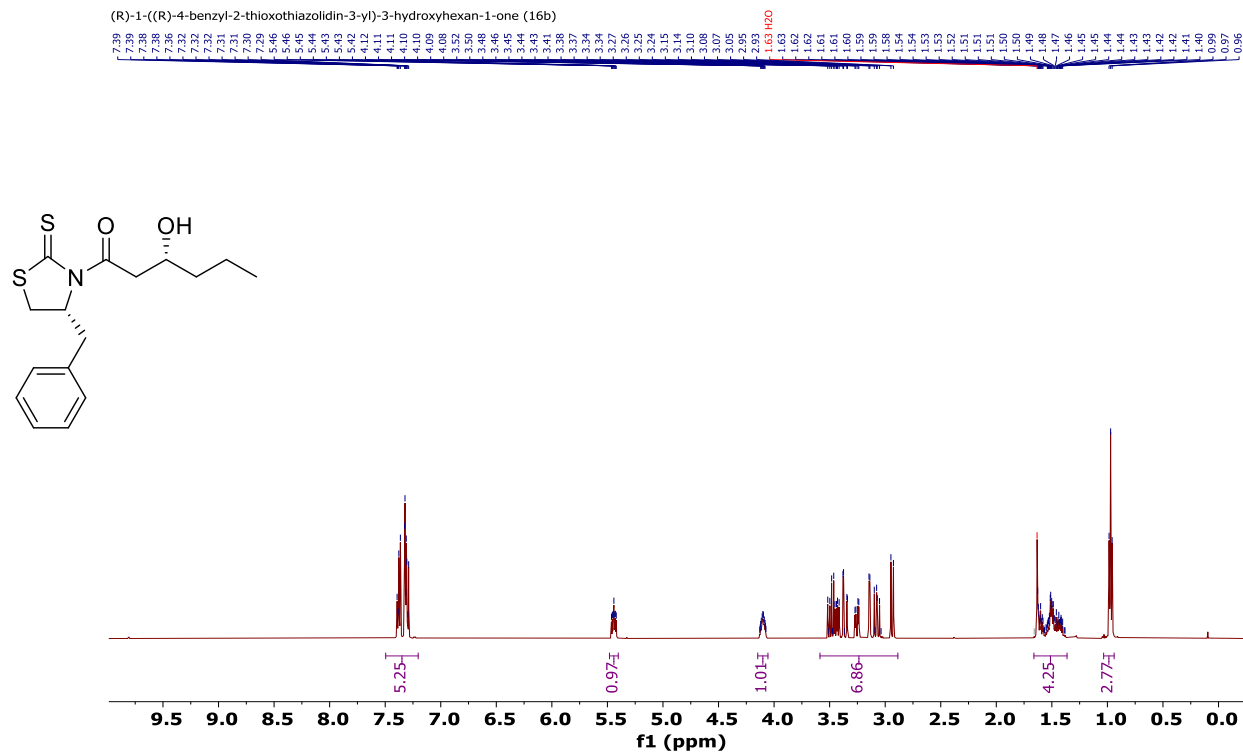
^{13}C NMR of compound **16b** on 125 MHz at 298 K in CDCl$_3$.

(R)-1-((R)-4-benzyl-2-thioxothiazolidin-3-yl)-3-hydroxyhexan-1-one (16b)
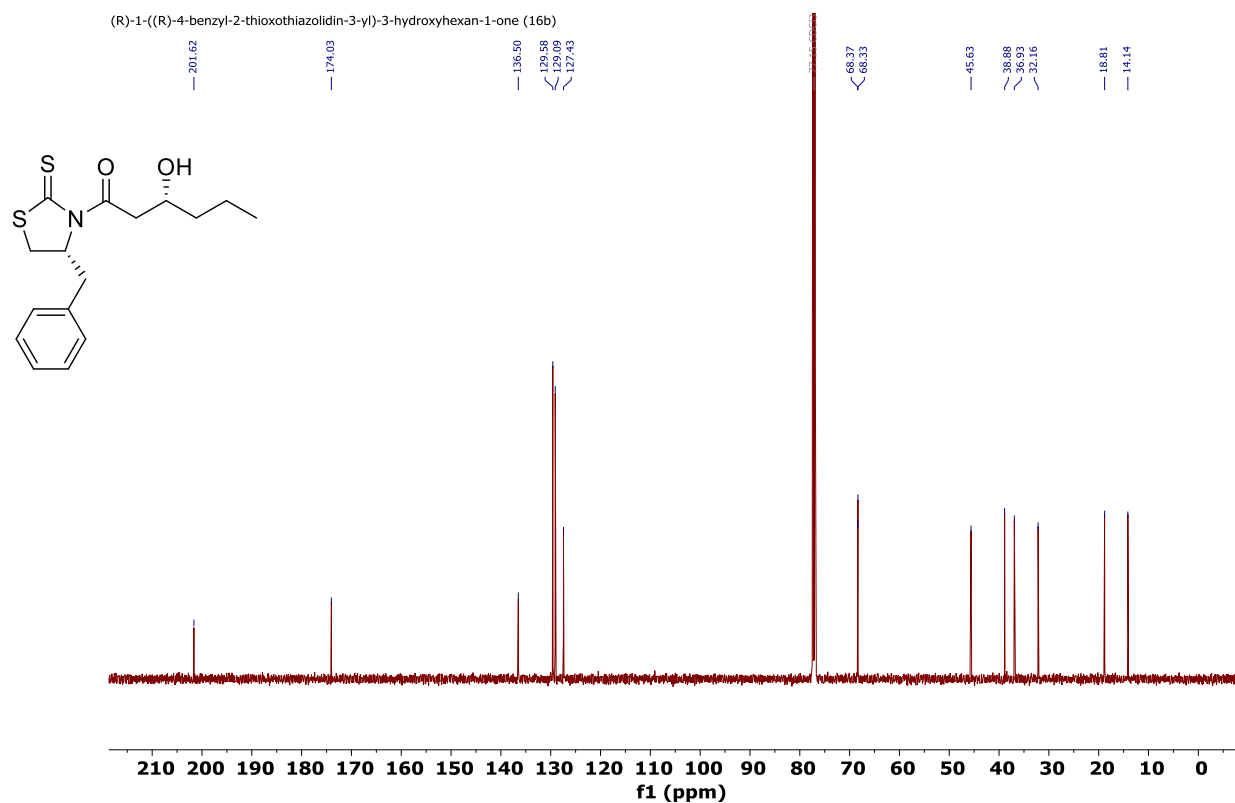
^{1}H NMR of compound **16c** on 400 MHz at 298 K in CDCl$_3$.

(R)-1-((R)-4-benzyl-2-thioxothiazolidin-3-yl)-3-hydroxyoctan-1-one (16c)

^{13}C NMR of compound **16c** on 100 MHz at 298 K in CDCl$_3$.

(R)-1-((R)-4-benzyl-2-thioxothiazolidin-3-yl)-3-hydroxyoctan-1-one (16c)

201.62
174.03
136.52
129.58
129.09
127.43
77.16 CDCl3
68.63
68.38
45.64
36.95
36.76
32.18
31.89
25.30
22.74
14.18

^{1}H NMR of compound **16d** on 400 MHz at 298 K in CDCl$_3$.

(R)-1-((R)-4-benzyl-2-thioxothiazolidin-3-yl)-3-hydroxydecan-1-one (16d)

^{1}H NMR of compound **16e** on 400 MHz at 298 K in CDCl$_3$

(R)-1-((R)-4-benzyl-2-thioxothiazolidin-3-yl)-3-hydroxydodecan-1-one (16e)

^{13}C NMR of compound **16e** on 100 MHz at 298 K in CDCl$_3$

(R)-1-((R)-4-benzyl-2-thioxothiazolidin-3-yl)-3-hydroxydodecan-1-one (16e)

^{1}H NMR of compound **16f** on 500 MHz at 298 K in CDCl$_3$.

(R)-1-((R)-4-benzyl-2-thioxothiazolidin-3-yl)-3-hydroxytetradecan-1-one (16f)
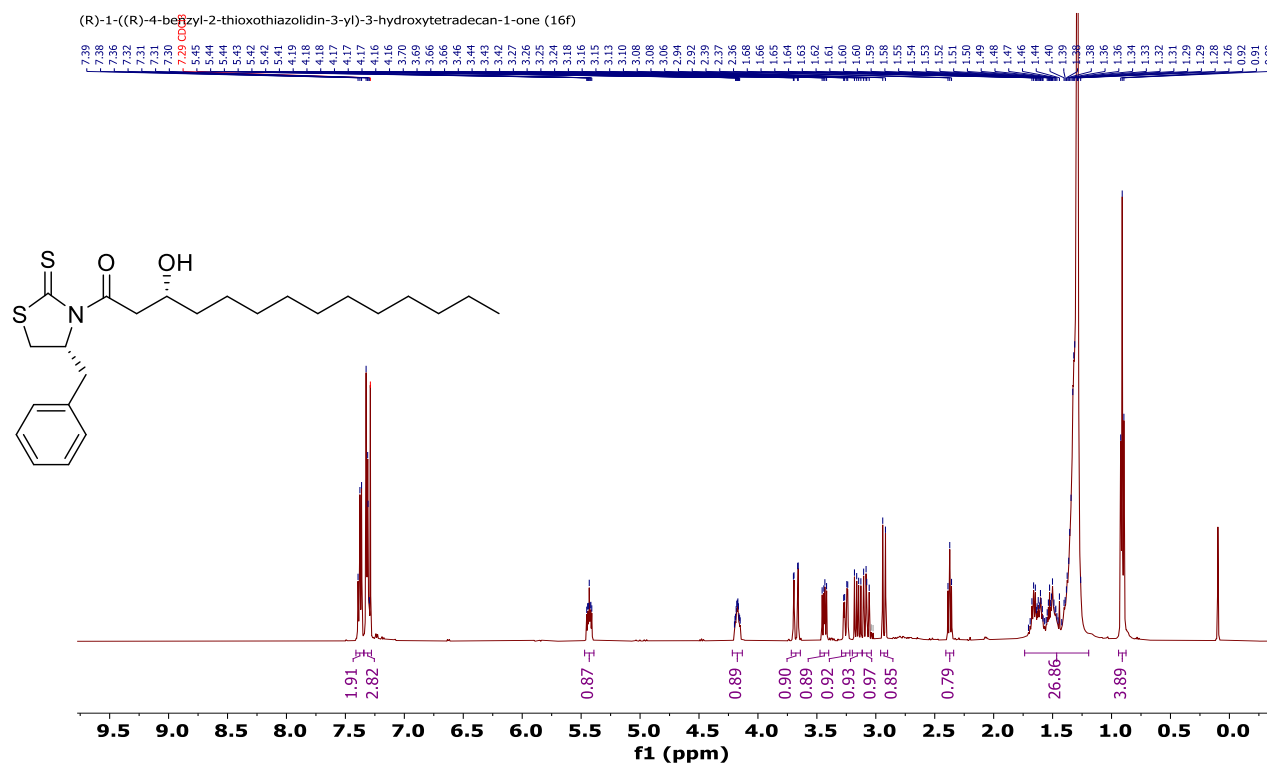
^{13}C NMR of compound **16f** on 125 MHz at 298 K in CDCl$_3$.

(R)-1-((R)-4-benzyl-2-thioxothiazolidin-3-yl)-3-hydroxytetradecan-1-one (16f)
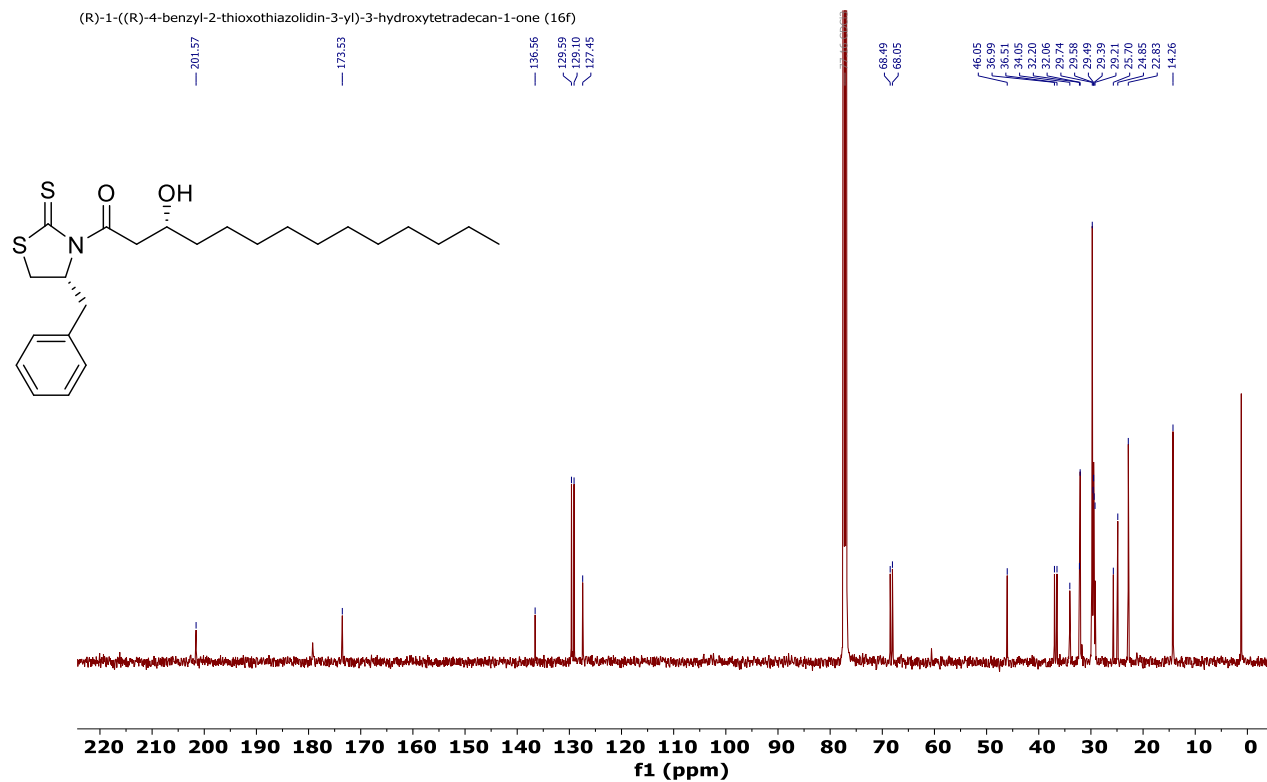
^{1}H NMR of compound **16g** on 700 MHz at 298 K in CDCl$_3$.

(R)-1-((R)-4-benzyl-2-thioxothiazolidin-3-yl)-3-hydroxy-4-methylpentan-1-one (16g)
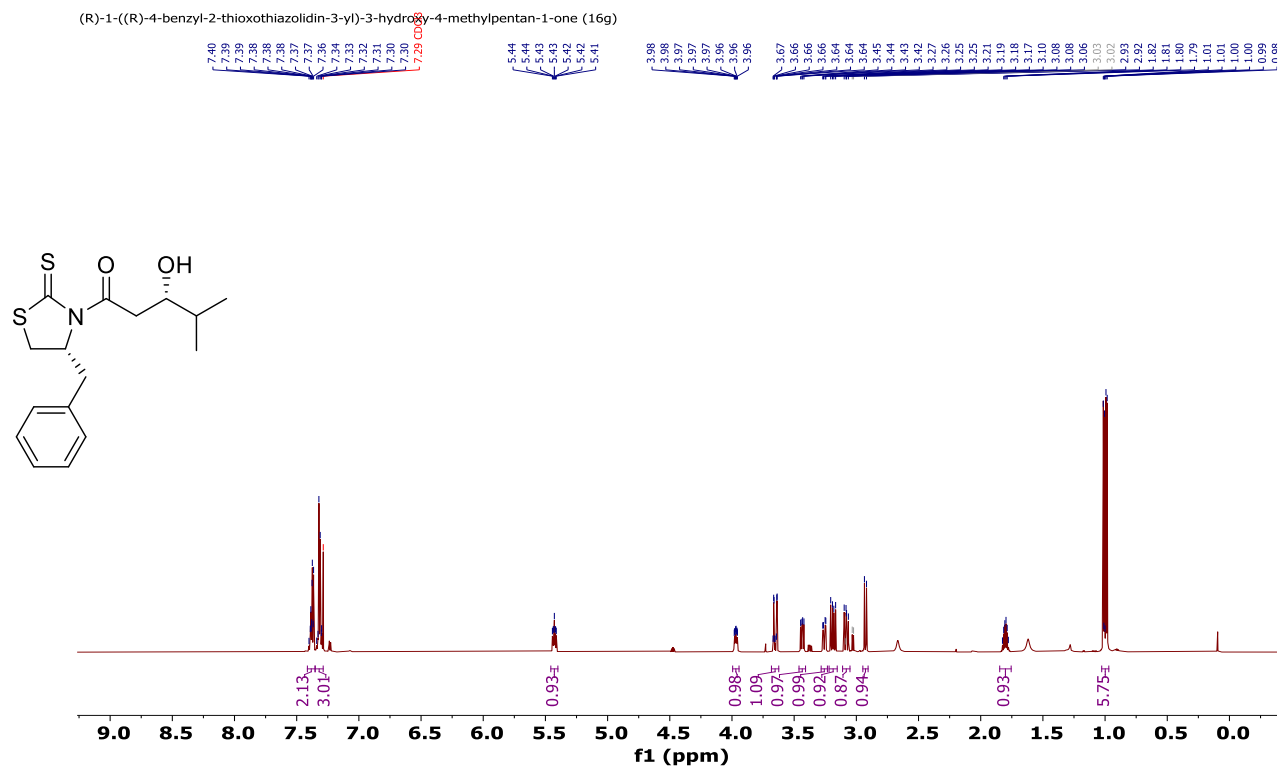
^{13}C NMR of compound **16g** on 175 MHz at 298 K in CDCl$_3$

(R)-1-((R)-4-benzyl-2-thioxothiazolidin-3-yl)-3-hydroxy-4-methylpentan-1-one (16g)
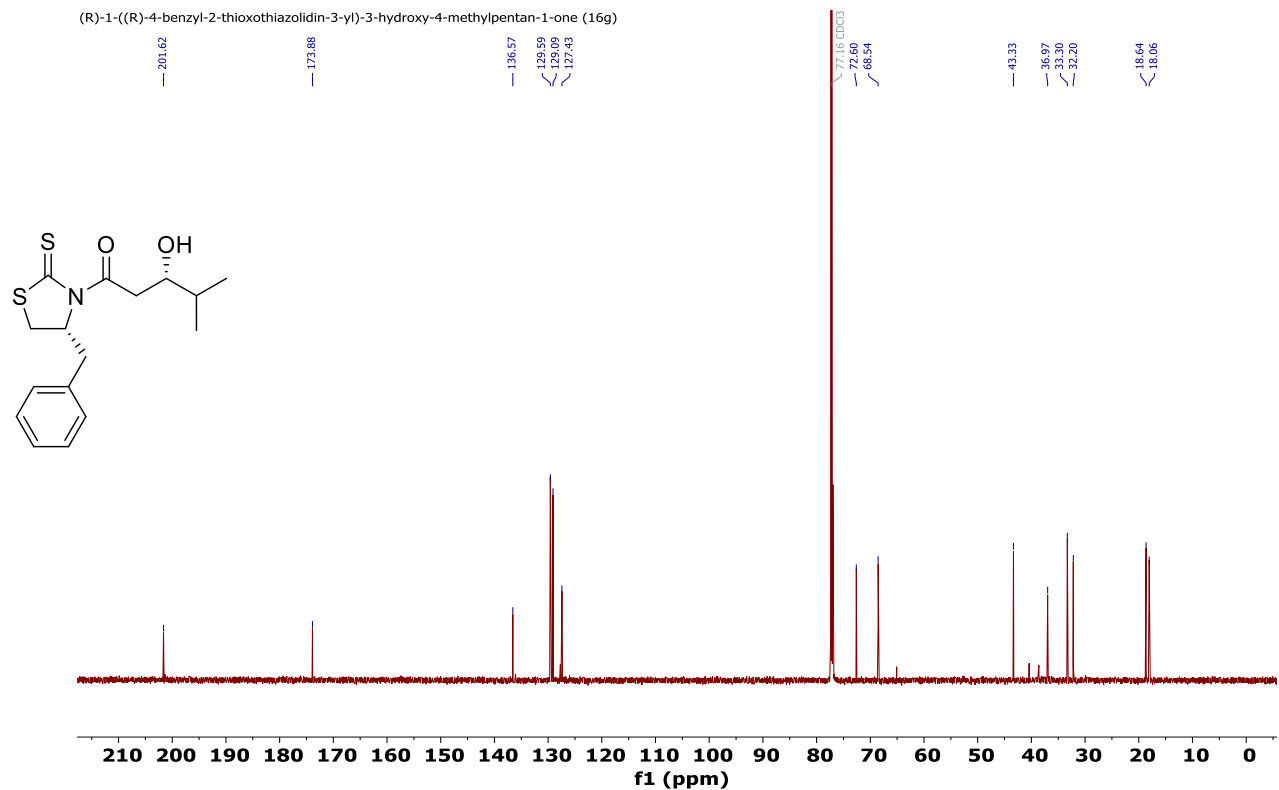
¹H NMR of compound **16h** on 700 MHz at 298 K in CDCl₃.

(R)-1-((R)-4-benzyl-2-thioxothiazolidin-3-yl)-3-cyclopropyl-3-hydroxypropan-1-one (16h)
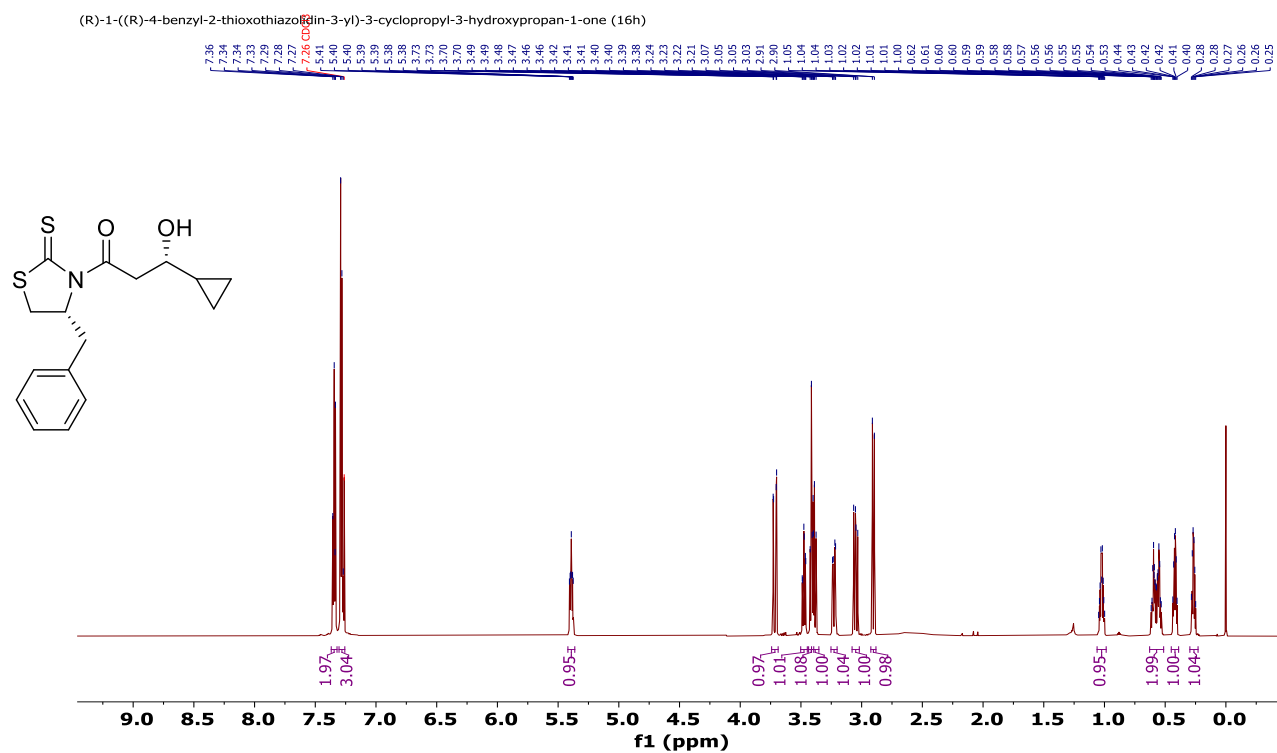
¹³C NMR of compound **16h** on 175 MHz at 298 K in CDCl₃.

(R)-1-((R)-4-benzyl-2-thioxothiazolidin-3-yl)-3-cyclopropyl-3-hydroxypropan-1-one (16h)

235
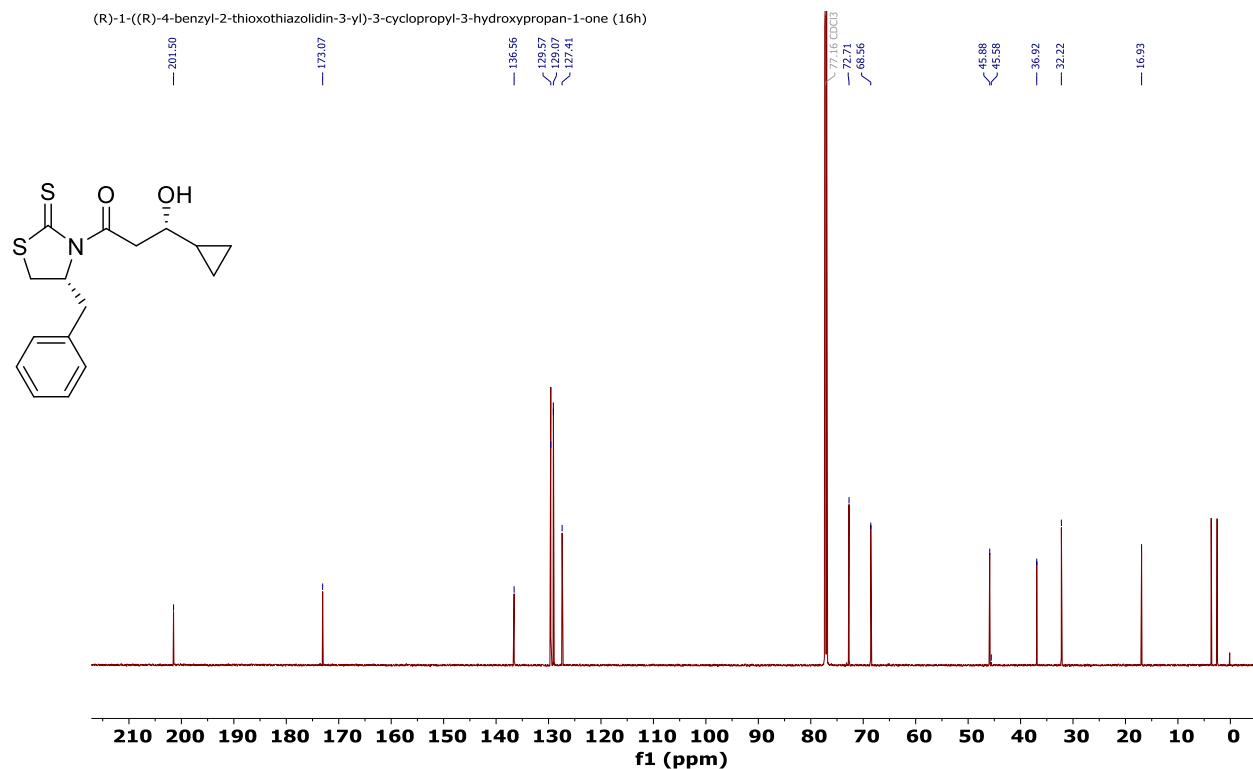
¹H NMR of **17a** on 500 MHz at 298 K in CDCl₃.
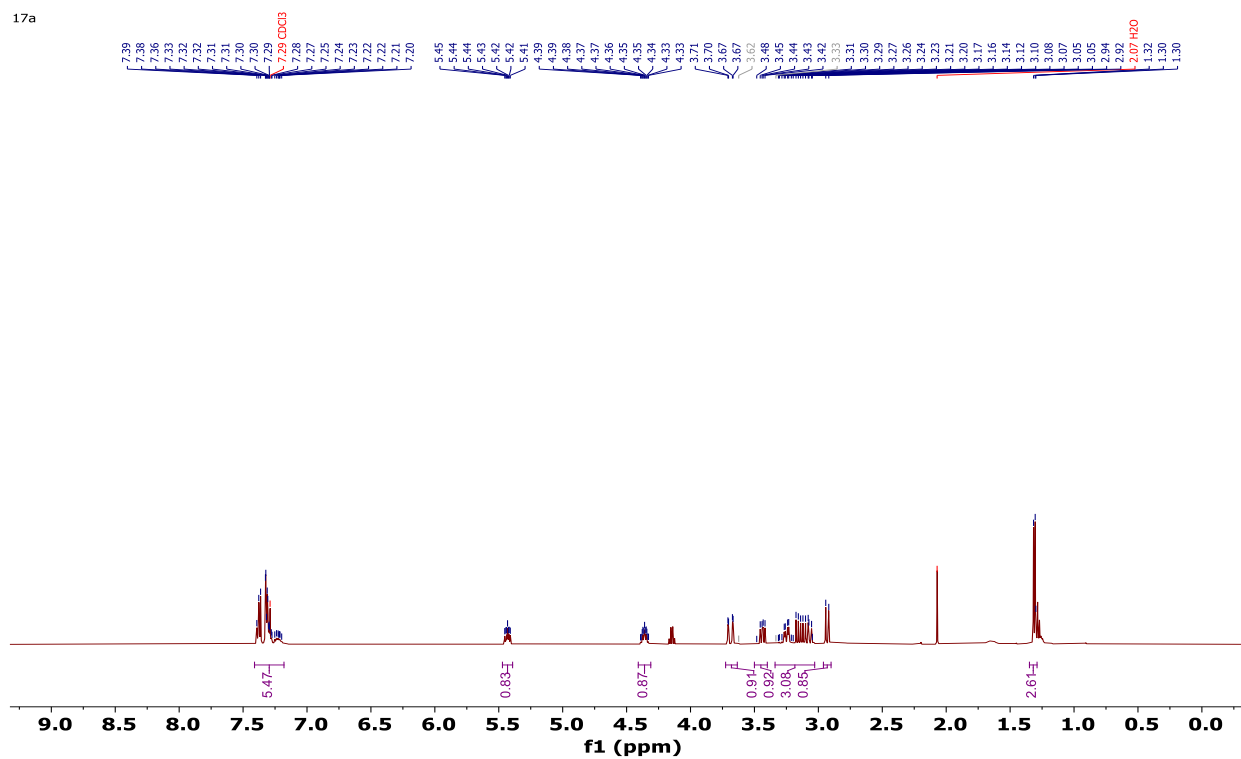
¹³C NMR of **17a** on 500 MHz at 298 K in CDCl₃.

^{1}H NMR of **17b** on 500 MHz at 298 K in CDCl$_3$.

^{13}C NMR of **17b** on 500 MHz at 298 K in CDCl$_3$.
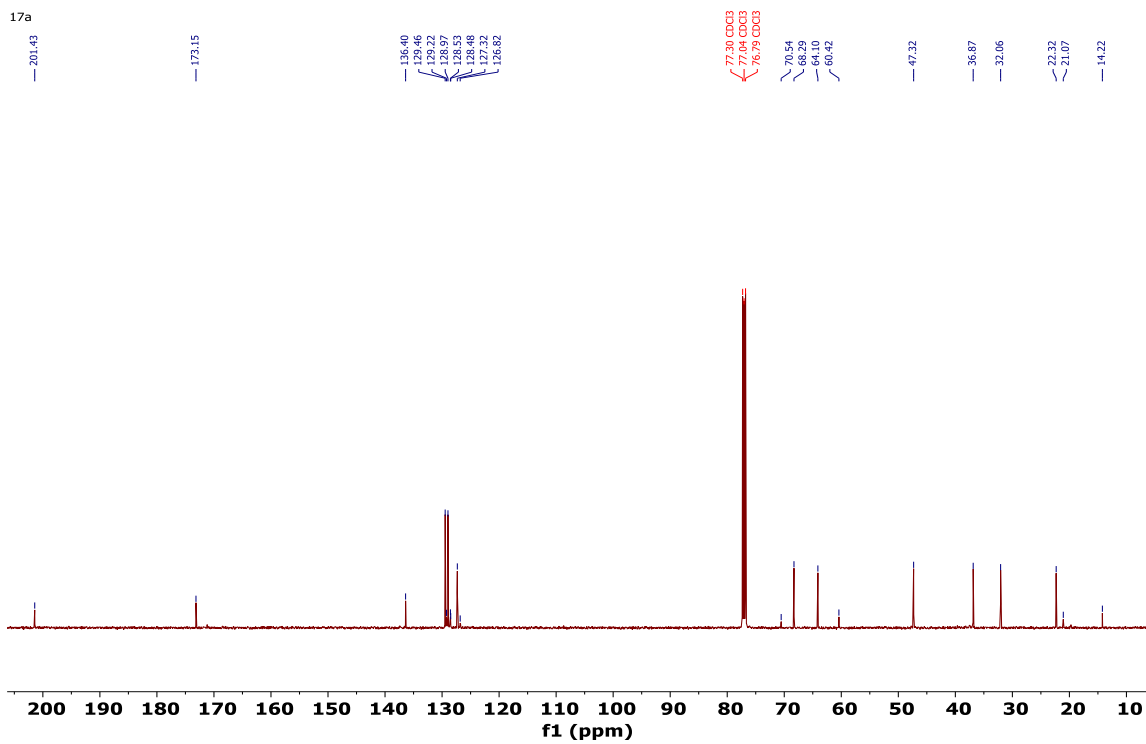
¹H NMR of **17c** on 500 MHz at 298 K in CDCl₃.
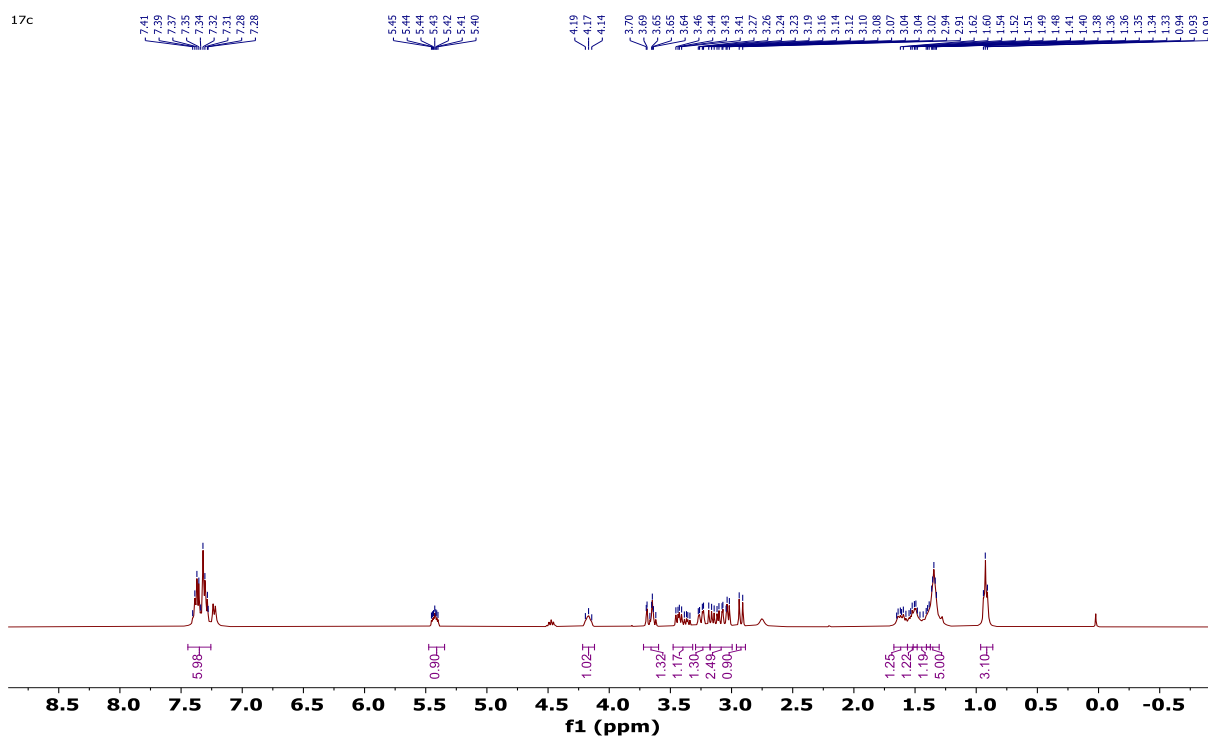
¹³C NMR of **17c** on 500 MHz at 298 K in CDCl₃.
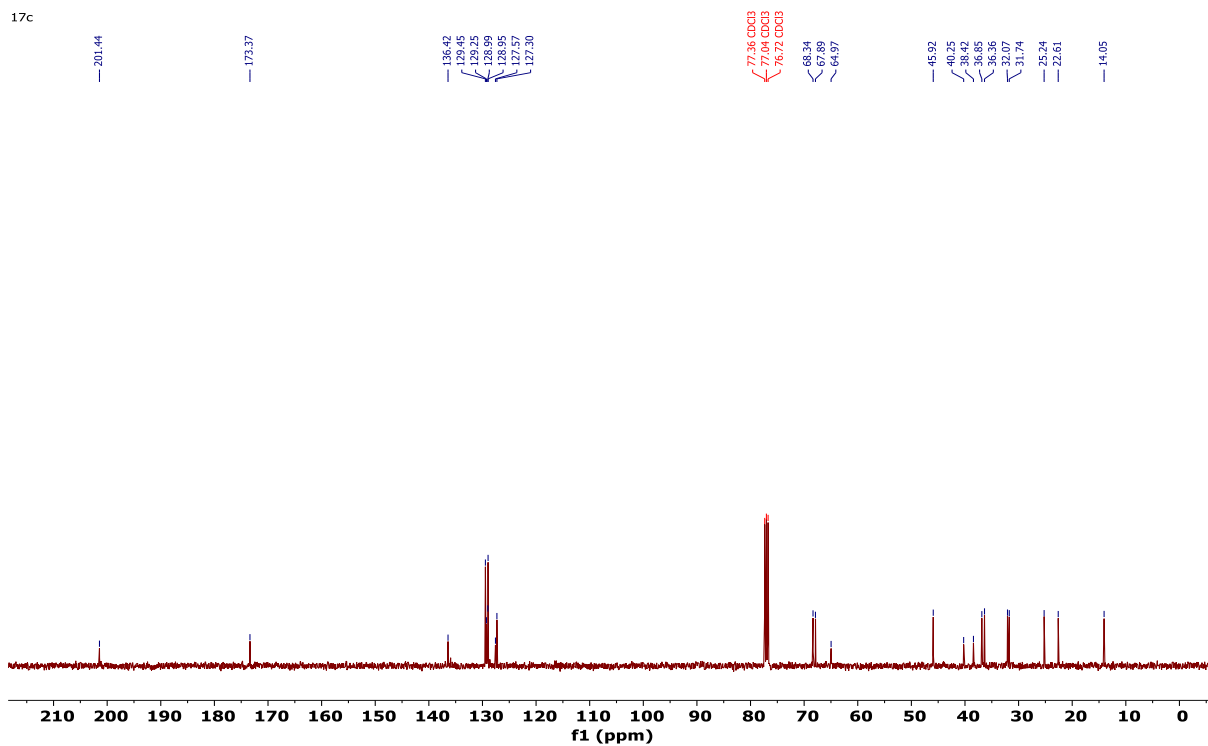
¹H NMR of **17d** on 500 MHz at 298 K in CDCl₃.
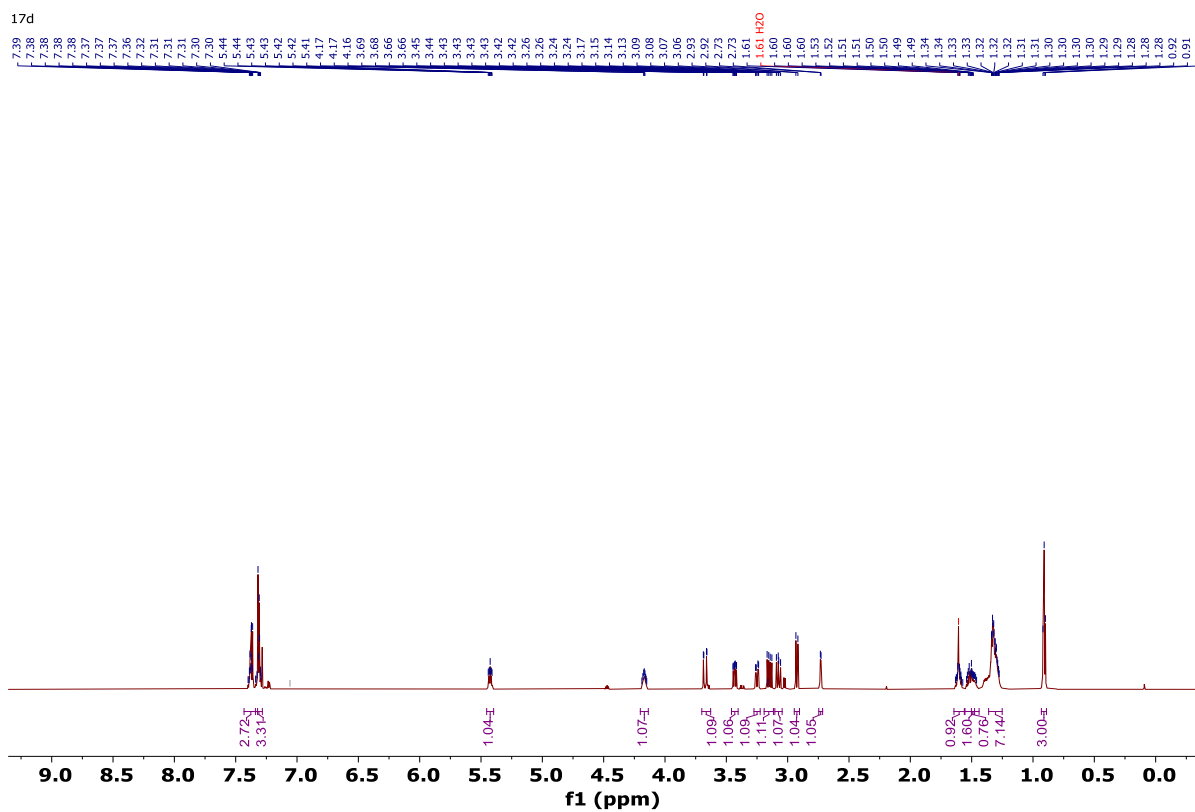
¹H NMR of **17e** on 500 MHz at 298 K in CDCl₃.
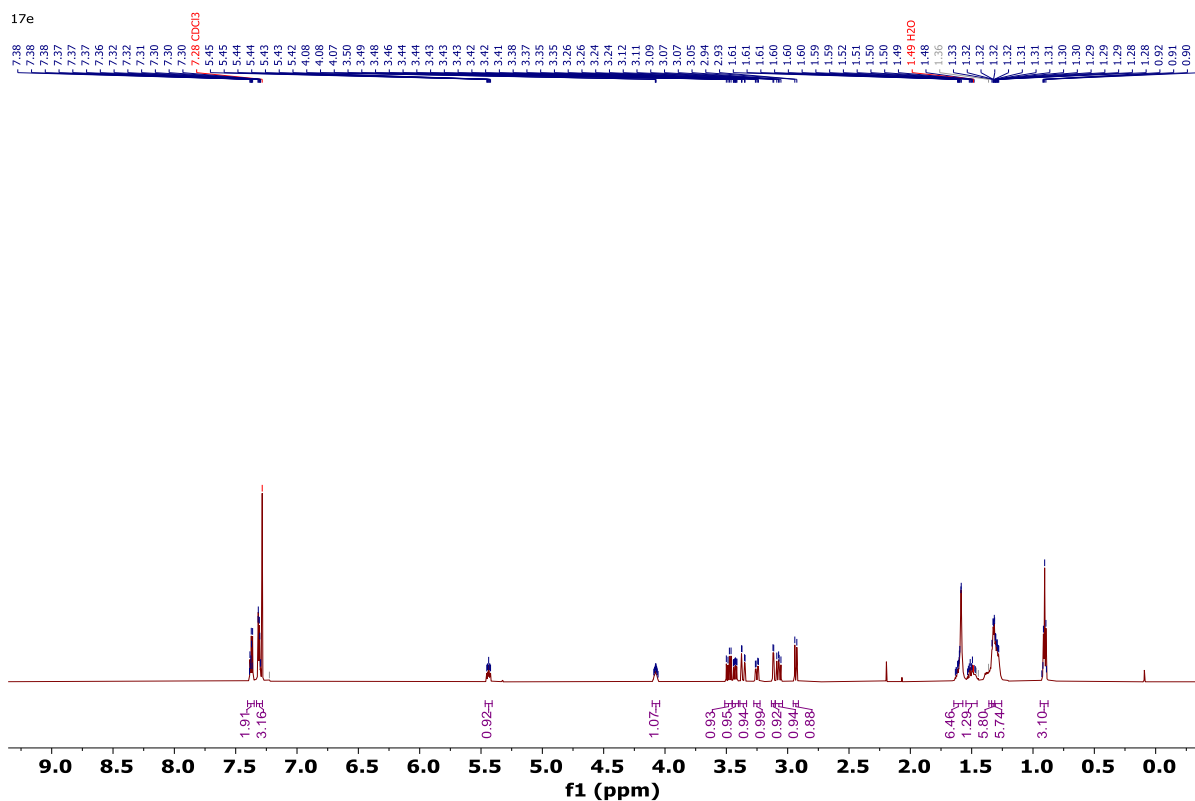
^{1}H NMR of **17f** on 500 MHz at 298 K in CDCl$_3$.
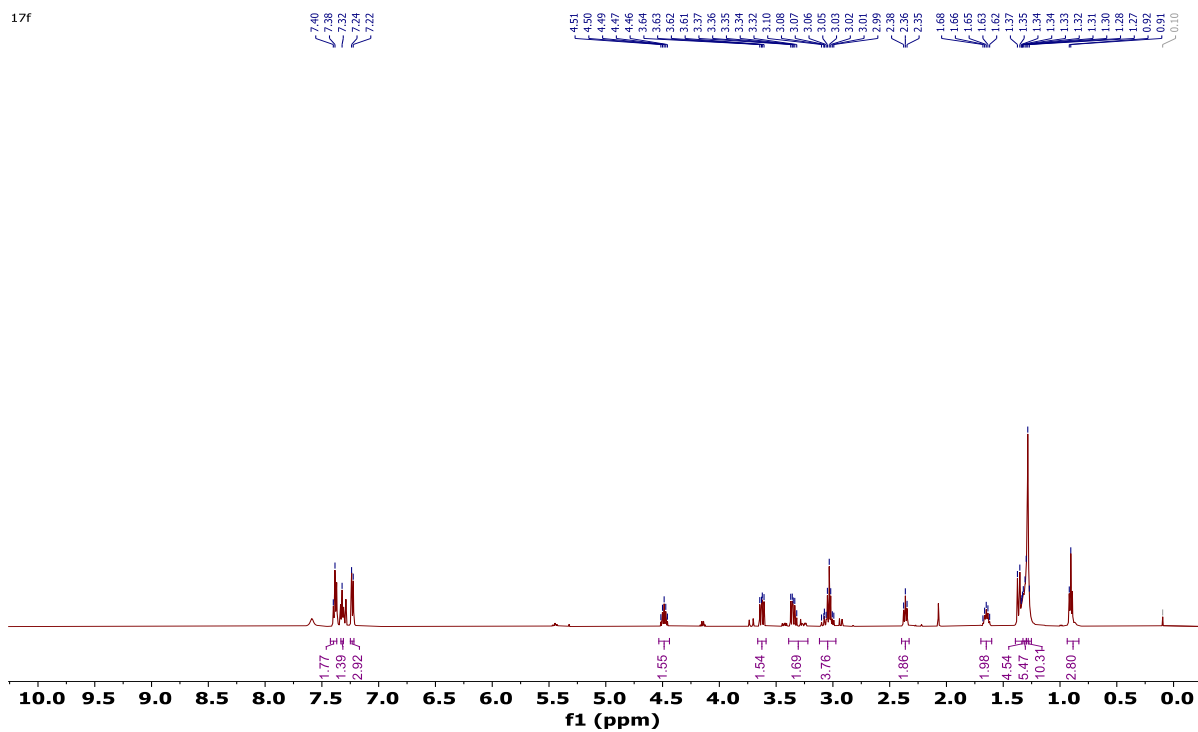
^{1}H NMR of compound **18b** on 500 MHz at 298 K in CDCl$_3$.

(R)-3-hydroxyhexanoic acid (18b)
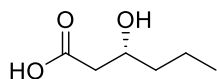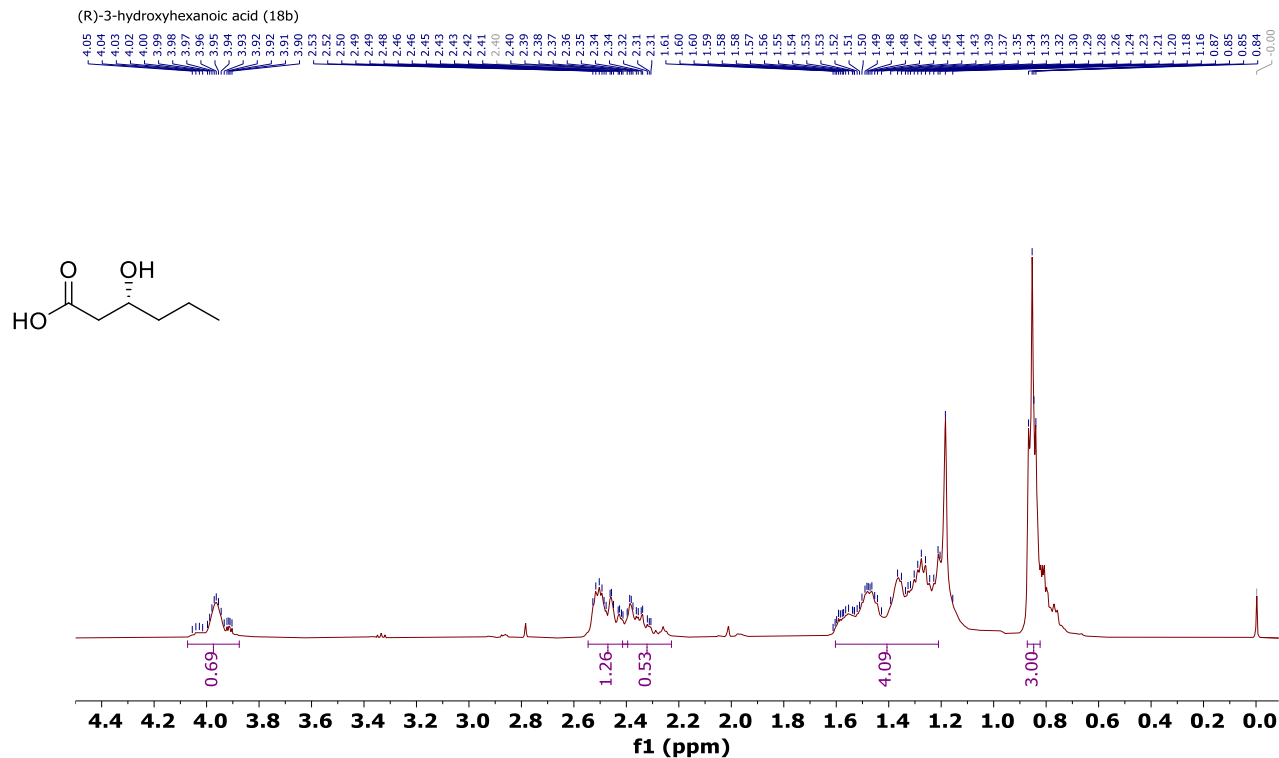
^{13}C NMR of compound **18b** on 125 MHz at 298 K in CDCl$_3$.

(R)-3-hydroxyhexanoic acid (18b)
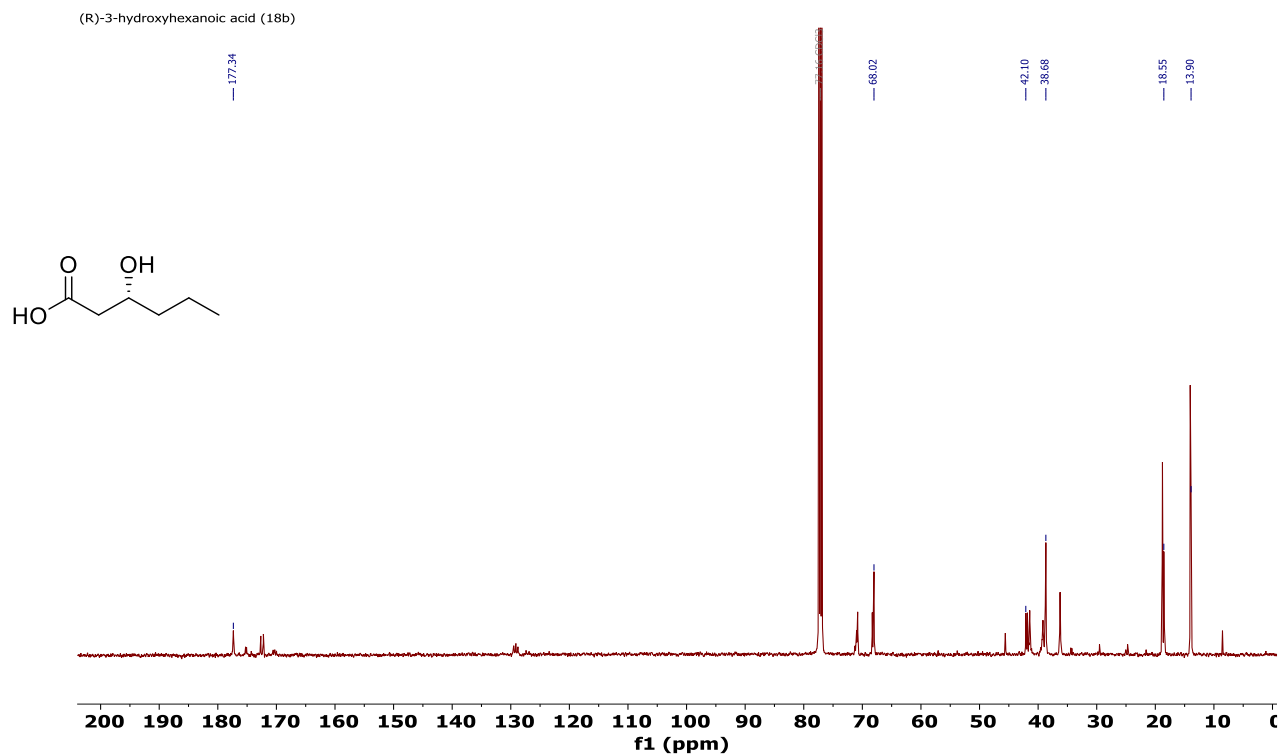
^{1}H NMR of compound **18c** on 500 MHz at 298 K in CDCl$_3$.

(R)-3-hydroxyoctanoic acid (18c)
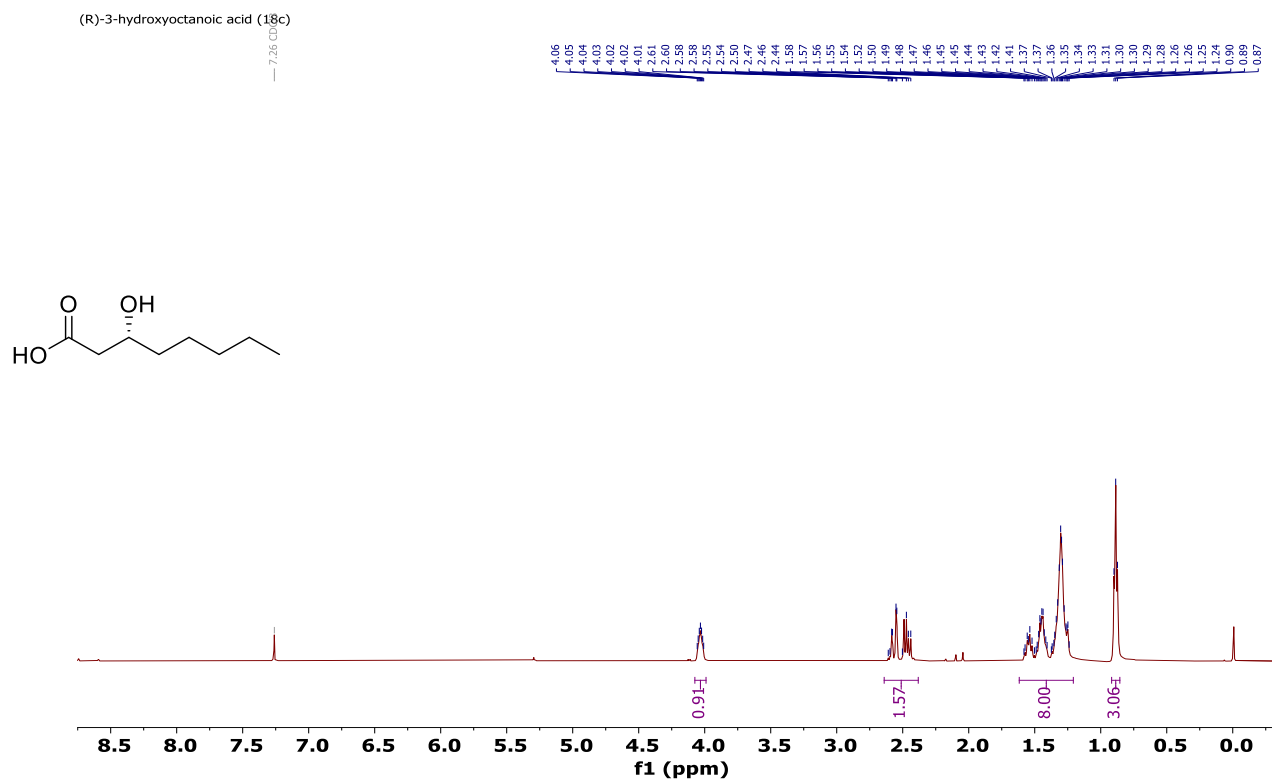
^{1}H NMR of compound **18c** on 125 MHz at 298 K in CDCl$_3$.

(R)-3-hydroxyoctanoic acid (18c)
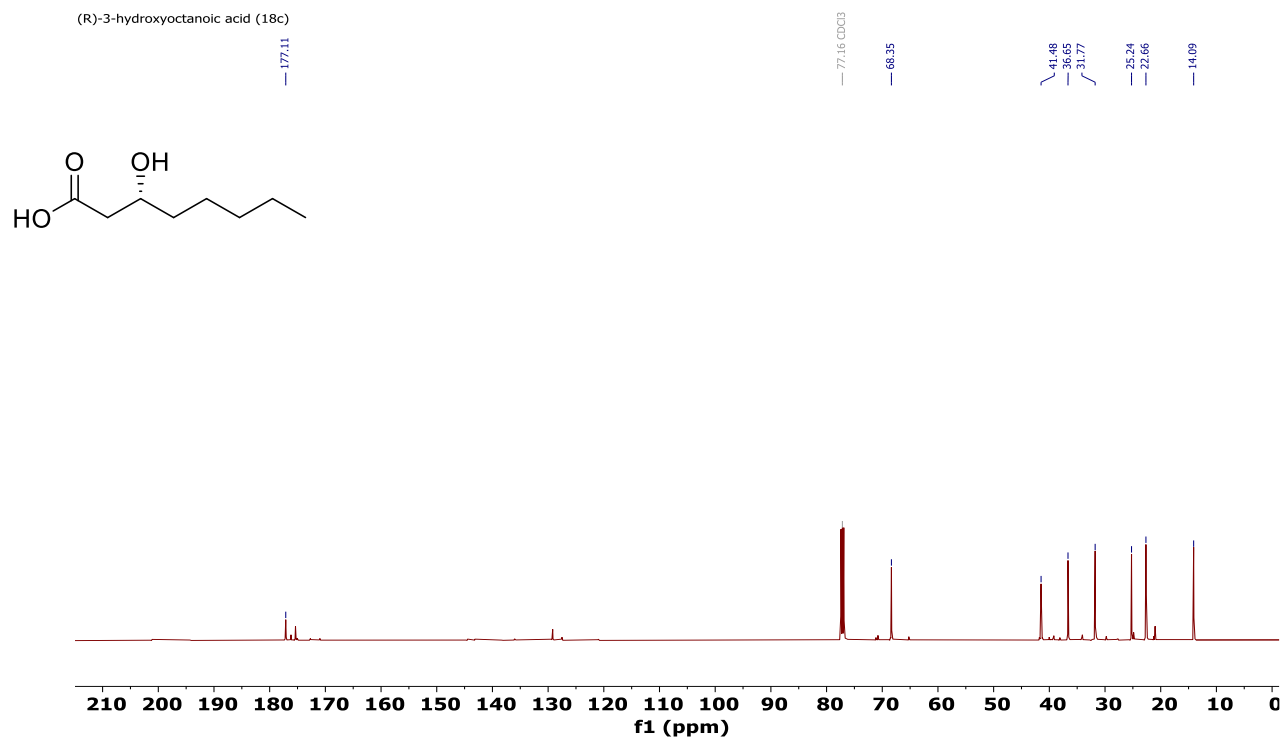
^{1}H NMR of compound **18d** on 700 MHz at 298 K in CDCl$_3$.

(R)-3-hydroxydecanoic acid (18d)
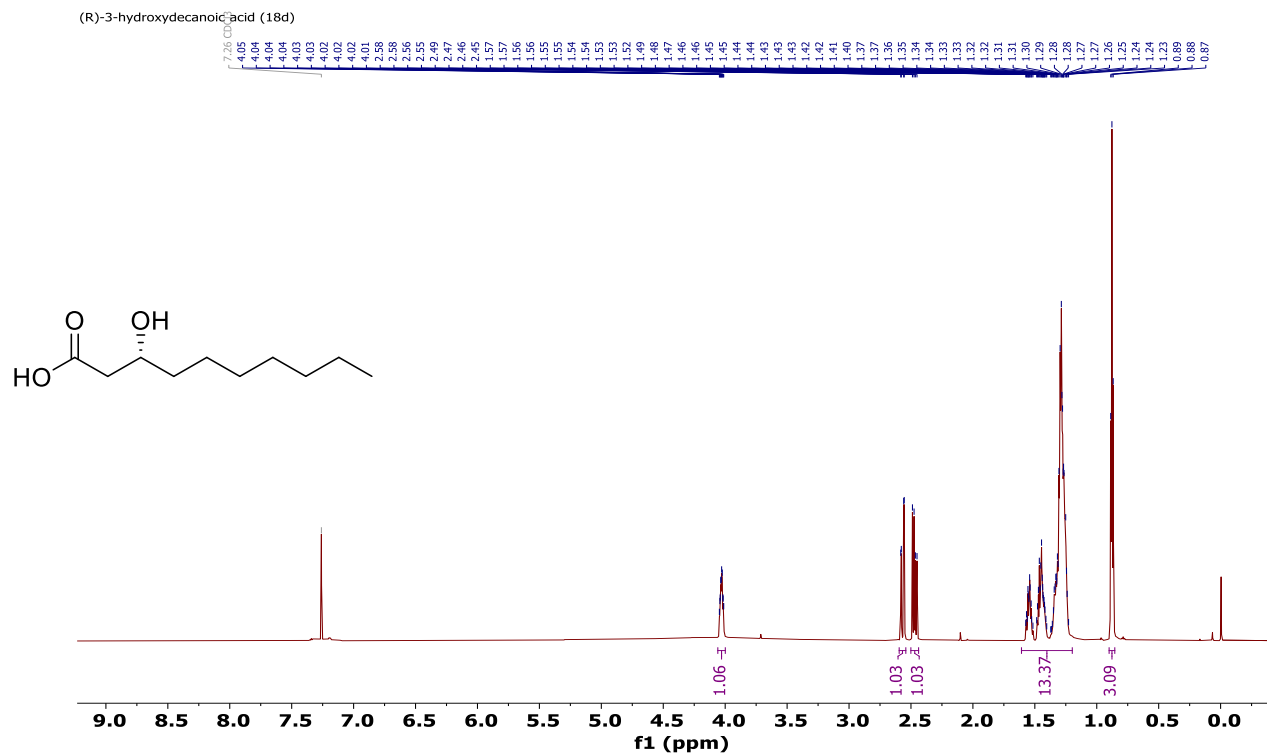
^{13}C NMR of compound **18d** on 175 MHz at 298 K in CDCl₃.

(R)-3-hydroxydecanoic acid (18d)

[1]H
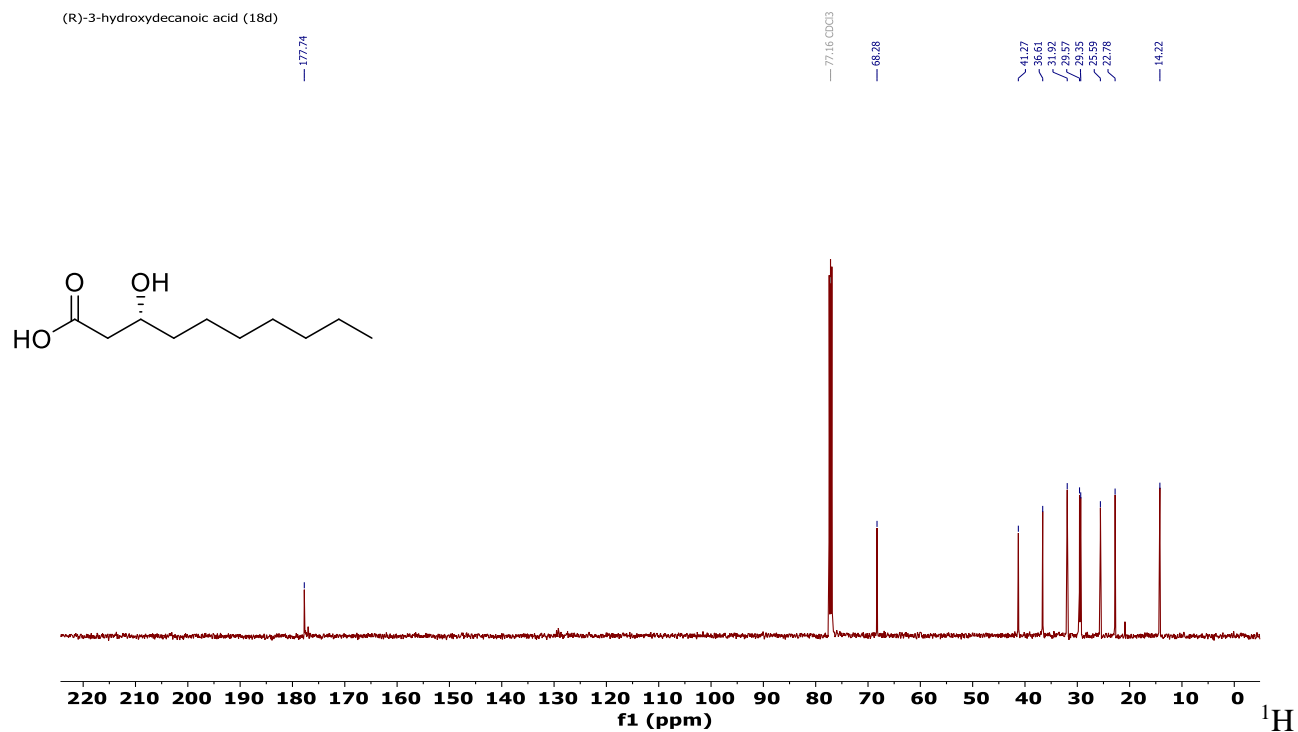
NMR of compound **18e** on 500 MHz at 298 K in CDCl₃.

(R)-3-hydroxydodecanoic acid (18e)
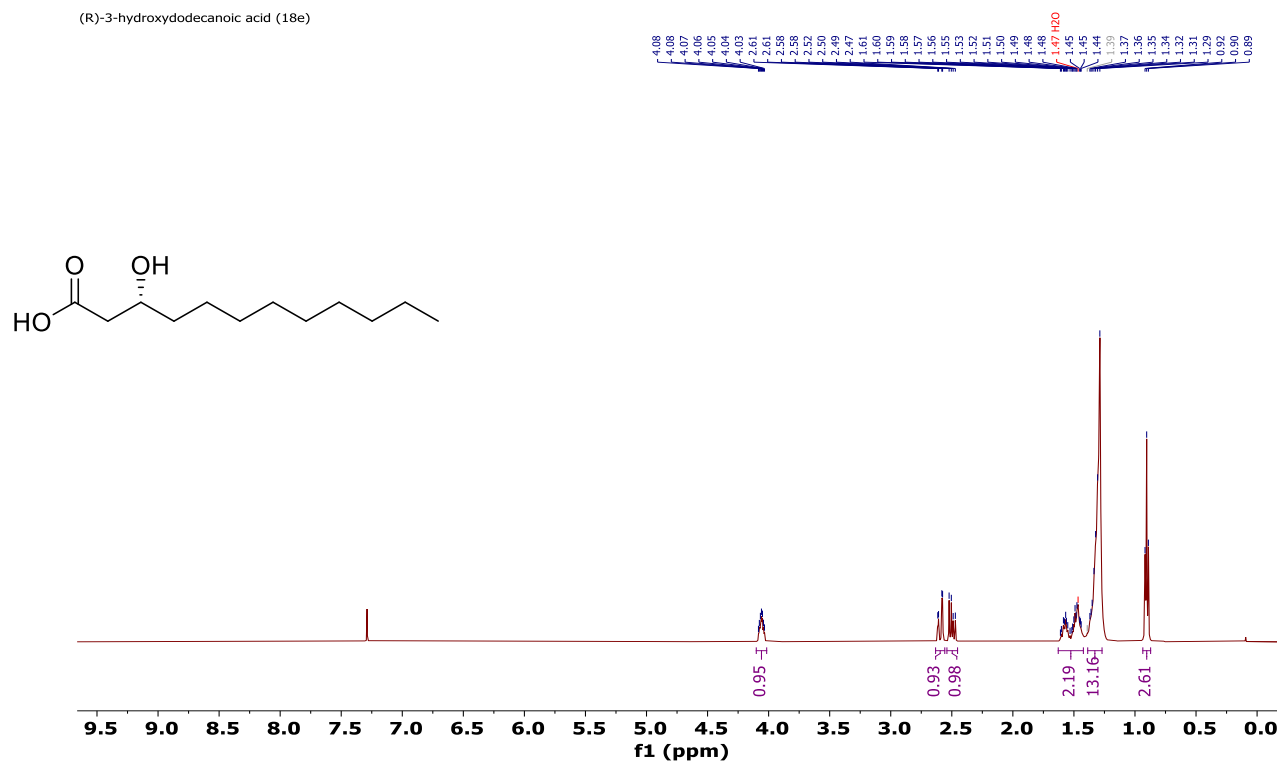
^{13}C NMR of compound **18e** on 125 MHz at 298 K in CDCl$_3$.

(R)-3-hydroxydodecanoic acid (18e)
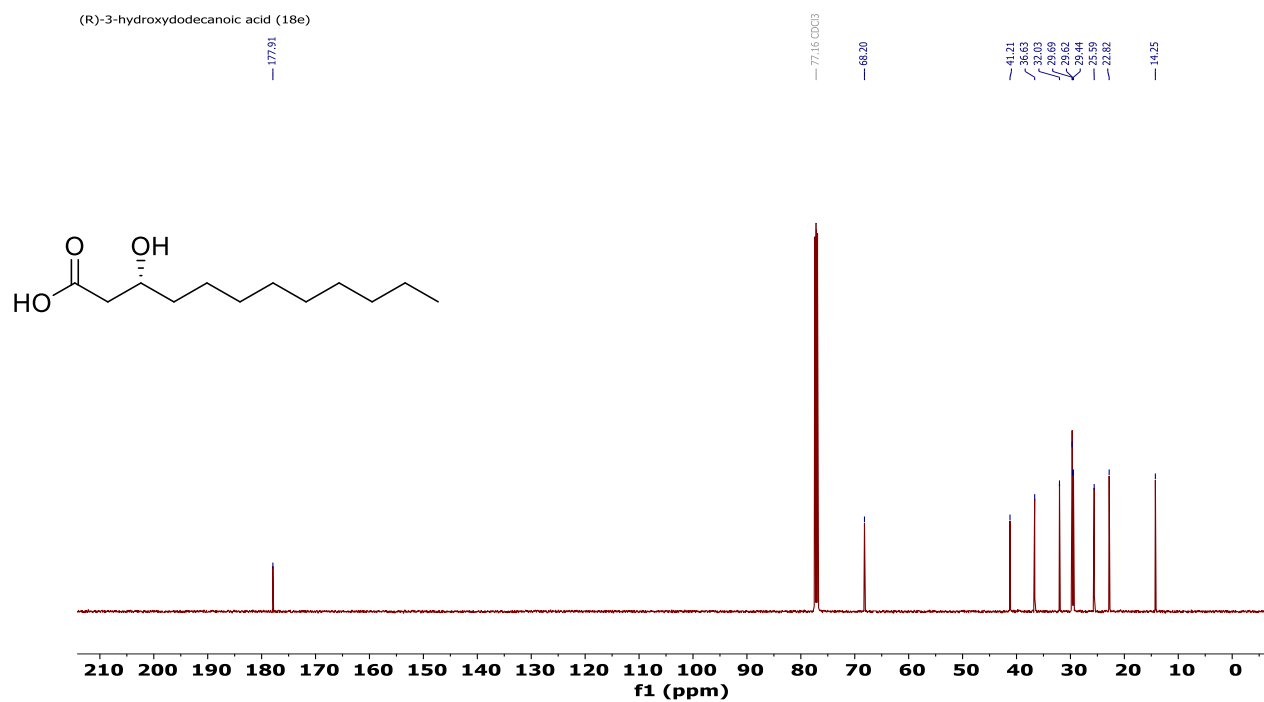
^{13}C NMR of compound **18g** on 700 MHz at 298 K in CDCl$_3$.

(R)-3-hydroxy-4-methylpentanoic acid (18g)
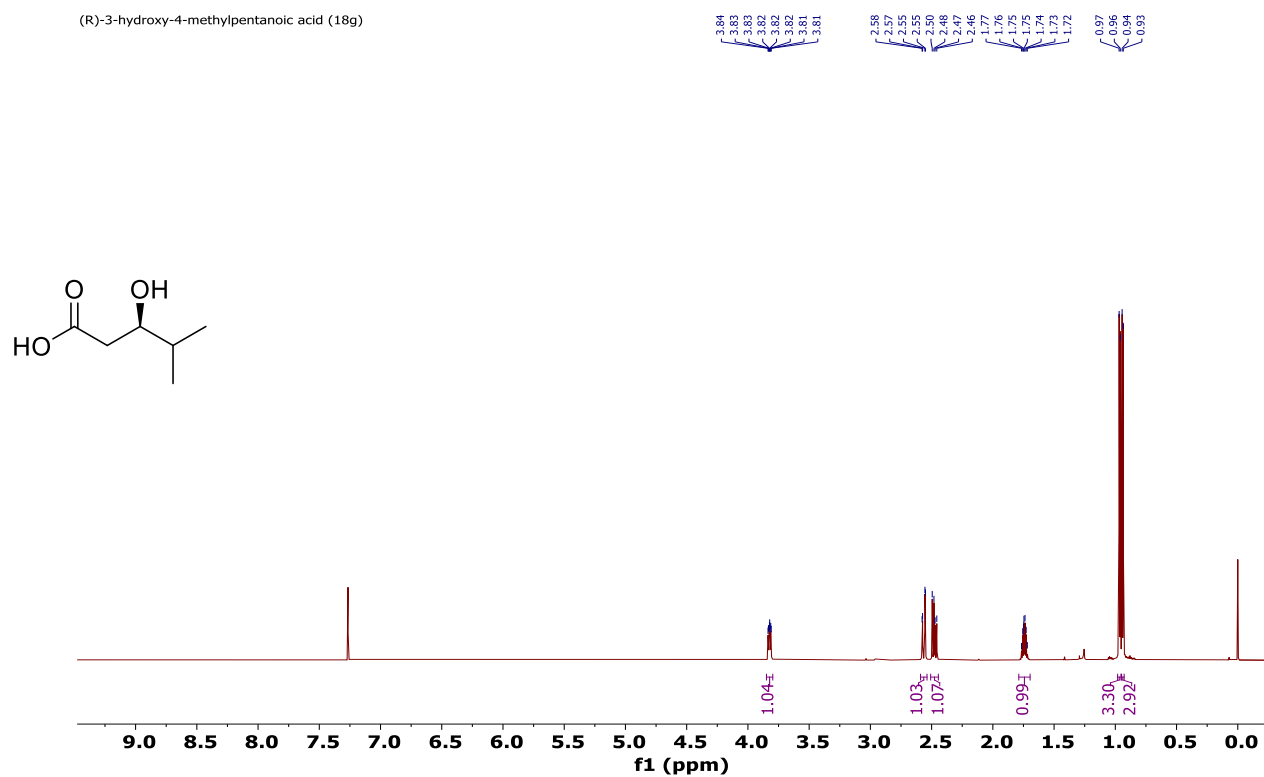
¹³C NMR of compound **18g** on 125 MHz at 298 K in CDCl₃.

(R)-3-hydroxy-4-methylpentanoic acid (18g)
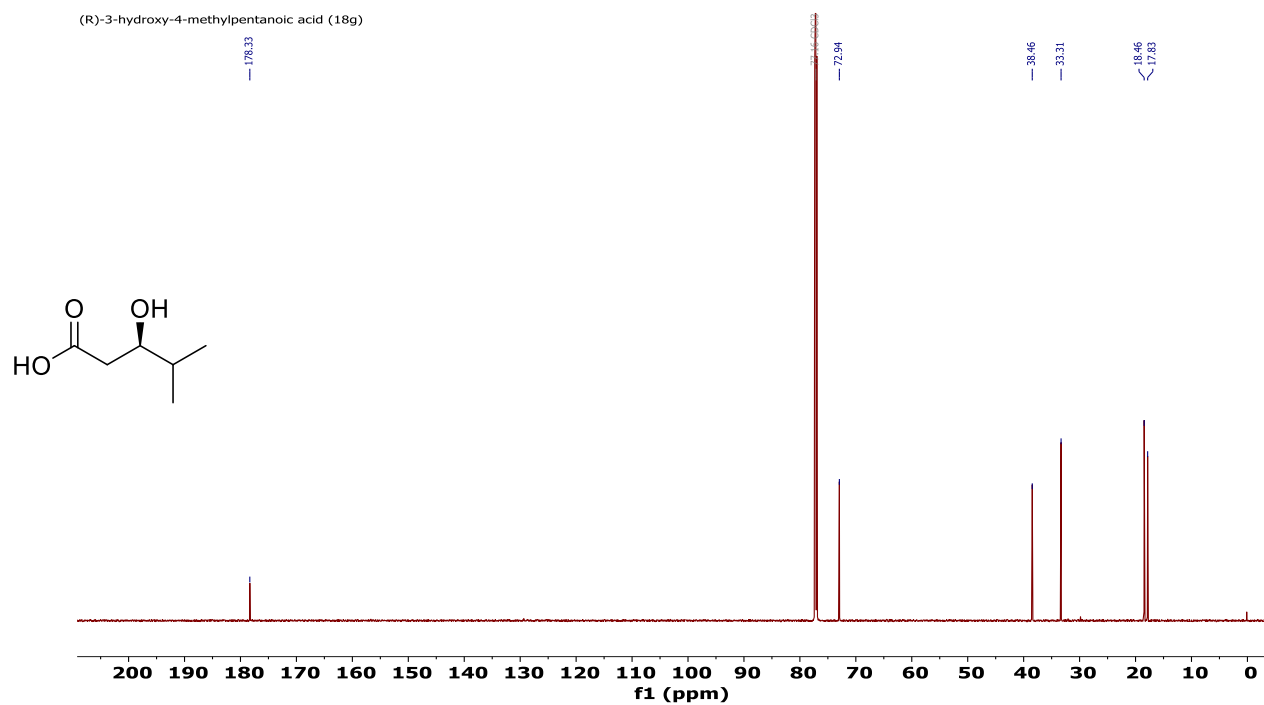
¹H NMR of compound **18h** on 500 MHz at 298 K in CDCl₃.

(R)-3-cyclopropyl-3-hydroxypropanoic acid (18h)

245
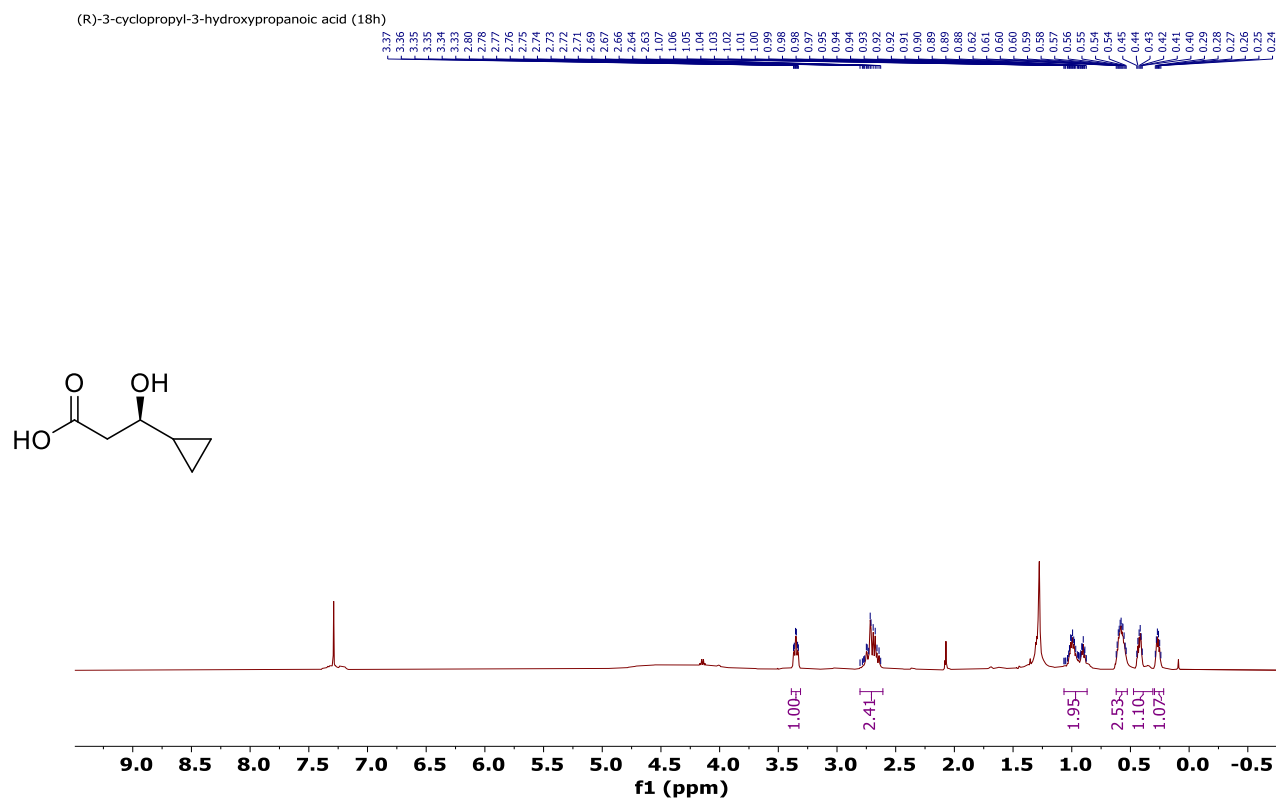
¹³C NMR of compound **18h** on 125 MHz at 298 K in CDCl₃.

(R)-3-cyclopropyl-3-hydroxypropanoic acid (18h)
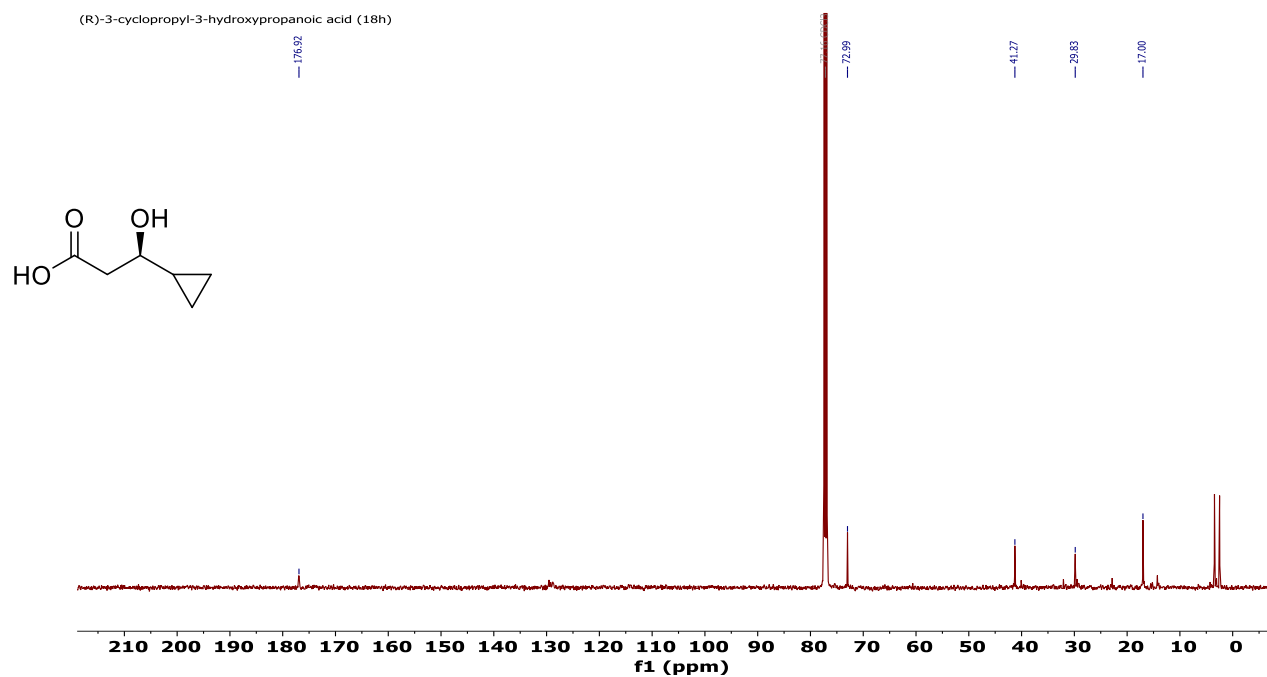
¹H NMR of compound **20c** on 700 MHz at 298 K in CDCl₃.

Beta lactum octanoic acid (20c)
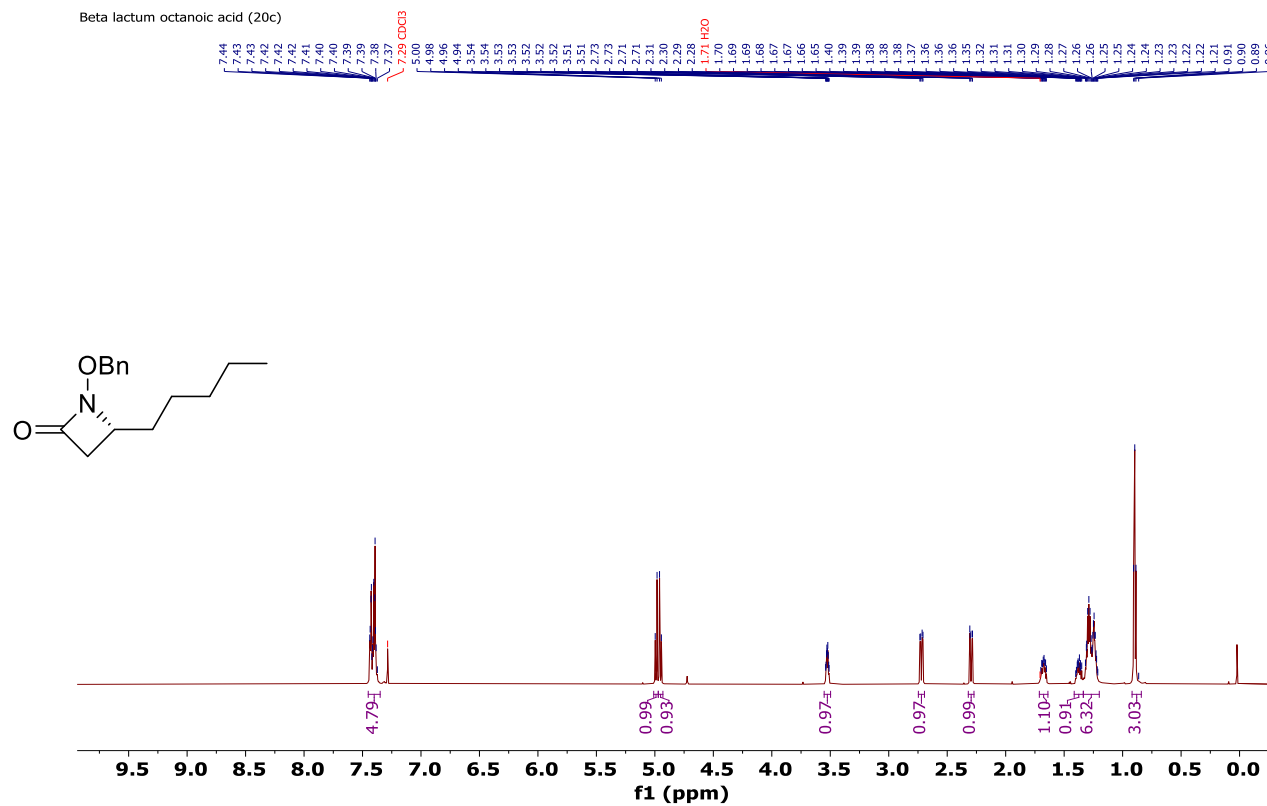
^{13}C NMR of compound **20c** on 175 MHz at 298 K in CDCl$_3$.

Beta lactum octanoic acid (20c)
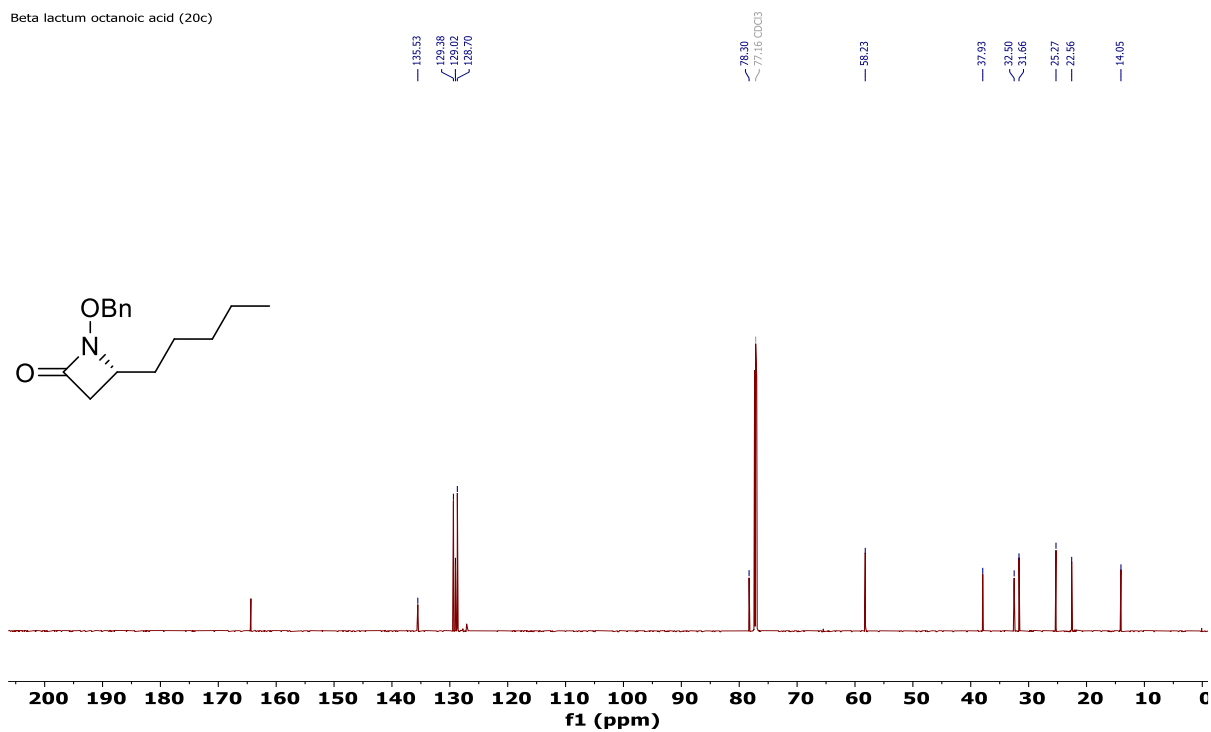
^{1}H NMR of compound **20d** on 500 MHz at 298 K in CDCl$_3$

Beta lactum decanoic acid

247
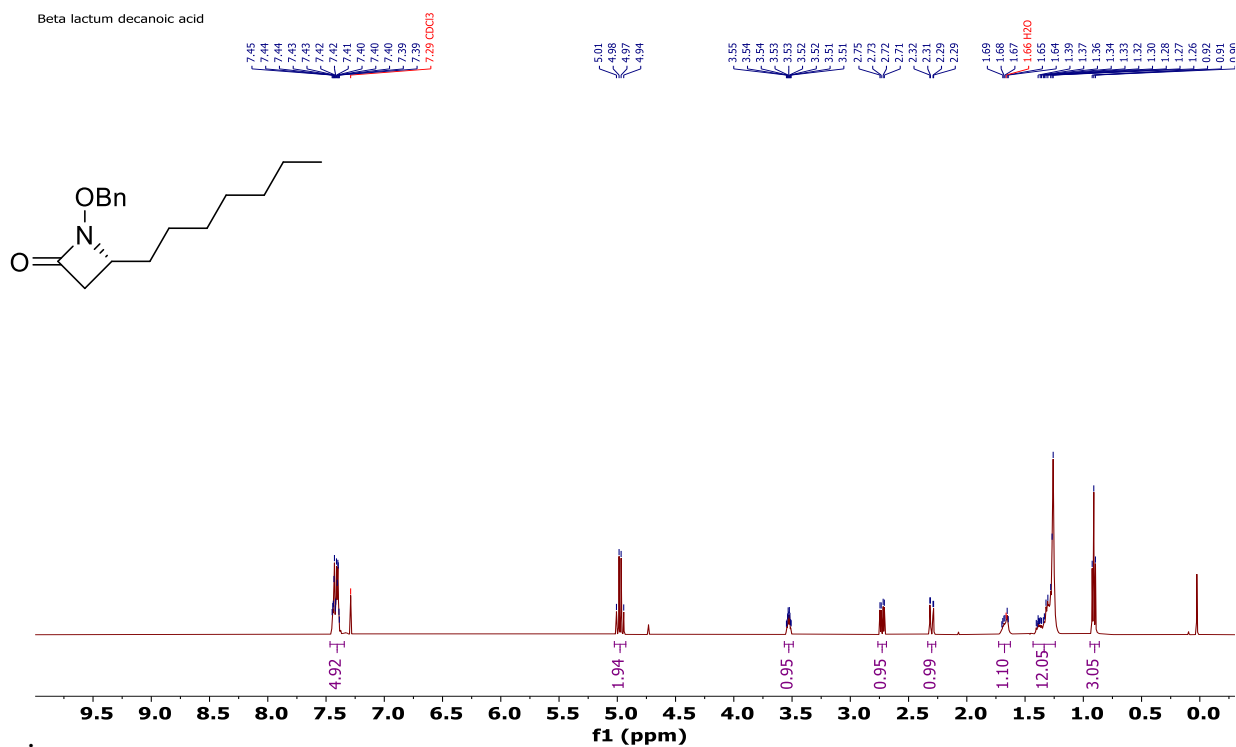
^{1}H NMR of compound **23c** on 500 MHz at 298 K in CDCl$_3$.

(R)-3-((((9H-fluoren-9-yl)methoxy)carbonyl)amino)octanoic acid (23c)
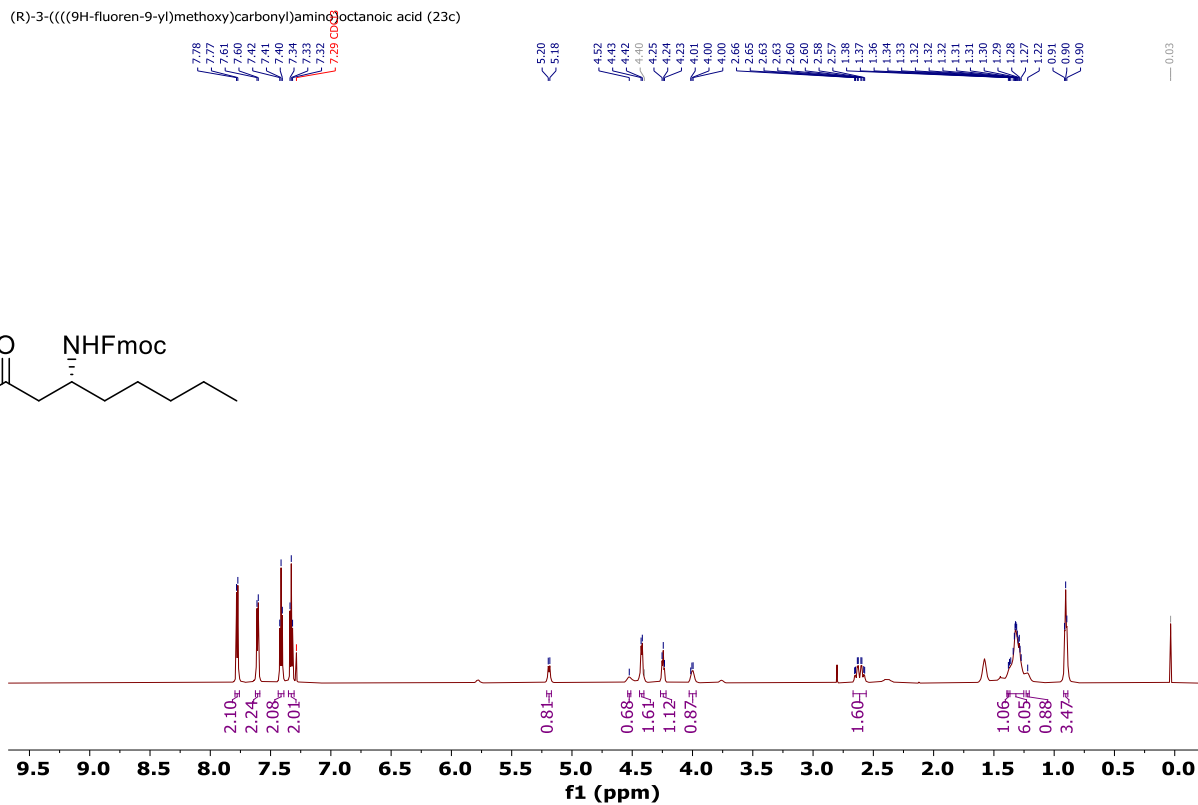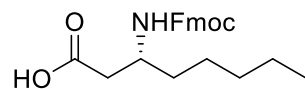
^{13}C NMR of compound **23c** on 125 MHz at 298 K in CDCl$_3$.

(R)-3-((((9H-fluoren-9-yl)methoxy)carbonyl)amino)octanoic acid (23c)
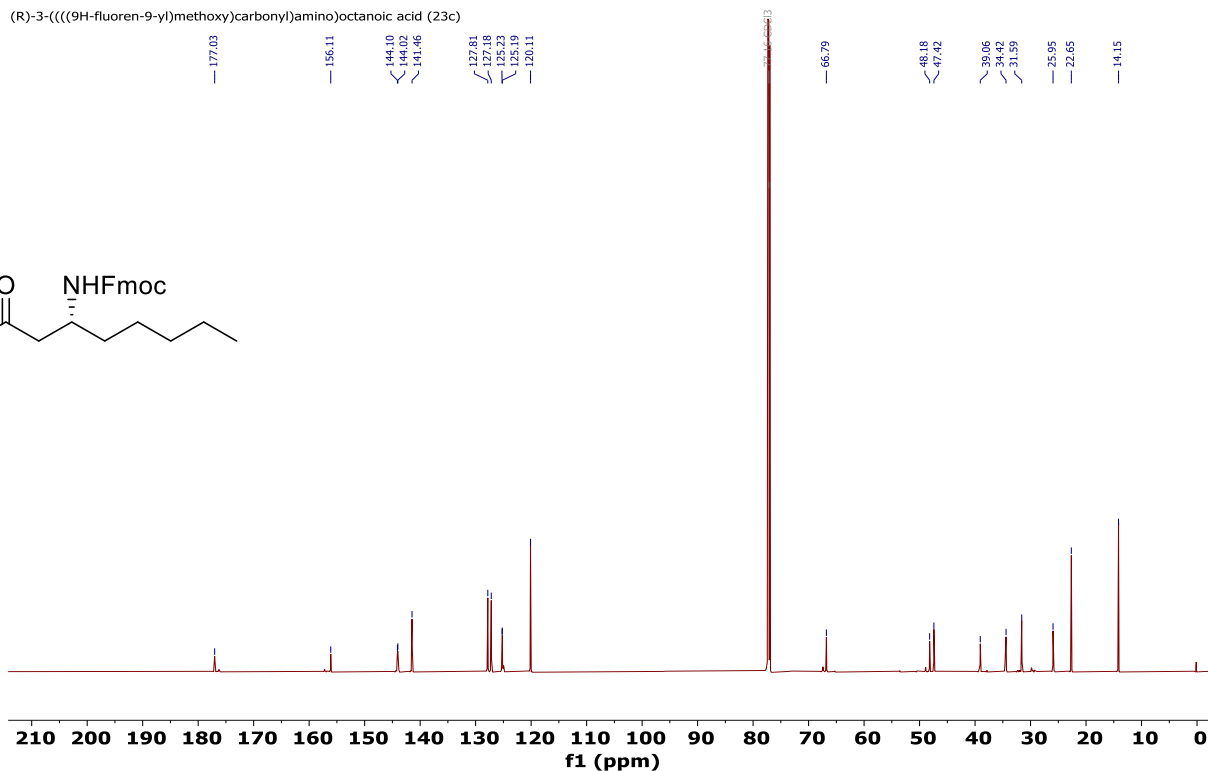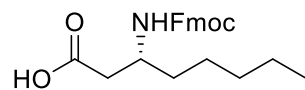
^{1}H NMR of compound **23d** on 700 MHz at 298 K in CDCl₃.

(R)-3-((((9H-fluoren-9-yl)methoxy)carbonyl)amino)decanoic acid (23d)
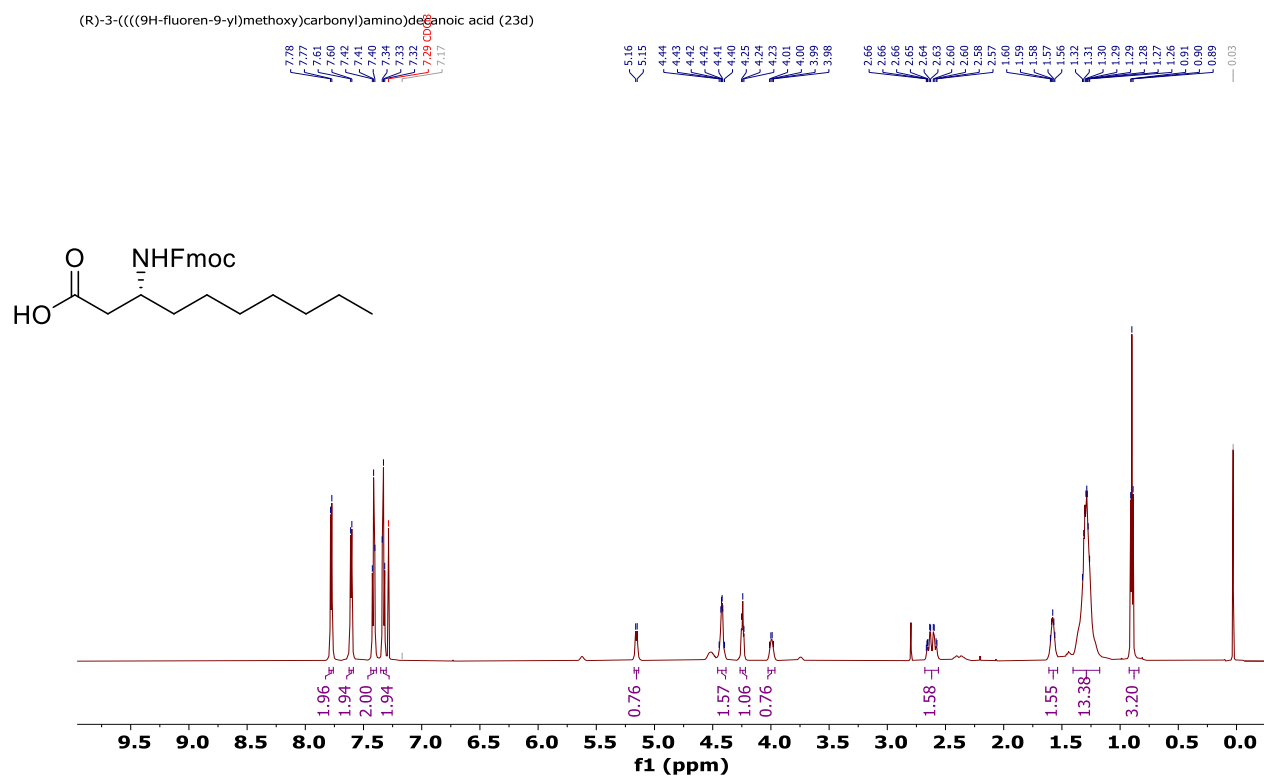
¹³C NMR of compound **23d** on 175 MHz at 298 K in CDCl₃.

(R)-3-((((9H-fluoren-9-yl)methoxy)carbonyl)amino)decanoic acid (23d)

249
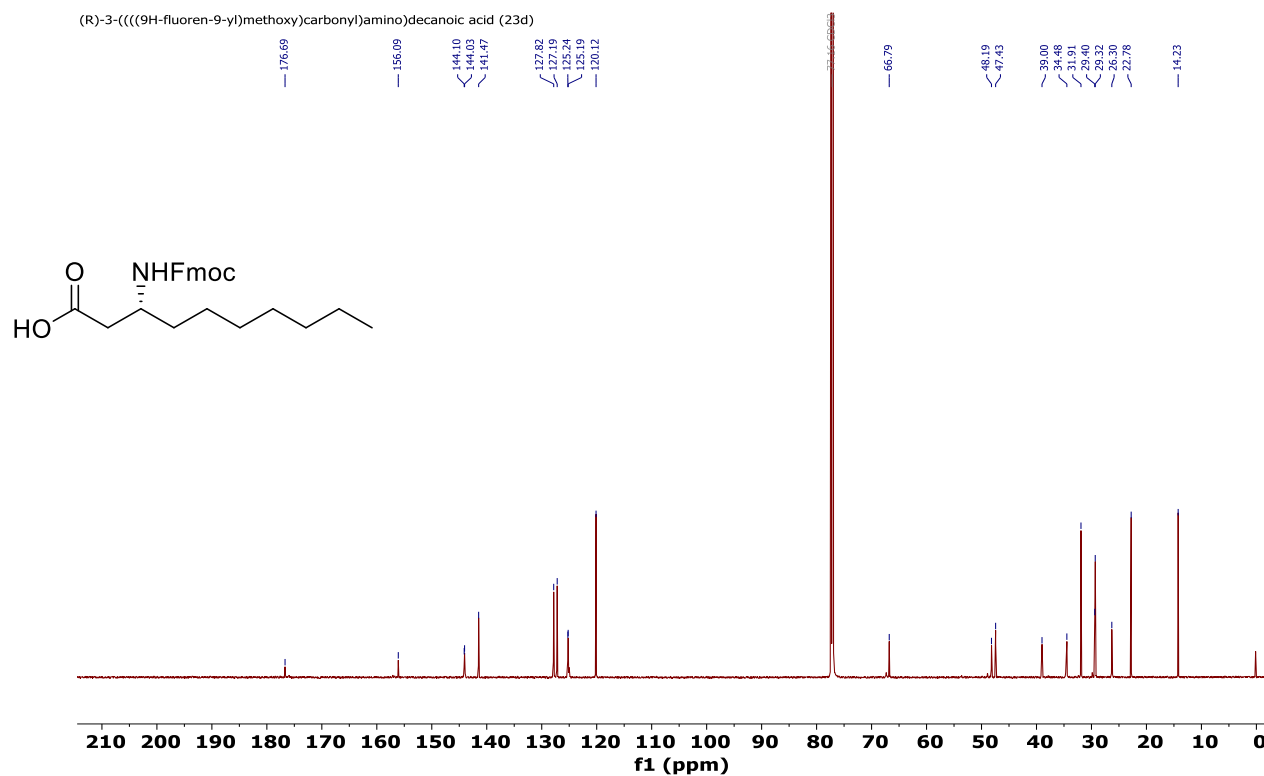
2D COSY NMR of Icosalide **1a** on 500 MHz at 298 K in DMSO-d_6.
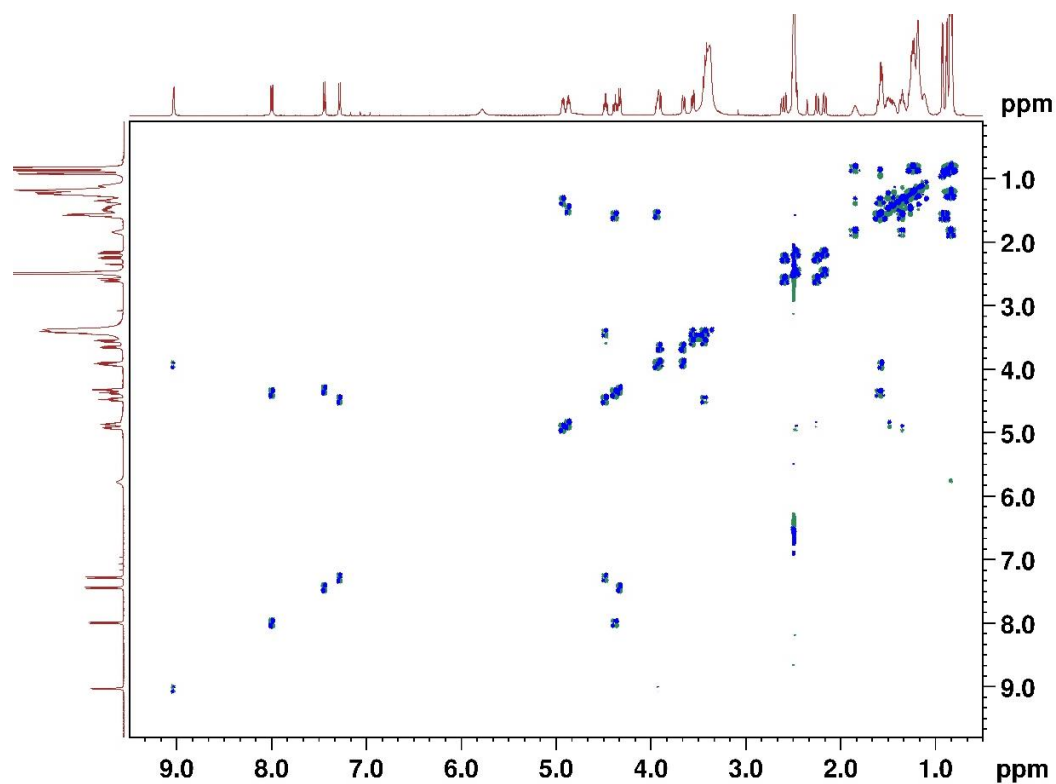
2D TOCSY NMR of Icosalide **1a** on 500 MHz at 298 K in DMSO-d_6.
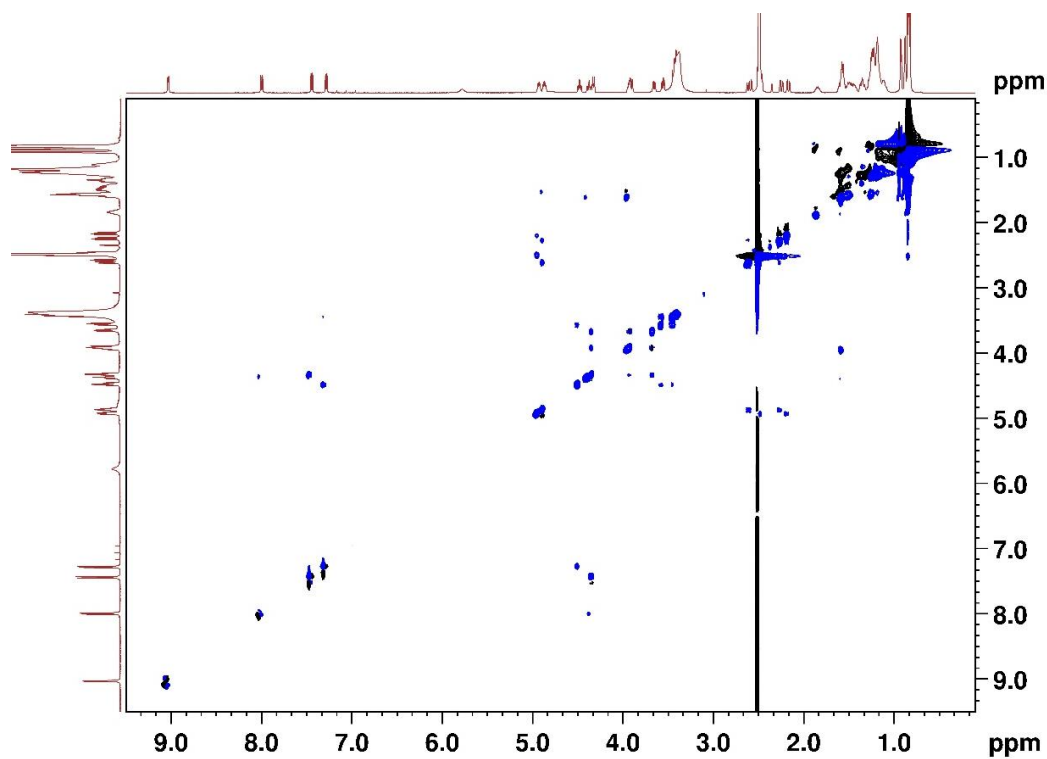
2D ROESY NMR of Icosalide **1a** on 500 MHz at 298 K in DMSO-*d*$_6$.
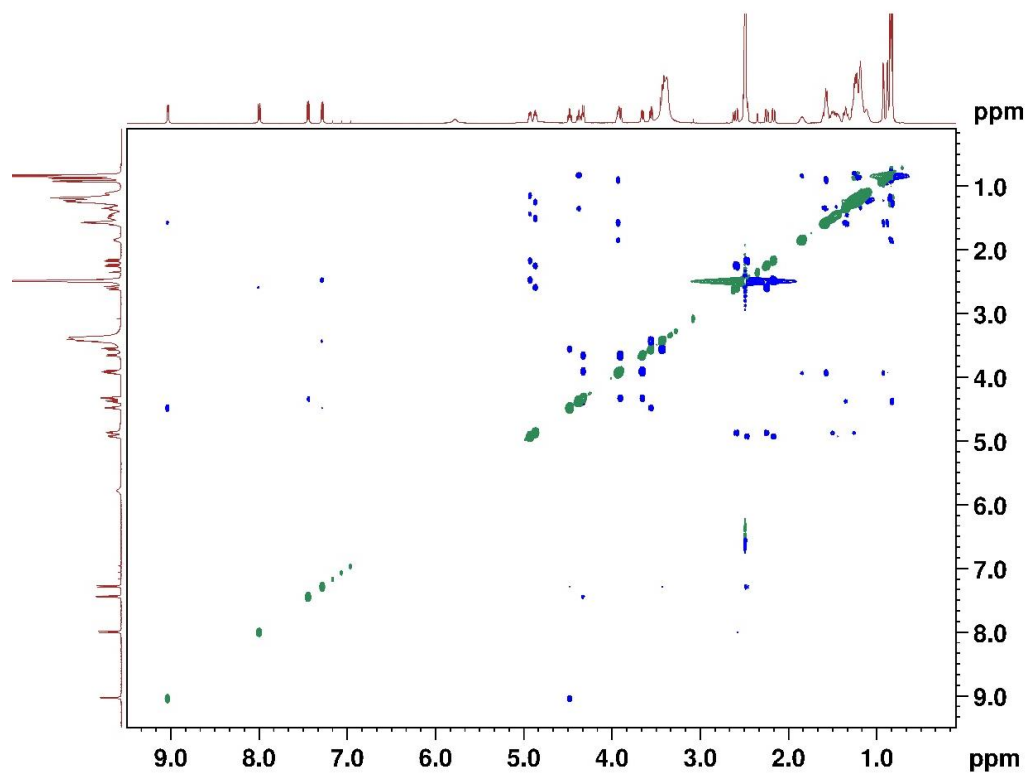
2D HSQC NMR of Icosalide **1a** on 500 MHz at 298 K in DMSO-*d*$_6$.
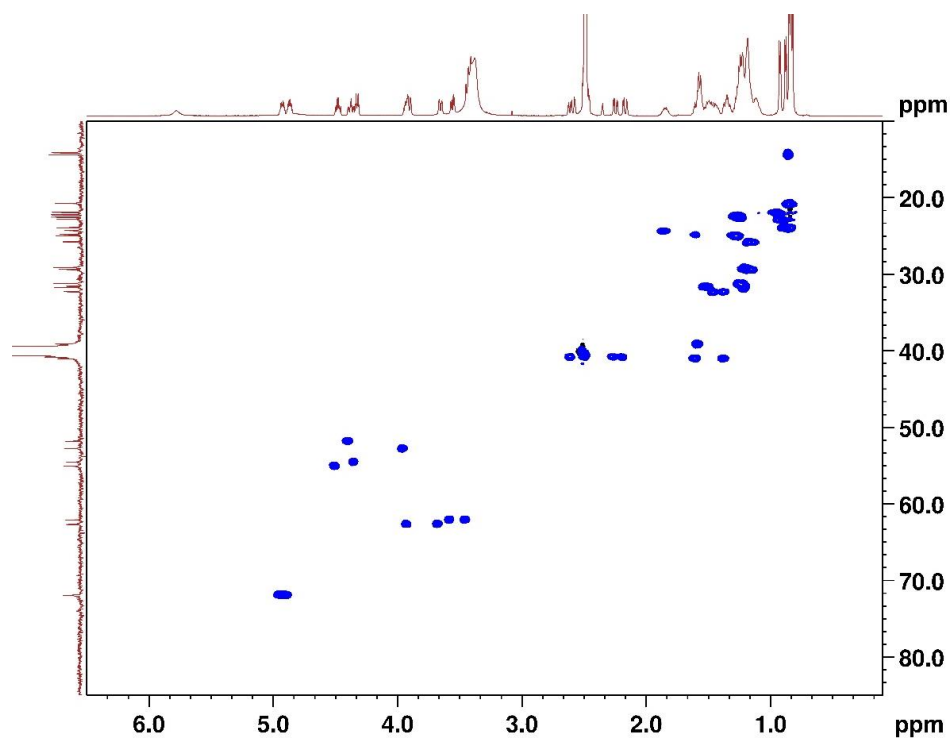
2D HMBC NMR of Icosalide **1a** on 500 MHz at 298 K in DMSO-*d*₆.
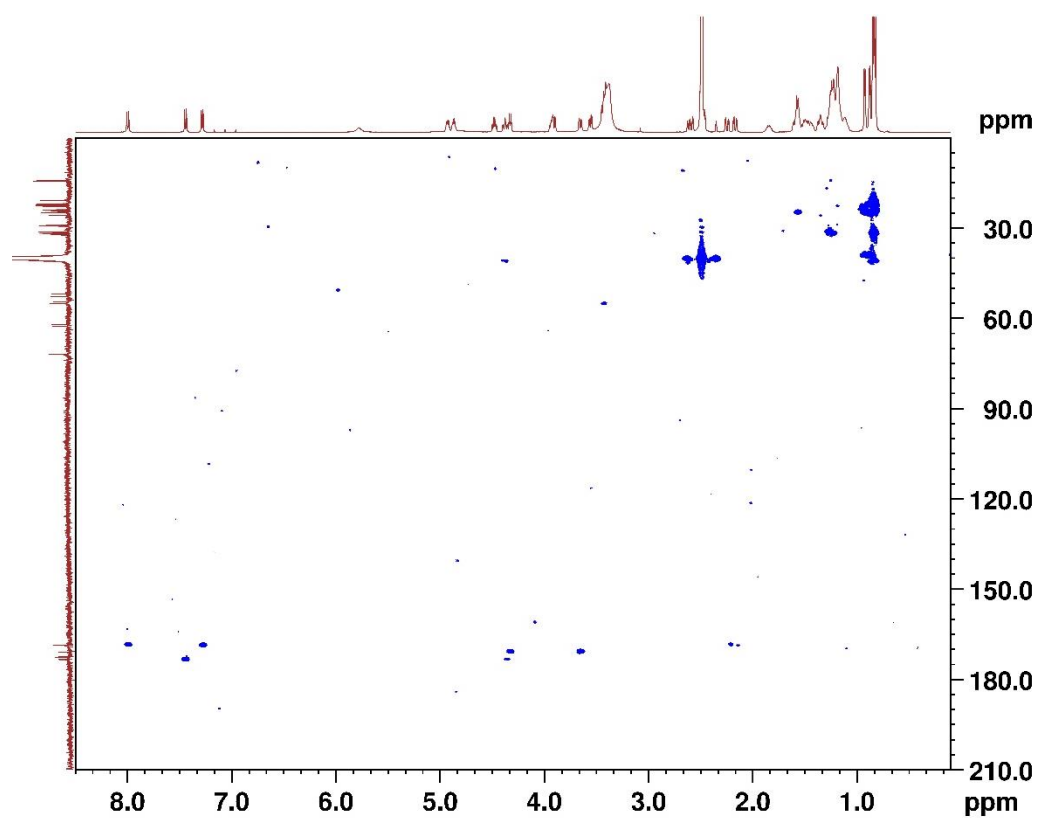
4.5. References

(1)   Aminov, R. I. A Brief History of the Antibiotic Era: Lessons Learned and Challenges for the Future. *Front. Microbiol.* **2010**, *1* (DEC), 1–7. (2)   Ventola C. L. The Antibiotic Resistance Crisis - Causes and Threats. *P T J.* **2015**, *40* (4), 277–283.

(3)   Sengupta, S.; Chattopadhyay, M. K.; Grossart, H. P. The Multifaceted Roles of Antibiotics and Antibiotic Resistance in Nature. *Front. Microbiol.* **2013**, *4* (MAR), 1–13.

(4)   Zaman, S. Bin; Hussain, M. A.; Nye, R.; Mehta, V.; Mamun, K. T.; Hossain, N. A Review on Antibiotic Resistance: Alarm Bells Are Ringing. *Cureus* **2017**, *9* (6).

(5)   Larsson, D. G. J.; Flach, C. F. Antibiotic Resistance in the Environment. *Nat. Rev. Microbiol.* **2022**, *20* (5), 257–269.

(6)   Murray, C. J.; Ikuta, K. S.; Sharara, F.; Swetschinski, L.; Robles Aguilar, G.; Gray, A.; Han, C.; Bisignano, C.; Rao, P.; Wool, E.; Johnson, S. C.; Browne, A. J.; Global Burden of Bacterial Antimicrobial Resistance in 2019: A Systematic Analysis. *Lancet* **2022**, *399* (10325), 629–655.

(7)   Schilling, N. A.; Berscheid, A.; Schumacher, J.; Saur, J. S.; Konnerth, M. C.; Wirtz, S. N.; Beltrán-Beleña, J. M.; Zipperer, A.; Krismer, B.; Peschel, A.; Kalbacher, H.; Brötz-Oesterhelt, H.; Steinem, C.; Grond, S. Synthetic Lugdunin Analogues Reveal Essential Structural Motifs for Antimicrobial Action and Proton Translocation Capability. *Angew. Chemie Int. Ed.* **2019**, *58* (27), 9234–9238.

(8)   Greber, K. E.; Dawgul, M. Current Topics in Medicinal Chemistry The International Journal for In-Depth Reviews on Current Topics in Medicinal Chemistry Impact Factor: 2.9. *Curr. Top. Med. Chem.* **2017**, *17*, 620–628.

(9)   Mahlapuu, M.; Håkansson, J.; Ringstad, L.; Björn, C. Antimicrobial Peptides: An Emerging Category of Therapeutic Agents. *Front. Cell. Infect. Microbiol.* **2016**, *6* (DEC), 1–12.

(10)   De La Fuente-Núñez, C.; Korolik, V.; Bains, M.; Nguyen, U.; Breidenstein, E. B. M.; Horsman, S.; Lewenza, S.; Burrows, L.; Hancock, R. E. W. Inhibition of Bacterial Biofilm Formation and Swarming Motility by a Small Synthetic Cationic Peptide. *Antimicrob. Agents Chemother.* **2012**, *56* (5), 2696–2704.

(11)   Rütschlin, S.; Böttcher, T. Inhibitors of Bacterial Swarming Behavior. *Chem. - A Eur. J.* **2020**, *26* (5), 964–979.

(12)   Uddin, S. J.; Shilpi, J. A.; Nahar, L.; Sarker, S. D.; Göransson, U. Editorial: Natural Antimicrobial Peptides: Hope for New Antibiotic Lead Molecules. *Front. Pharmacol.* **2021**, *12* (February), 10–12.

(13)   Atanasov, A. G.; Zotchev, S. B.; Dirsch, the I. N. P. S. T.; Supuran, C. T. Natural Products in Drug Discovery: Advances and Opportunities. *Nat. Rev. Drug Discov.* **2021**, *20* (3), 200–216.

(14)   Huang, S.; Liu, Y.; Liu, W.; Neubauer, P.; Li, J. The Nonribosomal Peptide Valinomycin: From Discovery to Bioactivity and Biosynthesis. *Microorganisms* **2021**, *9* (4), 1–22.

(15)   Gunjal, V. B.; Thakare, R.; Chopra, S.; Reddy, D. S. Teixobactin: A Paving Stone toward a New Class of Antibiotics? *J. Med. Chem.* **2020**, *63* (21), 12171–12195.

(16)   Ling, L. L.; Schneider, T.; Peoples, A. J.; Spoering, A. L.; Engels, I.; Conlon, B. P.; Mueller, A.; Schäberle, T. F.; Hughes, D. E.; Epstein, S.; Jones, M.; Lazarides, L.; Steadman, V. A.; Cohen, D. R.; Felix, C. R.; Fetterman, K. A.; Millett, W. P.; Nitti, A. G.; Zullo, A. M.; Chen, C.; Lewis,

K. A New Antibiotic Kills Pathogens without Detectable Resistance. *Nature* **2015**, *517* (7535), 455–459.

(17)   Guan, Q.; Huang, S.; Jin, Y.; Campagne, R.; Alezra, V.; Wan, Y. Recent Advances in the Exploration of Therapeutic Analogues of Gramicidin S, an Old but Still Potent Antimicrobial Peptide. *J. Med. Chem.* **2019**, *62* (17), 7603–7617.

(18)   Hamada, Y.; Shioiri, T. Recent Progress of the Synthetic Studies of Biologically Active Marine Cyclic Peptides and Depsipeptides. *Chem. Rev.* **2005**, *105* (12), 4441–4482.

(19)   Adrio, J.; Cuevas, C.; Manzanares, I.; Joullié, M. M. Total Synthesis and Biological Evaluation of Tamandarin B Analogues. *J. Org. Chem.* **2007**, *72* (14), 5129–5138.

(20)   Kaur, H.; Harris, P. W. R.; Little, P. J.; Brimble, M. A. Total Synthesis of the Cyclic Depsipeptide YM-280193, a Platelet Aggregation Inhibitor. *Org. Lett.* **2015**, *17* (3), 492–495.

(21)   Lemmens-Gruber, R.; Kamyar, M.; Dornetshuber, R. Cyclodepsipeptides - Potential Drugs and Lead Compounds in the Drug Development Process. *Curr. Med. Chem.* **2009**, *16* (9), 1122–1137.

(22)   Belofsky, G. N.; Jensen, P. R.; Fenical, W. Sansalvamide: A New Cytotoxic Cyclic Depsipeptide Produced by a Marine Fungus of the Genus Fusarium. *Tetrahedron Lett.* **1999**, *40* (15), 2913–2916.

(23)   Otrubova, K.; Lushington, G.; Vander Velde, D.; McGuire, K. L.; McAlpine, S. R. Comprehensive Study of Sansalvamide A Derivatives and Their Structure-Activity Relationships against Drug-Resistant Colon Cancer Cell Lines. *J. Med. Chem.* **2008**, *51* (3), 530–544.

(24)   Vera, M. D.; Joullie, M. M. Natural Products as Probes of Cell Biology: 20 Years of Didemnin Research. *Med. Res. Rev.* **2002**, *22* (2), 102–145.

(25)   Belof, J. L. Survey of the Didemnins: A Class of Depsipeptide Natural Products with Promising Biomedical Applications. **2006**, No. January 2007.

(26)   Bionda, N.; Stawikowski, M.; Stawikowska, R.; Cudic, M.; López-Vallejo, F.; Treitl, D.; Medina-Franco, J.; Cudic, P. Effects of Cyclic Lipodepsipeptide Human Cell Toxicity. *ChemMedChem* **2012**, *7* (5), 871–882.

(27)   Driggers, E. M.; Hale, S. P.; Lee, J.; Terrett, N. K. The Exploration of Macrocycles for Drug Discovery - An Underexploited Structural Class. *Nat. Rev. Drug Discov.* **2008**, *7* (7), 608–624.

(28)   Zhang, H.; Nielsen, A. L.; Boesgaard, M. W.; Harpsøe, K.; Daly, N. L.; Xiong, X. F.; Underwood, C. R.; Haugaard-Kedström, L. M.; Bräuner-Osborne, H.; Gloriam, D. E.; Strømgaard, K. Structure–Activity Relationship and Conformational Studies of the Natural Product Cyclic Depsipeptides YM-254890 and FR900359. *Eur. J. Med. Chem.* **2018**, *156*, 847–860.

(29)   Bionda, N.; Pitteloud, J. P.; Cudic, P. Cyclic Lipodepsipeptides: A New Class of Antibacterial Agents in the Battle against Resistant Bacteria. *Future Med. Chem.* **2013**, *5* (11), 1311–1330.

(30)   Craik, D. J.; Fairlie, D. P.; Liras, S.; Price, D. The Future of Peptide-Based Drugs. *Chem. Biol. Drug Des.* **2013**, *81* (1), 136–147.

(31)   Boros, C.; Smith, C. J.; Vasina, Y.; Che, Y.; Dix, A. B.; Darveaux, B.; Pearce, C. Isolation and Identification of the Icosalides - Cyclic Peptolides with Selective Antibiotic and Cytotoxic Activities. *J. Antibiot. (Tokyo).* **2006**, *59* (8), 486–494.

(32)   Wilkinson, L. V.; Alford, M. A.; Coleman, S. R.; Wu, B. C.; Lee, A. H. Y.; Blimkie, T. M.;

Bains, M.; Falsafi, R.; Pletzer, D.; Hancock, R. E. W. Peptide 1018 Inhibits Swarming and Influences Anr-Regulated Gene Expression Downstream of the Stringent Stress Response in Pseudomonas Aeruginosa. *PLoS One* **2021**, *16* (4 April), 1–18.

(33) Dose, B.; Niehs, S. P.; Scherlach, K.; Flórez, L. V.; Kaltenpoth, M.; Hertweck, C. Unexpected Bacterial Origin of the Antibiotic Icosalide: Two-Tailed Depsipeptide Assembly in Multifarious Burkholderia Symbionts. *ACS Chem. Biol.* **2018**, *13* (9), 2414–2420.

(34) Jenner, M.; Jian, X.; Dashti, Y.; Masschelein, J.; Hobson, C.; Roberts, D. M.; Jones, C.; Harris, S.; Parkhill, J.; Raja, H. A.; Oberlies, N. H.; Pearce, C. J.; Mahenthiralingam, E.; Challis, G. L. An Unusual: Burkholderia Gladioli Double Chain-Initiating Nonribosomal Peptide Synthetase Assembles "fungal" Icosalide Antibiotics. *Chem. Sci.* **2019**, *10* (21), 5489–5494.

(35) Bionda, N.; Fleeman, R. M.; Shaw, L. N.; Cudic, P. Effect of Ester to Amide or N-Methylamide Substitution on Bacterial Membrane Depolarization and Antibacterial Activity of Novel Cyclic Lipopeptides. *ChemMedChem* **2013**, *8* (8), 1394–1402.

(36) Merrifield, R. B. Solid Phase Peptide Synthesis. *Excerpta Med., I.C.S.* **1976**, *No.374*, 29–39.

(37) Kitir, B.; Baldry, M.; Ingmer, H.; Olsen, C. A. Total Synthesis and Structural Validation of Cyclodepsipeptides Solonamide A and B. *Tetrahedron* **2014**, *70* (42), 7721–7732.

(38) Jin, Y.; Kim, D. H. A Practical Method for the Conversion of β-Hydroxy Carboxylic Acids into the Corresponding β-Amino Acids. *Synlett* **1998**, *33* (11), 1189–1190.

(39) Schrödinger Release 2022-2: MacroModel, Schrödinger, LLC, New York, NY, **2021**.

(40) Cierpicki, T.; Otlewski, J. Amide Proton Temperature Coefficients as Hydrogen Bond Indicators in Proteins. *J. Biomol. NMR* **2001**, *21* (3), 249–261.

(41) Castilho, A. L.; Caleffi-Ferracioli, K. R.; Canezin, P. H.; Dias Siqueira, V. L.; de Lima Scodro, R. B.; Cardoso, R. F. Detection of Drug Susceptibility in Rapidly Growing Mycobacteria by Resazurin Broth Microdilution Assay. *J. Microbiol. Methods* **2015**, *111*, 119–121.

(42) Yeware, A.; Sarkar, D. Novel Red Fluorescence Protein Based Microplate Assay for Drug Screening against Dormant Mycobacterium Tuberculosis by Using Paraffin. *Tuberculosis* **2018**, *110*, 15–19.

(43) Langdon, S. P. Cancer Cell Culture. *Cancer Cell Cult.* **2003**, *731*, 237–245.

(44) Pirrung, M. C.; Zhang, F.; Ambadi, S.; Gangadhara Rao, Y. Total Synthesis of Fellutamides, Lipopeptide Proteasome Inhibitors. More Sustainable Peptide Bond Formation. *Org. Biomol. Chem.* **2016**, *14* (35), 8367–8375.

(45) Mountford, S. J.; Mohanty, B.; Roberts, K. D.; Yu, H. H.; Scanlon, M. J.; Nation, R. L.; Velkov, T.; Li, J.; Thompson, P. E. The First Total Synthesis and Solution Structure of a Polypeptin, PE2, a Cyclic Lipopeptide with Broad Spectrum Antibiotic Activity. *Org. Biomol. Chem.* **2017**, *15* (34), 7173–7180.

(46) Stawikowski, M.; Cudic, P. Depsipeptide Synthesis. *Methods Mol. Biol.* **2007**, *386* (4), 321–339.

(47) CLSI. M45. Methods for Antimicrobial Dilution and Disk Susceptibility Testing of Infrequently Isolated or Fastidious Bacteria ; Proposed Guideline; **2015**; Vol. 35.

(48) CLSI, Methods for Antimicrobial Dilution and Disk Susceptibility of Infrequently Isolated or Fastidious Bacteria, Approved Guideline, 2nd. Ed., CLSI Document M45-A2.

ABSTRACT

Name of the Student: Abha Dangi   **Registration No.:** 10CC17J26034

Faculty of Study: Chemical Science   **Year of Submission:** 2023

AcSIR academic center/CSIR Lab: **Name of the Supervisor**: Dr. Udaya Kiran

CSIR-National Chemical Laboratory, Pune   Marelli

Title of the thesis: "Study of conformations in *N*-substituted peptides beyond *N*-methylation & Development of bioactive peptide analogs based on Tau derived AcPHF6 and AcPHF6*, and Icosalide A"

Peptides, a distinct class of molecules placed between small molecules and antibodies, have occupied a therapeutic niche due to their unique biochemical and therapeutic properties. The advantages of high receptor specificity and low toxicity make peptides superior drug candidates, and their limitations such as low *in vivo* stability and low membrane permeability are major roadblocks to their drug development process. As the biological activity of peptides results from their conformations, peptide-based drug design focuses on optimizing the bioactive peptide sequences and their conformations to elicit all the desirable functions required to be a lead or drug. Based on these aspects, this thesis discusses the development of new synthetic modifications in peptides for the modulation of their conformations; and employs peptide design strategies to obtain new bioactive peptides and to study their structure-activity relationships. Chapter 1 of the thesis discussed the general introduction and therapeutic significance of peptides. In Chapter 2, we explored the *N*-arylation of backbone amides in peptides as a conformational modification tool for peptides. In Chapter 3, we investigated the aggregation propensity of each amino acid in the amyloidogenic hexa peptides (PHF and PHF*) derived from Tau protein. By using these results and peptide design principles, we designed, synthesized and investigated the aggregation nature of 10 macrocyclic peptides. The study resulted in two peptides that selectively modulate Tau aggregation- an aggregation promoter and an inhibitor. In Chapter 4, we discussed the total synthesis of Icosalide A and its structure elucidation. We established the NMR conformation of Icosalide A that showed an amphiphilic structure with a unique disposition of sidechains. Further, we explored the SAR studies of Icosalide A and its analogues while also establishing the antitubercular and anticancerous activity of Icosalide A.

(1) List of publications emanating from the thesis work

1. **Dangi, A** Marelli, U. K.; Pande, B.; Agrawal, S.; Sarkar, D.; Vamkudoth, K. R. Total Synthesis, Structure Elucidation and Expanded Bioactivity of Icosalide A: Effect of Lipophilicity and Ester to Amide Substitution on Its Bioactivity. *Org. Biomol. Chem.* **2023**. https://doi.org/10.1039/D3OB00809F.

2. **Dangi, A**.; Kiran Marelli, U. Exploration of N-Arylation of Backbone Amides as a Novel Tool for Conformational Modification in Peptides. *Cover Feature Article Chem. A Eur. J.* 2023.

3. **Dangi, A**.; Balmik, A. A.; Ghorpade, A. K.; Gorantla, N. V.; Sonawane, S. K.; Chinnathambi, S.; Marelli, U. K. Residue-Based Propensity of Aggregation in the Tau Amyloidogenic Hexapeptides AcPHF6∗ and AcPHF6. *RSC Adv.* **2020**, *10* (46), 27331-27335.

4. **Dangi, A**.; Tazeen Qureshi, Subashchandrabose Chinnathambi U. Macrocyclic peptides derived from AcPHF6* and AcPHF6 to selectively modulate the Tau aggregation. (**Under review**)

(2) List of publications non-emanating from the thesis work

5. Meena, C. L.; Singh, D.; Weinmüller, M.; Reichart, F.; **Dangi, A**.; Marelli, U. K.; Zahler, S.; Sanjayan, G. J. Novel Cilengitide-Based Cyclic RGD Peptides as Avβ3 Integrin Inhibitors. *Bioorganic and Medicinal Chemistry Letters*. **2020**

6. Sonawane, S. K.; Chidambaram, H.; Boral, D.; Gorantla, N. V.; Balmik, A. A.; **Dangi, A**.; Ramasamy, S.; Marelli, U. K.; Chinnathambi, S. EGCG Impedes Human Tau Aggregation and Interacts with Tau. *Sci. Rep.* **2020**, *10* (1), 1–17.

7. Balmik, A. A.; Chidambaram, H.; **Dangi, A**.; Marelli, U. K.; Chinnathambi, S. HDAC6 ZnF UBP as the Modifier of Tau Structure and Function. *Biochemistry* **2020**, *59* (48), 4546–4562.

8. Balmik, A. A.; Das, R.; **Dangi, A**.; Gorantla, N. V.; Marelli, U. K.; Chinnathambi, S. Melatonin Interacts with Repeat Domain of Tau to Mediate Disaggregation of Paired Helical Filaments. *Biochim. Biophys. Acta - Gen. Subj.* **2020**, *1864* (3), 23–26.

9. Di Leva, F. S.; Tomassi, S.; Di Maro, S.; Reichart, F.; Notni, J.; **Dangi, A**.; Marelli, U. K.; Brancaccio, D.; Merlino, F.; Wester, H. J.; Novellino, E.; Kessler, H.; Marinelli, L. From a Helix to a Small Cycle: Metadynamics-Inspired αvβ6 Integrin Selective Ligands. *Angew. Chemie Int. Ed.* **2018**, *57* (44), 14645–14649.

(3) List of posters presented with details

1. Poster presentation at 26th National Magnetic Resonance Society Meeting & International Conference on NMR from "Molecules to Human Behavior and Beyond" Organized by Department of Chemistry, Saurashtra University, Rajkot, (Feburary 18-21 2020).

Title: Residue-Based Propensity of Aggregation in Tau Amyloidogenic Hexapeptides AcPHF6* and AcPHF6

Abstract: In Alzheimer`s disease and related Tauopathies, aggregation of microtubule-associated protein Tau occurs *via* association of two hexapeptides motifs PHF* ^{275}VQIINK^{280} and PHF ^{306}VQIVYK^{311} present in second and third repeat regions, respectively. The PHF and PHF* form the core of Tau fibrils by forming stable β-sheet structure. To understand the role of constituent amino acids of PHF and PHF* in their aggregation, a library of 12 peptides was synthesized using solid phase peptide synthesis by replacing each amino acid with alanine. The peptides were subjected to aggregation and their aggregation propensity, the morphology of aggregates was characterized by using ThS/ANS fluorescence assay and TEM. The NMR data and CD spectroscopy indicated the absence of any robust conformation in all peptides. While the aggregation was found to be suppressed in most of the alanine substituents, replacement of glutamine by alanine in both PHF and PHF* resulted in enhanced fibrillization. Overall, the study provides key insights of PHF*/PHF peptide aggregation with alanine mutation and their potential in therapeutics against Tau aggregation.

2. Poster presentation at National Science Day Poster Presentation at CSIR-National Chemical Laboratory, Pune (February 25-27, 2020)

Title: Residue-Based Propensity of Aggregation in Tau Amyloidogenic Hexapeptides AcPHF6* and AcPHF6

Abstract: In Alzheimer`s disease and related Tauopathies, aggregation of microtubule-associated protein Tau occurs *via* association of two hexapeptides motifs PHF* ^{275}VQIINK^{280} and PHF ^{306}VQIVYK^{311} present in second and third repeat regions, respectively. The PHF and PHF* form the core of Tau fibrils by forming stable β-sheet structure. To understand the role of constituent amino acids of PHF and PHF* in their aggregation, a library of 12 peptides was synthesized using solid phase peptide synthesis by replacing each amino acid with alanine. The peptides were subjected to aggregation and their aggregation propensity, the morphology of aggregates was characterized by using ThS/ANS fluorescence assay and TEM. The NMR data and CD spectroscopy indicated the absence of any robust conformation in all peptides. While the aggregation was found to be suppressed in most of the alanine substituents, replacement of glutamine by alanine in both PHF and

PHF* resulted in enhanced fibrillization. Overall, the study provides key insights of PHF*/PHF peptide aggregation with alanine mutation and their potential in therapeutics against Tau aggregation.

Ms. Abha Dangi

Research Student

Dr. Udaya Kiran Marelli

Research Supervisor

Check for updates

Residue-based propensity of aggregation in the Tau amyloidogenic hexapeptides AcPHF6* and AcPHF6†

Abha Dangi,‡[abc] Abhishek Ankur Balmik,‡[cd] Archana Kisan Ghorpade,[ab] Nalini Vijay Gorantla,[cd] Shweta Kishor Sonawane,[cd] Subashchandrabose Chinnathambi [ID] *[cd] and Udaya Kiran Marelli [ID] *[abc]

In Alzheimer's disease and related tauopathies, the aggregation of microtubule-associated protein, Tau, into fibrils occurs via the interaction of two hexapeptide motifs PHF* [275]VQIINK[280] and PHF [306]VQIVYK[311] as β-sheets. To understand the role of the constituent amino acids of PHF and PHF* in the aggregation, a set of 12 alanine mutant peptides was synthesized by replacing each amino acid in PHF and PHF* with alanine and they were characterized by nuclear magnetic resonance (NMR) spectroscopy, circular dichroism (CD), transmission electron microscopy (TEM) and ThS/ANS fluorescence assay. Our studies show that while the aggregation was suppressed in most of the alanine mutant peptides, replacement of glutamine by alanine in both PHF and PHF* enhanced the fibrillization.

Conformational misfolding of proteins leading to protein aggregates, also known as amyloids, is a prime trait of neurodegenerative diseases such as Alzheimer's (AD) and Parkinson's disease (PD).[1,2] Amyloid protein aggregates are also observed in other disease conditions such as diabetes and arthritis.[1,3–7] Deposition of amyloids in AD leads to irreversible cell death and chronic dementia, resulting in the loss of vital bodily functions, severe behavioural disorders and ultimately death. The search for an effective cure for AD is in persistent progress and interfering with the protein deposition mechanisms in neuronal cells and tissues is a rational target[8–13] for the majority of studies focused on the drug discovery research for AD.

Two proteins, amyloid beta (Aβ) and Tau, have been identified to form protein deposits linked with AD. Aβ are various small length protein fragments derived from amyloid precursor protein (APP), among which Aβ-42 has been proven to be toxic and form amyloid plaques.[8,14] However, in recent times, increasing evidence for the pathological role of Tau protein in AD was found.[15–19] Tau, a microtubule-binding protein, forms neurofibrillary tangles (NFTs) in AD via soluble oligomers, which are stabilized by beta-sheet interactions. Tau is 441 amino acids long with an N-terminus region, a proline rich region, a key microtubule-binding domain consisting of 3 or 4 repeat regions depending on the Tau isoform, and a C-terminus domain.[20] A high resolution cryo-EM structure of Tau filaments from the brain of an AD patient was recently established and highlighted the presence of beta sheet structures stabilized by hydrogen bonds and hydrophobic interactions.[21] Interestingly, the cryo-EM structure of Tau filaments obtained from the brain of a patient with Pick's disease revealed a different fold for Tau, suggesting disease specific conformational misfolding of Tau.[22]

Two hexapeptide regions, [275]VQIINK[280] and [306]VQIVYK[311], residing in the second and third repeat units of Tau, respectively, form the core beta sheet structure in Tau, a structural feature responsible for Tau oligomerization and the formation of NFTs.[16,23–26] Synthetic analogues of both these hexapeptides, Ac-VQIINK-NH$_2$ (AcPHF6*, **1**; PHF stands for paired helical filaments) and Ac-VQIVYK-NH$_2$ (AcPHF6, **1'**), which has acetyl protection on the N-terminus and amidation on the C-terminus, are known to form structurally similar fibrils akin to those of Tau. Due to this structural mimicry, AcPHF6 and AcPHF6* stand out as model peptides to study the promotion or inhibitory effect of various ligands on Tau aggregation[27–29] and for the development of any peptide based Tau aggregation inhibitors.[30–39] Previous studies have shown that even shorter fragments from AcPHF6 are also capable of fibril formation but with a lower rate of polymerization and only upon nucleation with known fibrils.[40] The aggregation properties in lysine mutants of AcPHF6 were explored by the Goux research group and the results showed variable fibril formation tendency for the

[a]Central NMR Facility, CSIR-National Chemical Laboratory, Dr HomiBhabha Road, 411008 Pune, India

[b]Division of Organic Chemistry, CSIR-National Chemical Laboratory, Dr HomiBhabha Road, 411008 Pune, India

[c]Academy of Scientific and Innovative Research (AcSIR), 110025 New Delhi, India

[d]Neurobiology Group, Division of Biochemical Sciences, CSIR-National Chemical Laboratory, Dr HomiBhabha Road, 411008 Pune, India

† Electronic supplementary information (ESI) available: Experimental details, HRMS, HPLC, cell morphology and cell viability data. See DOI: 10.1039/d0ra03809a

‡ Equal contribution.

mutants subject to buffer and salt conditions.[40,41] Recently, Chemerovski-Glikman *et al.* demonstrated that proline mutants of AcPHF6 inhibited the aggregation of AcPHF6.[42]

In general, AcPHF6* remains less explored compared to AcPHF6, although the recent studies attribute a higher role to [275]VQIINK[280] in Tau aggregation.[27] Despite several studies on these hexapeptides, to our knowledge, the contribution of individual amino acids in AcPHF6 and AcPHF6* towards Tau aggregation has not been examined hitherto, which information is fundamentally important for the design of Tau aggregation inhibitors. Hence, in the present study, the residue specific propensity of amino acids constituting AcPHF6* and AcPHF6 in their aggregation is investigated. For our study, alanine mutation peptides of AcPHF6* and AcPHF6 were synthesized, and their conformational and aggregation properties were characterized using various biophysical and biochemical techniques.

A set of twelve peptides consisting of parent peptides AcPHF6* (**1**) and AcPHF6 (**1′**) and their sequential single site alanine mutant peptides (**2–6** and **2′–6′**) were synthesized by employing Fmoc-based solid phase peptide synthesis using rink amide MBHA resin (Fig. 1). All of the peptides were subsequently purified by reverse phase semi preparative HPLC for further studies. Although mutant peptides of **1** and **1′** in which lysine is substituted by alanine were synthesized, they could not be purified because of partial solubility in an acetonitrile–water combination and other buffers.

Under normal physiological conditions, Tau protein exists in a random coil conformation or a natively disordered state.[43,44] CD spectroscopic study of all of the twelve peptides was carried out at 1 mg mL^{-1} concentration in plain 5 mM 3-(*N*-morpholino)propanesulfonic acid (MOPS) buffer (Fig. 2) under non-aggregating conditions. All of the peptides exhibited a similar pattern of CD absorption with only negative mode absorption. Peptides **1** and **4** had similar CD spectra with negative absorption at ~203 nm and a very weak shoulder at around 225 nm, whereas **2**, **3**, **5** and **6** exhibited slightly intense CD spectra
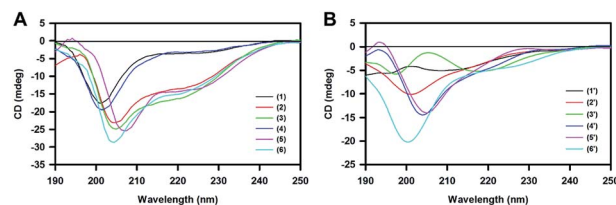
Fig. 2 Circular dichroism (CD) analysis for (A) **1–6** and (B) **1′–6′** recorded at 1 mg mL^{-1} concentration in 5 mM MOPS buffer at 298 K in non-aggregating conditions. None of these peptides showed the CD characteristics of a well folded alpha helix or a beta sheet. All of the peptides, in general, showed a random coil conformation with negative absorption at approx. 205 nm, while **1′** and **3′** indicated more inclination towards a β-sheet structure.

compared to **1** and **4**, with negative absorption at 205 nm and a weak negative shoulder at around 225 nm. This shift for **1** and **4** could be due to the presence of mixed secondary structures. Overall, the described CD analysis is mostly indicative of a random coil structure.[40,41] Hence, a possible random coil population may be inferred for all of the peptides **1–6**. A similar trend was observed for the conformation of the peptides in the **1′–6′** series, wherein the **2′**, **4′**, **5′** and **6′** peptides exhibited negative absorptions at around ~203–205 and ~225 nm, with the latter being weak in intensity. A slight rightward shift for **4′** and **5′** compared to **2′** and **6′** could indicate a possible mixed population of random coils and beta sheets. Peptides **1′** and **3′** did not have a characteristic CD pattern corresponding to any of the standard peptide secondary structural scaffolds. The signatures obtained for peptides **1′** and **3′** indicate a structural orientation towards β-sheets.

^{1}H NMR spectra for the compounds **1–6** and **1′–6′** were recorded in DMSO-d_6 (Fig. 3) and phosphate buffer (see the ESI†) at 298 K at 5 mM concentration. The chemical shift dispersion of the amide and alpha proton regions in ^{1}H NMR reflect the folded secondary structural nature of the linear peptides. It is evident from the overlay of these regions for
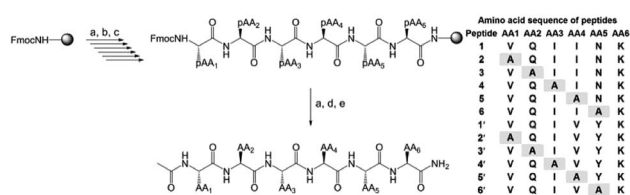
Fig. 1 Scheme showing the synthesis of peptides (**1–6** and **1′–6′**) using Fmoc-based solid phase peptide synthesis on rink amide MBHA resin (150 mg with 0.6 mmol g^{-1} loading capacity). Reaction conditions: (a) Fmoc deprotection in 20% piperidine in DMF (2* 10 min); (b) Fmoc-pAA6-OH (2 eq.), HCTU (2 eq.), HOAt (2 eq.), DIPEA (2 eq.) in NMP, 1.5 h; (c) capping of free NH groups on resin using acetic anhydride (1.2 mL) and pyridine (0.8 mL), 30 min. Steps (a) and (b) were repeated for the coupling of the rest of the amino acids in sequential order until a linear chain of the hexamer was achieved on the resin. (d) Acetic anhydride (1 mL), DIPEA (100 μL) in DMF, 1 h; (e) TFA : H2-O : TIPS in a 9 : 0.5 : 0.5 volume ratio (3 times for 30 min) for global deprotection of the peptide and cleavage from the resin. pAA stands for the side chain protected form of the corresponding amino acid.
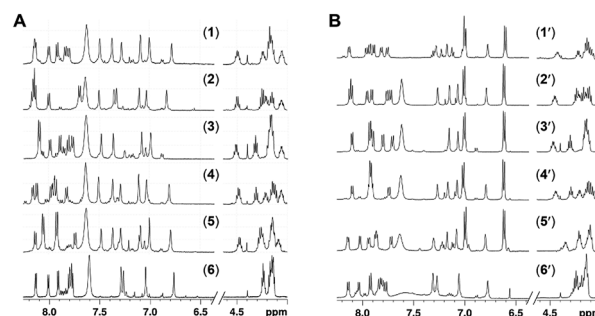
Fig. 3 Overlay of ^{1}H NMR spectra of **1–6** and **1′–6′** recorded in DMSO-d_6 at 298 K at 5 mM concentration. For clarity, the amide NH region (6.5–8.25 ppm) and alpha proton region (4–4.6 ppm), which signify the folded nature of the peptides, are shown. An absence of a robust solution state conformation in these peptides was supported by the lack of resonance dispersion for both the amide and alpha proton regions.

peptides **1–6** and **1′–6′** (Fig. 3, ESI Fig. 1–24†) that none of the peptides have significant chemical shift dispersion, either for amide or alpha protons. For all of the peptides, the amide and alpha proton chemical shifts were found to be distributed within a range of 0.2–0.5 ppm and have severe overlaps, supporting the absence of a well folded conformation among these peptides. This is in concurrence with the CD spectroscopic studies, which indicated a random coil structure for **1–6** and **1′–6′** in monomeric form. ^{1}H NMR based hydrogen bonding coefficients (calculated based on the change in the chemical shift over a temperature range; see the ESI†) for the amide NHs conveys information about the involvement of NHs in hydrogen bonding or solvent shielding. Constituent backbone amide NH resonances from all of the peptides have shown high temperature coefficients (in the range of −3.4 to −7.6 ppb K^{-1}; see the ESI†), implying their non-involvement in strong hydrogen bonding. This complements the lack of chemical dispersion for amide and alpha protons, further supporting the absence of a robust conformation for any of the twelve peptides, **1–6** and **1′–6′**. Therefore, based on the above results it can be stated that mutation with alanine neither promoted a robust helical or beta sheet conformtion nor brought any significant changes in the original conformtion of peptides **1–6** and **1′–6′**.

The self-aggregation properties of peptides **1–6** and **1′–6′** were characterized by TEM analysis (Fig. 4). The aggregation for all of the peptides was set up at 100 μM concentrations in 20 mM BES buffer at pH 7.4 with 25 μM heparin as an inducer. After incubation for 168 h at 37 °C, TEM images were recorded for 2 μM peptides on carbon coated copper grids. The parent peptides, AcPHF6* (**1**) and AcPHF6 (**1′**) formed aggregates as expected. Out of ten mutant peptides, peptides **3** and **3′** both with glutamine substituted by alanine showed filamentous aggregates similar to **1** and **1′**, while no aggregates were observed for the rest of the peptides.
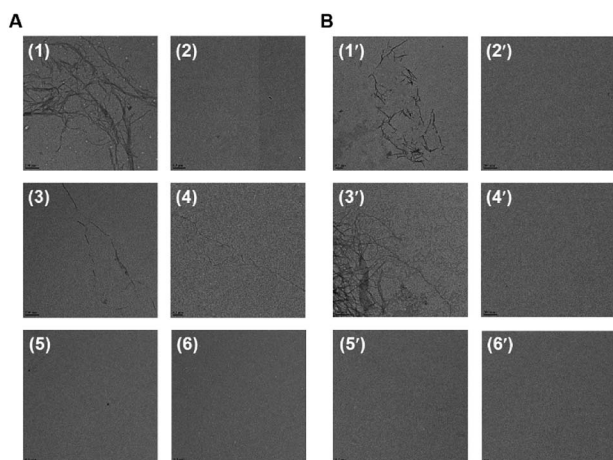
Aggregation of the **1–6** peptides was also monitored by ThS and ANS fluorescence. It was observed that the substitution of valine or isoleucine with alanine in **1** diminished the aggregation propensity of hexapeptides as compared to the native peptide **1**. However, substituting glutamine with alanine in peptide **3** increased the aggregation propensity (Fig. 5A), while a marginally higher aggregation propensity was also observed for **6**, in which alanine is substituted for asparagine. On comparing them at 168 h, **3** and **6** exhibited 83 and 60 au fluorescence, respectively, compared to 30 au for **1** (ESI Fig. 25C†). Similar results were observed for the aggregation assay carried out for the **1′–6′** peptides and their mono-substituted variants (Fig. 5B). The aggregation propensity was found to be suppressed for **2′**, **4′**, **5′** and **6′** when compared to **1′** and **3′**. The aggregation propensity of **3′** was found to be greatly increased compared to all hexapeptides. At 168 h, **3′** exhibited an absolute fluorescence of 100 au, compared to **1′** where a fluorescence value of 48 au was obtained (ESI Fig. 25D†). In agreement with this, peptides **1′** and **3′**, which showed high aggregation propensity in the ThS fluorescence assay, did not present any prominent signature for random coiling but showed orientation towards β-sheet structure in their CD spectra (Fig. 2). However, the ANS fluorescence assay for monitoring hydrophobicity changes over time did not show any significant difference between **1** and its variants (ESI Fig. 25E†). **1′** and its variants in the ANS fluorescence assay followed the pattern of the corresponding ThS assay, suggesting that glutamine to alanine substitution was associated with increased hydrophobicity (ESI Fig. 25F†). Overall, the current aggregation assay suggests that substitution of glutamine to alanine in **1** and **1′** elevates the aggregation propensity, while alanine replacements for the majority of all the other residues suppress the aggregation propensity.

Thus, it is interesting to note that out of the first five residues in **1** and **1′** (namely VQIIN in **1** and VQIVY in **1′**) substitution of any amino acid except for glutamine with alanine nullified their aggregation properties. Conversely, it may be stated that except for glutamine (and asparagine as per the fluorescence assay results), the rest of the residues (V and I in **1**, and V, I and Y in **1′**)

Fig. 4   TEM images for peptides **1–6** and **1′–6′** at the aggregation assay end-point (168 h). The **1** and **1′** hexapeptides can form fibrillar aggregates similar to the full-length Tau protein as they consist of the core upon which aggregates of Tau form. Except for the parent peptides **1** and **1′** and the modified peptides **3** and **3′**, none of the other peptides were observed to form aggregates.
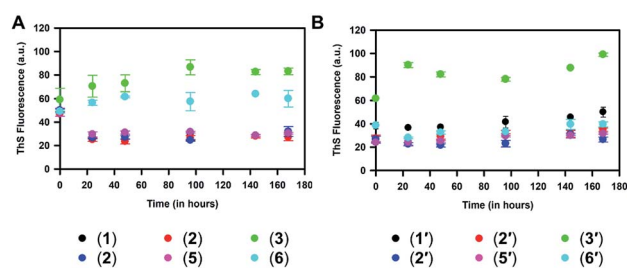
Fig. 5   (A) Aggregation of peptides **1–6** monitored using ThS fluorescence shows the effect of alanine incorporated at various positions in the VQIINK hexapeptide. VQIINK aggregation was found to be affected by substitution of Glu or Asn residues, where these substitutions enhanced the aggregation propensity. (B) Peptides **1′–6′** showed a similar trend in their aggregation propensity, as peptide **3′** with Glu to Ala substitution showed increased aggregation compared to the other peptides in the group.

have a higher propensity to aggregate than alanine when present in **1** and **1′**. Interestingly, in one of the recent studies where proline, a beta sheet breaker, is substituted for each amino acid in **1′**, it was reported that the peptide with glutamine to proline substitution inhibited the aggregation properties of **1′** while the mutant peptide itself was non-aggregating in nature.[42] We speculate that the glutamine in the PHF peptides might be in a conformationally favorable position for beta sheet formation and aggregation, which was disturbed by the cyclically constrained amino acid proline but not by an alanine in our case.

Furthermore, the aggregated **1–6** and **1′–6′** peptides after 168 h were studied in terms of their toxicity in neuro2a cells (see the ESI, Fig. 26†). The aggregated **1–6** peptides did not show toxicity to neuro2a cells up to 5 µM concentration.

In conclusion, Alzheimer's disease is characterized by the deposition of intracellular Tau aggregates and extracellular amyloid-beta plaques. Various treatment strategies have been designed to inhibit or revert this protein aggregation. In particular, PHF6* and PHF6 peptide based inhibition therapies have gained focus due to their structural mimicry to Tau aggregation. To understand the aggregation nature of these two peptides at an individual residue level, here we have synthesized alanine mutant libraries of AcPHF6* and AcPHF6, and characterized them using various biochemical and biophysical methods. The results showed that all of the mutant peptides, except for those with glutamine to alanine substitution (**3** and **3′**), did not aggregate as per the general conditions used for the parent peptides **1** and **1′**. While asparagine to alanine mutation (**6**) showed aggregation propensity in fluorescence assays, no aggregates were observed in the TEM images. Therefore, it was inferred that except for glutamine, the residues V and I in AcPHF6* **1**, and V, I and Y in AcPHF6 **1′** impart a higher aggregation propensity than alanine in the parent peptides. These results are also in alignment with the higher beta sheet propensity of alanine compared to Q but lower than that of V, I and Y.[45,46] Mutational studies using other amino acids that have higher beta sheet/alpha-helical propensities may provide more details on the conformational and aggregation properties of PHF peptides. Overall, alanine substitution in PHF peptides reduces their aggregation propensity without any major change in their conformation. Studying the aggregation properties of these alanine based PHF peptide derivatives provides important and site specific insight into the aggregation behavior of PHFs, *i.e.* PHF6 and PHF6*. Hence, this strategy can be potentially employed to selectively control the aggregation in PHFs *via* the rational choice of alanine mutations. While further extended studies are in progress in our research group, we hope that the current results can form the basis for designing PHF based Tau aggregation inhibitors using suitable mutations.

Conflicts of interest

There are no conflicts to declare.

Acknowledgements

Notes and references

1 C. Soto and S. Pritzkow, *Nat. Neurosci.*, 2018, **21**, 1332–1340.
2 C. A. Ross and M. A. Poirier, *Nat. Med.*, 2000, **10**, S10.
3 D. Eisenberg and M. Jucker, *Cell*, 2012, **148**, 1188.
4 Y. S. Eisele, C. Monteiro, C. Fearns, S. E. Encalada, R. L. Wiseman, E. T. Powers and J. W. Kelly, *Nat. Rev. Drug Discovery*, 2015, **14**, 759.
5 G. G. Glenner and C. W. Wong, *Biochem. Biophys. Res. Commun.*, 1984, **122**, 1131.
6 C. L. Masters, G. Simms, N. A. Weinman, G. Multhaup, B. L. McDonald and K. Beyreuther, *Proc. Natl. Acad. Sci. U.S.A.*, 1985, **82**, 4245.
7 M. Goedert, *Science*, 2015, **349**, 1255555.
8 J. Hardy and D. J. Selkoe, *Science*, 2002, **297**, 353–356.
9 D. M. Holtzman, J. C. Morris and A. M. Goate, *Sci. Transl. Med.*, 2011, **3**(77), 77sr1.
10 C. Li and J. Götz, *Nat. Rev. Drug Discovery*, 2017, **16**, 863.
11 M. Necula, R. Kayed, S. Milton and C. G. Glabe, *J. Biol. Chem.*, 2007, **282**, 10311.
12 M. Pickhardt, M. von Bergen, Z. Gazova, A. Hascher, J. Biernat, E.-M. Mandelkow and E. Mandelkow, *Curr. Alzheimer Res.*, 2005, **2**, 219.
13 K. L. Sciarretta, D. J. Gordon and S. C. Meredith, *Methods Enzymol.*, 2006, **413**, 273.
14 M. P. Murphy and H. LeVine III, *J. Alzheim. Dis.*, 2010, **19**, 311.
15 K. S. Kosik, C. L. Joachim and D. J. Selkoe, *Proc. Natl. Acad. Sci. U.S.A.*, 1986, **83**, 4044.
16 M. Von Bergen, P. Friedhoff, J. Biernat, J. Heberle, E.-M. Mandelkow and E. Mandelkow, *Proc. Natl. Acad. Sci. U.S.A.*, 2000, **97**, 5129.
17 M. Goedert, F. Clavaguera and M. Tolnay, *Trends Neurosci.*, 2010, **33**, 317.
18 S. J. Jackson, C. Kerridge, J. Cooper, A. Cavallini, B. Falcon, C. V. Cella, A. Landi, P. G. Szekeres, T. K. Murray and Z. Ahmed, *J. Neurosci.*, 2016, **36**, 762.
19 P. Friedhoff, M. von Bergen, E.-M. Mandelkow and E. Mandelkow, *Biochim. Biophys. Acta, Mol. Basis Dis.*, 2000, **1502**, 122.
20 E.-M. Mandelkow and E. Mandelkow, *Cold Spring Harbor Perspect. Med.*, 2012, **2**, a006247.
21 A. W. Fitzpatrick, B. Falcon, S. He, A. G. Murzin, G. Murshudov, H. J. Garringer, R. A. Crowther, B. Ghetti, M. Goedert and S. H. Scheres, *Nature*, 2017, **547**, 185.
22 B. Falcon, W. Zhang, A. G. Murzin, G. Murshudov, H. J. Garringer, R. Vidal, R. A. Crowther, B. Ghetti, S. H. Scheres and M. Goedert, *Nature*, 2018, **561**, 137.
23 M. von Bergen, S. Barghorn, L. Li, A. Marx, J. Biernat, E.-M. Mandelkow and E. Mandelkow, *J. Biol. Chem.*, 2001, **276**, 48165.
24 P. Friedhoff, J. Biernat, J. Heberle, E.-M. Mandelkow and E. Mandelkow, *Proc. Natl. Acad. Sci. U.S.A.*, 2000, **97**, 5129.

25 H. Inouye, D. Sharma, W. J. Goux and D. A. Kirschner, *Biophys. J.*, 2006, **90**, 1774.

26 M. von Bergen, S. Barghorn, J. Biernat, E.-M. Mandelkow and E. Mandelkow, *Biochim. Biophys. Acta, Mol. Basis Dis.*, 2005, **1739**, 158.

27 P. Seidler, D. Boyer, J. Rodriguez, M. Sawaya, D. Cascio, K. Murray, T. Gonen and D. Eisenberg, *Nat. Chem.*, 2018, **10**, 170.

28 M. Perez, I. Santa-María, E. Tortosa, R. Cuadros, M. Del Valle, F. Hernández, F. J. Moreno and J. Avila, *J. Neurochem.*, 2007, **103**, 1447.

29 T. Mohamed, T. Hoang, M. Jelokhani-Niaraki and P. P. Rao, *ACS Chem. Neurosci.*, 2013, **4**, 1559.

30 J. Zheng, A. M. Baghkhanian and J. S. Nowick, *J. Am. Chem. Soc.*, 2013, **135**, 6846.

31 A. Belostozky, M. Richman, E. Lisniansky, A. Tovchygrechko, J. H. Chill and S. Rahimipour, *Chem. Commun.*, 2018, **54**, 5980.

32 M. Frenkel-Pinter, M. Richman, A. Belostozky, A. Abu-Mokh, E. Gazit, S. Rahimipour and D. Segal, *Chem.–Eur. J.*, 2016, **22**, 5945.

33 C. K. Wang, S. E. Northfield, Y. Huang, M. C. Ramos and D. J. Craik, *Eur. J. Med. Chem.*, 2016, **109**, 342.

34 C. Dammers, D. Yolcu, L. Kukuk, D. Willbold, M. Pickhardt, E. Mandelkow, A. H. Horn, H. Sticht, M. N. Malhis and N. Will, *PLoS One*, 2016, **11**, e0167432.

35 S. A. Sievers, J. Karanicolas, H. W. Chang, A. Zhao, L. Jiang, O. Zirafi, J. T. Stevens, J. Münch, D. Baker and D. Eisenberg, *Nature*, 2011, **475**, 96.

36 J. Zheng, C. Liu, M. R. Sawaya, B. Vadla, S. Khan, R. J. Woods, D. Eisenberg, W. J. Goux and J. S. Nowick, *J. Am. Chem. Soc.*, 2011, **133**, 3144.

37 V. G. KrishnaKumar, A. Paul, E. Gazit and D. Segal, *Sci. Rep.*, 2018, **8**, 71.

38 A. Paul, S. Kalita, S. Kalita, P. Sukumar and B. Mandal, *Sci. Rep.*, 2017, **7**, 40095.

39 T. D. Vaden, S. A. Gowers, T. S. De Boer, J. D. Steill, J. Oomens and L. C. Snoek, *J. Am. Chem. Soc.*, 2008, **130**, 14640.

40 W. J. Goux, L. Kopplin, A. D. Nguyen, K. Leak, M. Rutkofsky, V. D. Shanmuganandam, D. Sharma, H. Inouye and D. A. Kirschner, *J. Biol. Chem.*, 2004, **279**, 26868.

41 F. A. Rojas Quijano, D. Morrow, B. M. Wise, F. L. Brancia and W. J. Goux, *Biochemistry*, 2006, **45**, 4638.

42 M. Chemerovski-Glikman, M. Frenkel-Pinter, R. Mdah, A. Abu-Mokh, E. Gazit and D. Segal, *Chem.–Eur. J.*, 2017, **23**, 9618.

43 A. L. Fink, *Curr. Opin. Struct. Biol.*, 2005, **15**, 35.

44 S. Jeganathan, M. von Bergen, E.-M. Mandelkow and E. Mandelkow, *Biochemistry*, 2008, **47**, 10526.

45 D. L. Minor Jr and P. S. Kim, *Nature*, 1994, **367**, 660.

46 K. Fujiwara, H. Toda and M. Ikeguchi, *BMC Struct. Biol.*, 2012, **12**, 18.

Cover Feature:

A. Dangi and U. Kiran Marelli

Exploration of N-Arylation of Backbone Amides as a Novel Tool for Conformational Modification in Peptides

N-aryl amide restricted amide bond rotation

D-Ala
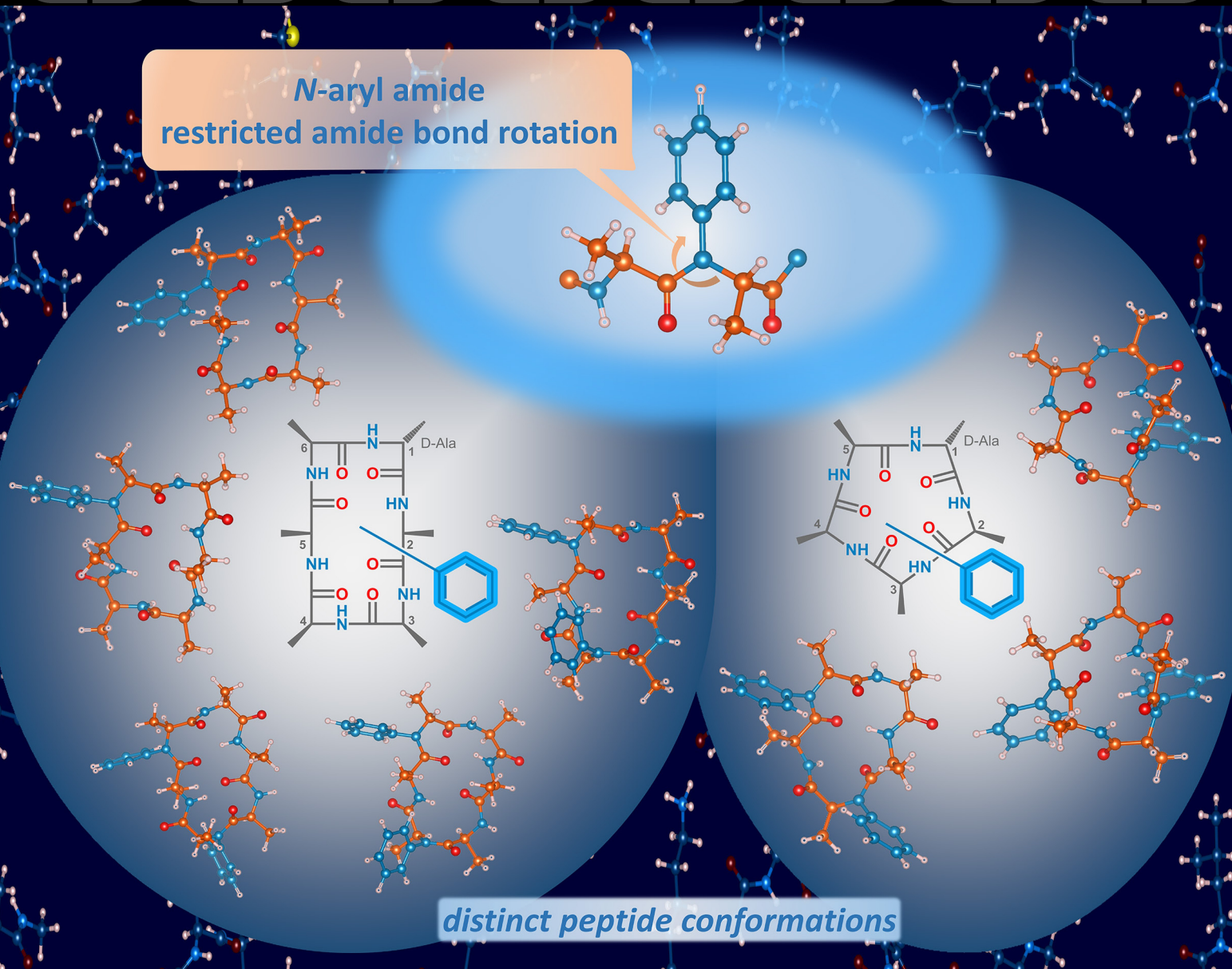
distinct peptide conformations

COVER

N-aryl amide bonds for peptide conformation: In the universe of peptides, the N-aryl amide bond, with its large steric and electronic effects and ability to restrain amide bond rotation, is represented as a new star. By employing N-arylation as a backbone amide modification strategy in peptides, we could unravel the different worlds of distinct and predominantly homogeneous conformations in cyclic hexa- and cyclic pentapeptides containing one or two N-aryl amide bonds. More information can be found in the Research Article by A. Dangi and U. Kiran Marelli (DOI: 10.1002/chem.202300753).

A. Dangi, Dr. U. Kiran Marelli*

1 – 2

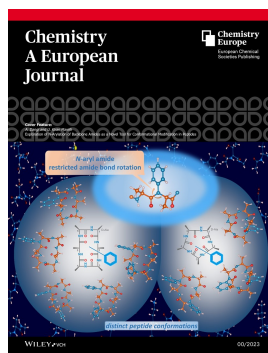**Exploration of N-Arylation of Backbone Amides as a Novel Tool for Conformational Modification in Peptides**

Exploration of N-Arylation of Backbone Amides as a Novel Tool for Conformational Modification in Peptides

Abha Dangi[a, b] and Udaya Kiran Marelli*[a, b]

Abstract: A set of 15 cyclic-hexaalanine and 10 cyclic-pentaalanine peptides containing one or two backbone N-aryl amide bonds were synthesized by following a combination of solution-phase and solid-phase peptide synthesis. NMR-based conformation studies of these N-aryl cyclic-hexaalanine peptides revealed five distinct template conformations with an antiparallel β-sheet structure; for N-aryl cyclic-pentaalanine peptides three template structures were revealed. All the template structures have distinct peptide-turn features. The conformations in these N-aryl peptides were compared to those in the commonly studied N-methyl peptide analogues. We observed that the N-aryl peptides exhibit a considerable conformational homogeneity, and their conformations differ significantly from those in N-methyl analogues. We anticipate that the N-arylation of backbone amides has the potential for application as a novel tool for conformation and physicochemical modification in peptides.

Obtaining a stable, orally available bioactive peptide is a challenging task in the field of peptide therapeutics.[1–6] The biological aspects of peptides are primarily a result of their conformation.[7–9] Conformations in peptides determine the orientation of the constituent residues and corresponding stereoelectronic and physicochemical features responsible for the biological function of the peptides.[10] Hence, optimizing a peptide's conformation while also bringing in specific functional group changes is a crucial part of the peptide-based drug design.[10] A multitude of peptide design strategies, such as the use of homologous or nonproteinogenic amino acids, cyclization, stereo-inversion, foldamers, stapled peptides, and disulfide bridged peptides are some methods that have been developed and followed to architect peptide folding.[11–19]

Cyclic peptides are undoubtedly one of the most successful class of peptides that has offered numerous peptide ligands and therapeutics.[20,21] A growing number of peptide drugs that have received drug approval in recent times are based on cyclic peptides.[22] The conformational robustness of cyclic peptides enhances their binding affinity and selectivity for specific receptors. As they lack amino and carboxyl terminals, cyclic peptides are resistant to exopeptidase hydrolysis.[23] Cyclic peptides can show good permeability and are able to pass through cell membranes as compared to linear peptides.[24,25]

These characteristics have made cyclic peptides with a stable conformation more drug-like than their linear counterparts.

Tailoring the conformations in cyclic peptides is majorly achieved by shaping the turns in the cyclic peptides.[26–28] Because of their cyclic nature, most cyclic peptides display robust structures with well-defined conformational scaffolds such as turns, hairpins, and hydrogen bonding patterns in general. In the last couple of decades, N-methylation of the backbone amide protons has emerged as one of the multi-purpose tools for the chemical modification of cyclic peptides.[29–34] N-Methylation has been demonstrated to modify the conformations, bioactivity, lipophilicity, or bioavailability in cyclic peptides.[29,35–37] Cyclosporine, a natural bioavailable peptide and immunosuppressant drug, and Cilengitide, a synthetic peptide from Kessler's research group, are prime examples that portray how a combination of cyclization, stereo inversion, and N-methylation can be used to optimize a peptide sequence for a targeted biological activity.[38,39] Kessler's research group has widely employed N-methylation as a strategy to develop selective peptide ligands for multiple integrin receptor subtypes, somatostatin and melanocortin receptors, and imaging.[40–42] In parallel, both Kessler and Lokey's group have demonstrated the potential of N-methylation in improving the permeability and bioavailability of the peptides.[33,41,43]

Kessler's group reported extensive conformational studies of N-methyl containing oligo-alanine cyclic peptides and used them as templates to investigate the structural requirements for permeability.[43–48] They developed two highly permeable scaffolds from a library of 54 cyclic-hexaalanine peptides, proved the conformational reliance of permeability, and suggested that the multiple N-methylation can dramatically improve the permeability of peptides.[43,45] Biron et al. studied the effect of multiple N-methylation on the intestinal permeability and enzymatic stability of somatostatin analogue, the Veber-Hirschmann peptide, and showed that multiple N-methylation improved its oral bioavailability without altering its

[a] A. Dangi, Dr. U. Kiran Marelli
Central NMR Facility and Division of Organic Chemistry
CSIR-National Chemical Laboratory
Dr. Homi Bhabha Road, 411008 Pune (India)
E-mail: m.udayakiran@ncl.res.in
Homepage: http://academic.ncl.res.in/m.udayakiran

[b] A. Dangi, Dr. U. Kiran Marelli
Academy of Scientific and Innovative Research (AcSIR)
CSIR-HRDC Campus
Sector 19, Kamla Nehru Nagar, Ghaziabad, UP, 201002 (India)

Chemistry–A European Journal

Research Article
doi.org/10.1002/chem.202300753

Chemistry Europe
European Chemical
Societies Publishing

bioactivity.[41] Lokey's group developed a highly membrane permeable orally available (cyclo[Leu-*N*Me-D-Leu-*N*Me-Leu-Leu-D-Pro-*N*Me-Tyr]) scaffold.[33] These investigations proved that varying the position and number of N-methylations on the backbone amides of a cyclic peptide can significantly impact their permeability and bioactivity.

Other than N-methylation, a few individual backbone amide modifications were discussed in the literature recently. Del Valle's group has shown the effect of N-amination and N-hydroxylation on conformations and activity of peptides.[49–52] Fernando Albericio's group studied the *N*-TEG and *N*-OEG as a surrogate of *N*-Me and found an increase in lipophilicity of the *N*-TEG peptides as compared to the N-methylated peptides.[53,54] In an interesting approach, Sando's research group pioneered the synthesis of oligo(N-substituted alanine) peptoids via reductive amination of amines in the amino acids with various aldehydes to result in peptoids containing diverse *N*-alkyl groups. These *N*-alkyl peptoids exhibited extended conformations in water and cell permeability.[55,56] As evident by this discussed literature, the backbone amide modifications are quite versatile in subtle and controlled alteration of the conformations and the resulting stereoelectronic attributes in peptides.[57] Compared to backbone N-methylation of amide bonds, other backbone N-modifications are underexplored, and new modifications are warranted.

In this direction, we have hypothesized and explored the backbone amide N-arylation as a novel chemical modification in peptides. We speculate that N-arylation would impart the peptides with large steric effects, polarity changes, and π-π interaction-based conformational changes. For instance, earlier reports on the N-alkylated anilides,[58] oligo(*N*-aryl glycines),[59] and peptoids with *N*-aryl groups[60] have indicated a strong preference of the *N*-aryl amide groups to stay in *trans*-amide geometry.[58–61] Furthermore, N-arylation would have a much broader substrate scope because of a variety of choices of the aryl groups. In this context, herein we discuss the design, synthesis, NMR-based conformational characterization of 15 cyclic-hexaalanine and ten cyclic-pentaalanine peptides containing backbone *N*-aryl amide groups.
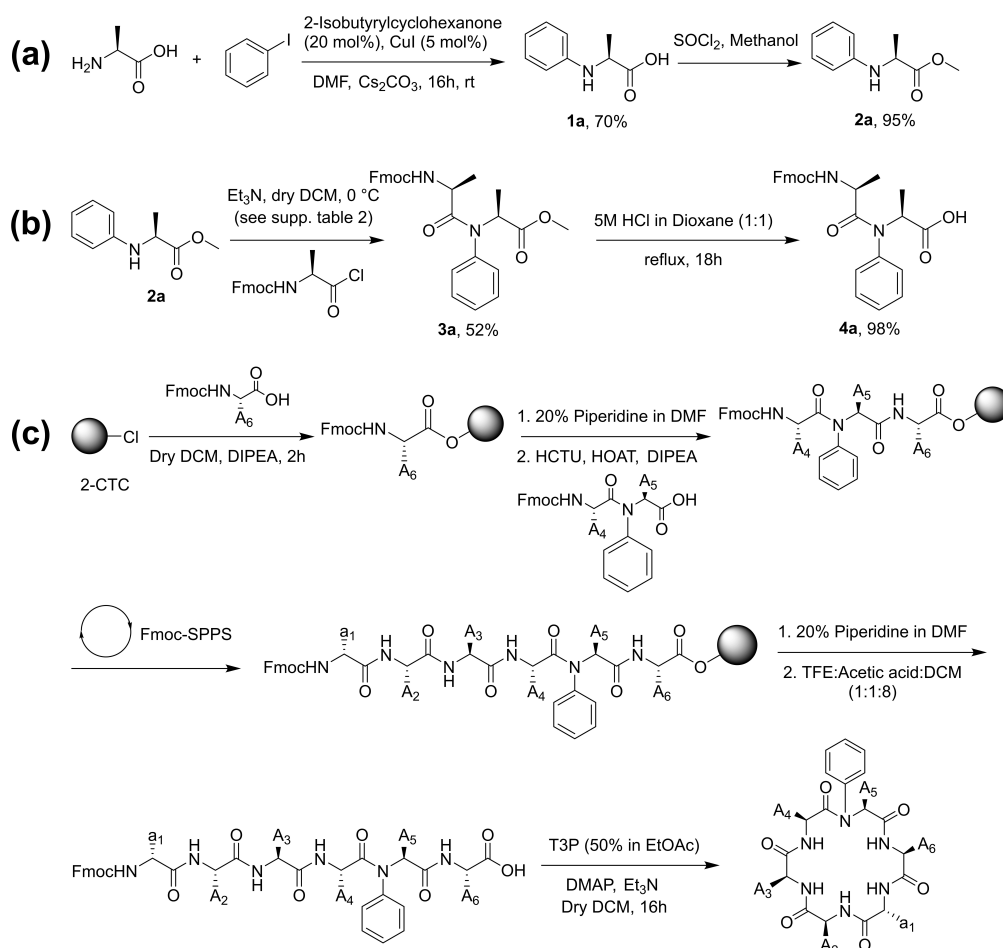
For our studies, we have considered two model cyclic peptides as parent templates – a cyclic-hexaalanine (CHA) and a cyclic-pentaalanine (CPA) – both containing a D-alanine residue that brings in the configurational heterogeneity (Figure 1). We synthesized a library of 15 *N*-phenyl containing cyclic-hexaalanine peptides (NPCHA; 6 peptides containing one *N*-phenyl-L- or D-alanine and 9 peptides with two *N*-phenyl-L- or D-alanine residues) and 10 *N*-phenyl containing cyclic-pentaalanine peptides (NPCPA; 5 peptides containing one *N*-phenyl-L- or D-alanine and 5 peptides with two *N*-phenyl-L- or D-alanine residues) (Figure 1e). The 25 peptides were synthesized by combining solution and solid-phase peptide synthesis chemistry. For the synthesis, N-arylation of L- or D-alanine was carried out in solution by following Buchwald–Hartwig method using Iodobenzene to obtain *N*-phenyl-L- or D-alanine (**1a**, Scheme 1a).[62] Thus obtained, *N*-phenyl-L- or D-alanine (**1a**) was protected with Fmoc to generate Fmoc-*N*-phenyl-L- or D-alanine
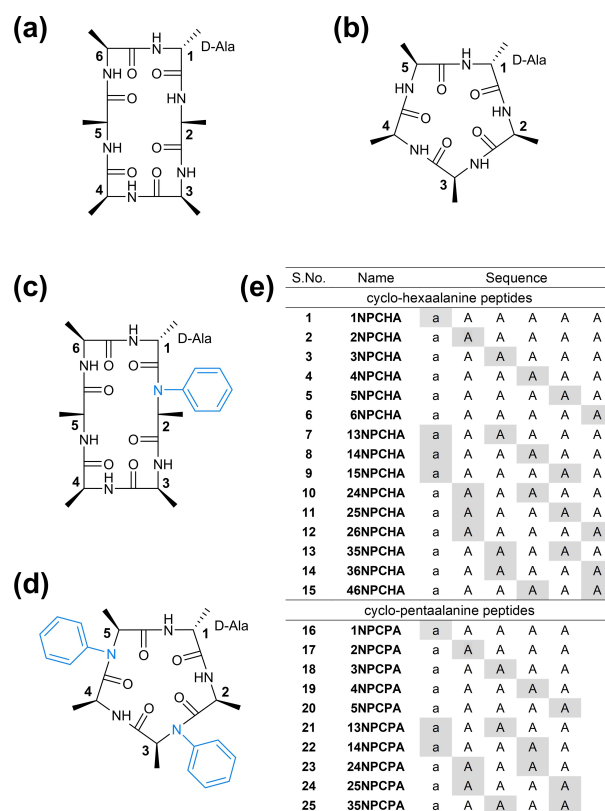
Figure 1. a) and b) Parent template peptides used for N-arylation. The residues are numbered starting from D-alanine as position 1. representative examples of *N*-phenyl peptides c) 2NPCHA and d) 35NPCPA containing one and two *N*-phenyl residues, respectively. e) List of the *N*-phenyl containing peptides characterized in this work. The numbers at the start of the peptide name and the amino acid labels highlighted in gray in the sequences indicate the position of the residues with *N*-phenyl amide group.

S.No.	Name	Sequence					
		cyclo-hexaalanine peptides					
1	1NPCHA	a	A	A	A	A	A
2	2NPCHA	a	A	A	A	A	A
3	3NPCHA	a	A	A	A	A	A
4	4NPCHA	a	A	A	A	A	A
5	5NPCHA	a	A	A	A	A	A
6	6NPCHA	a	A	A	A	A	A
7	13NPCHA	a	A	A	A	A	A
8	14NPCHA	a	A	A	A	A	A
9	15NPCHA	a	A	A	A	A	A
10	24NPCHA	a	A	A	A	A	A
11	25NPCHA	a	A	A	A	A	A
12	26NPCHA	a	A	A	A	A	A
13	35NPCHA	a	A	A	A	A	A
14	36NPCHA	a	A	A	A	A	A
15	46NPCHA	a	A	A	A	A	A
		cyclo-pentaalanine peptides					
16	1NPCPA	a	A	A	A	A	
17	2NPCPA	a	A	A	A	A	
18	3NPCPA	a	A	A	A	A	
19	4NPCPA	a	A	A	A	A	
20	5NPCPA	a	A	A	A	A	
21	13NPCPA	a	A	A	A	A	
22	14NPCPA	a	A	A	A	A	
23	24NPCPA	a	A	A	A	A	
24	25NPCPA	a	A	A	A	A	
25	35NPCPA	a	A	A	A	A	

to use as a building block in Fmoc solid-phase peptide synthesis protocol using 2-CTC resin.[63]

However, the low nucleophilicity of the arylated amine in *N*-phenyl-L- or D-alanine (**1a**) had posed an insurmountable challenge in its solid-phase peptide couplings to Fmoc-L- or D-Ala-OH despite our trials with various reagent conditions (Table S1 in the Supporting Information). Hence, we attempted to synthesize the dipeptide Fmoc-L-Ala-*N*-phenyl-L-Ala-OH (**4a**) in solution-phase under multiple peptide coupling conditions (Table S2). While most coupling conditions have produced nil or trace amounts of the required compound, the activation of Fmoc-L-Ala-OH to Fmoc-L-Ala-Cl as an acid chloride and coupling to *N*-phenyl-L-Ala-OMe (**2a**) in presence of triethyl amine in dry DCM resulted in reasonable quantities of the dipeptide ester Fmoc-L-Ala-*N*-phenyl-L-Ala-OMe (**3a**) in approximately 55% reaction yield. This dipeptide ester upon ester hydrolysis with 1:1 aqueous 5 M HCl and dioxane under reflux yielded the required dipeptide Fmoc-L-Ala-*N*-phenyl-L-Ala-OH in ~98% yield (**4a**, Scheme 1b).[64] With the success of dipeptide synthesis in the solution phase, we decided to use such suitable *N*-phenyl containing dipeptides as one of the building blocks for solid-phase synthesis, instead of Fmoc-*N*-phenyl-L- or D-alanine monomer. Using a dipeptide building block and the

Chem. Eur. J. **2023**, e202300753 (2 of 8)

© 2023 Wiley-VCH GmbH

Chemistry–A European Journal

Research Article
doi.org/10.1002/chem.202300753

Chemistry Europe
European Chemical
Societies Publishing

Scheme 1. a) Synthesis of *N*-phenyl-L-alanine (**2a**). b) Synthesis of one of the *N*-phenyl containing dipeptides, Fmoc-L-Ala-*N*-phenyl-L-Ala-OH (**4a**), which are used as the building blocks in c) Fmoc-based solid-phase peptide synthesis of the required peptides (Figure 1) on 2-CTC resin, exemplified for 5NPCHA.

lack of N terminus coupling reactivity of *N*-phenyl-L-or D-alanine on the solid phase, therefore, channeled the library to a select 25 peptides (Figure 1e). As required by the planned sequence of the 25 target peptides, we separately obtained the suitable dipeptides Fmoc-L-Ala-*N*Ph-L-Ala-OH (**4a**), Fmoc-D-Ala-*N*Ph-L-Ala-OH (**4b**) and Fmoc-L-Ala-*N*Ph-D-Ala-OH (**4c**) by solution-phase chemistry (see the Experimental Section) to use as coupling units for solid-phase peptide synthesis. All the target peptides **1–25** were synthesized by Fmoc-solid-phase peptide synthesis using 2-CTC resin (Scheme 1c) and were purified by reversed-phase HPLC (see the Experimental Section; Tables S3–S8).

For NMR spectroscopic characterization and structure elucidation, 5 mg of each peptide was dissolved in 500 μL of [D₆]DMSO, and data were recorded on Bruker Avance 500 or 700 MHz NMR spectrometers. We used Schrödinger Maestro and MacroModel for the structure calculations of all the peptides with NMR data inputs.[65]

The ¹H NMR spectra of all the compounds have shown only one set of chemical shifts implying, in general, either a single predominant conformation or fast-exchanging conformations on the NMR chemical shift timescales (Tables S9–S33). Thirteen

out of the 15 NPCHA peptides and nine of the ten NPCPA peptides exhibited distinct antiparallel β-sheet conformations with characteristic β- or γ-turns (Figures 2–5 and S1–S11, Tables S34–S43). The said conformations are supported by representative NOE correlations and amide chemical shift temperature coefficients that indicated solvent shielding/hydrogen bonding or exposure to the solvent (Figures 2–5 and S1–11, Tables S34 and 35). Based on the position of the D-alanine in the conformations, the amide NHs that exhibited hydrogen bonding nature or orientated into the peptide macrocycle, and the type of turns, the conformations observed in NPCHA peptides are broadly classified into five different templates and those in NPCPA peptides into three templates (Figures 2 and 4).

NPCHA peptides exhibited antiparallel β-sheet structures with two β-turns at either end of the 18-atom macrocycle. The NPCHA template 1 (Figures 2a, f, 3a, S1 and S3) conformation is made up of two β-turns; the first β-turn is of type II' or I' positioned between residues 1 and 2, and the second β-turn between residues 4 and 5 is of type II or I. The D-configured residue (D-Ala or *N*-Ph-D-Ala) is occupying the *i*+1 position of the first β-turn. The NHs from residues 3 and 6 have internal orientation into the macrocycle with a possibility of hydrogen

Figure 3. Stereoviews of the NMR-derived 3D conformations of the select peptides representing each NPCHA template. a) NPCHA template 1 conformation represented by 14NPCHA peptide; b) NPCHA template 2 conformation represented by 6NPCHA peptide; c) and d) NPCHA template 3 conformations represented by 26NPCHA peptide illustrating the possibility of a peptide bond flip linking residues 5 and 6 that results in β-turns II and I; e) NPCHA template 4 conformation represented by 15NPCHA peptide; and f) NPCHA template 5 conformation represented by 35NPCHA peptide.

conformations in NPCHA peptides				
NPCHA Templates	Turn 1	Turn 2	solvent shielded NH	peptides
Template 1 (Fig 2a)	β turn II'/I'	β turn II/I	3 and 6	1, 2, 5, 14, 24 and 25
Template 2 (Fig 2b)	β turn II'/I'	β turn II/I	2 and 5	3, 4, 6, 13 and 36
Template 3 (Fig 2c)	β turn II	β turn II/I	4 and 1	26
Template 4 (Fig 2d)	β turn II'	β turn VI	3 and 6	15
Template 5 (Fig 2e)	β turn II'	β turn VI	1 and 4	35

Figure 2. Five different conformational templates observed for NPCHA peptides. The first three templates, (a)–(c), contain only β-turns with *trans* peptide bonds, whereas the last two types, (d) and (e) consist of one β VI turn with a *cis* peptide bond. All the residues are numbered, starting with the D-Ala residue as position 1. Wherever the amide group is given as NR, R can be either H or phenyl group depending on the peptide sequence. The possibility of hydrogen bonding for the NHs oriented into the macrocycle is indicated in dashed lines. f) Summary of the types of conformation observed in NPCHA peptides, the type of turns in each conformation, and the amide NHs that are solvent shielded, as indicated by the NMR chemical shift temperature coefficients. The last column shows a list of peptides (named after the position of the *N*-phenyl group) exhibiting the conformations corresponding to each NPCHA template type.
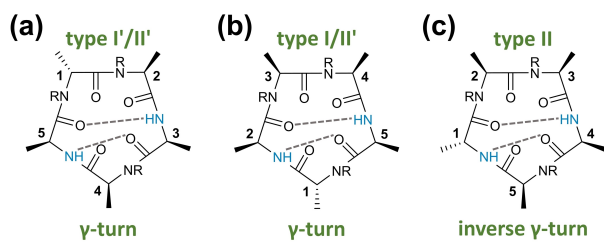
bonding to the carbonyl of residues 6 and 3, respectively. This is supported by amide NMR chemical shift temperature coefficients > -2.4 ppb/K for the NHs from residues 3 and 6. Out of the six NPCHA peptides, two peptides, 1NPCHA and 14NPCHA (Figures 3a and S3), have exhibited a single conformation with type II′ first turn and type II second turn in the structure calculation. The peptide 2NPCHA, has a conformation in which the second β-turn is of type I and the first β-turn between residues 1 and 2 is either type II′ or I′, which are a result of 180° peptide bond flip (Figures S3 and S7a). The distinct observation of type II′ or I′ turns for the first turn in this peptide could be because of the high energy barrier of rotation for the peptide bond involving the *N*-phenyl amide bond between residues 1 and 2. In support of this peptide bond flip, we have also observed distinct NOEs from the phenyl ring protons to either face of the peptide plane (Figure S7a). Such peptide bond flip for an unmodified amide bond would be energetically more favorable and thus lead to averaged conformations and NMR data.[44,45,66,67] On similar lines, the

conformation for 5NPCHA and 25NPCHA showed a type II′ first turn while the second turn between residues 4 and 5 is either type II or I (Figure S7b). For 24NPCHA conformation, the first turn being either of the type II′ or I′ and the second turn is observed to be type II. For the peptides showing the NPCHA template 1 fold, there are two *N*-methyl CHA peptides whose NMR conformations were discussed by Beck et al.[45] 5*N*MeCHA, which is an *N*-methyl analogue of 5NPCHA, had a single conformation with a first β-type II′ turn between residues 1 and 2, and a second β-type VI turn between residues 4 and 5 with a *cis* peptide bond (Figures S3 and S12). In contrast, for 5NPCHA we did not find any signs of *cis* peptide bond and instead observed a population of type II or I turn between residues 4 and 5. For 1*N*MeCHA, Beck et al. had speculated two fast-exchanging conformations with less distinct NMR temperature coefficients for the amide NHs, while the analogous 1NPCHA discussed here has a dominant NPCHA template 1 conformation.

The NPCHA template 2 (Figures 2b, f, 3b, S1, and S4a, b) structure comprises the first β-turn between residues 6 and 1, which is of type II or I′ and the second β-turn of type II/I around residues 3 and 4, with the D-amino acid occupying the $i+2$ position of the first turn. The amide NHs of the residues at positions 2 and 5 of the NPCHA template 2 structure are involved

Chemistry–A European Journal

Research Article
doi.org/10.1002/chem.202300753

Chemistry Europe
European Chemical
Societies Publishing

(a) type I'/II'   **(b)** type I/II'   **(c)** type II

γ-turn   γ-turn   inverse γ-turn

(d)

conformations in NPCPA peptides				
NPCPA Templates	Turn 1	Turn 2	solvent shielded NH	peptides
Template 1 (Fig 3a)	β turn I'/II'	classical γ-turn	3 and 5	2, 4, 5, 14 and 24
Template 2 (Fig 3b)	β turn I/II'	classical γ-turn	5 and 2	1, 3, and 13
Template 3 (Fig 3c)	β turn II	inverse γ-turn	4 and 1	25

Figure 4. a)–c) Three different conformational templates observed for NPCPA peptides. While (a) and (b) have a β-turn with a *trans* peptide bond in combination with a γ-turn, (c) differs in having an inverse γ-turn along with a β-turn having a *trans* peptide bond. All the residues are numbered, starting with the D-residue as position 1. Wherever the amide group is given as NR, R can be either H or a phenyl group depending on the peptide sequence. The possibility of hydrogen bonding for the NHs oriented into the macrocycle is indicated in dashed lines. d) Summary of the types of conformation observed in NPCPA peptides along with the type of turns in each conformation and the amide NHs that are solvent shielded, as indicated by the NMR chemical shift temperature coefficients. The last column lists the peptides (named after the position of the *N*-phenyl group) exhibiting the conformations corresponding to each NPCPA template type.

(a) NPCPA Template 1

2NPCPA

(b) NPCPA Template 2

13NPCPA

(c) NPCPA Template 3

25NPCPA
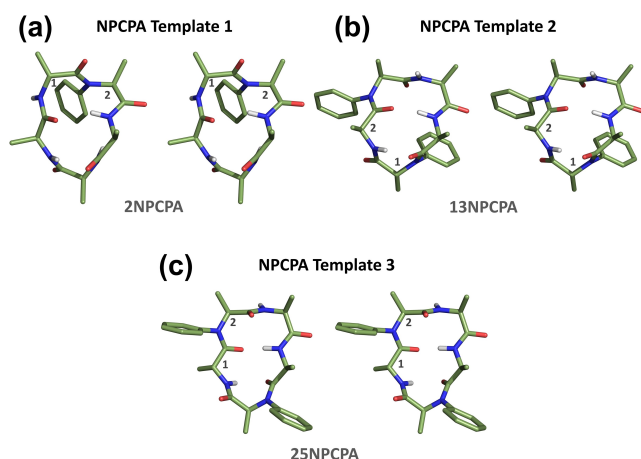
Figure 5. Stereoviews of the NMR-derived 3D conformations of the select peptides representing each NPCPA template. a) NPCPA template 1 conformation represented by 2NPCPA peptide; b) NPCPA template 2 conformation represented by 13NPCPA peptide; and c) NPCPA template 3 conformation represented by 25NPCPA peptide.

in hydrogen bonding with the C=O of residues 5 and 2, respectively. Among 3NPCHA, 4NPCHA, 6NPCHA, 13NPCHA, and 36NPCHA that have exhibited the NPCHA template 2 conformation, 6NPCHA and 36NPCHA have predominantly shown one particular β-turn type for each end of the cyclic antiparallel β-sheet conformation (Figure S4a). 4NPCHA populated peptide bond flip conformations with β-type II first turn and the second turn flipping between type II and type I (Figures S4a and 7c). For 3NPCHA and 13NPCHA, the ROE data and temperature coefficients could be

more satisfactorily explained when NPCHA template 2 conformation and NPCHA template 3 conformation (Figures 2, 3, and S4a, b) are considered in a fast exchange on the NMR chemical shift timescales.

Only one peptide, 26NPCHA, displayed the NPCHA template 3 (Figures 2c, f, 3c, d, S1, S5, and 7d) conformation with type II first turn between amino acids 2 and 3, and a type II/I β-turn around positions 5 and 6 with *N*-phenyl amide bond flipping. The D-amino acid in this conformation is simultaneously a part of the first turn as i^{th} residue and as $i+3$ residue for the second turn. The amide protons of amino acids 4 and 1 are involved in hydrogen bonding with the C=O groups of each other across the macrocycle.

The last two conformations observed for NPCHA peptides, the NPCHA template 4 and NPCHA template 5 (Figures 2d-f, f, S1, S6, and S8), are represented by one peptide each, specifically 15NPCHA and 35NPCHA, respectively. These two templates are distinct from the other NPCHA templates in having a β VI turn with a *cis* peptide bond as one of the turns. Both the templates have a β II' and β VI turn however the position of these turns differ. While the β II' turn for 15NPCHA is populated around residues 1 and 2, that for 35NPCHA is between residues 5 and 6. In accordance, the β VI turns are centered around residues 4 and 5 for 15NPCHA and amino acids 2 and 3 for 35NPCHA. Similarly, the hydrogen bonding pattern for 15NPCHA is between the amide NHs and C=O groups of residues 3 and 6, while it is between those of amino acids 1 and 4 in 35NPCHA. To draw parallels, for 15NPCHA, the analogous 15*N*MeCHA peptide (Figures S6 and S12) had the exact same conformation as NPCHA template 4, which is interesting.[45] On the other hand, the 35NPCHA differs starkly from its analogous 35*N*MeCHA in populating a single conformation. In contrast, the methyl analogue of 35NPCHA, the 35*N*MeCHA had exhibited two conformations (Figures S6 and S12),[45] one conformation (56%) with two *cis* peptide bonds between residues 2 and 3, and 4 and 5, and the other conformation (44%) with only one *cis* peptide bond between residues 2 and 3 and β II' turn between residues 5 and 6. This could be attributed to the role of *N*-aryl group substitution as a bulky restraint on the peptide bond flipping, which leads to distinct conformations.[44,45,66,67]

In N-methylation studies of the CHA scaffold, it was observed that the *N*Me at position 5 played a crucial role in conformational control (Figure S12).[45] When N-methylation was present at position 5, the presence or absence of *N*Me at positions 1, 2, 4, and to a certain extent at 3 and 6, had retained the parent conformation observed for 5*N*MeCHA (which is similar to the NPCHA template 4 conformation). However, in the current studies, although the size of the library is limited, we did not observe any such control over the conformation by the *N*-phenyl group at position 5 or any other position. Especially, the four peptides 5NPCHA, 15NPCHA, 25NPCHA, and 35NPCHA have revealed conformations that are entirely different from each other (Figures 2 and 3). While the analogous 5*N*MeCHA, 15*N*MeCHA, 25*N*MeCHA, and partially the 35*N*Me-CHA had identical conformational features (Figure S12).

The NPCPA compounds displayed three template structures containing one β-turn and a γ-turn (Figures 4, 5, S2 and S9-S11). Five peptides, 2NPCPA, 4NPCPA, 5NPCPA, 14NPCPA, and 24NPCPA folded into NPCPA template 1 structure. The NPCPA template 1 (Figures 4a, d, 5a, and S9) conformation consists of a β-turn type I'/II' connecting residues 1 and 2 with the D-residue at the $i+1$ position, and classical γ-turn centered around residue 4. This arrangement leads to the internal orientation and hydrogen bonding of NH of residue 3 with the C=O of residue 5 in a β-turn and hydrogen bonding between NH of residue 5 (except for 5NPCPA, where NH at position 5 is modified to *N*-phenyl) with the C=O of residue 3 in the classical γ-turn. While peptides 2NPCPA and 24NPCPA showed a type I' β-turn, the others, 4NPCPA, 5NPCPA, and 14NPCPA have a type II' turn.

1NPCPA, 3NPCPA, and 13NPCPA displayed NPCPA template 2 conformation (Figures 4b and d, 5b, S2 and S10) with a type I/II' β-turn around 3 and 4 positions and a classical γ-turn centered at position 1, which is a D-amino acid. The hydrogen bonding pattern involves NH of amino acid 5 with the C=O of residue 2 in the β-turn and vice versa in the γ-turn. Among the three peptides of the NPCPA template 2 structure, the 1NPCPA populated a type I turn, whereas 3NPCPA and 13NPCPA have a type II' β-turn.

Only one peptide, 25NPCPA, has exhibited NPCPA template 3 folding (Figures 4c, 4d and 5c, S2,11) consisting of a type II β-turn around residues 2 and 3 with D-amino acid occupying the ith position of the turn. In contrast to the NPCPA templates 1 and 2 discussed here, the NPCPA template 3 has an inverse γ-turn centered around amino acid 5. The NPCPA template 3 has NH of amino acid 4 involved in hydrogen bonding with C=O of residue 1 in the β II' turn and the NH of amino acid 1 hydrogen bonded to C=O of 4 in an inverse γ-turn. We speculate that probably due to the ring constraint in the cyclic-pentaalanine peptides, the peptide bond flipping in the β-turns containing *N*-phenyl groups could be restricted. Therefore, we failed to observe an amide bond flipping-based equilibrium of β-turns in the NPCPA peptides, unlike that in NPCHA series.

It is appealing that in the *N*Me analogues of NPCPA compounds, except for 1*N*MeCPA and 12*N*MeCPA, none has exhibited a conformational homogeneity (Figure S13).[44] Furthermore, it is noteworthy that for the NPCPA series, we observed relatively distinct amide NMR chemical shift temperature coefficients (Table S34) that strongly support a pattern of solvent shielding and involvement in hydrogen bonding. In contrast, the amide NMR chemical shift temperature coefficients for the *N*Me analogues of NPCPAs were ambiguous (Table S44).[44] We think the large size of the *N*-aryl group, acts as a barrier for the bond rotation and peptide bond flipping, thus restricting the conformational heterogeneity and rotamer populations, in general, for the *N*-aryl peptides.

In summary, we have explored the *N*-aryl modification of amide protons in peptides as a novel approach for peptide modifications beyond N-methylation. We have designed, synthesized, and carried out the structural characterization of a series of 15 cyclic-hexaalanine peptides and 10 cyclic-pentaalanine peptides containing one or two *N*-phenyl-amino acids. Our studies have shown that the *N*-phenyl peptides are noticeably conformationally homogeneous on the NMR chemical shift timescales. Structural studies on *N*-phenyl series peptides revealed cyclic antiparallel β-sheet conformations with well-defined β- and γ-turns, and hydrogen bonding patterns supported by NMR data. The *N*-phenyl series peptides showed superior conformational homogeneity to their *N*-methyl analogues and exhibited different conformations in the corresponding analogues. We hope that *N*-aryl modification of amide NHs has the potential to be employed as a versatile peptide modification tool in peptide-based drug design.

Experimental Section

Synthesis of *N*-phenyl-L/D-Ala-OH (1a/1b):[62] Into a predried round bottom flask L-alanine (1.2 equiv.) Cs$_2$CO$_3$ (2.0 equiv.) and CuI (5 mol%) were weighed in air. After that, argon was flushed into the flask two to three times, and the flask was sealed under argon. The contents in the flask were dissolved in dry DMF. To this mixture, aryl iodide (2 mmol, 1.0 equiv.), and 2-isobutyrylcyclohexanone (20 mol%) were added, and the reaction was stirred at RT for 18 h. After the completion of the reaction, the reaction mixture was worked up with cold water and ethyl acetate to remove the DMF. The ethyl acetate layer was washed with 1 N NaOH (twice). The aq. phase was acidified with 1 N HCl up to 2–3 pH and then extracted with ethyl acetate. The combined organic layer was dried over sodium sulfate and purified by flash column chromatography to obtain the compound in 78% yield, as a brown oil. ^{1}H NMR (400 MHz, CDCl$_3$): $\delta = 7.23$ (t, $J = 7.6$ Hz, 2H), 6.82 (t, $J = 7.3$ Hz, 1H), 6.66 (d, $J = 7.9$ Hz, 2H), 4.16 (q, $J = 7.1$ Hz, 1H), 1.57 (d, $J = 7.0$ Hz, 3H). ^{13}C NMR (125 MHz, CDCl$_3$): $\delta = 178.39$, 146.34, 129.61, 119.22, 113.80, 52.58, 19.02. HRMS (ESI-TOF) m/z calcd for C$_9$H$_{13}$NO$_2$: 166.0790 [$M+$H$^+$]; found: 166.0868.

Following the same procedure, D-alanine was also N-arylated.

Synthesis of *N*-phenyl-L/D-Ala-OMe (2a/2b): In a round bottom flask *N*-phenyl-L-alanine (1 equiv.) was dissolved in MeOH and cooled to 0 °C. To the cooled mixture, SOCl$_2$ (1.5 equiv.) was added very slowly, and the reaction was stirred at RT overnight. After the completion of the reaction, thionyl chloride was evaporated to achieve the *N*-phenyl-L-Ala-OMe (2a) with 95% yield as a brown solid. ^{1}H NMR (500 MHz, CDCl$_3$): $\delta = 7.75–7.69$ (m, 2H), 7.40 (m, 3H), 4.26 (q, $J = 7.2$ Hz, 1H), 3.65 (s, 3H), 1.70 (d, $J = 7.2$ Hz, 3H). ^{13}C NMR (126 MHz, CDCl$_3$): $\delta = 168.79$, 134.53, 129.80, 129.23, 124.36, 59.89, 53.07, 15.05. HRMS (ESI-TOF) m/z calcd for C$_{10}$H$_{14}$NO$_2$: 180.09460 [$M+$H$^+$]; found: 180.1016.

Following the same procedure, esterification of **1b** was also carried out with 96% yield to achieve **2b**. ^{1}H NMR (500 MHz, CDCl$_3$): $\delta = 7.25–7.17$ (m, 2H), 6.81–6.74 (m, 1H), 6.67–6.61 (m, 2H), 4.19 (q, $J = 6.9$ Hz, 1H), 3.76 (s, 3H), 1.51 (d, $J = 7.0$ Hz, 3H). ^{13}C NMR (126 MHz, CDCl$_3$): $\delta = 175.24$, 146.64, 129.45, 118.42, 113.44, 52.34, 52.01, 19.06. HRMS (ESI-TOF) m/z calcd for C$_{10}$H$_{14}$NO$_2$: 180.09460 [$M+$H$^+$]; found: 180.1016.

General procedure for the synthesis of dipeptides (3a, 3b, and 3c): For the synthesis of the dipeptide, Fmoc-L/D-Ala-OH (1 equiv.) was activated by refluxing it with SOCl$_2$ (5 equiv.) in dry DCM for 3 h. After 3 h, the solvent was evaporated on a rotatory evaporator. To remove the excess thionyl chloride, the contents were dissolved in toluene and were evaporated 3 or 4 times. In an oven-dried round bottom flask *N*-phenyl-L/D-Ala-OMe (1 equiv.) was dissolved in dry DCM. Et$_3$N (1.2 equiv.) was added to the solution and stirred for 15 min. Then the Fmoc-L/D-Ala-Cl (2 equiv.) dissolved in dry DCM was added slowly at 0 °C to the reaction mixture. The reaction mixture was stirred for 1.5 h.

Chemistry–A European Journal

Research Article
doi.org/10.1002/chem.202300753

**Chemistry
Europe**
European Chemical
Societies Publishing

After the completion of the reaction, the contents in the flask were washed with 5% Na$_2$CO$_3$ solution followed by brine. The organic fraction was dried with Na$_2$SO$_4$ and concentrated on a rotatory evaporator and purified by column chromatography to get the desired dipeptide as a white solid (51–56% yield).

Synthesis of Fmoc-L-Ala-N-phenyl-L-Ala-OMe (3 a): The dipeptide Fmoc-L-Ala-N-phenyl-L-Ala-OMe was synthesized by following the above general procedure with a yield of 52%. ^{1}H NMR (400 MHz, CDCl$_3$): δ = 7.75 (d, J = 7.5 Hz, 2H), 7.59 (t, J = 6.7 Hz, 2H), 7.41 (dt, J = 14.8, 6.6 Hz, 7H), 7.34–7.26 (m, 2H), 5.55 (d, J = 8.4 Hz, 1H), 5.11 (q, J = 7.5 Hz, 1H), 4.35–4.24 (m, 3H), 4.20 (t, J = 7.3 Hz, 1H), 3.78 (s, 3H), 1.23–1.15 (m, 6H). ^{13}C NMR (101 MHz, CDCl$_3$): δ = 173.50, 172.75, 155.73, 144.13, 144.01, 141.44, 138.31, 129.87, 129.25, 127.84, 127.22, 125.36, 120.12, 67.09, 54.92, 52.55, 48.13, 47.30, 18.78, 15.31.

Synthesis of Fmoc-D–Ala-N-phenyl-L-Ala-OMe (3 b): The dipeptide Fmoc-D-Ala-N-phenyl-L-Ala-OMe was synthesized by following the above general procedure with a yield of 55%. ^{1}H NMR (500 MHz, CDCl$_3$): δ = 7.76 (d, J = 7.5 Hz, 2H), 7.59 (t, J = 6.5 Hz, 2H), 7.49–7.38 (m, 6H), 7.36 (s, 1H), 7.31 (t, J = 7.4 Hz, 2H), 5.60 (d, J = 8.2 Hz, 1H), 4.63 (q, J = 7.3 Hz, 1H), 4.34–4.24 (m, 3H), 4.20 (t, J = 7.3 Hz, 1H), 3.77 (s, 3H), 1.41 (d, J = 7.2 Hz, 3H), 1.18 (d, J = 6.8 Hz, 3H). ^{13}C NMR (126 MHz, CDCl$_3$): δ = 173.05, 171.74, 155.49, 144.11, 143.98, 141.39, 139.62, 130.02, 129.37, 129.18, 127.78, 127.17, 125.32, 120.07, 77.41, 77.16, 76.91, 67.01, 57.81, 52.50, 47.92, 47.24, 18.99, 15.35.

Synthesis of Fmoc-L-Ala-N-phenyl-D-Ala-OMe (3 c): The dipeptide Fmoc-L-Ala-N-phenyl-D-Ala-OMe was synthesized by following the above general procedure with a yield of 55%. ^{1}H NMR (500 MHz, CDCl$_3$): δ = 7.76 (d, J = 7.6 Hz, 2H), 7.59 (t, J = 6.5 Hz, 2H), 7.49–7.38 (m, 6H), 7.38 (s, 1H), 7.31 (t, J = 7.5 Hz, 2H), 5.59 (d, J = 8.4 Hz, 1H), 4.63 (q, J = 7.1 Hz, 1H), 4.35–4.24 (m, 3H), 4.19 (t, J = 7.4 Hz, 1H), 3.77 (s, 3H), 1.40 (d, J = 7.4 Hz, 3H), 1.18 (d, J = 6.8 Hz, 3H). ^{13}C NMR (126 MHz, CDCl$_3$): δ = 173.08, 171.76, 155.50, 144.13, 143.99, 141.41, 139.62, 130.03, 129.20, 127.80, 127.18, 125.34, 120.08, 67.03, 57.82, 52.52, 47.94, 47.26, 29.84, 19.01, 15.36.

General procedure for the ester hydrolysis of dipeptides:[64] For the ester hydrolysis, the dipeptide ester (3 a/3 b/3 c) was dissolved in 5 M HCl and dioxane (1:1) and the reaction mixture was refluxed for 18 h. After completion of the reaction, the reaction contents were diluted with 5% Na$_2$CO$_3$, and the resulting solution was washed two times with diethyl ether. Further, the aqueous layer was acidified with 3 M HCl up to pH 1. The aqueous phase was extracted with DCM 3 or 4 times, concentrated on rotovap, and purified by column chromatography to get the desired dipeptide as a white fluffy solid (92–95%).

Fmoc-L-Ala-N-phenyl-L-Ala-OH (4 a): By following the above general procedure, the ester hydrolysis of dipeptide 3 a has been carried out with a yield of 90%. ^{1}H NMR (500 MHz, CDCl$_3$): δ = 7.75 (d, J = 7.5 Hz, 2H), 7.60 (t, J = 8.0 Hz, 2H), 7.49–7.36 (m, 7H), 7.33–7.27 (m, 2H), 5.79 (d, J = 8.5 Hz, 1H), 5.10 (q, J = 7.4 Hz, 1H), 4.37–4.27 (m, 3H), 4.21 (t, J = 7.3 Hz, 1H), 1.24 (d, J = 7.5 Hz, 3H), 1.21 (d, J = 7.0 Hz, 3H). ^{13}C NMR (126 MHz, CDCl$_3$): δ = 175.41, 174.43, 155.92, 144.11, 143.99, 141.42, 138.09, 129.97, 129.39, 127.82, 127.20, 125.38, 120.10, 67.14, 55.11, 48.22, 47.25, 18.41, 15.04. HRMS (ESI-TOF) m/z calcd for C$_{27}$H$_{27}$N$_2$O$_5$: 459.1842 [M+H$^+$]; found: 459.1914.

Fmoc-D-Ala-N-phenyl-L-Ala-OH (4 b): By following the above general procedure, the ester hydrolysis of dipeptide 3 b has been carried out to get the desired dipeptide with a yield of 91%. ^{1}H NMR (500 MHz, CDCl$_3$): δ = 7.77 (d, J = 7.5 Hz, 2H), 7.63 (t, J = 7.2 Hz, 2H), 7.52–7.37 (m, 8H), 7.32 (t, J = 7.5 Hz, 2H), 5.82 (d, J = 8.2 Hz, 1H), 4.64 (q, J = 7.2 Hz, 1H), 4.39–4.27 (m, 3H), 4.22 (t, J = 7.4 Hz, 1H), 1.46 (d, J = 7.2 Hz, 3H), 1.24 (d, J = 6.8 Hz, 3H). ^{13}C NMR

(126 MHz, CDCl$_3$): δ = 174.52, 173.77, 155.66, 143.98, 143.84, 141.27, 139.41, 130.01, 129.18, 127.67, 127.06, 125.26, 119.94, 77.28, 77.02, 76.77, 67.00, 58.01, 47.92, 47.09, 18.38, 14.96. HRMS (ESI-TOF) m/z calcd for C$_{27}$H$_{27}$N$_2$O$_5$: 459.1842 [M+H$^+$]; found: 459.1814.

Fmoc-L-Ala-N-phenyl-D-Ala-OH (4 c): By following the above general procedure, the ester hydrolysis of dipeptide 3 c was carried out with a yield of 89%. ^{1}H NMR (500 MHz, CDCl$_3$): δ = 7.77 (d, J = 7.5 Hz, 2H), 7.63 (t, J = 7.2 Hz, 2H), 7.52–7.37 (m, 7H), 7.32 (t, J = 7.4 Hz, 2H), 5.85 (d, J = 8.4 Hz, 1H), 4.62 (q, J = 7.2 Hz, 1H), 4.34 (s, 1H), 4.33 (d, J = 2.1 Hz, 1H), 4.30 (d, J = 10.7 Hz, 1H), 4.22 (t, J = 7.3 Hz, 1H), 1.46 (d, J = 7.2 Hz, 3H), 1.23 (d, J = 6.9 Hz, 3H). ^{13}C NMR (126 MHz, CDCl$_3$): δ = 174.80, 173.89, 155.80, 144.11, 143.96, 141.39, 139.57, 130.14, 129.31, 127.80, 127.19, 125.39, 120.07, 67.13, 58.20, 48.04, 47.22, 18.50, 15.09. HRMS (ESI-TOF) m/z calcd for C$_{27}$H$_{27}$N$_2$O$_5$: 459.1842 [M+H$^+$]; found: 459.1914.

General protocol for the solid-phase peptide synthesis of N-aryl peptides 1–25: Synthesis of peptides 1–25 started with the loading of the required C terminus Fmoc-protected amino acid or dipeptide building block Fmoc-L/D-Ala-N-phenyl-L/D-Ala-OH (4 a/4 b/4 c, 1.2 equiv.) as required by their target linear sequences given in Tables S4 and S5 onto the 2-chloro trityl chloride resin (150 mg, 1.6 mmol/g, 0.24 mmol) in dry DCM and DIPEA (3 equiv.) for 2 h (e.g., see Scheme 1 for 5NPCHA). After loading of the first building block, capping of the unreacted active sites of the resin was done by MeOH (0.5 mL) and DIPEA (30 μL) for 30 min. After completing the capping, the resin was washed 3 times with DCM, 3 times with NMP, and then the Fmoc deprotection was done with 20% piperidine in DMF (2x10 min) followed by washing the resin 4 times with NMP. The peptide chain was elongated by coupling the appropriate Fmoc-protected amino acid or dipeptide building block Fmoc-L/D-Ala-N-phenyl-L/D-Ala-OH (2 equiv.) using HCTU (2 equiv.), HOAt (2 equiv.), DIPEA (3 equiv.) in NMP for 1.5 h following which Fmoc deprotection was done with 20% piperidine in DMF (2× 10 min) and washing the resin with NMP. The process of coupling of amino acids or dipeptide building blocks and Fmoc deprotection was repeated until the desired length of the peptides was achieved (Tables S4 and S5). After obtaining the complete linear peptide sequence, Fmoc deprotection of the terminal residue was carried out with 20% piperidine in DMF (2×10 min), and then the resin was washed 4 times with NMP, 4 times with DCM. The linear peptide was cleaved from the resin by using TFE: Acetic acid: DCM (1:1:8) for 1.5 h (3×30 min). The filtrate was collected and concentrated by removing the excess acetic acid as an azeotrope using chloroform. After the solvent removal, the head-to-tail cyclization of the linear peptide was performed by 50% 1-propane-phosphonic acid cyclic anhydride (T3P) in ethyl acetate. For cyclization, the linear peptide was dissolved in dry DCM (15 mL) and the Et$_3$N (2 equiv.) and DMAP (0.2 equiv.) were added at 0 °C. After that, the T3P (1.5 equiv.) reagent was added dropwise. The reaction mixture was brought to room temperature and stirred overnight. After completion of the reaction, the solvent was evaporated on rotovap and the residue was purified by reversed-phase HPLC. Following this procedure, all the mono and diarylated cyclic peptides 1–25 were synthesized.

Detailed data on synthesis, HRMS, HPLC and NMR are included in the Supporting Information.

Acknowledgements

Chemistry–A European Journal

Research Article
doi.org/10.1002/chem.202300753

Chemistry Europe
European Chemical
Societies Publishing

Conflict of Interests

The authors declare no conflict of interest.

Data Availability Statement

The data that support the findings of this study are available in the supplementary material of this article.

[1] A. Henninot, J. C. Collins, J. M. Nuss, *J. Med. Chem.* **2018**, *61*, 1382–1414.
[2] K. Fosgerau, T. Hoffmann, *Drug Discovery Today* **2015**, *20*, 122–128.
[3] J. L. Lau, M. K. Dunn, *Bioorg. Med. Chem.* **2018**, *26*, 2700–2707.
[4] L. Wang, N. Wang, W. Zhang, X. Cheng, Z. Yan, G. Shao, X. Wang, R. Wang, C. Fu, *Signal Transduct. Target. Ther.* **2022**, *7*, 48.
[5] P. Vlieghe, V. Lisowski, J. Martinez, M. Khrestchatisky, *Drug Discovery Today* **2010**, *15*, 40–56.
[6] A. C. L. Lee, J. L. Harris, K. K. Khanna, J. H. Hong, *Int. J. Mol. Sci.* **2019**, *20*, 1–21.
[7] C. Lamers, *Futur. Drug Discov.* **2022**, *4*, 2.
[8] M. Muttenthaler, G. F. King, D. J. Adams, P. F. Alewood, *Nat. Rev. Drug Discovery* **2021**, *20*, 309–325.
[9] D. J. Craik, D. P. Fairlie, S. Liras, D. Price, *Chem. Biol. Drug Des.* **2013**, *81*, 136–147.
[10] J. E. Bock, J. Gavenonis, J. A. Kritzer, *ACS Chem. Biol.* **2013**, *8*, 488–499.
[11] L. K. Buckton, M. N. Rahimi, S. R. McAlpine, *Chem. Eur. J.* **2021**, *27*, 1487–1513.
[12] A. Bhat, L. R. Roberts, J. J. Dwyer, *Eur. J. Med. Chem.* **2015**, *94*, 471–479.
[13] M. Moiola, M. G. Memeo, P. Quadrelli, *Molecules* **2019**, *24*, 3654.
[14] S. Rinaldi, *Molecules* **2020**, *25*, 3276.
[15] Z. C. Girvin, S. H. Gellman, *J. Am. Chem. Soc.* **2020**, *142*, 41, 17211–17223.
[16] S. P. Roche, A. D. Richaud, *J. Org. Chem.* **2020**, *85*, 12329–12342.
[17] N. Tsomaia, *Eur. J. Med. Chem.* **2015**, *94*, 459–470.
[18] T. Kimmerlin, D. Seebach, *J. Pept. Res.* **2005**, *65*, 229–260.
[19] A. F. B. Räder, M. Weinmüller, F. Reichart, A. Schumacher-Klinger, S. Merzbach, C. Gilon, A. Hoffman, H. Kessler, *Angew. Chem. Int. Ed.* **2018**, *57*, 14414–14438.
[20] A. Zorzi, K. Deyle, C. Heinis, *Curr. Opin. Chem. Biol.* **2017**, *38*, 24–29.
[21] D. Gang, D. W. Kim, H. S. Park, *Genes* **2018**, *9*, 557.
[22] H. Zhang, S. Chen, *RSC Chem. Biol.* **2022**, *3*, 18–31.
[23] D. S. Nielsen, N. E. Shepherd, W. Xu, A. J. Lucke, M. J. Stoermer, D. P. Fairlie, *Chem. Rev.* **2017**, *117*, 8094–8128.
[24] O. S. Gudmundsson, S. D. S. Jois, D. G. Vander Velde, T. J. Siahaan, B. Wang, R. T. Borchardt, *J. Pept. Res.* **1999**, *53*, 383–392.
[25] T. Rezai, B. Yu, G. L. Millhauser, M. P. Jacobson, R. S. Lokey, *J. Am. Chem. Soc.* **2006**, *128*, 2510–2511.
[26] R. Pelay-Gimeno, A. Glas, O. Koch, T. N. Grossmann, *Angew. Chem. Int. Ed.* **2015**, *54*, 8896–8927.
[27] R. Jwad, D. Weissberger, L. Hunter, *Chem. Rev.* **2020**, *120*, 9743–9789.
[28] T. A. Hill, N. E. Shepherd, F. Diness, D. P. Fairlie, *Angew. Chem. Int. Ed.* **2014**, *53*, 13020–13041.
[29] Y. Li, W. Li, Z. Xu, *Mar. Drugs* **2021**, *19*, 311.
[30] A. Sharma, A. Kumar, S. A. H. Abdel Monaim, Y. E. Jad, A. El-Faham, B. G. de la Torre, F. Albericio, *Biopolymers* **2018**, *109*, e23110.
[31] J. Chatterjee, C. Gilon, A. Hoffman, H. Kessler, *Acc. Chem. Res.* **2008**, *41*, 1331–1342.
[32] J. Chatterjee, F. Rechenmacher, H. Kessler, *Angew. Chem. Int. Ed.* **2013**, *52*, 254–269.
[33] T. R. White, C. M. Renzelman, A. C. Rand, T. Rezai, C. M. McEwen, V. M. Gelev, R. A. Turner, R. G. Linington, S. S. F. Leung, A. S. Kalgutkar, J. N. Bauman, Y. Zhang, S. Liras, D. A. Price, A. M. Mathiowetz, M. P. Jacobson, R. S. Lokey, *Nat. Chem. Biol.* **2011**, *7*, 810–817.
[34] R. A. Turner, N. E. Hauksson, J. H. Gipe, R. S. Lokey, *Org. Lett.* **2013**, *15*, 5012–5015.
[35] S. Liu, W. Gu, D. Lo, X. Z. Ding, M. Ujiki, T. E. Adrian, G. A. Soff, R. B. Silverman, *J. Med. Chem.* **2005**, *48*, 3630–3638.
[36] A. M. T. Nguyen, S. Brettell, N. Douanne, C. Duquette, A. Corbeil, E. F. Fajardo, M. Olivier, C. Fernandez-Prada, W. D. Lubell, *Molecules* **2021**, *26*, 3606.
[37] S. Sciabola, G. H. Goetz, G. Bai, B. N. Rogers, D. L. Gray, A. Duplantier, K. R. Fonseca, M. A. Vanase-Frawley, N. M. Kablaoui, *Bioorg. Med. Chem.* **2016**, *24*, 3513–3520.
[38] C. Mas-Moruno, F. Rechenmacher, H. Kessler, *Anti-Cancer Agents Med. Chem.* **2011**, *10*, 753–768.
[39] C. K. Wang, J. E. Swedberg, P. J. Harvey, Q. Kaas, D. J. Craik, *J. Phys. Chem. B* **2018**, *122*, 2261–2276.
[40] M. Weinmüller, F. Rechenmacher, U. K. Marelli, F. Reichart, T. G. Kapp, A. F. B. Räder, F. S. Di Leva, L. Marinelli, E. Novellino, J. M. Muñoz-Félix, K. Hodivala-Dilke, A. Schumacher, J. Fanous, C. Gilon, A. Hoffman, H. Kessler, *Angew. Chem. Int. Ed.* **2017**, *56*, 16405–16409.
[41] E. Biron, J. Chatterjee, O. Ovadia, D. Langenegger, J. Brueggen, D. Hoyer, H. A. Schmid, R. Jelinek, C. Gilon, A. Hoffman, H. Kessler, *Angew. Chem. Int. Ed.* **2008**, *47*, 2595–2599.
[42] M. Cai, U. K. Marelli, J. Bao, J. G. Beck, F. Opperer, F. Rechenmacher, K. R. McLeod, M. R. Zingsheim, L. Doedens, H. Kessler, V. J. Hruby, *J. Med. Chem.* **2015**, *58*, 6359–6367.
[43] O. Ovadia, S. Greenberg, J. Chatterjee, B. Laufer, F. Opperer, H. Kessler, C. Gilon, A. Hoffman, *Mol. Pharm.* **2011**, *8*, 479–487.
[44] J. Chatterjee, D. Mierke, H. Kessler, *J. Am. Chem. Soc.* **2006**, *128*, 15164–15172.
[45] J. G. Beck, J. Chatterjee, B. Laufer, M. U. Kiran, A. O. Frank, S. Neubauer, O. Ovadia, S. Greenberg, C. Gilon, A. Hoffman, H. Kessler, *J. Am. Chem. Soc.* **2012**, *134*, 12125–12133.
[46] U. K. Marelli, O. Ovadia, A. O. Frank, J. Chatterjee, C. Gilon, A. Hoffman, H. Kessler, *Chem. Eur. J.* **2015**, *21*, 15148–15152.
[47] U. K. Marelli, J. Bezençon, E. Puig, B. Ernst, H. Kessler, *Chem. Eur. J.* **2015**, *21*, 8023–8027.
[48] A. F. B. Räder, F. Reichart, M. Weinmüller, H. Kessler, *Bioorg. Med. Chem.* **2018**, *26*, 2766–2773.
[49] K. C. Tillett, J. R. Del Valle, *RSC Adv.* **2020**, *10*, 14331–14336.
[50] B. M. Rathman, J. L. Rowe, J. R. Del Valle, *Methods Enzymol.* **2021**, *656*, 271–294.
[51] B. M. Rathman, J. L. Allen, L. N. Shaw, J. R. Del Valle, *Bioorg. Med. Chem. Lett.* **2020**, *30*, 127283.
[52] M. P. Sarnowski, C. W. Kang, Y. M. Elbatrawi, L. Wojtas, J. R. Del Valle, *Angew. Chem. Int. Ed.* **2017**, *56*, 2083–2086.
[53] A. I. Fernández-Llamazares, J. García, V. Soto-Cerrato, R. Pérez-Tomás, J. Spengler, F. Albericio, *Chem. Commun.* **2013**, *49*, 6430–6432.
[54] A. I. Fernández-Llamazares, J. Adan, F. Mitjans, J. Spengler, F. Albericio, *Bioconjugate Chem.* **2014**, *25*, 11–17.
[55] J. Morimoto, Y. Fukuda, D. Kuroda, T. Watanabe, F. Yoshida, M. Asada, T. Nakamura, A. Senoo, S. Nagatoishi, K. Tsumoto, S. Sando, *J. Am. Chem. Soc.* **2019**, *141*, 14612–14623.
[56] Y. Fukuda, M. Yokomine, D. Kuroda, K. Tsumoto, J. Morimoto, S. Sando, *Chem. Sci.* **2021**, *12*, 13292–13300.
[57] M. Erak, K. Bellmann-Sickert, S. Els-Heindl, A. G. Beck-Sickinger, *Bioorg. Med. Chem.* **2018**, *26*, 2759–2765.
[58] N. H. Shah, G. L. Butterfoss, K. Nguyen, B. Yoo, R. Bonneau, D. L. Rabenstein, K. Kirshenbaum, *J. Am. Chem. Soc.* **2008**, *130*, 16622–16632.
[59] J. R. Stringer, J. A. Crapster, I. A. Guzei, H. E. Blackwell, *J. Org. Chem.* **2010**, *75*, 6068–6078.
[60] G. J. Pros, A. J. Bloomfield, *J. Phys. Chem. A* **2019**, *123*, 7609–7618.
[61] A. Itai, Y. Toriumi, S. Saito, H. Kagechika, K. Shudo, *J. Am. Chem. Soc.* **1992**, *114*, 10649–10650.
[62] K. K. Sharma, S. Sharma, A. Kudwal, R. Jain, *Org. Biomol. Chem.* **2015**, *13*, 4637–4641.
[63] R. B. Merrifield, *Excerpta Med., I. C. S.* **1976**, *374*, 29–39.
[64] F. Sladojevich, A. Trabocchi, A. Guarna, *J. Org. Chem.* **2007**, *72*, 4254–4257.
[65] a) *Schrödinger Release 2023–1: MacroModel*, Schrödinger, LLC, New York, NY, **2021**; b) *Schrödinger Release 2023–1: Maestro*, Schrödinger, LLC, New York, NY, **2021**.
[66] S. Hayward, *Protein Sci.* **2008**, *10*, 2219–2227.
[67] D. F. Mierke, H. Kurz, H. Kessler, *J. Am. Chem. Soc.* **1994**, *116*, 1042–1049.

RESEARCH ARTICLE

As an inquisitive approach, cyclic peptides containing *N*-aryl alanine amino acids were synthesized. Their conformations in solution were determined by NMR spectroscopy and compared with those of other *N*-modified peptides. The compounds showed relatively high conformational homogeneity and populated well-characterized antiparallel β-sheet structures having discrete β- and γ-turns and hydrogen bonding patterns; these have been classified into different templates.
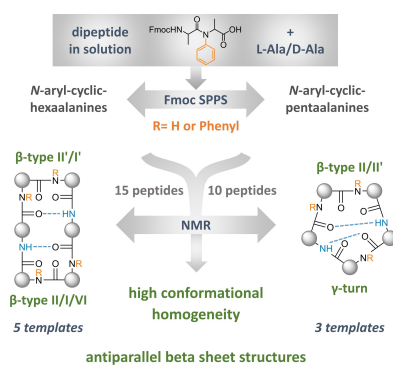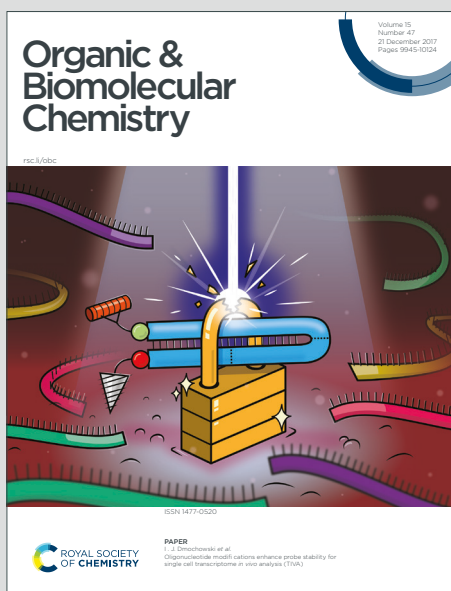

A. Dangi, Dr. U. Kiran Marelli*

1 – 9

Exploration of N-Arylation of Backbone Amides as a Novel Tool for Conformational Modification in Peptides

Organic & Biomolecular Chemistry

Accepted Manuscript

Organic & Biomolecular Chemistry

Volume 15
Number 47
21 December 2017
Pages 9945-10124

rsc.li/obc

ISSN 1477-0520

ROYAL SOCIETY OF CHEMISTRY

PAPER
I. J. Dmochowski et al
Oligonucleotide modifications enhance probe stability for single cell transcriptome in vivo analysis (TIVA)

This is an Accepted Manuscript, which has been through the Royal Society of Chemistry peer review process and has been accepted for publication.

Accepted Manuscripts are published online shortly after acceptance, before technical editing, formatting and proof reading. Using this free service, authors can make their results available to the community, in citable form, before we publish the edited article. We will replace this Accepted Manuscript with the edited and formatted Advance Article as soon as it is available.

You can find more information about Accepted Manuscripts in the Information for Authors.

ROYAL SOCIETY OF CHEMISTRY

rsc.li/obc

COMMUNICATION

Total synthesis, structure elucidation and expanded bioactivity of Icosalide A: Effect of lipophilicity and ester to amide substitution on its bioactivity

Abha Dangi,[a,b,c] Bharat Pande,[c,d] Sonia Agrawal,[b,d] Dhiman Sarkar,[b] Koteswara Rao Vamkudoth,[c,d] Udaya Kiran Marelli*[a,b,c]

The first total synthesis of Icosalide A, an antibacterial depsipeptide unique in containing two lipophilic beta hydroxy acids has been achieved by following Fmoc solid-phase peptide synthesis in combination with solution-phase synthesis. The ambiguity in the absolute stereochemistry of Icosalide A has been resolved by synthesizing the reported structures and the other relevant diastereomers of the icosalides and comparison of their NMR data. NMR-based structure elucidation of Icosalide A has revealed a well-folded structure with cross-strand hydrogen bonds similar to an anti-parallel beta-sheet conformation in peptides and displayed a synergistic juxtaposition of the aliphatic sidechains. 12 analogues of Icosalide A were synthesized by varying the constituent lipophilic beta hydroxy acid residue, and their biological activities against *Bacillus thuringenesis* and *Paenibacillus dendritiformis* were explored. Most of these Icosalide analogues displayed their MIC at 12.5 µg/mL against both bacteria. Swarming inhibition by Icosalides was least in *B. thuringiensis* (8.3%) compared to that in *P. dendritiformis* (33%). Further, this is the first report of Icosalides showing assured inhibitory action (MIC between 2 to 10 µg/mL) against the active stage of *Mycobacterium tuberculosis*, and cancer cell lines such as HeLa and ThP1. This study could help optimize icosalides for anti-TB, antibacterial, and anti-cancer activities.

Introduction

a. Central NMR Facility, CSIR-National Chemical Laboratory, Dr. Homi Bhabha Road, 411008 Pune, India.

b. Division of Organic Chemistry, CSIR-National Chemical Laboratory, Dr. Homi Bhabha Road, 411008 Pune, India.

c. Academy of Scientific and Innovative Research (AcSIR), CSIR-HRDC Campus, Sector 19, Kamla Nehru Nagar, Ghaziabad, UP, 201002, India.

d. Biochemical Sciences Division, CSIR-National Chemical Laboratory, Dr.Homi Bhabha Road, 411008 Pune, India.

† Footnotes relating to the title and/or authors should appear here.

Electronic Supplementary Information (ESI) available: Supplementary Information contains materials and methods, synthetic procedures for all the compounds, HRMS, HPLC, NMR data, NMR conformation details, description and data of biological assays. See DOI: 10.1039/x0xx00000x

Infectious diseases, as witnessed by the Covid-19 pandemic, are always a major threat to human health. In addition, antibiotic resistance, an impending reality caused by the inappropriate use of the existing antibiotics and the growing virulence of the microbes, is a challenge to overcome in front of the scientific and medical community.[1–4] A repertoire of antibiotic molecules that act by distinct mechanisms and are not extensively used would help tackle infectious diseases more effectively in times of pandemics or widely spreading infections.[5–7] Hence, searching for newer antibiotic substances belonging to different structural classes that act efficiently and by novel mechanisms of action is a continuous process.[8,9] Among the various ways of communication among bacterial colonies, swarming behaviour in bacteria is a vital phenomenon that has significance in signalling, virulence, pathogenicity, colonization, and antibiotic tolerance.[10] The display of antibiotic activity by inhibiting the swarming behaviour of bacteria is a new mechanism of action that has gained significant interest in recent times.[11] Many existing antibiotic drugs and isolated natural products, as reviewed by Retschlin *et al*., were tested for their swarming behaviour.[11] However, the search is persistently underway for molecules that could inhibit bacterial swarming at less than hundreds of millimolar concentrations.

Nature is the limitless source of discovering several bioactive compounds, including peptides and depsipeptides, for antibiotic activity.[12,13] Many antimicrobial peptides (AMPs) such as defensins, gramicidin S, valinomycin, nisin, phalloidin, amanitins, teixobactin[14–17] are all isolated from nature and have shown good Gram-positive and Gram-negative bacterial inhibitory action.

Cyclic depsipeptides are a class of cyclic peptides in which one or more amide bonds are replaced with ester bonds.[18–20] Numerous cyclic depsipeptides have been discovered that displayed anticancer, antibacterial, antifungal, and anti-inflammatory activities.[21–23] Since the discovery of the didemnins, this class of natural compounds has sparked ongoing study in synthetic and medicinal chemistry, clinical

COMMUNICATION

Journal Name

oncology, and cell biology.[24,25] For instance, Daptomycin 1 and Ramoplanin are excellent antibiotic depsipeptides examples that act by a different mechanism of action and have proved their clinical potential in drug development.[26,27] While Daptomcin 1 acts by disrupting the cell membrane functions, Ramoplanin acts by interfering with cell wall synthesis. Multiple naturally occurring cyclic depsipeptides exhibiting distinct structural features responsible for antibiotic activity were identified over the years and used as parent scaffolds for structure-activity optimization.[28–30]
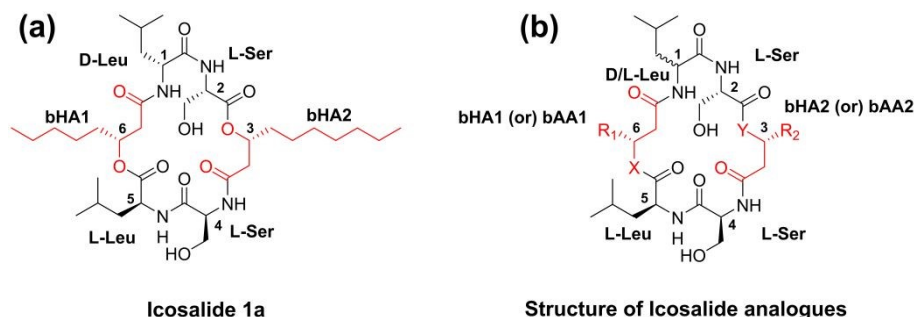
Figure 1. (a) The structure of Icosalide **1a**, whose analogues were developed in this study; and (b) General structure representing the Icosalide analogues.

Icosalides (Figure **1**), new members of the peptolide class of cyclic depsipeptides, were discovered by Boros *et al.* as isolated from a fungal culture.[31] Icosalides are lipodepsipeptidic comprised of six residues, namely, L-Serine, L/D-Leucine alongside beta hydroxy acids having 8 or 10 carbon chains, which form a 20 atom macrocycle core. Unlike most lipopeptides, which contain only one fatty acid chain, the Icosalides are considered unusual for possessing two lipophilic chains as beta-hydroxy acids. Among the three isolated Icosalides (**1a**, **1b** and **1c**, Table **1**), Icosalide **1a** exhibited an antimicrobial activity of MIC 8-16 µg/ml against *Streptococcus pyogenes, S. pneumoniae (Felton),* and *Enterococcus faecalis*. Interestingly, Icosalide **1a** was also found to inhibit the swarming behaviour of the bacteria,[31] a mechanism of antibiotic activity, which is being thoroughly explored.[11,32]

The stereochemistry of the constituent beta hydroxy acids in Icosalides was not identified initially when isolated by Boros *et al.* However, recently, Dose *et al.*[33] studied the genomic, metabolic profiling of *Burkholderia gladioli* bacteria and attributed the origin of the Icosalides to the bacteria rather than fungi. Further, they assigned the stereochemistry of beta hydroxy acids as 3-*S*-hydroxy decanoic acid and 3-*R*-hydroxy octanoic acid based on Moscher ester analysis and molecular modeling.[33] In contrary, Jenner *et al.*[34] established the biosynthetic pathway of Icosalides and reported the configurations of both beta hydroxy acids in Icosalide **1a** as *R*.[34] These two studies have left the stereochemistry of the beta hydroxy acids in Icosalides ambiguous.

The swarming inhibitive nature, unusual lipophilic composition, antibiotic activity of the Icosalide **1a,** and the ambiguity in its structure have attracted us to investigate it. Through this study, we established its precise stereochemical structure via its total synthesis, NMR-based three-dimensional conformation, and further the influence of the lipophilic sidechains and the ester bonds on its activity.

Table 1. Residue sequences of isolated and synthesized Icosalides (the residue numbering is as given in Figure **1**).

Icosalides	Residues					
	1	2	3 (bHA2) Y=O, R2=	4	5	6 (bHA1) X=O, R1=
1a	l	S	C_7H_{15}	S	L	C_5H_{11}
1a'	l	S	C_7H_{15}*	S	L	C_5H_{11}
1a''	l	S	C_7H_{15}	S	L	C_5H_{11}*
1a'''	l	S	C_7H_{15}*	S	L	C_5H_{11}*
1b	L	S	C_7H_{15}	S	L	C_5H_{11}
1c	L	S	C_5H_{11}	S	L	C_5H_{11}
Ester containing Icosalide analogues						
2	l	S	C_3H_7	S	L	CH_3
3	l	S	C_5H_{11}	S	L	C_3H_7
4	l	S	C_9H_{19}	S	L	C_7H_{15}
5	l	S	$C_{11}H_{23}$	S	L	C_9H_{19}
6	l	S	*i*-Pr	S	L	*i*-Pr
7	l	S	Cp	S	L	Cp
Amide containing Icosalide analogues						
	1	2	3 (bHA2) Y=O, R2=	4	5	6 (bAA1) X=NH, R1=
8	l	S	C_7H_{15}	S	L	H
9	l	S	C_7H_{15}	S	L	C_5H_{11}
	1	2	3 (bAA2) Y=NH, R2=	4	5	6 (bHA1) X=O, R1=
10	l	S	H	S	L	C_5H_{11}
11	l	S	C_7H_{15}	S	L	H
	1	2	3 (bAA2) Y=NH, R2=	4	5	6 (bAA1) X=NH, R1=
12	l	S	H	S	L	H
13	l	S	C_7H_{15}	S	L	C_5H_{11}

L = L-Leucine; l = D-Leucine; S = L-Serine; bHA = beta hydroxy acid; bAA = beta amino acid; *= Chiral centre of this beta hydroxy acid is *S*
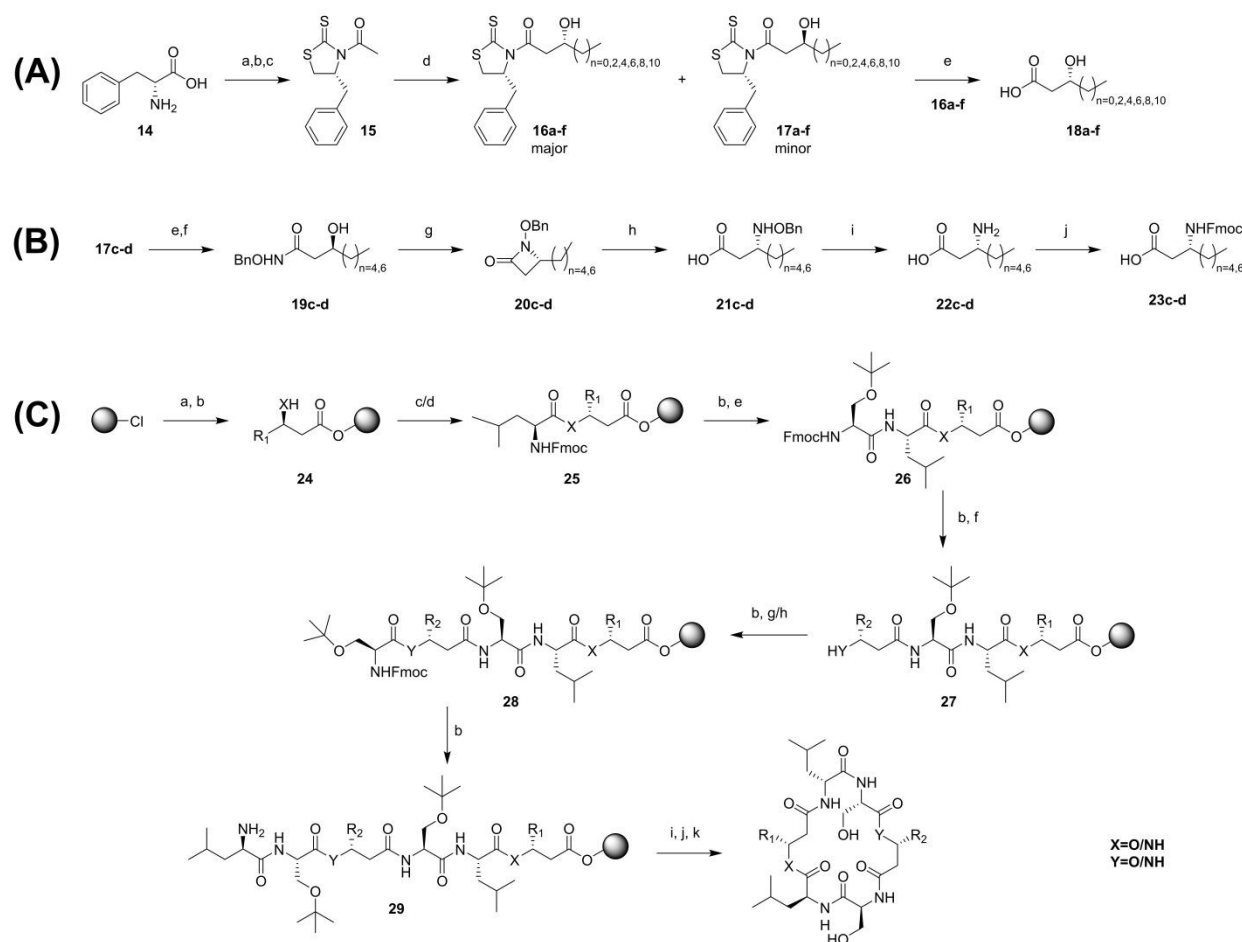
Journal Name

Herein, we report the synthesis of Icosalide **1a** and its analogues (Figure **1**, Table **1**), NMR-based structural studies of Icosalide **1a**, and the structure-activity studies of its analogues. The Icosalide **1a** analogues (peptides **1a**, **2**-**13**, Table **1**) planned for the biological study vary (a) in the length of the beta hydoxy fatty acid chains (peptides **2**-**7**) and (b) substitution of the beta hydroxy acid with beta amino acid (peptides **8**-**13**), which is inspired by the earlier reports on the influence of ester to amide switching on bioactivity.[26,35]

Results and discussion

The Icosalide **1a** and its analogues were synthesized by employing the solid phase peptide synthesis protocol using Fmoc strategy (see scheme **1** and experimental section).[36] The basic L- and D- amino acid building blocks and reagents were obtained from commercial sources. The required *R*-beta hydroxy acids (**18a-h**) and *R*- beta amino acids (**22c-d**) needed for the analogues were synthesized by stereoselective aldol condensation using chiral auxiliary (see scheme **1** and experimental section).[37]

Scheme 1. Synthetic schemes, reagents, and conditions (yields). (**A**) **stereoselective synthesis of *R*-beta hydroxy acid (bHA)**[37]; (a) LAH (1.7 eq.), Dry THF 12 h reflux; (b) CS$_2$ (5 eq.), KOH (5 M); (c) AcCl (1.5 eq.), DMAP (0.1 eq), NEt$_3$ (1.5 eq.), Dry DCM; (d) aldehyde (1 eq.), TiCl$_4$ (1.8 eq.), DIPEA (1.8 eq.), Dry DCM; (e) LiOH (4 eq., 1M, H$_2$O), THF. (**B**) **stereoselective synthesis of R-beta amino acid (bAA)**,[38] (f) EDCI (1.5 eq.), BnONH$_2$ (2.0 eq.), THF-H$_2$O (90%); (g) DEAD (1.0 eq.), PPh$_3$ (1.1 eq.), Dry THF (80%); (h) LiOH, THF MeOH-H$_2$O, 0 °C (95%); (i) Pd/C, H$_2$, MeOH (98%); (j) Fmoc-Cl (1.1 eq.), 10% Na$_2$CO$_3$, dioxane:water (1:1) (95%) (**C**) **solid phase peptide synthesis of Icosalide 1a-1a''' and analogues (2-13)**; (a) bHA1 or Fmoc-bAA1 (1.2 eq.), DIPEA (3 eq.), DCM 1.5 h (b) 20% piperidine in DMF 20 min (2*10 min) (c) Fmoc-Leu (2 eq.), DIPEA (3 eq.), HCTU (2 eq.), HOAt (2 eq.), NMP 2 h (d) Fmoc-Leu (2 eq.), DIC (2 eq.) DMAP (0.2 eq.) DCM (e) Fmoc-Ser(*t*Bu) (2 eq.), DIPEA (3 eq.), HCTU (2 eq.), HOAt (2 eq.), NMP (f) bHA2 or Fmoc-bAA2 (2 eq.), DIPEA (3 eq.), HCTU (2 eq.), HOAt (2 eq.), NMP 2 h (g) Fmoc-D-Leu (2 eq.), DIPEA (3 eq.), HCTU (2 eq.), HOAt (2 eq.), NMP 2 h (h) Fmoc-D-Leu (2 eq.), DIC (2 eq.) DMAP (2 eq.) DCM 2 h (i) TFE: AcOH: DCM (1:1:8) (j) HCTU (1.1 eq.) HOAt (1.1 eq), DIPEA (k) 50% TFA in DCM.

To determine the correct stereochemistry of the constituent beta hydroxy acids in the Icosalide **1a**, we synthesized Icosalide **1a** containing beta hydroxy octanoic acid and beta hydroxy decanoic acid both in *R* configuration (3*R*6*R* isomer) as per Jenner *et al*. and the analogue Icosalide **1a'** (3*S*6*R* isomer) containing 3-*R*-hydroxy octanoic acid and 3-*S*-hydroxy decanoic acid as per Dose *et al*. Further, we have also synthesized the other two diastereomers of Icosalide **1a** in which the beta

hydroxy acid configuration at residue positions 3 and 6 are 3*R*6*S* (**1a''**) and 3*S*6*S* (**1a'''**) (Figure **2**, supplementary figure **1**). Our synthesis studies and the comparison of all the four diastereomers with the isolated Icosalide **1a** have shown that Icosalide **1a** with both hydroxy acids in *R* configuration has matched the NMR data (Figure **2**, supplementary figure **2**) reported by Boros *et al*., Dose *et al*., and Jenner *et al*. Thus, the

COMMUNICATION

structural ambiguity associated with Icosalide **1a** has been resolved while also achieving its total synthesis.

To understand the three-dimensional folding in Icosalide **1a**, NMR-based conformation of Icosalide **1a** (Figure **3a**) was determined in DMSO-d_6 at 298 K on Schrodinger Maestro macro model 13.1[39] using inter-proton distance restraints derived from ROESY experiments. The depsipeptide exhibited a conformation akin to an anti-parallel beta-sheet structure in cyclic peptides. The conformation shows the possibility of three amide NHs, namely, 1-D-Leu-NH, 2-Ser-NH, and 4-Ser-NH, internally oriented into the macrocycle and involved in hydrogen bonding with the ester oxygen of *R*-3-hydroxy octanoic acid, 4-Ser-CO, and the ester oxygen of *R*-3-hydroxy decanoic acid, respectively. The ROE between 2-Ser-NH and 4-Ser-NH supports the internal orientation of the Serine NHs (see supplementary figure **7**). The involvement in hydrogen bonding or solvent shielding of these three amide NHs is also supported by the low values (-2.8, -0.4, and -1.6 ppb/K for 1-D-Leu-NH, 2-Ser-NH, and 4-Ser-NH, respectively) of NMR chemical shift temperature coefficients (supplementary table **3**) calculated in DMSO-d_6.[40] 3-Leu-NH is externally oriented, and its solvent-accessible nature is supported by a high (-6.8 ppb/K) chemical shift temperature coefficient.
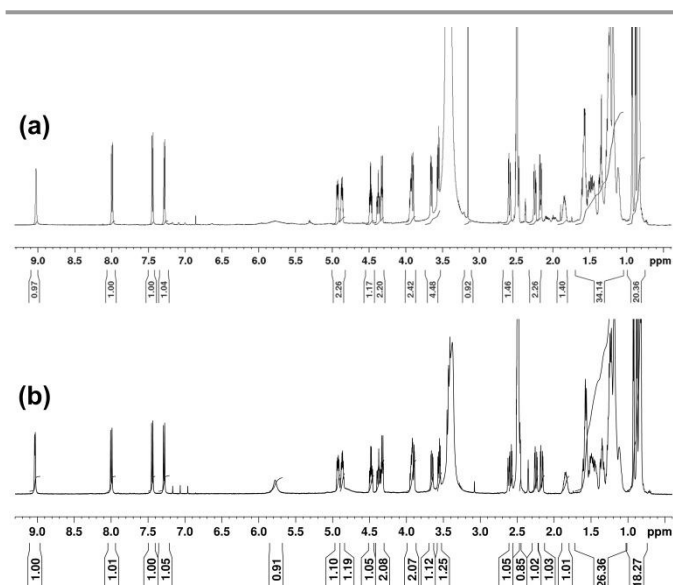

Figure 2. Comparison of the NMR spectra of **(a)** the Icosalide **1a** isolated from cell culture,[6] and (**b**) the synthesized Icosalide **1a**.

A unique feature of the Icosalide **1a** conformation (Figure **3b**) is the amphiphilic orientation of all the lipophilic chains (from 1-D-Leu, 3-*R*-hydroxy octanoic acid, 3-*R*-hydroxy decanoic acid, and 5-Leu) towards one face of the macrocycle ring and the orientation of the polar sidechains of 2-Ser and 4-Ser towards the opposite face. It is very likely that such orientation promotes Van der Waals interactions and leads to a stable conformation. Further, the sidechains of 2-Ser and 4-Ser face each other from the opposite sides of the macrocyle ring, which is supported by the ROEs, 4-Ser-NH to 2-Ser-Hβ protons, and 2-Ser-NH to 4-Ser-Hβ protons (supplementary figure **7a**). A similar face-to-face position is also observed for the sidechains of 1-D-

Leu and 5-Leu and is supported by the ROE between the 5-Leu-Hα proton and 1-D-Leu-Hγ proton (supplementary figure **7b**). The turn regions are occupied by *R*-3-hydroxy octanoic acid, *R*-3-hydroxy decanoic acid. (Figure **3**).

Bioactivity assays

The common appearance of a typical Icosalide complex in different *Burkholderia spp.* indicates that the peptolide has a key role in ecology as evidenced by its lipopeptidic nature that harms the swarming process resulting in its antimicrobial activity. The Icosalide isolated from *Burkholderia* symbionts has swarming inhibitory activity and it also showed antibacterial activity against *Bacillus thuringenesis* and *Paenibacillus larvae* with MIC of 12.5 μg/mL and 3.1 μg/mL respectively. Previous study by Boros *et al.* (2006) reported the activity of Icosalide **1a** against *Streptococcus pneumoniae*, *Enterococcus faecalis* and an MIC of 8-16 μg/mL against *Streptococcus pyogenes*. To understand the effect of the chain length of the lipophilic sidechain and the ester to amide modification on the activity of Icosalide **1a**, we have investigated their structure-activity relationship (SAR) studies against *B. thuringenesis* and *P. dendritiformis*.
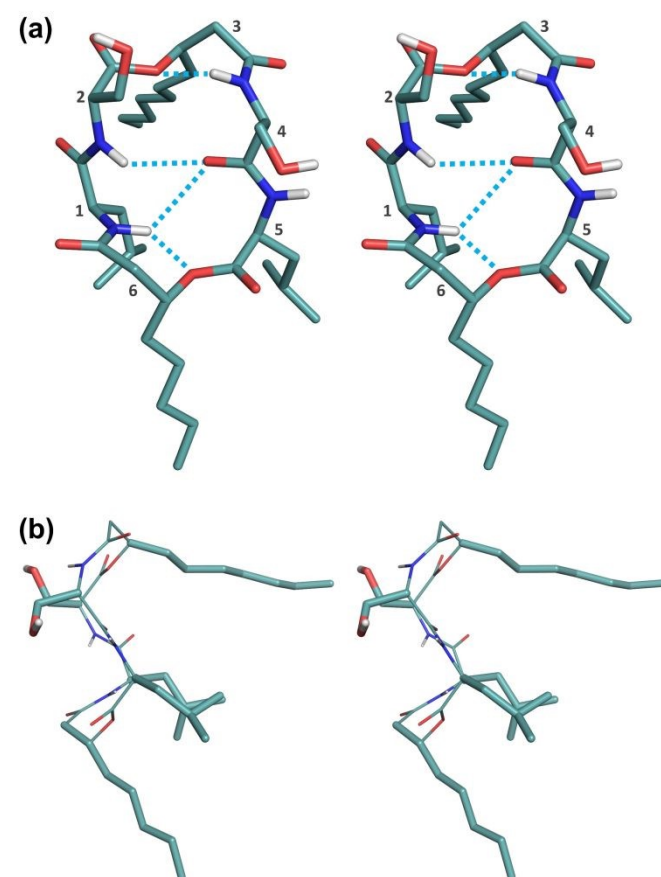
Figure 3. (a) Stereoview (top view) of the solution state conformation of Icosalide **1a**. For clarity, all the non-polar hydrogens are omitted. The possible hydrogen bonds are indicated as dashed lines in cyan. (**b**) Stereoview (side view) of the NMR-derived conformation of Icosalide **1a**.

For the SAR study, 12 analogues (**2**-**13**) of **1a** were designed and synthesized. The analogues **2**-**7** have the ester linkages but vary

in the length of the lipophilic sidechains. **2** and **3** have shorter lipophilic sidechains than those in Icosalide **1a**, whereas **4** and **5** have longer lipophilic sidechains than those in Icosalide **1a**. Analogue **6** has branched isopropyl sidechains, and **7** has cyclopropyl sidechains. Analogues **8-11** contain one amide bond, and **12**-**13** have two amide bonds instead of the ester groups. While **8** and **9** have amide linkage between residues 5 and 6, **10** and **11** have amide linkage between residues 2 and 3. **8** and **10** used β-Alanine for amide bond, **9** and **11** have 3-*R*-amino octanoic acid and 3-*R*-amino decanoic acid, respectively. **12** has two amide bonds from two β-Alanines and **13** has two amide bonds made from the amide analogues of respective beta hydroxy acids at positions 3 and 6. In principle, **12** is the amide analogue of **1a** without lipophilic chains, and **13** is the amide analogue of **1a** with all the original side chain groups.

Time-kill test

In this study, synthesized Icosalide **1a** analogues were primarily evaluated for their antimicrobial activity against *B. thuringenesis* as model strain. All the tested 13 icosalide analogues showed antibacterial activity at 50 μg/mL. The Icosalide **1a** showed the least CFU indicating the highest growth inhibition of the tested bacteria, followed by **4** and **5** containing the longest beta hydroxy acid chains and analogues **10** and **12** (supplementary figure **8**). Analogues **3**, **8**, **9**, and **13** showed moderate activity. The rest of the analogues showed the least inhibitory activity against *B. thuringenesis*. Further, we evaluated their MIC using dilution and resazurin assay.[41]

Determination of MIC

MIC assay was carried out for all the Icosalide analogues against *B. thuringenesis* and *P. dendritiformis* (supplementary figure **9**, and supplementary table **6, 7**). Against *B. thuringenesis*, **1a**, **2**, **8** and **9** displayed MIC at 25.0 μg/mL, while **3**, **4**, **5**, **6**, **7**, **12**, and **13** showed MIC at 12.5 μg/mL, which is better than the activity of Icosalide **1a**. The least MIC was noticed for **10** at MIC 50 μg/mL and no or partial activity was observed with **11**. Against *P. dendritiformis*, Icosalide **1a** showed MIC at 0.8 μg/mL, followed by analogues **5, 6, 7, 9, 10, 11**, and **12** that showed MIC at 12.5 μg/mL while the peptides **2, 3, 4, 8** and **13** exhibited the least MIC at 25 μg/mL.

Swarming assay

A swarming inhibition assay was performed to determine the chemotoxicity of the Icosalide analogues towards *B. thuringiensis* and *P. dendritiformis* (supplementary figure **10**). In this study, Icosalide **1a** has shown complete inhibition against both the bacterial strains at 25 μg/mL. Analogues **2**, **5**, and **8** inhibited about ~8.3% of the swarming activity of *B. thuringiensis* when compared with the Icosalide **1a**. On the other hand, for *P. dendritiformis*, analogue **2** demonstrated ~33% of swarming inhibition, followed by **3**, and **4** which demonstrated ~25% inhibition. The rest of the Icosalides displayed about 16–24% inhibition of the swarming area of *P. dendritiformis*.

Drop collapse assay

Further, the drop collapse assay was performed to determine the surfactant activity of the various Icosalide analogues on *B. thuringiensis* on Parafilm 'M'. The results showed that most

Icosalide analogues displayed drop collapsing except **2, 4, 5,** and **11** (supplementary figure **11**).

In a further expansion of the biological activity screening of the Icosalides, we have also screened the Icosalides for their anti-mycobacterium and anti-cancer activities.

Antitubercular activity

The Icosalide **1a** and its analogues were screened for *in vitro* antitubercular activity against *M. tuberculosis* H37Ra RFP strain by an established paraffin red fluorescence microplate assay.[42] The MIC of each screened Icosalide (supplementary table **8**) against *Mycobacterium tuberculosis* is in between 2 to 10 μg/mL except **2** and **9**. Here, Rifampicin and Isoniazid were used as standard molecules for anti-TB studies with MIC 0.005±0.001 & 0.047±0.021 μg/mL.

Anticancer activity

Furthermore, anticancer activity for Icosalides was performed on Hela cervical cancerous cell lines and Thp1 monocytic cell lines by using the anticancer drug Doxorubicin as the standard (supplementary table **8**).[43] Among all, Icosalide **1a** has shown IC_{50} of (4.612±0.389) μg/mL on HeLa and, (4.125±1.271901) μg/mL against ThP1 cell lines.

Through the current SAR study, we could showcase the expanded biological activities of the Icosalide **1a** and its analogues. Amongst all, compound **5** having the longest lipophilic sidechains, had shown positive activity in the majority of the tests (Time-kill test, MIC against *B. thuringenesis* and *P. dendritiformis*, Swarming inhibition assay and antitubercular activity). Analogues of **1a** with beta-branched sidechains, **6** and **7**, also displayed a competitive MIC against both the tested bacterial strains. Compound **12**, the all amide analogue of **1a,** containing two β-Alanines and no lipophilic sidechains showed better Time-kill and MIC activity than compound **13**, which is an all amide compound with lipophilic sidechains as in **1a**. Interestingly, most of the modifications studied here have not affected the newly found antitubercular activity of Icosalide **1a**. However, pronounced trends in the bioactivities to the changes in lipophilic sidechains or amide substitutions in Icosalide **1a** were elusive.

Conclusions

In summary, we have developed a hybrid synthetic route comprising solid-phase and solution-phase synthesis methods to access Icosalide **1a**, a natural antibacterial product, and its analogues. We have also unequivocally confirmed the stereochemistry of the two hydroxy acids in Icosalide **1a** as *R*-configuration. We have synthesized a set of analogues of Icosalide **1a**, which varied in the length of the constituent lipophilic beta-hydroxy acids and/or have the ester bonds replaced by amide bonds. We found that the ester analogues containing longer beta-hydroxy acid chains (**4** and **5**) have shown antibacterial activity similar to Icosalide **1a**, however, the ones with shorter beta hydroxy acid chain lengths have shown a lower activity. On the other hand, Icosalide **1a** and most of its analogues, except for **2** and **9,** have exhibited antitubercular activity within 10 μg/mL. Icosalide **1a** is found to be anticancerous against HeLa and ThP1 cell lines. The work

described here lays the foundation for generating analogues of Icosalide **1a** with a view to optimize their activity for tuberculosis and Gram-positive infections.

View Article Online
DOI: 10.1039/D3OB00809F

Conflicts of interest

There are no conflicts to declare.

Acknowledgements

Abbreviations

CCR2, CC chemokine receptor 2; CCL2, CC chemokine ligand 2; CCR5, CC chemokine receptor 5; TLC, thin layer chromatography.

Notes and references

1 R. I. Aminov, *Front. Microbiol.*, 2010, **1**, 1–7.
2 C. L. Ventola, *P T J.*, 2015, **40**, 277–283.
3 S. Sengupta, M. K. Chattopadhyay and H. P. Grossart, *Front. Microbiol.*, 2013, **4**, 1–13.
4 S. Bin Zaman, M. A. Hussain, R. Nye, V. Mehta, K. T. Mamun and N. Hossain, *Cureus*, 2017, **9**, e1403.
5 D. G. J. Larsson and C. F. Flach, *Nat. Rev. Microbiol.*, 2022, **20**, 257–269.
6 Antimicrobial Resistance Collaborators, *Lancet*, 2022, **399**, 629–655.
7 N. A. Schilling, A. Berscheid, J. Schumacher, J. S. Saur, M. C. Konnerth, S. N. Wirtz, J. M. Beltrán-Beleña, A. Zipperer, B. Krismer, A. Peschel, H. Kalbacher, H. Brötz-Oesterhelt, C. Steinem and S. Grond, *Angew. Chemie Int. Ed.*, 2019, **58**, 9234–9238.
8 K. E. Greber and M. Dawgul, *Curr. Top. Med. Chem.*, 2017, **17**, 620–628.
9 M. Mahlapuu, J. Håkansson, L. Ringstad and C. Björn, *Front. Cell. Infect. Microbiol.*, 2016, **6**, 1–12.
10 C. De La Fuente-Núñez, V. Korolik, M. Bains, U. Nguyen, E. B. M. Breidenstein, S. Horsman, S. Lewenza, L. Burrows and R. E. W. Hancock, *Antimicrob. Agents Chemother.*, 2012, **56**, 2696–2704.
11 S. Rütschlin and T. Böttcher, *Chem. - A Eur. J.*, 2020, **26**, 964–979.
12 S. J. Uddin, J. A. Shilpi, L. Nahar, S. D. Sarker and U. Göransson, *Front. Pharmacol.*, 2021, **12**, 10–12.
13 A. G. Atanasov, S. B. Zotchev, the I. N. P. S. T. Dirsch and C. T. Supuran, *Nat. Rev. Drug Discov.*, 2021, **20**, 200–216.
14 S. Huang, Y. Liu, W. Liu, P. Neubauer and J. Li, *Microorganisms*, 2021, **9**, 1–22.
15 V. B. Gunjal, R. Thakare, S. Chopra and D. S. Reddy, *J. Med. Chem.*, 2020, **63**, 12171–12195.
16 L. L. Ling, T. Schneider, A. J. Peoples, A. L. Spoering, I. Engels, B. P. Conlon, A. Mueller, T. F. Schäberle, D. E. Hughes, S. Epstein, M. Jones, L. Lazarides, V. A. Steadman, D. R. Cohen, C. R. Felix, K. A. Fetterman, W. P. Millett, A. G. Nitti, A. M. Zullo, C. Chen and K. Lewis, *Nature*, 2015, **517**, 455–459.
17 Q. Guan, S. Huang, Y. Jin, R. Campagne, V. Alezra and Y. Wan, *J. Med. Chem.*, 2019, **62**, 7603–7617.
18 Y. Hamada and T. Shioiri, *Chem. Rev.*, 2005, **105**, 4441–4482.
19 J. Adrio, C. Cuevas, I. Manzanares and M. M. Joullié, *J. Org. Chem.*, 2007, **72**, 5129–5138.
20 H. Kaur, P. W. R. Harris, P. J. Little and M. A. Brimble, *Org. Lett.*, 2015, **17**, 492–495.
21 R. Lemmens-Gruber, M. Kamyar and R. Dornetshuber, *Curr. Med. Chem.*, 2009, **16**, 1122–1137.
22 G. N. Belofsky, P. R. Jensen and W. Fenical, *Tetrahedron Lett.*, 1999, **40**, 2913–2916.
23 K. Otrubova, G. Lushington, D. Vander Velde, K. L. McGuire and S. R. McAlpine, *J. Med. Chem.*, 2008, **51**, 530–544.
24 M. D. Vera and M. M. Joullie, *Med. Res. Rev.*, 2002, **22**, 102–145.
25 Y. Xu, R. D. Kersten, S.-J. Nam, L. Lu, A. M. Al-Suwailem, H. Zheng, W. Fenical, P. C. Dorrestein, B. S. Moore and P.-Y. Qian, *J. Am. Chem. Soc.*, 2012, **134**, 8625–8632.
26 N. Bionda, M. Stawikowski, R. Stawikowska, M. Cudic, F. López-Vallejo, D. Treitl, J. Medina-Franco and P. Cudic, *ChemMedChem*, 2012, **7**, 871–882.
27 E. M. Driggers, S. P. Hale, J. Lee and N. K. Terrett, *Nat. Rev. Drug Discov.*, 2008, **7**, 608–624.
28 H. Zhang, A. L. Nielsen, M. W. Boesgaard, K. Harpsøe, N. L. Daly, X. F. Xiong, C. R. Underwood, L. M. Haugaard-Kedström, H. Bräuner-Osborne, D. E. Gloriam and K. Strømgaard, *Eur. J. Med. Chem.*, 2018, **156**, 847–860.
29 N. Bionda, J. P. Pitteloud and P. Cudic, *Future Med. Chem.*, 2013, **5**, 1311–1330.
30 D. J. Craik, D. P. Fairlie, S. Liras and D. Price, *Chem. Biol. Drug Des.*, 2013, **81**, 136–147.
31 C. Boros, C. J. Smith, Y. Vasina, Y. Che, A. B. Dix, B. Darveaux and C. Pearce, *J. Antibiot.*, 2006, **59**, 486–494.
32 L. V. Wilkinson, M. A. Alford, S. R. Coleman, B. C. Wu, A. H. Y. Lee, T. M. Blimkie, M. Bains, R. Falsafi, D. Pletzer and R. E. W. Hancock, *PLoS One*, 2021, **16**, 1–18.
33 B. Dose, S. P. Niehs, K. Scherlach, L. V. Flórez, M. Kaltenpoth and C. Hertweck, *ACS Chem. Biol.*, 2018, **13**, 2414–2420.
34 M. Jenner, X. Jian, Y. Dashti, J. Masschelein, C. Hobson, D. M. Roberts, C. Jones, S. Harris, J. Parkhill, H. A. Raja, N. H. Oberlies, C. J. Pearce, E. Mahenthiralingam and G. L. Challis, *Chem. Sci.*, 2019, **10**, 5489–5494.
35 N. Bionda, R. M. Fleeman, L. N. Shaw and P. Cudic, *ChemMedChem*, 2013, **8**, 1394–1402.
36 R. B. Merrifield, *Excerpta Med., I.C.S.*, 1976, **No.374**, 29–39.
37 B. Kitir, M. Baldry, H. Ingmer and C. A. Olsen, *Tetrahedron*, 2014, **70**, 7721–7732.
38 Y. Jin and D. H. Kim, *Synlett*, 1998, **33**, 1189–1190.
39 a) Schrödinger Release 2023-1: MacroModel, Schrödinger, LLC, New York, NY, 2021. b) Schrödinger Release 2023-1: Maestro, Schrödinger, LLC, New York, NY, 2021.
40 T. Cierpicki and J. Otlewski, *J. Biomol. NMR*, 2001, **21**, 249–261.
41 A. L. Castilho, K. R. Caleffi-Ferracioli, P. H. Canezin, V. L. Dias Siqueira, R. B. de Lima Scodro and R. F. Cardoso, *J. Microbiol. Methods*, 2015, **111**, 119–121.
42 A. Yeware and D. Sarkar, *Tuberculosis*, 2018, **110**, 15–19.
43 S. P. Langdon, *Cancer Cell Cult.*, 2003, **731**, 237–245.

Organic & Biomolecular Chemistry Accepted Manuscript